Final Report

Study to Understand and Assess the Non- Putrefying Nature of Ganga Water

Sponsor

National Mission of Clean Ganga (NMCG)
Ministry of Water Resources and River Rejuvenation (MoWR),
Government of India, New Delhi

CSIR-National Environmental Engineering Research Institute (NEERI)
Under Council of Scientific & Industrial Research
Nehru Marg, Nagpur – 440 020

November 2023

Project Team

- CSIR-National Environmental Engineering Research Institute (NEERI), Nagpur
- CSIR – National Chemical Laboratory, Pune
- Indian Institute of Technology – Roorkee
- IIT – BHU, Varanasi
- University of Patna, Patna
- All India Institute of Medical Sciences, Delhi

CONTENTS

Sl. No.	Title			Page No.
Chapter -1 : Introduction				1
1.0	Introduction			2
1.1	Background			2
1.2	Previous Studies			4
Chapter-2 : Physico-chemical Aspects				9
2.0	Physico-chemical Aspects			10
2.1	Water Quality along the Ganga River at select locations			11
	2.1.1	Scope of Work		12
	2.1.2	Methodology		12
	2.1.3	Physico-chemical characteristics of River Ganga		15
		2.1.3.1	Electrical conductivity (EC)	16
		2.1.3.2	Total Hardness (Calcium & Magnesium)	17
		2.1.3.3	Total Alkalinity	17
		2.13.4	Dissolved Oxygen	18
		2.1.3.5	Chemical Oxygen Demand	18
		2.1.3.6	Biochemical Oxygen Demand	19
Chapter-3 : Dissolved Oxygen				31
3.0	Monitor the dissolved oxygen in the Ganga, and examine the dissolved oxygen profile for saturation levels and depleted levels, simultaneously correlating with other influencing parameters (such as zoo and phytoplankton population) and to study the re-aeration of the river			32
3.1	Introduction			32
3.2	Objectives			33
3.3	Study Area			33
	3.3.1	Kanpur		33
	3.3.2	Prayagraj (Allahabad)		34
	3.3.3	Varanasi (Banaras)		35
3.4	Methodology			36
	3.4.1	Dissolved Oxygen Profiling		36

Sl. No.	Title		Page No.
	3.4.2	Reaeration Rate Experiment	37
	3.4.3	Biochemical Oxygen Demand Monitoring	37
	3.4.4	Diurnal Variation	38
3.5	Results and Discussion – Pre Monsoon Season		38
	3.5.1	Dissolved Oxygen Profiling	38
	3.5.1.1	Kanpur	38
	3.5.1.2	Prayagraj	41
	3.5.1.3	Varanasi	41
	3.5.2	Reaeration Rate Experiment	44
	3.5.2.1	Kanpur	44
	3.5.2.2	Prayagraj	47
	3.5.2.3	Varanasi	49
3.6	Results ansd Discussion – Post Monsoon Season		51
	3.6.1	Dissolved Oxygen Profiling	51
	3.6.2	BOD monitoring	52
	3.6.2.1	Prayagraj	52
	3.6.2.2	Varanasi	53
	3.6.3	Reaeration Rate Experiment	54
3.7	Conclusions		55
Chapter-4 : Quantitative Risk Assessment			56
4.0	Quantitative Risk Assessment in River Ganga to assess hot spots in the river and associated health risk		57
4.1	Introduction		57
4.2	Methodology		58
	4.2.1	Study Site	58
	4.2.2	General Quantitative Microbial Risk Assessment Framework	59
4.3	Study Considerations for QMRA		62
	4.3.1	Problem Formulation	62
	4.3.2	Exposure Assessment	64
	4.3.3	Health Effects Assessment	68

Sl. No.	Title			Page No.
	4.3.4	Risk Characterization		69
	4.3.5	Limitations and Recommendations		70
4.4	Results			70
	4.4.1	Exposed Population Characteristics		70
	4.4.2	Exposure Patterns in the Study Area		71
	4.4.3	Health Risks Linked to Farming Activities and Salad Consumption		71
	4.4.4	Conclusion		77
4.5	References			77
Chapter-5 : Geo-chemical Partitioning of Metals				80
5.0	Geo-Chemical Partitioning of Metals in River Ganga:Preliminary Trends of Various Trace Metals and their Partitioning in Upper Stretches of River Ganga			81
5.1	Background			81
5.2	Methods and Materials			82
	5.2.1	Collection of Samples		83
	5.2.2	Digestion Procedure for Total Metal Analysis		83
	5.2.3	Calibration and Standardization		86
5.3	Results and Discussions			91
	5.3.1	Distribution of Metals		92
	5.3.2	Distribution of Various Metals Along the Entire Stretch of River Ganga		94
		5.3.2.1	Arsenic	94
		5.3.2.2	Silver	95
		5.3.2.3	Barium	96
		5.3.2.4	Cadmium	97
		5.3.2.5	Cobalt	98
		5.3.2.6	Copper	99
		5.3.2.7	Chromium	100
		5.3.2.8	Manganese	101
		5.3.2.9	Lead	102
		5.3.2.10	Selenium	103

Sl. No.	Title			Page No.
		5.3.2.11	Zinc	104
5.4	Variations at Different Points of Sampling			105
5.5	Variations of Metal Concentrations at Various Depths in Tehri Reservoir			106
5.6	Salient Findings			107
Chapter-6 : Sediment Characterization				108
6.0	Sediment Characterization			109
6.1	Sampling Locations : Area of Study			109
6.2	Sediment Sampling			119
6.3	Pre-Treatment of the Sample			119
6.4	Analytical Techniques used for Sediment Characterization			119
	6.4.1	Grain Size Distribution		119
	6.4.2	Laser Light Experiments		119
	6.4.3	Dynamic Light Scattering (DLS) and Zeta potential Experiments		120
	6.4.4	Transmission Electron Microscopy (TEM)		121
	6.4.5	Powder X-Ray Diffraction (pXRD) Study		121
	6.4.6	X-Ray Fluorescence (XRF) Study		122
	6.4.7	Inductively Coupled Plasma Mass Spectroscopy (ICP-MS) Analysis		122
	6.4.8	Antibacterial Activity Test		122
6.5	Results and Discussion			123
	6.5.1	Grain size distribution		123
	6.5.2	Laser Light Scattering Experiment		127
	6.5.3	Dynamic Light Scattering (DLS) Analysis		131
	6.5.4	Zeta Potential Study		133
	6.5.5	Transmission Electron Microscopy (TEM)		134
	6.5.6	X-Ray Diffraction (XRD)		148
	6.5.7	Elemental Analysis		154
		6.5.7.1	X-Ray Fluorescence (XRF)	154
		6.5.7.2	Inductively Coupled Plasma Mass Spectroscopy (ICP-MS) Analysis Results	157
	6.5.8	Assay for antibacterial of sediments, suspended sediments, and river		160

Sl. No.	Title			Page No.
		water of Ganga		
6.6	Salient Findings			166
6.7	Future Studies			169
6.8	References			170
Chapter-7 A: Chemical-biological Interactions				177
7.0	Investigation of chemical-biological interactions of plant-originated organics for self-purification properties of River Ganga			178
7.1	Introduction			178
	7.1.1	Phytochemicals of Plant Origin		179
	7.1.2	Sample Collection		182
	7.1.3	Materials and Methods		189
	7.1.4	Experimental Details		189
		7.1.4.1	Simulated Experiments using Plant Parts	189
		7.1.4.2	Ganga Water, Soil, Sediment and Litter Analysis	191
		7.1.4.3	Non-putrefaction properties: Prevention of protein Denaturation using Phytochemicals	191
	7.1.5	Analytical Results		191
		7.1.5.1	FTIR Analysis	195
		7.1.5.2	Total Phenolic Content	197
		7.1.5.3	GC-MS Analysis: Terpenes and Terpenoids Leached	199
		7.1.5.4	Ganga Sample Analysis	201
		7.1.5.5	Results of FTIR Analysis	201
		7.1.5.6	GC-MS/MS Analysis	202
	7.1.6	Non-Putrefaction Properties of Phytochemicals		207
	7.1.7	Salient Findings		210
	7.1.8	References		212
7 B. Phytochemical Component				215
7.2	Phytochemical Component			216
	7.2.1	Background		216

Sl. No.	Title		Page No.
	7.2.2	Plant based Leaching Experiments	221
	7.2.3	TOC and CHNS of the Samples before leaching experiments	225
	7.2.4	Antibacterial properties of plant-leaf litter-soil leachate from Lysimeter study	229
Chapter –7C : Salient Findings			231

Chapter-8 : Biological and Health Component		
7.3	Metaviromics approach for understanding viral diversity, taxonomy and functional analysis	1-78
7.4	To deduce diversity, community and metabolic potential of uncultured bacteriophages in Ganga water and sediments using metavirome approach	
7.5	Assessment for distribution of bacteriophage communities with respect to their hosts and seasonal factors	
7.6	Assessing the Non-Putrefying Properties of GANGA Microbiome using High resolution Structural Techniques	1-103
7.7	Transmission electron microscopy (TEM) analysis of bacteriophages isolated from Ganga waters	
7.8	Structural and functional characterization of Pseudomonas phage endolysin detected by NEERI from Ganga bacteriophages	
7.9	NMR based metabolic analysis of bacteriophage endolysin producing bacteria	
8.0	Heavy metal remediation characteristics of microalgal species detected from Ganga waters near Haridwar	

8.1	Identification of bacteriophages against health care associated bacterial strains, clinical isolates, multi drug resistant bacterial strains, anaerobic and special pathogen bacteria of clinical significance.	1-33
8.2	Assessment of bacteriophage enriched water as an anti-infective agent to clean infected hospital setup including wards, ICU and operation theatre.	

8.3	Monitoring of source and spectrum of pathogenic and so called non pathogenic bacteria that interfere with the water quality of Ganga round the year in Varanasi.	1-38
8.4	Study on relevant bacteriophages (enumeration, isolation, characterization) with different seasonal variations.	
8.5	Study on potentials of bacteriophage therapy in the infections caused by multidrug-resistant bacterial pathogens in animal and human infections.	

List of Tables

Table No.	Title	Page No.
2.1	Table 2.1: Parameters analysed to assess the chemical characteristics of River Ganga	13
2.2	Table 2.2: Water quality data for the samples collected from entire stretch of River Ganga during Post-Monsoon seasons (Oct-2017)	26
2.3	Table 2.3: Water quality data for the samples collected from entire stretch of River Ganga during Pre-Monsoon seasons (May 2018)	28
4.1	Table 4.1: Key Exposure Groups included in the Study	62
4.2	Table 4.2: Reference Pathogens and Conversion Factors	63
4.3	Table 4.3: Exposure Assessment for Quantitative Risk Assessment	65
5.1	Table 5.1: Operating Conditions of ICP-MS	84
5.2	Table 4.2: Calibration Standards	86
5.3	Table 5.3 :Elements measured simultaneously using NexION 300X ICP-MS	87
5.4	Table 5.4 : Digestion Recovery Data	88
5.5	Table 5.5: Method Recovery Data	89
5.6	Table 5.6: Average Recoveries and Standard Deviation for Various Elements	90
6.1	Table 6.1: Details of the Sampling Location across the Stretch of River Ganga	109
6.2	Table 6.2: Depth Sampling At Selected Locations of River Ganga	115
6.3	Table 6.3: Grain Size Distribution and the approximate	124

Table No.	Title	Page No.
	percentage composition of sediment	
6.4	Table 6.4: Relation between Relative centrifugal (g) force and revolution per minute (rpm)	127
6.5	Table 6.5: Composition of mineral phases found in p-XRD profile of sediments at Gangotri	149
6.6	Table 6.6: Distribution of mineral phases obtained from pXRD analysis of 25 µm sediment fraction at the first stretch of River Ganga	150
6.7	Table 6.7: Composition of mineral phases obtained from pXRD analysis of the sediment samples	151
6.8	Table 6.8: The presence of elements in the selected sediments collected from the River Ganga	155
6.9	Table 6.9: ICP-MS analysis of a selected fraction of the sediments collected from River Ganga	158
6.10	Table 6.10: Antibacterial activity of various sediments and SS from River Ganga	161
6.11	Table 6.11: Antibacterial activity of their sediment sample form river Ganga	161
6.12	Table 6.12: Antibacterial activity of water samples from river Ganga devoid of sediments	163
7.1	Table 7.1: Significant Phytochemical Groups	180
7.2	Table 7.2: Project Milestones	181
7.3	Table 7.3: Sampling locations for the collection of plant parts and water	183
7.4	Table 7.4: TOC Results of Leaching Study in Distilled Water	193
7.5	Table 7.5: TOC Results of Leaching Study in Ganga Water	194
7.6	Table 7.6: Functional Groups Identified in Leaching Studies	195
7.7	Table 7.7: Phenolics in Leaf Extracts	198

Table No.	Title	Page No.
7.8	Table 7.8: LODs based on neat standards injected in GC-MSMS	200
7.9	Table 7.9: Blue Pine Leachate	200
7.10	Table 7.10: Deodar Leachate	201
7.11	Table 7.11: GC-MS Analysis of Ganga Water Samples	205
7.12	Table 7.12: Terpenes detected in water, sediment, litter and soil samples	206
7.13	Table 7.13: Protein putrefaction studies with Plant extracts	208
7.14	Table 7.14: Protein putrefaction studies with Ganga Water	209
7.15	Table 7.15: Protein putrefaction studies with Individual Phytochemicals	209
7.16	Table 7.16: Prominent secondary metabolites/phytochemicals reported from plant based sources	217
7.17	Table7.17: Selected plants collected for leaching experiments in Ganga water as well as distilled water	222
7.18	Table 7.18. Qualitative assessment of secondary metabolites from Cedrus deodara (Deodar) tree soil (Harsil) profile from single run leachate	226
7.19	Table 7.19. Qualitative assessment of secondary metabolites from Pinus wallichiana (Blue Pine) tree soil (Harsil) profile from multiple run leachate	227
7.20	Table 7.20: Qualitative assessment of secondary metabolites from Cedrus deodara (Deodar) and Pinus wallichina tree (blue pine) tree soil (Harsil) profile from multiple run leachate	228

List of Figures

Figure No.	Title	Page No.
2.1	Fig. 2.1: Physico-chemical component	11
2.2	Fig. 2.2: Selected major sampling locations along the river Ganga	15
2.3	Fig. 2.3: Seasonal variation of Electrical conductive along the stretch of River Ganga	20
2.4	Fig. 2.4: Seasonal variation of Total Hardness along the stretch of River Ganga	21
2.5	Fig. 2.5: Seasonal variation of Total Alkalinity along the stretch of River Ganga	22
2.6	Fig. 2.6: Seasonal variation of Dissolved Oxygen along the stretch of River Ganga	23
2.7	Fig.2.7: Seasonal variation of Chemical Oxygen Demand along the stretch of River Ganga	24
2.8	Fig. 2.8: Seasonal variation of Biochemical Oxygen Demand along the stretch of River Ganga	25
3.1	Fig. 3.1: Selected cities along river Ganga and the respective sewage loads	33
3.2	Fig.3.2: Monitoring locations at Kanpur	34
3.3	Fig. 3.3: Monitoring locations at Prayagraj	35
3.4	Fig. 3.4: Monitoring locations at Varanasi	36
3.5	Fig. 3.5: DO Monitoring locations near the nallah (drain)	37
3.5a	Fig. 3.5a: DO and Temperature profiling at various locations at surface of Ganga River at Kanpur (May, 2019)	39
3.5b	Fig. 3.5b: DOand Temperature profiling at various locations at 2 m depth of Ganga River at Kanpur (May, 2019)	40

Figure No.	Title	Page No.
3.5c	Fig. 3.5c: DOand Temperature profiling at various locations at 4 m depth of Ganga River at Kanpur (May, 2019)	40
3.5d	Fig. 3.5d: DO and Temperature profiling at various locations at 6 m depth of Ganga River at Kanpur (May, 2019)	40
3.6	Fig. 3.6: DO and Temperature profiling at various locations at surface of Ganga River at Prayagraj (May, 2019)	41
3.7a	Fig. 3.7a: DO and Temperature profiling at various locations at surface of Ganga River at Varanasi (May, 2019)	42
3.7b	Fig. 3.7b: DO and Temperature profiling at various locations at 2 m depth of Ganga River at Varanasi (May, 2019)	43
3.7c	Fig. 3.7c: DO and Temperature profiling at various locations at 4 m depth of Ganga River at Varanasi (May 9-12, 2019)	43
3.7d	Fig. 3.7d: DO and Temperature profiling at various locations at 6 m depth of Ganga River at Varanasi (May 9-12, 2019)	44
3.8a	Fig. 3.8a: Day time Reaeration at Bhagwat Das Nallah Kanpur (May,2019)	45
3.8b	Fig. 3.8b: Night time Reaeration at Bhagwat Das Nallah Kanpur (May,2019)	45
3.8c	Fig. 3.8c: Day time Reaeration at Kalwari Nallah Kanpur (May,2019)	46
3.8d	Fig. 3.8d: Night time Reaeration at Kalwari Nallah Kanpur (May,2019)	46
3.8e	Fig. 3.8e: Day time Reaeration at Golaghat Nallah Kanpur (May,2019)	47
3.8f	Fig. 3.8f: Day time Reaeration at Baba Nallah Kanpur (May,2019)	47
3.9a	Fig. 3.9a: Day time Reaeration at Resoolabad Nallah Prayagraj (May,2019)	48
3.9b	Fig. 3.9b: Day time Reaeration at Daragang, Prayagraj (May,2019)	49
3.10a	Fig. 3.10a: DO Reaeration at Assi Nallah- Pre-Monsoon	50

Figure No.	Title	Page No.
	(May,2019)	
3.10b	Fig. 3.10b: Day time Reaeration at Varuna Nallah (May, 209)	50
3.11a	Fig. 3.11a: DO Montoring at surface and at 1.5 m depth for 48 hrs at Rajghat Varanasi (Nov, 2019)	51
3.11b	Fig. 3.11b: Temparature Montoring at surface and at 1.5 m depth for 48 hrs at Rajghat Varanasi (Nov, 2019)	52
3.11c	Fig. 3.11c: BOD Variation in Prayagraj (Nov, 2019)	53
3.11d	Fig. 3.11d: BOD Variation in Varanasi (Nov, 2019)	54
3.12	Fig 3.12: DO Reaeration at Assi Nala- Post-Monsoon Day/Night (November, 2019)	55
4.1	Fig. 4.1: Illustration Of study site- Varanasi with Waste Water Treatment Plants Details Source: (a) Google Maps and (b) Sangat Mochan Foundation	59
4.2	Fig. 4.2: QMRA Framework outline (Hajare R.et.al 2021)	62
4.3	Fig. 4.3: Varanasi Map in 2-D excel format with GPS Coordinates	66
4.4	Fig. 4.4: Input for Model used for caluculation of concentration of Thermo Tolerant Coliform Count	67
4.5	Fig. 4.5: Irrigation Risk Map of Varanasi with Water Quality Data of 2017	72
4.6	Fig. 4.6: Irrigation Risk Map of Varanasi with Water Quality Data of 2023	73
4.7	Fig. 4.7: Pre-Monsoon and Post-Monsoon accidental ingestion risk on Bathing Risk for Childrens and Adults with Water Quality Data of 2017	74
4.8	Fig. 4.8: Pre-Monsoon and Post-Monsoon accidental ingestion risk on Bathing Risk for Childrens and Adults with Water Quality Data of 2023	76
5.1	Fig. 5.1: Methodology adopted for Sample Collection and Analysis	83

Figure No.	Title	Page No.
5.2	Fig. 5.2: Dissolved Fractions of Pre-Monsoon Season	92
5.3	Fig. 5.3: Dissolved Fractions of Post-Monsoon Season	93
5.4	Fig. 5.4: Suspended Fractions of Pre-Monsoon Season	94
5.5	Fig.5.5: Suspended Fractions of Post-Monsoon Season	94
5.6	Fig. 5.6: Variation in As at various locations and geo-chemical partitioning during pre and post monsoon season	95
5.7	Fig. 5.7: Variation in Ag at various locations and geo-chemical partitioning during pre and post monsoon season	96
5.8	Fig. 5.8: Variation in Ba at various locations and geo-chemical partitioning during pre and post monsoon season	97
5.9	Fig. 5.9: Variation in Cd at various locations and geo-chemical partitioning during pre and post monsoon season	98
5.10	Fig. 5.10: Variation in Co at various locations and geo-chemical partitioning during pre and post monsoon season	99
5.11	Fig. 5.11: Variation in Cu at various locations and geo-chemical partitioning during pre and post monsoon season	100
5.12	Fig. 5.12: Variation in Cr at various locations and geo-chemical partitioning during pre and post monsoon season	101
5.13	Fig. 5.13: Variation in Mn at various locations and geo-chemical partitioning during pre and post monsoon season	102
5.14	Fig. 5.14: Variation in Pb at various locations and geo-chemical partitioning during pre and post monsoon season	103
5.15	Fig. 5.15: Variation in Se at various locations and geo-chemical partitioning during pre and post monsoon season	104
5.16	Fig. 5.16: Variation in Zn at Various Locations and Geo-Chemical Partitioning during Pre and Post Monsoon Season	105
5.17	Fig. 5.17: Variations in Dissolved Concentration of Cu at Different Points of Sampling	106
5.18	Fig. 5.18: Variations of metal concentrations at different depths in Tehri reservoir	107

Figure No.	Title	Page No.
6.1	Fig 6.1: Overall study area and sampling locations details across the stretch of Indo-Gangetic plain	117
6.2	Fig. 6.2: Depth sampling at Tehri reservoir and Chinyalisaur	118
6.3	Fig. 6.3: Particle size distribution analysis of the SS samples collected from various locations of River Ganga	121
6.4	Fig. 6.4: TEM analysis plan of SS samples collected from River Ganga	121
6.5	Fig. 6.5: Antibacterial activity test for the samples collected from the first stretch of River Ganga	123
6.6	Fig. 6.6: Size distribution of various sediment samples across the entire stretches of River Ganga	126
6.7	Fig. 6.7: Laser Light scattering of SS samples collected from various locations across River Ganga	129
6.8	Fig. 6.8: Laser Light scattering of the SS samples before and after centrifugation at 75000 rpm	130
6.9	Fig. 6.9: Average particle size distribution (Z_A) of SS samples collected from Gangotri	131
6.10	Fig. 6.10: Average particle size (ZA) of SS samples collected from Tehri left Bhagirathi stream	132
6.11	Fig. 6.11: Zeta potential values for the samples collected from the whole stretch of River Ganga	133
6.12	Fig. 6.12: TEM images of the as-collected SS samples collected from Gomukh	134
6.13	Fig 6.13: TEM images of the SS sample collected from Gomukh after centrifugation	135
6.14	Fig. 6.14: TEM images of the SS samples collected from Gangotri without centrifugation	136
6.15	Fig. 6.15: TEM images of SS sample collected from Gangotri after centrifugation	137
6.16	Fig. 6.16: TEM images of SS sample collected from	138

Figure No.	Title	Page No.
	Koteshwar without centrifugation	
6.17	Fig. 6.17: TEM images of selected SS samples collected from Koteshwar after centrifugation	139
6.18	Fig. 6.18: TEM images of SS sample collected from Tehri 50m depth without centrifugation	140
6.19	Fig. 6.19: TEM images of SS sample collected from Tehri 50 m depth after centrifugation	141
6.20	Fig. 6.20: TEM images of SS sample collected from Tehri 70 m depth without centrifugation	142
6.21	Fig. 6.21: TEM images of SS sample collected from Tehri 70 m depth after centrifugation	143
6.22	Fig. 6.22: TEM images of SS sample collected from Chinyalisaur without centrifugation	144
6.23	Fig. 6.23: TEM images of SS sample collected from Chinyalisaur after centrifugation	145
6.24	Fig 6.24: (a) TEM images of samples collected from Chinyalisaur after centrifugation. (b)Histogram profile of the particles of sample collected from Chinyalisaur after centrifugation	146
6.25	Fig. 6.25: Antibacterial activity Tehri samples. 1) Control Plate 2) Tehri SS 3) Tehri SS 4) Tehri SS	162
6.26	Fig. 6.26: Antibacterial activity of water samples from river Ganga devoid of sediments	163
6.27	Fig. 6.27: Antibacterial activity of the sediment samples collected from River Yamuna and Narmada	164
7.1	Fig. 7.1: Experimental Design and Analysis	189
7.2	Fig. 7.2: Experimental Setup of Leaching Study	190
7.3	Fig. 7.3: Variation In Ph During Leaching Study With Distilled Water	192
7.4	Fig. 7.4: Variation in Conductivity during leaching study with distilled water	192

Figure No.	Title	Page No.
7.5	Fig.7.5: pH Variation during Leaching Studies in Ganga Water	194
7.6	Fig. 7.6: Conductivity Variation during Leaching Studies in Ganga Water	195
7.7	Fig. 7.7: Calibration Curve for Total Phenols (Gallic Acid Equivalent)	197
7.8	Fig. 7.8: Polyphenolic Compounds in Leachates and Ganga water samples	198
7.9	Fig 7.9: Leaching of phenolic compounds from senescent leaves (Yule et al. Carbon Balance Manage (2018) 13:3)	199
7.10	Fig. 7.10: Combined FTIR spectra for water, soil, sediment and leaf samples from Upper stretches of River Ganga	202
7.11	Fig. 7.11: GC-MS Chromatogram of deodar stem sample indicating presence of vanillin	203
7.12	Fig. 7.12: GC-MS Chromatogram of Harsil 9 water sample indicating presence of vanillin	204
7.13	Fig. 7.13: GC-MS Chromatogram of Harsil 2 water sample indicating presence of Beta Pinene	204
7.14	**7B**Fig. 7.14 Types of forest in UGRB and the Dominant Tree Species as per their presence in percentage Total Geographical Area (TGA)	218
7.15	Fig 7.15: Different forest types in UGRB	218
7.16	Fig. 7.16: Number of plant species under different groups and habits reviewed for plant based phytochemicals/secondary metabolites	219
7.17	Fig. 7.17: Important group of secondary metabolites analyzed and reported from Trees in UGRB (Data collated from literature review)	220
7.18	Fig. 7.18: Important group of secondary metabolites analyzed and reported from herbs and shrubs in UGRB (Data collated from literature review)	220
7.19	Fig. 7.19: Graphical Representation of Lysimeter Setup to study the phytochemical leaching from leaf litter in the soil	223

Figure No.	Title	Page No.
	profile	
7.20	Fig. 7.20: Lysimeter Setup to study the phytochemical leaching from leaf litter (Deodar and Blue Pine) in the soil profile of Harsil	224
7.21	Fig. 7.21: Collected Leachate Samples of first trial and second trial	225
7.22	Fig. 7.22. TOC of plants, litter and soil from different depths of Harsil forest	225
7.23	Fig 7.23: of plants, litter and soil from different depths of Harsil forest	226
7.24	Fig. 7.24: Antibacterial test of leachates using Agar Disc Diffussion Agar Well Diffusion method showing no inhibition zone	230

List of Plates

Plate No.	Title	Page No.
7.1	Harsil	185
7.2	Harsil Side stream	185
7.3	Harsil Side Stream	186
7.4	Gangotri	186
7.5	Harsil and side streams (Sample codes H and HSS respectively)	187
7.6	Gangotri and Side streams (sample codes G and GSS)	187
7.7	Litter sample	188
7.8	Litter and Soil samples	188
7.9	Habitat and dense formations of Deodar and Blue Pine forests in Upper Ganga Catchment of Bhagirathi basin	221

CHAPTER -1

INTRODUCTION

1.0 Introduction

1.1 Background

Rivers are easily accessible, and useful in multiple facets. Most perennial rivers are primary renewable water resource for agriculture, domestic and industrial use. Additionally, they are vital for navigation, aquatic life, and generation of hydroelectricity. In short, rivers are indispensable in maintaining environmental equilibrium and for human development. Accordingly, it is clearly evident that all the civilizations, since ancient times till date, have thrived along the major rivers of the world (Hillel, 1992)(Winner, 2012). Consequently, the rivers held the position prima in all parts of the ancient world. As the world entered the modern era, on the advent of technology and industrialization, the essentiality of rivers and our dependence on them has increased (Hillel, 1992).

The Ganga is not just a River; the mythological importance associated with the River is deep-rooted in the Indian culture and is considered as 'Holy River'. The status and recognition which River Ganga has attained in the minds of the population residing in the vicinity as well as thousands of kilometres away cannot be articulated in words. It is a combination of faith and necessity. Demystifying this river is a mammoth task but can be attempted if followed a logical path. The various aspects of the river including river flow dynamics, micro / macro flora and fauna, diversity in vegetation and its impact on the River can be both mystically as well as scientifically studied and explained. For centuries together, the nature of this river has been explained through the age old scriptures in a spiritual setting but never been attempted to explain these observed phenomena through a lens of modern science.

River Ganga is part of the Ganga-Brahmaputra-Meghana composite river system, which drains a massive 1.7 million KM2, and is one of the larges river syst3ems in the world by drainage area (Arnold, 2000). The trans-border basin spreads across four nations – India, Nepal, China and Bangladesh. River Ganga is fed by snow-melt water from Himalayan Glaciers and also by sub surface flows and plateau rivers; and

flows perennially. The main stem of the river flows for 2,525 KM1 making it the 39th longest2 in the world and second in terms of the total suspended load which is 524 Mega tonnes/year (Tandon, Sinha, Gibling, Dasgupta, & Ghazanfari, 2008)(IIT Consortium, 2013).This perennially flowing River has spurred development in the entire basin. Dams and barrages have been built with an intention of providing energy and massive increases in food production. Some parts of the River are used for navigation. For centuries, the River carries fertile alluvial sediment from the Himalayas and deposits in the plains of the Uttar Pradesh, turning the later in to an one of the most fertile alluvial plains in the world (Taneja et al., 2014). Due to availability of water and fertile land, the Ganga basin supports a population of about 600 million and generating over 40% of India's GDP in this region (The World Bank Report No. STEP705, 2011). All these physical and natural attributes of the river Ganga already make it an important and special river system of the world. The river is central to the culture of the region and has gained importance as someone who has created this entire civilization and nurtured life of the centuries. As it nurtures the civilization, the River is believed to also possess beneficial properties such as its ability to remain fresh for long periods and positive effects on one's health; properties which are believed to be unique and venerable.

Therefore, the generally supposition includes two facets to the reputation surrounding the River Ganga. Firstly, the natural aspects which are primarily tangible, such as the vastness, flow, vegetation and the physical aspects associated with the river itself, along with the massive population it supports. The second is the uniqueness, mysticism and the beneficial properties which are believed to be in Ganga River and yet not looked into by modern science. However, the detailed understanding of this river system reveals that these two aspects are not necessarily disjoint but are integrated in to one another. The manifestation of the physical aspects at the scientific as well as spiritual level has led to the belief of uniqueness to the river water. It is very plausible argument that the sheer diversity within the Ganga River

[1]The Merriam Webster Geographical dictionary (Merriam Webster, 1997) and Berga.L. (Berga et al., 2006) have indicated the length of the River Ganga as 2,505 km and 2,550 km respectively.

[2]The rank is based on comparing the lengths of other major rivers reported in peer reviewed literature.

basin, are causative in imbibing certain beneficial properties. The Ganga basin is diverse – in geology, climate, vegetation, and aquatic ecology to mention a few.

However, The Ganga basin, and especially the region along the River Ganga, has been characterized by rapid urbanisation and industrialization in the past few decades. The River has been tapped as an indispensable natural resource, and thereby impacting most or all of its natural and physical characteristics. These anthropogenic pressures over the years also played part in creating the artificial stress over the entire river ecology. The distinction between the original characteristics of the river, its validity in the today's context and factors, if corrected, which would bend the curve of changing river characteristics, is paramount.

1.2 Previous Studies

Isolated scientific studies have been undertaken to understand the ability of Ganga Water to kill/inactivate microorganisms and rapid rejuvenation of river despite of tremendous pollution load entering the river. Ernest Hankin (Abedon et al., 2011), Felix d'Herelle observed and studied the ability of river to kill / inactivate microorganisms and linked it to viruses. Prof. A.C.Shukla, from Christ Church College Kanpur, worked further on the action of these viruses. Jay Ramachandran, an ex-executive at the famous pharmaceutical firm – AstraZeneca, argued that phages exist at all parts of the River and in all rivers. According to his report, the bacterial load from anthropogenic factors may act as a catalyst to phage growth and a wider variety of phage strains (Independent Broadcasting Associates, 2007). The work of Chandra Shekar Nautiyal from CSIR-National Botanical Research Institute, India, has investigated the bactericidal property of the Ganga (Nautiyal, 2009). In an experiment undertaken by Dr. Nautiyal, bactericidal ability of Ganga water was evaluated using fresh, 8-year-old, and 16-year-old Ganga water samples spiked with pathogenic Escherichia coli serotype O157:H7. It was seen that survival of E. coli O157:H7 over the course of the experiment was 3, 7, and 15 days for fresh, 8-year-old, and 16-year-old Ganga waters, respectively. On the contrary, in Milli Q (Ultrapure Water branded by Millipore Corporation®) water the decline in viable count of E. coli O157:H7 up to 30 days was only 2 log units. These findings suggest that Ganga water has certain novel antimicrobial attributes(Nautiyal, 2009).

The second important property of the Ganga water is the ability to retaining high concentrations of dissolved oxygen in the river (Bhargava D. , 1983) (Bhargava D. , 1987)(Alley, 2010). Devendra Swaroop Bhargava is a retired Professor from the University of Roorkee who has worked exclusively about the high re-aeration rates which the Ganga exhibits and also about its superior capacity to assimilate organic matter. Definitive causal science behind this special property is yet to be established (Bhargava D. , Most rapid BOD assimilation in Ganga and Yamuna rivers, 1983)(Bhargava D. , Most rapid BOD assimilation in Ganga and Yamuna rivers, 1983).

CSIR-NEERI worked extensively to assess impacts of Tehri Dam on water quality of the River Bhagirathi. A study was carried out in 2004 on the impact of Tehri Dam on self-purification capacity of the River Bhagirathi (CSIR-NEERI, 2004). Another study was carried out in 2013 to present a water quality management plan for the Tehri reservoir. It was observed that faecal contamination with increasing settlements. The metal concentration in the sediment was found to be much higher than the crustal average. A study of the radioactive isotopes indicated a significant difference in the radium isotope presence.

Given this background, it can be seen that the River Ganga has been extensively studied and researched upon, with also a regular monitoring framework in place as part of the 2014 study. This study on identifying special characteristics of River Ganga concluded that high and near saturation concentration of DO throughout the River Ganga, in spite of substantial organic load being discharged into the River. The presence of phytoplanktons contributed significantly towards an intraday variation of about 5 mg/L. Further, it concluded that the diversity of phytoplankton is equally important as it is also an indicator of pollution.

Another important aspect during monitoring was microbial diversity and presence of bacteriophages in River Ganga. The study identified the trend of bacteriophages against pathogenic, non-pathogenic and opportunistic pathogenic bacterial isolates in water and sediment was same. The fresh water sedimentary metagenome-viromes differed from the earlier viromes collected from other fresh water sediments. The fresh water sediments from the River Ganga not only housed novel viromes, but also

included unexplored double stranded DNA viruses. Importantly, Ganga River house important bacteriophages and other microbiomes which can be related to its non-putrefying properties. Being highly analytics and interdisciplinary intensive, this project will provide a strong scientific rationale to understand bacteriophage and microbial population diversity, purifying properties of the Ganga and disease predications. This study will provide a model system and validatable parameters for other rivers of India. The bacteriophages as antimicrobial agent may prove to have important role in non-putrefying and self-cleansing properties of Ganga.

Further, the role and importance of huge quantity of sediment carried by the river from Himalayas to the plains needs to be assessed in depth.

The study also highlighted riparian and upland vegetation likely introduces secondary metabolites to adjacent lateral streams coming from forests and finally merging in Bhagirathi and Alaknanda. Organic fingerprinting leading to presence of terpenes and related compounds/ phytochemical/secondary metabolites was pronounced at nearly all the confluences in the upper stretch. The possible sources of these phytochemical signatures can thus be attributed to rich and bio diverse mega watersheds and landscapes of this stretch. Dilution plays a crucial role for the effective concentrations of these phytochemicals at different locations of river and ultimately determines the potential of their possible contributions to impart any significant medicinal or special properties to river water.

Complexity of the intra-ecosystem interactions warrants further in-depth assessment of the scenarios and drivers controlling the leaching and persistence of these phytochemicals in the Ganga water. The role of these phytochemicals needs to be understood in imparting any unique characteristics as the riparian vegetation in the upper catchment of river Ganga is unique in itself. These initial leads from various studies carried out on properties needs to be researched to unveil the science behind these properties in order to formulate a strategy to retain these characteristics.

Therefore, there was a need to understand the nature of the special properties which the River Ganga believed to possess, and in extension, understand the manner in which they interact with the dynamic environment. Subsequently, the impact of

anthropogenic activities and pollution on water quality and these properties has to be realized, so that the River and its uniqueness can be suitably conserved. Extensive research has been undertaken in various elements pertaining to this River such as hydraulic flow, aquatic life, sediment constituent and transportation, contaminant toxicology and rudimentary Physico-chemical parameters. However, dedicated research to unearth special properties of the river has been initiated as part of this study. This study is designed to be comprehensive in terms of analysing various parameters, as well as cover the entire stretch of the River Ganga, over a complete seasonal cycle.

The study undertaken has three major components (Chemical, Biological and Health aspects) and nine sub components to understand the specific characteristics of the river Ganga.

Physico - Chemical Aspects (CSIR-NEERI)	**Biological Aspects (CSIR-NEERI, CSIR-NCL & IIT-R)**	**Health Aspects (ICMR-AIIMS, ICMR-BHU)**
1. Water Quality Monitoring for Physico-chemical parameters 2. Dissolved oxygen profile for saturated and depleted levels in the River Ganga and its correlation with other influencing parameters 3. Sediment characterization to unveil non-putrefying property of Ganga	1. Unravelling the role of bacteriophages / micro biome in non-putrefying and self-cleaning properties of River Ganga (CSIR - NEERI) 2. Structural and metabolomics studies on bacteriophages / micro biome to unravel the non-putrefying and self-cleaning properties of River Ganga (IIT-R) 3. Metaviromics approach	1. Identification of bacteriophages against health care associated bacterial strains, clinical isolates, multi-drug resistant bacterial strains, anaerobic and special pathogen bacteria of clinical significance. (ICMR-AIIMS) 2. Assessment of bacteriophage enriched water as an

Physico - Chemical Aspects (CSIR-NEERI)	Biological Aspects (CSIR-NEERI, CSIR-NCL & IIT-R)	Health Aspects (ICMR-AIIMS, ICMR-BHU)
water 4. Geochemical partitioning of trace metals and their influence on non-putrefying properties of river Ganga ecosystem 5. Investigation of chemo-biological interactions of plant – originated organics for self-purification properties of River Ganga **6.** Quantitative Risk Assessment in River Ganga to assess hot spots in the river and associated health risk	for understanding viral diversity, taxonomy and functional analysis (CSIR-NCL)	anti-infective agent to clean infected hospital setup including wards, ICU and operation theaters. (ICMR-AIIMS) 3. Phage therapy center for pre-clinical investigations (ICMR-BHU)

CHAPTER -2

PHYSICO-CHEMICAL ASPECTS

2.0 Physico-chemical Aspects

The characteristics of any river vary significantly over seasons. Though Ganga is a perennial river, there is an appreciable difference inflow of the river in the summer and post-monsoon. In addition to the flow of the river, factors such as runoff from the catchment, temperature, cropping patterns and migratory fish have substantial influence on the water quality parameters. Therefore, the study stretched across at least one season cycle (pre- and post-monsoon). The framework which addresses the water quality issues of the Ganga should derive information from seasonal data, as something insignificant during one part of the year will turn out to be a key driver for water quality in the other.

Following sites were selected for details study:

- Gangotri / Gomukh
- Harsil
- Maneri
- Tehri
- Devprayag
- Rishikesh / Haridwar
- Kanpur
- Allahabad / Prayagraj
- Varanasi
- Bhagalpur / Patna

The sampling and monitoring sites varied based on its relevance to the specific component. The frequency of sampling was also dependent on the factor of variability and the information which needed to be collected and its impact / correlation with other parameters. The Physico-chemical component of the project is dived in six sub components shown in the figure below:

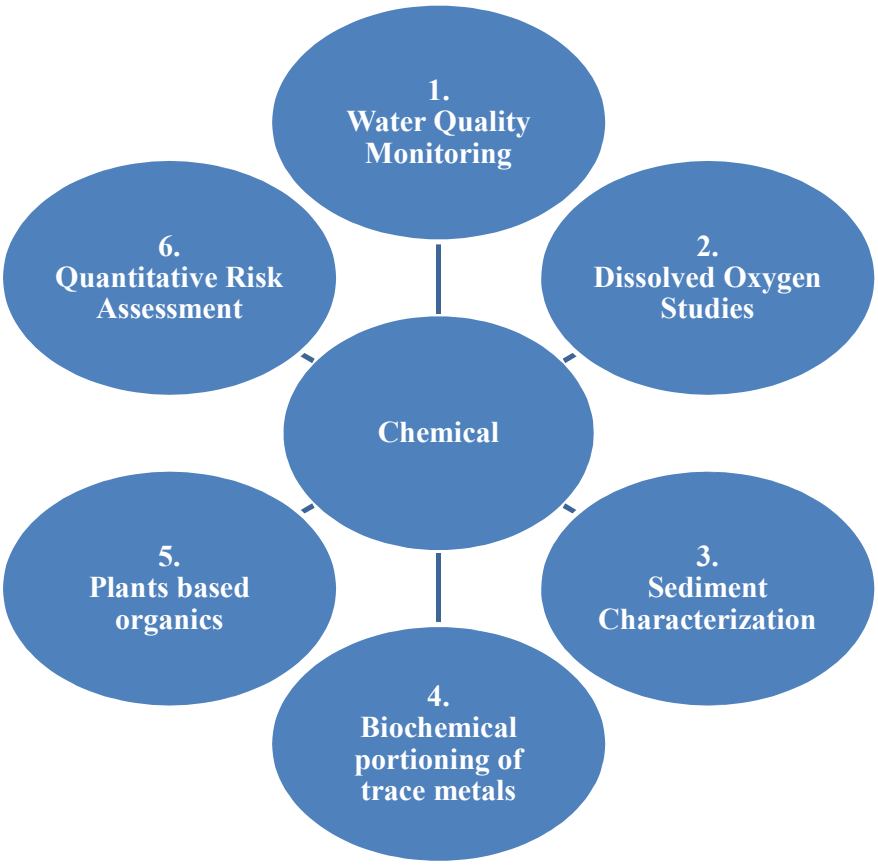

Fig. 2.1:Physico-chemical component

2.1 Water Quality along the Ganga River at select locations

The objective of this study understands the water quality of river Ganga along the stretch with the specific focus on parameters that indicates the interactions of river with its varied environment. Various ongoing activities along the entire stretch of river impart the significant effect on the water quality like the impact of anthropogenic activities, urban centres on the bank of the River, discharge and geology as well as hydro-geological process. The goal of this objective was met by carrying out the compressive study of physic-chemical parameters at select locations along the entire stretch of river Ganga. The changing environmental conditions and seasonal variation also affect the water quality of river. To understood the seasonal variation on the water quality of the river Ganga the samples were collected in during pre and post monsoon session. The detailed water quality data along the river stretch

and with seasonal variation will help to correlate the various other parameters to understand the non-putrefying properties of river Ganga.

2.1.1 Scope of Work

- To assess the existing seasonal water quality status of Ganga River for one complete cycle (post monsoon and pre monsoon seasons).
- To monitor water quality for rudimentary and specific physico-chemical in River Ganga at select locations and along the river Ganga at about twenty (13) identified sampling locations.
- To undertake extensive literature, search and survey restricting to water quality in River Ganga from peer reviewed literature and credible sources.

2.1.2 Methodology

Keeping in the view the aim of project all environmental features along the entire stretch of the river Ganga were closely scrutinized before closely indentifying sampling locations. The characteristics of River Ganga in terms of its flow, temperature, climate, vegetation, altitude and river bed geology vary significantly as it flows from Gomukh to Ganga Sagar. The hydraulics of the River Ganga varies distinctly when it flows in Himalayas, alluvial pains and in the delta. The geography, temperature and climate also follow a distinct variation in these three stretches of the river. Thus, entire stretch of the River Ganga can be divided into following two stretches based on the environmental diversity along the course of the river:

- **Stretch I** – Upper stretch (Gomukh, Gongotri, Harshil, Maneri, Tehri, Devprayag, Rishikesh/ Haridwar)
- **Stretch II** – Lower Stretch (Bijnor, Kanpur, Allahabad, Varanasi, Patna and Bhagalpur)

13 sampling locations were finalized and the details sampling was done at all selected locations. Samples were collected on the left and right bank of river and in the middle of river as well as where possible samples were collected from certain depth by using depth sampler. Upstream and downstream samples were collected approximately

within the5-15 km of tentative boundary of the main city/ inhabitation / industry / human activity zone. Water samples were collected within 3-60 meter from bank, depending on the bank characteristics and local conditions, depth of river and accessibility of the most appropriate locations. Depth sampling was done where there is sufficient depth to river water was found. In upper stretch upto Haridwar the river flow with very high intensity and depth sampling is not possible in such situation due to highly turbulent water with hardly any depth to flowing water.

Ganga is a perennial river, there is an appreciable difference in flow of the river along the course in the pre-monsoon and post-monsoon seasons. In addition to that a variation in flow, factors such as dilution due to runoff from the catchments, temperature, cropping patters and water withdrawal also exhibit this seasonal variation and have considerable effect on all water quality parameters. Henceforth, it is necessary to perform the water quality analysis for pre and post-monsoon seasons.

The collection of water samples along the entire stretch of river Ganga is challenging task and sampling was done by 3 teams simultaneously. The post-monsoon sampling was completed in month of September and October 2017 whereas the pre-monsoon sampling was conducted last week of May 2018 and first week of June 2018. Samples were collected from all the locations as described earlier during pre-monsoon and post monsoon seasons. A detailed protocol was prepared to ensure sample integrity, common methodology for sample collection, and optimal conditions during transport of these samples.

Table 2.1: Parameters analysed to assess the chemical characteristics of River Ganga

Sl. No.	Parameter	Methodology	Standard Method Number
1.	Temperature (0C)	Thermometer	2550B, APHA, 2012
2.	Conductivity	EC Probe on-site/Conductivity meter in lab	2510B, APHA, 2012

Sl. No.	Parameter	Methodology	Standard Method Number
3.	pH	pH Probe on-site/pH meter in lab	4500-H+ B, APHA, 2012
4.	Turbidity	Turbidimeter	2130B, APHA, 2012
5.	Alkalinity	Titrimetric method	2320B, APHA, 2012
6.	Total Hardness	Complexometric Titration	2340C, APHA, 2012
7.	Calcium	Complexometric Titration	2340C, APHA, 2012
8.	Magnesium	Complexometric Titration	2340C, APHA, 2012
9.	Chloride	Argentometric Titration	4500-Cl^- B, APHA, 2012
10.	Nitrate	Spectrophotometry	4500-$NO3^-$ B, APHA, 2012
11.	Sulphate	Spectrophotometry	4500-$SO42^-$ E, APHA, 2012
12.	Sodium	Flame Photometer	3500-Na B, APHA, 2012
13.	Potassium	Flame Photometer	3500-K B, APHA, 2012
14.	Phosphate	Spectrophotometry	4500-P C, APHA, 2012
15.	Fluoride	Specific Ion meter	4500-F^- C, APHA, 2012
16.	Dissolved Oxygen	DO Probe and Titration by Winkler's Method	4500 – O C/G, APHA, 2012
17.	Biochemical Oxygen Demand	Incubation followed by titration	5210 B, APHA, 2012
18.	Chemical Oxygen Demand	Acid digestion followed by titration	5220 B/C, APHA, 2012

Fig. 2.2: Selected major sampling locations along the river Ganga

2.1.3 Physico-chemical characteristics of River Ganga

The water quality of River Ganga monitored during pre-monsoon and post-monsoon seasons are presented and discussed in detail in this section. Total of 13 locations was selected for assessment of water quality throughout the entire length of River Ganga to undertake a comparative study of water quality. These locations were selected based on specific criteria which would bring forth information about the water quality of the Rivers Ganga, throughout its stretch, as well as the effect of city and ultimately anthropogenic activities, discharges from the particular city on the river water quality. In addition, details of causative factors such as quantum of flow, the abstraction of water, impoundment, and urban centers were collected.

The chemical characteristics of a River provide valuable information about the water quality at any given point. A comprehensive study was undertaken to assess the water

quality characteristics of River Ganga, taking into consideration different points that represent the changing environment of the River as it flows across different States. The changing physiographical features alter the environment and hence water quality needs to be assessed by analysing the River for parameters which encompass all the possible impacts of this diverse environment of which the River is a part. Water samples collected for chemical analysis were brought to CSIR-NEERI, Nagpur, All parameters were analysed as per standard procedures described in the APHA manual with required quality control checks to ensure the reliability of data (APHA, AWWA & WEF Standard Methods 22nd Edition, 2012).

2.1.3.1 Electrical conductivity (EC)

Electrical conductivity is an indirect measure of the dissolved ionic elements and compounds in the water. The sources of these compounds in the river are either geogenic as natural rock formations are constituted of various minerals and are weathered by the River; or are anthropogenic as point-source effluents from cities and industries, and non-point source runoff from agricultural fields. The EC is expected to increase as the River interacts with sediment and flows through different topographic regions. Further, anthropogenic activities like agriculture, landfill, industries, etc. also increase the quantum of total dissolved solids (TD S). This increase in TDS is directly reflected by an increase in the conductivity.

The increase in EC was found up to Harshil in both pre and post-monsoon session with certain natural variation (Fig. 2). EC slightly drop down at Tahri for both the seasons and increase constantly with increasing anthropogenic activities up Varanasi and slightly drop down from Patna to Bhagalpur, this probably because of dilution due to tributaries entering into River Ganga before to Patna.

The EC in Upper stretch is low during the pre-monsoon season as compared to the post-monsoon season (Fig. 1), and this might be attributed to the change in discharge in the River and the consequent change in the dissolution of rock minerals. The variation in EC remained within a narrow band of 80 - 180 µS/cm at most of the locations of Upper Stretch. However, the trend is reversed after Devprayag mainly due to less quantum of water compared to post-monsoon season. As the river flows through the first major urban centers - Haridwar and Rishikesh, electrical conductivity

starts increasing. The EC in Lower Stretch was almost more than double as that of Upper Stretch. This trend was observed in both seasons.

2.1.3.2 Total Hardness (Calcium & Magnesium)

The dissolution of Calcium and Magnesium minerals account for the hardness of the water. Hardness is an important parameter which decides the suitability of the River water for various purposes. River weathers rock formations which are constituted by Calcium and Magnesium minerals in significant proportion. In addition, groundwater also dissolves appreciable amounts of Calcium and Magnesium and eventually finds its way into the River when the groundwater interacts with River Ganga. A higher level of hardness does not pose any direct adverse health effects but it affects the taste and acceptability as a drinking water source.

Hardness during pre-monsoon and post-monsoon seasons show a similar trend, as it ranges from 50 to 1000 mg/L in upper stretch with the exception of the location Devprayag, Rishikesh & Haridwar during pre-monsoon season (Fig. 3). The main reason behind such behavior might be ongoing road construction under Chardham yojna and increased tourism during the summer season. A slight increase in hardness in the pre-monsoon season in lower stretch can be attributed to higher discharge and subsequent erosion. Comparatively total hardness for lower stretch increases continuously up to Patna and then gets stabilized for both the seasons.

2.1.3.3 Total Alkalinity

Hardness and alkalinity are the major contributors to the change in conductivity in inland surface water. The rivers fed by snow/glacier melt have limited interaction with rocks and thus have lower values of hardness and alkalinity as compared to rivers inland. This trend was observed when hardness and alkalinity were compared between upper and lower stretch. As the river flows through the lower stretch, the subsurface lateral movement of groundwater and its influx into the river contributes to an increase in hardness and alkalinity.

A gradual increasing trend is observed in alkalinity of the River in upper Stretch as the River flows from Gomukh to Haridwar ((Fig. 4), for both pre-monsoon and post-monsoon seasons. Comparatively higher alkalinity is observed downstream of

Haridwar in both pre-monsoon and post-monsoon seasons. Alkalinity increases significantly in the lower stretch from Kanpur onwards and maximum alkalinity of around 250 mg/L is observed downstream of Allahabad. Alkalinity during the post-monsoon season is found to comparatively higher than pre-monsoon season at almost all locations.

2.13.4 Dissolved Oxygen

Dissolved oxygen in a river system is governed by complex interrelated processes, it is reduced by two important factors in a River most importantly respiration by aquatic biota and stabilization of organic matter in the River. As the River naturally draws oxygen from the atmosphere, turbulence i.e., good mixing at the surface of the River enhances dissolved oxygen concentration. The maximum concentration of dissolved oxygen attainable by the atmosphere is a function of water temperature and atmospheric pressure.

The upper stretch of River Ganga up to Devprayag shows the appreciable concentration of DO ranging from 7.5 to 9.5 mg/L (Fig. 5). The slightly lower temperatures and high turbulence in this region allow more oxygen to be gets dissolved in the River. Negligible organic load due to anthropogenic activity compared to the quantum of water flows is also not affect the health of the River system.

In lower Stretch the River has a DO concentration ranging from 6 to 8.5 mg/L, However, this region has a hotter climate, and thereby a lower saturation concentration. The high-density population centers situated on the bank of river Ganga in lower stretch do not reduce down the DO concentration much below in spite of the intrusion of organic load and industry effluent. Most of the locations had dissolved oxygen near saturation levels in both pre- and post-monsoon seasons. A marginal increase was observed in post-monsoon in both stretches which correlate with lower water temperature.

2.1.3.5 Chemical Oxygen Demand

The oxygen required to chemically oxidise the all organic/inorganic matter in the river water is termed as a Chemical oxygen demand. It is also an indicator of pollution, and

especially reflects the anthropogenic and industrial pollution load on the River. In the upper stretch, up to Rishikesh, the value of COD is in between 10 to 40 mg/L (Fig. 6). The COD value increases continuously up to Tehri and droops down slightly. The COD values in the upper stretch is due to combine effect of organic load and suspended sub-micron size particles of sediment remaining into water samples after filtration through Whatman's filter paper. After Tehri, most of the sediment gets to settle down which resulted in the lower COD values after Tehri. The COD increases continuously Bijnor onward and found to be highest at Kanpur downstream, Allahabad upstream and downstream and reduced down further. For lower stretch COD ranged between 20 and 70 mg/L both in pre-monsoon and post-monsoon seasons. The possible reasons for not observing an appreciable increase in COD as River flows through the industrial belt could be the increased dilution and settling of the chemical constituents along with sediment due to low velocity.

2.1.3.6 Biochemical Oxygen Demand

Biochemical oxygen demand is a measure of oxygen consumed by the biological activities in the River water. It also the indicator of organic load entering into the River and respiration from aquatic biota leads to oxygen consumption. The BOD was measured as 3-day BOD.

Samples collected from upper stretch up to Rishikesh had a BOD less than 2 mg/L during both the season (Fig.7). The BOD at Haridwar is slightly more than 2 mg/L in both the seasons and increases continuously in the entire second stretch for both the seasons. In second stretch the BOD ranges from 3 to 6 mg/L, except for downstream of Kanpur where exceptionally high BOD of around 14 mg/l and 24 mg/l was found during the post- & pre-monsoon seasons respectively.

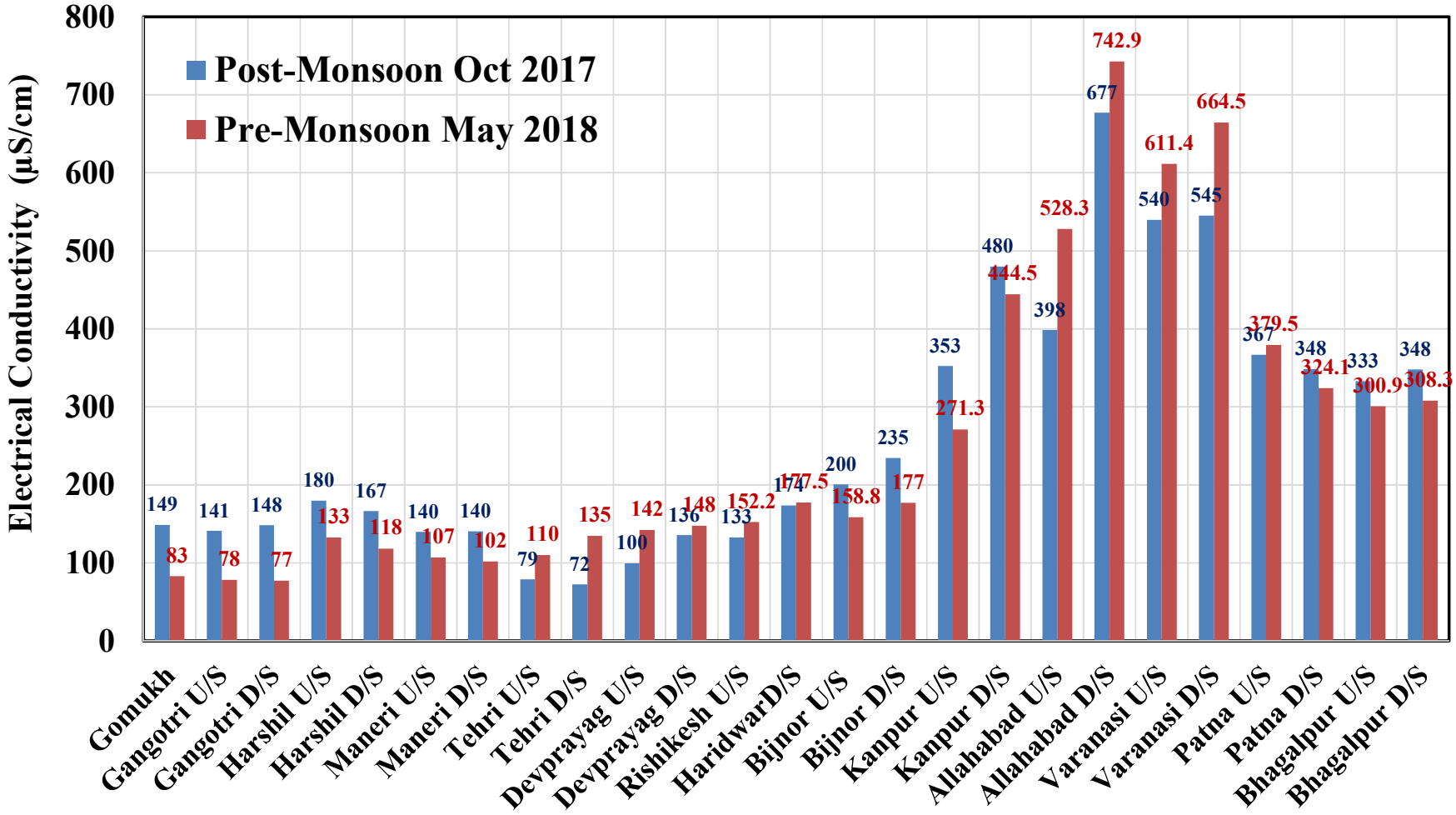

Fig. 2.3: Seasonal variation of Electrical conductive along the stretch of River Ganga

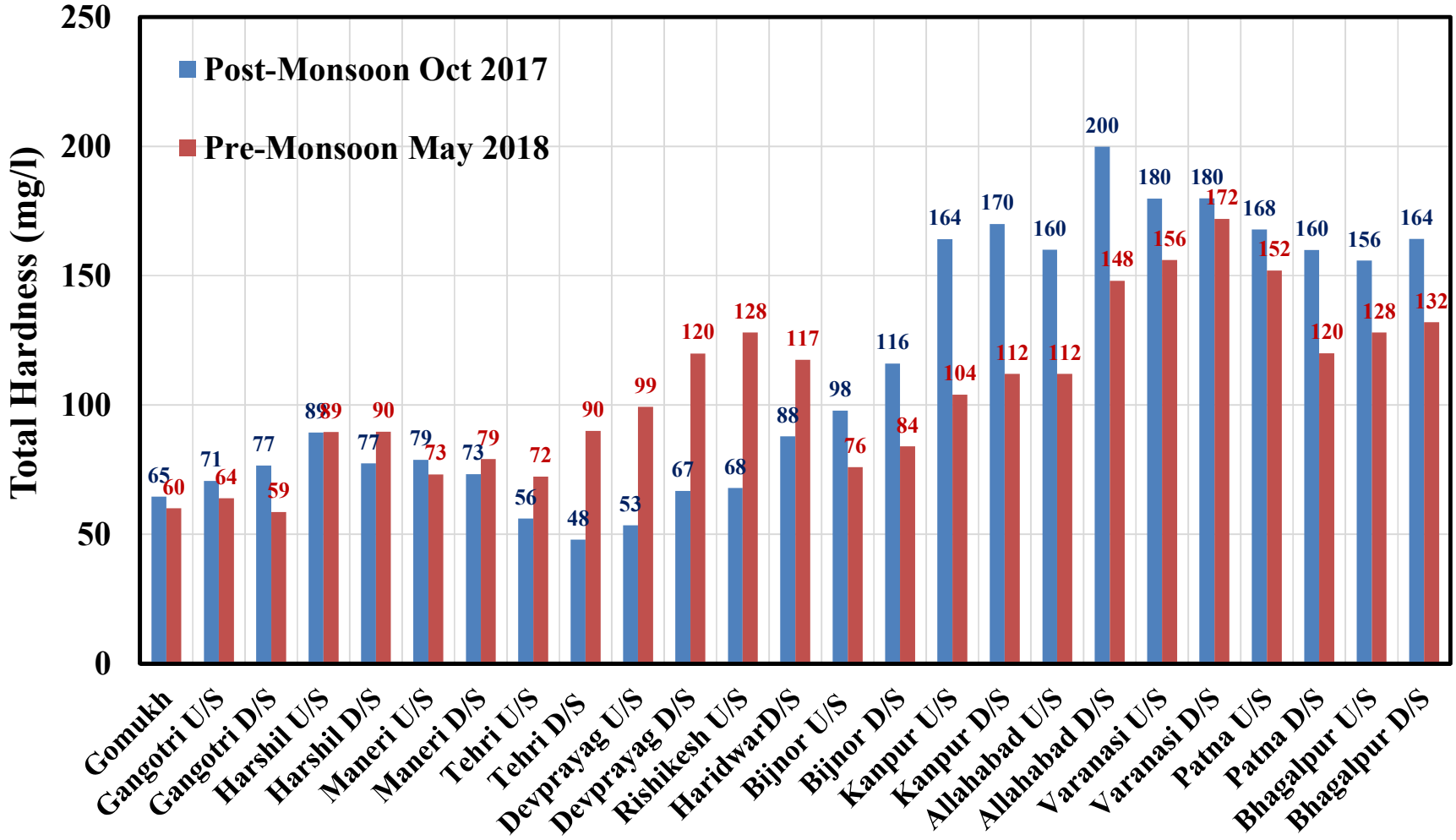

Fig. 2.4: Seasonal variation of Total Hardness along the stretch of River Ganga

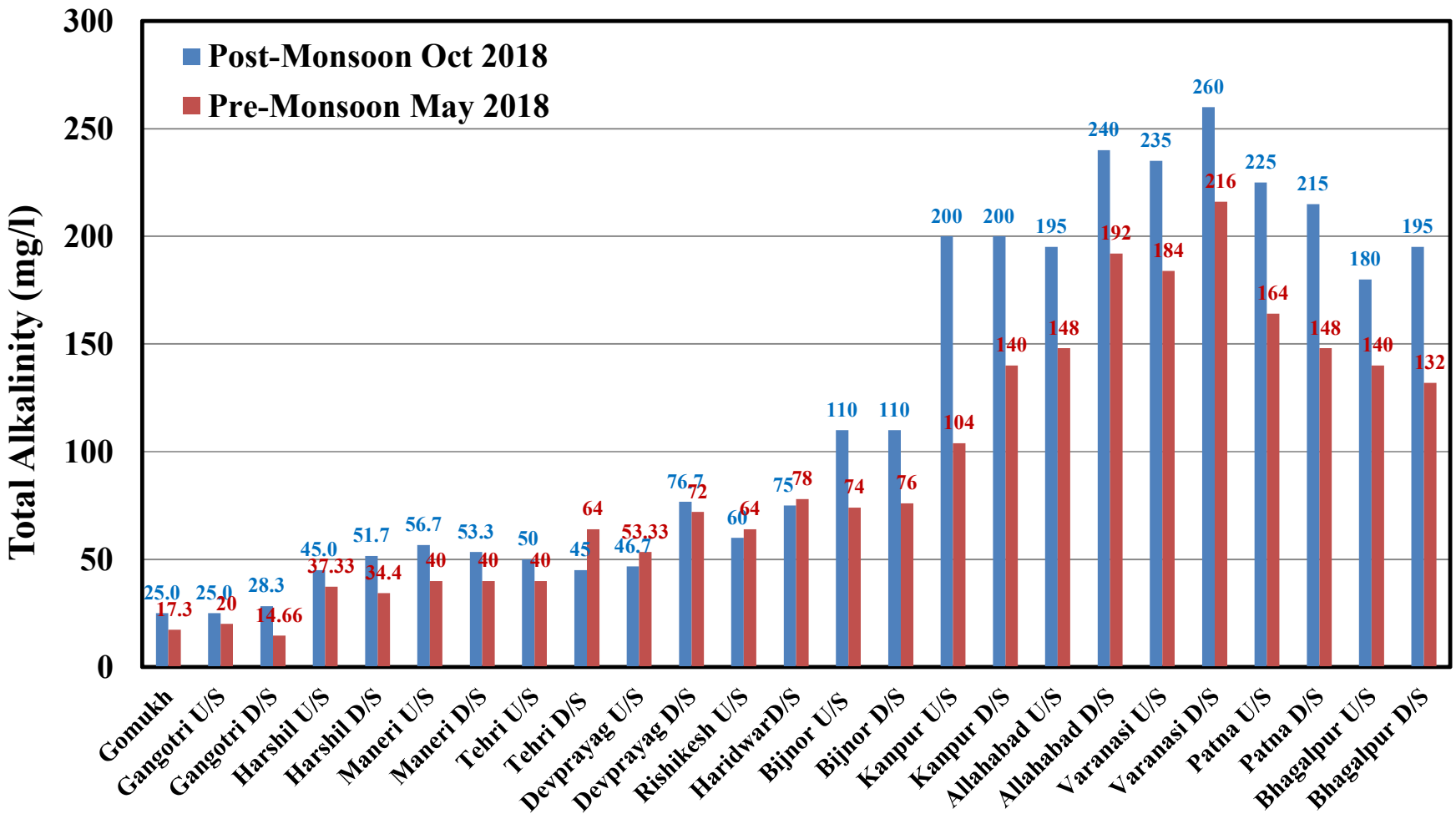

Fig. 2.5: Seasonal variation of Total Alkalinity along the stretch of River Ganga

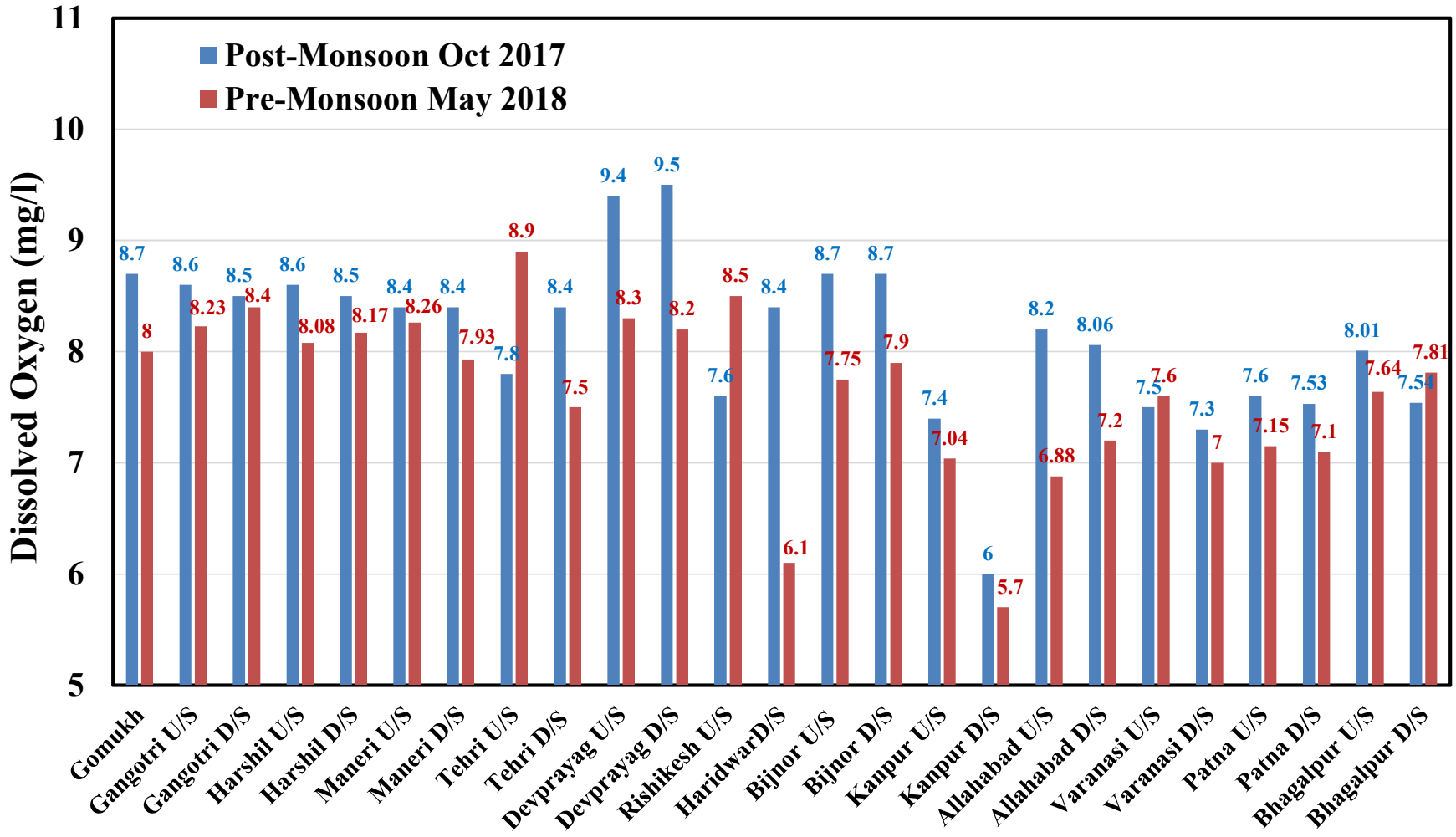

Fig. 2.6: Seasonal variation of Dissolved Oxygen along the stretch of River Ganga

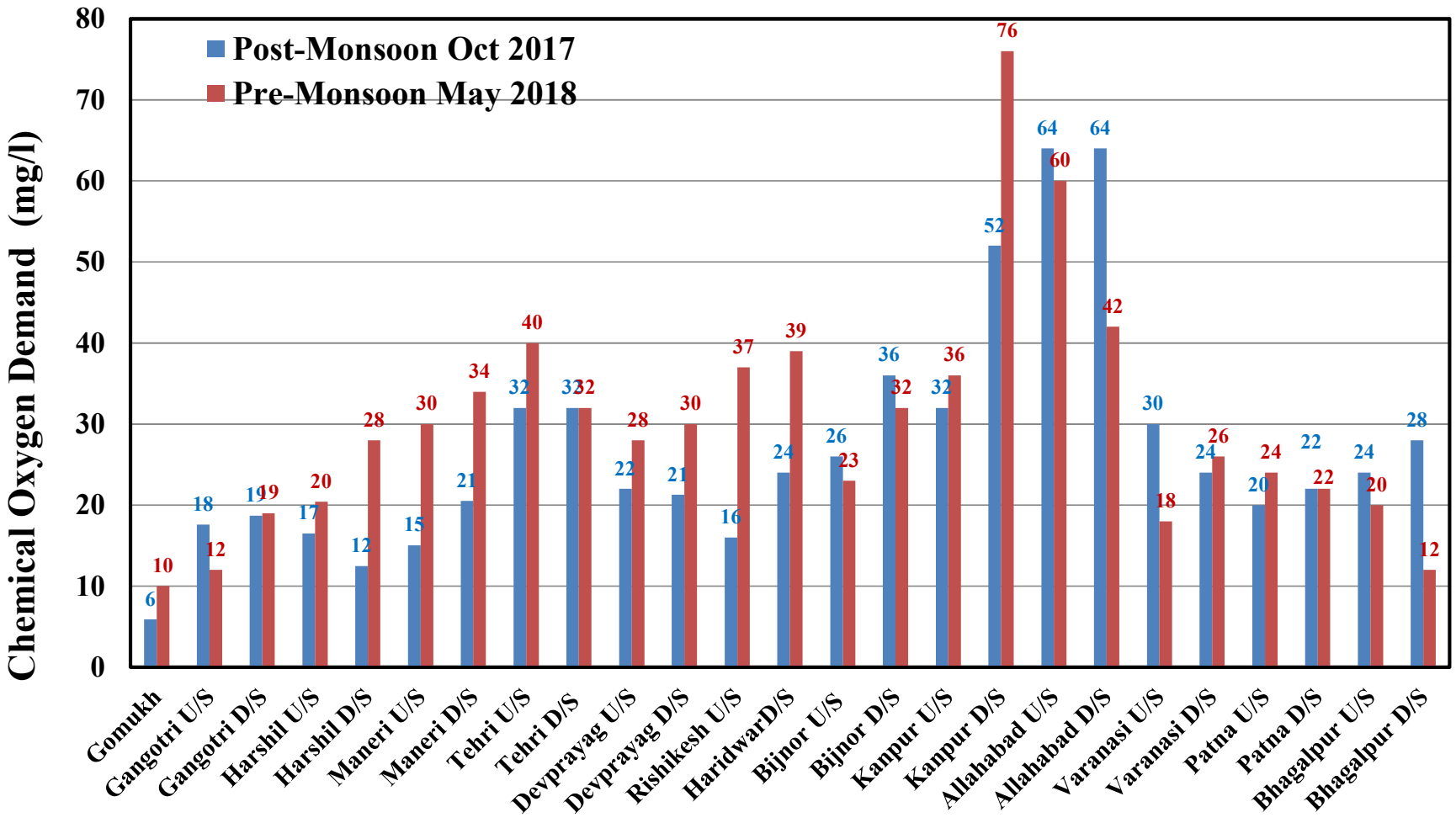

Fig.2.7: Seasonal variation of Chemical Oxygen Demand along the stretch of River Ganga

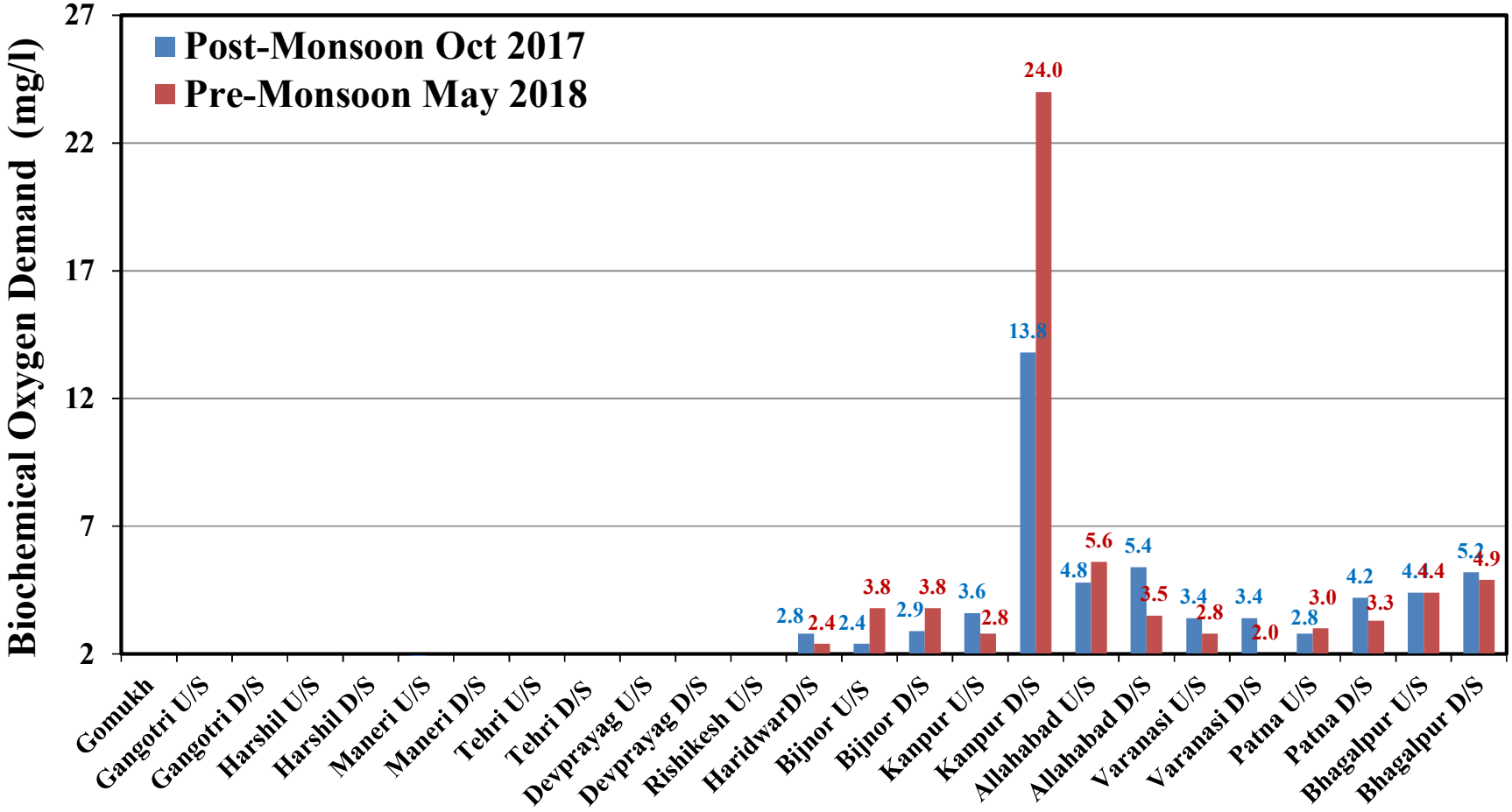

Fig. 2.8: Seasonal variation of Biochemical Oxygen Demand along the stretch of River Ganga

Table 2.2: Water quality data for the samples collected from entire stretch of River Ganga during Post-Monsoon seasons (Oct-2017)

Sl. No.	Sample Locations	Onsite pH	EC (µS/cm)	Total Hardness (mg/l)	Sodium (mg/l)	Potassium (mg/l)	Total alkalinity (mg/l)	Sulphate (mg/l)	Chloride (mg/l)	Nitrate (mg/l)	COD (mg/l) (Filtered COD)	BOD (5 Days) (mg/l)	DO (mg/l)
1	Gomukh	7.0	149	65	2.4	2.2	25.0	56.8	4.0	0.4	6	<2	8.7
2	Gangotri U/S	6.8	141	71	2.8	1.8	25.0	51.8	3.4	0.5	18	<2	8.6
3	Gangotri D/S	7.0	148	77	2.5	2.0	28.3	56.7	2.0	1.5	19	<2	8.5
4	Harshil U/S	7.1	180	89	2.5	1.3	45.0	54.9	3.4	0.8	17	<2	8.6
5	Harshil D/S	7.5	167	77	2.3	1.3	51.7	45.6	3.4	0.8	12	<2	8.5
6	Maneri U/S	7.3	140	79	2.9	1.5	56.7	33.2	2.7	0.9	15	<2	8.4
7	Maneri D/S	7.3	140	73	3.3	1.7	53.3	33.7	4.0	0.8	21	<2	8.4
8	Tehri U/S	7.8	79	56	4.2	2.3	50	15	2	1.2	32	<2	7.8
9	Tehri D/S	8.3	72	48	3.9	2.2	45	8	6	1.2	32	<2	8.4
10	Devprayag U/S	7.6	100	53	2.3	1.5	46.7	16.6	2.7	0.5	22	<2	9.4
11	Devprayag D/S	7.7	136	67	2.9	1.6	76.7	16.6	4.03	0.78	21	<2	9.5
12	Rishikesh U/S	8.1	133	68	4.8	2.7	60	24	4	1.1	16	<2	7.6
13	HaridwarD/S	8.4	174	88	6.5	3.2	75	32	6	1.7	24	2.8	8.4
14	Bijnor U/S	8.58	200	98	7	3.6	110	28	4	2.1	26	2.4	8.7

Sl. No.	Sample Locations	Onsite pH	EC (µS/cm)	Total Hardness (mg/l)	Sodium (mg/l)	Potassium (mg/l)	Total alkalinity (mg/l)	Sulphate (mg/l)	Chloride (mg/l)	Nitrate (mg/l)	COD (mg/l) (Filtered COD)	BOD (5 Days) (mg/l)	DO (mg/l)
15	Bijnor D/S	8.1	235	116	9.8	4.2	110	39	15	2.8	36	2.9	8.7
16	Kanpur U/S	8.9	353	164	24.2	7.3	200	33	14	4.5	32	3.6	7.4
17	Kanpur D/S	8.95	480	170	42	7.2	200	45	28	7.8	52	13.8	6
18	Allahabad U/S	9.1	398	160	35.4	9.8	195	48	28	6.3	64	4.8	8.2
19	Allahabad D/S	7.8	677	200	83.7	9.9	240	69	76	9.6	64	5.4	8.06
20	Varanasi U/S	8.67	540	180	58.3	8.2	235	40	50	6.8	30	3.4	7.5
21	Varanasi D/S		545	180	56.9	8.2	260	74	54	6.9	24	3.4	7.3
22	Patna U/S	8.73	367	168	26.3	4.7	225	30	20	2	20	2.8	7.6
23	Patna D/S	8.56	348	160	24.6	4.7	215	27	16	2.1	22	4.2	7.53
24	Bhagalpur U/S	8.64	333	156	22.4	4.8	180	27	16	2	24	4.4	8.01
25	Bhagalpur D/S	8.43	348	164	22.8	4.9	195	35	14	1.8	28	5.2	7.54

Table 2.3: Water quality data for the samples collected from entire stretch of River Ganga during Pre-Monsoon seasons (May 2018)

Sl. No.	Sample Locations	Onsite pH	EC (µS/cm)	Total Hardness (mg/l)	Sodium (mg/l)	Potassium (mg/l)	Total alkalinity (mg/l)	Sulphate (mg/l)	Chloride (mg/l)	Nitrate (mg/l)	COD (mg/l) (Filtered COD)	BOD (5 Days) (mg/l)	DO (mg/l)
1	Gomukh	10.9	83	60	1.36	1	17.3	30.64	7.33	1.05	10	<2	8
2	Gangotri U/S	8.3	78	64	1.36	1	20	27.17	6	1.15	12	<2	8.23
3	Gangotri D/S	8.0	77	59	1.16	0.9	14.66	28.15	7.33	0.86	19	<2	8.4
4	Harshil U/S	8.0	133	89	1.53	0.6	37.33	36.8	6	1.43	20	<2	8.08
5	Harshil D/S	7.6	118	90	1.56	0.6	34.4	30.88	6	1.47	28	<2	8.17
6	Maneri U/S	7.9	107	73	2.16	0.7	40	25.11	1.9	1.4	30	<2	8.26
7	Maneri D/S	7.9	102	79	2.3	0.7	40	25.05	6	1.34	34	<2	7.93
8	Tehri U/S	8.2	110	72	2	0.8	40	24.65	8	1.39	40	<2	8.9
9	Tehri D/S	8.7	135	90	5	1.1	64	22.6	8	6.07	32	<2	7.5
10	Devprayag U/S	8.0	142	99	2.9	0.9	53.33	21.99	7.33	1.57	28	<2	8.3
11	Devprayag D/S	8.0	148	120	3.63	1	72	19	1.8	1.56	30	<2	8.2

Sl. No.	Sample Locations	Onsite pH	EC (µS/cm)	Total Hardness (mg/l)	Sodium (mg/l)	Potassium (mg/l)	Total alkalinity (mg/l)	Sulphate (mg/l)	Chloride (mg/l)	Nitrate (mg/l)	COD (mg/l) (Filtered COD)	BOD (5 Days) (mg/l)	DO (mg/l)
12	Rishikesh U/S	8.6	152.2	128	2.7	0.9	64	27.53	6	1.68	37	<2	8.5
13	HaridwarD/S	8.3	177.5	117	4.1	1	78	22.67	8	5.14	39	2.4	6.1
14	Bijnor U/S	7.6	158.8	76	3.8	2.7	74	21.7	8	0	23	3.8	7.75
15	Bijnor D/S	7.7	177	84	3.6	2.8	76	20.54	6	0	32	3.8	7.9
16	Kanpur U/S	9.2	271.3	104	25.6	7.8	104	22.33	16	0	36	2.8	7.04
17	Kanpur D/S	9.15	444.5	112	56.8	9.2	140	34.35	46	0	76	24	5.7
18	Allahabad U/S	9.81	528.3	112	74	10.4	148	26.68	64	0	60	5.6	6.88
19	Allahabad D/S	9.52	742.9	148	102	10.8	192	55.72	96	0	42	3.5	7.2
20	Varanasi U/S	8.66	611.4	156	85.8	8.9	184	43.66	70	0	18	2.8	7.6
21	Varanasi D/S	8.47	664.5	172		8.9	216	40	70	0	26	2	7
22	Patna U/S	9.2	379.5	152	36.2	5.3	164	19.73	26	0	24	3	7.15
23	Patna D/S	9.15	324.1	120	13.3	4.5	148	32.06	10	0	22	3.3	7.1

Sl. No.	Sample Locations	Onsite pH	EC (µS/cm)	Total Hardness (mg/l)	Sodium (mg/l)	Potassium (mg/l)	Total alkalinity (mg/l)	Sulphate (mg/l)	Chloride (mg/l)	Nitrate (mg/l)	COD (mg/l) (Filtered COD)	BOD (5 Days) (mg/l)	DO (mg/l)
24	Bhagalpur U/S	9.9	300.9	128	18.8	4.8	140	31.36	14	0	20	4.4	7.64
25	Bhagalpur D/S	9.31	308.3	132	22.8	5.6	132	30.42	16	0	12	4.9	7.81

CHAPTER - 3

DISSOLVED OXYGEN

3.0 Monitor the dissolved oxygen in the Ganga and examine the dissolved oxygen profile for saturation levels and depleted levels, simultaneously correlating with other influencing parameters (such as zoo and phytoplankton population) and study the reaeration of the river

3.1 Introduction

The level of dissolved oxygen in water is one of the most critical parameters in determining its quality as it indicates the level of pollution in any water body. The amount of free, non-compound oxygen in water refers to dissolved oxygen (DO), which measures the number of free oxygen molecules in water. The general water quality of any river is gauged by the dissolved oxygen present in it. Many factors affect the dissolved oxygen and depend upon the river hydrology, climatic conditions and seasonal patterns besides organic pollution. DO decreases with higher temperature, salinity, and elevation. However, phytoplankton in water produces oxygen as a by-product and increases DO levels, even in warmer water during the day.

Common processes that pollute surface waters include the discharge of organic matter derived from municipal sewage or industrial wastes and runoff from agricultural fields and livestock feedlots. In addition, the release of warm or hot discharges from industrial cooling towers induces what is known as thermal pollution. The organic waste entering the river is assimilated by microorganisms that consume oxygen. Rivers, however, draw oxygen from the atmosphere through diffusion, replenishing oxygen levels. The oxygen generally dissolves in water by the diffusion of atmospheric air and turbulence. An adequate amount of DO is a prerequisite for the aquatic species to continue their survival. DO levels in the water below 5.0 mg/L can stress the aquatic life, and levels below 2-3 mg/L for few hours can result in the death of fish on a large scale. In recent times, excessive pollution has caused massive fish deaths. The discharges of organics or nutrients favour the accelerated eutrophication or productivity process with algal blooms.

Focused field-based investigations were carried out to gather in-depth information about the relationship between Dissolved Oxygen (DO) and the special non-putrefying properties in the Ganga river water. These extensive sampling and monitoring were based on the relationship between DO and the river's health and water quality.

Three major cities with excessive anthropogenic organic load discharged in the Ganga River are Kanpur, Prayagraj and Varanasi (**Figure 3.1**). This study focused on the diurnal variation of DO, monitoring of DO, BOD, and reaeration rate in the Ganga River in three cities.

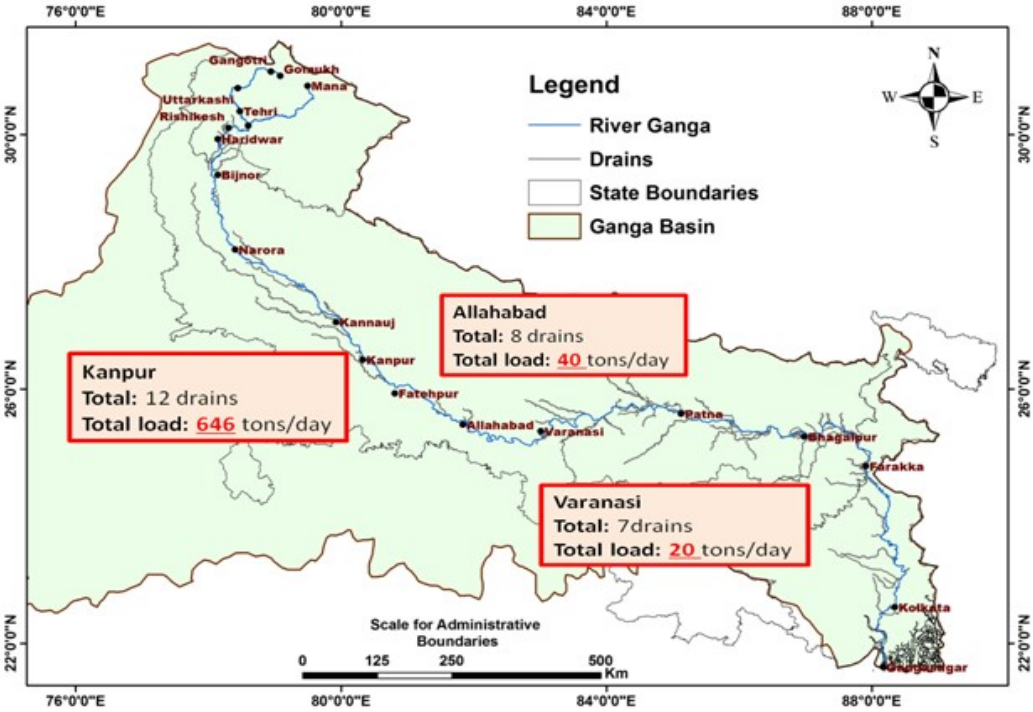

Figure 3.1: Selected cities along river Ganga and the respective sewage loads

3.2 Objectives

The study focused on the following aspects of the River Ganga at Kanpur, Varanasi and Prayagraj:

i. Dissolved oxygen profiling
ii. Reaeration rate experiments near sewer outfalls
iii. Biochemical Oxygen Demand (BOD) monitoring

3.3 Study Area

Three cities, Kanpur, Prayagraj and Varanasi, were selected for the study as these cities receive the maximum organic load in the entire stretch of Ganga. A brief description of the cities is given below.

3.3.1 Kanpur

In Uttar Pradesh, Kanpur is the most important industrial centre, which lies on the bank of river Ganga and has an area of about 1040 km^2 and is 126 meters above mean sea level. The total stretch is around 32 km from Bithoor to Jajmau. Leather and textile goods are manufactured in Kanpur, one of our country's most important cities with aviation, leather and wool industries, vegetable oil, flour and cotton mills, and chemical and sugar refineries. It is known as Manchester of India and is also called the state's commercial capital. The Jajmau area has the maximum number of tanneries and factories. Due to the domestic and industrial wastewater generation and discharge, there is an extensive impact on the water quality of river Ganga. The stretch from Bithoor to Jajmau was monitored as several nallahs are meeting River Ganga, but most are in tapped condition except a few like Permia and Bhagwat Das Nallah. Extensive DO mapping and reaeration experiments were carried out in the stretch between Bithoor and Jajmau to depict DO's longitudinal, lateral and depth-wise variation and determine the relation with temperature, as shown in **Figure 3.2**.

Figure 3.2: Monitoring locations at Kanpur

3.3.2 Prayagraj (Allahabad)

Prayagraj, also called Prayag or Allahabad, is situated in the southern part of Uttar Pradesh and lies on the confluence of the Ganga and Yamuna rivers. Triveni Sangam is the confluence of three rivers: Ganga, Yamuna and Sarasvati. According to Hindu legends, the Sarasvati River wells up from underground. The world's most significant historical gathering, Kumbh, occurs at this site. Prayagraj is at an elevation of about 90m above the mean sea

level. The total stretch of Prayagraj is approximately 20.37 km from upstream to downstream, as shown in **Figure 3.3**.

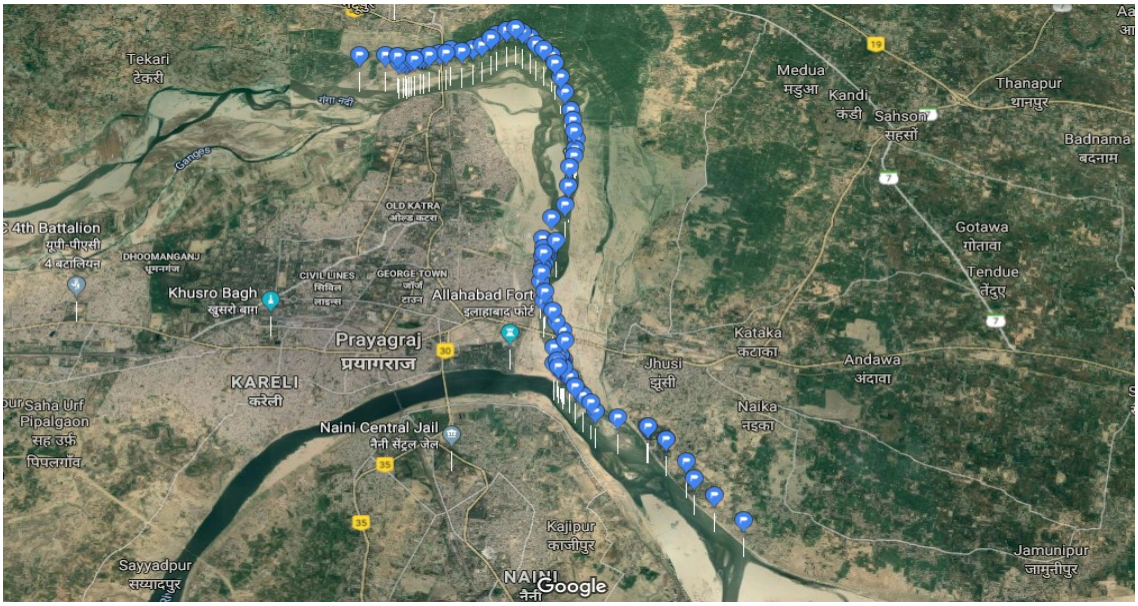

Figure 3.3: Monitoring location at Prayagraj

3.3.3 Varanasi (Banaras)

Varanasi is one of the holiest and oldest continually inhabited cities on the bank of Ganga River. It is also called Banaras or Kashi and is situated at an elevation of 80.7 m above mean sea level east of Uttar Pradesh. It is famous for the 84 riverfronts or Ghats aligned beside the left bank and agricultural practices over the right bank of the river Ganga. The total stretch is about 12 km and the river Ganga enters from Ramnagar upstream and flows from Rajghat downstream. There are many small drains (often called nalla or nallah), mainly two prominent sewage drainages, Varuna and Assi, which carry large quantities of organic waste and garbage. An extensive DO mapping and reaeration experiment was carried out from 1 km before Ramnagar to 1 km after Rajghat to depict the variation across and depth-wise and determine its relationship with temperature. BOD samples were collected from the various points at the conjunction of river Ganga with Assi and Varuna nallah. The monitoring locations at Varanasi are shown in **Figure 3.4**.

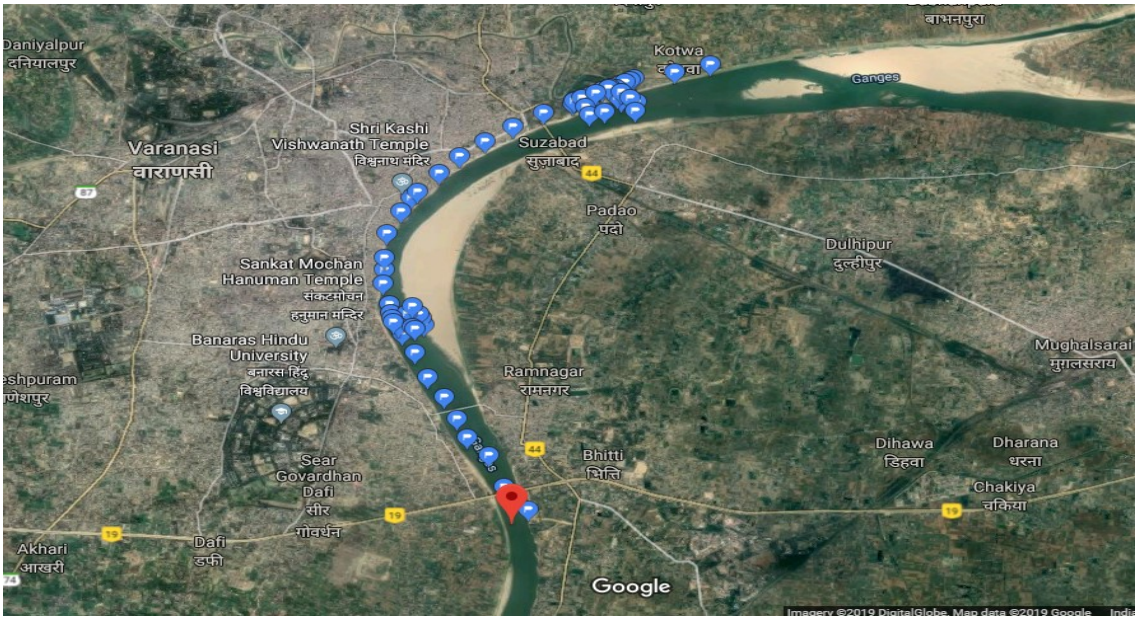

Figure 3.4: Monitoring location at Varanasi

3.4. Methodology

The studies on mapping and DO profiling, reaeration rate experiments and BOD monitoring in the Ganga River were extensively carried out in the pre-monsoon season (May 2019). Based on the results and the previous studies, further DO reareration experimentation studies were carried out at Varanasi during daytime and nighttime in the post-monsoon season (October-November 2019) as per the suggestions of NMCG.

3.4.1 Dissolved oxygen profiling

In this study, the measurement of dissolved oxygen in the Ganga River was carried out by electro-analytical and titration Methods. About 80% of samples were analysed by the electro-analytical method, whereas the remaining 20% were analysed by Winkler's Method. The DO was monitored along the surface of the riverbank and across at the nallah at 2m, 4m and maximum depths. The device used for in situ monitoring of DO was HANNA-HI 98193, a handheld DO meter. It was calibrated after every 50 readings to ensure measurement confidence and precision. The overall DO maps of each city were generated to find out high DO or an abrupt dip at specific sites. Sampling and experiments were conducted during the pre-monsoon season of 2019, i.e., May.

3.4.2 Reaeration Rate Experiment

Reaeration is the physicochemical process by which oxygen is transferred across the surface of a water body from the atmosphere. It is a crucial element within the biochemical oxygen cycle in natural water bodies. It is an important pathway by which any deficit in dissolved oxygen (DO) concentration gets reduced over time. The reaeration rate depends on the surface flux of oxygen and is controlled by a complex interaction of molecular diffusion and turbulent exchange processes near the interfaces. The reaeration rate experiment was conducted near the river sewer outfall points. DO measurements were carried out, and water samples were collected initially at a place before the confluence where sewage mixes with the river and consecutively at every 300-350 m after the mixing point along with the flow at the bank of the river, as shown in **Figure 3.5**. Samples were collected, safely packed, transported and detailed analysis was performed in the laboratory.

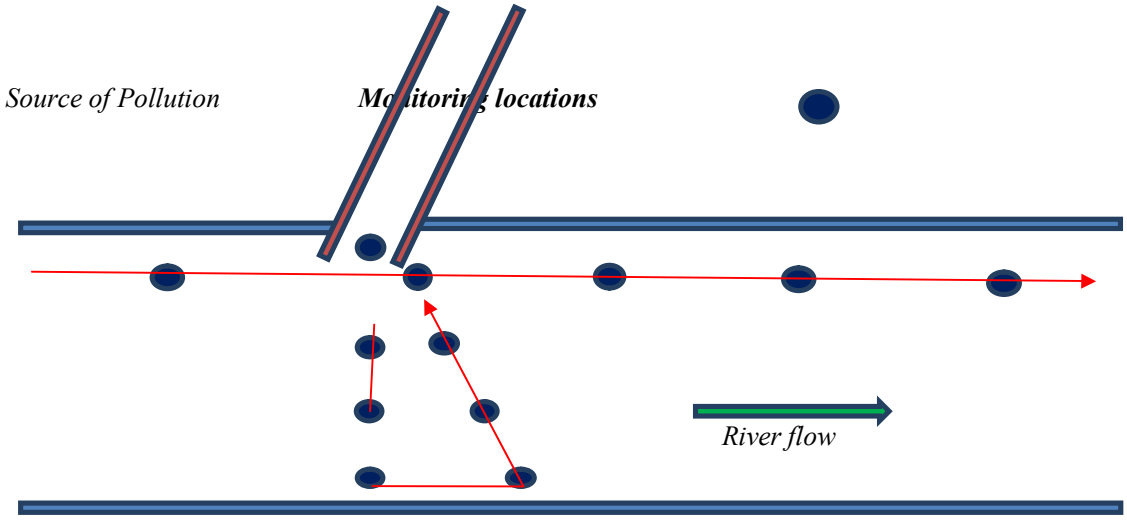

Figure 3.5. DO Monitoring locations near the Nallah (drain)

The observations mentioned above and studies were carried out to understand the dynamics of dissolved oxygen and the causative factors for high dissolved oxygen. In this regard, a framework was developed, and experiments were planned and undertaken at Kanpur, Prayagraj (previously Allahabad), and Varanasi to investigate this aspect of river Ganga.

3.4.3 Biochemical Oxygen Demand Monitoring

The Biochemical Oxygen Demand (BOD) is referred as "The amount of oxygen per unit volume of water required to oxidise (stabilise) the oxidisable matter in water bacterially". Microorganisms like bacteria act on organic waste for decomposition. The aerobic bacteria are responsible for the breakdown of organic material such as leaves, manure, dead plants, grass clipping, sewage or food waste in the water body. Aerobic bacteria consume dissolved oxygen during decomposition. At the same time, some other aquatic organisms also consume available oxygen from water bodies for sustenance. A large quantity of organic matter in the water body also has a massive load of bacteria to decompose the waste material. The BOD samples were collected from various locations along the river before, at and after the confluence with nalla.

3.4.4 Diurnal Variation

This experiment was carried out at Rajghat in Varanasi, where light and dark bottles were placed at two depths. The monitoring was carried out for 24 hours. The main focus of this experiment was to study the variation in DO concerning depth and time in the presence and absence of sunlight. It also determines the effect of the existence of phytoplankton on DO.

3.5 Results and Discussion-Pre Monsoon season

As stated earlier, extensive study related to DO profiling, reaeration rate experiments and BOD monitoring was carried out in pre-monsoon seasons. Details of the study related to these aspects are presented subsequently.

3.5.1 Dissolved Oxygen Profiling

3.5.1.1 Kanpur

The DO was measured at various locations along the bank of river Ganga upstream and downstream of Kanpur. The average DO concentration was found to be below <2 mg/L at the drain mixing point and about 6-7 mg/L at the river surface (**Figures 3.5a-3.5d**). The drains carry sewage into the river, the main reason for the significant DO sink. The Kanpur stretch showed significant depth variation of River Ganga, and the maximum depth was 6m. DO was measured at the surface, 2m, 4m and 6m depth. DO at 2m, 4m and 6m depth showed minor variation. The maximum DO at the surface was 7.29 mg/L, and the minimum DO was 1.54 mg/L. The surface DO was higher than the DO at 2m, 4m, and 6m depth because of turbulence, mixing of atmospheric oxygen and photosynthesis due to phytoplankton. The DO

concentration at 2m depth ranged from 5.16 mg/L to 7.3 mg/L, and DO at 4 m ranged from 5.21 mg/L to 6.93 mg/L. The DO at 6m depth was found to be varying from 5.25 mg/L to 6.56 mg/L.

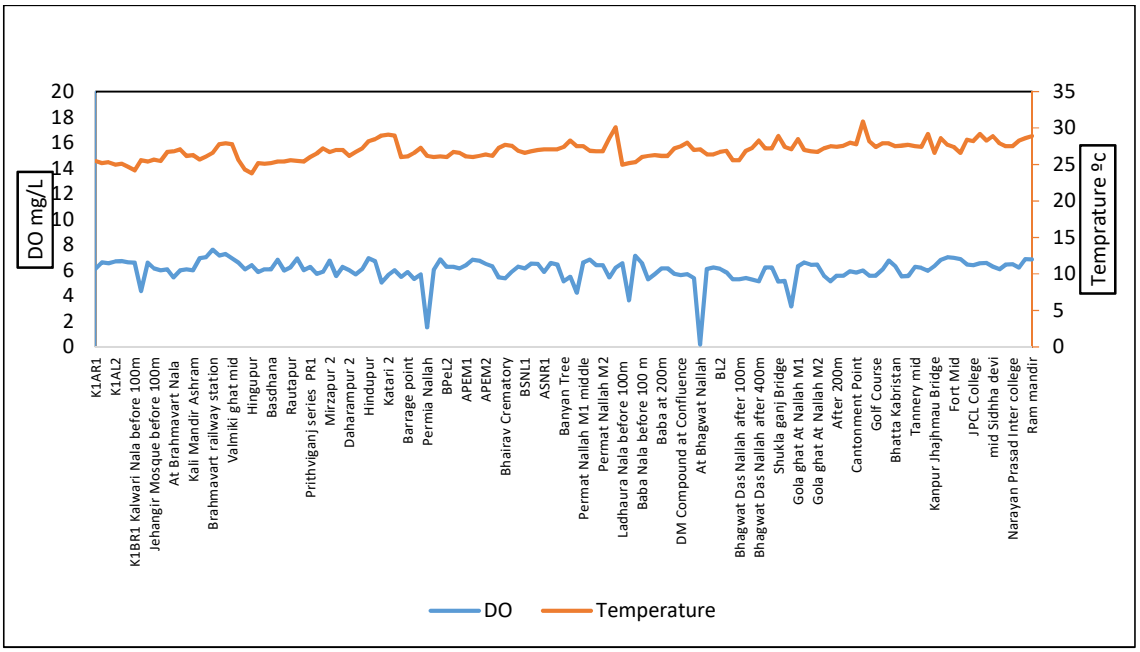

Figure 3.5a: DO and Temperature profiling at various locations at surface of Ganga River at Kanpur (May, 2019)

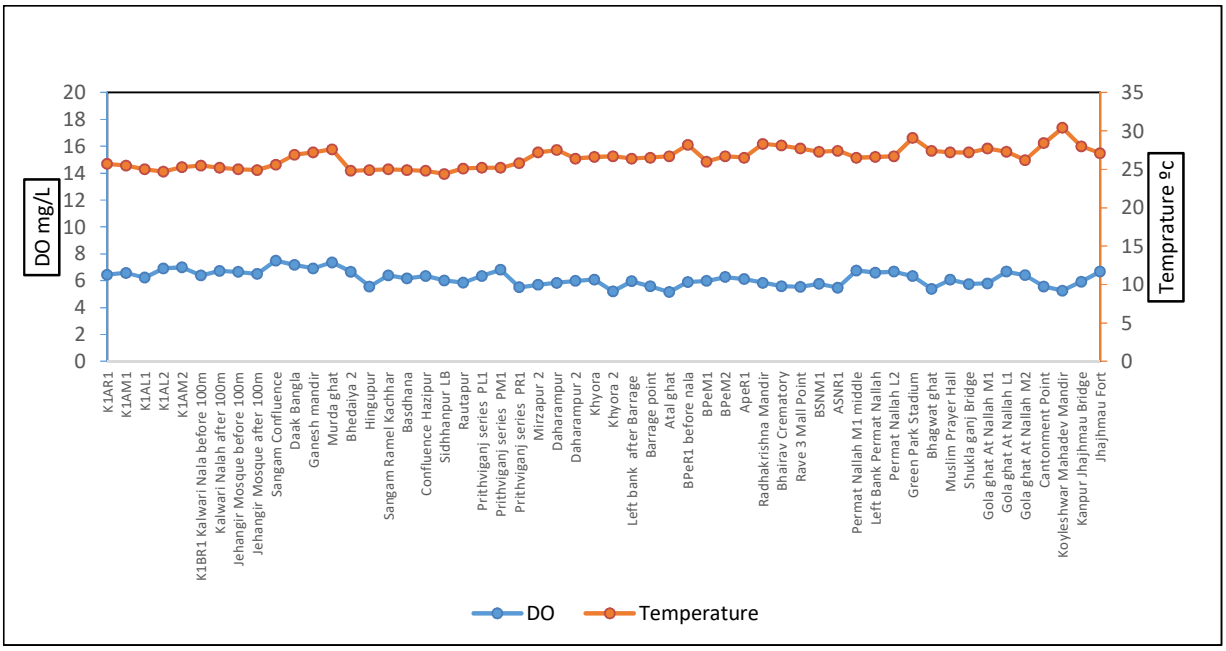

Figure 3.5b: DO and Temperature profiling at various locations at 2m depth of Ganga River at Kanpur (May, 2019)

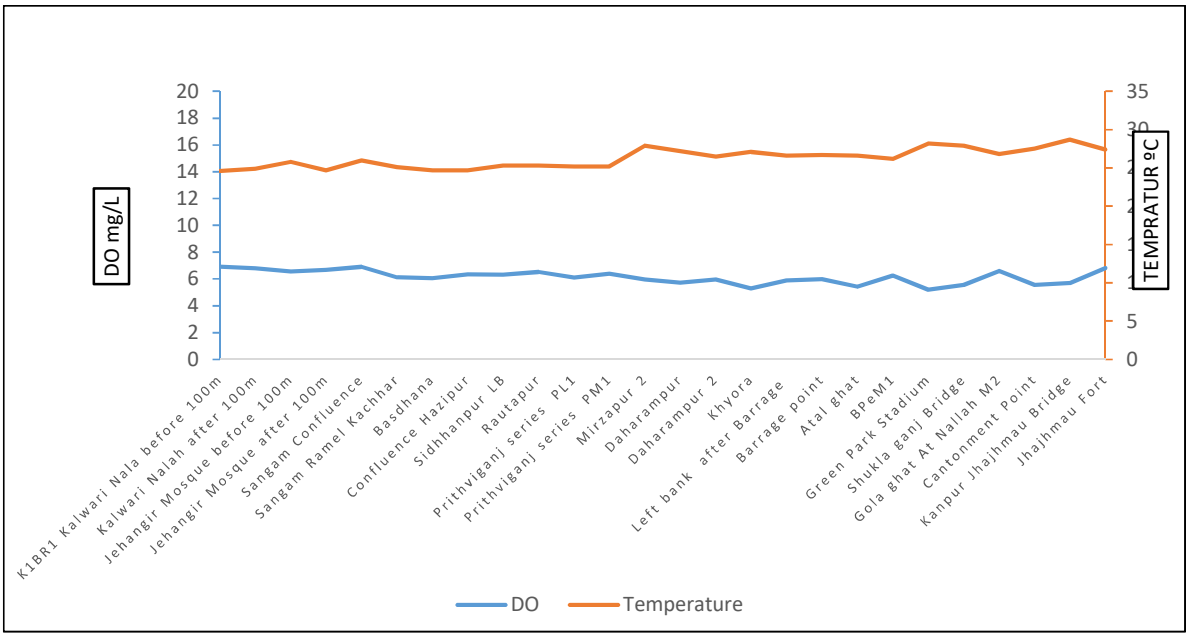

Figure 3.5c: DO and Temperature profiling at various locations at 4m depth of Ganga River at Kanpur (May, 2019)

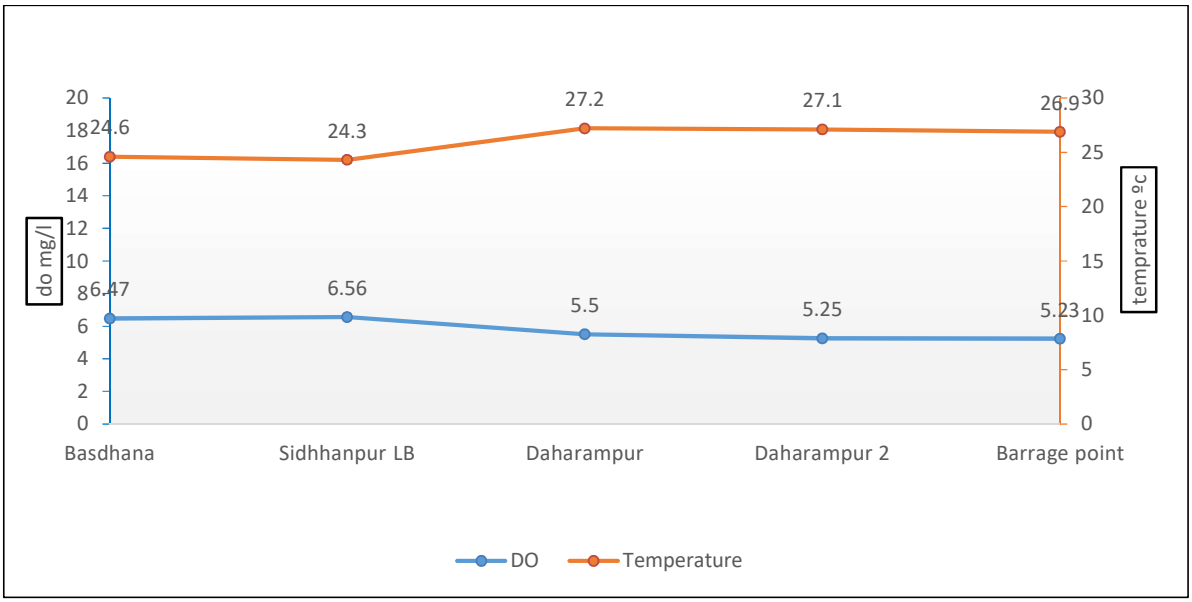

Figure 3.5d: DO and Temperature profiling at various locations at 6m depth of Ganga River at Kanpur (May, 2019)

3.5.1.2 Prayagraj

The water depth at Allahabad was shallow, i.e. not more than 1m, due to the Kumbh festival. The concerned State Government agency tapped every drain over 1 MLD and artificially increased the flow of Ganga. Due to this shallow depth, monitoring was carried out only at the surface. In the upper stretches of Prayagraj, some drainage may be due to the sewers opening at night time. The DO of Prayagraj was found to be varying from 3.48 mg/L to 7.80 mg/L as shown in **Figure 3.6**.

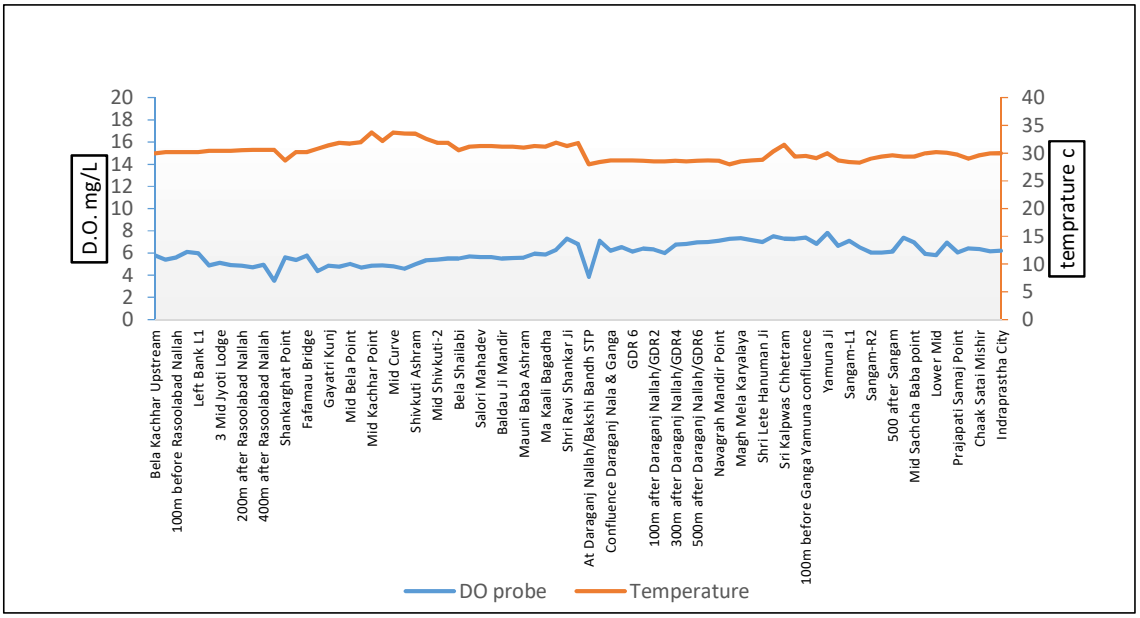

Figure 3.6: DO and Temperature profiling at various locations at surface of Ganga River at Prayagraj (May, 2019)

3.5.1.3 Varanasi

The DO at the surface of Assi and Varuna confluences with the Ganga River were less than 2 mg/L. DO at various locations shown in the **Figure 3.7a** were found to be more than 6mg/L. DO at 2m, 4m, and 6m depths (**Figures 3.7b and 3.7d**) also did not show any significant variation as the measured DO was >4mg/l at all the locations except the places where there was a confluence with nallah. The organic matter from the sewage settles down at the bottom of the river near the confluence of the sewage and river, forming layers of sediments.

Significant DO sinks were observed due to sediments and zooplankton at 6m depths. It might be due to the tapping of most of the sewers in Varanasi that could have led to the reduced organic load. The DO values along the stretch of about 15 km ranged from 3.55 mg/L to 11.50 mg/L. All the DO values at different depths are shown in **Figures 3.7a-3.7d**.

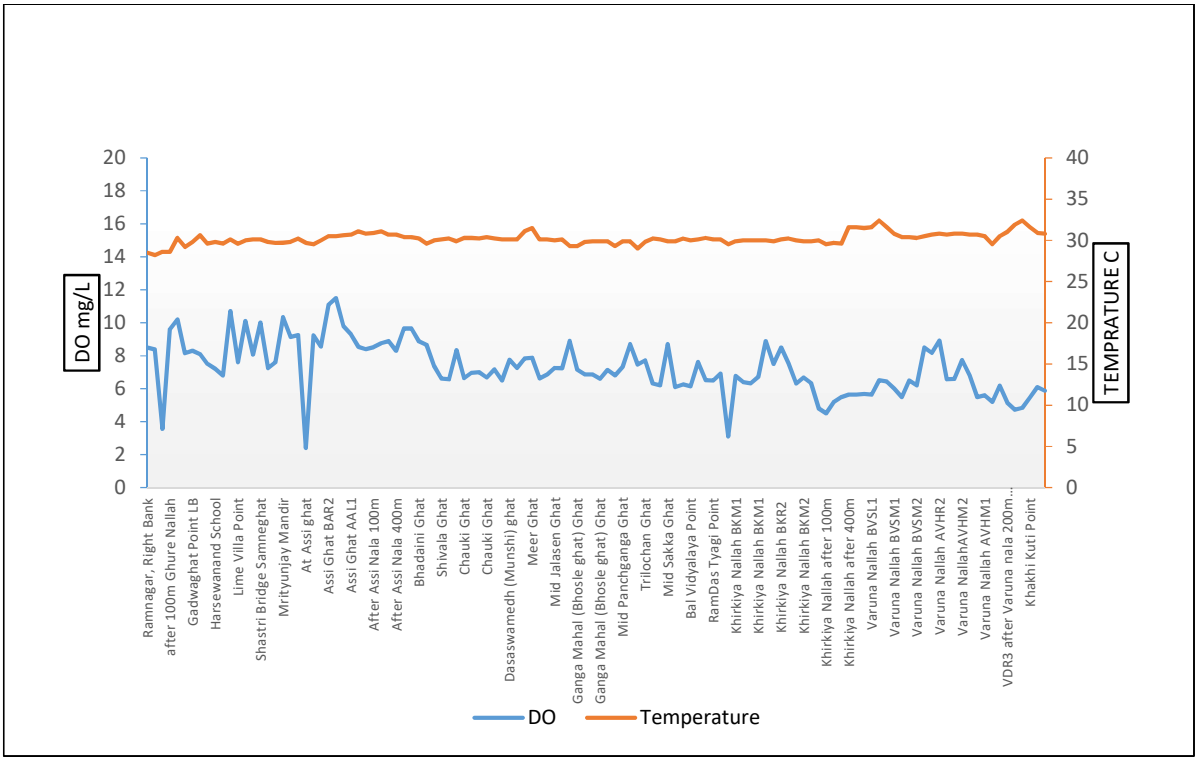

Figure 3.7a: DO and Temperature profiling at various locations at surface of Ganga River at Varanasi (May, 2019)

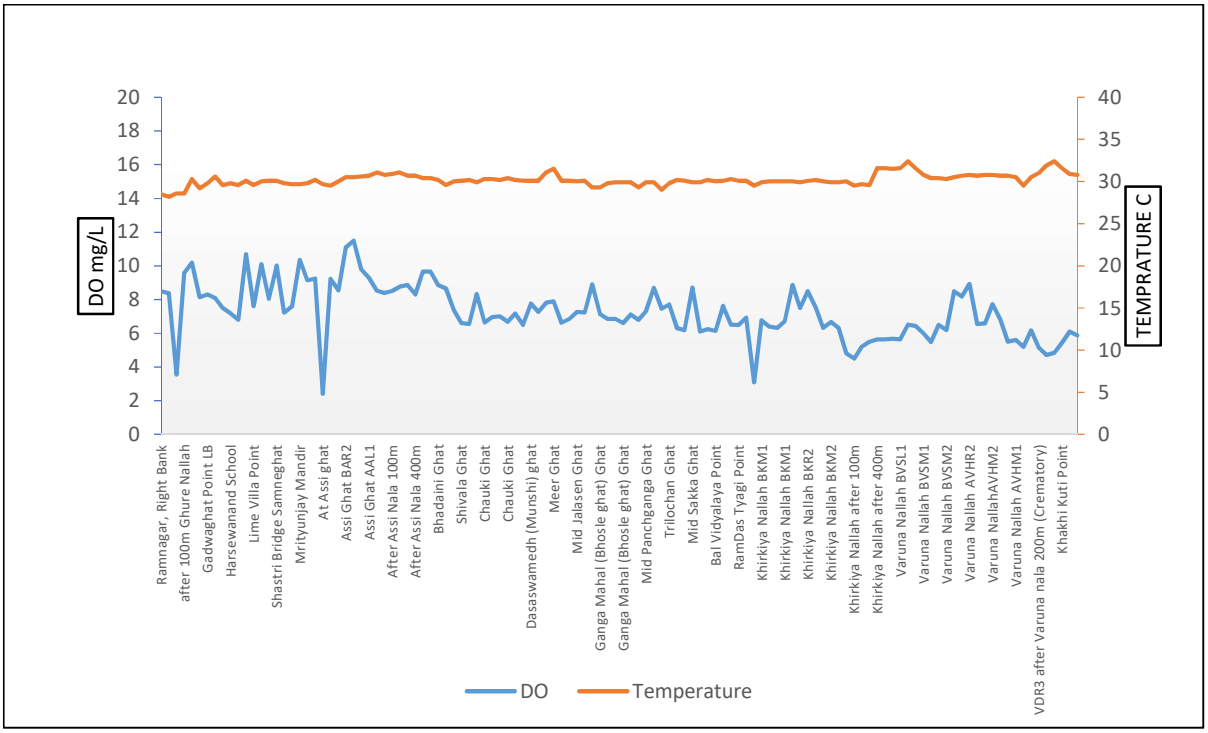

Figure 3.7b: DO and Temperature profiling at various locations at 2m depth of Ganga River at Varanasi (May, 2019)

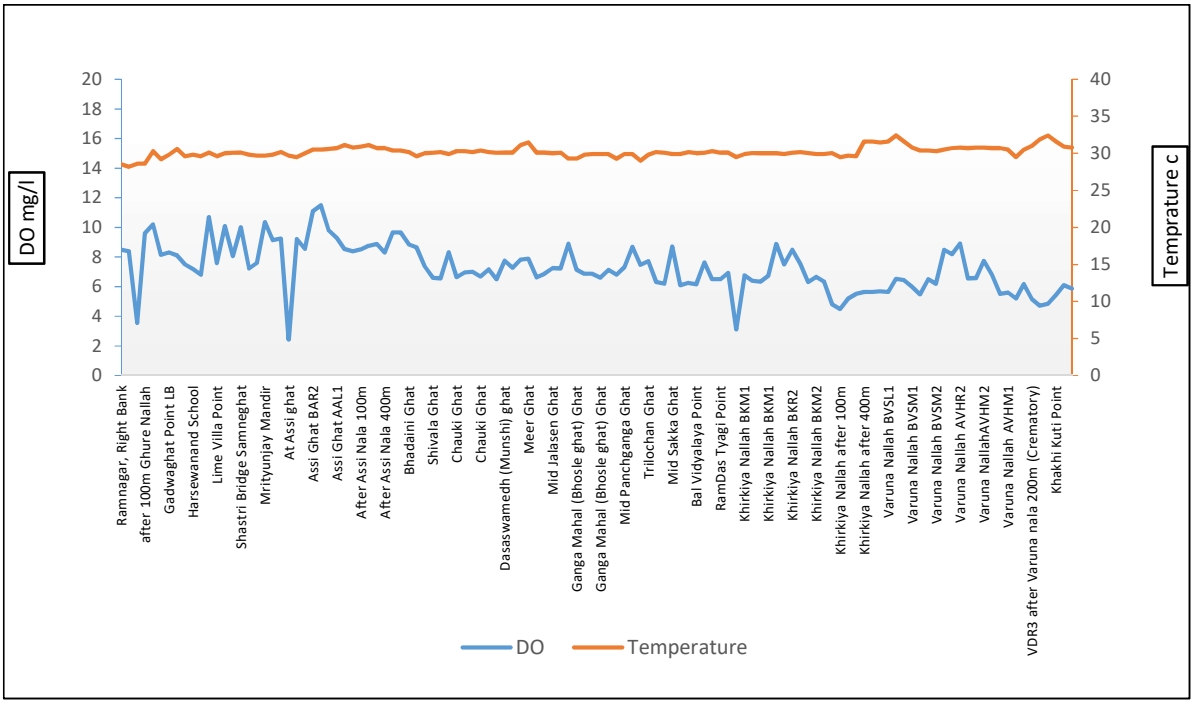

Figure 3.7c. DO and Temperature profiling at 4m depth at Varanasi (May 9-12, 2019)

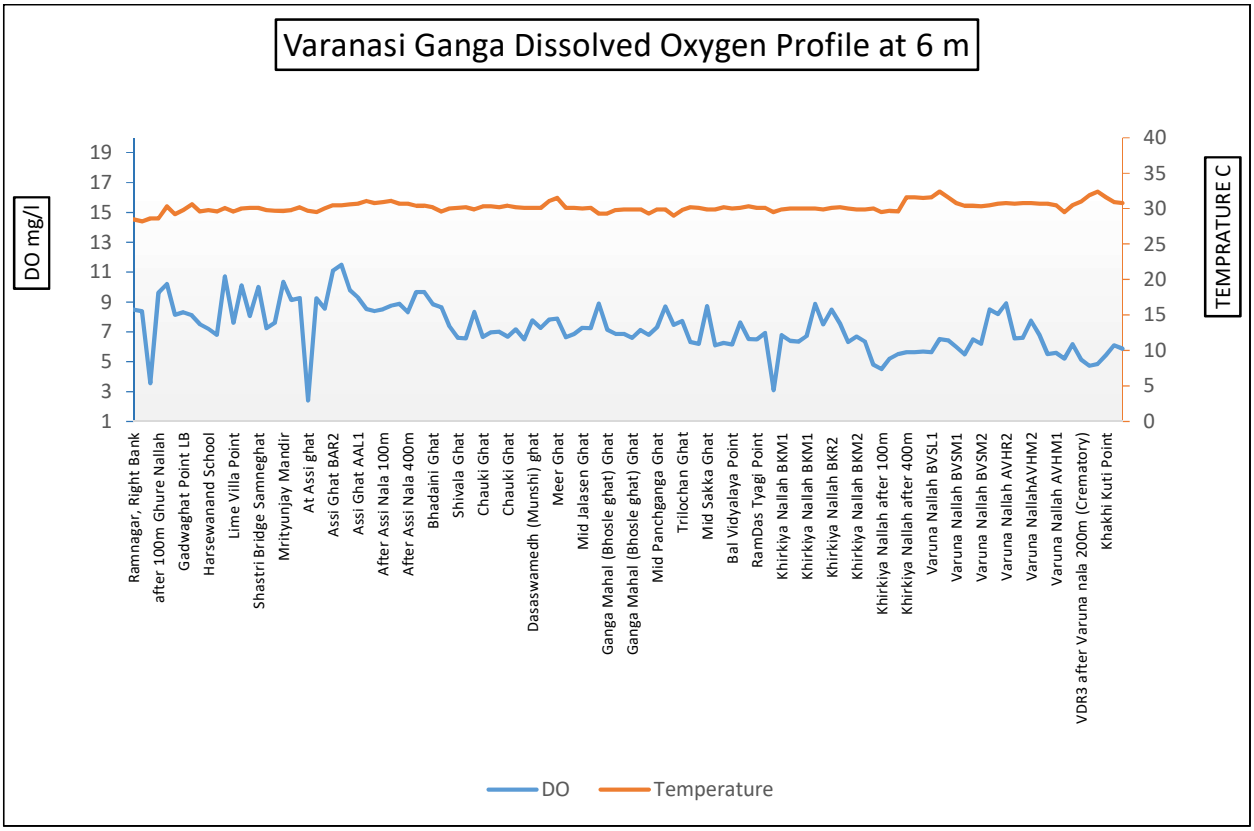

Figure 3.7d. DO and Temperature profiling at 6m depth at Varanasi (May 9-12, 2019)

3.5.2 Reaeration Rate Experiment

3.5.2.1 Kanpur

Reaeration rate experiments were carried out near the sewer outfall locations in the river. DO was monitored initially at a place before the point where the sewage mixes with the river and every 300-350m after the mixing point along the river. At Kanpur, the reaeration experiment was performed on four nallahs, Bhagwat nallah, Kalwari nallah, Gola Ghat nallah and Baba nallah. Out of this, day and night comparative reaeration experiments were carried out at Bhagwat nallah and Klawari nallah. DO levels before Bhagwat nallah in daytime and nighttime were measured as 5.39 mg/L and 5.68 mg/L, respectively. DO was found to be significantly low, i.e. 0.2 mg/L and 0.4 mg/L at the mixing point of Bhagwat nallah during day and night, respectively. The DO levels increased to 5-6 mg/l within a distance of 700 m from the mixing point of sewage. At Kalwari nallah, DO levels measured at the mixing point during the day and night were 4.38 mg/L and 2.12 mg/L, respectively. The DO levels increased to 6-6.5 mg/L within 100 m. All four nallahs get reaerated quickly due to

substantial flow in River Ganga. **Figures 3.8a to 3.8f** show the reaeration graphs of four nallahs of Kanpur.

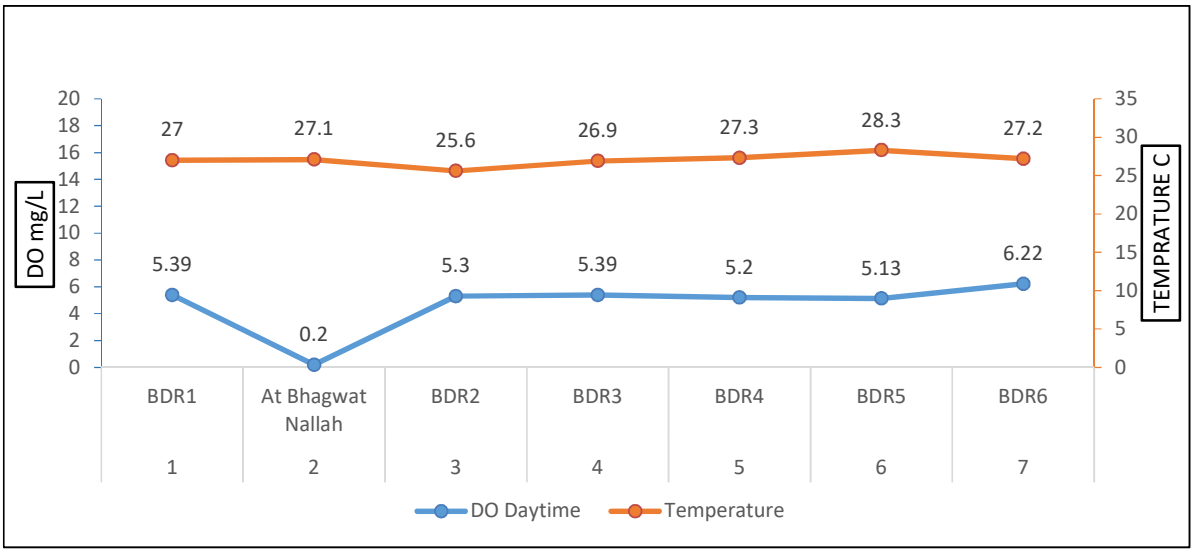

Figure 3.8a: Day time Reaeration at Bhagwat Das Nallah Kanpur (May, 2019)

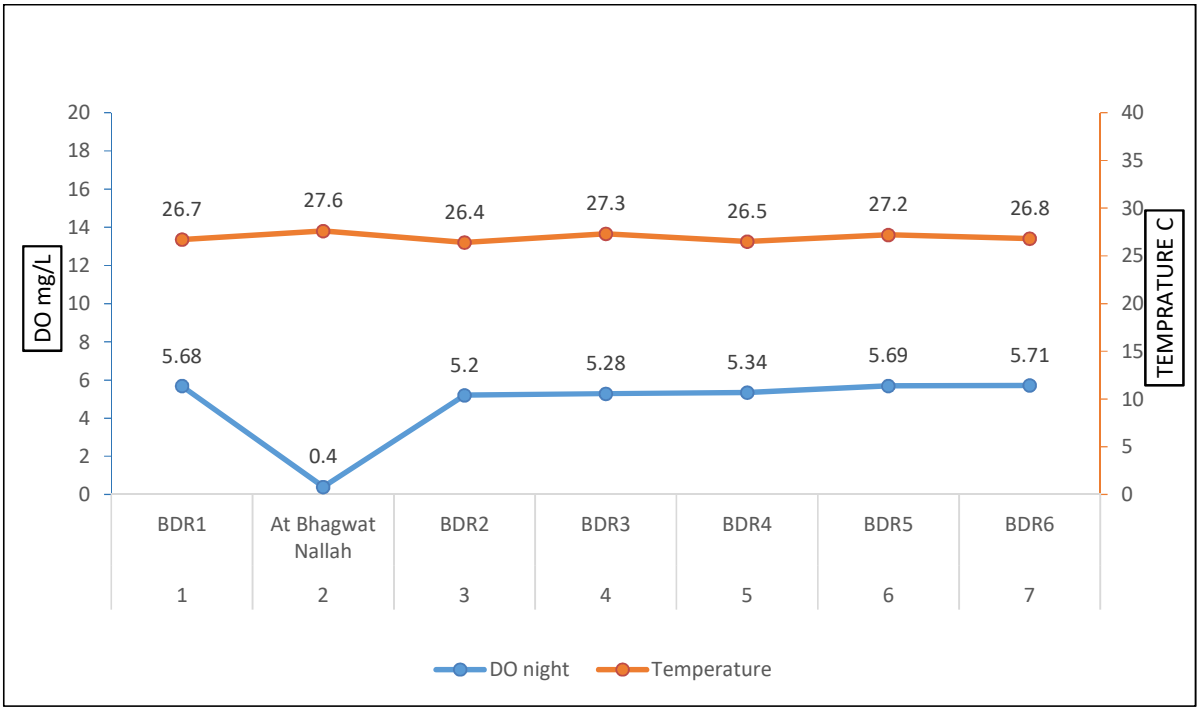

Figure 3.8b: Night time Reaeration at Bhagwat Das Nallah Kanpur (May, 2019)

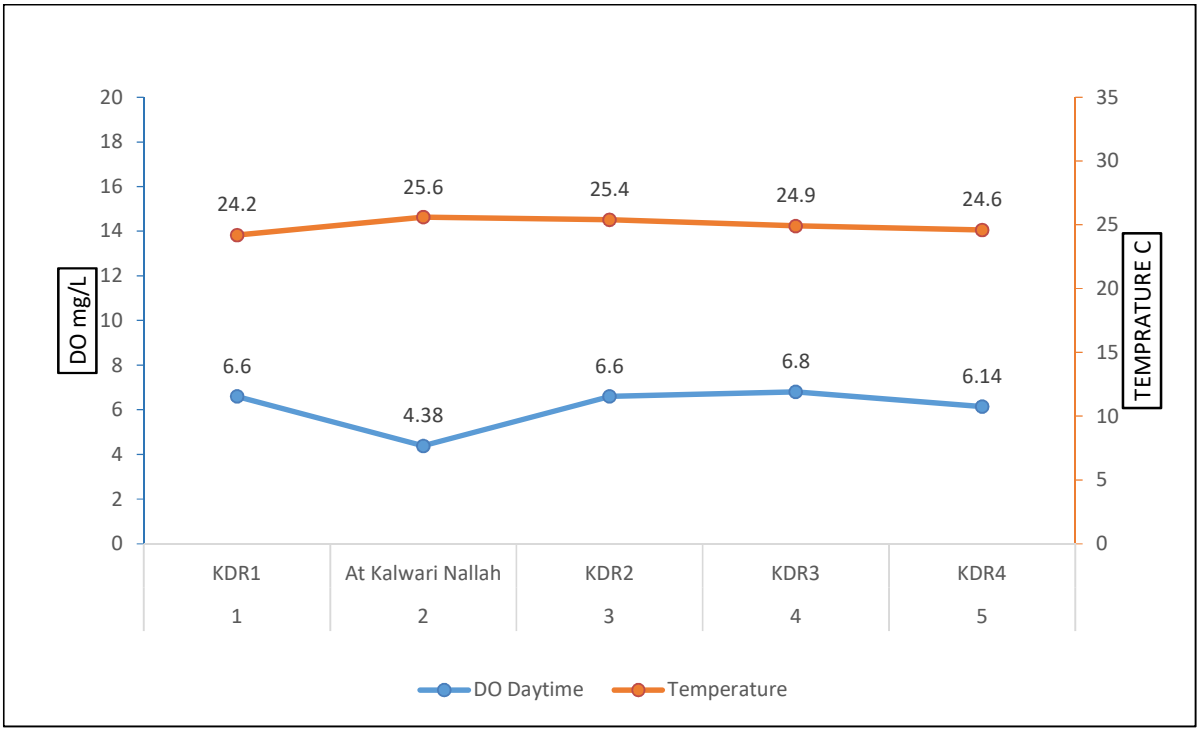

Figure 3.8c: Day time Reaeration at Kalwari Nallah Kanpur (May, 2019)

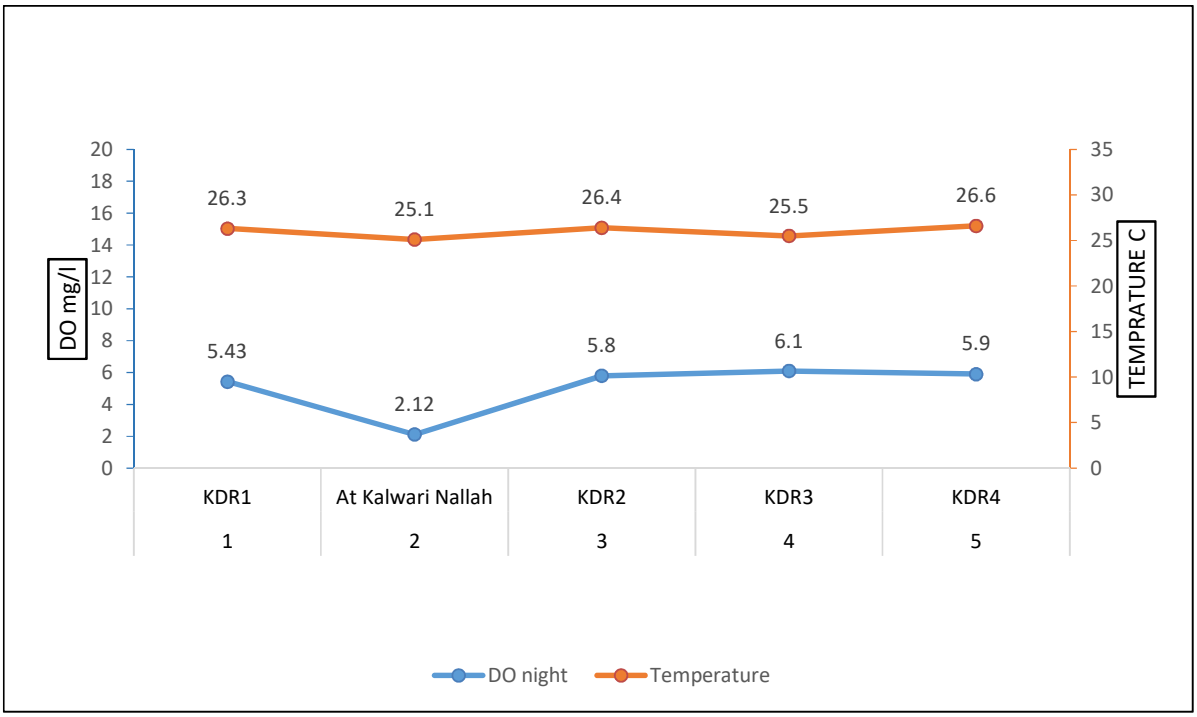

Figure 3.8d: Night time Reaeration at Kalwari Nallah Kanpur (May, 2019)

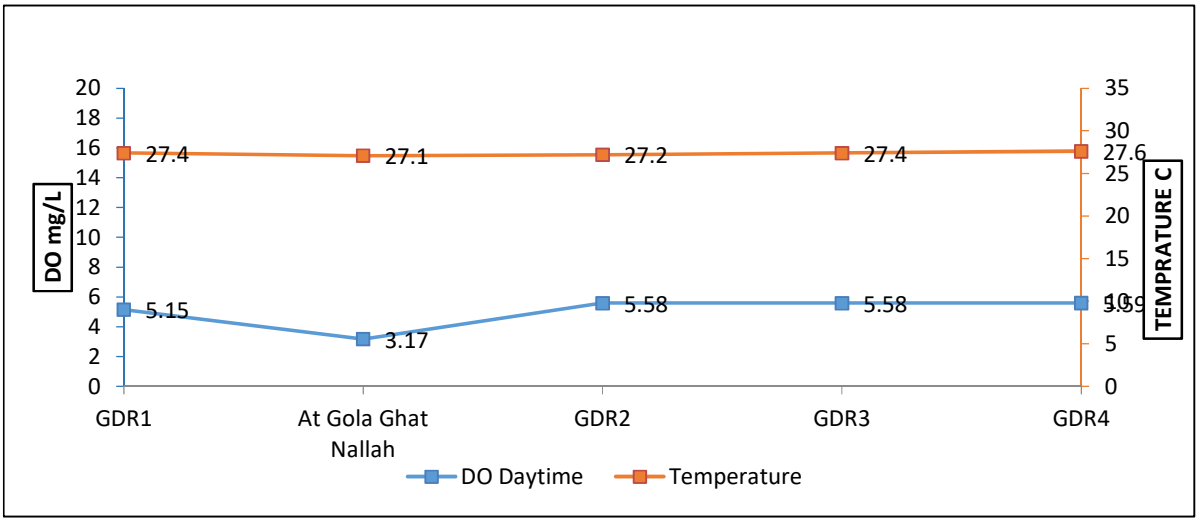

Figure 3.8e: Day time Reaeration at Gola Ghat Nallah Kanpur (May, 2019)

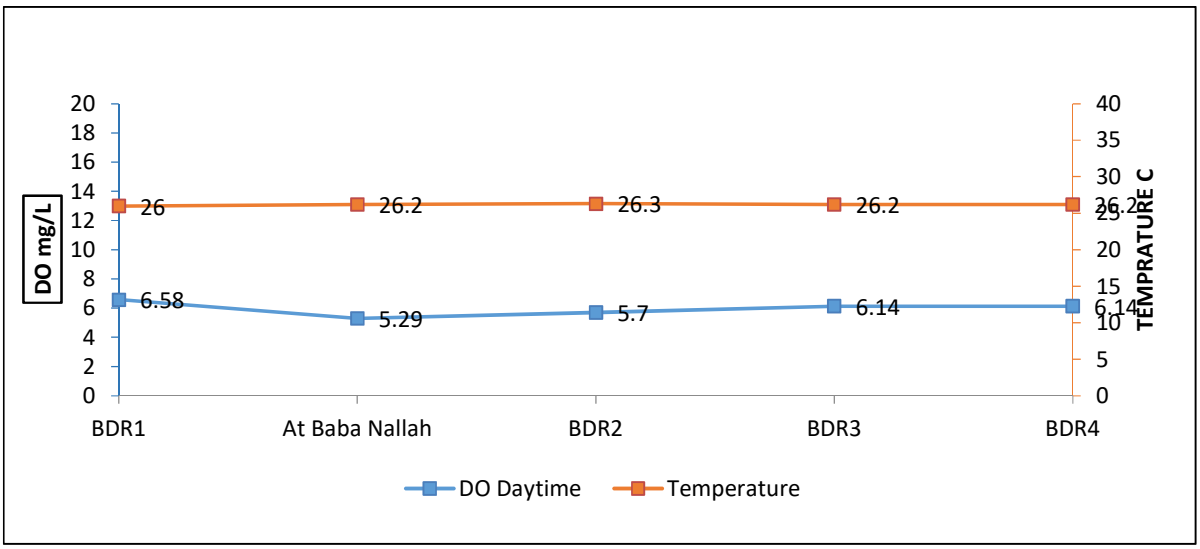

Figure 3.8f: Day time Reaeration at Baba Nallah Kanpur (May, 2019)

3.5.2.2 Prayagraj

The total stretch of Prayagraj along Ganga is about 21 km, and there are several drain outlets, but most of them were tapped due to the Kumbh festival 2019. Therefore, the reaeration experiment in the daytime at Prayagraj was carried out only at two nallahs, i.e. Rasoolabad nallah and Daraganj nallah. Before Rasoolabad nallah, the DO was 5.60 mg/L but at the mixing point, the DO decreased to 4.10 mg/L; after 100 m, it increased 4.89 mg/L. However, DO again decreased to 3.48 mg/L after 400m due to the confluence of Chhohara mandir nallah. At about 600 m from Rasoolabad nallah, the DO increased to 5.61 mg/L, as shown in

Figure 3.9a. In Daraganj nallah, the DO before the confluence was measured as 7.10 mg/L. At the mixing point, DO was 3.85 mg/L and increased to 7.10 mg/L at 700m downstream of the mixing point, as shown in **Figure 3.9b**.

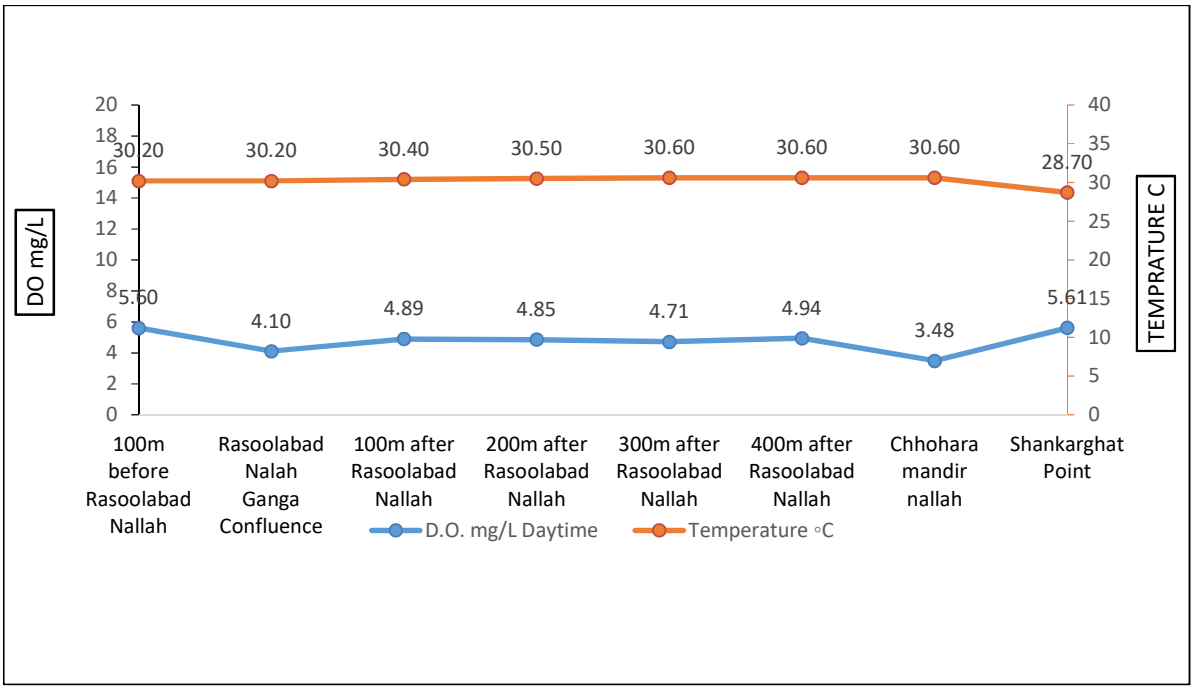

Figure 3.9a: Day time Reaeration at Rasoolabad Nallah, Prayagraj (May, 2019)

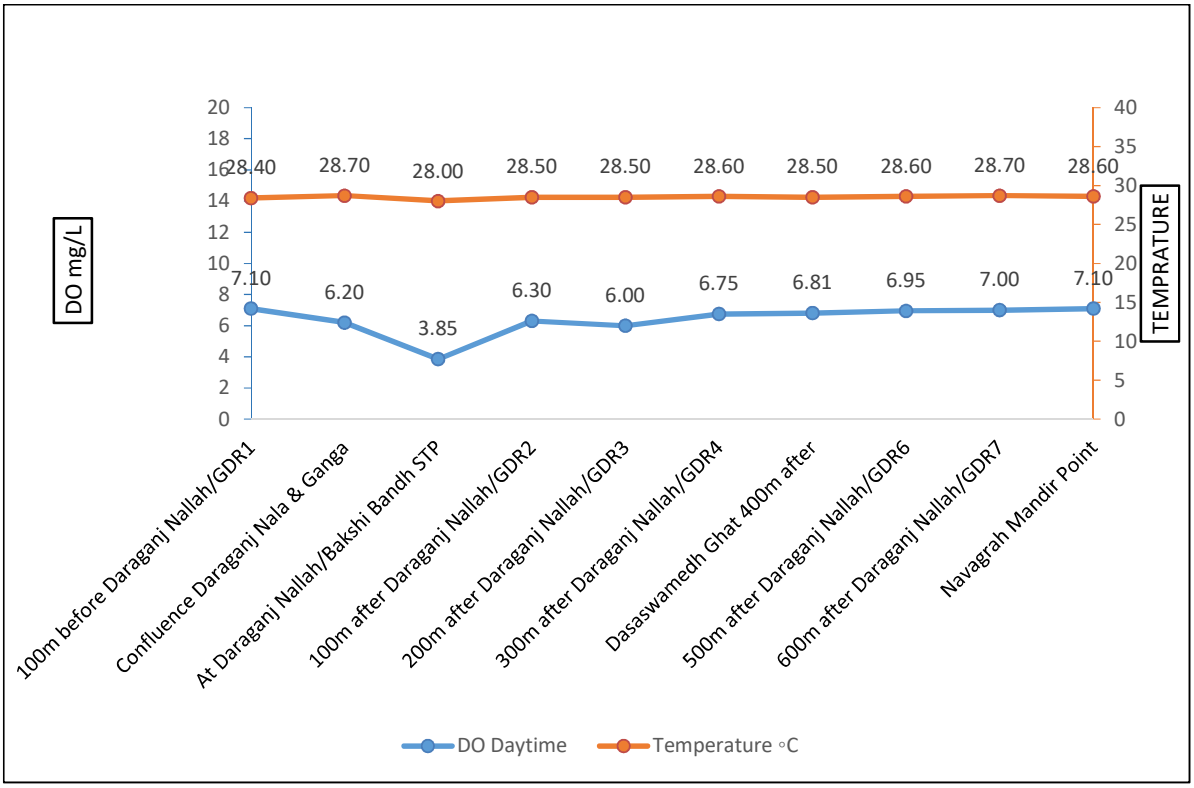

Figure 3.9b: Day time Reaeration at Daragang, Prayagraj (May, 2019)

3.5.2.3 Varanasi

There are two major nallahs at Varanasi: i) Assi nallah upstream and ii) Varuna nallah downstream. Both nallahs have a heavy pollution load. The DO at Assi ghat, Varanasi confluence and along the bank of the river was measured till the DO was restored to the level before the confluence of nallahs with the river. The results showed that DO before mixing Assi nala sewage into river Ganga is around 7mg/l and decreases to 0.4mg/l immediately after mixing. It takes approximately 2.5 km to restore DO level of 7mg/L during the pre-monsoon period. The phytoplankton and zooplankton were monitored only at Varanasi for the following reasons:

- Based on the findings of previous studies,
- most polluted stretches
- have more significant variation and sink of DO compared to other locations like Kanpur and Prayagraj.

The variation in DO, BOD, phytoplankton and zooplankton were studied to assess the microenvironment that played a major role in the reaeration. The phytoplankton increases after the influx of sewage as it brings nutrients and organic matter. Consequently, phytoplankton decreases as the nutrients move away from the mixing point, and there is also an increase in the zooplankton density that feeds on the phytoplankton. **Figures 3.10a-3.10b** show the DO monitoring at Assi ghat and Varuna nallah. The DO value measured before Vruna nallah was 5.68 mg/L, and at the mixing point, it reduced to 3.20 mg/L, restored after a distance of about 500m.

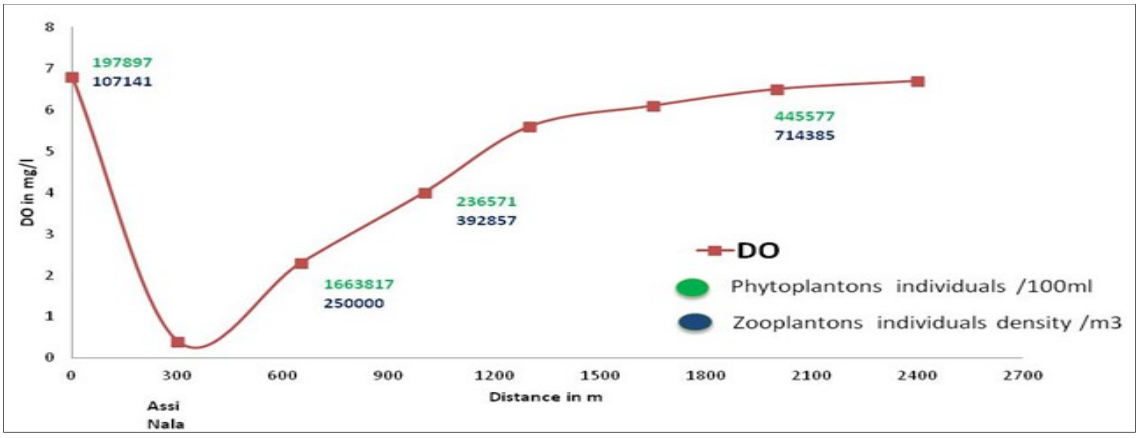

Figure 3.10a: DO reaeration at Assi nallah- Pre monsoon (May, 2019)

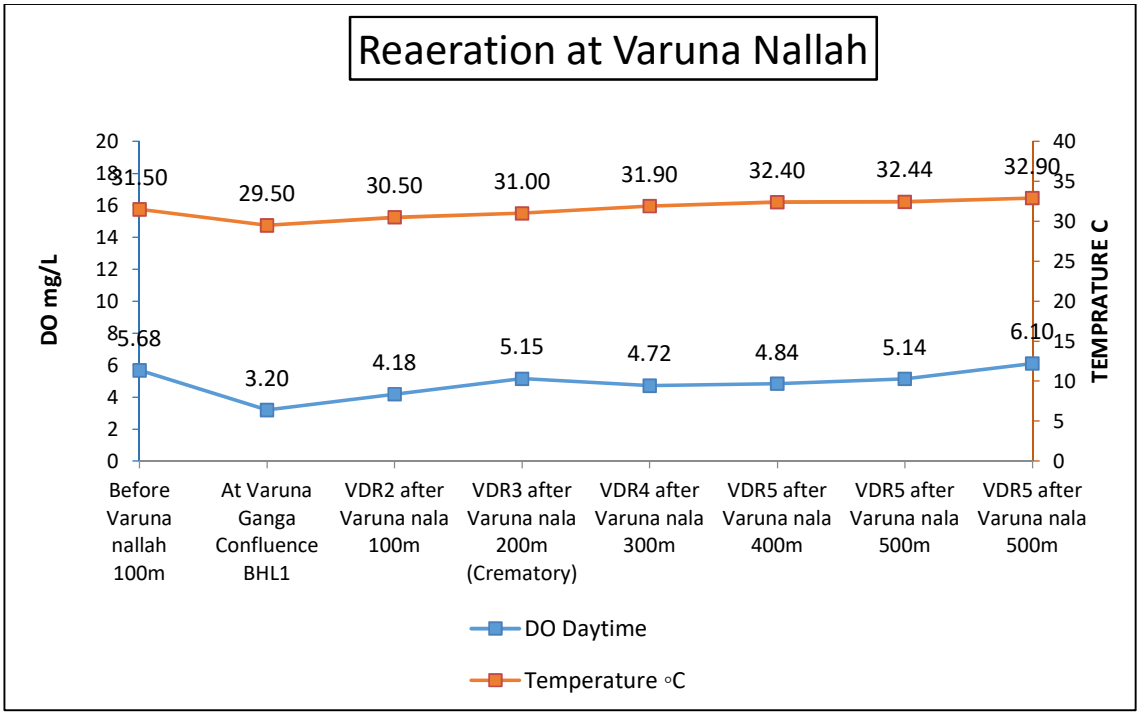

Figure 3.10b: Day time Reaeration at Varuna Nallah (May, 2019)

3.6 Results and Discussion – Post-monsoon season

The post-monsoon monitoring was carried out at a few locations at Assi nallah in Varanasi, which showed a significant improvement. Insignificant variation in the DO values was observed,possibly due to considerable flow resulting in sufficient dilution in the River Ganga. However, a major reason for comparatively higher DO values in Varanasi is sewage collection and treatment at all the locations and ghats. BOD monitoring was carried out at the Prayagraj and Varanasi locations only.

3.6.1 Dissolved Oxygen Profiling

Figures 3.11a and 3.11b show the results of post-monsoon DO monitoring at Rajghat, Varanasi, at the surface and 1.5m depth. The results show no significant variation in DO; the average DO was around 7.5 mg/l. There are no major pollution sources near Rajghat except the pollution due to activities like bathing, washing etc. The water temperature recorded at around 2.00 pm in the daytime was 25°C and around 17°C at night. No significant variation was found in the temperature at the surface and 1.5m depth.

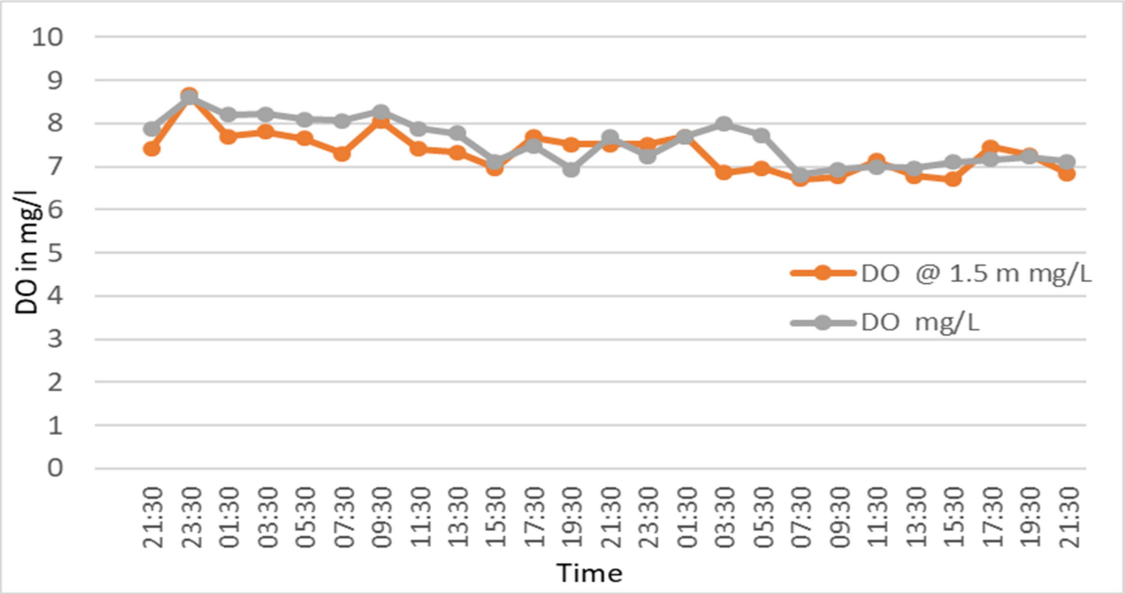

Figure 3.11a: DO monitoring at surface and at 1.5m depth for 48 hrs at Rajghat Varanasi (Nov 2019)

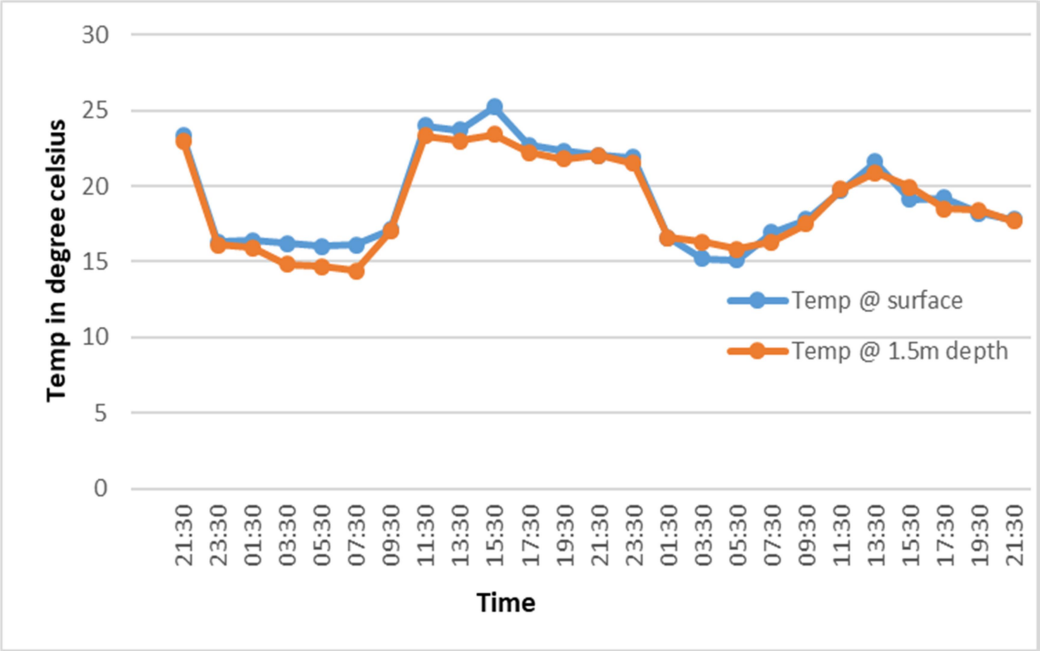

Figure 3.11b: Temperature monitoring at surface and at 1.5m depth for 48 hrs at Rajghat Varanasi (Nov-2019)

3.6.2. BOD monitoring

A comparative study of BOD variation along the Ganga River was conducted at only two locations, i.e. Prayagraj and Varanasi, during the post-monsoon season.

3.6.2.1 Prayagraj

The BOD monitoring at Prayagraj showed no significant variation; the observed values were 1.93-7.10 mg/l. The maximum value of 7.10 mg/l was observed at Sangam, as shown in **Figure 3.11c**.

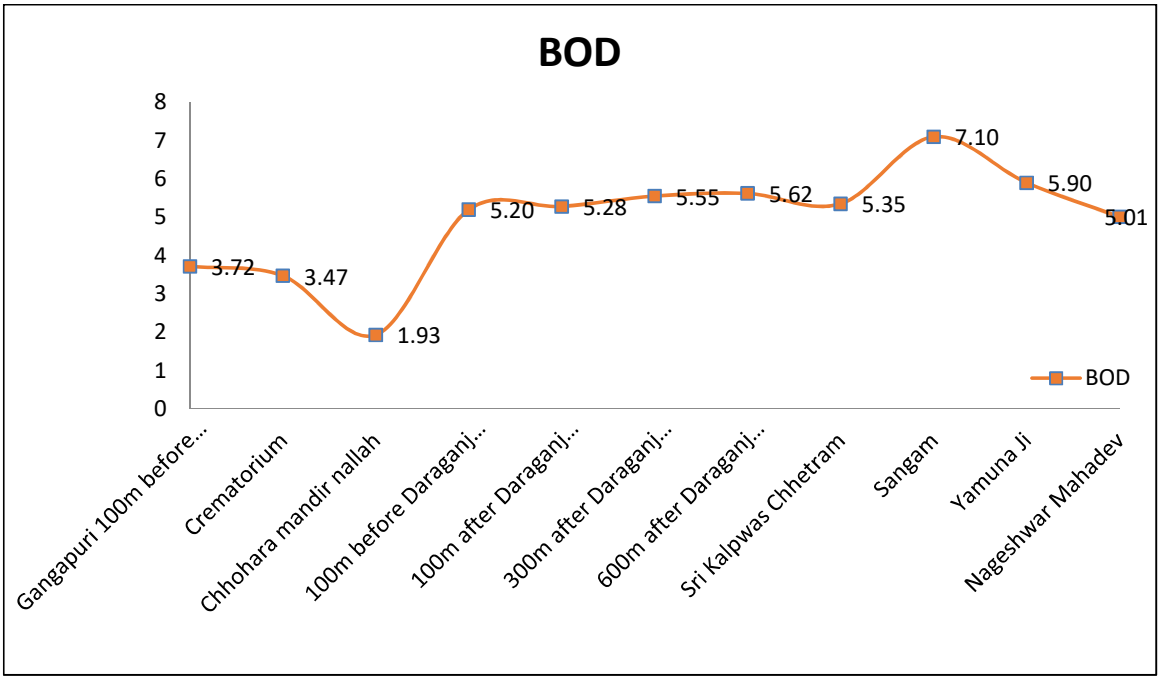

Figure 3.11c. BOD variation in Prayagraj (Nov, 2019)

3.6.2.2 Varanasi

A similar trend was observed in Varanasi, as the maximum values of BOD did not exceed 10 mg/l. The maximum value of 9.21 mg/l was recorded at Assi nallah confluence, and water qualitygradually improved as we moved away from the nallah as shown in **Figure 3.11d**. The other nallahs such as Varuna and Khirkiya did not impact the water quality. The BOD values were less than 3 mg/l at most locations except at immediate confluence with nallahs.

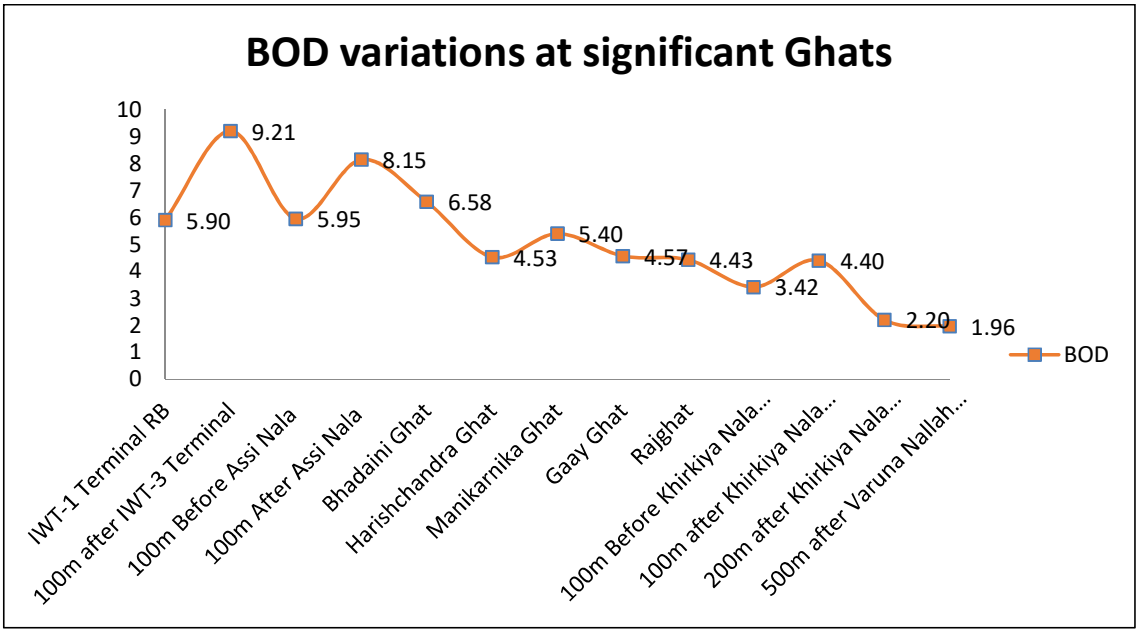

Figure 3.11d. BOD variation in Varanasi (November, 2019)

3.6.3 Reaeration Rate Experiments

During the post-monsoon season, the sink in DO at the confluence of Assi nala was less compared to the pre-monsoon season. A similar trend in DO, phytoplankton and zooplankton was observed during the monitoring in post-monsoon season. The DO sink was lower in the nighttime compared to the daytime. The initial DO before mixing of sewage was recorded as 9mg/l and decreased to 3mg/l and 5mg/l in the day and night times (fig 3.12). In both cases, the DO was restored to around 7 mg/l within 1km. The BOD of Assi nala sewage was approximately 50 mg/l, and it slowly reduced to 3mg/l at 1.5 km downstream. The zooplankton concentration during the night was found to be more significantthan that in the day. It may be due to the tapping of the sewage outlets at multiple locations and dilution due to an increase in the volume of water (as a result of monsoon) in the river. However, there is a significant overall improvement in the quality of water after nallahs were tapped and treated before discharge to the Ganga River.

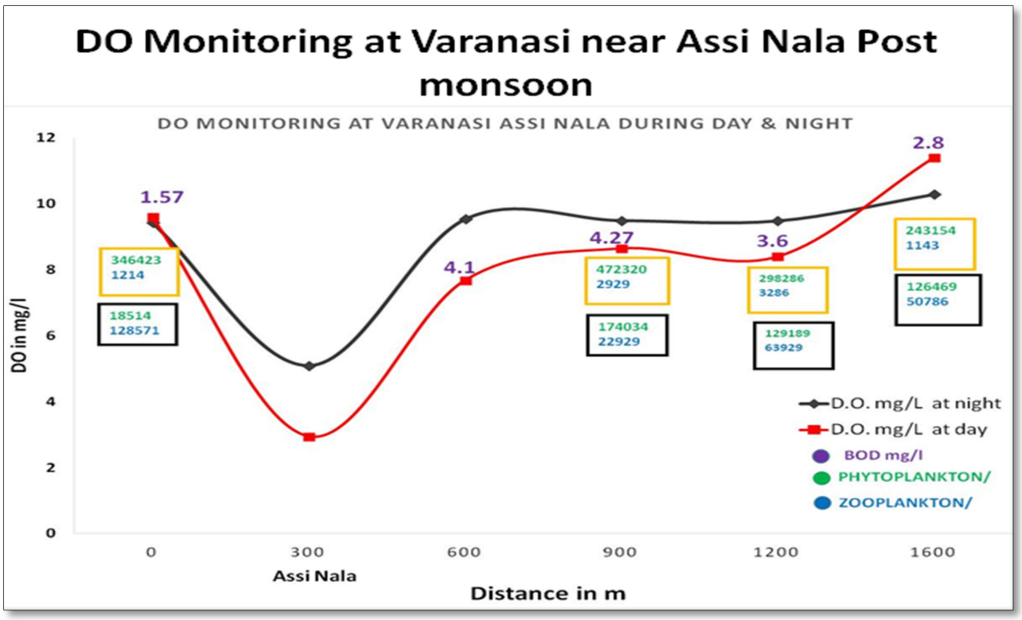

Figure 3.12: DO reaeration at Assi nala- Post monsoon Day/Night (November, 2019)

3.7 Conclusions

The following conclusions can be drawn based on the studies:

- There is no significant variation in the DO levels at the surface and 1.5 m depths during both day and night. The results of the diurnal variation experiments showed that the average DO value was 7-8mg/l day and night over 48 hours. It may be due to stopping all the sewage from mixing into Ganga.
- The DO at the surface decreased to < 2mg/l during the sewage mixing but did not significantly decrease at 2m and 4m depths. It may be due to factors such as reduction in organic load, shallow depth of river, high water velocity (> 0.3m/s) and the river profile.
- The DO was restored to 7-8mg/l within a distance of 1.6 km from the mixing point of sewage and the river during the post-monsoon season compared to the pre-monsoon season. It could be due to the control and treatment of the sewage infusing river Ganga.

Sewage is the primary source of contamination in the monitored locations in the river Ganga. The dip in the DO values was not observed after the sewage was stopped from entering the river. However, at a few locations, the sewage mixes with the river in petite proportions, which doesn't significantly affect the DO of the river Ganga.

CHAPTER - 4

QUANTITATIVE RISK ASSESSMENT

4.0 Quantitative Risk Assessment in River Ganga to assess hot spots in the river and associated health risk

4.1 Introduction

The conservation and protection of Ganga water quality is of critical importance. The rapid industrialization, economic development and agricultural activities, combined with limited precipitation contribute to the quantitative and qualitative degradation of freshwater resources (Mok and Hamilton 2014; Pandey et al. 2014). Major factor for degradation of River Ganga is faecal contamination due to underdeveloped sanitation and sewerage networks in nearby areas where River Ganga flows, release of untreated wastewater discharges, anthropogenic activities, agricultural discharge, septic leakages and wildlife populations (Mishra and Mohapatra 2009). However, there is substantial improvement in terms of sewage treatment as sewage treatment plants are commissioned. Based on the water quality data of the river collected in 2023 as part of Indian National Aquatic Resources program indicates that water quality of River Ganga improved substantially.

The major concern is when humans come in contact with contaminated water bodies during recreational activities, irrigation, bathing, and religious activities in the river. For this purpose, a series of risk estimates are studied including environmental health risk assessment and vulnerability mapping that can depict key exposure groups, key areas or hot spots, exposure pathways and routes which needs attention, protection and/or implementation measures (Timm et al. 2016).

In broad perspective, quantitative risk assessment (QRA) is a systematic framework in which the risks or ill-effects of an entity or agent on humans and ecosystems is quantified (Busgang et al. 2018; Haas et al 1999; Regli et al 1991). The framework covers a range of risks or hazards or receptors: biological, chemical, radiation and/or physical risks towards impacts on receptors such as human beings (individuals or population), fauna and flora (single species or whole ecosystems). For each of these risk receptors different end-points are defined for example, probability of infection, illness or death, etc.

Unlike the earlier guidelines, which focused on water quality compliance, this framework advocates a preventative, risk management approach with focus on assessing, managing and reducing risks. In this study, QRA approach was used to predict the risks of pollutants (microbial, chemical and metals) in Ganga water. The objectives of this sub-component are as follows:

1. Assess microbial risk from human-associated activities which contaminate Ganga river water
2. Identify key exposure groups and exposure pathways that cause waterborne disease in humans
3. Estimate health risk among exposed population
4. Map health risk zones

4.2 Methodology

4.2.1 Study site

Varanasi one of the oldest city inhabited continuously, is located on the banks of the river Ganga in Uttar Pradesh, India. It is mainly famous for religious activities and is said to be the holiest of the seven sacred cities (Sapta Puri) in Hinduism and Jainism. A report of then Ministry of Urban Development, Government of Indiain 2013 states thatriver Ganga provides approximately 38% of the total water supply to the city, while the rest comes from 220 tube, 16 mini-tube wells and 41 tube wells. According to the report, the city draws a total 270 million litres of water per day from Ganga to meet population water demands.

Sewerage network is also not sufficient and wastewater finds its way into treated water due to leakages in pipes. Insufficient water treatment plant capacity and lack of elevated service reservoirs add to water supply woes of the city. The water treatment plant at Bhelupura, which extract and treat water drawn from the Ganga, has a capacity of 250 million litres per day. Another treatment plant is located as Dinapur and has a capacity to treat 100MLD. In addition, two auxiliary treatment plants are installed at Banaras Hindu University and Diesel Locomotive work. According to CPCB report (2013), only 30% of city's wastewater is treated and discharged properly into the River Ganga while rest goes without any treatment

At Varanasi, the quality of river water has consistently deteriorated over the years until 2019. The Ganga river basin at Varanasi is used for range of land uses including agriculture (primarily vegetables), densely urbanised areas, industries etc.People mostly use river Ganga for recreational purposes like swimming, bathing etc., and religious rituals. Hence, theriver water gets contaminated with microbial and chemical contaminants and pose threat to humans on exposure during its use. Moreover, Assi nallah and Varuna river, which carries urban wastewater and to small quantities of industrial wastewater, discharge water into River Ganga raw or partially treated. In recent years, several municipal sewage treatment plants are built to reduce the quantity released of untreated domestic sewage in the river Ganga. The industrial wastewater discharges have also been controlled. This has led to the reduction in microbial contamination in the river Ganga water.

The study site for risk assessment in Varanasi is shown in Figure 4.1.

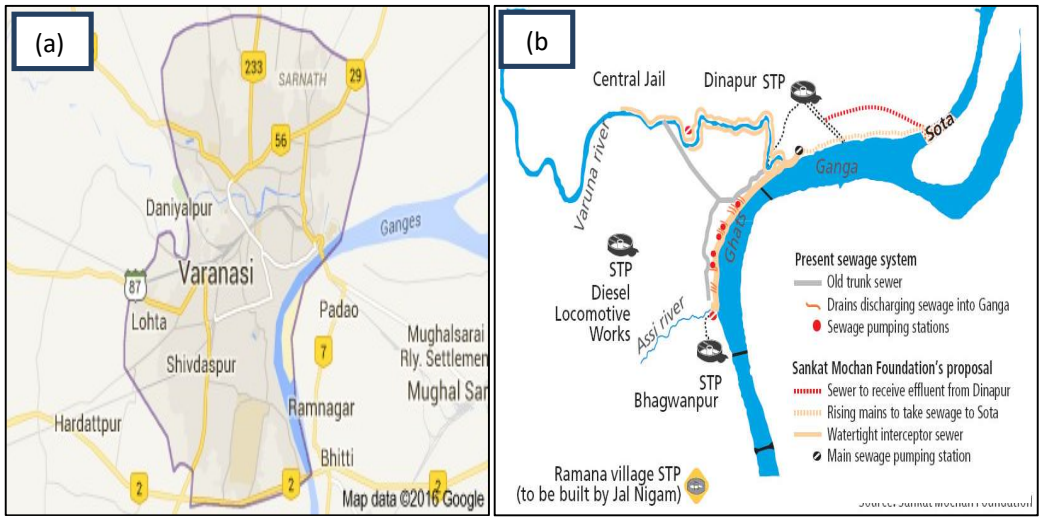

Fig. 4.1: Illustration of Study Site – Varanasi with Wastewater Treatment Plants Details
Source: (a) Google maps and (b) Sankat Mochan Foundation

4.2.2 General Quantitative Microbial Risk Assessment Framework

Quantitative Microbial Risk Assessment (QMRA) is a structured framework integrating science, data analysis, and mathematical modelling to predict infection/illness probability if exposed to the pathogen. The food sector initially used this approach to predict the disease burden upon consuming contaminated food

[Codex Alimentarius Commission, 1999]. It is now used in the environmental field to calculate the probability of infection/illness upon exposure to microorganisms during various waterreuse applications. QMRA builds on the chemical risk assessment approach, which involves five distinct steps; identifying a problem statement, exposure-assessment, dose-illness analysis, risk characterization and risk management as elaborated below.

1. Problem formulation for the risk assessment is the first step in which the purpose and the stakeholders, such as policymakers, consumers, academicians, researchers, treatment evaluators and innovators, are defined Haas et al. [Haas, Rose, Gerba 1999]. However, this requires an in-depth understanding of hazard/risk, intuition, creativity and experience [Haas, Rose, Gerba 1999]. It also, in some scenarios, lists microbiological agents of concern and the adverse health impacts. This step involves collating supporting information of the target microorganisms on the health impact (disease) from established literature, hospitalization data, or epidemiological studies.

2. Exposure assessment calculates the selected microorganism's daily intake by integrating their concentration and frequency for the defined exposure scenario. It considers the media through which the microorganisms travel from source to recipient (humans or animals) and the exposure mode. Air, water and food are the typical media through which microbial contamination can occur, while ingestion, inhalation and dermal contact are the most common exposure modes [Haas, Rose, Gerba 1999]. The media and the way in the exposure scenario govern the selection of microorganisms for the assessment. Microorganism numbers are either measured as part of the assessment or collated from the available literature, such as water quality monitoring data. This data help estimate exposure concentration accurately based on frequencies and intensity of infection.

3. Dose-response analysis calculates the probability of an impact (response) upon exposure to the microorganism. Dose-response is microorganism specific and defines the adverse effect (illness, infection and death) against a given dose[Shin & Ghosh 2017]. This step establishes a causal inference at a given

exposure dose (for example, how an increase in exposure dose can change health outcomes or responses). The dose-response relationship development process utilizes the data from disease outbreaks, epidemiological studies, or in-vitro animal studies (rats, guinea pigs, monkeys) [World Food Safety 2008]. The output is the dose-response curves derived from the curve fitting models using the data. The animals selected for establishing the dose-response curves are microorganisms specific, e.g., mice for the susceptibility to *Pseudomonas aeruginosa* infections [Hazlett et al 1978]; guinea pigs for *Bacillus spp*. The exponential and the Beta-Poisson are the most common models used for data fitting. The QMRAwiki webpage has a compiled list of the dose-response models for different pathogens from several studies [Mitchell et al 2014].

4. The risk characterization stage integrates the outcome from exposure assessment and dose-response analysis to estimate the health risk of reusing reclaimed water. The risk is calculated as a probability of infection or illness or death, depending upon the desired objective. This step involves using Monte Carlo simulations or probability simulation to reduce the uncertainty and variability in results.

5. Risk management, a final and most critical step in the QMRA framework, involves decision-making based on socio-economic, technical, ethical, political and regulatory factors. Risk management plans include measures to reduce, control, or eliminate risks. It consists of capital investments, process modifications or awareness among stakeholders to ensure continual safety under usual and emergency (worst case) scenario. It requires the decision-makers and managers to understand risk outcomes and apply sound judgment for effective decision-making [World foood safety 2008]. **Figure 4.2** summarizes all the steps involved in QMRA and lists the critical tasks within each step.

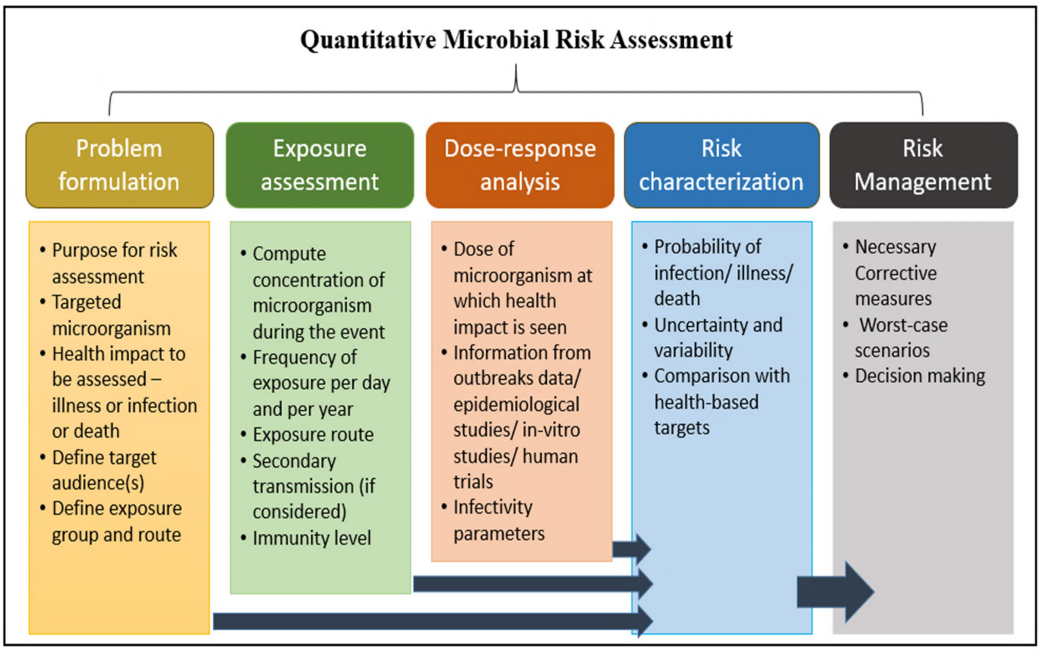

Fig. 4.2: QMRA framework outline (Hajare R. et al 2021)

4.3 Study Considerations for QMRA

4.3.1 Problem Formulation

Defining the scope

The main objective of this QMRA is to quantify the health risk posed by the day-to day use of River Ganga water for different human activities based faecal indicator organism (FIO) assays. The main focus of the risk assessment is to predict the impact on human health on exposure to pathogens present in water. The priority exposure groups vary according to application of Ganga water as listed in Table 4.1 will be the focus exposure group for this QMRA.

Table 4.5: Key Exposure Groups included in the Study

River Water Applications	Key Exposure Groups
Bathing/Laundry/ Recreational activities/Rituals	Children (<5yrs) and Adults
Agricultural (Food crops)	Farmers

Consumption of farm products	Farmers and Consumers

Hazard identification

Since it is impossible to consider all existing pathogens in a QMRA, reference pathogens are used that are of relevance for the defined system and exposure pathways of the risk assessment. The occurrence of reference pathogens represents the occurrence of other important pathogens within their class. It can be assumed that when reference pathogens are controlled, the important pathogens are also controlled. The selection of these reference pathogens in this study is listed in **Table 4.2.** Its concentration is calculated from *Thermotolerant coliform* (TTC) multiplied by conversion factor, recorded from previous Ganga report submitted by CSIR-NEERI in 2017.

Table 4.6: Reference Pathogens and Conversion Factors

Category	Reference pathogen	Conversion factor*	Purpose for Selection
Bacteria	*Escherichia coli O157H7*	8% of *E.coli* and *E.coli* = 95% of *TTC*	Quantitative enumeration by culture is possible. *E.coli* is a universal indicator.

Source: WHO, 2016. Quantitative microbial risk assessment: application for water safety management

Exposure Assessment

The main source focused on in this assessment is the river Ganga and drains, where untreated/partially treated wastewater is discharged. Other sources are direct contact with untreated waste, and drinking water sources which could be contaminated by the nearby water body.

The key routes of human exposure considered in this assessment are:

- Ingestion, direct by consuming contaminated products and drinking polluted water or indirect transferred via hands to mouth.

- Ingestion while bathing

Different exposure scenarios are shown, due to the scope of this study and the objective of this QMRA, not all possible exposure scenarios are included in the risk assessment. In this study, the assumption is made that the microbial risks of dermal contact, inhalation and exposure via vector breeding are minor compared to the risks posed by ingestion. Based on the semi-quantitative risk analysis, 3 important exposure events are chosen.

- **Accidental ingestion** of water **during farming/irrigation**
- Exposure to contaminants on **swimming/bathing/laundry/rituals** and other **recreational activities** in water through **ingestion**

Health outcomes

The final conducted health outcomes will be expressed in the annual probability of illness (Pill,a(d)). The human health outcomes of interests are the health outcomes corresponding with pathogenic *E.coli O157H7*. The most common health outcomes are Gastroenteritis and diarrhoea.

Level of certainty

QMRAs can be conducted on different levels of complexity. In this study, due to available data and knowledge, a screening-level deterministic risk assessment is adequate. The QMRA is based on probabilistic models and not static models. The main objective of this QMRA is to provide a broad overview of the level of risk in Varanasi. Variability of certain factors such as water quality, occurrence of pathogens are neglected. The executed assessment are highly dependent on assumptions based on comparable case studies and references. The outcome of this QMRA is therefore have a number of limitations and a more comprehensive QMRA would increase the validity of outputs. Nevertheless, this QMRA will provide a rough estimation of the health risk existing in the present scenario.

4.3.2 Exposure Assessment

Define the exposure pathways

Exposure pathways can be defined in terms of sources, control measures and intake. Sources define the initial point of the pathogen occurrence. Control measures can exist in different forms: environmental barriers, engineered barriers or regulatory control measures. In **Table 4.3**, the different aspects of the exposure pathways considered in this risk assessment are defined.

Table 4.7: Exposure Assessment for Quantitative Risk Assessment

Exposure route	Source	Exposure scenario	Control Measures	Intake (q)	References	Frequency (times per year)
Accidental Ingestion	Surface water: Ganga water/ Varuna river water	Exposure to drain/river water: during irrigation of farms	Worst case scenario: Direct use of water	10-50 ml	(Fuhrimann et al. 2016)	297 days
Accidental Ingestion	Drinking water or alternate water during swimming/ bathing	Exposure to pathogens via contaminated drinking water	Worst case scenario: Direct use of water	20-50 ml	(Fuhrimann et al. 2016)	10-12 days

Bacterial transport and fate modelling

To calculate the bacterial transport and fate, a 60X60 (15X15Km) grid map of Varanasi is created using Microsoft excel and each grid is GPS marked as shown in**Figure 4.3**. The land use pattern is marked and concentration of bacteria at each grid is calculated based on bacteria transport and fate model presented by Gao et al (2011) and four data inputs (**Figure 4.4**) which includei)TTC value at Upstream (U/S) location, ii)Convergence of Varuna river and Ganga river, iii)Convergence of Assi Nallah, and iv)Ganga river and small drain on right bank from Ram nagar area. The bacteria transport and fate model considers factors like sedimentation, re-suspension, dynamic growth/mortality mixing and advection. In this model the bacteria are demonstrated as a reactive tracer, wherein it is transported by the flow processes once

it enters the model domain and their concentrations are affected by specific processes like growth, die-off etc.

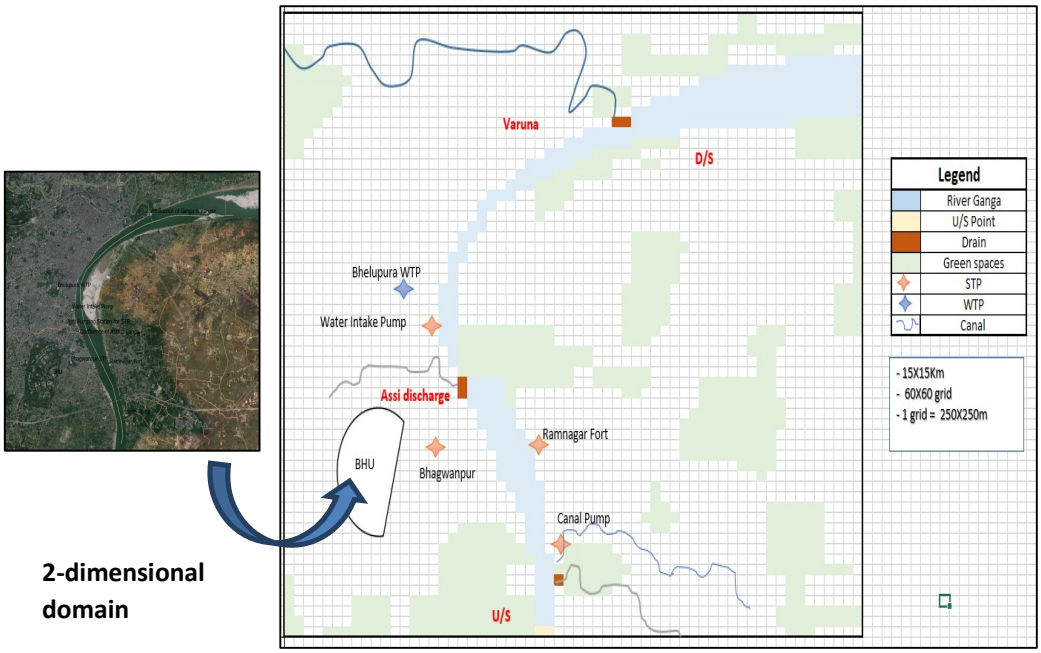

Fig. 4.3: Varanasi map in 2-D excel format with GPS coordinates

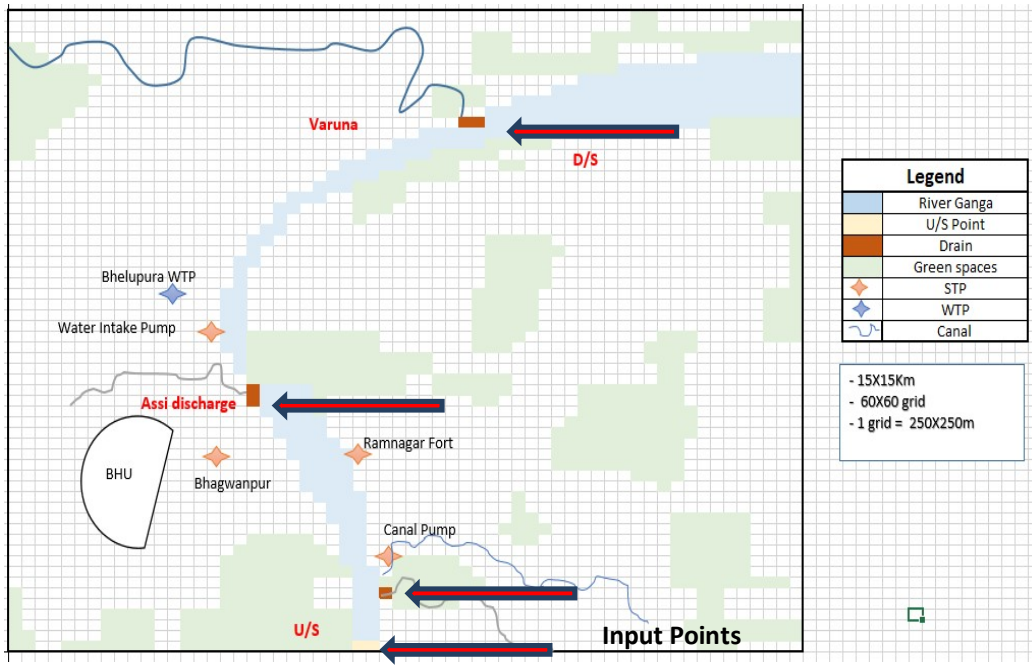

Fig. 4.4: Input for Model used for calculation of concentration of *Thermotolerant coliform* count

Thus, the bacteria transport equation is written as follows:

$$\frac{\partial AC}{\partial t} + \frac{\partial Q_R C}{\partial y} - \frac{\partial}{\partial y}\left(Ak_y \frac{\partial Q_R C}{\partial y}\right) = C_0 - kCA$$

where C = depth averaged bacteria concentration, Co = source or sink of bacteria; k = the decay rate for bacteria in the water, column; ∂y = depth-averaged dispersion coefficients in y direction, (we considered variation only in y direction) A = wetted cross-section area and QR = Discharge .

Here k is the decay constant and is said to be dependent on temperature, salinity, duration of darkness and sunlight and is calculated using equation:

$$k(I, S, T) = \{k_n + 0.02S + \alpha\, I(t)\theta^{T-20}$$

Where I = e I = Irradiance (cal/cm2/day); k20 = the decay rate at T = 20 °C; θ = a dimensionless temperature correction constant, 1.07; T = water temperature (°C); kn =

darkness condition decay rate at 20 °C; S = salinity; I = light intensity; and α = 0.00824 cm2/cal.

Quantify Source Concentration

The source concentration is quantified by taking samples and defining the quantity of TTC in the water samples in 2017. Samples from the upstream and downstream locations are considered. The conversion factors are used as stated in **Table 4.2**. Due to the chosen level of certainty, the data is used as distribution model, to generate more data and variability in source concentration. In second scenario, the latest data available with Indian National Aquatic Resources program in 2023 (provided by NMCG) were used.

Quantify Control Measures

The efficacy of the different identified control measures in reducing the concentration of reference pathogens and variability in performance should be considered. However, in present scenario, the worst case is considered with no control measure in order to calculate highest risk so that effective treatment barrier can be implemented.

Characterize magnitude and frequency exposure

Different exposure pathways and scenarios have different intake quantify. This quantity is not measured. The total coliform counts from the upstream and downstream collected under the continuous monitoring of Indian National Aquatic Resources program were used for the risk assessment. To define the quantity of intake, different literature is used and specified in Table 4.3.

To calculate the total exposure or dose (d) can be calculated using the following equation:

$D = (Iv \times Mc)$

In this equation, D is the ingested dose of pathogens, Iv the ingested volume and Mc the mean concentration of the targeted pathogens.

4.3.3 Health Effects Assessment

In this section the relation between intake of pathogens and the corresponding health effect will be assessed. Different dose-response relationships describe the correlation between exposure and the change on occurrence of specific infections or diseases.

The probability of occurrence and consequences of the different health outcomes are assessed and analysed.

Dose-Response Models

Different dose-response models exist, and different models are used for specific microbial species. The most commonly used dose-response models are the Beta-Poisson model and the exponential dose-response model. If all microorganisms are assumed to have the same probability of causing an infection, the exponential dose-response model is used. If the probability of infection varies between microorganisms (this variability is usually assumed to be beta distributed) the Beta-Poisson model is used.

The different dose-response models are described by the following equations:

Exponential Model:

$P_{inf,d} = 1 - \exp{-r \times D}$

Beta Poisson:

$P_{inf,d} = 1 - (1+D/\beta)^{-\alpha}$ or $P_{inf,d} = 1 - (1+d/N50\ (21/\alpha - 1)\ -\alpha$

Where:

$P_{inf,d}$ = Probability of infection for an individual exposed to dose 'd', d = Pathogen dose, r, α = Parameters describing the pathogen infectivity constant, the probability of infection, N50 = Medium infection dose, the dose (d) required to infect 50 % of the exposed population

n = Frequency per year

Based on literature and reference studies the most suitable dose-response models and their corresponding parameters (α and N50) are chosen for the selected hazards as presented below:

Pathogen	Constants	Reference
E.coli O157H7	α = 0.0571 β= 2.2183	Mok et al. 2014; Kouamé et al 2017

4.3.4 Risk Characterization

In the risk characterization, information from different parts of the conducted QMRA are combined to describe the risk quantitatively. The risks calculated are deterministic.

Risk characterization can be done by integrating hazard, exposure assessment and dose-response together. Since the main objective of this study is quantifying the health risk associated with exposure to use of river Ganga water for different uses and the outcome in this assessment is expressed in the probability of illness per person per year.

These probabilities of illness are calculated per exposure scenario.

Pill = Pinf,a x Pill|inf

Where, Pill = Annual probability of illness per person per year, Pinf,a = Calculated annual probability of infection, Pill|inf = Probability to get ill when infected. The corresponding Pill|inf value per hazardous contaminant, is again based on literature and comparable case studies.

4.3.5 Limitations and Recommendations

Firstly, the chosen scale of certainly and limitation in exposure pathways can be considered as the most significant limitation of this QMRA. A more comprehensive risk assessment and higher level of certainly results is more realistic and reliable risk values. The limited amount of data points makes this analysis uncertain. A human error made in the analysis of water samples or a variability in the concentration has a big influence on the outcome. The reliability on assumption is also very high in the current assessment, collecting data to decrease the needed assumption would improve the quality of the QMRA. Therefore, for a better and more reliable outcome the use of more data points is recommended.

4.4 Results

4.4.1 Exposed Population Characteristics

From field observations during water quality sampling following observations were made:

1. The majority of farmers had no formal education and use water from Ganga river for irrigation of vegetables. These farms grew leafy vegetables and farm produce was sold at nearby markets.

2. The area near Ghats was mainly used for discharge of ashes as part of religious rituals and people were observed to take bath

3. Adults and children were observed swimming in river Ganga.

4.4.2 Exposure Patterns in the Study Area

- The interactions revealed two main water sources: River Ganga and dug well were used for irrigating leafy vegetables in the study area.

- Farm produce primarily leafy vegetablesconsumption was found to be most important exposure route while studying health risks.

- In Varanasi, the most popular are early morning and evening boat cruises for the local people and the visitors. Hence one of the major pathway was listed to accidental ingestion during recreational activities.

4.4.3 Health Risks Linked to Farming Activities and Salad Consumption

- Concerning the probability of infection related to E.coliO157H7 based on the data collected by CSIR-NEERI in 2017, the results showed that region near convergence of Varuna river and stretch one kilometre downstream from the convergence was at highest risk. Hence it was advised that care should be taken that the water from this stretch should be avoided for irrigation of vegetables particularly leafy vegetables. However, use of the data of Indian National Aquatic Resources program in 2023 indicates that the overall risk for use of the Ganga water for irrigation without further treatment and accidental ingestion was below the acceptable value throughout the stretch from upstream to downstream of the Varanasi City.
- Similar result was obtained near Assi nallah convergence with River Ganga when data of CSIR-NEERI collected during 2017 were used. However based on the data collected in Indian National Aquatic Resources program in 2023 indicate that the region near convergence of Varuna river and a stretch500 m downstream from the convergence was at higher risk but below the acceptable value. The lower risk values observed are because of the improved water quality due to functioning of the sewage treatment plants and increase in river base flow. However, the

discharges from the Assi River and the Varuna River must be monitored to ensure no untreated sewage is discharged in the river which would result in higher risk.

- Based on the data collected by CSIR-NEERI in 2017, the annual risk linked to *E. coli O157:H7* with respect to leafy vegetables consumption ranged from the highest $3.83X10^{-3}$ per person per year (pppy) at River Varuna – River Ganga confluence to the lowest $9.64X10^{-8}$ pppy before Assi nallah discharge point (**Figure 4.5**). However, based on the data from Indian National Aquatic Resources program in 2023, the annual risk linked to *E. coli O157:H7* with respect to leafy vegetables consumption ranged from the highest 4.67×10^{-8} per person per year (pppy) at River Varuna – River Ganga convergence to the lowest $7.33x10^{-12}$pppy before Assi nallah release discharge (as illustrated in Figure 4.6).

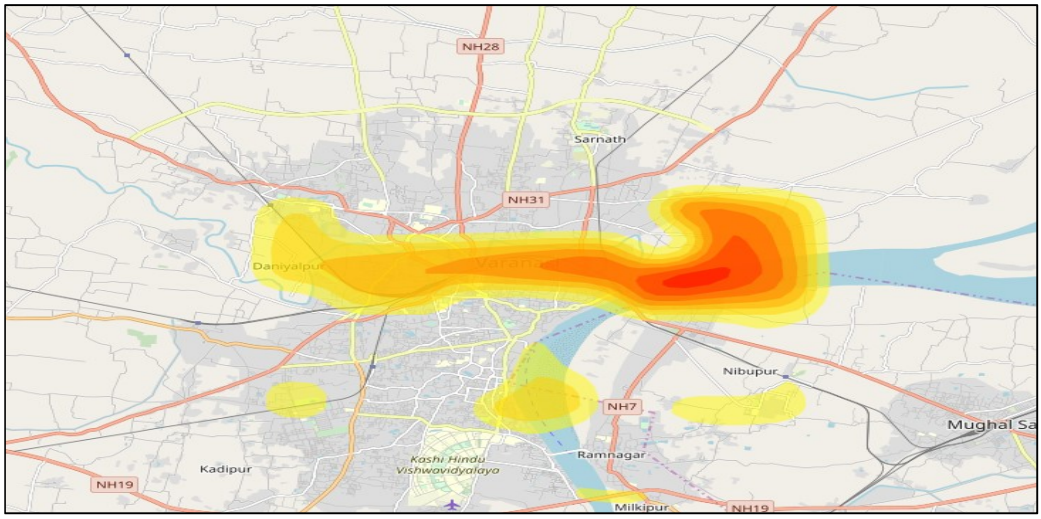

Fig. 4.5: Irrigation Risk Map of Varanasi with water quality data of 2017

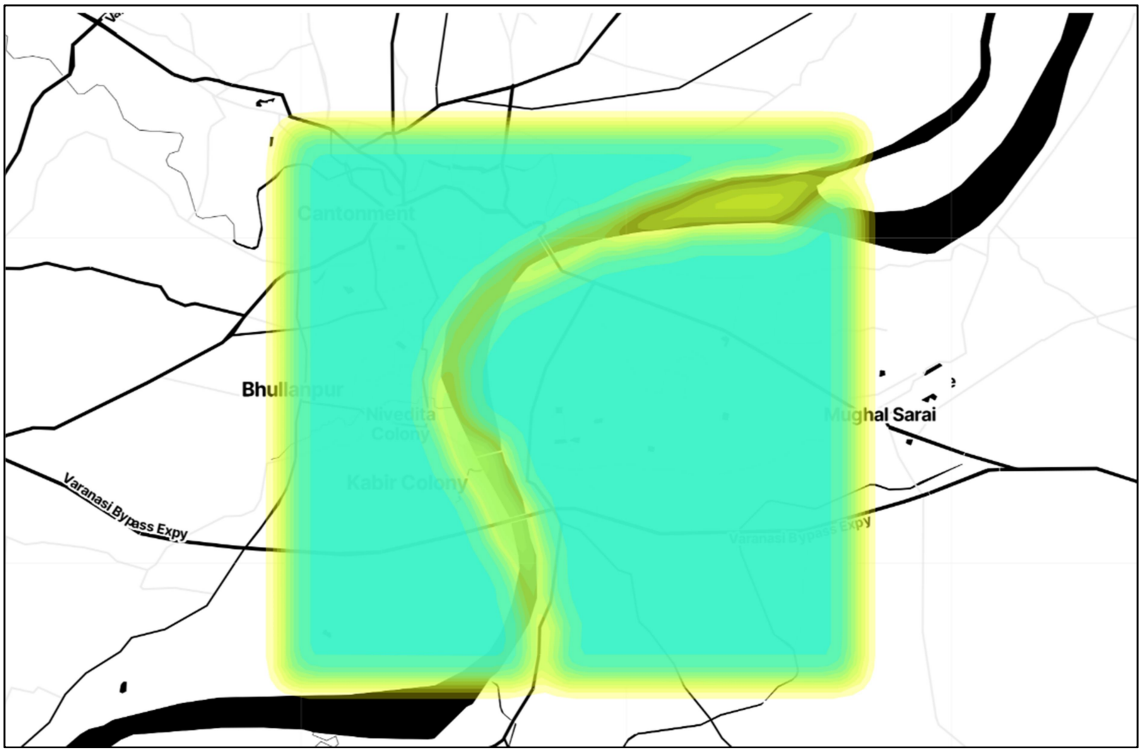

Fig. 4.6: Irrigation Risk Map of Varanasi with water quality data of 2023

- Further the risk due to accidental ingestion during recreational activities (bathing /swimming) is calculated. The Maps of the worst-case scenario based on the data collected by CSIR-NEERI in 2017 is illustrated in **Figure 4.7**. Further the risk is above the accepted value of $1x10^{-6}$ pppy.

  The Map of worst-case scenario based on the data from Indian National Aquatic Resources program in 2023is illustrated in **Figure 4.8**. The health risk in this case was below the acceptable value of $1x10^{-6}$ pppy.

Pre-Monsoon

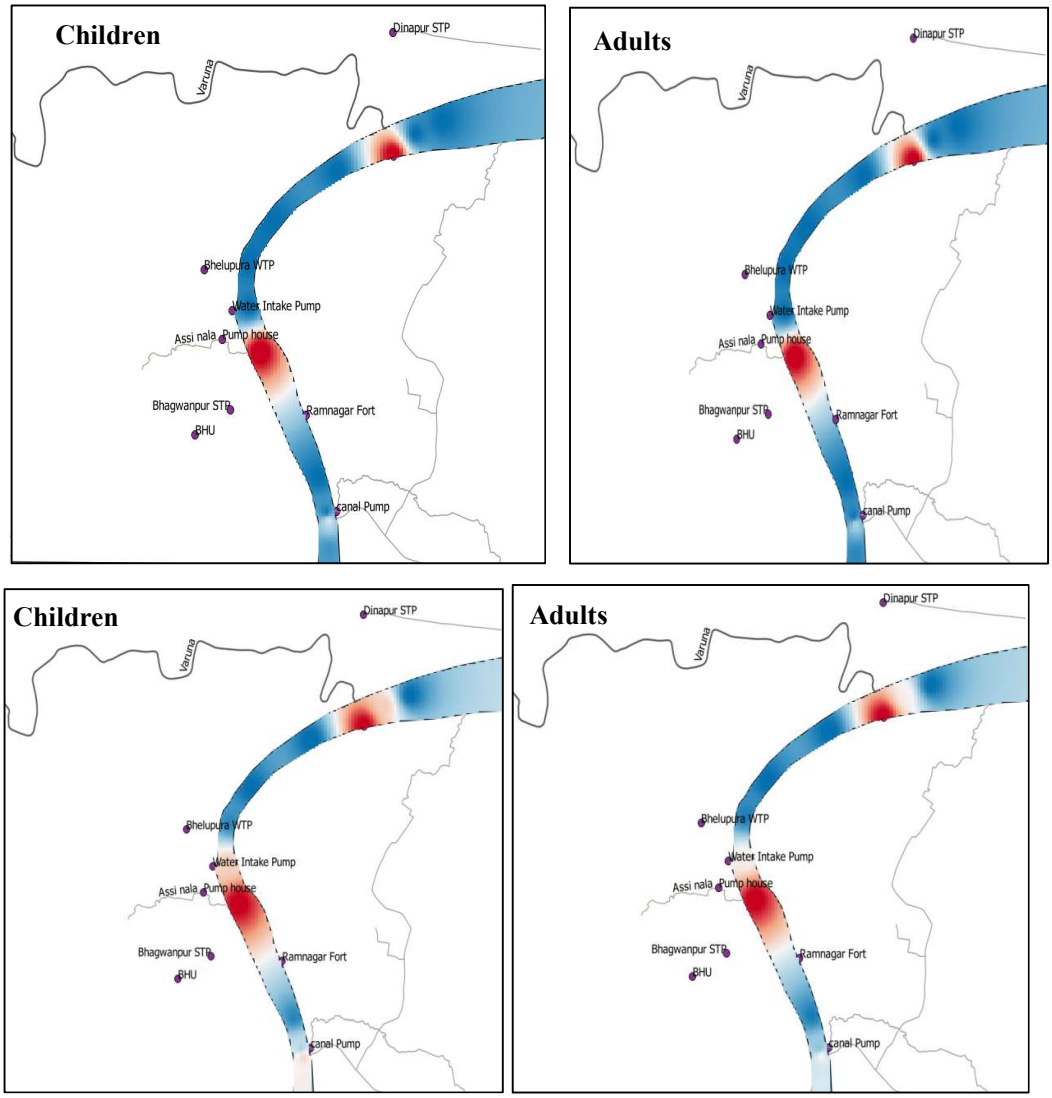

Fig.4.7: Pre-Monsoon and Post-Monsoon Accidental ingestion risk on Bathing Risk for Children and Adults with water quality data of 2017

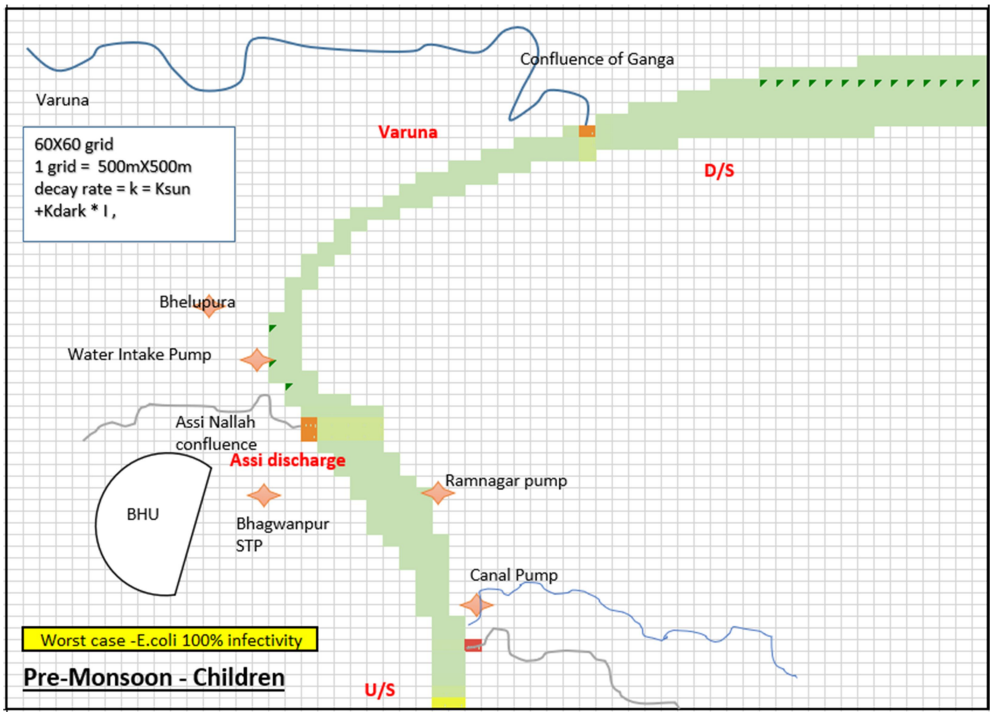
Confluence of Ganga
Varuna
Varuna
60X60 grid
1 grid = 500mX500m
decay rate = k = Ksun
+Kdark * I ,
D/S
Bhelupura
Water Intake Pump
Assi Nallah
confluence
Assi discharge
Ramnagar pump
BHU
Bhagwanpur
STP
Canal Pump
Worst case -E.coli 100% infectivity
Pre-Monsoon - Children
U/S

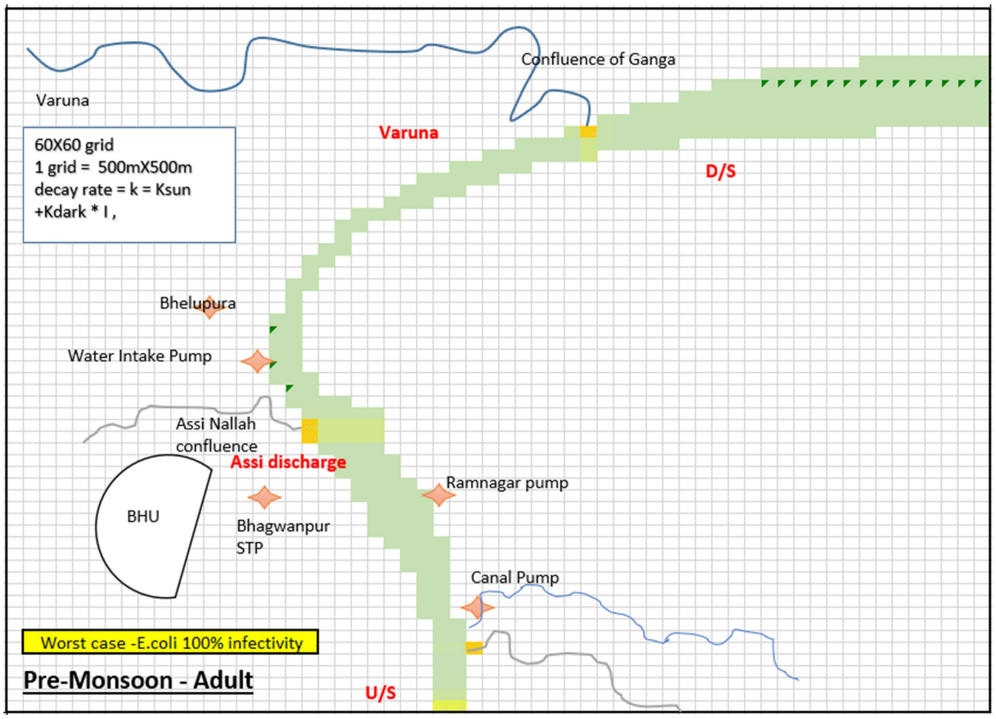
Confluence of Ganga
Varuna
Varuna
60X60 grid
1 grid = 500mX500m
decay rate = k = Ksun
+Kdark * I ,
D/S
Bhelupura
Water Intake Pump
Assi Nallah
confluence
Assi discharge
Ramnagar pump
BHU
Bhagwanpur
STP
Canal Pump
Worst case -E.coli 100% infectivity
Pre-Monsoon - Adult
U/S

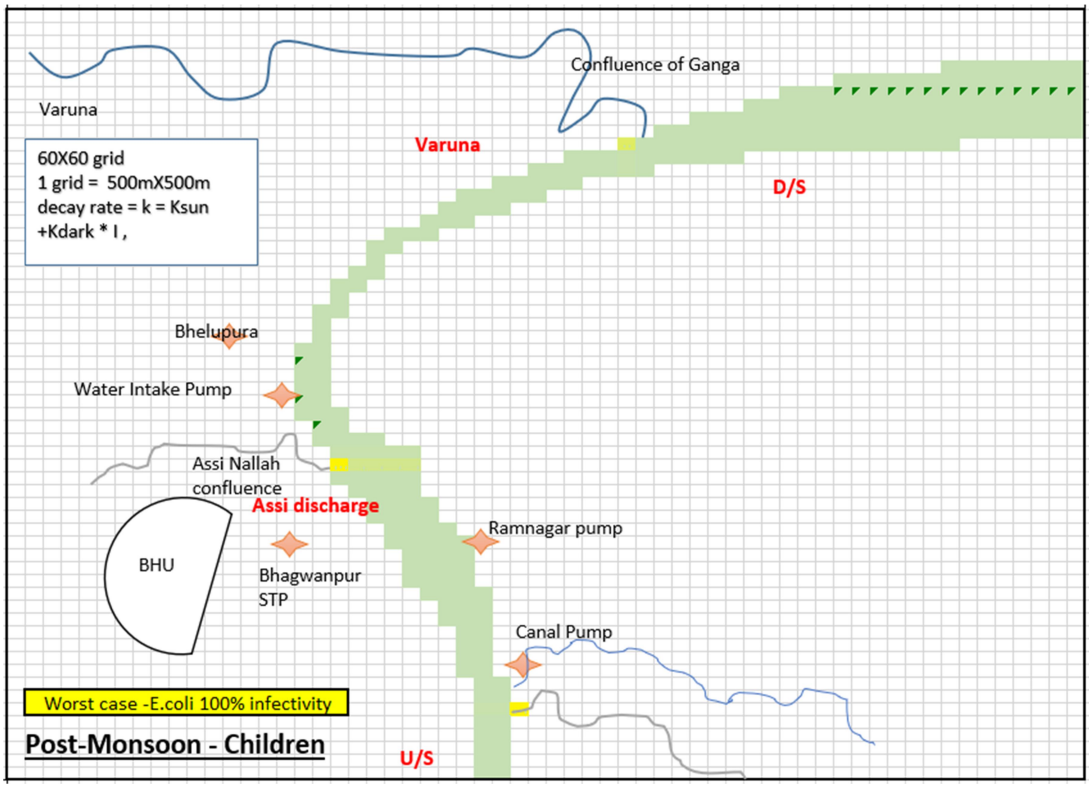

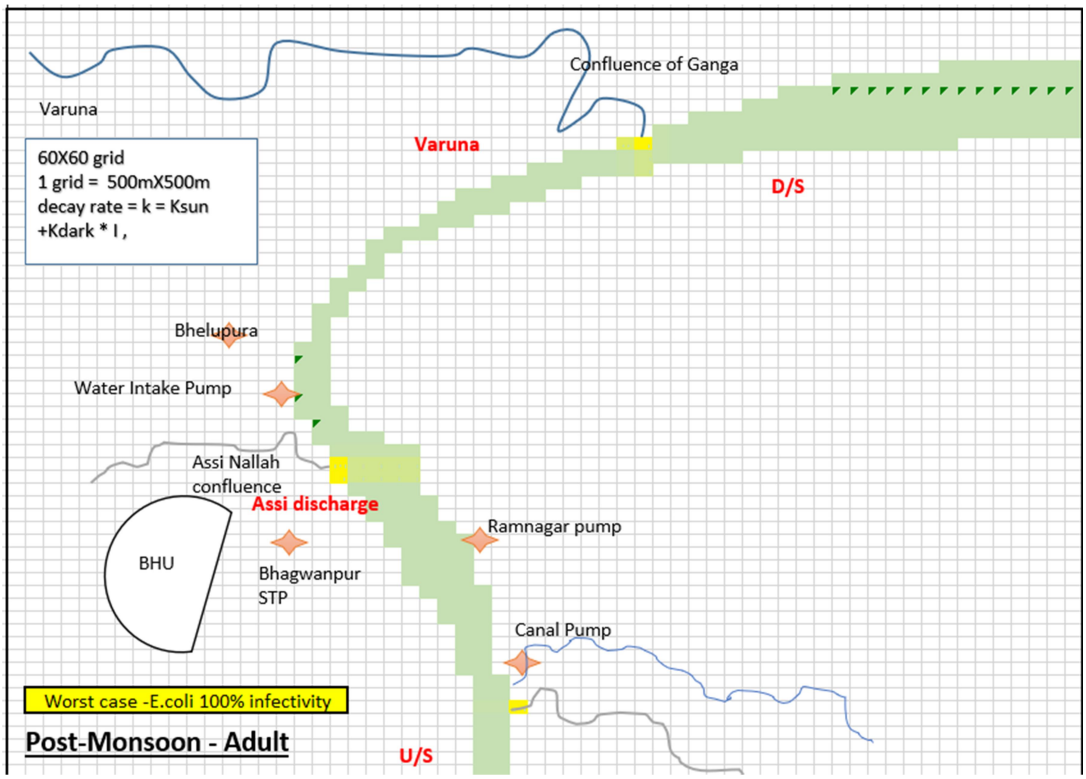

Fig.4.8: Pre-Monsoon and Post-Monsoon Accidental ingestion risk on Bathing Risk for Children and Adult with water quality data of 2023

4.4.4 Conclusion

- Only risk due to *E.coli O157:H7* is studied.
- The results of the QMRA confirmed the poor quality of Ganga River in 2017 for irrigation at certain patches which can possibly be controlled by use of certain preventive control measure.

  However, the results of the QMRA based on the data from Indian National Aquatic Resources program in 2023 confirmed the improved water quality of Ganga River for irrigation which is dueto commissioning of sewage treatment plants.
- The area near the discharge point of all the rivers and drains need to be continuously monitored.

4.5 References

- Busgang, Allison, Eran Friedler, Yael Gilboa, and Amit Gross. 2018. "Quantitative Microbial Risk Analysis for Various Bacterial Exposure Scenarios Involving Greywater Reuse for Irrigation." Water (Switzerland) 10(4): 1–15.
- Fuhrimann, Samuel et al. 2016. "Disease Burden Due to Gastrointestinal Pathogens in a Wastewater System in Kampala, Uganda." Microbial Risk Analysis 4: 16–28.
- Gao, Guanghai, Roger A. Falconer, and Binliang Lin. 2011. "Numerical Modelling of Sediment-Bacteria Interaction Processes in Surface Waters." Water Research 45(5): 1951–60.
- Haas, C. N., Rose, J. B., & Gerba, C. P. 1999. Quantitative Microbial Risk Assessment.
- Kouamé, Parfait K. et al. 2017. "Microbiological Risk Infection Assessment Using QMRA in Agriculture Systems in Côte d'Ivoire, West Africa." Environmental Monitoring and Assessment 189(11).

- Mishra, N. K., and S. C. Mohapatra. 2009. "Effect of Gangetic Pollution on Water Borne Diseases in Varanasi: A Case Study." Indian Journal of Preventive & Social Medicine 40(1). http://medind.nic.in/ibl/t09/i1/iblt09i1p39.pdf.
- Mok, Hoi Fei, and Andrew J. Hamilton. 2014. "Exposure Factors for Wastewater-Irrigated Asian Vegetables and a Probabilistic Rotavirus Disease Burden Model for Their Consumption." Risk Analysis 34(4): 602–13.
- Pandey, Pramod K. et al. 2014. "Contamination of Water Resources by Pathogenic Bacteria." AMB Express 4(1): 1–16.
- Regli, S., Rose, J. B., Haas, C. N., & Gerba, C. P. 1991. "Modeling the Risk from Giardia and Viruses in Drinking Water." Journal - American Water Works Association: 76–84.
- Sampson, Angelina et al. 2017. "Probabilistic Quantitative Microbial Risk Assessment Model of Farmer Exposure to Cryptosporidium Spp. in Irrigation Water within Kumasi Metropolis-Ghana." Microbial Risk Analysis 6(October 2016): 1–8.
- Timm, Christian et al. 2016. "Applying QMRA and DALY to Assess Health Risks from River Bathing." International Journal of Hygiene and Environmental Health 219(7): 681–92. http://dx.doi.org/10.1016/j.ijheh.2016.07.017.
- Shin SJ, Ghosh SK (2017) A comparative study of the dose-response analysis with application to the target dose estimation. J Stat Theory Pract 11:145–162 . https://doi.org/10.1080/15598608.2016.1261260
- Food Safety W (2008) Dose-response assessment. In: World Health Organization & Food and Agriculture Organization of the United Nations (ed) Principles and methods for the risk assessment in chemicals in food
- Codex Alimentarius Commission. (1999) Principles and guidelines for the conduct of microbiological risk assessment. CAC/GL-30.
- Brady J (2015) Risk Assessment: Issues and Challenges. Pharm Eng 35:1–8 . https://doi.org/10.1016/j.yebeh.2014.12.005

CHAPTER - 5

GEO-CHEMICAL PARTITIONING OF METALS

5.0 Geo-Chemical Partitioning of Metals in River Ganga : Preliminary Trends of Various Trace Metals and their Partitioning in Upper Stretches of River Ganga

5.1 Background

Metals are introduced in river waters from various sources, which can be both natural and/or anthropogenic. Naturally, trace metals originate from processes such as chemical weathering, soil erosion, fallout of aerosols from marine, volcanic or arid soils sources and most importantly dissolution of naturally occurring sediments. However, the level of these metals in the environment has increased tremendously due to human inputs and activities. For some metals, natural and anthropogenic inputs are of the same order (for example Hg and Cd), whereas for others (for example Pb) inputs due to human activities dwarf natural inputs. Heavy metals discharged into a river system by natural or anthropogenic sources during their transport are distributed between the aqueous phase and sediments. Heavy metals are of high ecological significance since they are not removed from water as a result of self-purification, but accumulate in reservoirs and enter the food chain.

The suspended and bed sediments of a river buffer higher metal concentrations of the water, particularly by adsorption and precipitation. Changing environmental conditions such as pH, redox potential or the presence of organic chelators in the system may render the remobilization of metals from sediments. Thus, sediment quality is a widely utilized method of environmental assessment. Natural sediment formed during weathering processes might be modified markedly during transportation and deposition by chemicals of anthropogenic origin. Apparently, higher the metal concentrations in the sediments, greater the quantity of metals that could be desorbed from the sediments into the water phase by physiochemical processes. River sediments are also a major sink as well as source of nutrients. Suspended sediments play an important role in the transport of nutrients and contaminants, in water–sediment interactions influencing the river water quality and as non-point source pollutants.

Trace metals are important in aquatic systems because of their demonstrated effects as both essential at low levels and toxic agents at higher levels for biota. Thus, the

presence of these metals in the aquatic ecosystem has far-reaching implications directly to the biota and the food chain. On the other hand, aquatic organisms may bio-accumulate and bio-concentrate environmental contaminants to more than 1,000,000 times the concentrations detected in the water column. Elements like Cu, Zn, Fe, Mn , and Co, which are required for normal biochemical functions, could become toxic when present in anomalous concentrations and may result in poisoning of enzyme. Interest in metals like Zn and Cu, which are required for metabolic activity in organisms, lies in the narrow "window" between their essentiality and toxicity, but others like Cd and Pb exhibit extreme toxicity even at trace levels. It has also been established that metals namely Ag, Cu, Cr, Co etc. when present in trace concentrations, imparts antimicrobial properties to the media. It has been observed in Phase I of the project that many of these elements are present in traces at several locations of the river Ganga. The previous study was focused on identifying the different metals present in Ganga river system and their influence on river water quality. It was observed in previous study that some of the metals are present in very trace concentrations and are also bound with suspended sediments.

It is therefore required to optimise the sample collection, processing and analytical methodology to achieve the desired levels of trace analysis. Based on these leads from previous study carried out by CSIR-NEERI and considering the several gaps in understanding the partitioning of metals in Ganga river ecosystem, and their possible influence on non-putrefying properties, the present study has been devised. The present study is also aimed at assessment of the present status of variety of trace metals in the Ganga River. The geo-chemical partitioning of metals in the form of dissolved and suspended fraction is also targeted.

5.2 Methods and Materials

Considering the trace metal analysis, extensive precautions were taken during sample collection, preservation, transportation, processing and analysis. All clean chemistry principles were followed including use of trace metal grade acids and reagents, deionised water additionally treated for removal of trace elemental impurities in ppt range, use of sampling bottles, glassware, plastic wares thoroughly pre-cleaned to remove all possible elemental impurities etc.

5.2.1 Collection of Samples

Considering the trace concentrations of various metals utmost care was taken while collection and preservation of samples. All metals exist in surface water in dissolved and suspended form bound to particulate and organic matter, although dissolved concentrations are generally low. As per Standard Methods (APHA), the dissolved metals can be defined as those metals present in a non-acidified sample that pass through 0.45 µ.m membrane filter whereas the suspended metals as one retained by the membrane filter. The total concentration of any particular metal is determined vigorous digestion of unfiltered samples. Representative samples from different locations were collected in polypropylene bottles thoroughly cleaned and rinsed with trace metal grade nitric acid. The samples for dissolved fraction were filtered in field and were immediately preserved by acidifying with trace metal grade HNO3 to pH< 2. Similar procedure wasadopted for samples for total metal concentration except for filtration step. The acid preserved samples were stored at > 4°C till transportation to laboratory and further analysis.

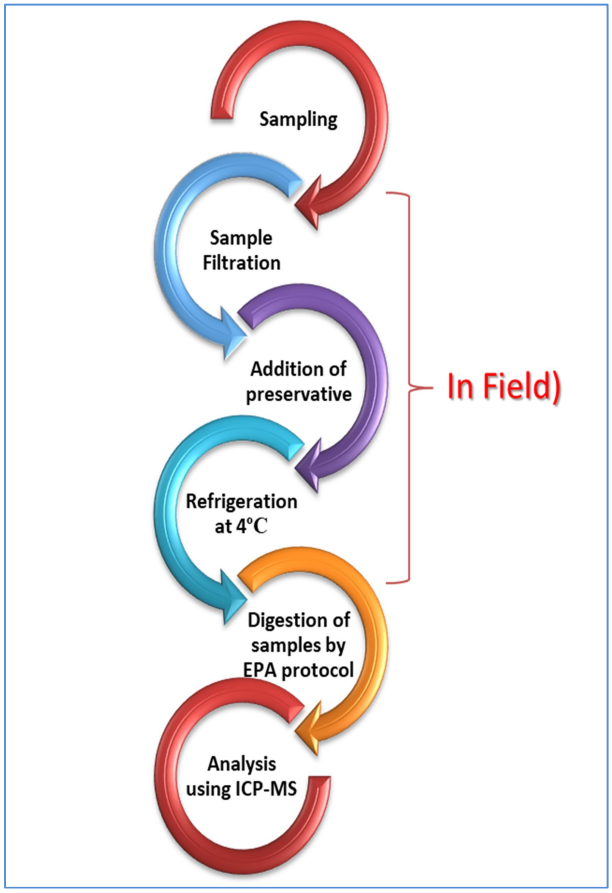

Fig. 3.1: Methodology Adopted for Sample Collection and Analysis

5.2.2 Digestion Procedure for Total Metal Analysis

Digestion of the acid preserved and unfiltered samples were done for analysis of total heavy metal concentrations. The digestion of the samples for total metals analysis was done by microwave acid digestion method. A representative aqueous sample is extracted with combination of concentrated nitric acid and concentrated hydrochloric

acid, using microwave heating with a suitable laboratory microwave unit. The sample and acid(s) are placed in a PTFA microwave vessels. The vessel is sealed and heated in the microwave unit for a specified period of time. After cooling, the vessel contents are filtered, centrifuged, or allowed to settle and then diluted to volume and analysed by ICPMS. Briefly, 15 ml of the sample was taken and 6 ml Nitric acid and 2 ml Hydrochloric acid was added. The program for complete acid digestion of sample were optimized and found to be 40 % power rating for 10 min, 80 % power rating for 10 min and 100 % power rating for 5 min. The solution was stored and diluted for further analysis. All the samples were digested in triplicates. The suspended fraction was determined from the difference between dissolved and total fractions.

Instrument Details

The Inductively Coupled Plasma-Mass Spectrometry (ICP-MS) is considered as best available technique for analysis of trace metals and metalloids in surface, ground and drinking water. The technique is also used for analysis of metals in wastewater, soils, sludge and biological samples after suitable digestion followed by dilution and/or clean-up. The instrument detection limits for many analytes varies between 1 to 100 ng/L. The ICPMS based analysis is best suited for the determination of metals in pristine fresh water matrices which is the case in present study. The method is suitable for most of the metals and metalloids.

Heavy metals and metalloids including Ag, As, B, Ba, Cd, Cr, Cu, Hg, Mn, Ni, Pb, Se, Si, Tl, U and Zn were analysed by ICP-MS (NexIon 300X, Perkin Elmer, USA). Different masses of the elements were selected to minimize the matrix interference. Prior to analysis the tubings were properly cleaned using acidified water. The operating conditions are listed below:

Table 5.1: Operating Conditions of ICP-MS

Mode	Standard
Sample introduction system:	Cyclonic spray chamber
Sample uptake rate:	0.5 mL/min
Nebulizer Gas flow rates: 0	0.95 L/min

Auxiliary Gas Flow: 1	0.2 L/min
Plasma Gas Flow:	17 L/min
ICP RF Power:	1600 W;
Sweep counts:	25
Dwell time:	100 mS
Detector Mode	Duel Detector

All the samples were analysed by external calibration method. Standard NIST traceable multi-elemental solutions of concentration 10 mg l-1 was procured from Inorganic Ventures, USA and working standard solutions of concentrations in the concentration range of 1 -100 µg L-1 were prepared from the stock solution by serial dilutions. Calibration was performed until a minimum regression coefficient of 0.999 was obtained. Concentration of elements exceeding the calibration range, were diluted for analysis. All the samples were analysed in triplicate to minimize the errors.

A protocol based upon US EPA method 200.8 was used and optimized to ensure the operating performance of the instrument. A summary of steps followed as per method 200.8 is given below:

- Ignite the plasma, allow 30 minutes to warm up
- Perform daily performance check – If fails perform other checks like torch adjustment, nebuliser gas flow, autolense etc. and check for the performance to pass
- Calibrate using blank and standards
- Monitor all masses necessary for interference correction
- Run instrument performance evaluation tests
- Run unknown sample (e.g. local tap water)
- Review results of quality control samples for pass/fail criteria

5.2.3 Calibration and Standardization

The operating conditions provided by the instrument manufacturer were followed. Pre-calibration routine was completed prior to analysis of samples. Warm up of the instrument was done for at least 30 minutes. The performance was checked using the tuning solution according to which the intensity for the analytes Be, Mg, In, U should not be less than 2000, 15000, 40000, 30000 CPS respectively and the background should not exceed beyond 1. All analysis was done unless these conditions are met.

Calibration standards

The multi-element calibration standards were prepared and used for the evaluation. The calibration blank is the acidified reagent water whose matrix is as same as matrix of standard and samples. It was treated as zero standards and was used to calibrate the ICP-MS instrument. Calibration standards were prepared using commercially available NIST traceable certified stock standards and prepared by dilution of the standard stock solution to the required concentration. These calibration standards are used to calibrate the instrument response with respect to analytes concentration. The samples were analysed immediately after calibration.

Table 8.2: Calibration Standards

Analytes	Standard 1 (µg/L)	Standard 2 (µg/L)	Standard 3 (µg/L)	Standard 4 (µg/L)	Standard 5 (µg/L)
As, Ag, Al, Cd, Cr, Co, Cu, Fe, Mn, Pb, Se, Zn	1	5	10	50	100

Details of various elements analysed and instrument detection limits (IDL), method detection limits (MDL) and method quantification limits (MQL) for the optimized method are presented in Table 5.3.

Table 5.3:Elements measured simultaneously using NexION 300X ICP-MS

Analyte	Symbol	Mass (amu)	IDL µg/L	MDL µg/L	MQL µg/L	Mode
Arsenic	As	75	0.007	0.12	0.35	Collision
Silver	Ag	107	0.002	0.09	0.27	Standard
Aluminium	Al	27	0.017	0.99	3.00	Standard
Cadmium	Cd	111	0.002	0.07	0.20	Standard
Cobalt	Co	59	0.002	0.17	0.51	Standard
Chromium	Cr	52	0.071	0.21	0.64	Standard
Copper	Cu	63	0.029	0.37	1.13	Standard
Iron	Fe	57	0.311	1.63	4.94	Collision
Manganese	Mn	55	0.031	0.25	0.75	Standard
Nickel	Ni	60	0.686	0.30	0.91	Standard
Lead	Pb	206,207,208	0.006	0.20	0.59	Collision
Selenium	Se	78,81	0.352	0.27	0.82	Collision
Zinc	Zn	66	0.067	1.59	5.92	Collision

Method detection limit was determined as follows: Seven laboratory reagent water samples were prepared and processed through the analytical procedure. The variance and standard deviation of the seven aliquot were calculated.

S2= $\frac{1}{n-1}\left[\left[\frac{\sum_{i=0}^{n} xi2 - \sum_{i=0}^{n} Xi^2}{n}\right]\right]$

Standard Deviation $S = (S^2)^{\frac{1}{2}}$

Where,

xi – Analytical results obtained from n sample aliquots

Xi – Mean of the n sample aliquots

n- Number of aliquot analyzed

The MDL is computed as

$MDL = t \times S$

Where,

MDL – Method detection limit

t- Students t value for 99% confidence level which is 3.14

S- Standard deviation of replicates analysed

Quality assessment and quality control

Comprehensive quality assurance and control checks were also performed by determining recoveries for digestion and analysis methods. The results of recoveries and other statistical parameters are presented in Tables 4-6 below:

Table 5.4: Digestion Recovery Data

Metals	Sample Concentration (µg/L)	Digestion recovery (µg/L)
Ag	2.82	2.88
As	2.5	2.42
Cd	3.55	3.48
Cu	1.44	1.57
Co	2.93	2.89
Cr	1.69	1.63
Mn	2.16	2.43
Pb	3.27	3.36

Metals	Sample Concentration (µg/L)	Digestion recovery (µg/L)
Se	4.88	4.76
Zn	8.5	9.15
Ni	3.96	4.42

Table 5.5:Method Recovery Data

Metals	Sample Conc µg/L	Recovery µg/L	Standard Deviation	Acceptance limit µg/L
Ag	10	10.06	0.03	9.96 -10.16
As	10	10.08	0.15	9.62-10.54
Al	10	10.54	0.41	9.31-11.77
Cd	10	9.93	0.02	9.88-9.98
Cu	10	10.13	0.06	9.95-10.31
Co	10	10.04	0.04	9.91-10.17
Cr	10	10.06	0.03	9.96-10.16
Mn	10	10.27	0.08	10.03-10.51
Pb	10	10.09	0.03	10.00-10.18
Ni	10	10.46	0.08	10.23-10.69
Zn	10	12.00	1.03	8.91-15.09

Table 5.6: Average Recoveries and Standard Deviation for Various Elements

Metal	Sample concentration (µg/L)	Low Spike µg/L	Average Recovery R (%)	Standard Deviation	High Spike (µg/L)	Average Recovery R (%)	Standard Deviation
Ag	0.00	10	91.00	0.08	300	92.00	2.47
As	0.00	10	106.00	0.22	300	101.00	1.1
Cd	0.01	10	91.91	0.05	300	96.97	1.16
Cu	0.00	10	101.00	0.07	300	97.67	1.06
Co	0.05	10	130.35	0.03	300	93.32	2.17
Cr	0.00	10	111.50	0.03	300	97.67	0.855
Mn	0.23	10	95.42	0.08	300	106.57	0.914
Pb	0.06	10	97.73	0.02	300	98.35	0.615
Se	0.00	10	91.00	0.10	300	97.33	1.96
Ni	0.12	10	112.99	0.11	300	101.18	0.647
Zn	5.40	10	109.68	3.33	300	100.33	1.06

The results of QA & QC exercise have established that both sample preparation (digestion) and analytical protocols are well optimised with recoveries in the range of 91-130 % in low range and 92-106 % in high spike range. These results also revealed that standard deviation varied between 0.8 to 3.3 and 0.6 to 2.47 in low and high spike

range respectively. All these data confirm that the performance data for both sample preparation and analysis are well below the acceptable ranges.

5.3 Results and Discussions

Amidst several metals which are considered dangerous for our health, 23 have been identified as heavy metals namely antimony, arsenic, bismuth, cadmium, cerium, chromium, cobalt, copper, gallium, gold, iron, lead, manganese, mercury, nickel, platinum, silver, tellurium, thallium, tin, uranium, vanadium, and zinc. Among these metals, the most hazardous are Mercury (Hg), Lead (Pb), Arsenic (As), Cadmium (Cd), Chromium (Cr), Copper (Cu), Zinc (Zn), Iron (Fe) and Nickel (Ni). Many trace elements are biologically beneficial at very low concentrations, but become toxic or otherwise detrimental to the health of organisms and plants at low to moderate concentrations. Long term exposure at sub-lethal concentrations to certain trace elements may result in chronic biological effects. Some trace elements can accumulate to potentially harmful levels in soils and sediment through chemical immobilization, in plants through bio- concentration, or via a food chain through bio magnifications. Further there are reports of antimicrobial and other medicinal properties of these metals, particularly in trace concentrations. There are several reports available on heavy metals in River Ganga, however detailed studies using highly sensitive instrumentation namely ICP-MS having very low detection limits in parts per trillion (ppt) range covering the entire stretch of river starting from Gomukh to Gangasagar has been undertaken for the first time in our previous study. Moreover, large number of trace metals and metalloids have been analysed for the first time in the study. Based on the leads obtained from the previous study conducted by CSIR-NEERI the present study was undertaken to determine the presence of metals/metalloids in trace concnetrations particularly in upper stretch of the river Ganga and also to determine the geo-chemical partitioning of these metals among suspended sediments.

The preliminary results obtained from the trace metal analysis of samples collected from various locations of Ganga River stretching from Gomukh to Varanasi are discussed in detail in following sections. The locations from Gomukh to Haridwar are categorized as stretch-I and from Bijnor to Varanasi in Stretch II. All the results are expressed in μg/L (Microgram per Litre) throughout the report. Results were statistically analysed and average, minimum, maximum, and range are also reported.

5.3.1 Distribution of Metals

The distribution of dissolved fractions of Ag, Cd, Cu, Cr, Co, and Pb at various locations during pre and post monsoon season are presented in figure5.2 and figure 5.3 respectively. The results indicate that although present in trace concentrations, comparatively higher concentrations are observed during pre-monsoon as compared to post monsoon season. Relatively high concentrations were observed for Cu, Cr and Co particularly at location including Gangotri, Harshil, Maneri etc. More strikingly it was also observed that majority of these elements are lost post Tehri reservior and started re-emerging after Koteshwar reserviors. This trend was more distinct during post monsoon season.

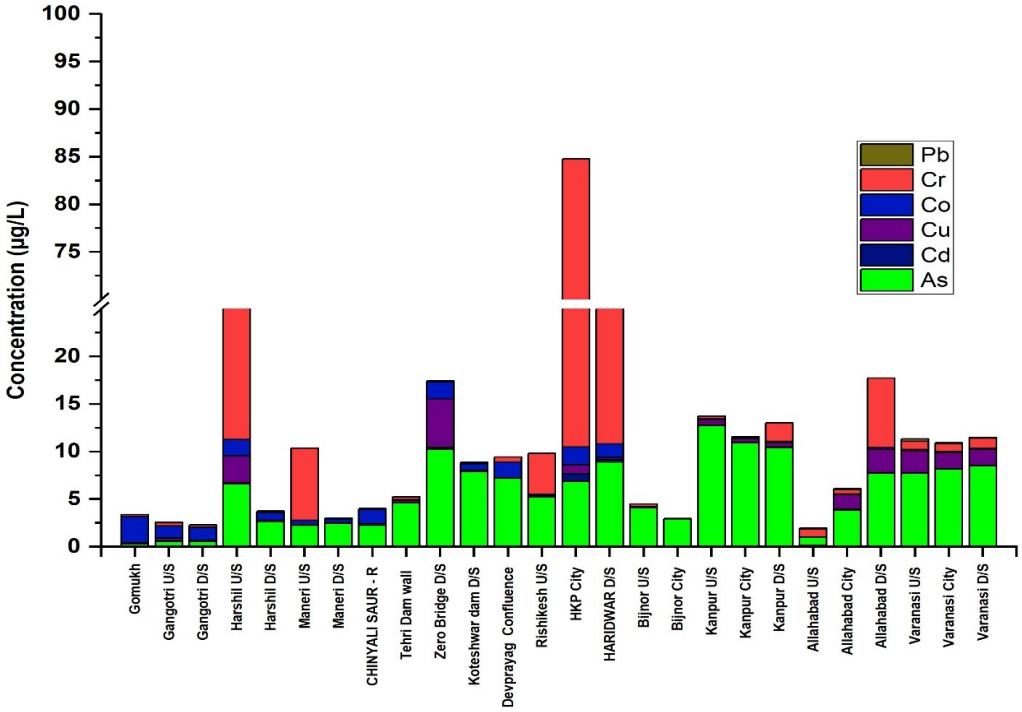

Fig. 5.2: Dissolved Fractions of Pre-Monsoon Season

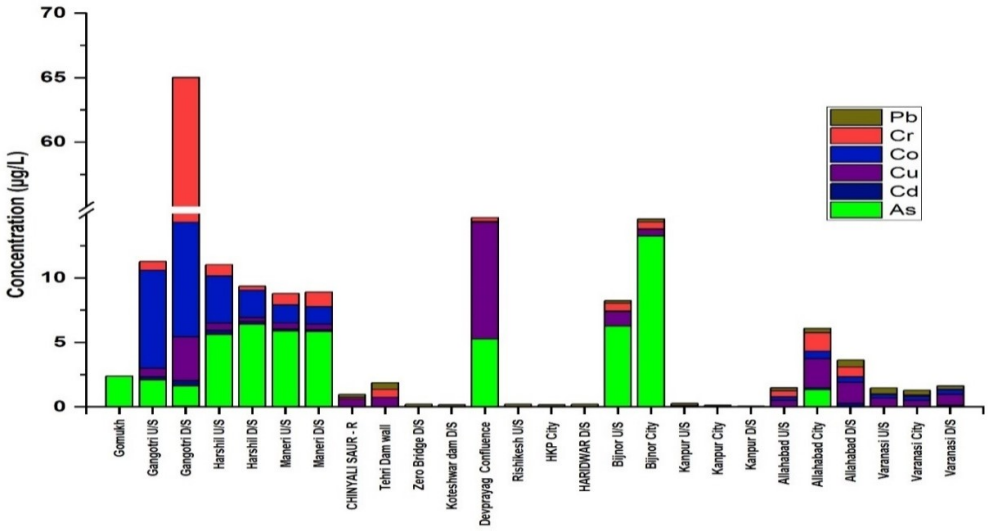

Fig.5.3: Dissolved Fractions of Post-Monsoon Season

Similar trend was observed for suspended fractions of these elements during pre and post monsson season as are presented in figure 5.4 and figure 5.5 respectively. The results indicate that comparatively the concentrations are higher during pre-monsoon as compared to post monsoon season. The suspended fractions also show relatively higher concentrations for Cu and Cr particularly at locations including Gangotri, Harshil, Maneri etc. The suspended fraction also shows the settling trends at Tehri reservior as the concentrations downstream of Tehri and Koteshwar are significantly lower as compared to other locations.

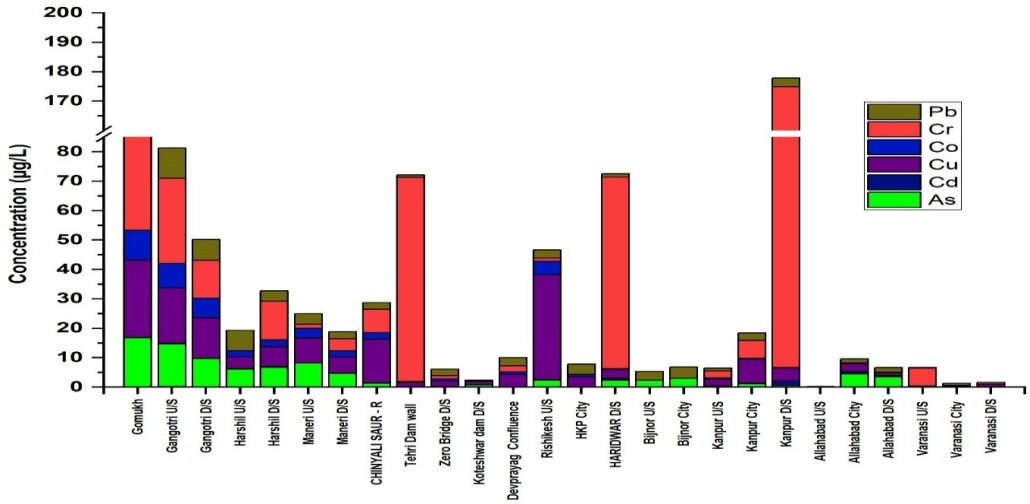

Fig.5.4: Suspended Fractions of Pre- Monsoon Season

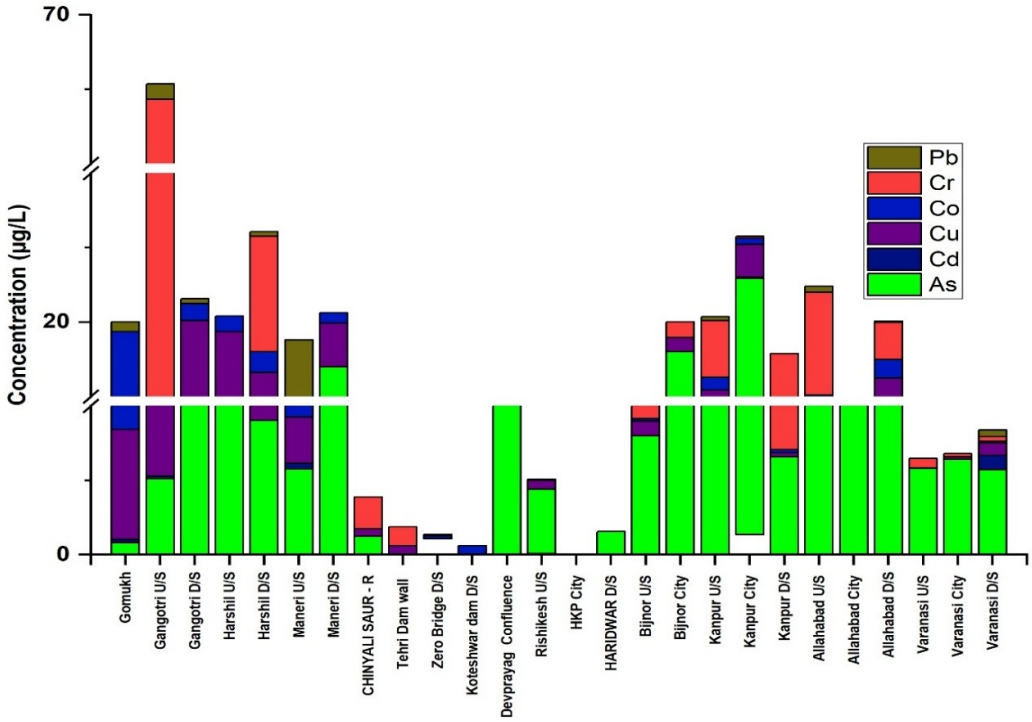

Fig. 5.5: Suspended Fractions of Post-Monsoon Season

5.3.2 Distribution of Various Metals Along the Entire Stretch of River Ganga

As mentioned in methodology section, metals can present as suspended or dissolved forms. The suspended metals are found bound to insoluble particulate matter which can be both organic and inorganic in nature. The dissolved forms are less prevalent and are present in free ionic form or bound to soluble metal complexing molecules or ligands. The concentrations of dissolved and total fractions were determined by analysing the filtered and digested unfiltered samples respectively. The suspended fraction was obtained from the difference between total and dissolved fractions. The effect of seasonal variation on different metals in various fractions are summarised here.

5.3.2.1 Arsenic

The occurrence of Arsenic in stretch I and II in both seasons in various fractions are presented in figure 5.6. As is present well below the permissible limits from Gomukh

to Varanasi in dissolved fraction in both seasons except at Bijnor and Kanpur with concentration of 10µg/L and 13µg/L respectively. Similarly; in suspended fractions the concentration exceeds the threshold limit (10-18µg/L) at Gomukh and Gangotri in pre-monsoon season and from Gangotri to Maneri and Bijnor to Allahabad in post monsoon season. The highest concentration of 18µg/L and 13.24 µg/L was recorded in suspended fraction and Dissolved fraction respectively at Bijnor City. Overall; As distinctly present in the suspended fraction of post monsoon season which may be due to the flow of sediments from upper to lower stretch in monsoon season.

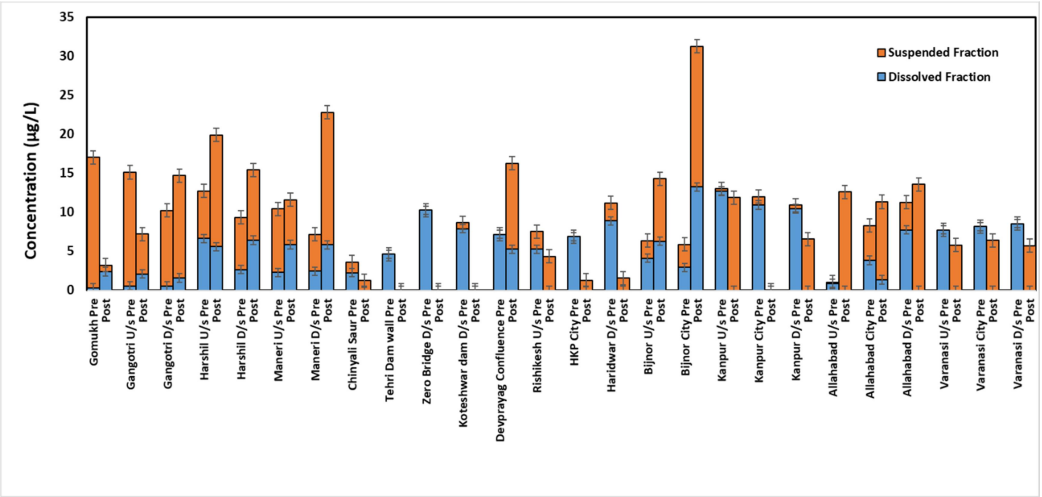

Fig. 5.6: Variation in As at various locations and geo-chemical partitioning during pre and post monsoon season

5.3.2.2 Silver

Silver is a precious metal and mostly present in traces in both stretches of river Ganga as depicted in figure 5.7. Interestingly the maximum concentration of 6.88µg/L was observed at Har ki Pauri in dissolved fraction. At Har Ki Pauri devotees offer coins of silver and gold to Ganga water and also silver particles present in the ashes of bone immersions accumulate below the surface of water. This might be the reason for the increased level of silver at this location. However, none of the locations showed concentration above the acceptable limit of 100 µg/L set by BIS 10500 (2012).

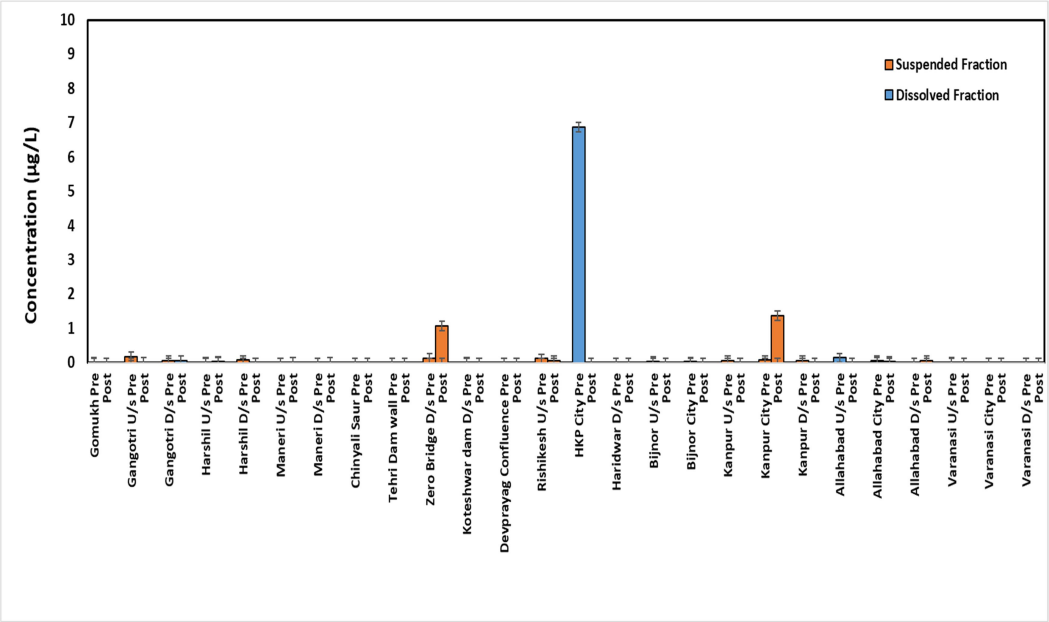

Fig. 5.7: Variation in Ag at various locations and geo-chemical partitioning during pre and post monsoon season

5.3.2.3 Barium

Along the entire stretch of river Ganga; Ba is present in the dissolved form in both seasons as presented in figure 5.8.Interestingly; like other metals Ba also observed in suspended fractions at Gomukh in both seasons. Concentration range of dissoved fractions is in decresing order from gomukh to Zero Bridge and again evolved after Haridwar. Maximum concentration occurred at Kanpur U/s, Varanasi City and downstream locations which are also exceeding the limit of BIS 10500 (2012). Overall, all the locations are well within the acceptable limits of BIS.

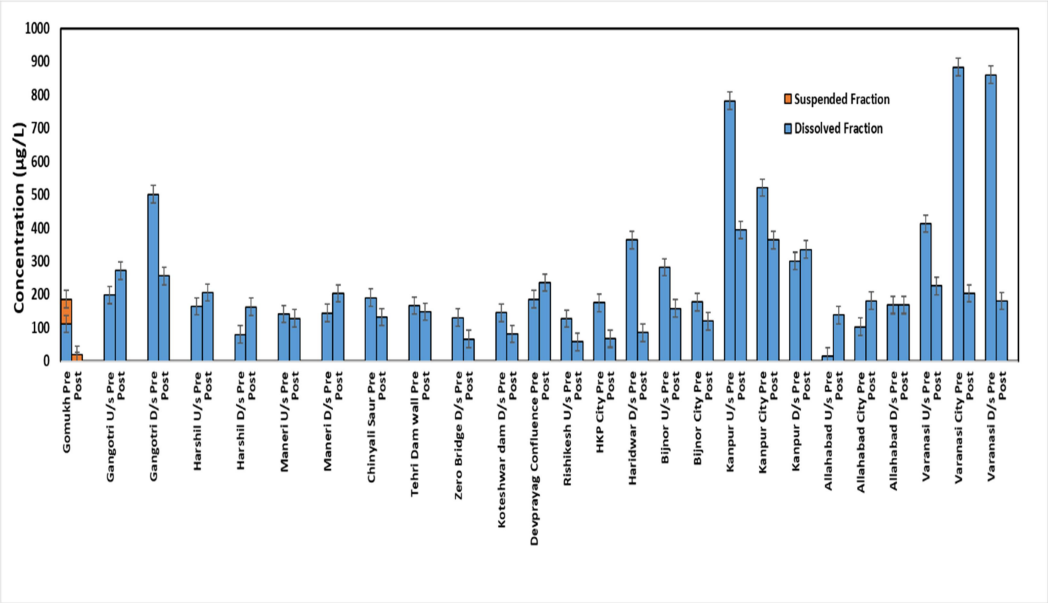

Fig. 5.8: Variation in Ba at various locations and geo-chemical partitioning during pre and post monsoon season

5.3.2.4 Cadmium

Cadmium is a rare element in earth's crust and occurs in very small levels. The increased levels may be contributed by introduction of the waste water from the metallurgical and textile industries to the water reservoirs. The occurrence of Cd in the different fractions is presented in figure 5.9. Cd is present in very low concentrations i.e. below 1µg/L throughout the stretch I and II in both seasons and fractions. The maximum concentration occurs at Kanpur downstream location in the suspended fraction of post monsoon season. Interestingly, compared to the values of Cd at other locations, higher values were observed after Kanpur in suspended fraction. However all the locations show concentrations well below the acceptable limit of BIS 10500 (2012).

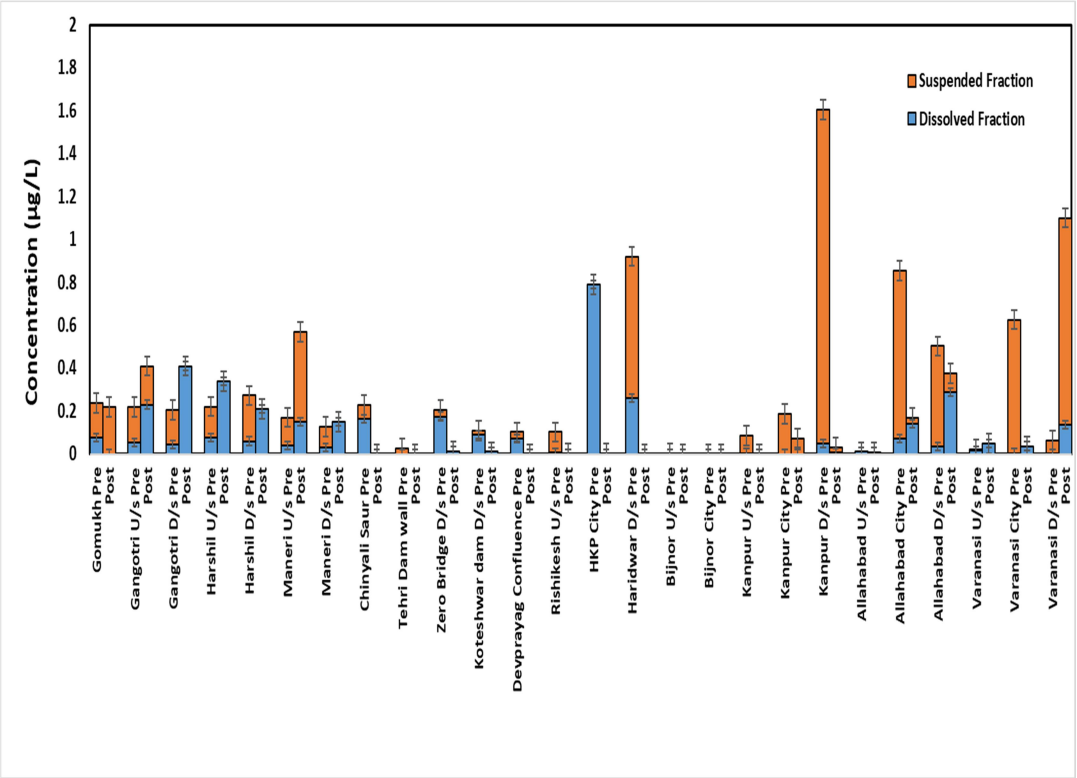

Fig. 5.9: Variation in Cd at various locations and geo-chemical partitioning during pre and post monsoon season

5.3.2.5 Cobalt

Cobalt distribution is measured in various fractions throughout the stretch I & II in both seasons which is presented in figure 5.10. The total concentration ranges between 0 to 10.96µg/L in different fractions. Majority of Co is present in upper stretch from Gomukh to Haridwar after that drastic decrease in concentration was observed. Highest concentration of approximately 11µg/L was observed at Gomukh in both seasons in suspended fraction. Majorly suspended Co is observed in pre monsoon season whereas in post monsoon season it was present in dissolved fraction in upper stretch. Interestingly; very trace concentration levels were available in stretch II in both fractions.

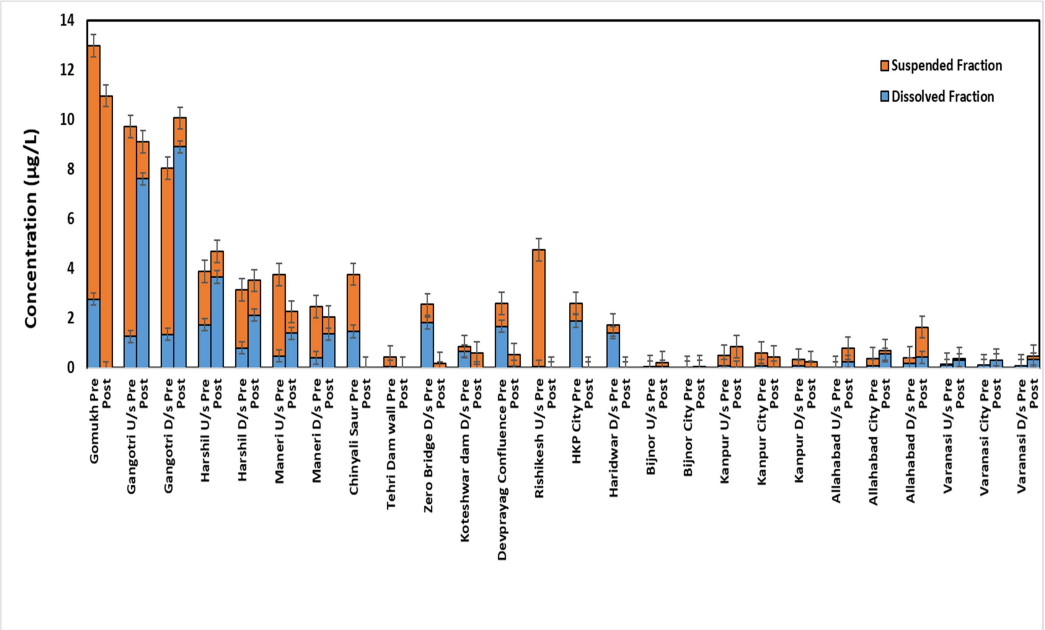

Fig. 5.10: Variation in Co at various locations and geo-chemical partitioning during pre and post monsoon season

5.3.2.6 Copper

The distribution and geochemical partitioning of Cu at various locations from Gomukh to Varanasi is presented in figure 5.11 for pre and post monsoon season respectively. As compared to other metals Cu was present in relatively high concentrations (5-40 µg/L) and is present mostly in suspended fraction. Comparatively higher concentrations in suspended form were observed in high altitude locations namely Gomukh, Gangotri and also at Chinyali Saur, and Rishikesh. Similar to trends observed for most of the metals, drastic decrease in Cu was observed post Tehri and almost negligible concentrations were observed downstream of Tehri. The Cu concentrations were regained after Devprayag almost reaching the same concentration range observed in upper locations. It was also observed that during pre-monsoon concentrations of Cu were higher as compared to post monsoon season.

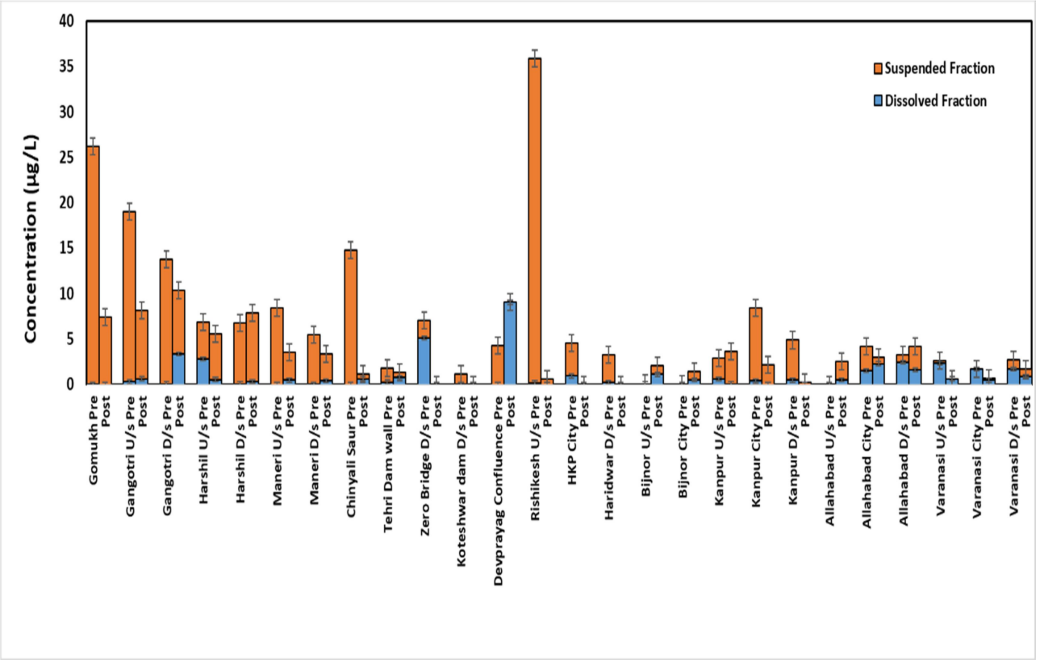

Fig. 5.11: Variation in Cu at various locations and geo-chemical partitioning during pre and post monsoon season

5.3.2.7 Chromium

Cr is another element which was observed in relatively higher concentrations as compared to other elements. The distribution of various fractions of Cr is presented in figure 5.12 for pre and post monsoon seasons. The total Cr concentration varied from less than 1 µg/L to more than 70 µg/L during pre-monsoon season and between 0.4 to 25 µg/L during post monsoon season. Majority of the fraction in both the seasons were present as suspended fraction; except for three locations namely Gangotri, Harshil downstream and Har ki Pauri where dissolved fraction of Cr predominated. Similar; trends were observed for most of the metals, drastic decrease in Cr was also observed post Tehri and almost negligible concentrations were observed downstream of Tehri which was regained after Rishikesh. The total concentration of Cr in all the samples remained below 50 µg/L except for Haridwar, Har ki Pauri and Kanpur downstream where the concentrations marginally exceeded the acceptable limit as per BIS 10500 (2012). Interestingly; Cr is present in traces in Stretch II except at Kanpur downstream which might be contributed by the industrialisation and or anthropogenic activities.

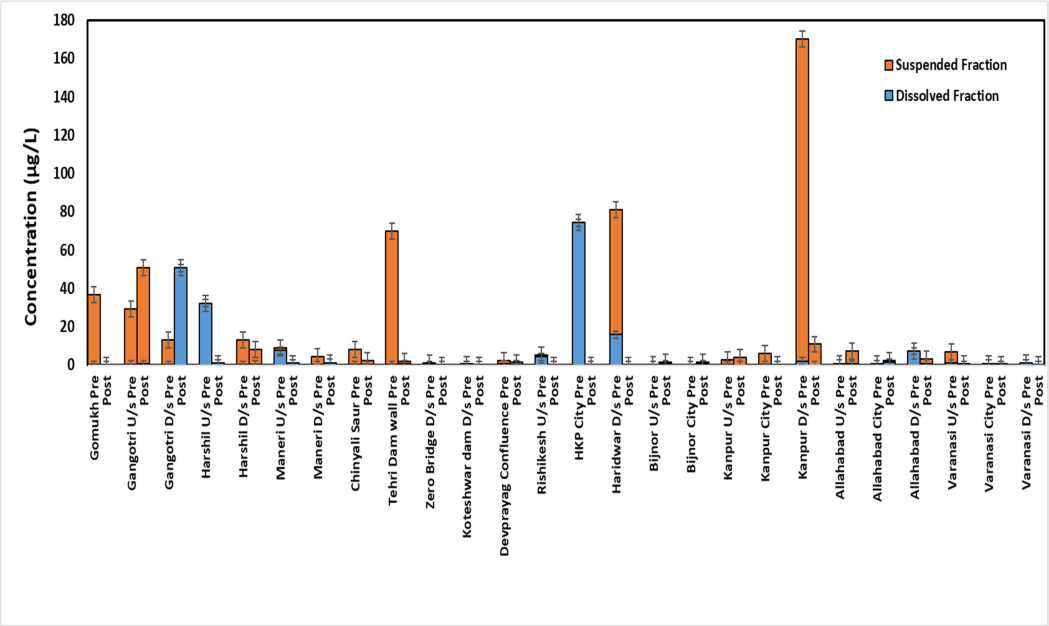

Fig. 5.12: Variation in Cr at various locations and geo-chemical partitioning during pre and post monsoon season

5.3.2.8 Manganese

Mn occur throughout the stretch of river Ganga and concentration ranges in different fractions was presented in figure5.13. Mn is present mostly in suspended form in the entire stretch of river Ganga from Gomukh to Varanasi. Dissolved form of Mn was predominant upto Tehri and after Haridwar it disappeared in the water samples. Similarly Suspended fractions were in decreasing trend from Gomukh to Tehri and it reappeared after Tehri in increasing trend. However, all the locations are well within the permissible limit of BIS 10500 (2012) except in suspended fractions at Gomukh and Gangotri locations.

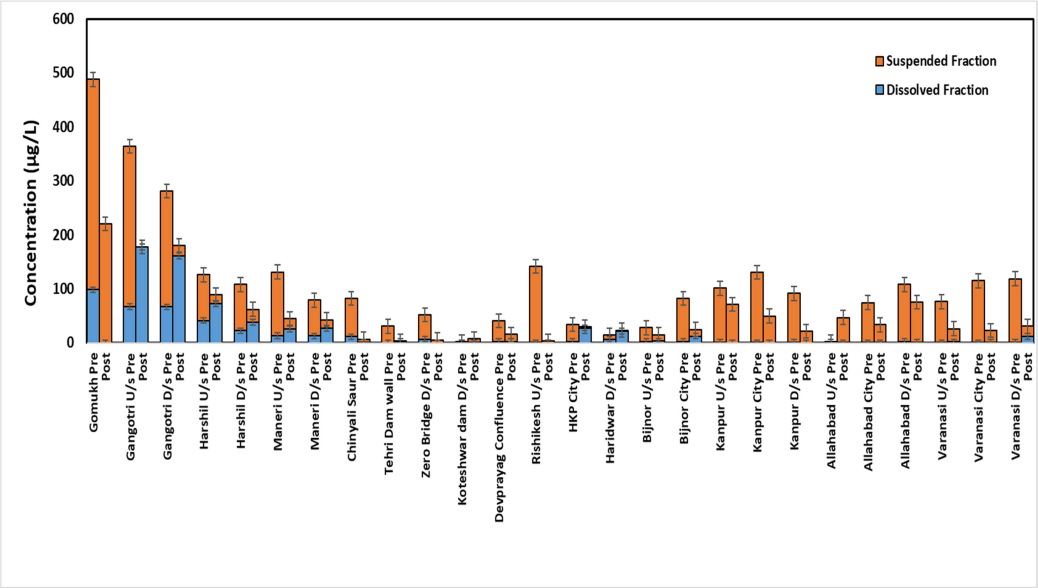

Fig. 5.13: Variation in Mn at various locations and geo-chemical partitioning during pre and post monsoon season

5.3.2.9 Lead

Pb is the most toxic metal present in the environment, originating from anthropogenic activities. The distribution of Pb is given in figure 5.14 which suggests dominance of Pb in suspended form along the entire stretch of river Ganga. Pb is present in trace concentration in post monsoon after Tehri however it is below detection limit in pre monsoon season in dissolved fraction. Maximum concentration of 13.53µg/L was measured at Gomukh which is in decreasing concentration upto tehri and again evolved in increasing concentration after Devprayag. However, except Gomukh, none of the locations are above acceptable limits of BIS 10500 (2012) for Pb.

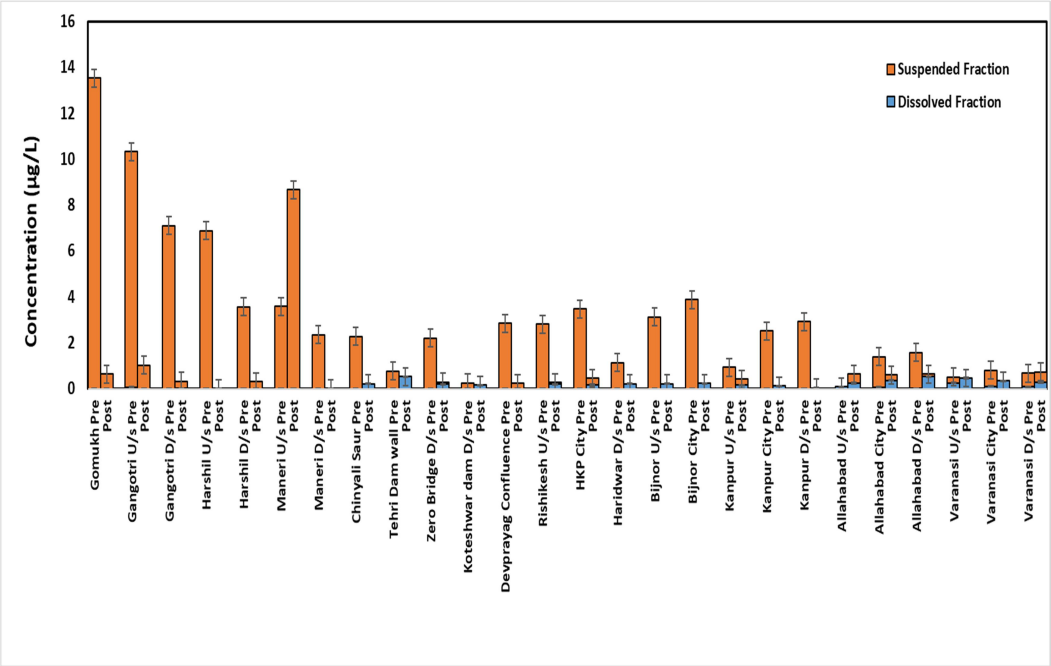

Fig. 5.14: Variation in Pb at various locations and geo-chemical partitioning during pre and post monsoon season

5.3.2.10 Selenium

Se is a micronutrient found in natural food and present as selenoproteins which protect cell from damage. Now a days Se is evolved as one of the emerging contaminant in the environment due to the increased industrialisation. The presence of Se in the river Ganga is in very trace levels as depicted in figure 5.15. Majority of Se is present in the dissolved fraction. Alike other metals it is also found in suspended form at higher altitude locations from Gomukh to Maneri. Interestingly it occurred in almost same concentration in both fractions at Chinyali Saur. Maximum concentration was observed in Allahabad and Varanasi. However, Se concentrations at all the locations are well below the permissible limits as per BIS 10500 (2012).

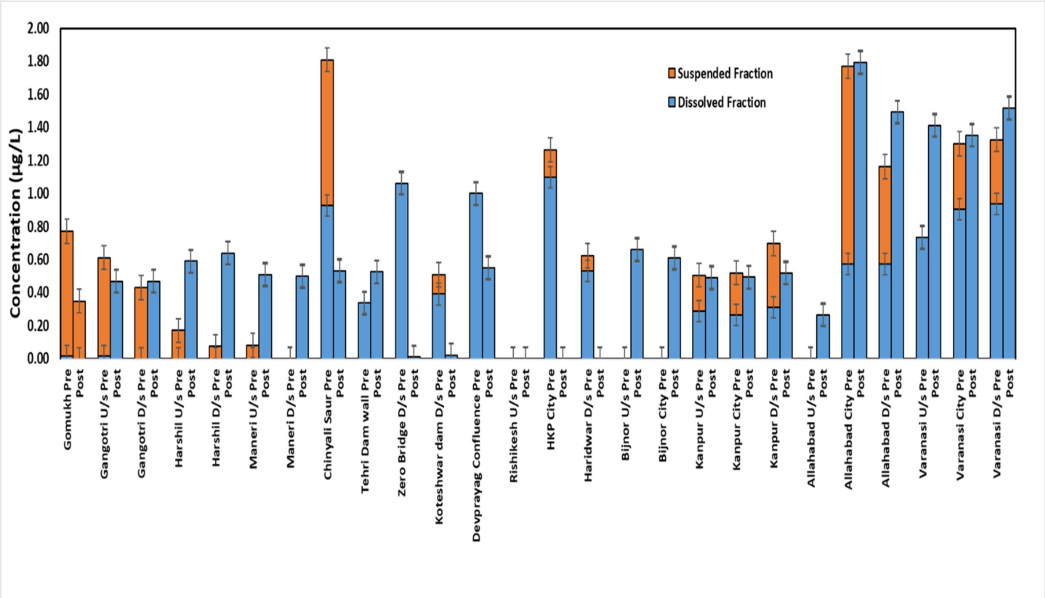

Fig. 5.15: Variation in Se at various locations and geo-chemical partitioning during pre and post monsoon season

5.3.2.11 Zinc

It is an essential micronutrient for plants and human metabolism. The acceptable limit of Zn in drinking water published by BIS is 5ppm. The presence of Zn in Stretch I and II is depicted in figure 5.16.The total concentration of Zn varied between 4 to 722.3µg/L . Zn is present majorly in dissolved form below 100µg/L in both pre and post monsoon seasons. Maximum presence in the suspended form occurs at Gomukh, Harshil and Rishikesh upstream locations with concentrations 239.8, 772.3 and 453.1µg/L respectively in pre monsoon season. Almost similar trends are observed in both seasons. However; none of the locations exceed the acceptable limit as per BIS 10500 (2012).

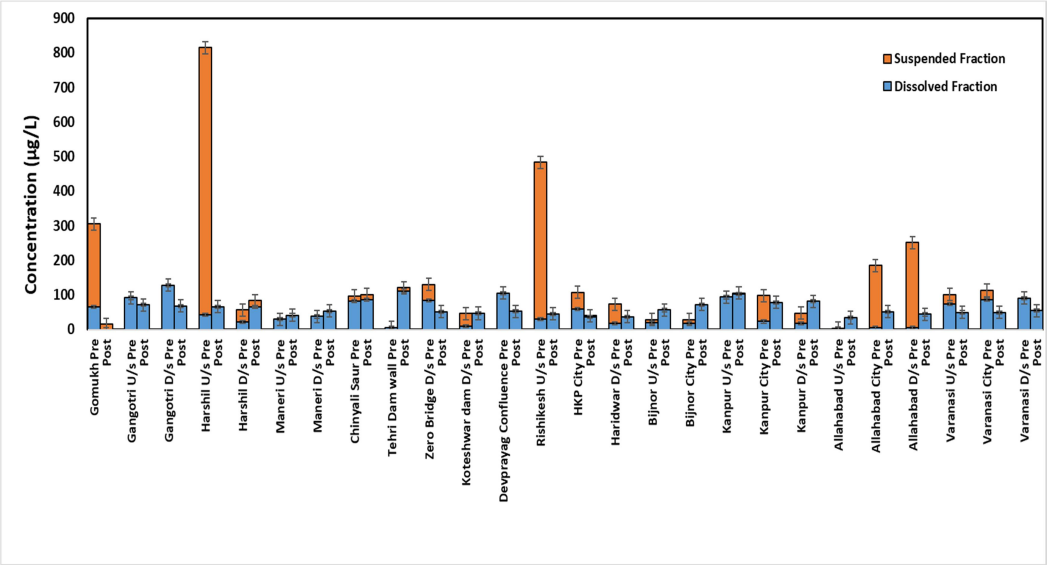

Fig. 5.16: Variation in Zn at Various Locations and Geo-Chemical Partitioning during Pre and Post Monsoon Season

5.4 Variations at Different Points of Sampling

As per the standard practice for collection of samples from river streams it is advisable to collect samples from both the banks and middle of the stream. Accordingly, attempts were made to collect samples from these three locations wherever possible. The representative results for dissolved fractions of Cu are presented in figure 5.17 which shows variation in concentration at different sampling point namely left and right banks and middle of the stream. It was observed that in stagnant streams (Tehri reservoir) the variations in concentrations are more pronounced as compared to flowing streams (locations at Rishikesh, Haridwar and Har ki Pauri).

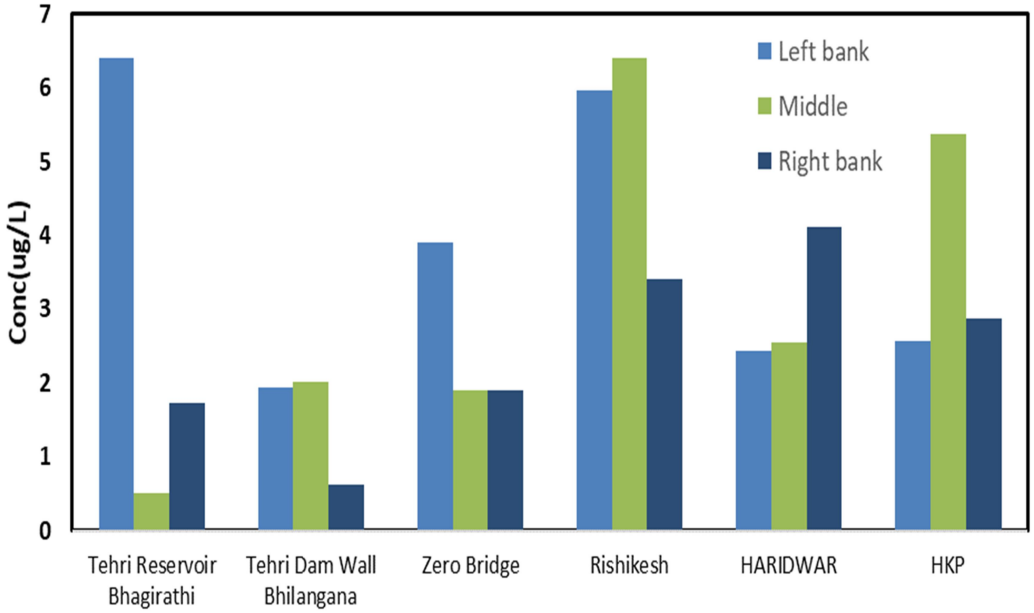

Fig. 5.17: Variations in Dissolved Concentration of Cu at Different Points of Sampling

5.5 Variations of Metal Concentrations at Various Depths in Tehri Reservoir

The majority of results for most of the metals indicate significant settling of suspended fractions of metals in Tehri reservoir leading to remarkably low concentrations immediately downstream of Tehri near Zero bridge location. In order to further confirm this trend, depth sampling was carried in Tehri reservoir for which samples at surface, 50 m and 70 m depth were collected using depth sampler. The representative results for Cu and Cr are presented in figure 5.18. It is clearly evident that concentrations of metals increase sharply with depth. The almost negligible concentrations on surface increases to 1.66 and 2.48 µg/L at 50 m which further significantly increases to 38.2 and 89.2 µg/L at 70 m depth for Cu and Cr respectively. These trends clearly indicate that there is noteworthy settling of suspended sediments leading to reduction in trace metal concentrations post Tehri reservoir. The above results are only representative results from huge set of results comprising of more than 25000 results of 200 samples collected, processed and analyzed.

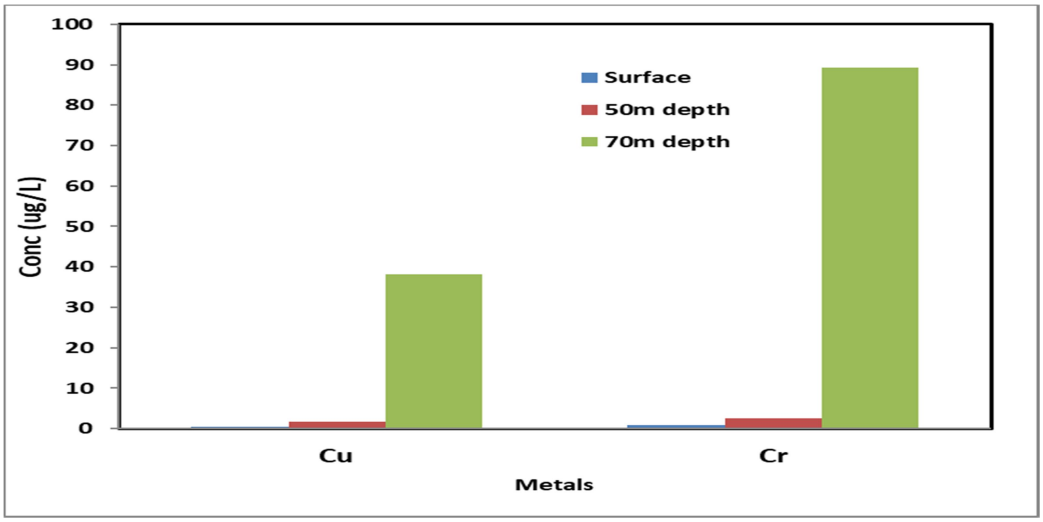

Fig. 5.18: Variations of metal concentrations at different depths in Tehri reservoir

5.6 Salient Findings

A comprehensive study of geochemical partitioning of metals in trace level along the entire stretch of river Ganga was undertaken for the first time. The results of the study reveals that several metals are present at Gomukh and Gangotri in elevated concentration ranges which may be due to the presence of heavy sediment load and geogenic origin. This was also observed in the Phase-I studies conducted by CSIR-NEERI. The suspended fractions sampled at the surface of the water body decrease post Tehri and this was also confirmed by depth sampling. The depth sampling and spatial trend of all the metals shows substantial settling of metals bound to suspended fractions in Tehri reservoir, however the trace levels of metals regain after Rishikesh. Maximum occurrence of metals such as As, Cu, Cr, Mn, and Pb is in suspended form whereas they are present in trace levels in dissolved fractions. Interestingly; Zn is predominantly present in dissolved fractions in both seasons. The religious activities happening at Har ki Pauri contributed to the elevated level of Ag at this location compared to other locations. It was also observed that many metals show higher levels in the pre-monsoon season which could be due to the dilution in the monsoon season. The anthropogenic activities contributed to the elevated levels of metals at Rishikesh and Haridwar. Overall; this study is one of its kind which will be useful for the identification of partitioning of various metals and their trends along the entire stretch of river Ganga.

CHAPTER - 6

SEDIMENTS CHARACTERIZATION

6.0 Sediment Characterization

6.1 Sampling Locations: Area of Study

For the comprehensive analysis of sediment and water of River Ganga, the respective samples were collected from various locations of the Indo-Gangetic plain, starting from Gomukh, the origin of River Ganga, to Bhagalpur (Table 6.1). The entire sampling area was divided into three stretches 1. The upper stretch 2. The middle stretch and 3. The lower stretch. From Gomukh to Haridwar and Rishikesh, the Ganges course is considered as the upper stretch (Figure 6.1). Sediments from various accessible spots (10-15 Nos) of a particular location were collected and mixed thoroughly to obtain representative sediment samples. Relatively more emphasis was placed on the sediment samples collected from the upper stretch to understand the non-putrefying property of the revered River as the upper stretch is considered relatively less contaminated (i.e., the minimum intervention of anthropogenic activities) compared to that of the other stretches. Depth profiling and core sampling were also performed at Tehri reservoir and Chinyalisaur, respectively, to understand the sediment characteristics. Sediment samples were collected from the Tehri reservoir at 50 and 70 m depth (Figure 2). Samples from a Chinyalisaur were collected at 1, 3, 5, 8, 11, 15, 25, and 30-35 ft as listed in Table 6.2.

Table 6.1: Details of the Sampling Location across the Stretch of River Ganga

Sl. No.	Location	Latitude	Longitude
1.	Gomukh	N30.93.11.27	E79.07.64.130
2.	Gangotri U/S	N30.59.39.18	E78.56.44.32
	Gangotri U/S	N30.59.38.53	E78.56.25.63
3.	Harshil U/S	N31.2.11.56	E78.45.34.90
	Harshil D/S	N31.1.8.91	E75.42.39.06
4.	Maneri U/S	N30.44.23.29	E78.32.23.51
	Maneri D/S	N30.44.14.42	E78.31.21.00
5.	Chinyalisaur left	N30º33'53.4"	E78º20'02.2"

Sl. No.	Location	Latitude	Longitude
	bank	N30º33'52.9"	E78º19'56.0"
	Chinyalisaur middle	N30º33'42.9"	E78º19'50.7"
	Chinyalisaur right bank		
6.	Koteshwar d/s left	N30º15'50.3"	E78º30'04.0"
	Koteshwar d/s middle	N30º15'46.2"	E78º30'01.5"
7.	Tehri dam wall left bank	N30º22'48.3"	E78º28'57.2"
	Tehri reservoir wall side middle	N30º22'46.7"	E78º28'55.2"
	Tehri dam wall right bank	N30º22'57.9"	E78º28'35.7"
	Bhilangana	N30º22'51.4"	E78º30'33.3"
	Tehri reservoir confluence	N30º23'14.9"	E78º28'52.2"
8.	Rishikesh u/s left	N30º07'35.4"	E78º21'10.6"
	Rishikesh u/s right	N30º07'37.4"	E78º21'11.5"
	Haridwar centre-left	N29º57'10.7"	E78º10'11.7"
	Haridwar centre middle	N29º57'12.2"	E78º10'10.2"
	Haridwar centre right	N29º57'13.1"	E78º10'08.7"
	Haridwar d/s	N29º51'27.3"	E78º08'51.4"

Sl. No.	Location	Latitude	Longitude
	right		
9.	Bijnor U/S (Bhagepurpatti Abdulla left side)	N29º26.206' N29º22.386' N29°26'25.94"	E78º3.654' E78º2.482' E78° 3'39.45"
	Bijnor U/S (Bijnor Barrage mid)	N29º26.650'	E78º3.495'
	Bijnor U/S (Bhagepurpatti Abdulla Middle depth)	N29º16.408'	E78º6.108'
	Bijnor U/S (Bhagepurpatti Abdulla Right side)		
	Bijnor D/S DaraNagar ghat		
10.	Kanpur U/S, Bithar brampavarta ghat	N26°37'1.68" N26°37'2.36" N26º36.809'	E80°16'26.11" E80°16'32.41" E80º16.520'
	Kanpur U/S, Bithar brampavarta ghat	N26º36.809'	E80º16.520'
	Kanpur U/S, Bithar brampavarta ghat (Middle stream)	N26º28.209' N26°28'14.02" N26°28'12.19" N26°28'12.19"N N26°22'42.61"N	E80º22.428' E80°22'26.82" E80°22'25.21" E80°22'25.21" E80°29'25.40"E
	KanpurU/S,		

Sl. No.	Location	Latitude	Longitude
	Bithar brampavarta ghat depth at middle stream 5.8 F)	N26°22'43.34" N26°22'44.08" N26º35.0414'	E 80°29'25.97" E80°29'26.43" E80º51.5601'
	Kanpur M/S, Ganga ghat (Right side)		
	Kanpur M/S, Ganga ghat (Left side)		
	Kanpur M/S, Ganga ghat (middle)		
	Kanpur M/S, Ganga ghat (middle depth)		
	Kanpur D/S, Dhondhi Ghat (Right side)		
	Kanpur D/S, Dhondhi Ghat (middle)		
	Kanpur D/S, Dhondhi Ghat (Left side)		
	Kanpur D/S, Katrirajapar ghat around 6 km downside of Dhondhi ghat		
11.	Allahabad U/S,	N25º51.6161'	E81º68.5440'

Sl. No.	Location	Latitude	Longitude
	Fatepur ghat (Ujihiniima)	N25º51.6161'	E81º68.5440'
	Allahabad U/S, Fatepur ghat (Ujihiniima)	N25°31'3.80"	E81°41'8.24"
	Allahabad U/S, Fatepur ghat (Ujihiniima)	N25°30'58.53"	E81°41'5.82"
	Allahabad U/S, Fatepur ghat (Ujihiniima)	N25º42.3628'	E81º88.8116'
	Allahabad U/S, Fatepur ghat (Ujihiniima)	N25º42.3628'	E81º88.8116'
	Allahabad M/S, sangam	N25º42.3628'	E81º88.8116'
	Allahabad M/S, sangam	N25º39.3014'	E81º91.2330'
	Allahabad M/S, Yamuna at sangam	N25º32.0510'	E81º78.9160'
	Allahabad M/S, Ganga at sangam		
	Allahabad D/S, (Mawaiya Uparhar)		
	Allahabad U/S (Deoria)		
12.	Varanasi u/s right bank	N25º13.778'	E83º01.513'
	Varanasi u/s middle	N25º13.760'	E83º1.636'
	Varanasi u/s right bank	N25º13.755'	E83º1.762'
		N25º18.418'	E83º0.688'
		N25º18.398'	E83º0.756'

Sl. No.	Location	Latitude	Longitude
	Varanasi centre left bank	N25º18.404'	E83º0.856'
	Varanasi centre middle		
	Varanasi centre right bank		
13.	Patna centre left bank	N25º36.965'	E85º12.976'
	Patna midstream centre	N25º36.871'	E85º12.705'
	Patna centre right bank	N25º36.827'	E85º12.375'
	Patna d/s left bank	N25º35.933'	E85º15.357'
	Patna d/s middle	N25º35.703'	E85º12.358'
	Patna d/s right bank	N25º35.492'	E85º15.207'
	Patna u/s left bank	N25º39.384'	E85º4.938'
	Patna u/s middle	N25º39.292'	E85º04.934'
	Patna u/s right bank	N25º39.135'	E85º5.130'
14.	Bhagalpur upstream right bank Sultanganj	N25º15.299'	E86º44.358'
	Bhagalpur centre left bank	N25º16.921'	E87º2.426'
	Bhagalpur centre midstream	N25º16.188'	E87º2.476'
	Bhagalpur centre	N25º15.316'	E87º2.873'
		N25º15.108'	E87º4.230'
		N25º14.971'	E87º4.326'

Sl. No.	Location	Latitude	Longitude
	right bank	N25º14.820'	E87º3.943'
	Bhagalpur downstream left bank		
	Bhagalpur downstream middle		
	Bhagalpur downstream right bank		

Table 6.2: Depth Sampling At Selected Locations of River Ganga

Sl. No	Location	Sampling depth	Latitude	Longitude
1.	Chinyalisaur	1 ft	N30º34'29.4"	E78º19'59.8"
		3 ft	N30º34'29.4"	E78º19'59.8"
		5 ft	N30º34'29.4"	E78º19'59.8"
		8 ft	N30º34'29.4"	E78º19'59.8"
		11 ft	N30º34'29.4"	E78º19'59.8"
		15 ft	N30º34'29.4"	E78º19'59.8"
		25 ft	N30º34'29.4"	E78º19'59.8"
		30-35 ft	N30º34'29.4"	E78º19'59.8"
2.	Koteshwar (near dam wall)	56 m	N30º15'35.1"	E78º29'49.4"
3.	Tehri reservoir (Bhagirathi river)	25 m	N30º26'14.8"	E78º29'49.4"
		50 m	N30º26'14.8"	E78º29'49.4"
		70 m	E78º29'49.4"	E78º29'49.4"

Samples were collected from Tehri reservoir, 10 km away from the reservoir wall at 25, 50 and 70 m depth. Sediment sample was also collected near the reservoir wall of Koteshwar at 56 m depth.

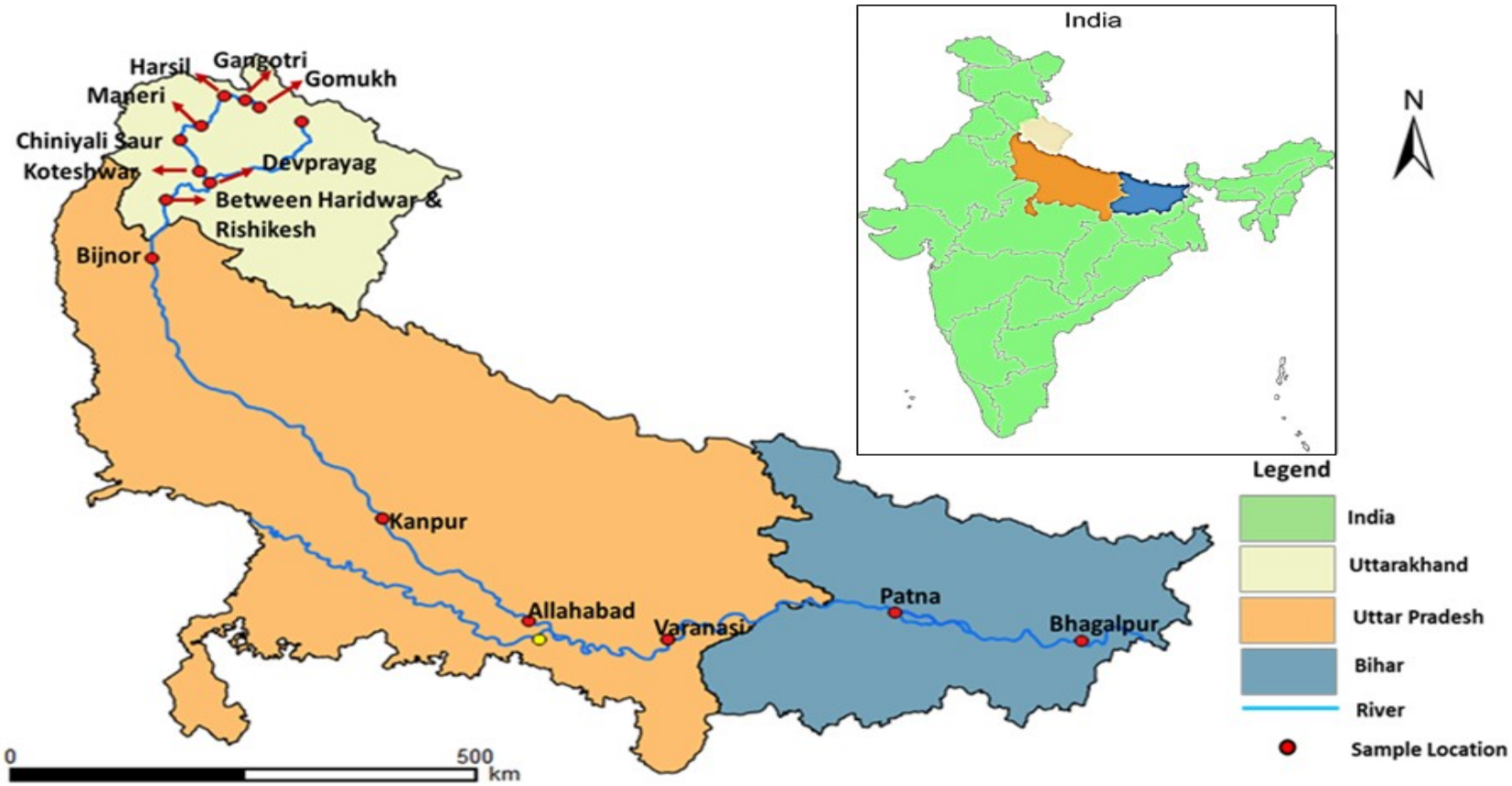

Fig 6.1: Overall study area and sampling locations details across the stretch of Indo-Gangetic plain

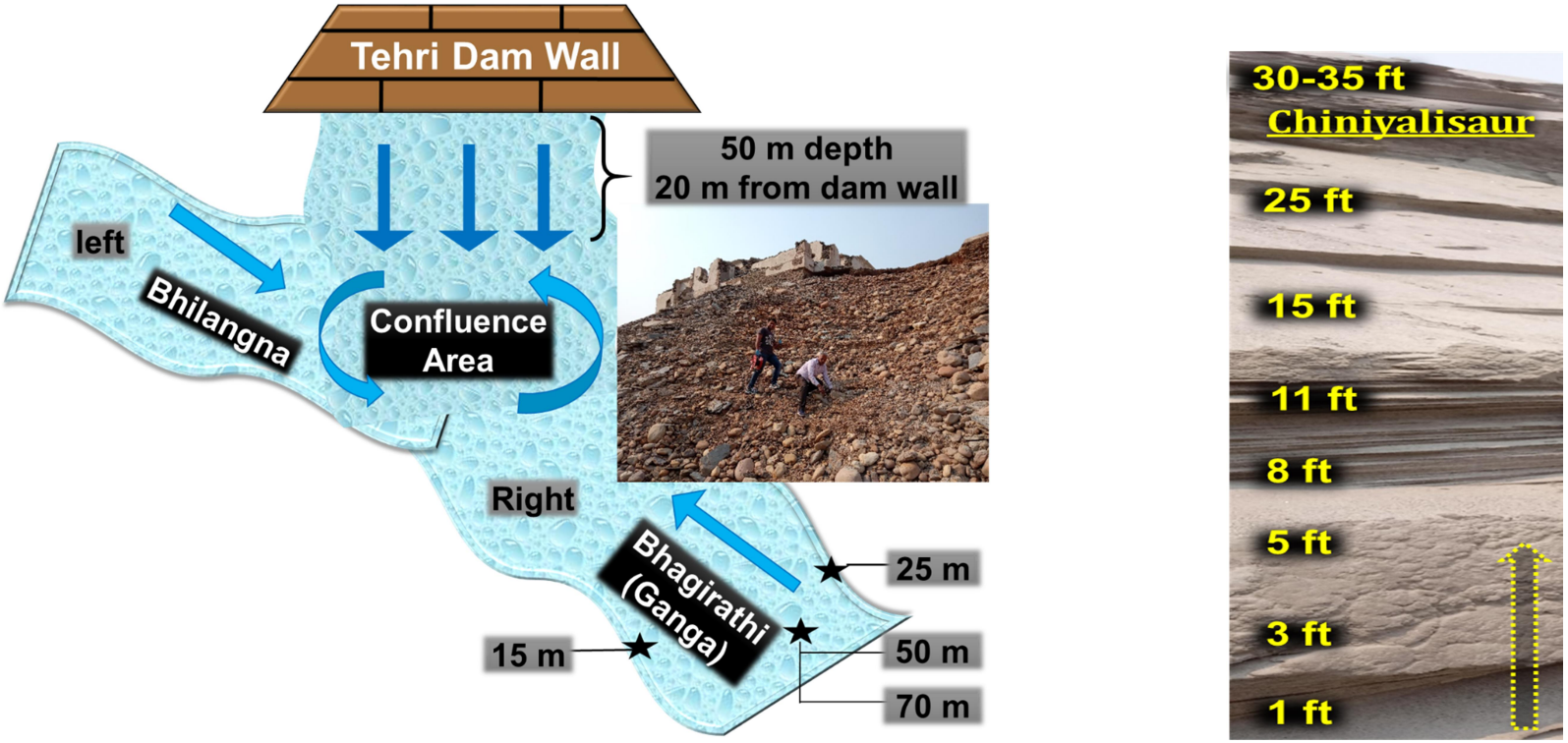

Fig. 6.2: Depth sampling at Tehri reservoir and Chinyalisaur

6.2 Sediment Sampling

Sediment samples were collected from 14 locations across the whole stretches of the River Ganga. The sediment samples were collected as per the standard SOP guidelines formulated by the Environmental Protection Agency (EPA) (LSASDPROC-200-R4, SOP#: 2016 DATE: 11/17/94 REV). The grab sampling procedure was adopted to collect the representative sediment samples using a scoop. Pre-cleaned polypropylene bottles of 1 liter capacity and the scoop were used to collect the sediment samples. After collection, the sediments were stored in a cool box and transported to the laboratory, followed by storage at 4 °C. A depth sampler device was used to collect samples from Chinyalisaur, Koteshwar- and Tehri- reservoirs.

6.3 Pre-Treatment of the Sample

The sediments collected from each spot of a particular location were transferred to a cleaned beaker, and they were mixed thoroughly. The mixed sample was then divided into two portions. The first aliquot is stored at 4 °C for bacteriological- and organic components- studies. The second aliquot of sediments was transferred to a cleaned glass Petri dish and dried **separately** under sunlight.

6.4 Analytical Techniques used for Sediment Characterization

6.4.1 Grain Size Distribution

After drying, the sediment samples were sieved mechanically into various fractions of different grain size (25 µm, 53 µm, 106 µm, 250 µm, 500 µm, and >500 µm) with the help of a sieve shaker (Bio Technics, India (BII-46) to separate the granular and finer particle portions. The fraction of each size present in the samples was then determined to identify their % composition that would aid to understand the heterogeneity of the sediment samples. The sieved samples were then ground using a mortar and pestle for 20 min and then used further for structural-, morphological- and elemental- analysis.

6.4.2 Laser Light Experiments

Laser light experiments (i.e., the subjection of laser light on the suspended sediment (SS) samples) were carried out to examine and confirm the presence of colloidal particles. The SS sample was taken in a sealed glass vial and irradiated with a beam of

coherent laser light. A clear scattered path may be seen in the SS solution upon irradiation of laser light due to the scattering of laser light by randomly moving colloidal particles (i.e., Brownian motion of the particles) if any present in the SS. The SS samples were centrifuged at 500, 1000, 2000, and 4000 rpm using a benchtop centrifuge machine (REMI-RC) for 15 min and a supernatant solution of the SS sample was irradiated with laser light. A few SS samples from the upper stretch of River Ganga (Gangotri, Harsil, Maneri, Tehri, etc.) were ultra-centrifuged (Sorvall M50 SE) at 75000 rpm at 4°C for 30 min to separate very fine suspended particles from the suspensions.

6.4.3 Dynamic Light Scattering (DLS) and Zeta potential Experiments

Particle size distribution and zeta potential (SZ-100 Horiba scientific nanopartica) experiments were carried out using 30 ml of the SS samples. The SS samples were sonicated, and the resultant suspensions were analyzed to determine the average particle size and surface charge of the SS samples. The SS samples were centrifuged at 1500, 2500, 3500, and 4500 rpm, and their particle size distribution is determined, as shown in Figure 6.3.

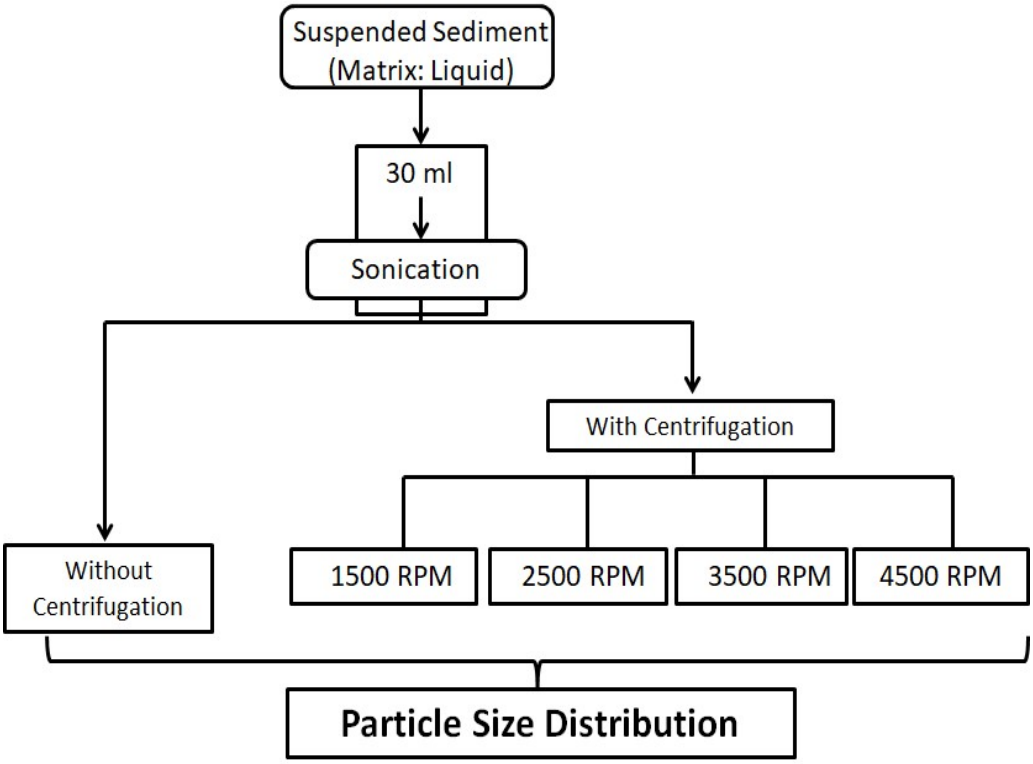

Fig. 6.3: Particle size distribution analysis of the SS samples collected from various locations of River Ganga

6.4.4 Transmission Electron Microscopy (TEM)

A high-resolution transmission electron microscope (HR-TEM) (JEOL JEM-1400 instrument operated at the acceleration voltage of 120 kV) was used to analyze the morphology and size of particles and their distributions present in the SS samples collected from Gomukh, Gangotri, Koteshwar, Chinyalisaur, and Tehri at 50 m and 70 m depth. Before the TEM analysis, the SS samples were homogenized using an ultrasonicator. Elemental analysis/mapping of the collected sediment samples was performed using, XRD, XRF, and ICP-MS techniques. Also, the SS samples were centrifuged at 8000 RPM again and performed the TEM analysis (Figure 6.4).

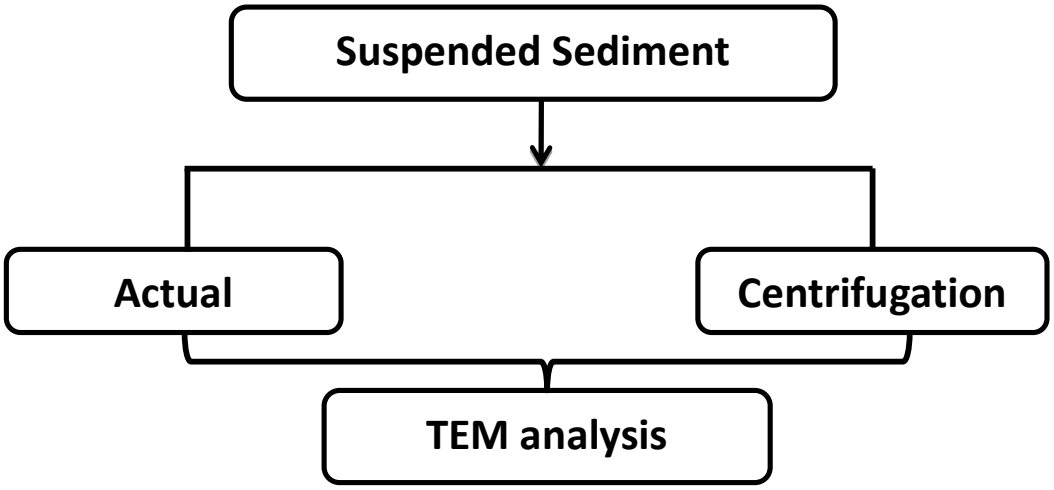

Fig. 6.4: TEM analysis plan of SS samples collected from River Ganga

6.4.5 Powder X-Ray Diffraction (pXRD) Study

The pXRD analysis essentially provides information about mineral contents and their crystallographic structures present in the sediments. pXRD analysis of the SS samples was carried out using a benchtop X-ray diffractometer (Rigaku Miniflex). The Cu Kα radiation generated at 30 kV and 15mA was used to scan (2 □ range) the sediment samples between 10° and 90° at a step size of 0.02° sec-1. The sediment samples were sun-dried for 8 h, followed by mixing them thoroughly. The various fraction of the

sediments were analyzed to examine the presence of minerals. The sediment fractions (< 25 µm, 53 µm, 106 µm, 250 µm, 500 µm, and >500 µm) from all the 14 locations were analyzed to identify the phases of minerals present in it.

6.4.6 X-Ray Fluorescence (XRF) Study

The qualitative analysis of the sediments was performed initially by X-Ray Fluorescence spectroscopy. XRF is a non-destructive analytical technique used to determine the elemental and chemical composition of the material. Handheld X-ray Spectrometer (EDXRF Spectrometer; SPECTRO xSORT) was used to analyze the sediment composition qualitatively. The sediment fraction of 106 µm grain size was used for the XRF analysis. X-Ray transparent polypropylene cuvettes were used to analyze the sediment samples.

6.4.7 Inductively Coupled Plasma Mass Spectroscopy (ICP-MS) Analysis

ICP-MS analysis of the sediments was performed further to reliably quantify the elements present in the sediments. Standard EPA protocol was followed for sample preparation. The microwave digestion method was used to digest the sediments. A sediment fraction of 25 µm size was used for the analysis. 0.5 gm of sediment samples were digested using aqua regia solution followed by the addition of 1 ml of Hydrogen fluoride solution to the reaction mixture. The entire reaction mixture was allowed to react for 1 min, and then the reaction vessel was sealed gently. The vessel was then placed in a microwave oven and heated up to 180 °C for 10 min. After the complete digestion of sediments, aliquots of the digested sample were analyzed using an ICP-mass spectrophotometer (Perkin Elmer NexION 300)

6.4.8 Antibacterial Activity Test

Antibacterial activity test was performed using both the sediments and the SS of River Ganga, as shown in Figure 5. The samples collected from the upper stretch region (Gomukh, Gangotri, Harsil, Maneri, and Tehri) were used for the antibacterial test. The sample collected from Mana was also tested for reference purposes. Escherichia coli (E. coli), DH5α strain was used for this purpose. For each plate, 0.5 or 1 g of sediments and 5 ml of the SS were added to 20 or 15 mL of molten agar at a bearable warmth, after which the agar solution was poured onto empty, autoclaved plates.

After solidification, 100 µL of E. coli that would result in 7000 CFU per ml was plated. The plates were incubated at 37 °C overnight, and the residual bacterial cells were scored. A controlled experiment was also performed alongside i.e., without the addition of any suspended/bulk sediment.

The SS samples collected from Gangotri, Harsil, Maneri, and Tehri were also centrifuged at 75000 rpm to remove most of the suspended particles present in the SS samples. The antibacterial activity test of the supernatant solution was also again performed after centrifugation.

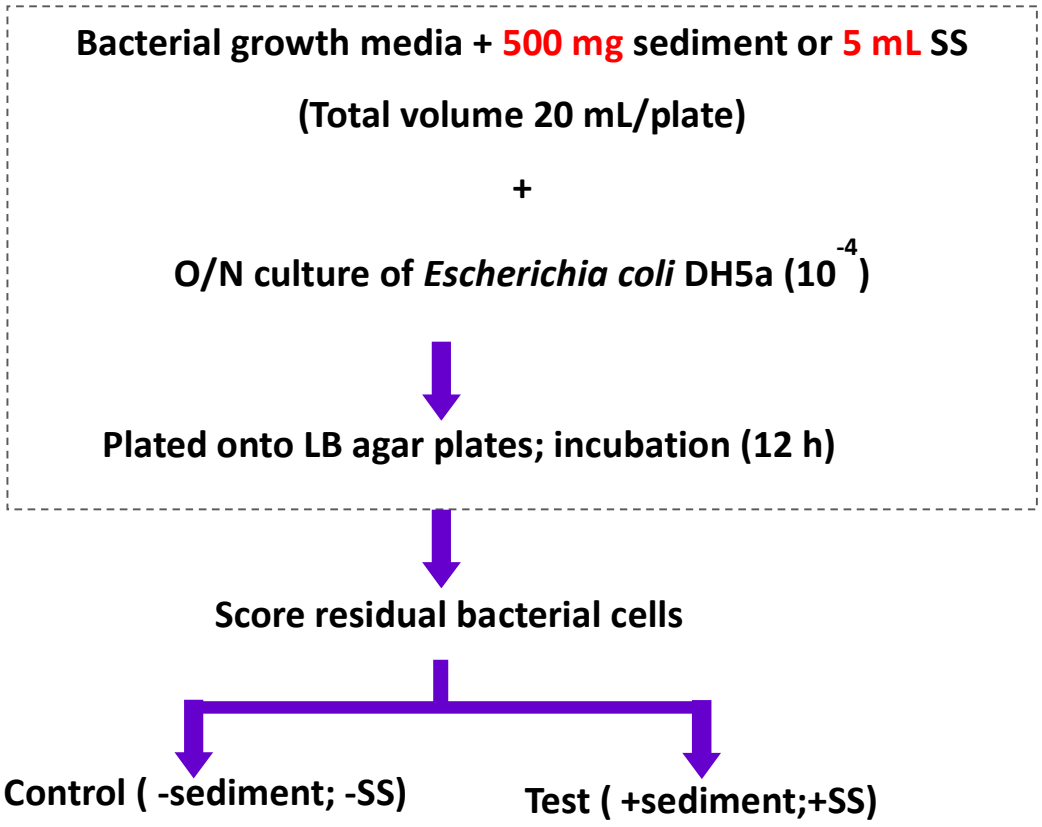

Fig. 6.5: Antibacterial activity test for the samples collected from the first stretch of River Ganga

6.5 Results and Discussion

6.5.1 Grain size distribution

Grain size and mineralogy of the sediments are responsible for controlling the mobility and dispersion of heavy metals in the River. The grain size distribution profile of various sediment fractions showed that the sediments are of a highly heterogeneous nature. Throughout the Indo-Gangetic plain, it was observed that the sediment fraction having a size of 250 µm is larger (approx. 45 %) compared with that of the other fractions, while the sediment fractions having the size of 25 and 53 µm account for only 3-4% of the total. However, the sediments collected from Koteshwar- and Tehri- reservoirs were fine in nature. As can be seen in more detail, the sediment fractions collected from Koteshwar showed mostly 25 µm size while the sediments collected from Tehri showed the size of 25, 53, and 106 µm. The presence of finer sediment fractions at these reservoirs can be attributed mainly to the inflow of silts and their gradual accumulation at the bottom of the water body over a period of time. Table 3 shows the composition of various fractions present (in percentage) in the sediments collected from the first stretch. The percent composition of each fraction of a particular location was first identified, and then the cumulative percent composition of each fraction was determined. Table 3 includes the cumulative percent composition of each fraction (25, 53, 106, 250, 500, and > 500 µm grain size) obtained from various locations across the entire stretch of River Ganga.

Table 6.3: Grain Size Distribution and the approximate percentage composition of sediment

S. No.	Grain Size (µm)	% Composition
1.	>500	9.2
2.	500	28.9
3.	250	45.0
4.	106	13.8
5.	53	1.8
6.	25	1.3

The % composition of Grain size across the stretch of River Ganga, as shown in Table 3 confirms the highly heterogeneous nature of the sediment samples. The sediment samples collected from Chinyalisaur at 1, 3, 5, 8, 11, 15, 25 and 30-35 ft depth showed predominantly the sediment fractions having 250 µm size followed by 106 µm fractions. All the other grain fractions contribute minimum to the sediment samples, as can be seen from Figure 6. 25 and 53 µm sediment fractions constitute only up to 1% of the total sediments collected at Chinyalisaur, in contrast to the sediment samples collected from Koteshwar and Tehri. Noticeable amounts of sediments with a size of > 500 nm were also observed when the sediment samples were collected at 1 ft of depth as the finer portion of sediment is washed away upon their contact with the flow of water. The rest of the sediment samples collected from other locations follow the general trend where sediment fraction having the size of 250 µm is predominantly present followed by the size of 106 and 500 µm.

The grain size distribution analysis of the sediments revealed that the sediments are highly heterogeneous. The sediments collected from the reservoirs (Tehri and Koteshwar) are fine due to the accumulation of silts at the bottom of the reservoirs over a period of time. From the depth analysis of the sediments of Chinyalisaur, the sediment fraction of the size > 500 µm was observed predominantly at the bottom of the water bodies due to the removal of finer sediments upon contact with the flow of river water.

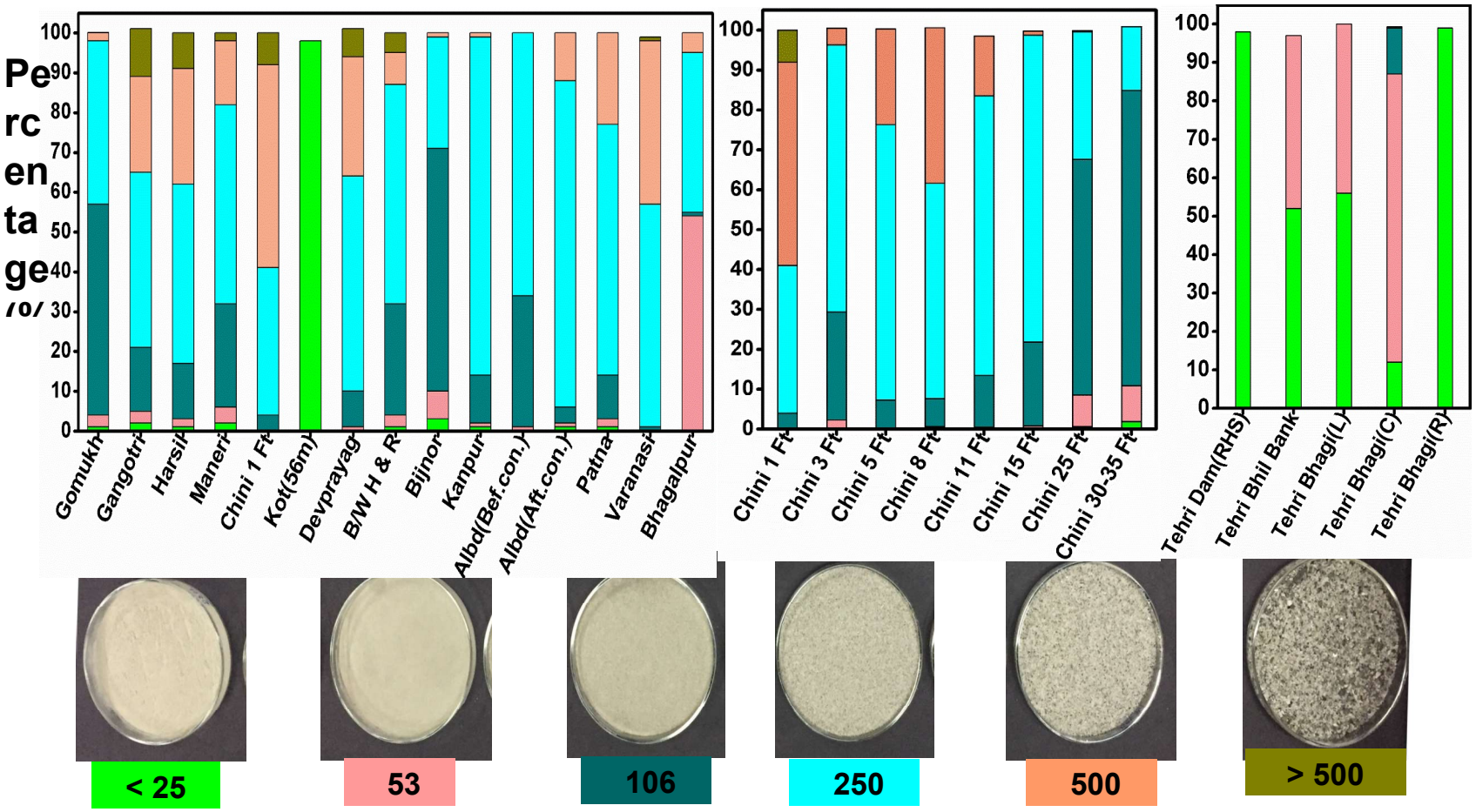

Fig. 6.6: Size distribution of various sediment samples across the entire stretches of River Ganga

6.5.2 Laser Light Scattering Experiment

A laser light scattering experiment is a preliminary technique that can be used to investigate whether the water samples contain any suspended components of sediments or not. Suspended components of the sediments in the solution can scatter laser light upon irradiation, which can show a scattered light path in the suspended solution. The collected SS samples were centrifuged at various set centrifugal forces to separate settleable components, followed by irradiation of laser light. It was observed that the SS after centrifugation at 4000 rpm showed a clear light scattering path, indicating that suspended components were still present in the solution even after centrifugation at 4000 rpm. As can be seen in more detail, Figure 9 shows the optical images of SS collected from various locations of Ganga River and after centrifugation at various set centrifugal forces. Relative centrifugal force is given by the formula:

$$g = (1.118 \times 10\text{-}5)*R*(rpm)2$$

Where R is the radius of the rotor in centimeters and rpm is the revolution per minute (Rotational speed). Centrifugal force is expressed as multiples of earth's gravitational field abbreviated as g.

Table 6.4: Relation between Relative centrifugal (g) force and revolution per minute (rpm)

Revolution per minute (rpm)	Centrifugal force (g)
500	2.795R
1000	11.18R
2000	44.72R
4000	178.88R
8000	715.52R
75000	62887.5R

The as-collected samples from all locations showed the dense light scattering path, which decreases with the increase of centrifugal force up to 4000 rpm (178.88 R). This is due to the separation of the large-sized components from the SS solution upon centrifugation.

Location / Size	Gomukh	Gangotri	Harsil	Maneri	Devprayag	Chiniyalisaur	Koteshwar	Bet. Hari & Rishikesh	Bijnor	Kanpur	Allahabad (Bef. Conflu.)
Actual											
500 RPM				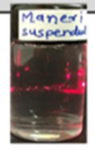							
1000 RPM											
2000 RPM											
4000 RPM	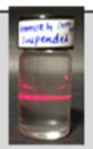										

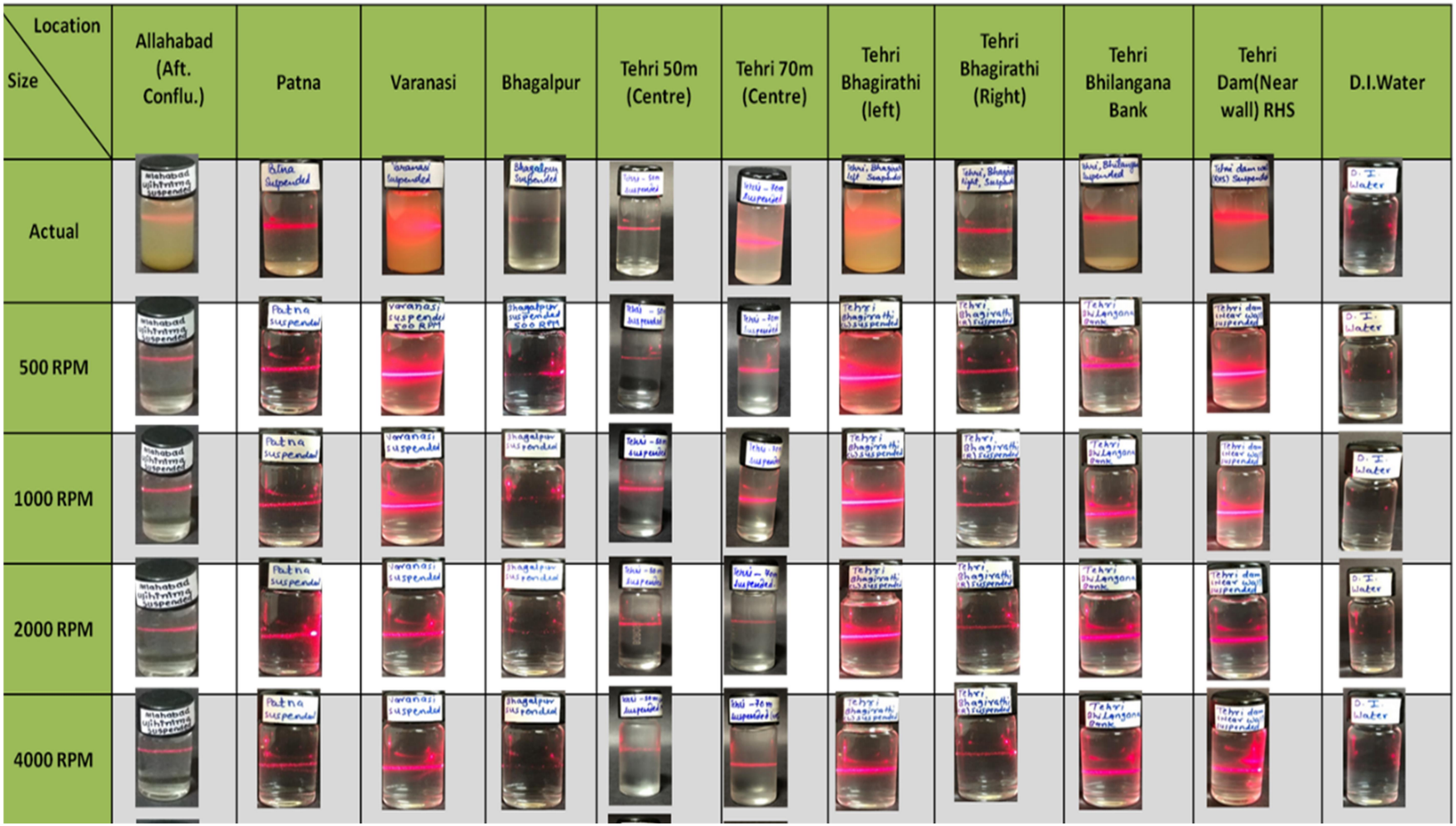

Fig. 6.7: Laser Light scattering of SS samples collected from various locations across River Ganga

Efforts were made to separate the suspended components further by ultra-high centrifugation at 75000 rpm (g = 62887.5 R). Figure 8 shows the comparison of the optical images taken before and after centrifugation at 75000 rpm of the suspended samples collected from Gangotri, Harsil, Maneri, and Tehri. It was observed from Figure 8 that the suspended colloidal particles in the sediment were settled down most likely at such a high centrifugal force, and therefore no light scattering path can be seen upon irradiation of laser light.

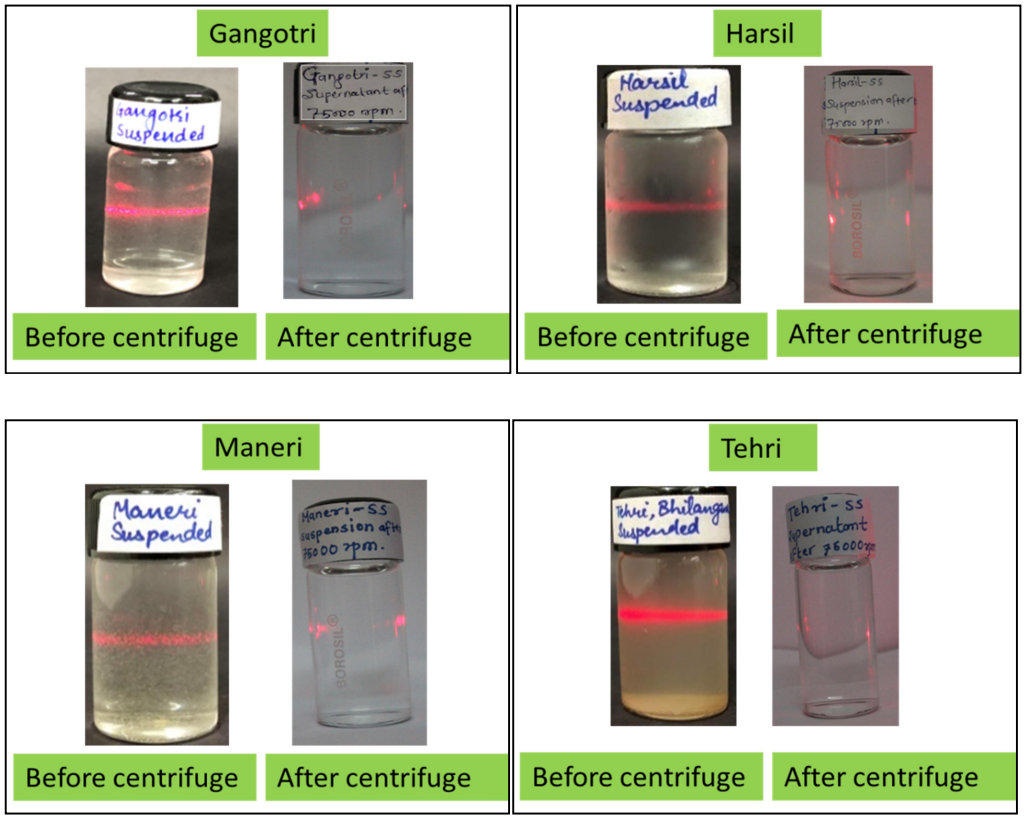

Fig. 6.8: Laser Light scattering of the SS samples before and after centrifugationat 75000 rpm

It is inferred from these results that suspended sediments are present in the samples as the light scattering path can be seen clearly upon irradiation of laser light. The large-sized suspended sediments were removed; however, a finer portion of the sediments wasn't removed upon centrifugation up to 4000 rpm as the light scattering path can be seen even after centrifugation. However, the finer portion of the suspended sediments was most likely removed completely upon centrifugation at 75000 rpm.

6.5.3 Dynamic Light Scattering (DLS) Analysis

DLS studies were used further to examine the average size of the SS in solution. Both as-collected SS samples and centrifuged samples were used to examine the average size of SS. It was observed that the average sediment size is in the range between 300 and 600 nm. The sediment size of the samples collected in most of the locations decreases with the increase of centrifugation up to 2500 rpm; however, it is increased again with the increase of centrifugation (3500 and 4500 rpm). It should be noted that the particle size is generally decreased with the increase of centrifugal force, which was not observed in the case of SS collected from the River Ganga (Figures 9 and 10). As can be seen in more detail in Figures 9 and 10, the average particle size (ZA) of the SS collected at Gangotri is decreased from 453.2 nm to 371.2 nm upon centrifugation up to 2500 rpm, which is, however, increased to 580.2 nm when the centrifugation is increased further up to 4500 rpm (Figure 9). A similar trend was also observed in the case of SS samples collected at Tehri (Figure 10) and other locations (Gomukh, Gangotri, Harsil, Maneri, Chinyalisaur, Devprayag, Bijnor, Kanpur,

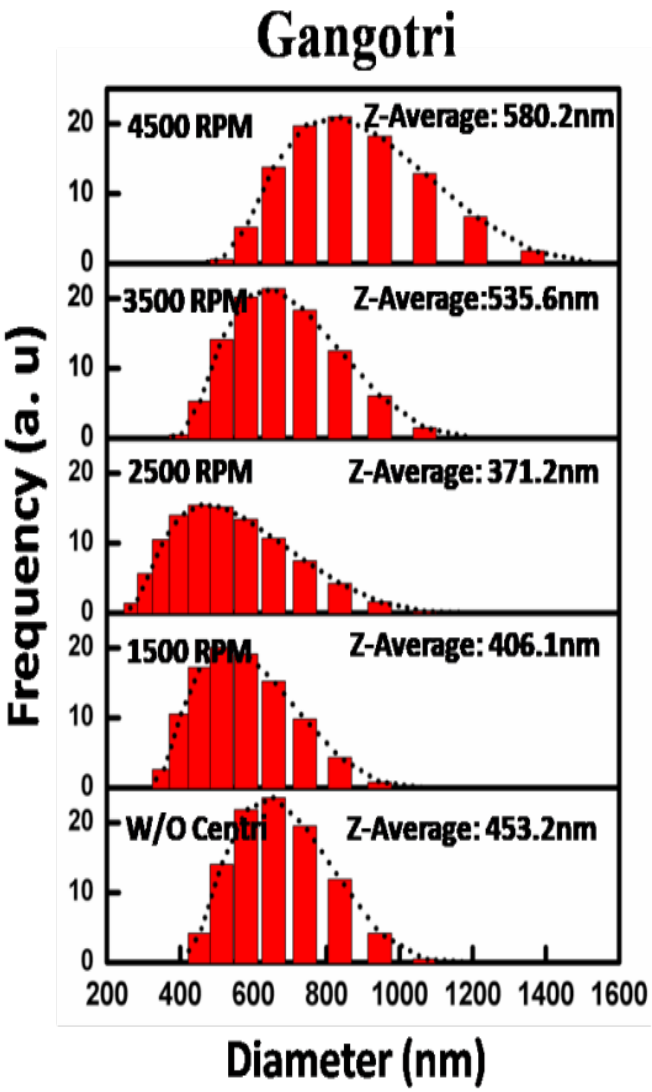

Fig. 6.9: Average particle size distribution (Z_A) of SS samples collected from Gangotri

Allahabad, Patna, Varanasi, and Phalapur). Although the possible attributes are not clear at present for this observed anomaly, the presence of amorphous and/or organic components along with the inorganic fractions in the SS samples may show this unusual behavior.

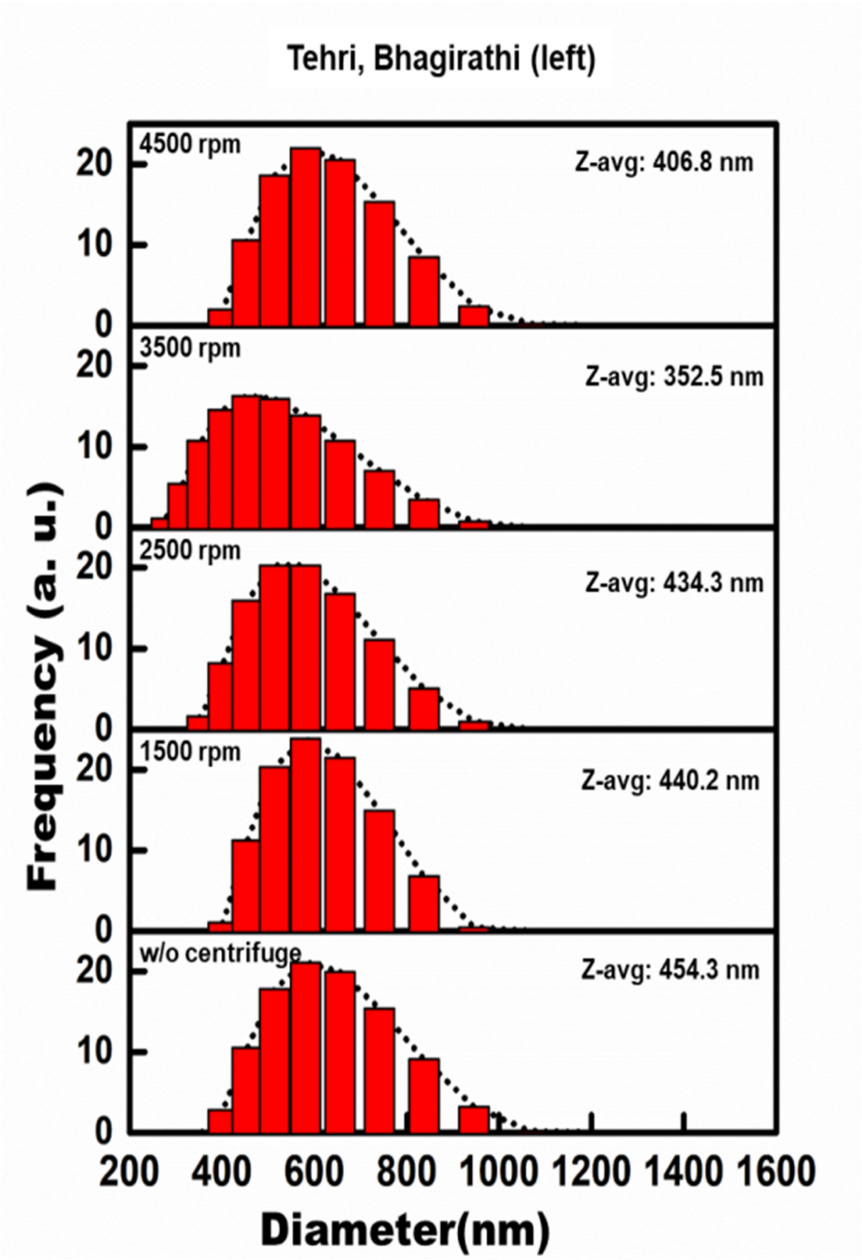

Fig. 6.10: Average particle size (ZA) of SS samples collected from Tehri left Bhagirathi stream

6.5.4 Zeta Potential Study

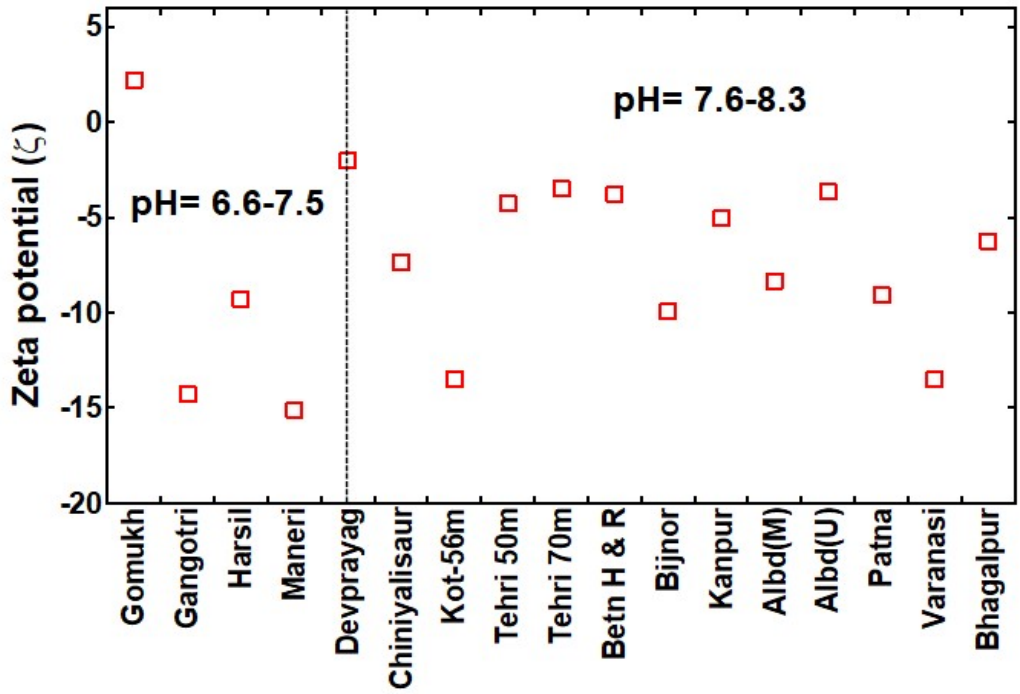

Fig.6.11: Zeta potential values for the samples collected from the whole stretch of River Ganga

Zeta potential is the difference between surface charges of the solid phase and mobile phase. The surface charge of the SS sample across the whole River stretch is observed between +5 and -15 mV. The Zeta potential value of Gomukh, Devprayag, Tehri, Between Haridwar and Rishikesh, Kanpur, and Allahabad are near neutral (Figure 11). Gangotri and Koteshwar Zeta potential values are fairly negative. Particles having surface charge values greater than ±35 mV form stable suspensions. However, the surface charge values of the SS samples collected were less than ±35 mV, hence, they will settle down at the bottom gradually which was observed in this case (reservoirs). Also, the surface charge values for the majority of the SS samples collected are near neutral values and are not at the extreme positive/negative side. Although the surface charge of the particles is relatively lower, the continuous flow of water in the Ganga River makes most of the fine particles will remain in the suspended form as evidenced from the laser light experiments.

6.5.5 Transmission Electron Microscopy (TEM)

TEM analysis of the as-collected SS and SS after centrifugation from the first stretch of the River Ganga was performed to understand the finer structures, morphology, size, and distribution. As-collected SS showed a mixture of large-sized, agglomerated sediments with different sizes, as shown in the TEM images (Figure 12). From the selective area electron diffraction (SAED) analysis, a fine spotted pattern with hexagonal symmetry (typical of alumina-silicate phases) was observed indicating polycrystalline particles in the suspension (Figure 12 (e)). In addition, the SS samples contain nano-sized crystalline solids as the fringes can be seen on the surface of the as-collected sediments (Figure 12 (f-i)).

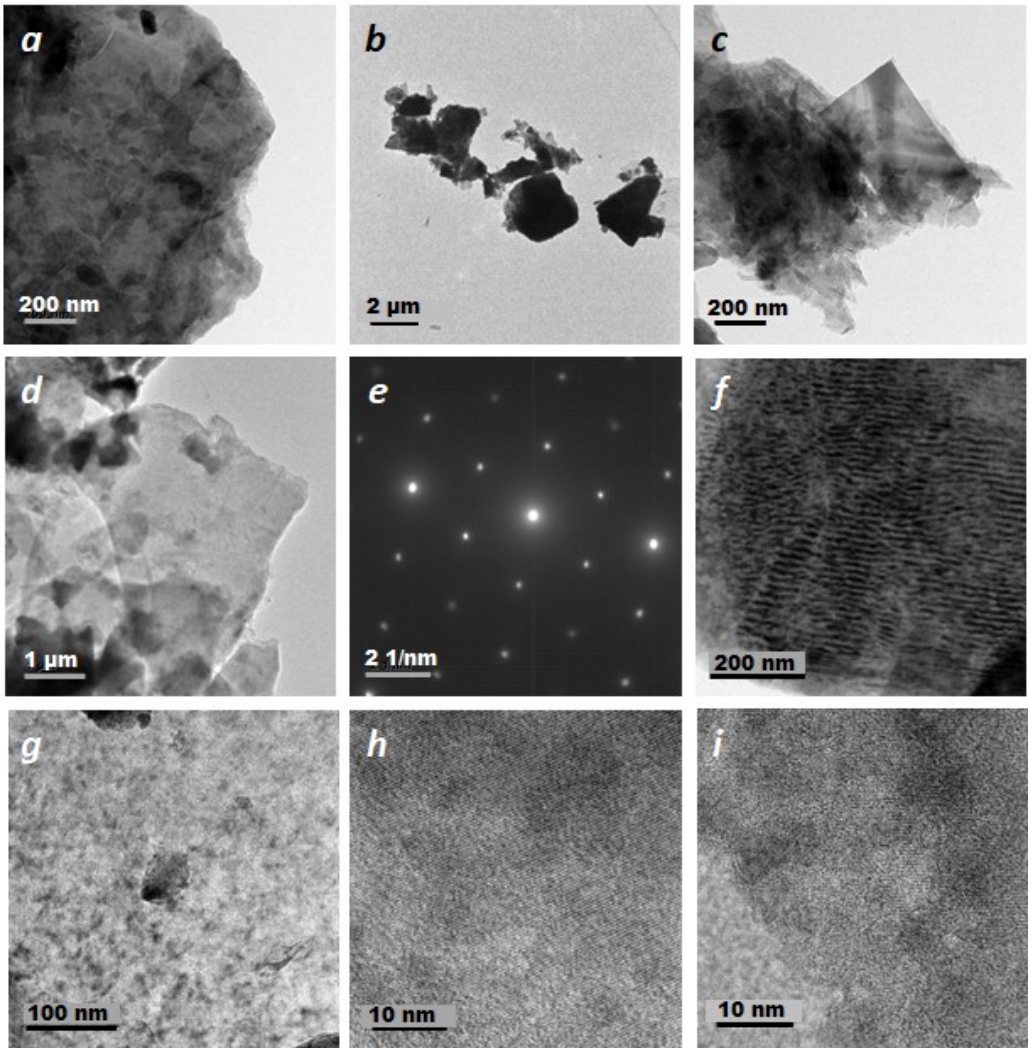

Fig. 6.12: TEM images of the as-collected SS samples collected from Gomukh

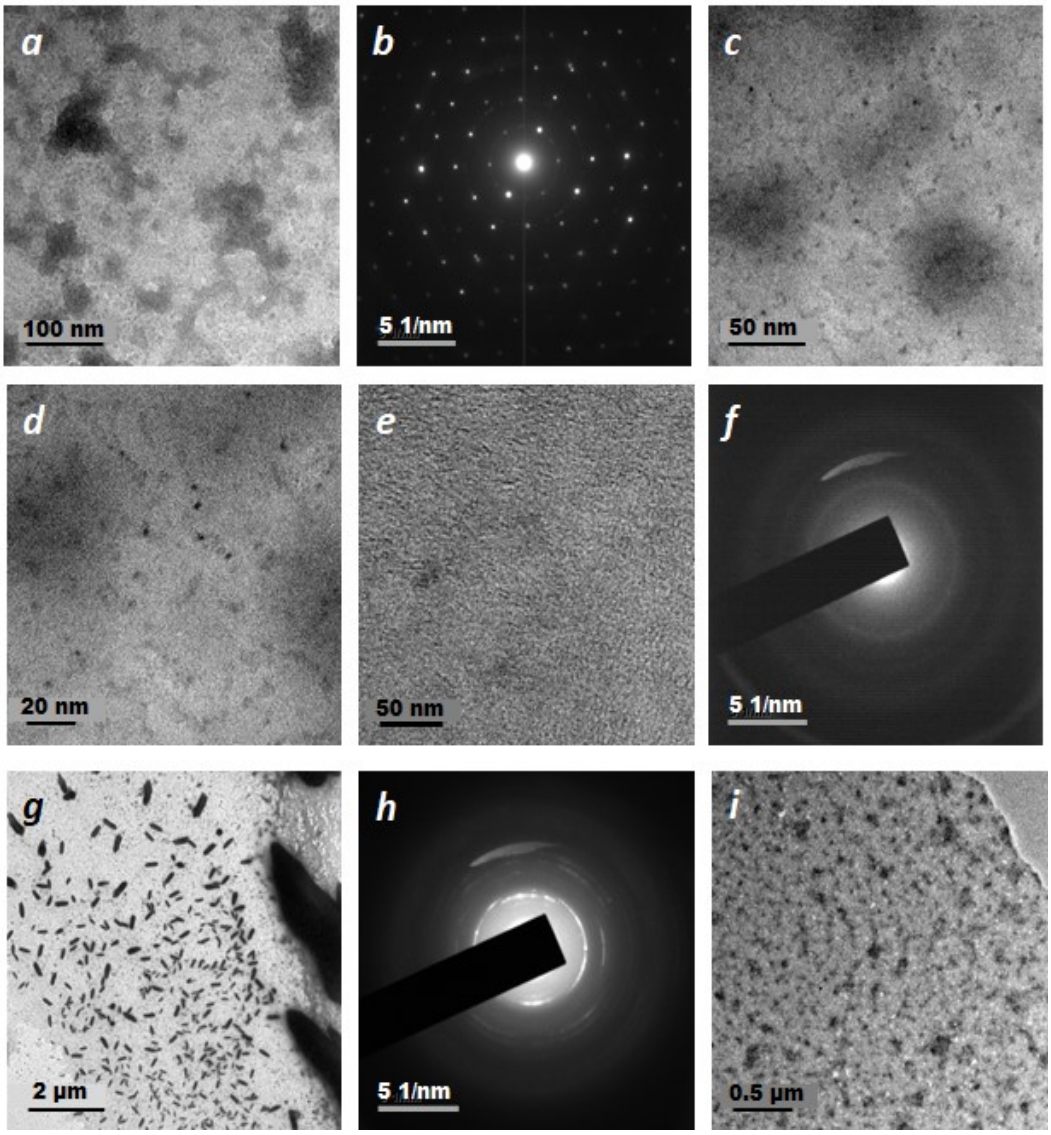

Fig 6.13: TEM images of the SS sample collected from Gomukh after centrifugation

The TEM analysis of the SS samples after centrifugation (8000 rpm) was performed to see the morphology, size, and distribution. It was found from Figure 13 (a-d), that relatively smaller-sized crystalline solid, single-crystalline thin sheets, etc., were observed after centrifugation of the as-collected sediment samples. In addition, highly mono-dispersed, nano-sediment particles with crystalline-like structures (Figure 13 (c-d)) were also observed in the case of centrifuged samples as the surface of these particles showed ordered structures. Apart from this, rod-like sediments having polycrystalline structures along with most likely volatile matters (e.g., organic

moieties) were also observed in the case of SS after centrifugation, as shown in Figure 13 (f-g). Moreover, homogeneously dispersed, amorphous-like nano-sediments were also present in the SS after centrifugation as no fringes and SAED patterns were observed when an electron beam was subjected to the select area of the sediment samples.

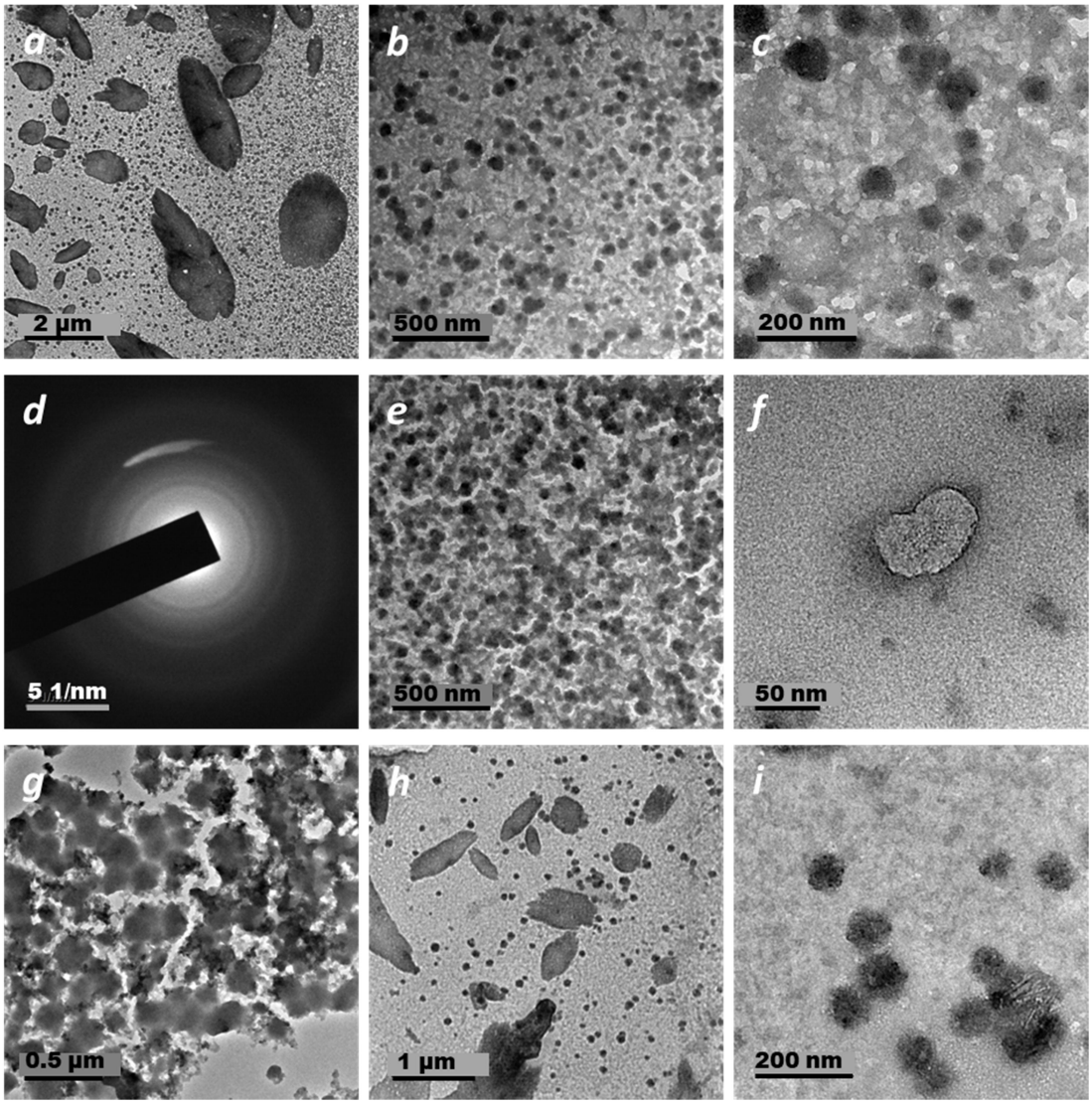

Fig. 6.14: TEM images of the SS samples collected from Gangotri without centrifugation

Similarly, the SS collected at Gangotri showed large-sized semi-elliptical and semi-spherical-shaped sediments (Figure 6.14a). In addition, the SS also contains

homogeneously dispersed nano-sediments, as shown in Figure 6.14b. It was found that these nano-sediments are polycrystalline structures as they showed a ring SAED pattern (Figure 6.14d). Some portions of the sediments contain volatile matters as they are burnt upon the subjection of an electron beam (Figure 6.14f). The spherical-shaped sediments contain a large number of nanoparticles that are agglomerated along with organic moieties.

The SS solution after centrifugation showed relatively smaller-sized thin sheets, rods, tubes, and agglomerated sediments having various shapes having crystalline structures. Interestingly, nano-sediments dispersed bacterial-like structures are also found in the SS after centrifugation, and they are amorphous. (Figure 6.15)

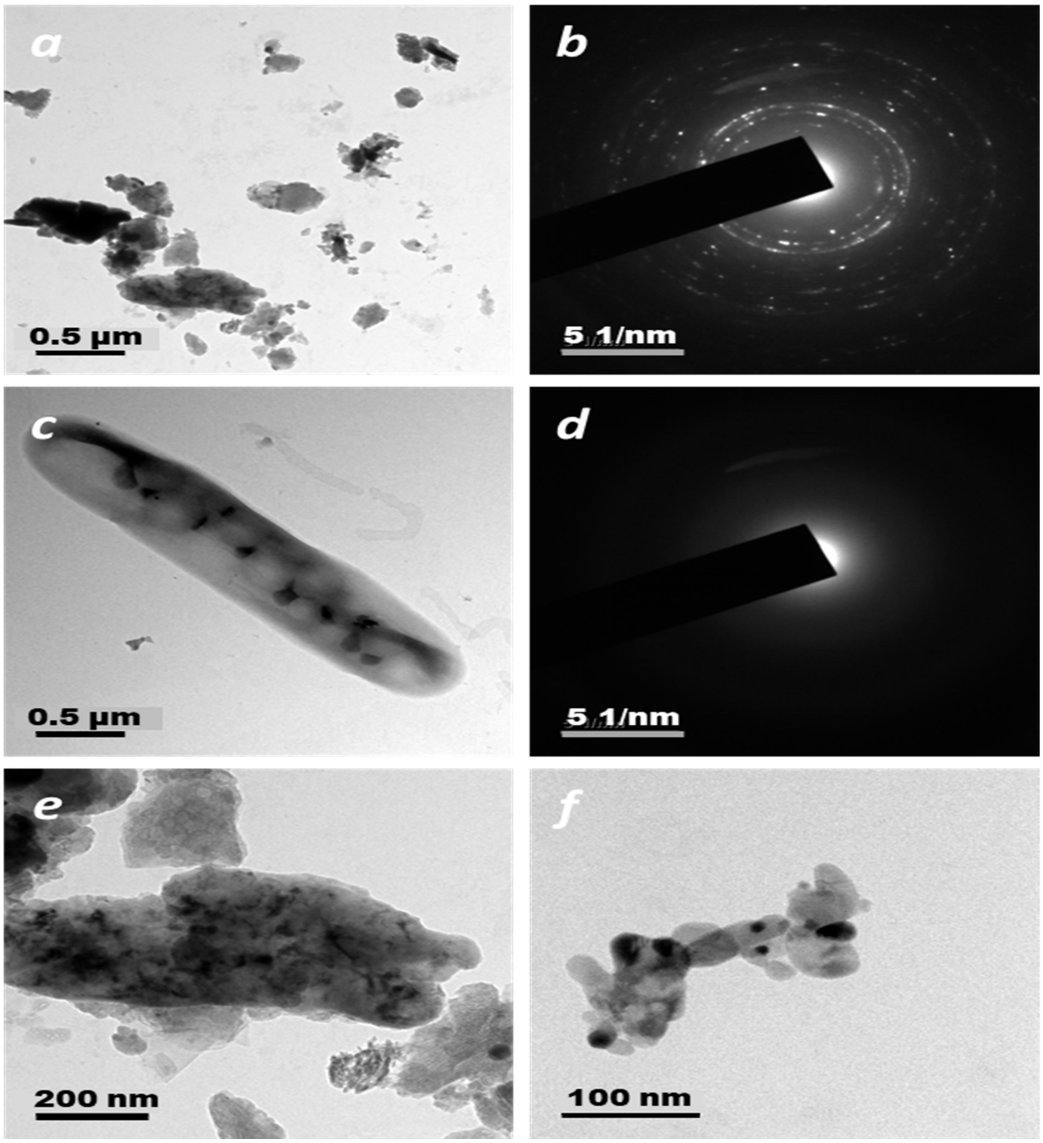

Fig. 6.15: TEM images of SS sample collected from Gangotri after centrifugation

Long-range agglomerated sediments having polycrystalline structures, fiber- as well as needle-like sediments, homogeneously dispersed semi-spherical shaped nano-sediments, etc., were observed in the case of as-collected SS at Koteshwar. (Figure 6.16)

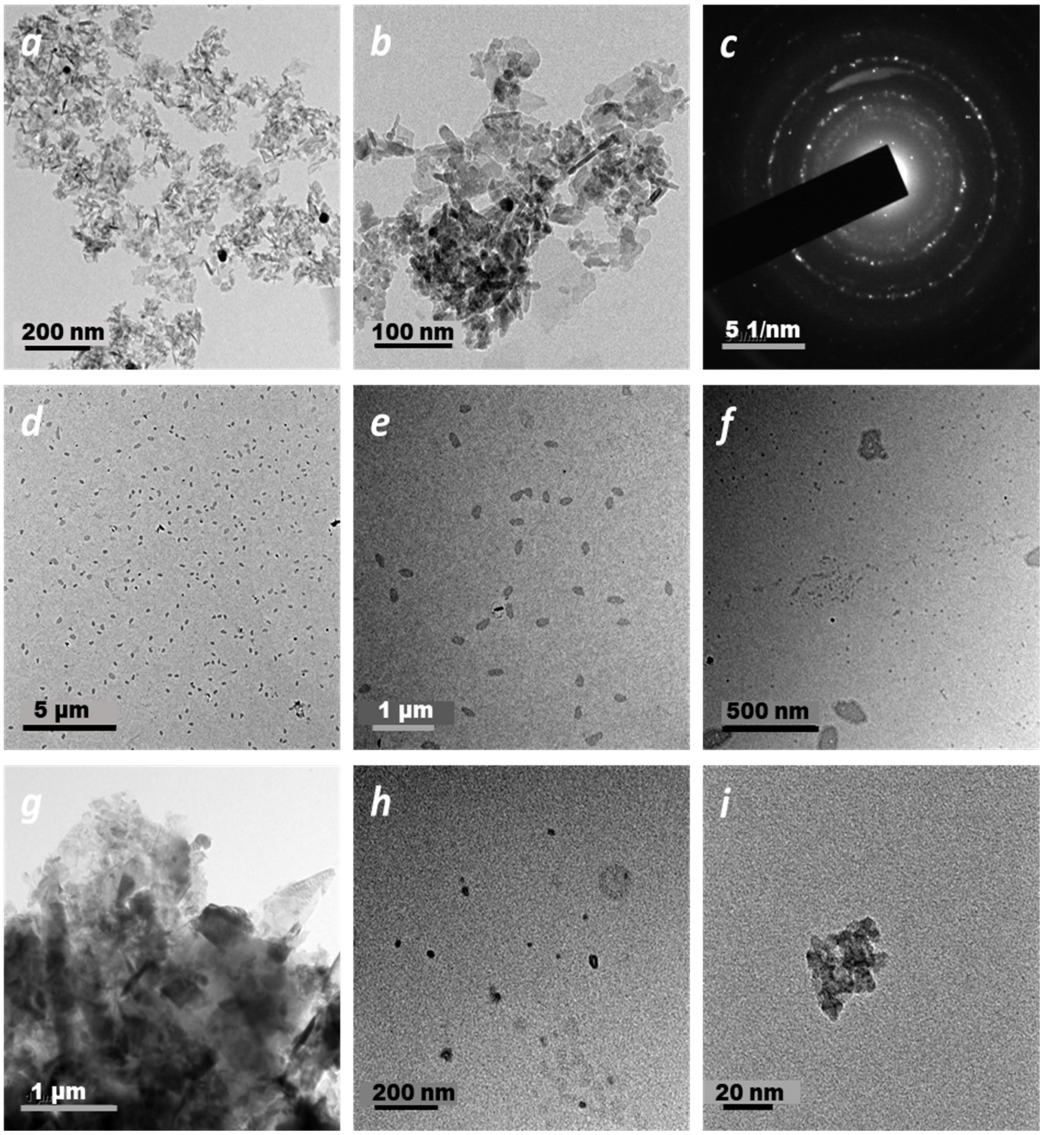

Fig. 6.16: TEM images of SS sample collected from Koteshwar without centrifugation

Nano-sediments with various definite shapes and crystalline structures were also found in the case of SS after centrifugation. Long-range amorphous tubes, as their

surface didn't show any SAED patterns, long-range roads with crystalline structure, homogenously dispersed nano sediments were also found in the case of SS after centrifugation. Interestingly, homogeneously dispersed, core-shell sediments with the elliptical structure were also observed in the sediments after centrifugation collected at Koteshwar. (Figure 6.17)

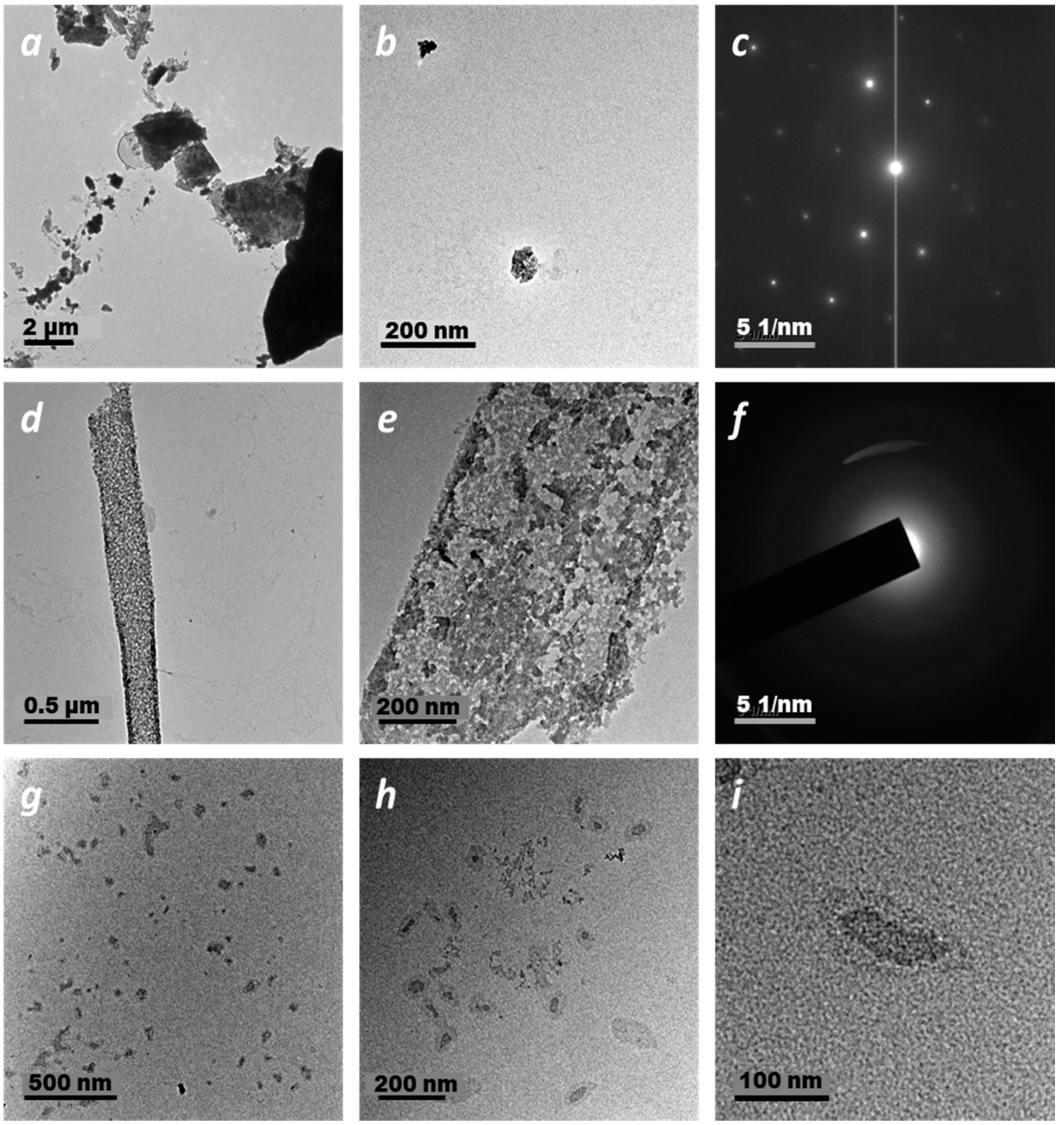

Fig. 6.17: TEM images of selected SS samples collected from Koteshwar after centrifugation

Evenly distributed, long-range fiber-like structures, nano-sediments without any definite shapes, however, having a polycrystalline structure, homogeneously

distributed nano-sediments, crumpled-like shape sediments having micron size order, etc. are present in the sediments collected at 50 m from Tehri reservoir. (Figure 18).

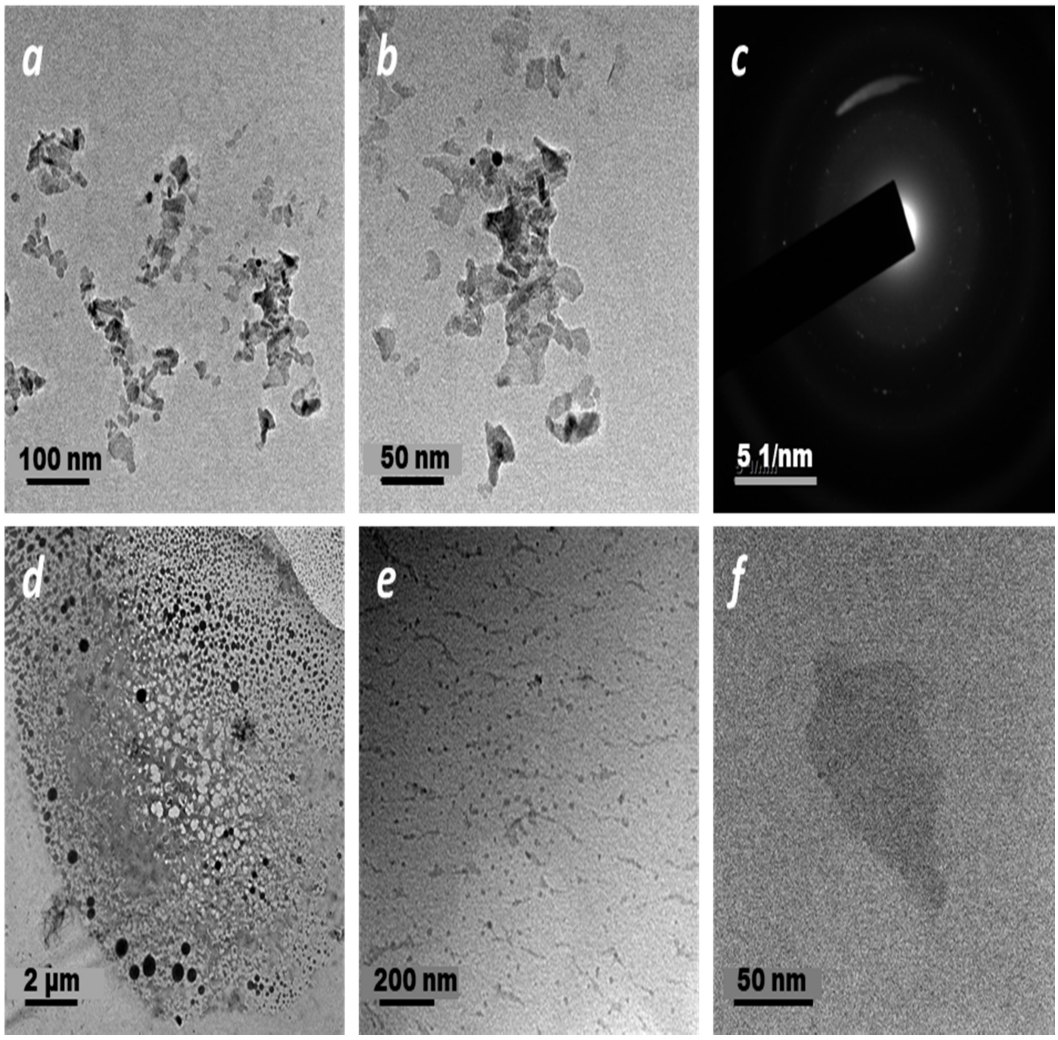

Fig. 6.18: TEM images of SS sample collected from Tehri 50m depth without centrifugation

Homogeneously distributed semi-spherical nanoparticles, long-range spherical nanoparticles that interacted with other particles, etc., were observed when the sediment samples were studied after centrifugation (Figure 6.19). Amorphous-like sediments with needle-type structures were also observed in the case of SS after centrifugation. Surprisingly, nano-particles embedded as well as nanoparticles (size: 5-10 nm) dispersed bacterial systems were also observed in this case (Figure 6.19 c-f).

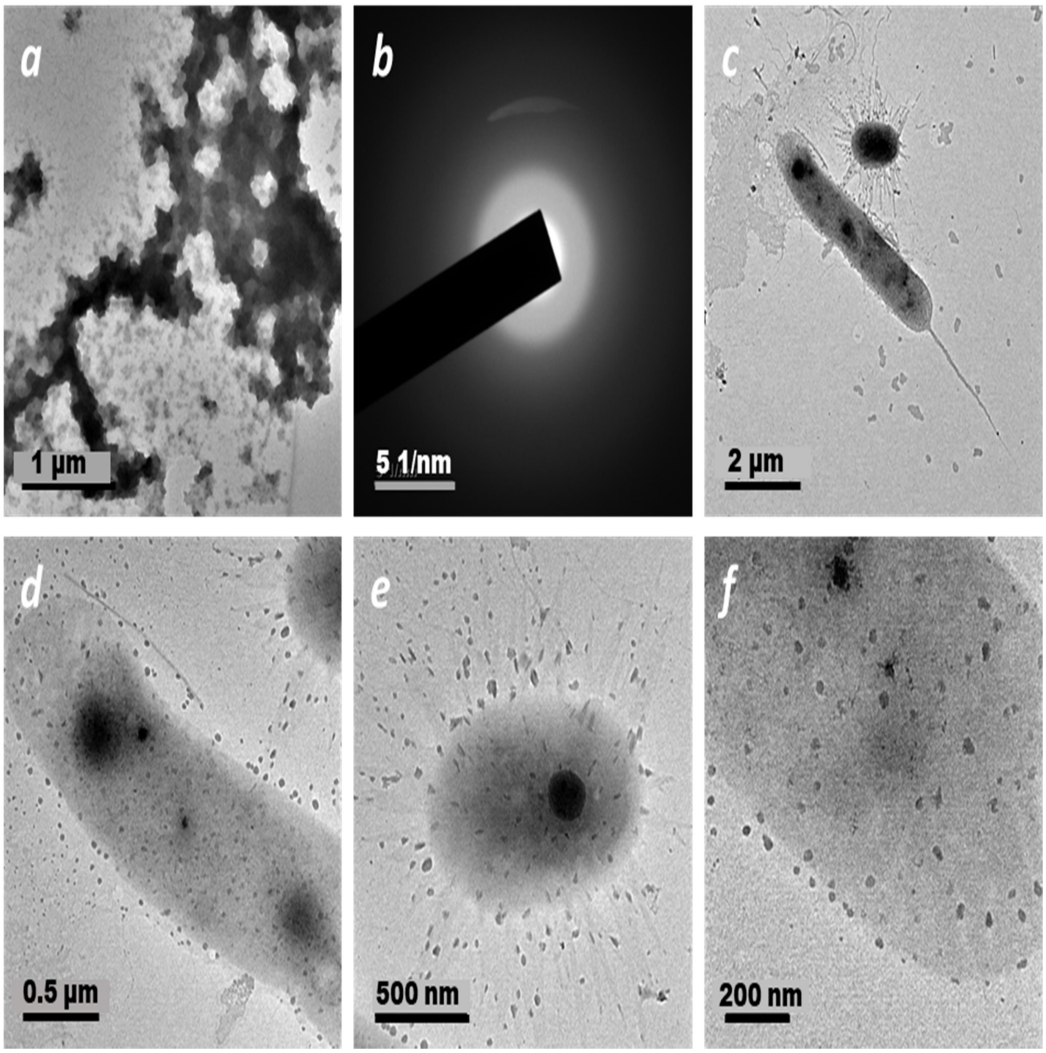

Fig. 6.19: TEM images of SS sample collected from Tehri 50 m depth after centrifugation

The SS sediment samples collected from Tehri at 70 m depth after centrifuge showed a highly crystalline, ordered filamentous structure as observed from Figure 6.20. The SEAD pattern shows the polycrystalline nature of a few filamentous samples. Some organic-like particles are also present in the sample which shows homogenous distribution throughout the SS sample.

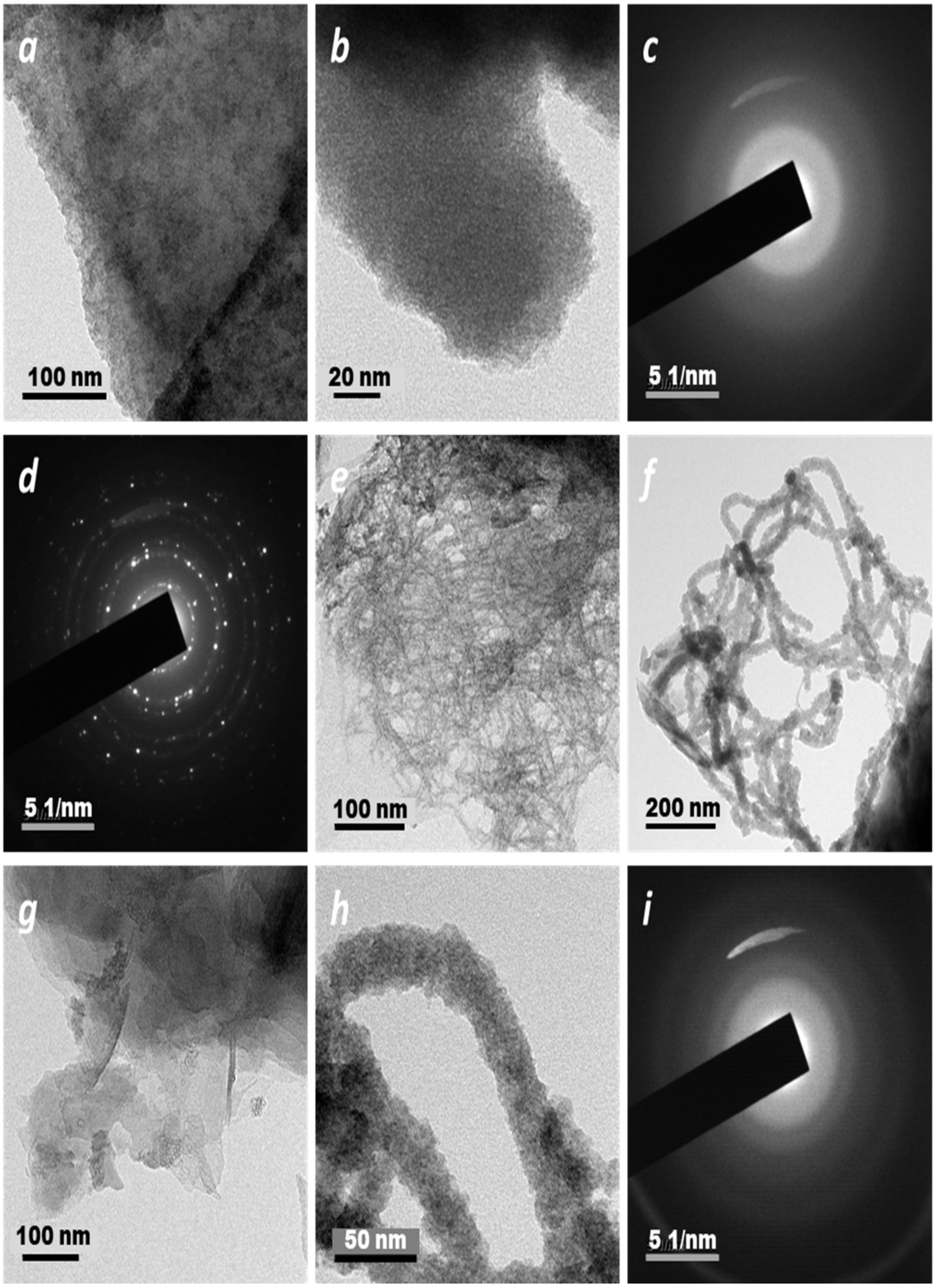

Fig. 6.20: TEM images of SS sample collected from Tehri 70 m depth without centrifugation

Further, highly crystalline sediments and amorphous-like ordered filamentous structures were observed in the case of SS collected at 70 m of Tehri reservoir. Highly dispersed, nanoparticles embedded amorphous or organic moieties were also present at 70 m depth of the reservoir. Long-range, interconnected spherical nanoparticles formed most likely under high pressure at a depth level of 70 m, which contains organic-like moieties, were also present in the samples. Highly crystalline sediments with various definite shapes and sheet-like structures were also observed in the case of SS collected at 70 m (bottom of the water body) of Tehri reservoir. (Figure 6.21)

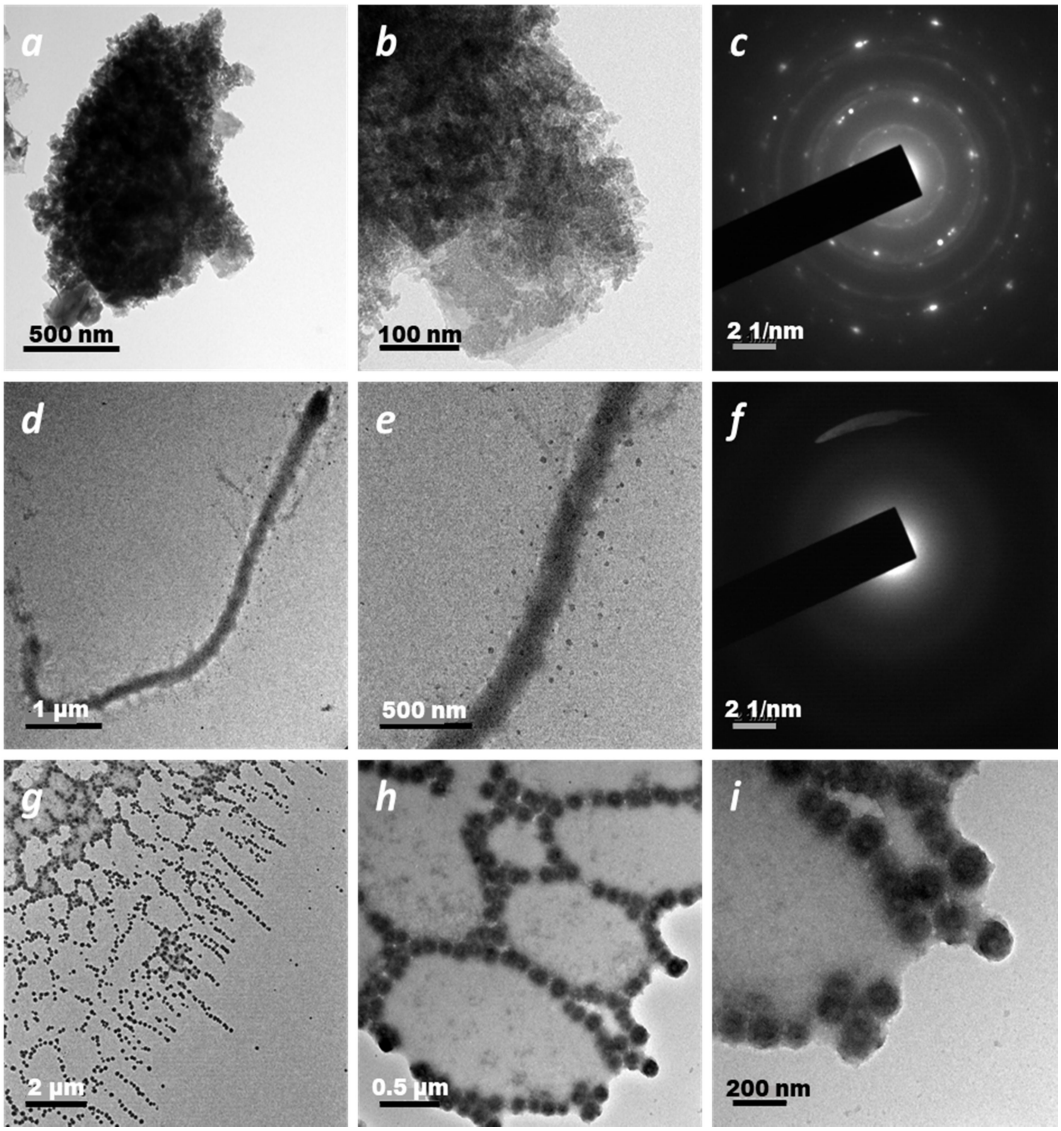

Fig. 6.21: TEM images of SS sample collected from Tehri 70 m depth after centrifugation

The as-collected Chinyalisaur SS contains mostly needle-like structures, as shown in Figure 6.22. In addition, needle-like structures embedded semi-spherical sediments were also observed in the SS solution. After centrifugation, the sample showed spherical shaped nano-sediments containing volatile matters, and ultra-high dispersion of nanoparticles was also found in the case of SS collected from Chinyalisaur. Such peculiar observations, however, may be limited to the collected sample and cannot be generalized although efforts were made to collect the representative sample to some extent from a very large mass of sediments present at almost every sample site.

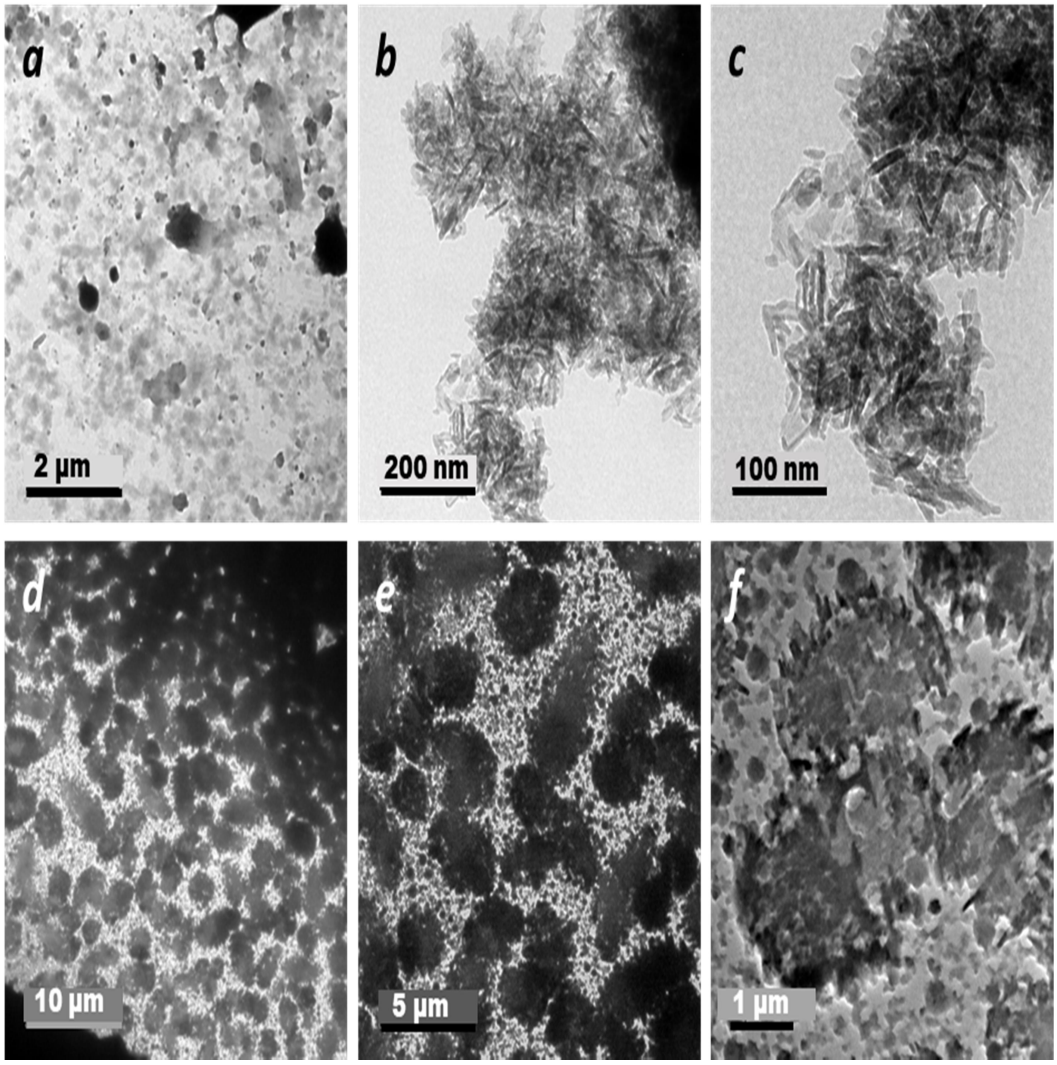

Fig. 6.22: TEM images of SS sample collected from Chinyalisaur without centrifugation

The SS sample collected from Chinyalisaur after centrifugation at 8000 rpm (Figure 6.23) shows a very homogenous distribution of fine particles. The particles show spherical morphology containing an uneven distribution of organic matter and volatile matter.

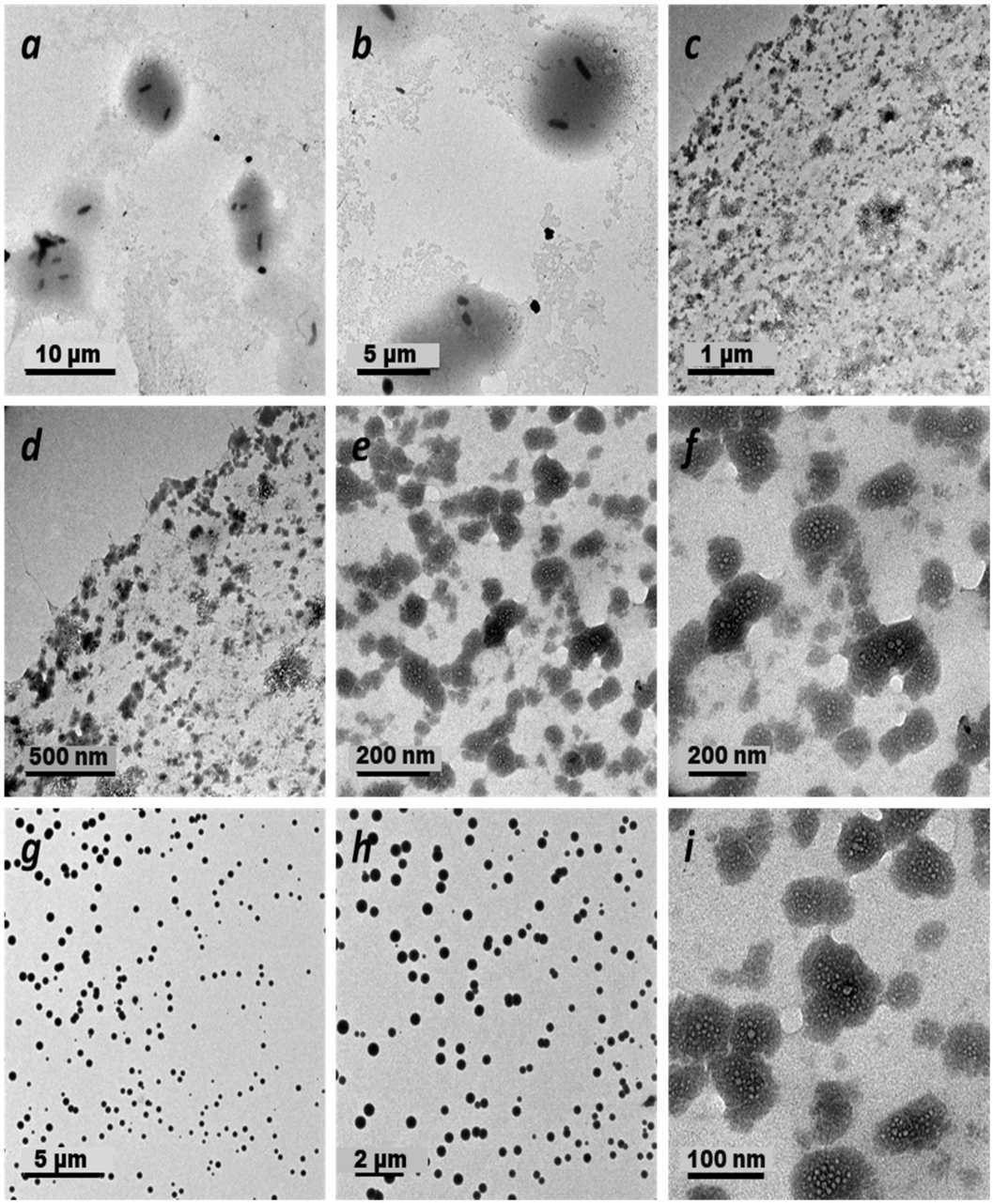

Fig. 6.23: TEM images of SS sample collected from Chinyalisaur after centrifugation

The histogram profile of the SS sample collected from Chinyalisaur after centrifugation shows particle size distribution. The particle size is in the range between 150 and 650 nm with an average particle size centered at around 450 nm. The TEM observation is consistent with DLS data, where Z-average is in the range between 200 and 600 nm (Figure6.24)

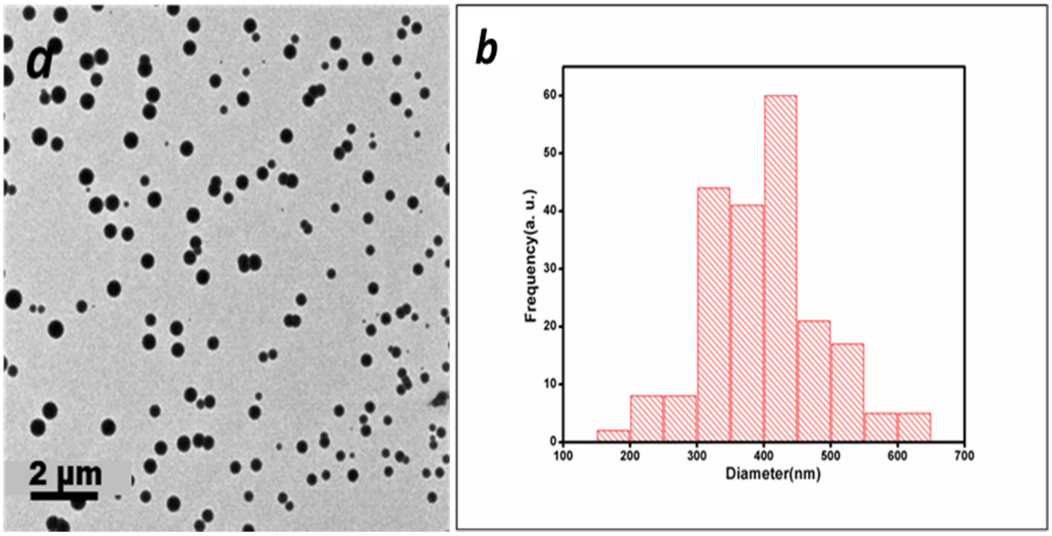

Fig 6.24: (a) TEM images of samples collected from Chinyalisaur after centrifugation. (b)Histogram profile of the particles of sample collected from Chinyalisaur after centrifugation

The TEM analysis of various sediments collected from the first stretch (Gomukh to Haridwar and Rishikesh) of the River Ganga showed that the SS are having a single and polycrystalline ordered structure which is in nano order. These nano suspended sediments are highly dispersed containing rod-like sediments along with most likely volatile matters (e.g., organic moieties). Interestingly nano sediments dispersed as well as embedded microbial-like structures are also found in the SS and they are amorphous. The as-collected SS from Koteshwar showed fiber- and needle-like structures. Long-range amorphous tubes, as well as rods, were observed in the SS samples after centrifugation at 8000 rpm as they didn't show any SAED pattern on their surface. Also, nanoparticles (5-10 nm) embedded microbial systems were observed when the SS samples were collected at the Tehri reservoir at 50 m. Long-

range interconnected spherical shaped organic moieties were observed in the SS samples collected at 70 m depth at Tehri reservoir.

It is a well-known fact that nanoparticles can show antimicrobial properties. Silver (Ag) nanoparticles, the most common and the widely exploited element, showed promising results towards multi-drug resistant microorganisms, which can kill them effectively. Metal and metal oxide nanoparticle exerts a varying degree of antimicrobial effect against microorganisms influenced by the metal involved. The antimicrobial property of nanoparticles depends on various parameters, one of the most important among them is the size of nanoparticles. A comparative study showed that smallest-sized silver nanoparticles (20 nm) have greater antimicrobial potential than that of their larger counterparts (50 nm) [27]. [28,29,30]. Gold colloidal particles [31,32], Copper, Zinc oxide, hematite (α-Fe2O3) [33], Titanium dioxide particles are reported to exhibit size-dependent antimicrobial activity, the anatase phase of Titania was investigated for this purpose. It was observed that titania nanoparticles having the particle size of 350-500 nm in dispersed solution inhibit the growth of several pathogens including E.coli, S.aureus, P.aeruginosa, C.albicans, and B.subtilis. The Minimum Inhibitory Concentration (MIC) for the Titania nanoparticles was found as low as 9.7 µg /ml for E. coli [34]. Furthermore, natural clays having particle size < 200 nm are very effective against microorganisms and are being used from ancient times as medicine to treat skin diseases [35]. The size-dependent antibacterial activities of three minerals, Alkali feldspar, Calcite, and Stibnite (without impurities) were examined against E. coli and S. aureus. The clay samples collected were ground into fine-sized fractions namely bulk, ball-milled, and nanosized with a particle size range of 500-2000 nm, 50-500 nm, 20-200 nm respectively. the minimum inhibitory concentration (MIC) for nanosized alkali feldspar and calcite mineral against E. coli and S. aureus was 0.8 and 0.6 mg/ml respectively [38]. This suggests that these minerals containing Na, Ca, K, Al, Si, etc. possess antimicrobial properties in nature. The plausible augmentation for bacterial cell mortality is the gradual increase of the Reactive Oxygen Species (ROS) as well as superoxide production from the bulk to a nanosized fraction. The finer mineral fraction can easily penetrate the bacterial cell membrane to reach the nuclear content of the cell causing the oxidation of cell organelles signifying the bacteriostatic effect of finer samples. Similarly, layered

Magnesium (Mg) minerals, Brucite (Mg(OH)2), Talc (Mg3Si4O10(OH)2), and Sepiolite (Mg4Si6O16(OH)26H2O) were examined for their antimicrobial, bacteriostatic, and bactericidal activity. Brucite and Talc acted as a bactericide for E. coli at 24 and 48 h with MIC of 20 µg/ml. the specific structural factors and availability of Mg of Brucite and Talc explain their bactericidal activity but not of Sepiolite. The study also reports the importance of microbial cell membrane composition while the surface charge plays a lesser role since the brucite layered structure is neutral [39]. Along with the reported results, these findings from the TEM analysis revealed that the presence of various nanoparticles along with ordered- as well as amorphous-like structure in the SS samples may influence the microbial systems upon contact, which may be corroborated to the non-putrefying property of River Ganga.

It is comprehensible from the above literature that the size of particles is an important factor to determine the antimicrobial properties of the nanomaterial. The suspended particles present in collected samples exhibit hydrodynamic particle size of nanometres range and are comprised of commonly found metallic elements. In correlation to the above discussion, the ZA value obtained for samples collected from the first stretch of the Ganga River is 400-600 nm, which can be expected to show antimicrobial activity. The finer sediment fraction was obtained at Tehri and hence can be expected to show a better antimicrobial property. Samples collected from the Tehri reservoir showed the highest antimicrobial potential as shall be discussed later. The toxicity of metallic nanoparticles depends upon the metal content of the material and accordingly, the mechanism of antimicrobial activity varies; some nanoparticles may cause toxic response directly at the cell membrane by their cellular uptake (MgO, Ag, ZnO) or by the release of dissolved metals in the solution from the surface. The generation of reactive oxygen species (ROS) leads to oxidative stress causing the damage of intracellular organelles, which in turn kills the microorganisms [36]. Despite the varying metallic content of nanoparticles, the common element among them is their small size, highly exposed surface area compared to the particle volume; hence, the metallic nanoparticles show size-dependent antimicrobial activity as the smaller-sized particles have a larger number of exposed surface particles.

6.5.6 X-Ray Diffraction (XRD)

XRD analysis of the sediments collected from the Ganga River was performed to understand their phases/mineral distribution. It was observed that the minerals/phases present in the first stretch of the Ganga River are significantly different from that of the second and third stretches. Also, they are very much different in the finer sediment fractions (25 and 53 µm) compared with that of the coarse sediment grains (500 µm). Table 6.5 shows the common mineral phases along with their chemical composition found at Gangotri for 25 µm sediment fraction. The minerals of potassium feldspar, muscovite, orthoclase, microcline, etc. are commonly found in the entire stretches of River Ganga. In addition, sodium-, potassium- and calcium aluminosilicates- are also found across the River Ganga.

Table 6.5: Composition of mineral phases found in p-XRD profile of sediments at Gangotri

Mineral phase found at Gangotri	Chemical composition
Merlinoite	K4.2Ca1.5Na0.6Ba0.4Fe2+0.2Si22.7Al9.3O64·22.7(H2O)/K5Ca2 (Al9Si23O64) ·24H2O/JCPDS no: 029-0989
Anorthite	NaAlSi3O8/Na.25Ca.71 (Al2Si2O8)/JCPDS no: 01-078-2330
Orthoclase	KAlSi3O8 /JCPDS no:01-075-1592
Feldspar	K2O,3Na2O,4Al2O3,8SiO2/ (K.871Na.120Rb.008Al0.94Si3.06O8)/JCPDS no: 01-076-0826
Albite	NaAlSi3O8 / (Na0.84Ca0.16) Al1.16Si2.84O8 /JCPDS no: 01-076-0927
Muscovite	KAl2(AlSi3O10) (FOH)2/(KF)2(Al2O3)3(SiO2)6(H2O)/JCPDS no:01-082-2450
Microcline	KAlSi3O8/JCPDS no: 019-0932
Quartz	SiO2

Table 6.6: Distribution of mineral phases obtained from pXRD analysis of 25 µm sediment fraction at the first stretch of River Ganga

Sample locations	25 µm																							
	Phases Identified																							
	Quartz	Microcline	Albite	Muscovite	Pot. Feldspar	Merlinoite	Cristobalite,syn	Anorthoclase	Anorthite	Nosean	Birnessite,syn	Sanidine,high,syn	Clinochlore-1	Dolomite	Xonotlite	Riebeckite	Rankinite	Gismondine	Ferrietite	Silica	Mallis Clay	Orthoclase	Silicon Oxide	Clinoenstatite
Gomukh	+	+	+	+	+	+	-	-	-	-	-	+	-	-	-	-	-	-	-	-	-	-	-	-
Gangotri	+	+	+	-	-	-	+	+	+	+	-	+	-	-	-	-	-	-	-	-	-	-	-	-
Harsil	+	+	+	+	-	-	-	-	-	-	+	+	-	-	-	-	-	-	-	-	-	-	-	-
Maneri	+	+	+	+	-	+	-	-	+	-	+	+	-	-	-	-	-	-	-	-	-	-	-	-
Devprayag	+	-	+	+	-	-	-	-	-	-	-	-	+	+	+	-	-	-	-	-	-	-	-	-
Chiniyalisaur	+	-	+	-	-	-	-	-	-	-	-	-	+	-	-	+	+	+	+	-	-	-	-	-
Bewtn Hari & Rishi	+	-	+	-	-	-	-	-	-	-	-	-	-	-	-	-	-	-	-	+	+	+	-	-
Bijnor	+	-	+	+	-	-	-	-	-	-	-	-	+	+	-	-	-	+	-	-	-	-	+	+
Kanpur	-	-	+	+	-	-	-	-	-	-	-	-	-	-	-	-	-	-	-	+	+	+	-	-

Table 6.6 shows the location-wise minerals present in the sediment samples having 25 µm fractions. The common minerals, e.g., quartz, Albite, muscovite, silica, etc., are found consistently across the first stretch of River Ganga.

Table 6.7: Composition of mineral phases obtained from pXRD analysis of the sediment samples

Mineral phase	Chemical composition
Clinoenstatite	Mg2Si2O6
Silicon Oxide	SiO2
Orthoclase	KAlSi3O8 /JCPDS no:01-075-1592
Mallis Clay	Ca - Mg - Al - Si – O/Calcium magnesium aluminium silicate/JCPDS no: 003-0418
Silica	SiO2
Ferrietite/ Ferrierite	(Na,K)2Mg(Si,Al)18O36(OH) 9H2O /(H18Na2O45Si18)/(Na , K , Mg)2, (Si , Al)18O36 ·9H2O)/JCPDS no:022-1238
Gismondine	CaAl2Si2O. 4(H2O)/JCPDS no: 020-0452
Rankinite	Ca3Si2O7 /JCPDS no: 022-0539
Riebeckite	Na2(Fe2+3Fe3+2) Si8O22(OH)2. (Na2Fe3Fe2Si8O22 (OH)2)/JCPDS no: 009-0436
Xonotlite	Ca6Si6O17(OH)2/Ca6Si6O17 (OH)2/JCPDS no:01-072-2396
Dolomite	CaMg(CO3)2/JCPDS no: 005-0622
Clinochlore-1	Mg3.75Fe2+1.25Si3Al2O10(OH)8 ((Mg, Fe, Al)6 (Si, Al)4O10 (OH)8) JCPDS no: 016-0362
Sanidine, High syn	K(AlSi3O8)/JCPDS no: 010-0353
Birnessite, syn	Na0.3Ca0.1K0.1Mn4+Mn3+O4•1.5(H2O)/K0.46Mn1.54Mn0.46O4(H2O)1.4/JCPDS no: 01-080-1098

Nosean	Na8Al6Si6O24(SO4). H2O/Na8Al6Si6O24SO4/JCPDS no: 01-073-1734
Anorthite	NaAlSi3O8/Na.25Ca.71 (Al2Si2O8)/JCPDS no: 01-078-2330
Anorthoclase	Na0.75K0.25AlSi3O8/ (Na, K) (Si3Al) O8/JCPDS no: 009-0478
Cristobalite, Syn	SiO2/JCPDS no: 039-1425
Merlinoite	K4.2Ca1.5Na0.6Ba0.4Fe2+0.2Si22.7Al9.3O64·22.7(H2O)/K5Ca2(Al9Si23O64) ·24H2O/JCPDS no: 029-0989
Pot. Feldspar	K2O, 3Na2O, 4Al2O3, 8SiO2/ (K.871Na.120Rb.008Al0.94Si3.06O8)/JCPDS no: 01-076-0826
Muscovite	KAl2(AlSi3O10) (FOH)2/(KF)2(Al2O3)3(SiO2)6(H2O)/JCPDS no:01-082-2450
Albite	NaAlSi3O8 / (Na0.84Ca0.16) Al1.16Si2.84O8 /JCPDS no: 01-076-0927
Microcline	KAlSi3O8/JCPDS no: 019-0932
Quartz	SiO2

Table 6.7 shows the minerals/phases obtained from the pXRD analysis of all the sediment samples collected from the entire stretches of the River Ganga. Silicon-based minerals/phases are found majorly from the pXRD analysis. Some mixed metal and a few iron-based oxides are also identified in trace quantities from the XRD analysis. Aluminum-, calcium-, sodium-, potassium- and magnesium-based minerals are very commonly found in the river sediment, as noted in Table 7. The sediment characteristics are dependent on the mineral ores present in a particular geographical location, and they vary significantly from one region to another. Hence, the minerals/phases found in the sediment samples are different considerably from the first stretch and other stretches. In addition to the commonly found aluminosilicate minerals, which generally show no microbial activity, however, Fe-, and manganese (Mn) (Riebeckite, Clinochlore-1, Clinoenstatite, Birnessitesyn, etc.) based minerals are also found, which are having variable oxidation states that may influence the microbial activity. It should be noted that clay and minerals have been used as remedies for various human diseases. Recently, a few studies were carried out using specific mineral phases to verify the antimicrobial potential of the minerals due to the continuous rise in the number of multidrug-resistant microorganisms. For this purpose, clay samples were collected from five different locations in Ghana that were tested for their antimicrobial potential against nine different pathogens namely P. aeruginosa, E. faecalis, C. albicans, E. coli, B. subtilis, S. typhi, S. aureus, K. pneumoniae, S. pneumoniae. It has been found that the leachates of the clay samples collected from various locations exhibit antimicrobial potential against these pathogens. Some of the clay samples (collected from Sogakope) exhibit antimicrobial potential against all these pathogenic organisms, while other samples collected from Keta, Anloga, Half-Assini, and Savietula prevent the growth of at least one of the test microbes. It has also been shown that the presence of Fe, Cu, Ni, Zn, etc. in the clay samples show significant bactericidal activity in in vitro studies, along with the pH of clay samples [37]. The cytotoxic effect of several clays and modified clays were examined such as Sepiolite [41], Bentonite, Kaolinite, Erionite [42], Kaolin [43], Halloysite, phyllosilicates [44], etc. These minerals are found to exhibit cytotoxic effects at variable physicochemical parameters. All the above-mentioned literature relates the presence of Iron, Aluminum, Magnesium, etc. containing minerals with their antibacterial assay as was found from the samples collected from various locations of River Ganga; aluminum-containing alkali Feldspar, albite microcline, muscovite, magnesium-containing clinoenstatite, mallis clay, dolomite as well as iron-containing riebeckite, clinochlore-1, etc. were found across the Indo-Gangetic plane.

The presence of these minerals may be associated with the antimicrobial potential of sediment samples (see microbial activity section).

6.5.7 Elemental Analysis

The detailed elemental analysis of sediment samples was performed using XRF and ICP-MS and this would further validate the hypothesis of antimicrobial potential of sediment samples due to the presence of certain metals in the sediments.

6.5.7.1 X-Ray Fluorescence (XRF)

XRF analysis was performed to ascertain the elements present in the sediment samples. As per the phases identified from XRD, the elements with the highest percentage found in sediments of Ganga are Si, Al, Na, K Mg, and Ca. Apart from these elements, other elements were quantified using XRD analysis (Table 6.8). It was found that Fe was present as a major element of the sediment samples collected from the first stretch of River Ganga. Although several elements are present in the sediment samples, Fe is found at the highest concentration throughout the locations of the River basin, among other elements, followed by Titanium (Ti). It should be noted that a few other transition metals (e.g., Zn, Cu, Ni, Zr, etc.) are also found in the sediment analysis. As can be seen in more detail, Fe concentration is highest at Tehri, followed by Chinyalisaur, Koteshwar and Haridwar, and Rishikesh. Ti element is the second major element found in the first stretch at a relatively higher concentration. Koteshwar showed the highest concentration of Ti among the tested sediment samples, followed by Tehri, Haridwar, and Rishikesh.

Interestingly, Barium, Cerium, Rubidium, Manganese, etc., are also found in minor quantities across the first stretch of River Ganga. Zinc, Strontium, Zirconium, Lead, etc., are also observed in a trace quantity. The concentration of these elements found at the first stretch of River Ganga is given in Table 8. The occurrence of a very high concentration of metals at Tehri and Koteshwar is due to the accumulation of incoming silts/mineral deposits from the upstream of reservoirs starting from Goumukh as the flow of water is generally lower at the reservoirs. The gradual deposition of minerals that are very fine at Tehri- and Koteshwar- reservoirs are responsible for the very high concentration of metals.

Table 6.8: The presence of elements in the selected sediments collected from the River Ganga

Locations / Conc (ppm)	Gomukh	Gangotri	Harsil	Maneri	Chinyali-saur	Tehri	Koteshwar	b/w Haridwar & Rishikesh
Ti	4300	4100	2900	3800	4800	5300	9100	6300
Mn	280	390	280	280	430	670	800	570
Fe	16700	15300	14700	26900	50400	55900	39900	25000
Ni	-	-	10	-	60	20	40	10
Cu	-	-	-	-	10	40	30	10
Zn	40	40	60	70	250	160	90	40
As	10	20	20	20	20	50	20	10
Rb	180	160	160	140	230	270	160	90
Sr	80	80	80	100	100	70	100	110
Y	20	40	20	20	30	20	30	50
Zr	220	490	140	110	140	70	240	810
Nb	10	10		10	20	10	20	20
Ag	-	-	-	-	30	-	-	-

Locations / Conc (ppm)	Gomukh	Gangotri	Harsil	Maneri	Chinyali-saur	Tehri	Koteshwar	b/w Haridwar & Rishikesh
Mo	-	-	-	-	-	-	10	20
In	-	10	-	-	30	-	-	-
Sb	20	-	-	-	-	-	10	-
Ba	1600	1900	1700	2600	2900	2600	1600	1600
La	240	-	-	-	-	-	-	440
Ce	500	540	390	-	370	280	450	730
W	-	20	-	-	-	-	-	10
Nd	-	-	650	-	-	490	-	-
Pr	-	-	-	-	-	-	610	-
Hg	-	-	-	10	10	10	-	10
Ta	10	-	30	-	-	-	-	-
Pb	20	20	20	10	40	40	20	10
Th	20	30	10	10	20	20	20	30

6.5.7.2 Inductively Coupled Plasma Mass Spectroscopy (ICP-MS) Analysis Results

ICP-MS analysis was carried out further to determine the presence of elements quantitatively in the sediment samples. The ICP-MS results, as given in Table 6.9, are found to be consistent with the XRF results. It was found that the concentration of Fe is higher among other elements present in the sediment samples, as high as 76700 ppm at Tehri, followed by Devprayag, Gangotri, Maneri, and the downstream of Haridwar. Magnesium is also found at Devprayag with a relatively higher concentration of 27000 ppm followed by Tehri and between Haridwar and Rishikesh. Ti is also present at a higher concentration at Tehri (5900 ppm), followed by Harsil and downstream of Rishikesh. It should be noted that the presence of Ti with an almost similar concentration range was observed throughout the upper stretch of River Ganga. The other transition metals are also found in considerable concentrations, such as Copper, Zinc, Chromium, Cobalt, Zirconium, Manganese, and Niobium. These results indicate that sediments of the Ganga River in the first stretch contain largely Fe, Ti, and other transition metals.

Table 6.9: ICP-MS analysis of a selected fraction of the sediments collected from River Ganga

Locations / Metalcontent (ppm)	Gomukh	Gangotri	Harsil	Maneri	Tehri	Devprayag	between Haridwar & Rishikesh
Iron (Fe)	16400	50200	40300	45300	76700	55800	45300
Magnesium (Mg)	6500	4200	9000	8600	17700	27000	17400
Niobium (Nb)	17.94	11.64	11.68	15.72	14.72	12.23	14.76
Copper (Cu)	37.51	21.89	41.5	58.02	66.19	46.31	32.04
Cerium (Ce)	709.87	430.69	257.43	264.04	82.09	231.91	322.28
Lead (Pb)	46.66	61.2	52.65	61.87	38.11	37.61	27.36
Chromium (Cr)	71.71	48.55	53.48	72.98	123.66	82.77	68.44
Cobalt (Co)	8.36	5.41	7.57	13.32	25.06	13.39	9.37
Zirconium (Zr)	1062.95	264.22	108.24	85.15	106.95	379.71	260.58
Titanium (Ti)	5400	3400	5500	5100	5900	5100	5600
Strontium (Sr)	111.49	76.65	71.06	102.32	53.87	92.81	82.9
Zinc (Zn)	527.42	147.89	208.76	223.24	293.15	247.76	146.37
Barium (Ba)	444.59	1242.47	441.35	490.48	517.5	318.43	338.31
Manganese (Mn)	479.01	290.2	305.6	525.91	563.06	640.523	557.79

Although the exact mechanism for the antimicrobial activity has not been identified yet, Williams et. al. proposed the role of Fe2+ in the bactericidal process of clay minerals [40]. A comparison of antibacterial activities was carried out using OMT clay with French Antibacterial Clay (ARG) and nonantibacterial clay (NAB). It was found that Al, P, V, Fe Cu, and Pb are associated with the bactericidal effect. The concentration of P, Fe, and Al was found to be significantly higher in the OMT clay that killed bacterial systems than in the control. The intracellular Fe concentration was found to be 8 times higher than control, which suggests that they are responsible for the bactericidal process. It was proposed that clay minerals in solution facilitate the Fe2+ solubility. Fe2+ overwhelmed outer membrane regulatory proteins, that can be oxidized when entering into the cell. Eventually, the Fe2+ ions precipitate as Fe3+ through the Fenton process and the Fenton reaction products (lethal hydroxyl radicals), which in turn oxidizes cell organelles and cell membrane causing bacterial death. The source of Fe in the clay minerals is Illite and Smectite as it was identified from quantitative X-Ray Diffraction. The OMT blue clay exhibited superior cytotoxicity against E. coli, Pseudomonas aeruginosa, Salmonella enterica subspecies enterica serovar Typhimurium, Staphylococcus aureus, Staphylococcus epidermidis, methicillin-resistant S. epidermidis, and methicillin-resistant S. aureus. This natural clay is dominated by illite-smectite, a group of clay minerals containing an expandable interlayer structure; as well as pyrite; Ca-plagioclase; and quartz. The interlayer smectite region acts as a reservoir from which metals are gradually released. The mechanism of antibacterial activity of OMT Blue clay supports the hypothesis that when clay containing reduced transition metal from the natural environment is oxygenated, soluble metals from minerals are dissolved (e.g., Fe2+, Al3+) which in turn damages bacterial cell membranes and excess Fe2+ causes intracellular protein damage by oxidation [45]. Selected elements have shown antibacterial activity that was found in trace quantities (e.g., Cu, Zn) while Ag was not found in all the sediment samples. Out of the metals found in XRF and ICP-MS analysis, Copper oxide (CuO), Zinc Oxide (ZnO), Alumina (Al2O3), Magnesium oxide (MgO) [58], Titanium Dioxide (TiO2), and Zero valent Iron (Fe0) nanoparticles were reported for their antimicrobial potential against several pathogens. The mechanism of cytotoxicity of these nanoparticles differs from one another, via surface charge interaction, free radical formation, or photocatalytic action [46].

The metal analysis of the sediment sample showed Fe, Ti, etc. as the most abundant elements consistently found throughout the whole stretch of River Ganga. Fe, Ti, and Mg were found to be in higher concentrations than that of the other elements (e.g., Zn, Cr, Cu, Ni, Mn), which were found at a trace concentration. All the above-mentioned literature relates the minerals containing Fe, Al, Mg, Ti, etc. may involve in the antibacterial activity of the sediment samples collected from various locations of River Ganga.

6.5.8 Assay for antibacterial of sediments, suspended sediments, and river water of Ganga

Time kill experiments were performed with sediments, SS, and river water of Ganga to determine antibacterial activity against Escherichia coli DH5□□□Experimental conditions were devised to directly incorporate sediments, SS, and river water in growth media and plating of appropriately diluted bacterial cultures onto the test plates followed by overnight incubation and scoring of residual bacterial cells post-incubation.

Initial trials were performed with samples from Gomukh, Gangotri, Harsil, Mana, Tehri, and Maneri wherein 500 mg of sediments were incorporated in growth media followed by plating of E. coli DH5□ cells at a concentration of ~ 6 x 108 on individual test plates. It was observed that samples from Harsil and Tehri resulted in a significant inhibitory effect of bacterial growth, and the results are summarised in Table 10.

Table 6.10: Antibacterial activity of various sediments and SS from River Ganga

Sl. No	Sample	Quantity	CFU (10-5) / 100µL
1	Gomukh	500 mg	480
2	Gangotri	500 mg	560
3	Harsil	500 mg	238
4	Mana	500 mg	600
5	Tehri	500 mg	95
6	Maneri SS	5 ml	535
7	Tehri SS	5 ml	104
8	Control	-	645

Further, sediment samples from Tehri were subjected to third-party verification/validation by performing similar experiments at the National Institute of Ocean Technology, Chennai. The results obtained confirmed the findings on the antibacterial activity of Tehri samples, and the results are summarised in Table 6.11.

Table 6.11: Antibacterial activity of their sediment sample form river Ganga

Sl. No	Sample	Quantity	CFU (10-4) / 100µL
1	Control	5 mL	396
2	Tehri SS	5 mL	35
3	Tehri SS	5 mL	30
4	Tehri SS	5 mL	28

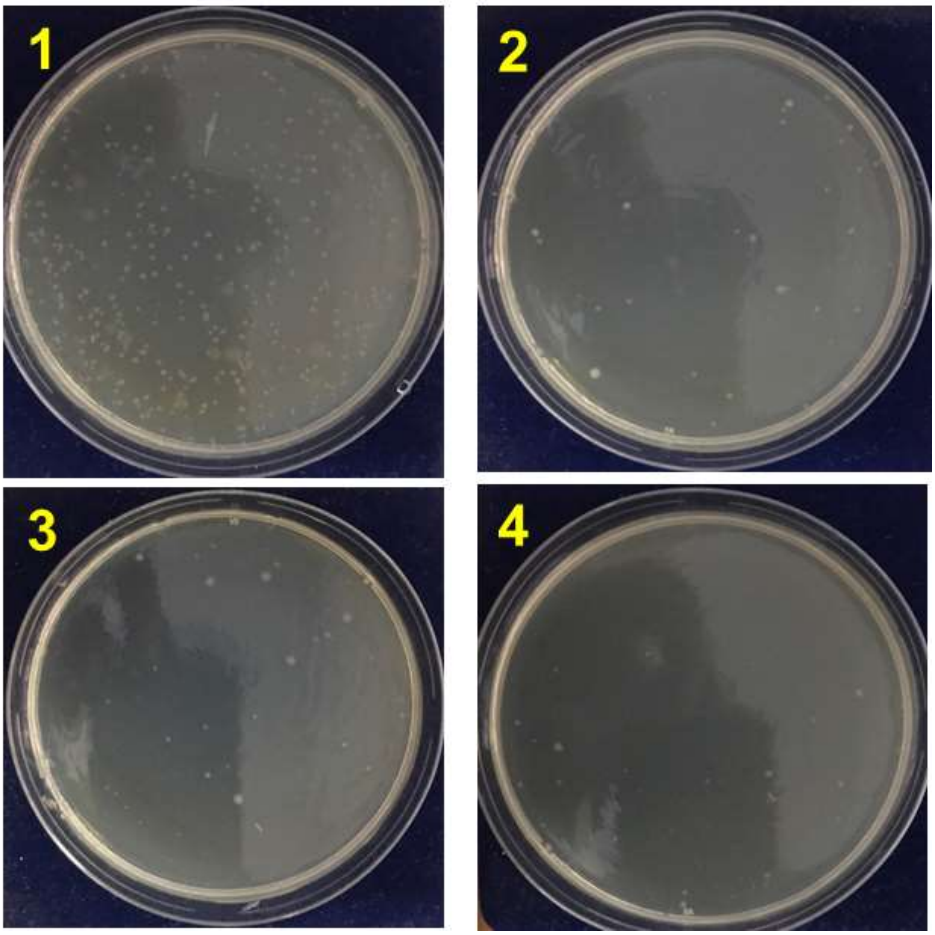

Fig. 6.25: Antibacterial activity Tehri samples. 1) Control Plate 2) Tehri SS 3) Tehri SS 4) Tehri SS

Further, to attribute the results to SS/sediment samples from Tehri, time-kill experiments were performed with river samples subjected to ultra-centrifugation at 85,000 g for 30 minutes. Upon confirmation by light scattering experiments that the samples are entirely devoid of any sediment particles, the water samples were incorporated in growth media, and the experimental trials were repeated. The results obtained indicated colony counts observed in test plates were similar to control samples confirming the absence of antibacterial activity. However, the colony counts are slightly lower than that of the other locations and control, which is due to most likely the presence of any dissolved fractions of metals or ultrafine particles present in the sediment suspensions. It is worthy to recall that the sediments are ultra-fine compared with that of the sediment samples collected from the other locations. The results are summarised in Table 6.12.

Table 6.12: Antibacterial activity of water samples from river Ganga devoid of sediments

Sample Nature	Sample name	CFU (10-5) / 100µL
Water suspension	Maneri	266
	Harsil	316
	Tehri	165
	Gangotri	259
	Control	247

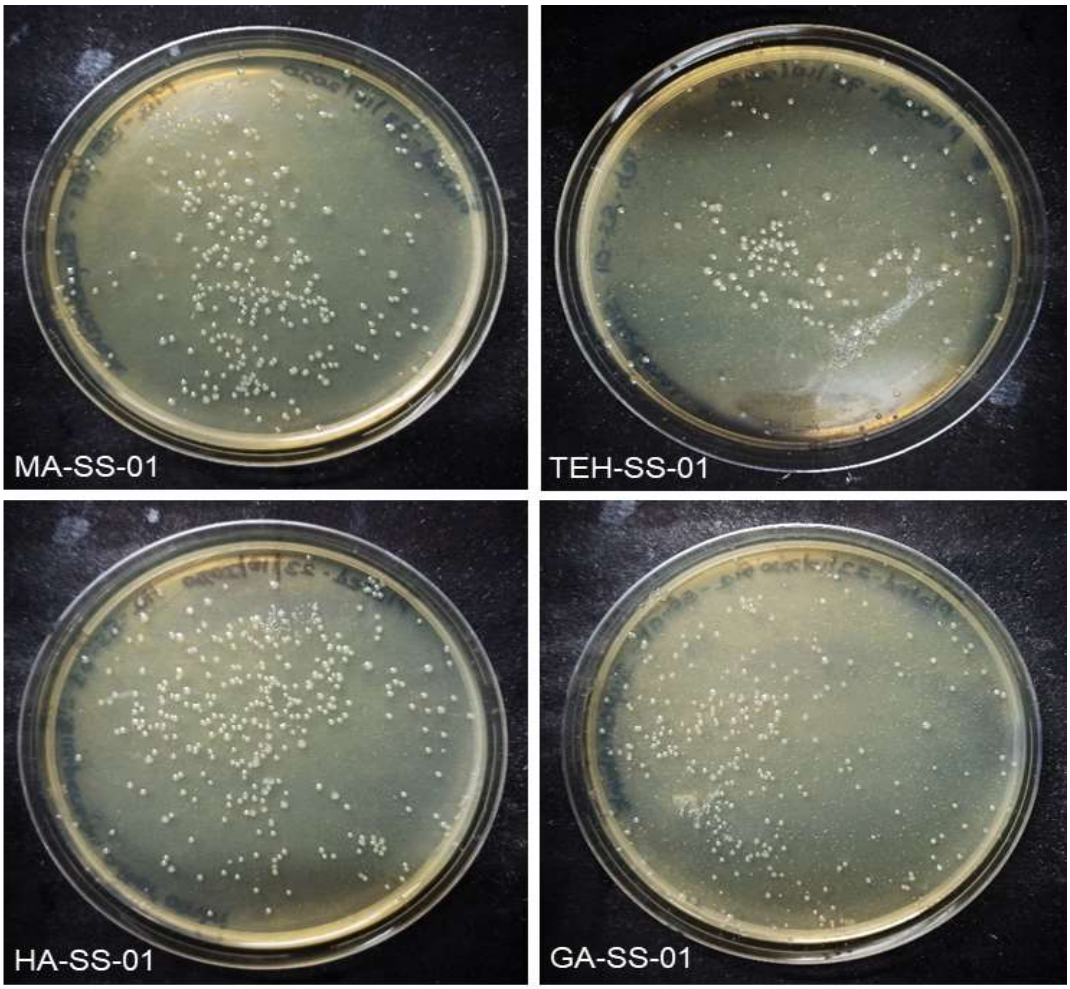

Fig. 6.26: Antibacterial activity of water samples from river Ganga devoid of sediment

For comparison, experiment trials for antibacterial activity were also performed with river water samples containing SS from Narmada and Yamuna. The sediment samples from Narmada and Yamuna were also performed for antibacterial activity, which showed virtually no antibacterial activity, as shown in Figure 6.27.

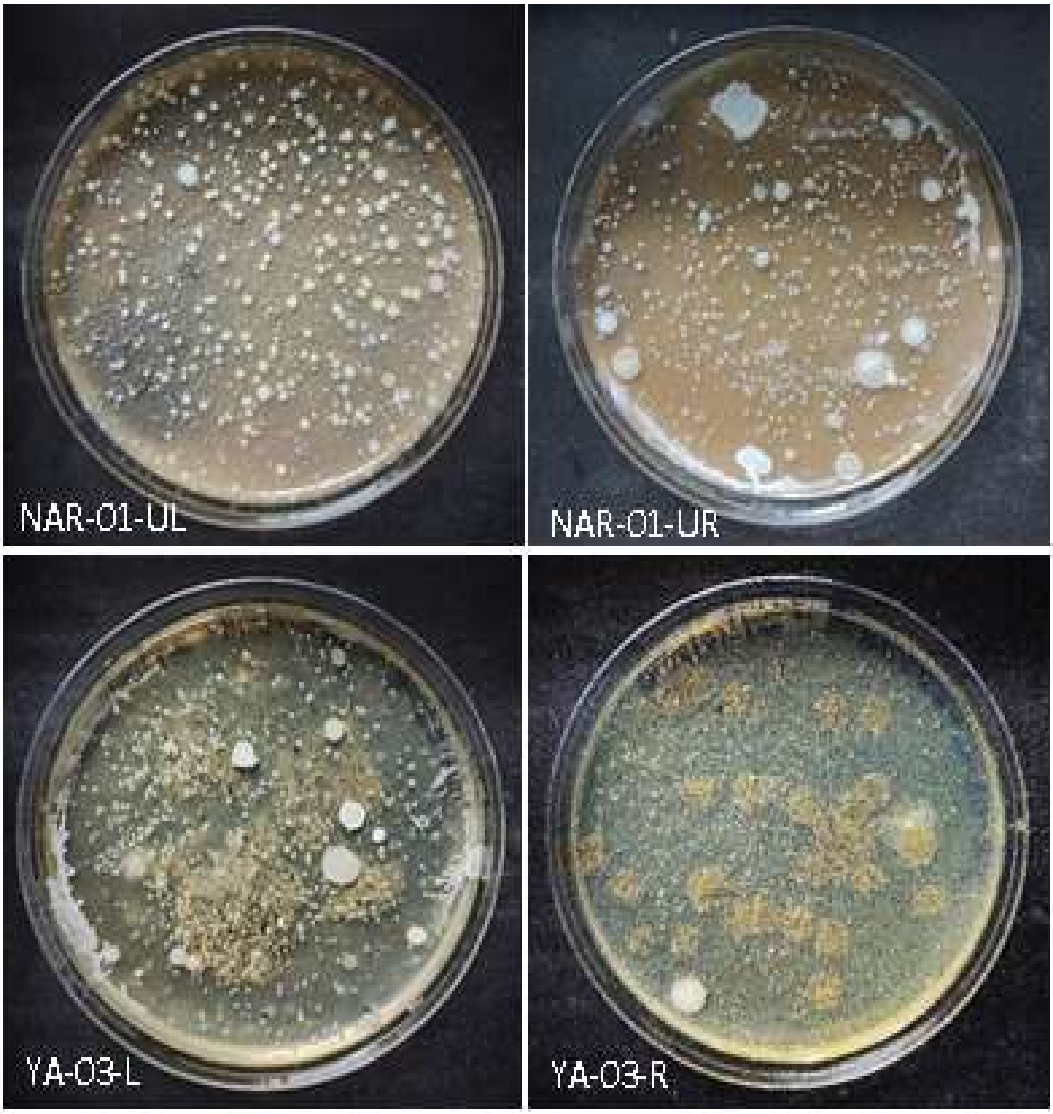

Fig. 6.27: Antibacterial activity of the sediment samples collected from River Yamuna and Narmada

The antibacterial activity test of the first stretch of River Ganga showed that samples collected from Tehri exhibited the highest antibacterial potential while Harsil, Gangotri, and Mana also showed antibacterial potential to some extent. From the metal analysis of these samples, it was found that the Fe- and Ti- the content of Tehri

is exceptionally higher compared with that of the other locations, which may be due to the accumulation of silt over time at the Tehri dam reservoir. This most probably accounts for the highest antibacterial potential of Tehri samples along with the finer grain size distribution. Many literatures are available indicating the microbicidal activity of Fe and Ti minerals as well as metal nanoparticles.

Size and concentration-dependent antibacterial activity of ZnO nanoparticles were examined. The results are consistent with our previous discussion that antibacterial activity increases with a decrease in particle size and increasing concentration. ZnO bulk powder showed no significant antibacterial activity while ZnO nanoparticles exhibit time-dependent antibacterial activity [55]. ZnO nanoparticles with a different particle size range showed significant antibacterial and antifungal properties [56]. Antibacterial activities of MgO, CaO, and ZnO were examined against S. aureus and E. coli wherein it was found that CaO was most effective for E. coli followed by MgO and ZnO, while ZnO was most effective against S. aureus [57]. TiO2 prepared from sonochemical method (anatase phase) having a particle size in the range of 300-900 nm (from Zetasizer analysis/DLS experiments) showed a clear zone of inhibition against E. coli, S. aureus, P. aeruginosa, C. albicans and B.subtilis with MIC of 9.7, 19.5, 19.0, 9.7 and 19.5 μg/ml respectively [47]. Synthesized TiO2/ZnO composite was found to be higher cytotoxic against E. coli, especially after UV light irradiation. It was reported that illuminated TiO2 samples having 90% Ti shows the bactericidal activity in about 20 minutes, while the samples having 50% Ti content took 45 minutes for the complete killing of bacteria. However, at dark conditions samples with 90%, Titania showed very low cytotoxicity compared to that of 50% Ti-sample. This indicates the photocatalytic behavior of TiO2 nanoparticles and the light-dependent antibacterial mechanism of TiO2 [48]. Hydrothermally synthesized and Ionic liquid assisted hydrothermally synthesized polycrystalline TiO2 was found to have an effective antibacterial ability against E. coli, K. aerogenes, S. aureus, P. desmolyticum [49,50]. The proposed mechanism of nano-TiO2 cytotoxicity is the inactivation of cellular enzymes and DNA by binding electron-donating groups such as carboxylates, amides, indoles, hydroxyls, thiols, etc. They cause little pores in bacterial cell walls, leading to increased permeability and cell death. CuO nanoflakes were also reported to show the antibacterial activity against S. flexneri and B. subtilis, the surface interactions are the primary cause of cytotoxicity of Cu2+ ions. The

copper ions show a higher affinity towards the carboxylic and amine group, which helps these ions to bind at the cell surface, which subsequently causes cell death [51]. ZnO nanoparticles are also reported to exhibit antibacterial activity against pathogenic organisms, which indicates the role of ROS in the oxidation of membrane lipids which eventually leads to bacterial death [52]. Other literatures are also available reporting the antibacterial property of these metal oxides [53,54].

The toxicity of metal ions depends on the reduction potential of the metals, their binding on the surface of the microbial structure (e.g., N, O, S, etc.) based on the principle of Hard-Soft Acid-Base interaction (HSAB) (Pearson's acid-base theory) and the speciation of metal ions. In any single milieu, metals can exist in variable oxidation states in the form of multiple different species, which depend on various parameters of the solution such as pH, ionic strength, temperature, etc. Reduction potential is an important characteristic of metals that depicts their capacity to participate in redox reactions. Reduction potential is a thermodynamic parameter that determines the tendency of metal species to acquire an electron from a donor and become reduced [59]. From the above discussion, it can be concluded that the presence of specific metal ions, metal oxides, or metal nanoparticles in the sediments is responsible for microbial cytotoxicity. The same can be related to the samples obtained from the Ganga River basin.

6.6 Salient Findings

Sediment samples were collected from 14 locations across the whole stretches of the River Ganga and investigated for the various physico-chemical characteristics, which can be corelated to its reported non-putrefying property. More emphasis was given to the sediment samples collected in the first stretch of the River Ganga, as it is relatively less influenced by anthropogenic activities and pollution. Different characterization techniques (Grain size distribution study, Laser light scattering experiment, DLS, Zeta potential analysis, TEM, XRD, XRF, ICP-MS) were used to understand the characteristics of the sediment samples.

The sediments were sieved mechanically into various fractions to determine their grain size distributions. It was found that the sediments are highly heterogeneous. It was observed that the sediment fraction having a size of 250 µm is larger (approx. 45 %) compared with that of the other fractions. However, the sediments collected from

Koteshwar- and Tehri- reservoirs show midget particle size distribution due to the inflow of silts and their gradual accumulation at the bottom of the water body over time. From the depth analysis of the sediments of Chinyalisaur, the sediment fraction of the size > 500 µm was observed predominantly at the bottom of the water bodies due to the removal of finer sediments upon contact with the flow of river water.

From the laser light scattering experiments, it was found that the suspended sediments are present in the samples as the light scattering path can be seen clearly upon irradiation of laser light. The large-sized suspended sediments were removed; however, the finer portion of the sediments wasn't removed upon centrifugation up to 4000 rpm as the light scattering path can be seen even after centrifugation. However, most of the finer portion of the suspended sediments were removed completely upon centrifugation at 75000 rpm.

Dynamic light scattering studies were performed to examine the average size of the suspended sediments in the water samples. It was observed that the average sediment size is in the range between 300 and 600 nm. The sediment size of the samples collected in most of the locations decreases with the increase of centrifugation up to 2500 rpm; however, it is increased again with the increase of centrifugation (3500 and 4500 rpm). Although the possible attributes are not clear at present for this observed anomaly, the presence of amorphous and/or organic components along with the inorganic fractions in the SS samples may show this unusual behavior.

Zeta potential analysis based studies were carried out to determine the surface charge of the colloidal particles present in suspension (at electrical double layer). The surface charge values obtained from Zeta potential studies were in the range of +5 to -15 mV; the charge at the particle surface is fairly near neutral (at neutral pH). Although the surface charge of the particles is relatively lower, the continuous flow of water in the Ganga River makes most of the fine particles will remain in the suspended form, which may influence the microbial systems present in the water.

From the HR-TEM analysis, it was observed that the suspended sediments contain nano-ordered single as well as polycrystalline structures. These nano suspended sediments are highly dispersed containing rod-like sediments along with most likely organic matter/ moieties. Interestingly nano sediments dispersed as well as embedded microbial-like structures are also found in the SS and they are amorphous. The as-

collected SS from Koteshwar showed fiber- and needle-like structures. Long-range amorphous tubes, as well as rods were observed in the SS samples after centrifugation. Also, nanoparticles (5-10 nm) embedded microbial systems were observed when the SS samples were collected at the Tehri reservoir from 50 m depth. Long-range interconnected spherical shaped organic moieties were observed in the SS samples collected at 70 m depth at Tehri reservoir. The presence of nano-ordered crystalline/amorphous sediments from the first stretch of River Ganga may likely is involved in the antimicrobial activity, which can be corroborated to the non-putrefying property of River Ganga [35, 37, 39, 42].

From the pXRD analysis, silicon-based minerals/phases, aluminum-, calcium-, sodium-, potassium- and magnesium-based minerals are very commonly found in the river sediment. In addition to the commonly found minerals, Fe-[45], Ti-[47] and manganese (Mn) [59] based minerals were also found, which are having variable oxidation states that may influence the microbial activity [45-50].

The elemental analysis of sediments was performed by XRF and ICP-MS techniques. Although several elements are present in the sediment samples, Si, Al, Ca, Mg, K, and Na are the most abundant. Apart from these elements, Fe is found with the highest concentration throughout the locations of the River basin, among other elements, followed by Ti. It should be noted that a few other transition metals (e.g., Zn, Cu, Ni, Zr, etc.) are also found in the sediment analysis. Magnesium is also found at Devprayag with a relatively higher concentration of 27000 ppm followed by Tehri and between Haridwar and Rishikesh. The occurrence of a high concentration of metals at Tehri and Koteshwar could be due to the accumulation of incoming silts/mineral deposits from the upstream of reservoirs starting from Goumukh as the flow of water is generally lower at the reservoirs. The gradual deposition of minerals that are very fine at Tehri- and Koteshwar- reservoirs are responsible for the very high concentration of metals. The minerals containing Fe, Al, Mg, Ti, etc. may be involved in the antibacterial activity of the sediment samples collected from various locations of River Ganga [36, 46, 57, 58].

The antimicrobial activity test of the first stretch of River Ganga showed that samples collected from Tehri exhibited the highest antibacterial potential while Harsil, Gangotri, and Mana also showed antibacterial potential to some extent. From the

metal analysis of these samples, it was found that the Fe and Ti content of Tehri is much higher compared with that of the other locations, maybe due to the accumulation of silt over time at the Tehri dam reservoir. This most probably accounts for the highest antibacterial potential of Tehri samples along with the finer grain size distribution.

From the detailed investigations of the sediment samples collected from the River Ganga, it was observed that the sediment samples collected from the first stretch showed antimicrobial activity which can be most likely corroborated to the non-putrefying property of River Ganga. Various explanations given above can be collectively responsible for anti-microbial activity, along with reasons as explained in other part of this study (including bacteriophage, metals etc.).

6.7 Future Studies

Several model studies using standard materials under simulated conditions noted below can further strengthen the possible attributes responsible for the non-putrefying properties of River Ganga.

- Zeta potential and particle size distribution studies using the reference nano-systems and organic moieties.
- Antimicrobial activity of reference pure minerals/phases observed in the pXRD studies.
- Metal ions leaching tests for the above-selected minerals/phases observed in the pXRD studies.
- Photo-catalytic activity studies using Fe- and/or Ti- containing minerals under sunlight.
- Basic studies by mimicking the results obtained from this work.

6.8 References

- Nautiyal, C. S. (2009). Self-purificatory Ganga water facilitates death of pathogenic Escherichia coli O157: H7. Current Microbiology, 58, 25–29.
- Singh, P. K., Parripati, A. P., Bareth, S., & Raja, R. B. (2011). Indian River water action on Streptococcus; a microbiological prospective. Annals of Biological Research, 2, 314–318.
- D'Herelle F (translated to English by Smith GH) (1922) The bacteriophage: its role in immunity. Williams and Wilkins/Waverly Press, Baltimore
- McMahan ZH, Dupont HL (2007) The history of acute infectious diarrhoea management—from poorly focused empiricism to fluid therapy and modern pharmacotherapy. Aliment Pharmacol Ther 25:759–769.
- D. Paul, S.N. Sinha, Assessment of various heavy metals in surface water of polluted sites in the lower stretch of River Ganga, West Bengal: a study for ecological impact, Discov. Nat. 6 (2013) 8e13.
- M.M. Rahaman, Principles of transboundary water resources management and Ganges treaties: an analysis, Water Resour. Dev. 25 (2009) 159e173.
- P. Das, K.R. Tamminga, The Ganges and the GAP: an assessment of efforts to clean a sacred river, Sustainability 4 (2012) 1647e1668.
- K.K. Vass, S.K. Mondal, S. Samanta, V.R. Suresh, P.K. Katiha, The environment and fishery status of the River Ganges, Aquat. Ecosyst, Health Manag. 13 (2010) 385e394.
- Agrawal, R.S. Pandey, B. Sharma, Water pollution with special reference to pesticide contamination in India, J. Water Resour. Prot. 2 (2010) 432e448.
- K. Biswas, D. Paul, S.N. Sinha, Prevalence of multiple antibiotic-resistant coliform bacteria in the water of river Ganga, Front. Environ. Microbiol. 1 (2015) 44e46.
- M.M. Rahaman, Integrated Ganges basin management: conflict and hope for regional development, Water Policy 11 (2009) 168e190.

- Paul, D., 2017. Research on heavy metal pollution of river Ganga: A review. Annals of Agrarian Science, 15(2), pp.278-286.
- Pandey, J., Shubhashish, K. and Pandey, R., 2009. Metal contamination of Ganga River (India) as influenced by atmospheric deposition. Bulletin of environmental contamination and toxicology, 83(2), pp.204-209.
- Dwivedi, S., Chauhan, P.S., Mishra, S., Kumar, A., Singh, P.K., Kamthan, M., Chauhan, R., Awasthi, S., Yadav, S., Mishra, A. and Mallick, S., 2020. Self-cleansing properties of Ganga during mass ritualistic bathing on Maha-Kumbh. Environmental Monitoring and Assessment, 192(4), pp.1-15.
- Dennis, M.W. and Middleton, D.J. eds., 2020. Navigating Deep River: New Perspectives on Shūsaku Endō's Final Novel. SUNY Press.
- Caldwell, J., 1965. "Effects of high partial pressures of oxygen on fungi and bacteria". Nature, 206(4981), p.321.
- ZoBell, C.E. and Hittle, L.L., 1967. "Some effects of hyperbaric oxygenation on bacteria at increased hydrostatic pressures". Canadian journal of microbiology, 13(10), pp.1311-1319.
- Dakin, H.D., 1915. "On the use of certain antiseptic substances in the treatment of infected wounds". British medical journal, 2(2852), p.318.
- Martin, R.S., Gates, W.H., Tobin, R.S., Grantham, D., Sumarah, R., Wolfe, P. and Forestall, P., 1982. "Factors affecting coliform bacteria growth in distribution systems". Journal-American Water Works Association, 74(1), pp.34-37.
- Straus, D.L., Farmer, B.D., Beck, B.H., Bosworth, B.G., Torrans, E.L. and Tucker, C.S., 2015. "Water hardness influences Flavobacterium columnare pathogenesis in channel catfish". Aquaculture, 435, pp.252-256.
- National Research Council and Safe Drinking Water Committee, 1977. Drinking water and health (Vol. 1). National Academies Press.

- Ellis, E.L. and Delbrück, M., 1939. "The growth of bacteriophage". The Journal of general physiology, 22(3), pp.365-384.
- Dizaj, S.M., Lotfipour, F., Barzegar-Jalali, M., Zarrintan, M.H. and Adibkia, K., 2014. "Antimicrobial activity of the metals and metal oxide nanoparticles". Materials Science and Engineering: C, 44, pp.278-284.
- Daglia, M., 2012. "Polyphenols as antimicrobial agents". Current opinion in biotechnology, 23(2), pp.174-181.
- Hajipour, M.J., Fromm, K.M., Ashkarran, A.A., de Aberasturi, D.J., de Larramendi, I.R., Rojo, T., Serpooshan, V., Parak, W.J. and Mahmoudi, M., 2012. "Antibacterial properties of nanoparticles". Trends in biotechnology, 30(10), pp.499-511.
- Stoimenov, P.K., Klinger, R.L., Marchin, G.L. and Klabunde, K.J., 2002. "Metal oxide nanoparticles as bactericidal agents". Langmuir, 18(17), pp.6679-6686.
- Kim, T.H., Kim, M., Park, H.S., Shin, U.S., Gong, M.S. and Kim, H.W., 2012. Size-dependent cellular toxicity of silver nanoparticles. Journal of biomedical materials research Part A, 100(4), pp.1033-1043.
- Li, J., Rong, K., Zhao, H., Li, F., Lu, Z. and Chen, R., 2013. Highly selective antibacterial activities of silver nanoparticles against Bacillus subtilis. Journal of nanoscience and nanotechnology, 13(10), pp.6806-6813.
- Lu, Z., Rong, K., Li, J., Yang, H. and Chen, R., 2013. Size-dependent antibacterial activities of silver nanoparticles against oral anaerobic pathogenic bacteria. Journal of Materials Science: Materials in Medicine, 24(6), pp.1465-1471.
- Raza, M.A., Kanwal, Z., Rauf, A., Sabri, A.N., Riaz, S. and Naseem, S., 2016. Size-and shape-dependent antibacterial studies of silver nanoparticles synthesized by wet chemical routes. Nanomaterials, 6(4), p.74.
- Mihai, S. and Malaisteanu, M., 2013. Size-dependent antibacterial of gold colloids. Revista de Chimie-Bucharest, 64, pp.105-107.

- Pan, Y., Neuss, S., Leifert, A., Fischler, M., Wen, F., Simon, U., Schmid, G., Brandau, W. and Jahnen-Dechent, W., 2007. Size-dependent cytotoxicity of gold nanoparticles. Small, 3(11), pp.1941-1949.
- Rufus, A., Sreeju, N., Vilas, V. and Philip, D., 2017. Biosynthesis of hematite (α-Fe2O3) nanostructures: size effects on applications in thermal conductivity, catalysis, and antibacterial activity. Journal of Molecular Liquids, 242, pp.537-549.
- Pişkin, S., Arzu, P. and Müge, S.Y., 2013, December. Antimicrobial activity of synthesized TiO2 nanoparticles. In International Conference on Emerging Trends in Engineering and Technology, ICETET, Patong Beach, Phuket, Thailand. http://dx. doi. org/10.15242/IIE (Vol. 1213004).
- Williams, L.B., Metge, D.W., Eberl, D.D., Harvey, R.W., Turner, A.G., Prapaipong, P. and Poret-Peterson, A.T., 2011. What makes a natural clay antibacterial? Environmental science & technology, 45(8), pp.3768-3773.
- Khan, S.A., 2020. Metal nanoparticles toxicity: role of physicochemical aspects. In Metal Nanoparticles for Drug Delivery and Diagnostic Applications (pp. 1-11). Elsevier.
- Borquaye, L.S., Ocansey, E. and Semenya, J., 2016. Inhibitory effect of selected Ghanaian clay leachates on some pathogenic microbes.
- Bardhan, S., Pal, K., Roy, S., Das, S., Chakraborty, A., Karmakar, P., Basu, R. and Das, S., 2019. Nanoparticle size-dependent antibacterial activities in natural minerals. Journal of nanoscience and nanotechnology, 19(11), pp.7112-7122.
- Zarate-Reyes, L., Lopez-Pacheco, C., Nieto-Camacho, A., Apán, M.T.R., Palacios, E., Kaufhold, S., Ufer, K., Garcia-Zepeda, E. and Cervini-Silva, J., 2017. Naturally occurring layered-mineral magnesium as a bactericidal against Escherichia coli. Applied Clay Science, 149, pp.87-96.

- Williams, L.B., Metge, D.W., Eberl, D.D., Harvey, R.W., Turner, A.G., Prapaipong, P. and Poret-Peterson, A.T., 2011. What makes a natural clay antibacterial? Environmental science & technology, 45(8), pp.3768-3773.
- Denizeau, F., Marion, M., Chevalier, G. and Cote, M.G., 1985. Absence of genotoxic effects of nonasbestos mineral fibers. Cell biology and toxicology, 1(2), pp.23-32.
- Murray, H.H., 2000. Traditional and new applications for kaolin, smectite, and palygorskite: a general overview. Applied clay science, 17(5-6), pp.207-221.
- Gao, N., Keane, M.J., Ong, T. and Wallace, W.E., 2000. Effects of simulated pulmonary surfactant on the cytotoxicity and DNA-damaging activity of respirable quartz and kaolin. Journal of toxicology and environmental health Part A, 60(3), pp.153-167.
- Han, H.K., Lee, Y.C., Lee, M.Y., Patil, A.J. and Shin, H.J., 2011. Magnesium and calcium organophyllosilicates: synthesis and in vitro cytotoxicity study. ACS applied materials & interfaces, 3(7), pp.2564-2572.
- Caflisch, K.M., Schmidt-Malan, S.M., Mandrekar, J.N., Karau, M.J., Nicklas, J.P., Williams, L.B. and Patel, R., 2018. Antibacterial activity of reduced iron clay against pathogenic bacteria associated with wound infections. International journal of antimicrobial agents, 52(5), pp.692-696.
- Rana, S. and Kalaichelvan, P.T., 2011. Antibacterial activities of metal nanoparticles. Antibacterial Activities of Metal Nanoparticles, 11(02), pp.21-23.
- Pişkin, S., Arzu, P. and Müge, S.Y., 2013, December. Antimicrobial activity of synthesized TiO2 nanoparticles. In International Conference on Emerging Trends in Engineering and Technology, ICETET, Patong Beach, Phuket, Thailand. http://dx. doi. org/10.15242/IIE (Vol. 1213004).
- Stoyanova, A., Hitkova, H., Bachvarova-Nedelcheva, A., Iordanova, R., Ivanova, N. and Sredkova, M., 2013. Synthesis and antibacterial activity of

TiO2/ZnO nanocomposites prepared via nonhydrolytic route. J. Chem. Technol. Metall, 48(2), pp.154-161.

- Alhadrami, H.A. and Al-Hazmi, F., 2017. Antibacterial activities of titanium oxide nanoparticles. J. Bioelectron. Nanotechnol, 2(5).
- Manjunath, K., Yadav, L.S.R., Jayalakshmi, T., Reddy, V., Rajanaika, H. and Nagaraju, G., 2018. Ionic liquid assisted hydrothermal synthesis of TiO2 nanoparticles: photocatalytic and antibacterial activity. Journal of materials research and technology, 7(1), pp.7-13.
- Pandiyarajan, T., Udayabhaskar, R., Vignesh, S., James, R.A. and Karthikeyan, B., 2013. Synthesis and concentration dependent antibacterial activities of CuO nanoflakes. Materials Science and Engineering: C, 33(4), pp.2020-2024.
- Dutta, R.K., Nenavathu, B.P., Gangishetty, M.K. and Reddy, A.V.R., 2012. Studies on antibacterial activity of ZnO nanoparticles by ROS induced lipid peroxidation. Colloids and Surfaces B: Biointerfaces, 94, pp.143-150.
- Top, A. and Ülkü, S., 2004. Silver, zinc, and copper exchange in a Na-clinoptilolite and resulting effect on antibacterial activity. Applied Clay Science, 27(1-2), pp.13-19.
- Naseem, T. and Farrukh, M.A., 2015. Antibacterial activity of green synthesis of iron nanoparticles using Lawsonia inermis and Gardenia jasminoides leaves extract. Journal of Chemistry, 2015.
- Emami-Karvani, Z. and Chehrazi, P., 2011. Antibacterial activity of ZnO nanoparticle on gram-positive and gram-negative bacteria. African journal of microbiology research, 5(12), pp.1368-1373.
- Sharma, D., Rajput, J., Kaith, B.S., Kaur, M. and Sharma, S., 2010. Synthesis of ZnO nanoparticles and study of their antibacterial and antifungal properties. Thin solid films, 519(3), pp.1224-1229.

- Sawai, J., 2003. Quantitative evaluation of antibacterial activities of metallic oxide powders (ZnO, MgO and CaO) by conductimetric assay. Journal of microbiological methods, 54(2), pp.177-182.
- Tang, Z.X. and Lv, B.F., 2014. MgO nanoparticles as antibacterial agent: preparation and activity. Brazilian Journal of Chemical Engineering, 31(3), pp.591-601.
- Chowdhury, A.N., Azam, M.S., Aktaruzzaman, M. and Rahim, A., 2009. Oxidative and antibacterial activity of Mn3O4. Journal of hazardous materials, 172(2-3), pp.1229-1235.

CHAPTER - 7

7A. CHEMICAL-BIOLOGICAL INTERACTIONS

7.0 Investigation of chemical-biological interactions of plant-originated organics for self-purification properties of River Ganga

Objective of Study

1. Exploration and identification of dominant flora as a source of river organics/metabolites
2. Investigating vital pathways, leaching mechanisms and associated bio-physico-chemical processes of introduction and influence of plant-origin organics in river system
3. Assessing chemo-biological interactions of plant-origin organics within river water and sediment contributing to non putrefaction/self purification properties of river Ganga.

7.1 Introduction

River Ganga is blessed to be in the lap of Himalayan ranges. Its terrain offers many special properties to the river. It traverses its way through the thick riparian vegetation rich pathways of Himalayan region. These riparian vegetations consist of trees of various kinds with many of them being species of very high medicinal value. The dominant flora of the area consists of trees, which generate many aromatic and medicinal compounds like is Cedrus deodara (Deodar) and Pinus wallichiana (Blue Pine) etc.

The leaves and other plant parts of these trees which contain various compounds with antimicrobial and medicinal properties, contribute substantial litter/debris and soil which in due course of time harbors rich microbial biodiversity. Part of the litter cover and the soil layers enters the river water from the slopes of the terrain. When the litter and other plant debris enter the river water and is anchored on the banks for longer times, it can leach these medicinal compounds to the water of the Ganga river. These compounds or phytoconstituents, are likely to enrich the pristine Ganga water especially in the upper stretches with denser vegetation and forest cover. The broader classes of these compounds are Terpenes, polyphenols, alkaloids etc. The highly oxygenated Ganga water can further enhance the solubility of terpenes and terpenoids from the plant parts and debris. Also, there are several large mountain streams carrying the terrain characteristics, which enter the river and may add phytochemicals

to river water. These side streams are also rich in the organic compounds with useful properties.

In the present study a systematic attempt is made, to establish the leaching of these phytochemicals from the prominent native plant species of that terrain, in order to understand the role of phytochemicals in imparting special properties to Ganga River Water.

To accomplish the objectives, sample collection has been done from the upper stretch of river Ganga and analysis has been performed for screening and identification of various phytochemicals originating from the medicinal plants of the terrain. An attempt has also been made to understand the leaching characteristics by performing simulated experiments at laboratory level to understand the introduction of the phytochemical organics into the river water.

The outcome of the study goes well with the hypothesis of leaching occurring in water in contact with leaves/plant parts and debris, with the leachates having a number of compounds from the plant parts, as evident from lab based leaching experiments using river water. Similar leaching mechanisms can be expected in the Ganga river water owing to its long forest trails, mountainous side streams and litter inputs of medicinal and other plants in the catchment areas.

7.1.1 Phytochemicals of Plant Origin

Phytochemicals are the compounds that exist naturally in the plants. They protect plants against disease and damage, and also contribute to the color, aroma and flavor of the plant. Phytochemicals are commonly referred to as plant chemicals that protect plants from environmental hazards such as pollution, stress, drought, UV exposure and pathogenic attack (Gibson, Edward.,et.al,1998) It has been clearly shown recently that they also protect human health when their dietary intake is substantial (Samrot Antony,et.al.,2009).

Phytochemicals are classified into two classes namely, primary and secondary metabolites according to their roles, in plant metabolism. The primary constituents consist of specific sugars, amino acids, proteins and chlorophyll, while the secondary constituents consist of alkaloids, terpenoids and phenolic compounds, and many others such as flavonoids, tannins, etc.(Krishnaiah Duduku, et.al.,2009)

Phytochemicals accumulate in various parts of plants, such as root , stem, leaf , flower, fruit and seed(Costa, M. A.,1999). To date, approximately 4,500 phytochemicals are identified and many of them have been categorized on the basis of their defensive functions and physical and chemical characteristics. (Koche.D, 2010)

Some important classes of phytochemicals are enlisted below:

Table 7.1: Significant Phytochemical Groups

Sl. No.	Group	Sub Groups	Features	Pharmacological Properties
1	Phenolic Compounds	Coumarins Lignin Flavonoids Isoflavonoids Tannins	Phenolic compounds, with at least one hydroxyl group attached to one or more aromatic rings in its chemical structure. Most of leaves have polyphenol content and these compounds being water soluble so easily leach out to water	Antioxidant, Antitumoral, Antibacterial, Antiviral and enzyme inhibitors. Main dietary phenolic compounds.
2	Alkaloids	Hormones Carotenoid Pigments Sterol Essential oils and latex	Nitrogen containing compounds, mainly amines	Anticancerous, sedative, Neuropharmaceuticals, antimicrobials, insecticidal.
3	Glycosides	Saponins Cardiac Glycosides Cyanogenic Glycosides Glucosinolates	They arise from a sugar molecule being condensed with another one containing a hydroxyl group	Antimicrobials, fungicides, insecticides, anticancer, anti-inflammatory and allelopathic

Sl. No.	Group	Sub Groups	Features	Pharmacological Properties
4	Terpenes and Terpenoids	Monoterpenes Diterpenes Triterpenes Tetraterpenes Sesquiterpenes Sesterterpenes Sesquaterpenes Polyterpenes	Basic Isoprene Structrure with functional groups	Antibacterial, antioxidant, Natural Food preservatives , Terpenes are believed to be involved in cannabinoid production(terpene blocks and phenol groups)

The project envisaged identification of organic compounds/phytochemicals of plant origin in the Ganga river water in context of imparting non-putrefaction properties.

A brief overview of the milestones and the status is presented below:

Table 7.2: Project Milestones

Milestone	Work Element
Identification of dominant flora as a possible source of river organics/metabolites	Screening and identification of floral components that impart organics/metabolites
Standardization of protocol for preparation of plant extracts and river water and sediment extracts for phytochemical characterization	Method development and standardization of phytochemical characterization
a. Qualitative phytochemical group analysis **b. Identification of individual compounds though advanced instrumentation**	Isolation and characterization of the phytochemical groups using FTIR and other parameters Identification of individual organics using GC-MS.

Milestone	Work Element
a. Experimental investigation of introduction of organics **b. Influence of phytochemicals on self-purification of river water**	a. Investigating leaching mechanisms and bio-physico-chemical processes of introduction of plant-origin organics in river systems. b.Simulated experiments for assessing self- purification
Assessing chemo-biological interactions of plant-origin organics within river water contributing to self-purification properties of River Ganga	Correlation of simulated experiments with natural processes for understanding chemo-biological interactions.

7.1.2 Sample Collection

Sample collection was majorly done from the upper stretch of Ganga River. The upper stretch of river Ganga has an extensive vegetation cover of the trees rich in medicinal value. Three samplings have been performed till date. First sampling was performed in December 2017 post-monsoon season. This was followed by pre-monsoon sampling in May 2018. Third sampling has been performed in pre-monsoon season (during April 2019).

Sample Collection has been done for river water, significant side streams meeting the river, sediment, soil, plant litter and plant parts. The sediment, soil, plant litter and plant parts (Blue Pine and Deodar needles and stems) have been collected from Harsil. The water sampling location details have been given in Table 7.3.

The water samples have been collected at various upstream and downstream location from Gangotri to Harsil. Major side streams, meeting the river were also identified and samples were collected for analysis. Besides this, selected downstream representative samples till Haridwar/Rishikesh have also been collected.

Table 7.3: Sampling locations for the collection of plant parts and water

Water Sample Code	Location	Latitude	Longitude	Altitude
G1	Gangotri U/S 500m from Gangotri temple	30°59' 38.9"N	78°59' 43.2"E	2999
G2	Stream opposite to Gangotri temple	30°59' 37.3"N	78°56' 27.7"E	3060
G3	Gangotri D/S	30°59' 41.5"N	78°56' 17.3"E	3043
GSS1	Gangotri side stream (1.5 km away from temple)	30°59' 55.4"N	78°55' 45.2"E	3074
GSS2	Gangotri side stream (4 km away from the temple)	31°00' 05.6"N	78°54' 14.8"E	3609
HSS1	Harshil Side stream (In front of Harsil gate)	31°01' 59.9"N	78°45' 23.1"E	2527
HSS2	Harshil side stream (Highway, 4km away from harshil)	31°00' 00.1"N	78°54' 14.5"E	3613
Dharali	Dharali	31°02' 26.5"N	78°40' 52.8"E	2715
HSS6	Side stream, Near mukhba temple	31°02' 43.7"N	78°46' 54.8"E	2600
HSS7	Side stream , 500 m before Mukhba temple on the way to temple	31°02' 27.2"N	78°45' 51.3"E	2599
HSS8	Side stream , 700m before mukhba temple	31°02' 26.0"N	78°45' 48.9''E	2603
H-1	Harsil Mid stream (From army camp)	31°02' 04.6"N	78°45' 10.2''E	2504
H-9	Harshil U/S (near halipad)	31°02' 13.0"N	78°45' 36.7"E	2506
H-10	Harshil D/S (Near Nilang Hotel)	31°02' 4.9"N	78°43'48.8"E	2424
H-11	Harshil 5 km D/s (Bhatwari pilot baba temple)	30°45'59.4"N	78°35'35.2"E	1331

H-12	Maneri D/S	30°44' 09.9"N	78°31' 06.4"E	1256
H-13	Chinyali Sour (cave towards chamba 74 km milestone)	30°34'18.8"N	78°19' 56.9"E	791
H- 14	Haridwar	29.57°08' 11.1"N	78°09' 58.162'E'	283
Tehari Dam	Tehari	30°29' 15.9"N	78°27' 49.5"E	764

Approximately, 1.5 litres water samples were collected from the upper stretches of Bhagirathi and were preserved in dry ice and brought back to laboratory for analysis. These samples were collected in 2 litre amber coloured glass bottles with Teflon lined stoppers. Grab sampling procedure was followed for all the samples collected ensuring a representative sample. Preparation of the sampling bottles was done which included several washings with detergent followed by rinsing with tap water, ultrapure water (Millipore) and lastly with solvent followed by air-drying. Samples were stored at 40C till extraction after transporting it to the laboratory.

Blue Pine and Deodar were two dominant tree species in the stretch from Gangotri to Harsil. Fresh stem and needle samples were collected from Harsil and were preserved in polyethylene bags and were refrigerated. For soil profile study, fresh litter, partially degraded litter, degraded litter, top soil and 0-10 layer soil samples have also been collected. Sediments samples were collected from selected water sampling sites.

Some representative photographs of sampling, terrain details and side streams are given below.

Representative photographs of sample Collection of plants, soil, litter and water from the mainstreams and sidestreams in the Upper Stretch of River Ganga

Plate 7.1: ***Harsil***

Plate 7.2: ***Harsil Side stream***

Plate 7.3: ***Harsil Side Stream***

Plate 7.4: ***Gangotri***

Plate 7.5: ***Harsil and side streams (Sample codes H and HSS respectively)***

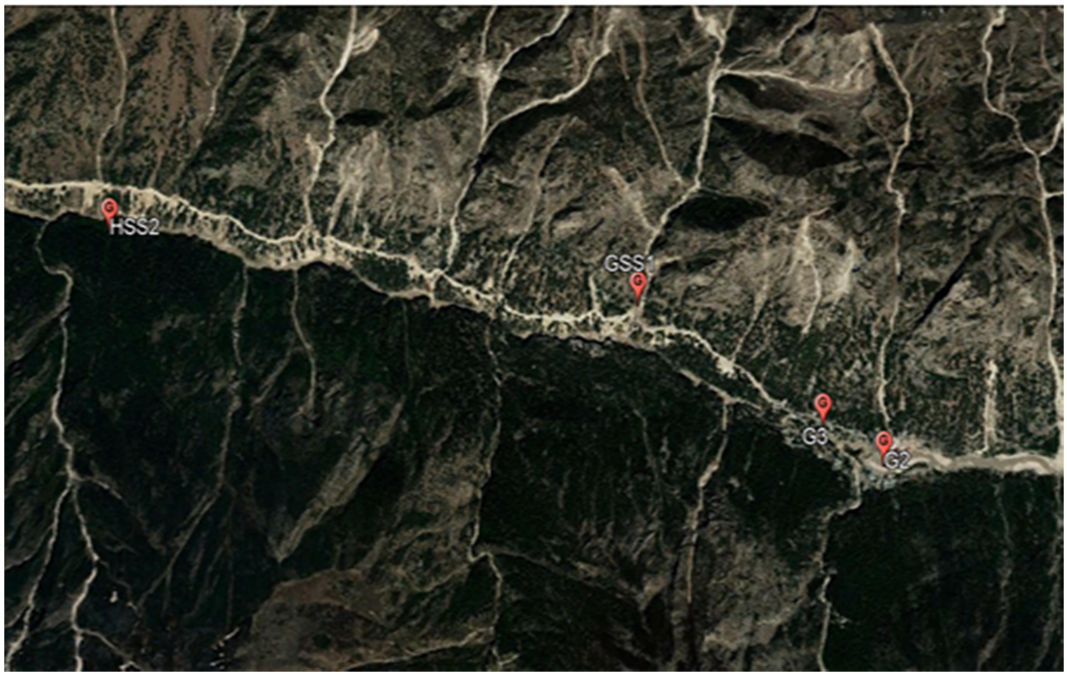

Plate 7.6: ***Gangotri and Side streams (sample codes G and GSS)***

Plate 7.7: ***Litter sample***

Plate 7.8: ***Litter and Soil samples***

7.1.3 Materials and Methods

Broadly the experimental work plan was included the following set of experiments

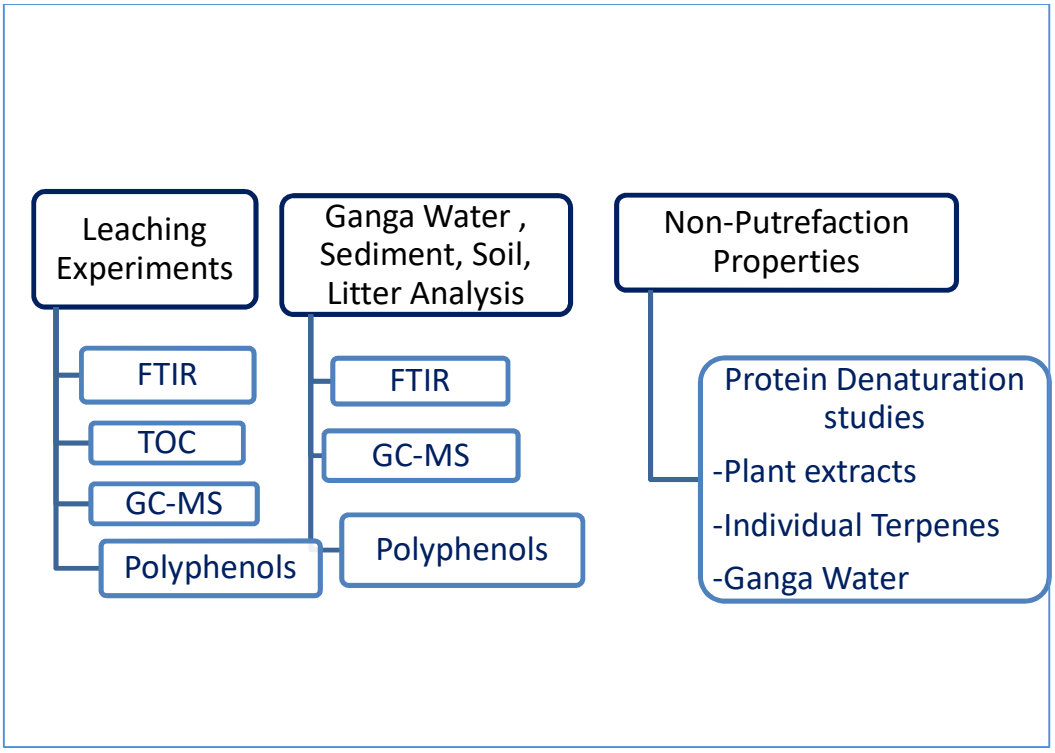

Fig.7.1: Experimental Design and Analysis

7.1.4 Experimental Details

7.1.4.1 Simulated Experiments using Plant Parts

To understand the leaching characteristic of phytochemicals from the plants into water a detailed study was performed. The experimental design is depicted in Figure 7.1. Two dominant tree species from Gangotri to Harsil locations that is Cedrus deodara (Deodar) and Pinus wallichiana (Blue Pine) were selected for the simulation experiments. The simulation experiments were carried out to observe the leaching of phytochemicals in Millipore water. Surface of the Leaves/needles of Blue pine and Deodar were washed and cleaned. The leaves were then immersed in Millipore water and periodic collection of leachates was done. In some experiments, Ganga water was also used as a reference. About 6 to 10gm of leaves were used with 350 ml of Distilled Water (Reference) and Ganga Water. Leachate was collected after completion of respective leaching days and fresh water was replenished. Besides,

Blue pine and Deodar, Jamun (Syzygium cumini) was also used as a control plant belonging to the non-coniferous group.

The leachates of the simulated experiments were analysed for various parameters including pH, conductivity, Total phenolics and TOC. FTIR and GC-MS/MS of the leachate samples was also performed. Total phenolic content determined by standard folin- ciocalteu reagent method using Gallic acid as a standard phenolic compound for calibration using UV-Visible spectrophotometer (765nm).

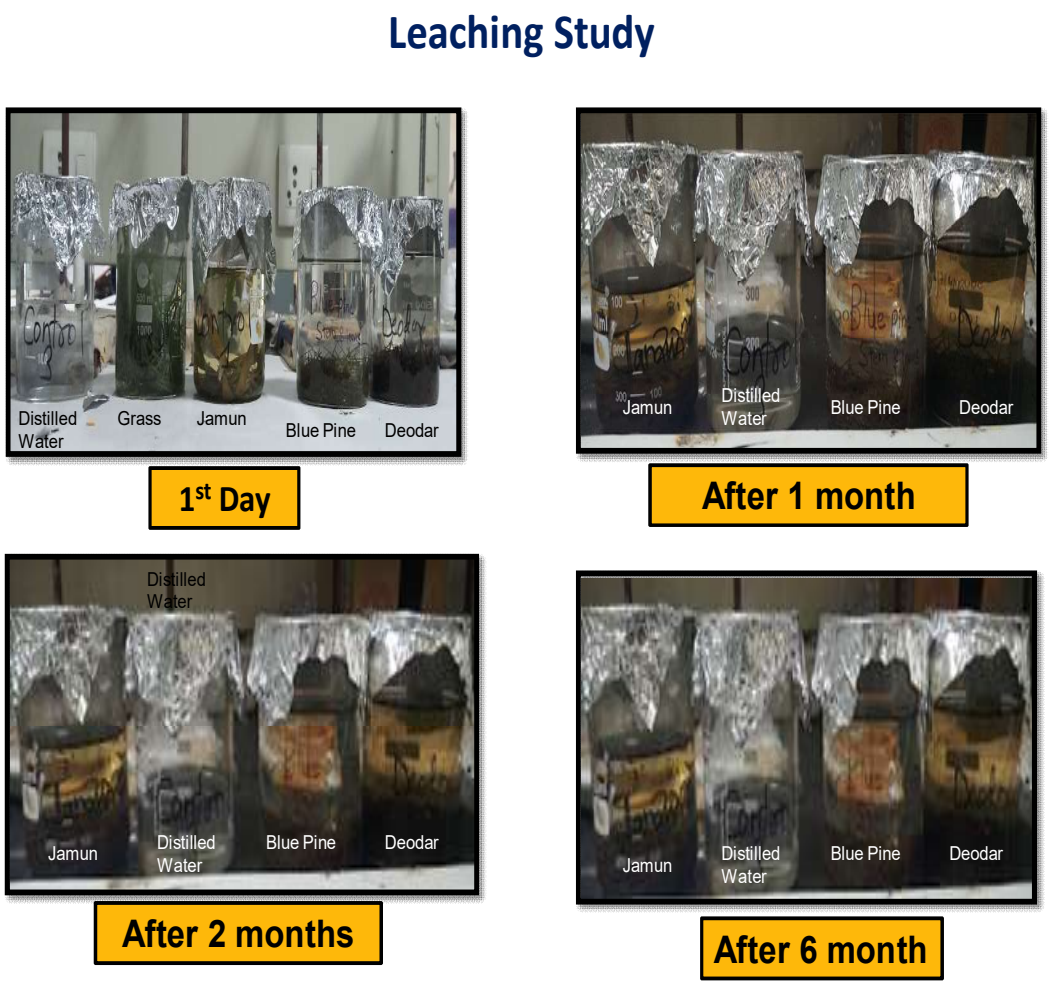

Fig. 7.2: Experimental Setup of Leaching Study

7.1.4.2 Ganga Water, Soil, Sediment and Litter Analysis

Different types of instrumentation techniques were used for exploring the presence of any plant based organic compound in river water samples and the screening of phytochemicals. The instrumental techniques like FTIR (Fourier Transform Infrared Spectroscopy) (for functional groups) and Gas Chromatography-Mass Spectrometry (GC-MS), were used. For GC-MS analysis, pre-processing of water samples using liquid-liquid extraction was performed for concentration of organic compounds.

The sediments, soil samples and plant leaves were also extracted using solvent (acetone and hexane 1:1) and the extract was analysed for organic parameters using FTIR and GC-MS

7.1.4.3 Non-putrefaction properties: Prevention of protein Denaturation using Phytochemicals

An experimental study was also performed to understand the non-putrefying properties of River Ganga. The basis of the study was that, putrefaction is chemically due to protein denaturation. So this study was performed in order to understand whether the presence of phytochemicals prevented protein denaturation. The protein denaturation was studied for the phytochemicals which were detected in the Ganga water samples like Alpha Pinene, Beta Pinene, 3-Carene etc . Beef extract media was used as the protein source in the experiment. Beef Extract solution (in distilled water) having a concentration of 3mg/ml was used. Individual terpenes/terpenoids mentioned above were used at different concentrations. Ganga water samples were also used for prevention of protein denaturation. Ganga water samples were taken in 1:1 ratio with the beef extract solution for the experiment. No phytochemicals were spiked in the Ganga water samples. Samples were incubated at 37°C for 24 and 48 hours after spiking of individual phytochemicals in water. Absorbance/Optical Density of the samples were recorded at 600nm using UV-Vis Spectrophotometer, before and after incubation.

7.1.5 Analytical Results

The parameters monitored during the leaching study helped understanding the leaching mechanism of phytochemicals from the plant parts. pH, conductivity and TOC was analysed for the leachates collected on different days.

The pH variations are mentioned in Figure 7.3. The day 0 indicated in the figure is the pH value recorded immediately after dipping the leaves/plant parts in water. Conductivity values showed a significant increase 423 µS, 321 µS and 259 µS for blue Pine , Deodar and Jamun respectively. After day 1, the increase in conductivity slowed down and on day 7 nearly stabilized to 11-12 µS. The conductivity changes indicate the inorganic release in water.

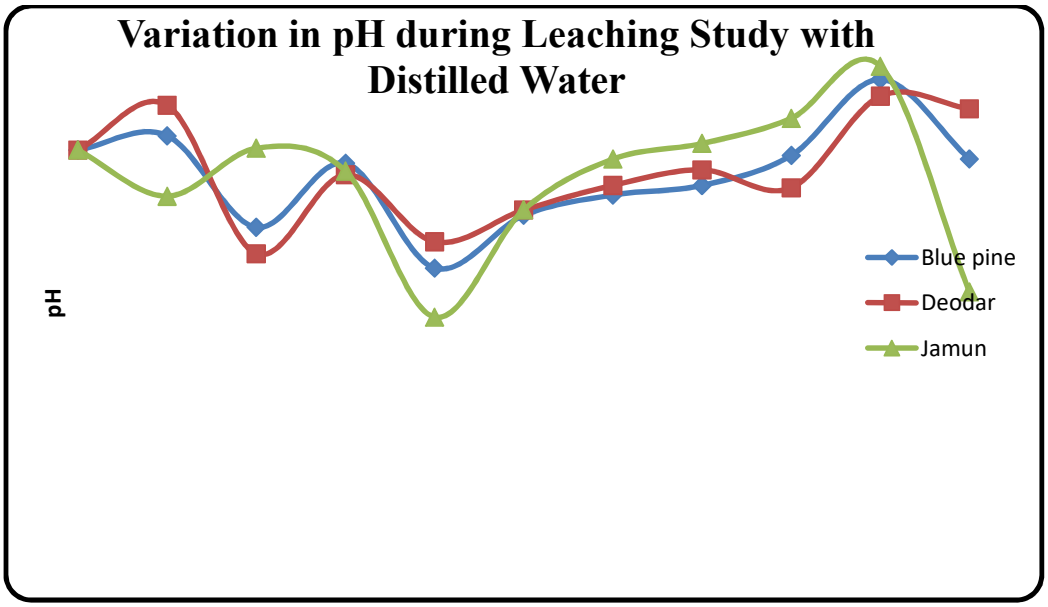

Fig. 7.3: Variation In Ph During Leaching Study With Distilled Water

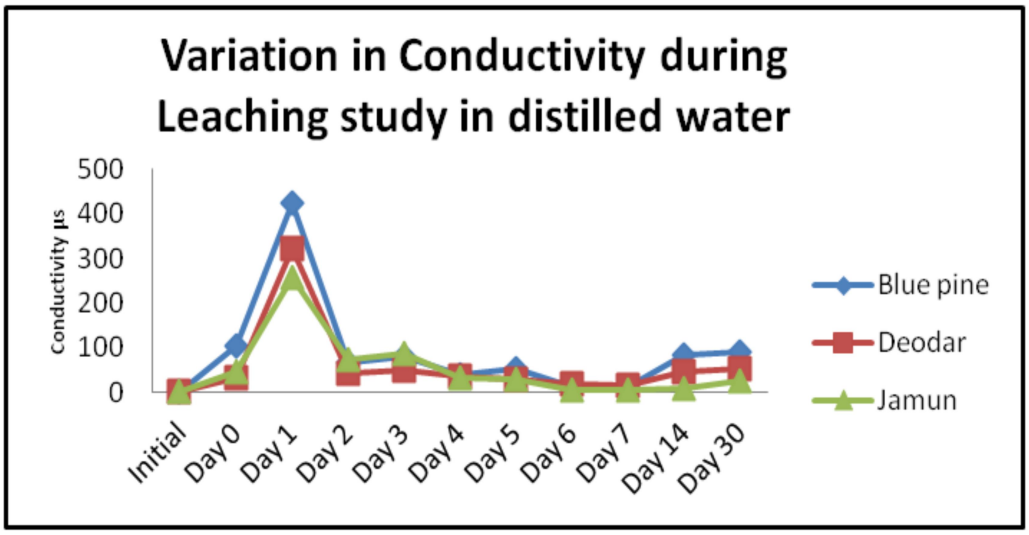

Fig. 7.4: Variation in Conductivity during leaching study with distilled water

The variations in the conductivity and Total Organic Carbon for the samples of leaching study indicated continued organic compound leaching in water. Changes in TOC of leachate was maximum on day 1 with a value of 630.7 mg/l (due to slight bacterial growth), 263.2 mg/l and 295.4 mg/l for Blue Pine, Deodar and Jamun respectively. Constant fresh TOC inputs were observed in leachate but in a declining trend as can be seen in Table 7.4 and Table 7.5

Similar leaching study was performed in Ganga river water with Blue Pine and Deodar needles. Leaching trends were similar to distilled water leaching as can be seen in figure 7.5 and 7.6.

Table 7.4: TOC Results of Leaching Study in Distilled Water

Leaching Days	TOC in ppm		
	Jamun in Distilled water	Blue Pine in Distilled water	Deodar in Distilled water
Day 1	295.4	630.7*	263.2
Day 2	163.6	162.5	85.8
Day 3	126.2	137.7	58.7
Day 4	70.8	86.4	39.5
Day 5	32.8	57.8	31.9
Day 6	20.5	41.5	25.1
Day 7	18.7	40.6	23.1
1 month	26.3	69.2	31.6
2 month	41.5	31.6	25.7

*Microbial growth

Table 7.5: TOC Results of Leaching Study in Ganga Water

Leaching Days	TOC in ppm	
	Blue Pine leaching with Ganga Water	Deodar leaching with Ganga Water
Day 1	217.9	212.8
Day 2	217.8	216.3
Day 3	56.7	60.9
Day 4	34.2	38.3
Day 5	28.2	29.7
1 month	49.4	46.6

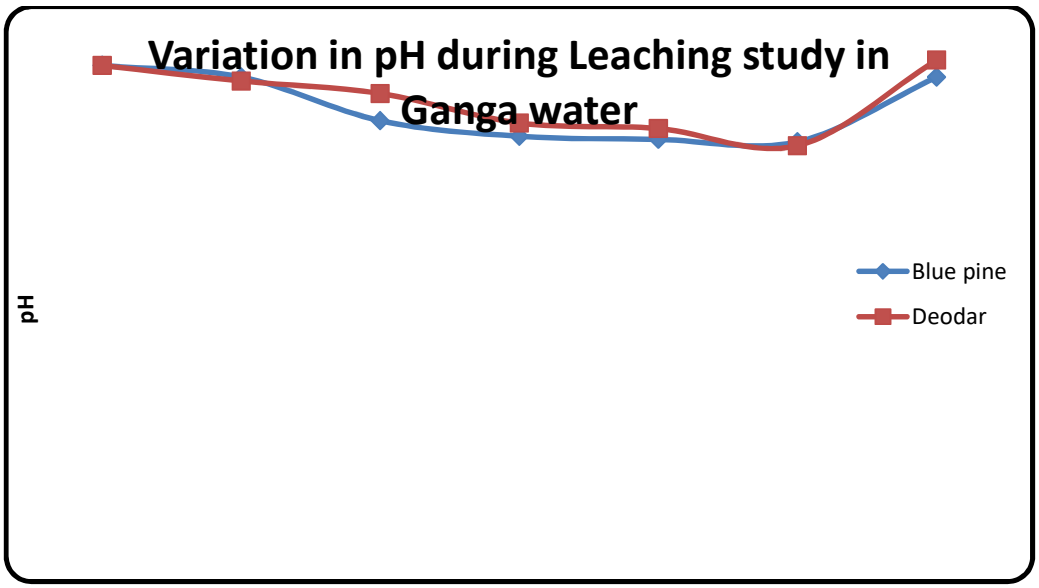

Fig.7.5: pH Variation during Leaching Studies in Ganga Water

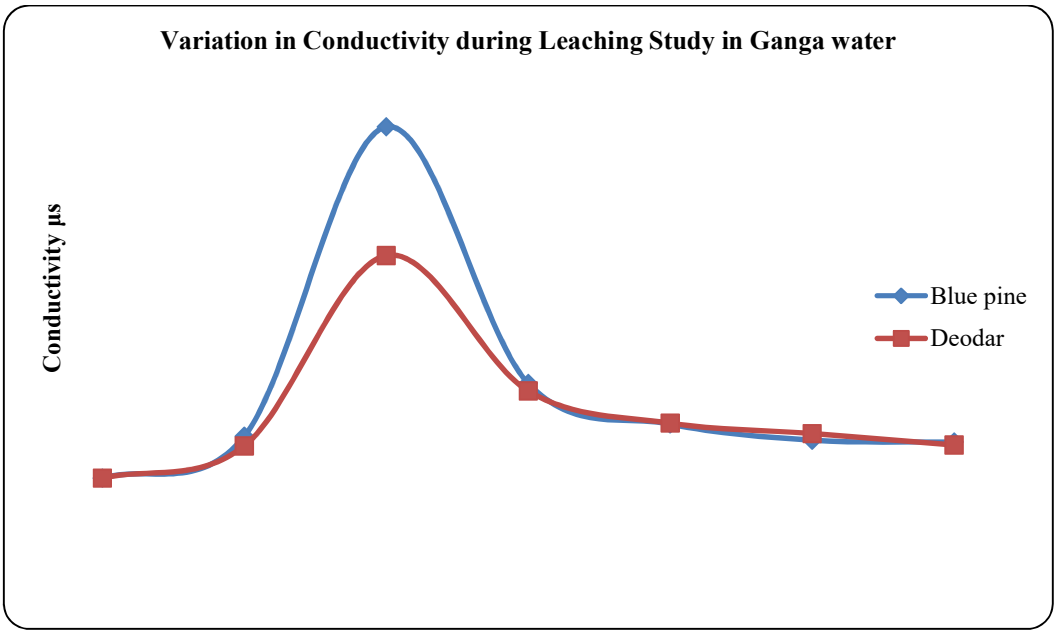

Fig. 7.6: Conductivity Variation during Leaching Studies in Ganga Water

7.1.5.1 FTIR Analysis

FTIR analysis gives an idea of the functional groups present in the samples. The phytochemicals usually belong to Amines, Alkanes, Esters, Amides, Alcohols or Phenolic groups, which are IR sensitive. The functional groups identified in different samples are given in Table 6. Aromatic groups and C=C were prominently present in all the leachate samples indicating presence of terpenes, besides Alcoholic, Phenolic (OH) and Ester groups

Table 7.6: Functional Groups Identified in Leaching Studies

Leaching Days	O-H	C-H Aromatic	C-H Aliphatic	C=O	C=C	C-N Amine	C-O
	(3500-3700)	(3000-3100)	(2840-3000)	(1670-1820)	(1620-1680)	(1266-1342)	(1000-1300)
Blue pine Day 1	+	+	+	-	+	-	+
Blue pine Day 2	+	+	+	-	-	-	+
Blue pine	+	+	-	-	+	-	+

Leaching Days	O-H	C-H Aromatic	C-H Aliphatic	C=O	C=C	C-N Amine	C-O
	(3500-3700)	(3000-3100)	(2840-3000)	(1670-1820)	(1620-1680)	(1266-1342)	(1000-1300)
Day 3							
Blue pine Day 4	+	+	+	+	+	+	+
Blue pine Day 5	+	+	+	+	+	-	+
Blue pine Day 6	+	+	+	-	+	-	+
Blue pine Day 7	+	+	-	-	+	-	+
Blue pine Day 14	+	+	-	-	-	-	+
Blue pine Day 32	+	+	+	-	+	-	+
Blue pine 6 months	+	+	+	+	+	+	+
Deodar Day 1	+	+	+	-	+	-	+
Deodar Day 2	+	+	+	-	+	-	+
Deodar Day 3	+	+	+	-	+	-	+
Deodar Day 4	+	+	+	-	+	-	+
Deodar Day 5	+	+	+	-	+	-	+
Deodar Day 6	+	+	+	-	+	-	+
Deodar Day 7	+	+	+	-	+	-	+
Deodar	+	+	+	-	+	-	+

Leaching Days	O-H	C-H Aromatic	C-H Aliphatic	C=O	C=C	C-N Amine	C-O
	(3500-3700)	(3000-3100)	(2840-3000)	(1670-1820)	(1620-1680)	(1266-1342)	(1000-1300)
Day 14							
Deodar Day 32	+	+	+	-	+	-	+
Deodar 6 months	+	+	+	-	+	-	+

7.1.5.2 Total Phenolic Content

Polyphenols are a class of secondary metabolites which play a key role as antioxidants. Besides, polyphenols are known to have many other functions (defense against herbivores and pathogens, repellence of insects, attraction of pollinators) Therefore, total phenolics, quantified in Ganga water sample as well as in leachate samples from the simulated experiments. Similar and higher ranges of total phenolics were also observed for the plant leachates of the simulated samples.

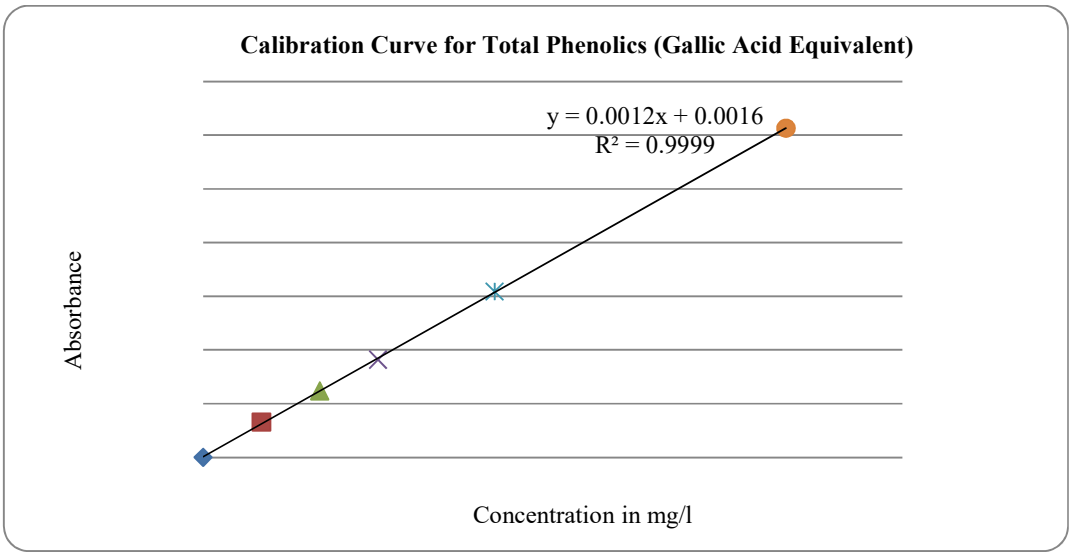

Fig. 7.7: Calibration Curve for Total Phenols (Gallic Acid Equivalent)

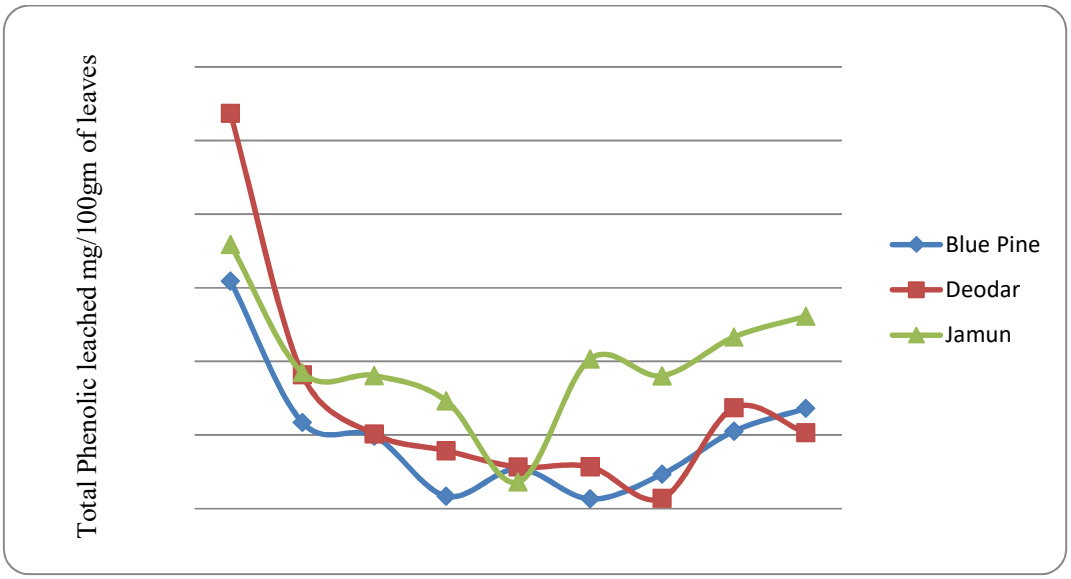

Fig. 7.8: Polyphenolic Compounds in Leachates and Ganga water samples

On comparing the cumulative leachate concentration with the Total Phenol Content in Leaf extracts it can be seen in Table 7 that more than 70% of Phenolics were leached out from Blue Pine and Jamun leaves. Deodar needles showed a slower leaching as compared to Blue Pine and Jamun.

Table 7.7: Phenolics in Leaf Extracts

Sample	Total Phenol Content in Leaf extracts (mg/100g of leaves)	Cumulative Total Phenol Content in Leachates for 30 days (mg/100g of leaves)
Blue Pine	639.12	448.39
Deodar	1095.1	633.31
Jamun	1175.8	892.43

A study reported by Yule et al. (2018) shows similar leaching trends of phenolic compounds from senescent leaves as given below.

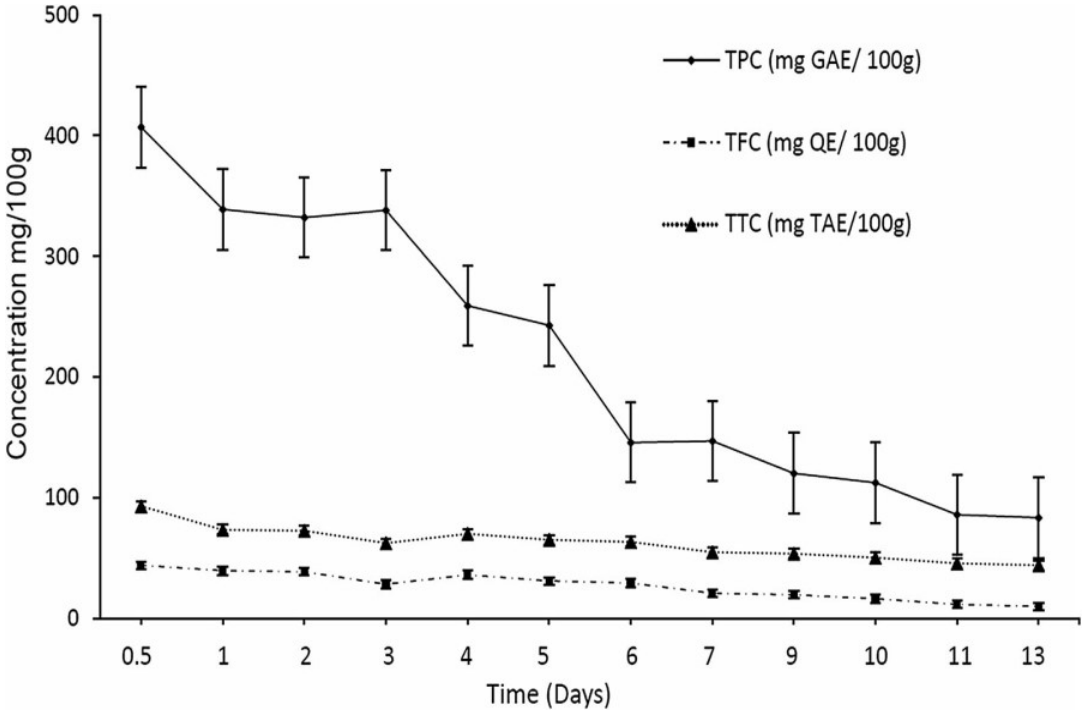

Fig 7.9: Leaching of phenolic compounds from senescent leaves (Yule et al. Carbon Balance Manage (2018) 13:3)

The total phenolic content of Gangotri water samples was in the range of 0.01-0.66 mg/l and Harsil: 0.76-1.16 mg/l. Literature value for river water range 0.5 to 1.1 mg/l (Fabrowska et al. , Wat. Res. 2018). The phenolics are reported to have food preservation properties thereby preventing putrefaction. (Plant Antimicrobial Polyphenols as Potential Natural Food Preservatives, 2019).

7.1.5.3 GC-MS Analysis: Terpenes and Terpenoids Leached

GCMS analysis was performed to understand the leaching of terpenes and terpenoids from the leaves. Table 8 gives the Limit of Detections (LOD) for the phytochemicals analysed. These LODs are based on the GC-MS response for the neat standards of these compounds.

Table 7.8: LODs based on neat standards injected in GC-MSMS

Phytochemical	LOD in ppm
Alpha Pinene	0.16
Camphene	0.15
Beta Pinene	0.51
3 carene	0.13
Eucalyptol	0.2
Fenchone	0.31
Menthol	0.14

The indicative concentration of terpenes and terpenoids in Leachate ahve been reported on the basis of LODs derived from calibrations of neat standards. The concentrations on various leaching Days are reported in Table 9 and 10.Indicative concentration of Terpenes and Terpenoids (µg/100gms of leaves) in Leachate on various leaching Days

Table 7.9: Blue Pine Leachate

Compound	Day 1	Day 2	Day 3	Day 4	Day 5	Day 7	Day 14	Day 32	Day 64
Alpha Pinene	-	-	BDL	24.60	7.17		-	-	-
Camphene	-	-	2.19	31.50	23.17	BDL	BDL	-	-
Beta pinene	-	-	-	39.30	-	-	BDL	-	-
3 carene	-	-	-		BDL			-	-
Eucalyptol	-	-	-		BDL			-	-
Fenchone	BDL	BDL	BDL	BDL	BDL		BDL	BDL	-
Menthol	3.74	24.59	BDL	4.21	-	-	-	-	-

Table 7.10: Deodar Leachate

Compound	Day 1	Day 2	Day 3	Day 5	Day 7	Day 16	Day 17	Day 32
Alpha Pinene	1.95	-	-	-	BDL	-	-	-
Camphene	5.37	-	-	BDL	1.46	-	-	-
Betapinene	-	-	-	-	BDL	-	-	-
3 carene	-	-	-	-	-	-	-	-
Eucalytptol	-	-	-	-	-	-	-	-
Fenchone	BDL	BDL	BDL	-	BDL	BDL	BDL	BDL
Menthol	-	2.42	1.43	-	-	-	-	-

In Jamun, the leaching was observed predominantly on Day 5. The important compounds leached were Alpha Pinene, Camphene and Beta pinene. In blue pine and deodar most of the studied compounds were observed in the leachates

7.1.5.4 Ganga Sample Analysis

The water, soil and sediment samples collected from the up were analysed for presence of any organic groups using FTIR. GC-MS/MS was used for specific identification of phytochemicals. Full scan screen on GC-MS/MS was performed. Reference standards (Purchased from Sigma-Aldrich) , of selected commonly occurring terpenes and terpenoids was used for a confirmatory qualitative analysis Some phytochemicals have been screened on the basis of NIST library confirmation on GC-MSMS (GCMS Varian 240).

7.1.5.5 Results of FTIR Analysis

Aromatic and alkene groups are detected in the samples indicating the presence of terpenes, terpenoids, phenolics and probably alkaloids as phytochemicals.

A combined FTIR scan for the water, soil sediment and litter samples is given in figure 7.10.

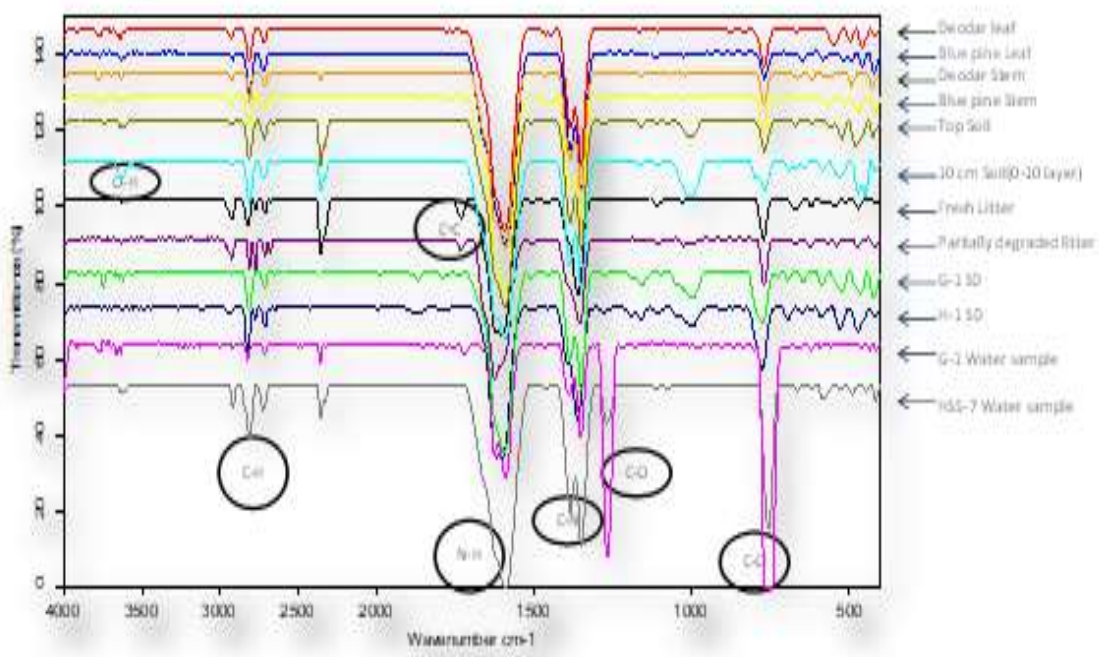

Fig. 7.10: Combined FTIR spectra for water, soil, sediment and leaf samples from Upper stretches of River Ganga

7.1.5.6 GC-MS/MS Analysis

Pre-processing of water samples was performed using Liquid Liquid extraction(LLE). For sediment, soil and litter extraction, automated soxhlet technique (Soxtherm) was used. Dichloromethane was used as an extraction solvent for LLE and for Soxhlet analysis a mixture of 1:1 acetone and hexane was used.

Many groups of phytochemicals like terpenes and terpenoids, alkaloids are reported to be present in the dominant plant species of the area. An attempt was made to screen commonly occurring phytochemicals like Alpha Pinene, beta pinene, Eucalyptol, menthol, Fenchone, 3-carene, Camphene, vanillin, squalene, limonene through GC-MS confirmation with the reference standards of these compounds.

A number of other phytochemicals were screened through GC-MS NIST library match which included various alkaloids, phenolic compounds, plant steroids, long chain alkenes/alcohols etc. which have been reported to exhibit medicinal properties.

Some of the representative GC-MS chromatograms with library matches are given below. Some typical compounds like vanillin were detected in the extracts. Vanillin is a commonly occurring compound in the plant species present in the sampling location and it is also reported to have with antimicrobial properties. A comparative representation of GC-MS chromatograms for the detection of Vanillin is as follows. The presence of vanillin can be observed both in the deodar stem and water sample collected from Harsil.

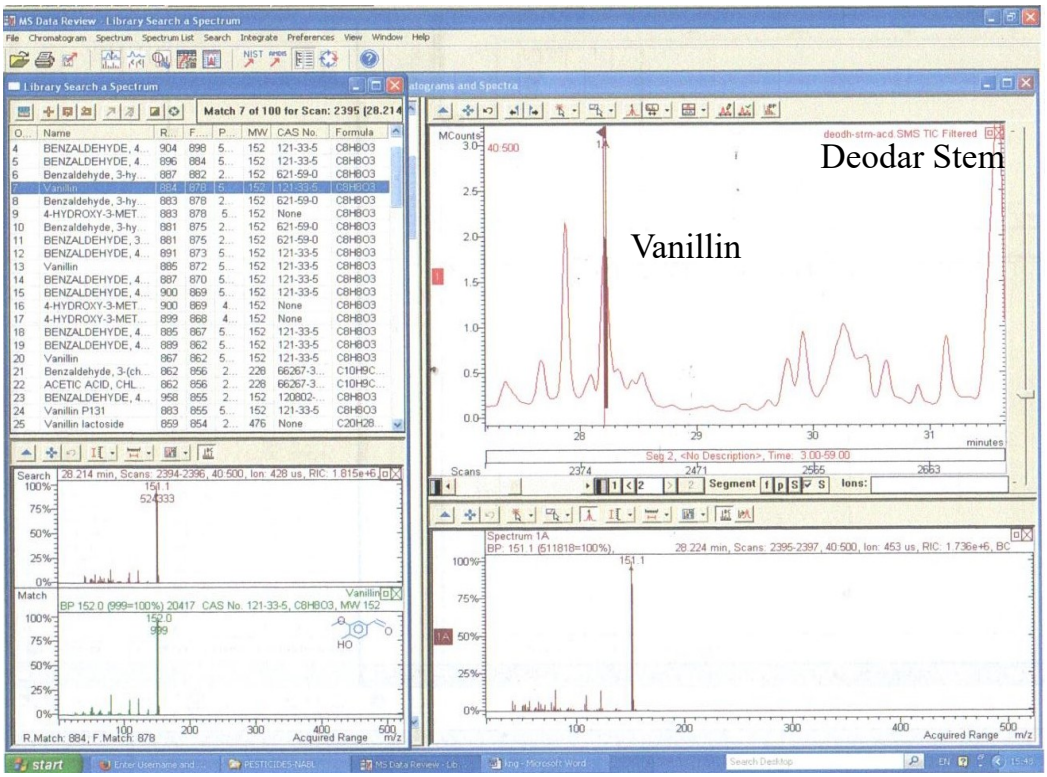

Fig. 7.11: GC-MS Chromatogram of deodar stem sample indicating presence of vanillin

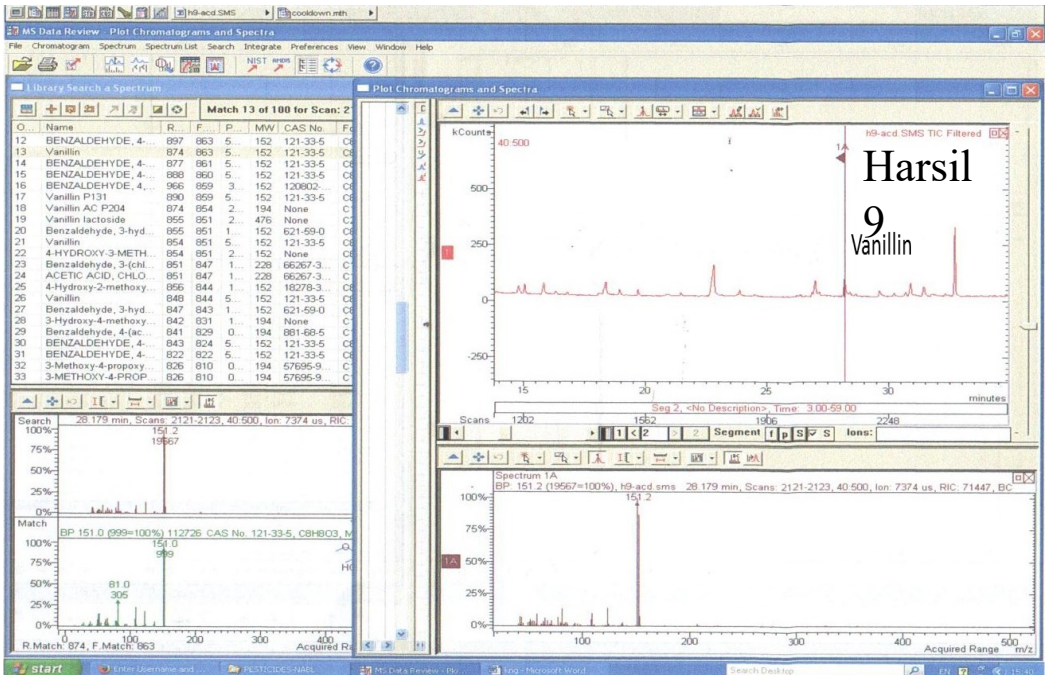

Fig.7.12: GC-MS Chromatogram of Harsil 9 water sample indicating presence of vanillin

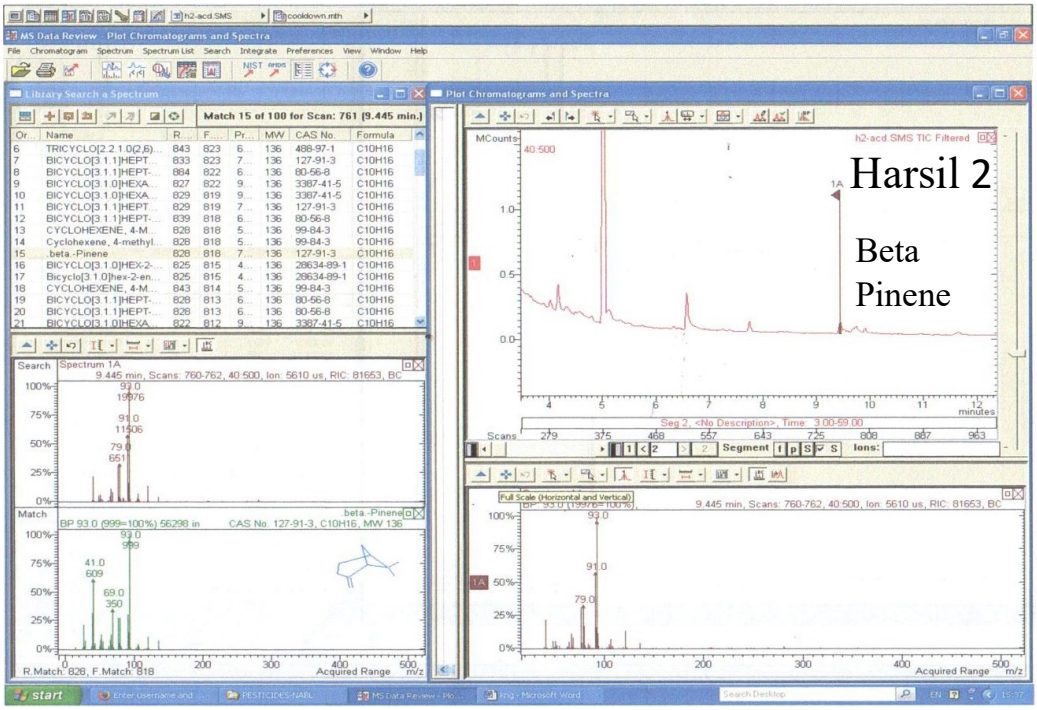

Fig. 7.13: GC-MS Chromatogram of Harsil 2 water sample indicating presence of Beta Pinene

The terpenes and terpenoids quantified in Ganga river samples were Alpha Pinene, beta pinene, Eucalyptol, menthol, Fenchone, 3-carene, Camphene. Sampling sites from Harsil showed presence of phytochemicals in most of samples collected. Alpha Pinene and/or Beta Pinene were prominently present in maximum samples. The side streams entering the river also showed presence of phytochemicals like camphene. Gangotri samples contained Alpha and Beta Pinene. (Table 7.11). Harsil has significant litter input due to upland terrain with a thick forest cover of Blue Pine and Deodar trees. The results relate well with the soil and the litter samples collected from Harsil as shown in Table 7.12.

Table 7.11: GC-MS Analysis of Ganga Water Samples

Sample Name	Compound
Harsil 1	Alpha pinene
	Beta pinene
Harsil 2	Beta Pinene
	Camphene
Harsil 3	Beta Pinene
Harsil 5	Beta Pinene
Harsil 9	Beta Pinene
	Camphene
Harsil 10	Beta Pinene
	Camphene
Harsil 11	Alpha pinene
	Beta pinene
Gangotri 1	Beta Pinene
	Camphene
Gangotri 2	Alpha-Pinene

Sample Name	Compound
	Beta-pinene
Dharali	Alpha-Pinene
	Beta-pinene
Tehri Dam	Alpha Pinene
	Beta pinene
Haridwar	Beta Pinene
Harsil Side stream 2	Beta-pinene
Harsil Side stream 8	Camphene

Table 7.12: Terpenes detected in water, sediment, litter and soil samples

Sample Name	Compound
Fresh litter	Menthol
	3-Carene
	Fenchone
	Alpha pinene
	Beta pinene
	Eucalyptol
	Camphene
Partially degraded	Fenchone
	Beta pinene
	Eucalyptol
Harsil Soil top layer	Alpha pinene
Soil top layer	Beta pinene
	3-Carene

Sample Name	Compound
	Menthol
	Eucalyptol
	Camphene
Harsil Soil (0-10 cm deep layer)	Alpha pinene
Soil (0-10 cm deep layer)	Beta pinene
	3-Carene
	Menthol
	Eucalyptol
	Fenchone
Harsil Sediment	Alpha pinene
	Beta pinene
Gangotri Sediment	Beta Pinene
Harsil Sidestream	Alpha Pinene

Other compounds like limonene,vanillin,squalene, azulene, borneol and some alkaloids were also screened in water samples based on the NIST library.

7.1.6 Non-Putrefaction Properties of Phytochemicals

Study on Non-putrefaction properties of different phytochemicals and Ganga water was performed using a protein source (beef extract) in water. This water containing protein would start putrefying in 24 to 48 hours due to bacterial growth. In the present study, water containing protein source was spiked with definite concentration of different phytochemicals (particularly terpenes and terpenoids) or Ganga water (which was likely to contain phytochemicals). Ganga water samples were taken in 1:1 ratio with the beef extract solution for the analysis. The bacterial growth was monitored in the samples spectrophotometrically by recording absorbance (indicating corresponding bacterial density) after incubation for 24 and 48 hours. The bacterial growth corresponding to increased optical density of solution was compared with the

optical density/absorbance of the blank sample with no spiked phytochemicals or Ganga water. Similar experiment was carried out using plant extracts. All the studies were carried out in triplicate .

It was observed that as compared to the blank sample containing beef extract, less putrefaction (as indicated by the bacterial density) was observed in the presence of plant extracts as can be observed by the absorbance values mentioned in Table 7.13 and 7.14.

Table 7.13: Protein putrefaction studies with Plant extracts

Sample	Initial Abs.	Abs.(24 hours)	Abs. (48 hours)
Blank	0.01	0.124	0.204
Blue Pine	0.081	0.031	*0.061 (After 72 hours)
Deodar	0.038	0.013	0.064

Initial

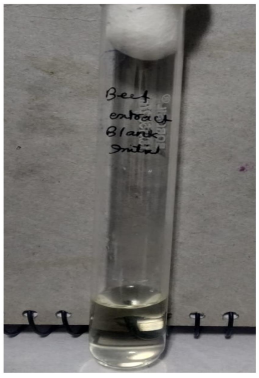

After 24 hrs

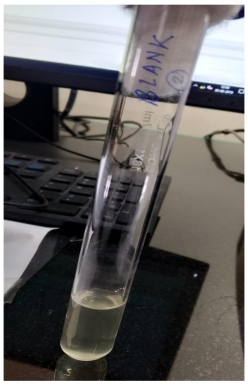

After 48 hrs

Table 7.14: Protein putrefaction studies with Ganga Water

Sample	Initial Abs(25/11/19)	Average Abs. After 24 hours
Blank (Beef Ext.)	0.052	0.26
Dharali +Beef Ext.	0.058	0.17
Harshil-10 + Beef Ext.	0.047	0.16
Tehri dam + Beef Ext.	0.07	0.20
Gangotri-1 + Beef Ext.	0.051	0.15

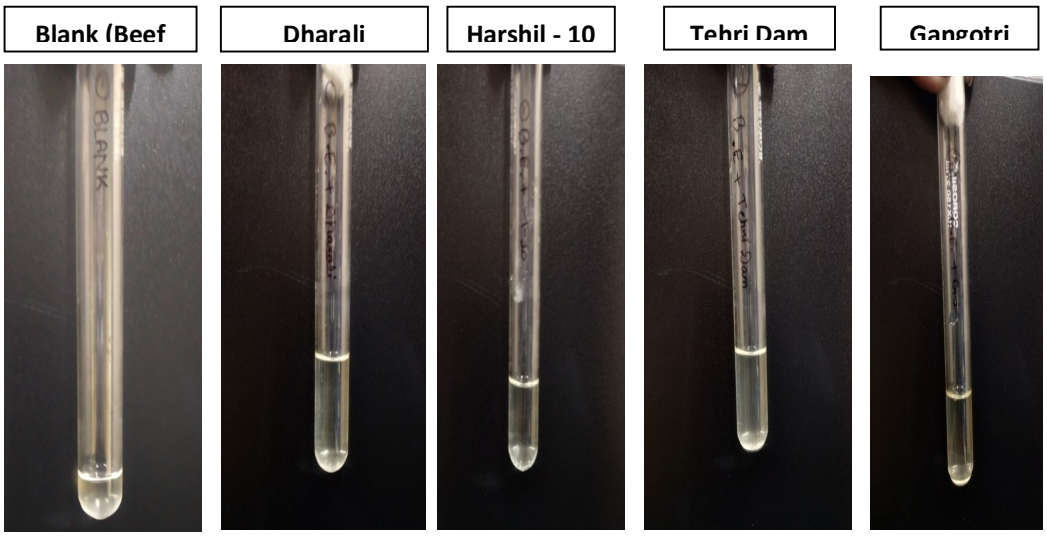

In case of individual phytochemical study carried out at 300 mg of phytochemical concentration. The relative values for spiked samples have been calculated with reference to the blank. Considering the growth of the blank to be maximum, it was denoted a value of 100% and the percentage growth with respect to blank sample have been given in Table 7.15.

Table 7.15: Protein putrefaction studies with Individual Phytochemicals

Phytochemicals	% Growth After 24 hours	% Growth After 48 hours
Blank	100.0	100.0

3-Carene	34.1	12.4
Alpha-Pinene	48.9	66.2
Beta-Pinene	62.4	-
Eucalyptol	38.2	-
Vanillin	30.3	46.7

7.1.7Salient Findings

A systematic attempt has been made to identify the presence of phytochemicals in Ganga water and understanding if they impart any special property to river Ganga water. Keeping in mind the complexity of river water composition due to the presence of large number of natural and anthopogenic compounds and their interactions, as well as huge dilution effect, the study was restricted to upper stretch of river. Another important reason for selecting this study area was due to the significant presence of riparian and upland vegetation in this catchment area of river, and the medicinal importance of these vegetation. To narrow down the list of probable compounds, the dominant vegetation parts of medicinally important trees were collected from the catchment areas and simulated experiments were performed to identify the presence of such compounds through leaching. These compounds and other phytochemicals in vegetation around the catchment area, were then targeted for their presence in river water by using advanced analytical techniques. Following are the important leads of this study, which needs further substantiation through an in-depth and more detailed investigations in future:

Riparian and upland vegetation likely introduces secondary metabolites to adjacent lateral streams coming from forests and finally merging in Bhagirathi and Alakhnanda.

Simulated experiments clearly inferred the presence and qualitative confirmation of organics/terpenes and related compounds/phytochemical/secondary metabolites in the leachates as indicated in FTIR and GC-MS analysis results. This also relates to the phytochemicals present in the plant species in riparian buffers.

Results of Ganga water sample analysis indicate confirmed organic fingerprinting leading to presence of terpenes and related compounds/phytochemical/secondary metabolites as interpreted through GC-MS/MS analysis.

Interestingly some of the probable compounds in the river water samples were those which were also observed in leachates of simulated experiments, thus strengthening the hypothesis of their origin from surrounding vegetation in the catchment area. The possible sources of these phytochemical signatures can thus be attributed to rich and biodiverse mega water sheds and landscapes of this stretch. However, at some places, the anthropogenic activities might also be a significant contributor to these compounds.

Dilution will play a crucial role for the effective concentrations of these phytochemicals at different locations of river and will ultimately determine the potential of their possible contributions to impart any significant medicinal or special properties to river water

The concentrations in Ganga water, however were mostly very low, to be able to impart any significant medicinal or non-putrefying properties, individually.

The special properties that these compounds impart in water is evidently concentration dependent, just like the doses of the medicines or antibacterial agents. Therefore, it may not be exaggeration to accept that during previous centuries the concentration of these compounds could be higher enough as the riparian forest cover in the upper stretches of river Ganga was enormous and subsequent deforestation has led to major loss of these forest covers. It can be therefore hypothesized that the course of river during early time would have added much more inputs of the phytochemicals in the water due to leaching from the forest and soil trails making the water much enriched with these phyto-constituents.

As stated before, this study had several limitations. Additionally complexity of the intra-ecosystem interactions, which requires an indepth assessment of the scenerios and drivers controlling the leaching and persistence of these phytochemicals in the Ganga water also need to be considered in future studies. However, these initial findings strongly suggest for a detailed related investigations in future.

7.1.8 References

- Silva, Ana & Lopes, Paula & Azevedo, Mariana & Costa, Danielle & Alviano, Celuta & Alviano, D.s. (2012). Biological Activities of a-Pinene and β-Pinene Enantiomers. Molecules (Basel, Switzerland). 17. 6305-16. 10.3390/molecules17066305.

- Perumalsamy, Haribalan & Jung, Moon & Hong, Seung & Ahn, Young-Joon. (2013). Growth-Inhibiting and morphostructural effects of constituents identified in Asarum heterotropoides root on human intestinal bacteria. BMC complementary and alternative medicine. 13. 245. 10.1186/1472-6882-13-245.

- Wang, Tong-Hong, et al. "Evaluation of the antibacterial potential of liquid and vapor phase phenolic essential oil compounds against oral microorganisms." PloS one 11.9 (2016).

- Odeyemi, Olumide & Oluwajoba, Solakunmi. (2011). Synergistic effect of menthol on in-vitro antibacterial activity of Garcinia kola against gram positive bacteria: A preliminary study. Journal of Applied Pharmaceutical Science. 1. 98-100.

- Roda, Rita & Taboada-Rodríguez, Amaury & Valverde-Franco, María & Marín, Fulgencio. (2010). Antimicrobial Activity of Vanillin and Mixtures with Cinnamon and Clove Essential Oils in Controlling Listeria monocytogenes and Escherichia coli O157:H7 in Milk. Food and Bioprocess Technology - FOOD BIOPROCESS TECHNOL. 5. 10.1007/s11947-010-0484-4.

- Panahi, Yunes & Sattari, Morteza & Babaie, Ahmad & Beiraghdar, Fatemeh & Ranjbar, Reza & Joo, Ali & Bigdeli, Mohsen. (2011). The Essential Oils Activity of Eucalyptus polycarpa, E. largiflorence, E. malliodora and E. camaldulensis on Staphylococcus aureus. Iranian journal of pharmaceutical research : IJPR. 10. 43-8.

- Allenspach, Martina & Valder, Claudia & Steuer, Christian. (2020). Absolute quantification of terpenes in conifer-derived essential oils and their antibacterial activity. Journal of Analytical Science and Technology. 11. 10.1186/s40543-020-00212-y.

- Yemiş, Gökçe & Pagotto, Franco & Bach, Susan & Delaquis, Pascal. (2011). Effect of Vanillin, Ethyl Vanillin, and Vanillic Acid on the Growth and Heat Resistance of Cronobacter Species. Journal of food protection. 74. 2062-9. 10.4315/0362-028X.JFP-11-230.

- Moreira, Ana & Lima, Edeltrudes & Souza, Evandro & Dingenen, Monique & Trajano, Vinicius. (2007). Inhibitory effect of Cinnamomum zeylanicum Blume (Lauraceae) essential oil and β-pinene on the growth of dematiaceous moulds. Brazilian Journal of Microbiology. 38. 33-38. 10.1590/S1517-83822007000100008.

- Dai, Jiali & Zhu, Liang & Yang, Li & Qiu, Jun. (2013). Chemical composition, antioxidant and antimicrobial activities of essential oil from Wedelia prostrata. EXCLI Journal. 12. 479-490. 10.17877/DE290R-7125.

- El Atki, Yassine & Aouam, Imane & Taroq, Amal & Gourch, Abdelkader & Badiaa, Lyoussi & el Kamari, Fatima. (2019). Antibacterial efficacy of Thymol, Carvacrol, Eugenol and Menthol as alternative agents to control the growth of nosocomial infection-bacteria. Journal of Pharmaceutical Sciences and Research. 11. 306-309.

- Soković, Marina & Glamoclija, Jasmina & Marin, Petar & Brkic, Dejan & Van Griensven, Leo. (2010). Antibacterial Effects of the Essential Oils of Commonly Consumed Medicinal Herbs Using an In Vitro Model. Molecules (Basel, Switzerland). 15. 7532-46. 10.3390/molecules15117532.

- Phanthong, Phanida & Lomarat, Pattamapan & Chomnawang, Mullika & Bunyapraphatsara, Nuntavan. (2013). Antibacterial activity of essential oils and their active components from Thai spices against foodborne pathogens. ScienceAsia. 39. 472. 10.2306/scienceasia1513-1874.2013.39.472.

- Montironi, Ivana & Cariddi, Laura & Reinoso, Elina. (2016). Evaluation of the antimicrobial efficacy of Minthostachys verticillata essential oil and limonene against Streptococcus uberis strains isolated from bovine mastitis. Revista Argentina de Microbiología. 48. 10.1016/j.ram.2016.04.005.

- Rasoul, Mona & Kh, Gehan & Marei, & Abdelgaleil, Samir. (2012). Evaluation of antibacterial properties and biochemical effects of monoterpenes on plant pathogenic bacteria. 6.
- Yule et al. Carbon Balance Manage (2018) 13:3 Leaching of phenolic compounds from senescent leaves
- Plant Antimicrobial Polyphenols as Potential Natural Food Preservatives, 2019J Sci Food Agric, Mar 15;99(4):1457-1474. Lynda Bouarab Chibane , Pascal Degraeve , Hicham Ferhout , Jalloul Bouajila , Nadia Oulahal
- Plant nutraceuticals as antimicrobial agents in food preservation: terpenoids, polyphenols and thiols , Int. J. Antimicrobial Agents 2018 , International Journal of Antimicrobial Agents, Volume 52, Issue 3, September 2018, Pages 309-315

7B. PHYTOCHEMICAL COMPONENT

7.2 Phytochemical Component

7.2.1 Background

Presences of MAPs (Medicinal & Aromatic Plants) in riparian and upland forests of Upper Ganga River Basin (UGRB) are extensively used for their special properties (medicinal and healing). Bhagirathi and Alakhnanda stretch forms Upper Ganga River Basin (UGRB) having dominant riparian vegetation forest and MAPs. The phytochemicals leaching from riparian and upland vegetation likely contribute to the properties of river Ganges. It has ready been reported and confirmed during our primary surveys that have wide variety of floral diversity in upland as well as riparian UGRB and many of them are MAPs.

Phytochemicals are broad term referring to plant (phyto) chemical referring to a wide variety of secondary metabolites or organic compounds that occur naturally in plants. They are non- nutritive organics that are plant based chemicals having protective or disease preventive properties. It is well-known that plants produce these secondary metabolites or chemicals to protect themselves but recent researches demonstrate that they can also protect humans against diseases. There are more than thousand known phytochemicals working differently such as acting as antioxidant, effecting hormonal actions, stimulation of enzymes, antibacterial effects, interference with DNA replication, physical effects etc. (https://www. phytochemicals.info/disclaimer.php). Table 16 provides an overview of different groups of secondary metabolites that are present and can be extracted from plants.

Table 7.16: Prominent secondary metabolites/phytochemicals reported from plant based sources

Polyphenols	Flavanoids	Quercitin
		Tanins
		Epigallactocatechin
	Phenolic acids	Vanillic Acid
		Gallic Acid
		Caffeic Acid
	Non-Flavanoid Polyphenols	Furanocoumarins
		Tanins
		Coumarins
Terpenoids	Carotenoid Terpenoids	Carotenoids
	Non-Carotenoid Terpenoids	Saponins
		Sterols/Steroids
		Ursolic acid
		Oils
Thiols	Glucosinolates	
	Allylic Sulphides	
	Indoles	

UGRB zone supports about 18,440 species of plants reported of which about 45% are having medicinal properties (total 1748 spp.) (http://forest.uk.gov.in/pages/display/99-medicinal- aromatic-plants). More than 125 are traded at large scale for various purposes for their phytochemical and healing properties. Figure 7.14 shows dominant forest type as well as dominant plants along the stretch and the MAPs that were preferred for study based on the dominance (% TGA i.e. Total Geographical Area) and presence of highly aromatic medicinal trees in these stretches. Cedrus deodara and Pinus wallichiana were selected for the study from these stretches.

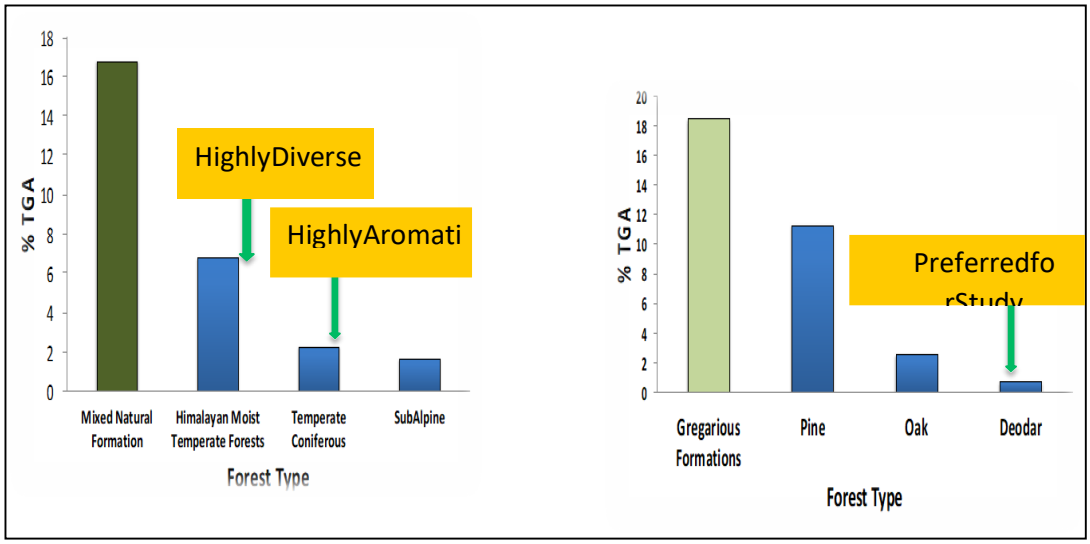

Source: IIRS, Dehradun 2016

Fig. 7.14 Types of forest in UGRB and the Dominant Tree Species as per their presence in percentage Total Geographical Area (TGA)

Various forest types were also reported in UGRB in which grasslands were dominant showing herbs and shrubs diversity and also the phytochemicals secreting from those plants were reviewed. Grasslands are habitat to a lot of herb and grasses that are medicinal and aromatic in nature. Figure 7.15 presents the dominant grasslands as per TGA in Uttarakhand.

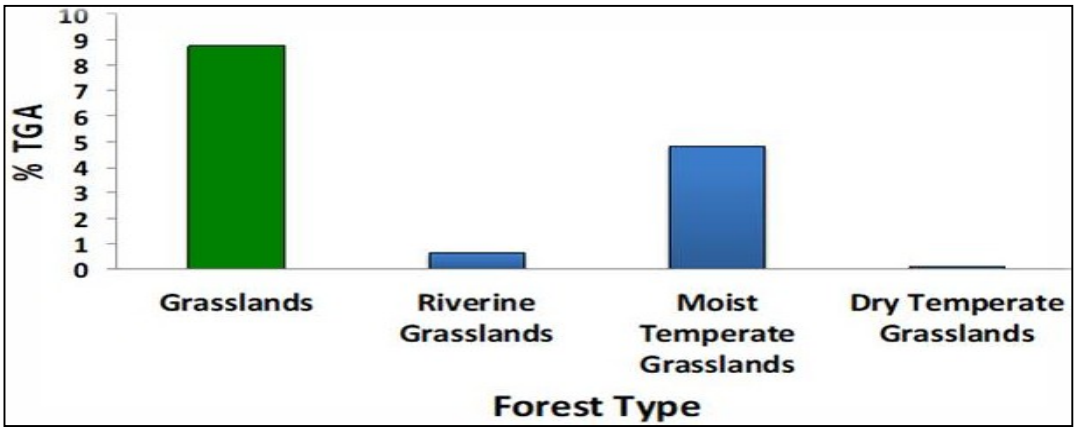

Fig 7.15: Different forest types in UGRB

More than 80 peer-reviewed publications were referred for phytochemicals reported from tree, shrub and herb species of Moist temperate, Dry Temperate and Alpine areas in Bhagirathi and Alakhnanda Catchment (For plant details please see the list in Appendix). Plants studied were from different plant groups that varied from broad-leaved trees, coniferous/gymnosperm trees as well herbs and shrubs present in forest types. Figure 7.16 shows the different plants (broad leaved, conifers/gymnosperms, herbs and shrubs) studied for their phytochemical components.

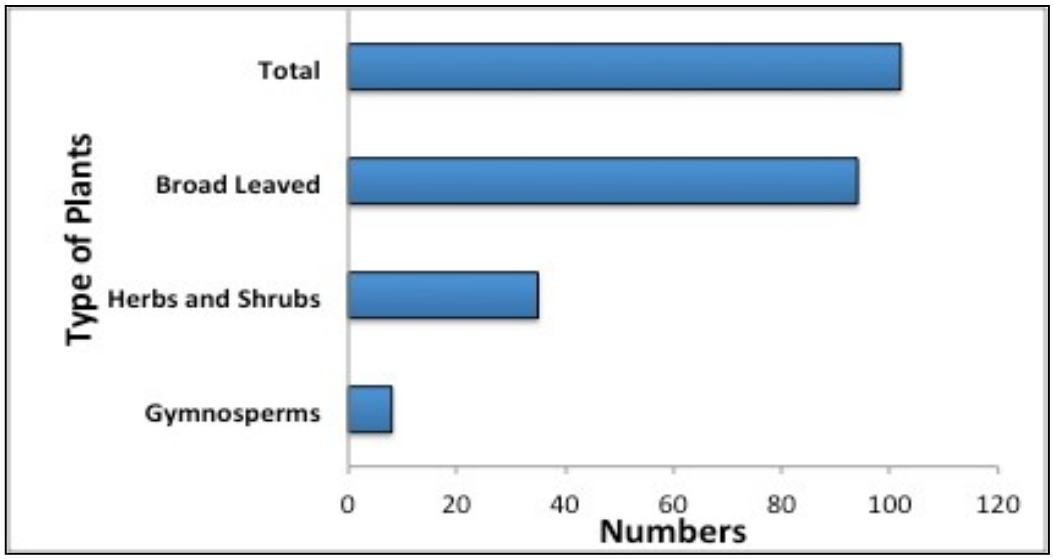

Fig.7.16: Number of plant species under different groups and habits reviewed for plant based phytochemicals/secondary metabolites

Broad group of phytochemicals reported from 54 trees of broad leaved, 6 coniferous and 50 MAPs (herbs and shrubs) were listed. Phytochemicals such as polyphenols, flavonoids etc were mostly studied and analyzed for plant based phytochemicals whereas lipids were less studied and analyzed for plant based secondary metabolites/phytochemicals. It was observed from extensive review of literature that mostly, Polyphenols and Terpenoids in plants were analyzed than other secondary metabolites. Alkaloids and Thiols were not at all reported and analyzed. A summary of our review with respect to phytochemicals in Trees as well as herbs and shrubs is presented in Figure 7.17and Figure 7.18 respectively.

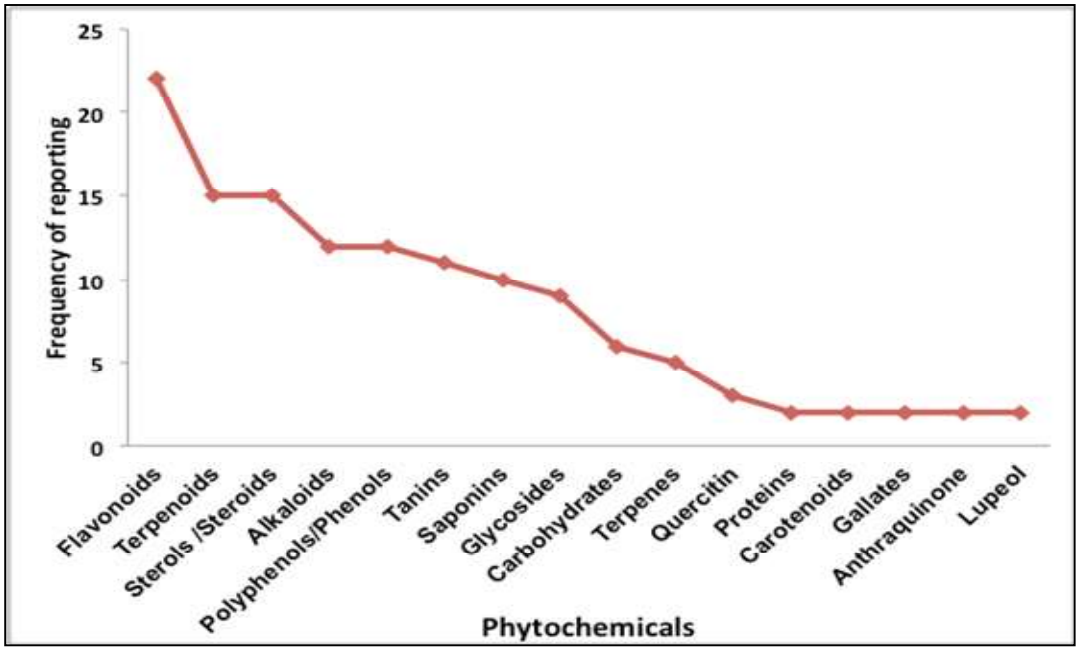

Fig.7.17: Important group of secondary metabolites analyzed and reported from Trees in UGRB (Data collated from literature review)

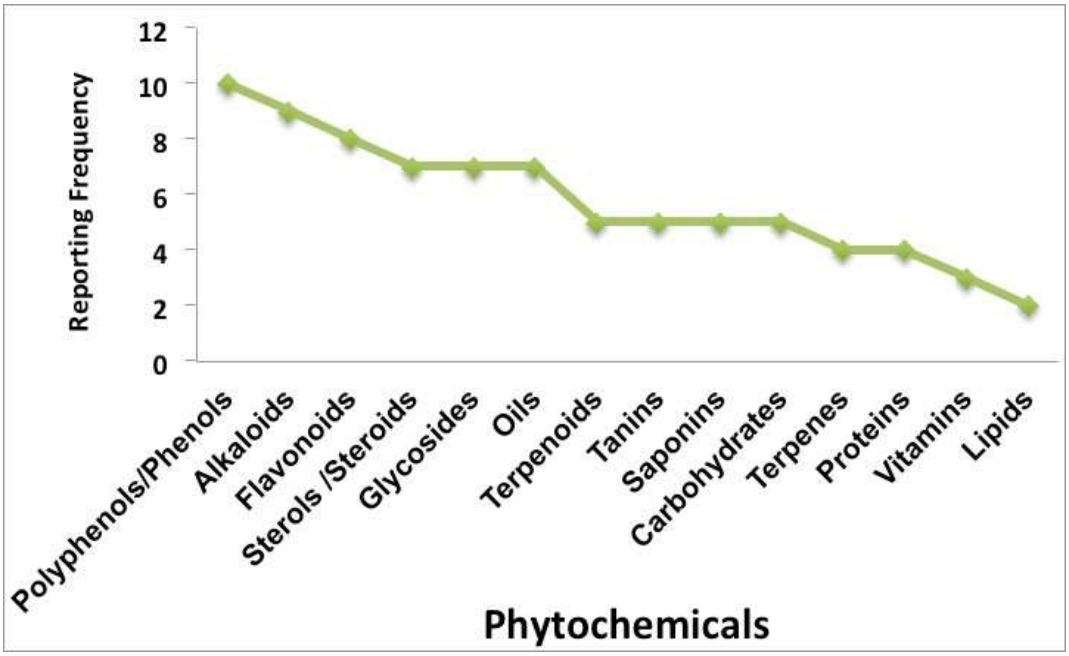

Fig.7.18: Important group of secondary metabolites analyzed and reported from herbs and shrubs in UGRB (Data collated from literature review)

Dense forest of Blue Pine and Deodar is found in Upper Ganga River Basin (UGRB). Considering Pine (Pinus roxburghii) in low altitude (400-1200 amsl) while, Blue Pine with Deodar (P. wallichiana with C. deodara) at high altitude (2000-3200 amsl) are dominant canopies (14% of gregarious patches) (Plate 1) hence, understanding the phytochemical/secondary metabolite leaching has been attempted in this stretch especially focused from Gangotri to Harsil in UGRB of Bhagirathi stretch.

Plate 7.9: Habitat and dense formations of Deodar and Blue Pine forests in Upper Ganga Catchment of Bhagirathi basin

7.2.2 Plant based Leaching Experiments

Plant based leaching experiment were carried out understand the leaching patterns of the plants growing in lower altitude in comparison to plants growing in UGRB. Selected plants based on their properties belonging to different groups were collected from NEERI campus as listed in Table 7.17. and leaching experiment was carried out using both Ganga water as well as Distilled water.

Table 7.17: Selected plants collected for leaching experiments in Ganga water as well as distilled water

S. No.	Scientific Name	Vernacular Name
1.	Thuja orientalis	**Thuja**
2.	Casuarina equisetifolia	**Whistling Pine**
3.	Polyalthia longifolia	**False Ashoka**
4.	Ziziphus maurtiana	**Ber**
5.	Punica granatum	**Pomegranate**
6.	Aloe vera	**Ghritkumari**
7.	Azadirachata indica	**Neem**
8.	Catharanthus roseus	**Sadaphuli**
9.	Ficus religiosa	**Peepal**
10.	**Leucaena leucocephala**	**Subabul**

Plants parts (especially leaves) were kept in distilled water and pH and EC of the samples were taken on daily basis. Ph range was found mostly between 4.5-7 (shown in Figure 7.19) and EC showed increase in range upto 1400 (shown in Figure 7.20). Casuarina equisetifolia survived longest upto 17 days however other plants got rotten in few days. This was due to specific lef characters of the leaves of Casuarina.

Column based leaching experiment using Lysimeter to understand leaching of secondary metabolites in high altitude soil at Harsil

Based on previous leaching based experiments in the beaker using leaves of Deodar and Blue Pine in laboratory, another set of improve experiment was set up using Lysimeter. Lysimeter is a device for measuring percolation of water through soils and sampling

soil water for chemical analyses (Figure 6). A lysimeter enables researchers to study and understand the natural environment by capturing the natural water gain and loss in a soil column under controlled conditions such as infiltration, runoff, and evapotranspiration.

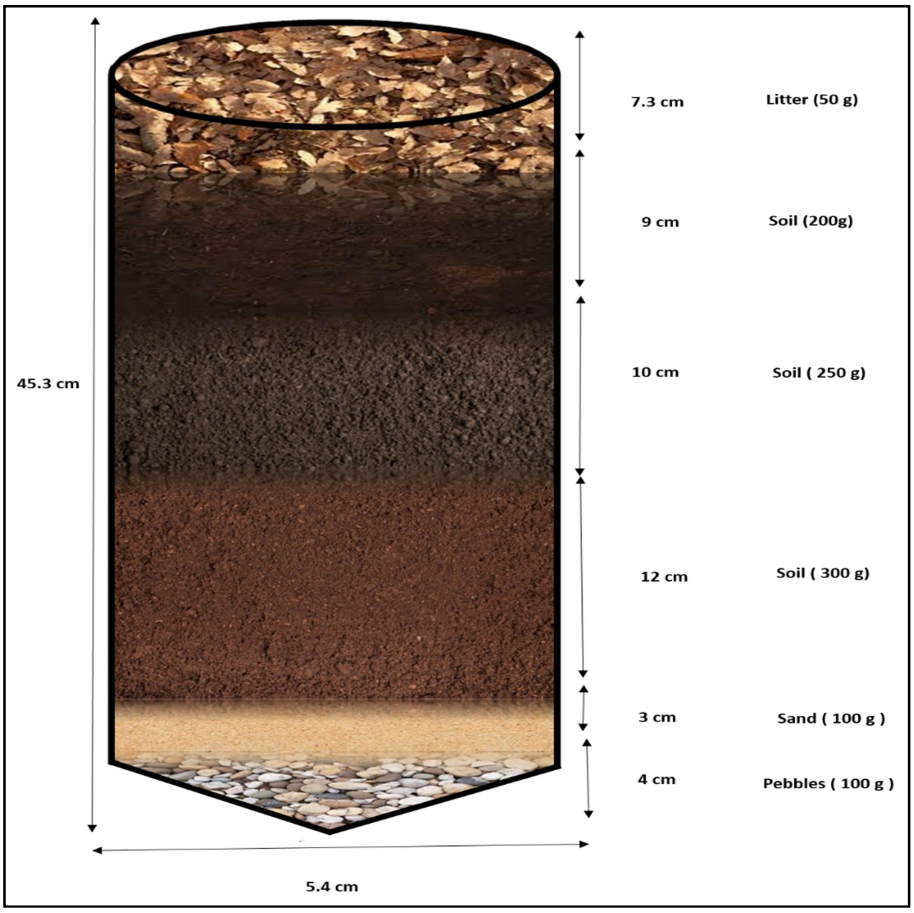

Fig. 7.19: Graphical Representation of Lysimeter Setup to study the phytochemical leaching from leaf litter in the soil profile

Leaching experiment was done using Lysimeter (column based experiments) for simulating the collection of leachate from litter-soil profile of Harsil (Higher altitude) and understanding the basic plant based secondary metabolites presence in the leachates. The soil profile (0-40 cm) of Deodar (Cedrus deodara) and Blue Pine (Pinus wallichiana) tree was collected from Harsil, Uttarakhand before Gangotri in the catchment of river Bhagirathi during the pre-monsoon survey in the month of May, 2019. The litter and soil profile upto 40 cm was collected for the experiments in Lysimeter columns (Fig. 6 and 7). Day time pre monsoon temperature and humidity

(approx. 25 degrees and approx. 48% humidity) was maintained in lab from August-October, 2019 that was little higher than the study area (Harsil minimum and maximum temperature varies from 5oC to 20 oC during summer months i.e. April-June though, occasional showers lower the temperature).

Collection of leachate was carried out in two ways first was using single time passed leachate that was less concentrated whereas, we also passed the leachate multiple (3-4) times from the same column so, that concentrated leachate can provide us better inferences about secondary metabolites from litter leaching. Lysimeter column used in the experiment had height of 45.3 cm and diameter of 5.4 cm. Study design included arranging soil profile of Harsil in Lysimeter with pebbles, sand, soil from 40 cm, 10 cm, 5 cm and leaf litter. Water used in the experiment was distilled and tap water and quantity was 1000 ml whereas, volume of leachate collected was 850 ml (approx.). Time taken for collection of leachate in first run was 4.5 hrs and for second run was 14 hrs (approx) (Fig. 7.21).

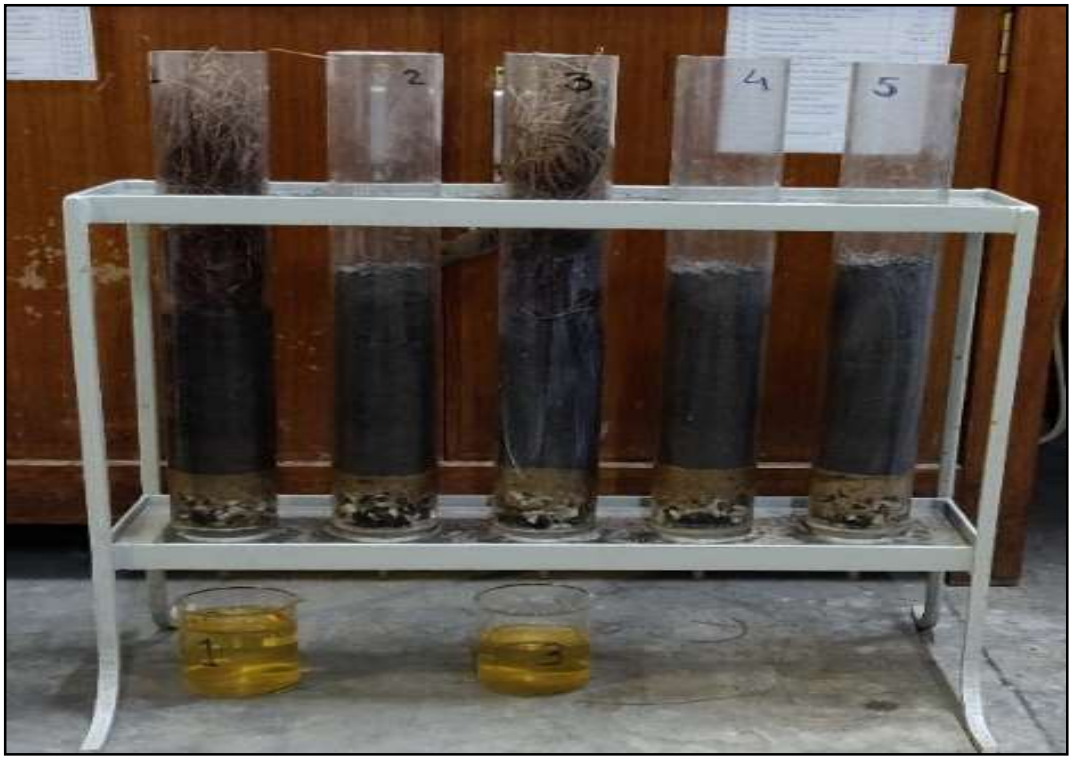

Fig. 7.20: Lysimeter Setup to study the phytochemical leaching from leaf litter (Deodar and Blue Pine) in the soil profile of Harsil

Fig. 7.21: Collected Leachate Samples of first trial and second trial

7.2.3 TOC and CHNS of the Samples before leaching experiments

Before carrying out column based leaching experiment, Total Organic Carbon (TOC) (Shimadzu, Japan Model TOC Vcph) and Carbon, Hydrogen, Nitrogen and Sulphur (CHNS) concentration in plant parts, litter and soil was analysed. TOC of the samples are presented in Fig. 7.22.

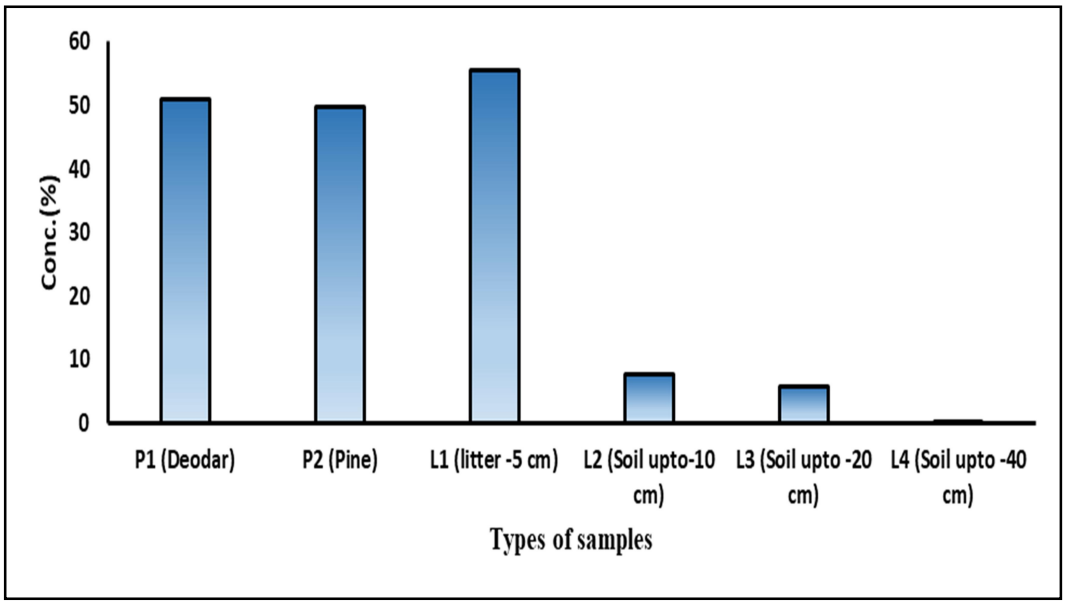

Fig.7.22. TOC of plants, litter and soil from different depths of Harsil forest

Figure7.22 represents the TOC concentration (%) in plant parts, litter and soil profile. Plants and litter showed presence of high amount of TOC that varied between 50-60

% while, it dropped down vertically in the soil profile. CHNS analysis was done by CHNS analyzer (Elementar Germany, Model Micro Select).

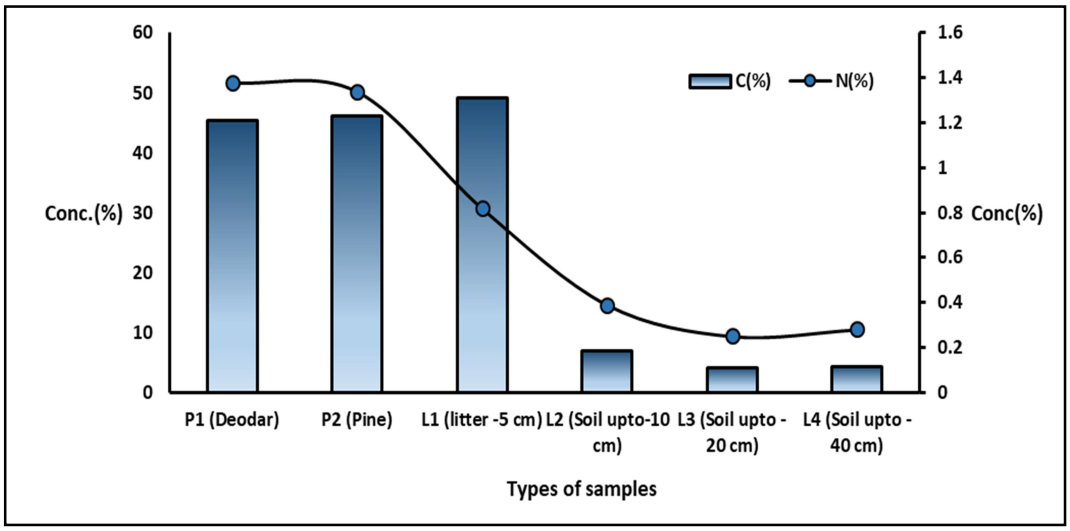

Fig 7.23: of plants, litter and soil from different depths of Harsil forest

Higher C: N ratio was observed in plants of Harsil forest reflecting to slow rate of litter decomposition (Fig. 7.23). Shafei et al., 2016 was followed for qualitative estimation of secondary metabolites present in the leachates collected from the column based lysimeter experiments. In the first trial Harsil (litter + soil) profile of Cedrus deodara tree was taken. Qualitative presence of secondary metabolites are presented in Table 7.18.

Table 7.18. Qualitative assessment of secondary metabolites from Cedrus deodara (Deodar) tree soil (Harsil) profile from single run leachate

Sl. No	Phyto-chemicals	Soil Leachate (Tap Water)	Soil Leachate (Distilled water)	Litter+Soil Leachate (Tap water)	Litter+Soil Leachate (Distilled water)	Deodar Leaves	Pine Leaves
1.	Flavonoids	-	-	-	-	+	+
2.	Terpenoids	+	-	-	-	+	+
3.	Tanins	-	+	+	+	+	+

Sl. No	Phyto-chemicals	Soil Leachate (Tap Water)	Soil Leachate (Distilled water)	Litter+Soil Leachate (Tap water)	Litter+Soil Leachate (Distilled water)	Deodar Leaves	Pine Leaves
4.	Carbohydrates	-	-	-	-	+	+
5.	Steroids	-	-	-	-	+	+
6.	Saponins	-	-	-	-	-	-

No positive results for secondary metabolities were observed in laechate from single run of water in lysimeter. Terpenoid and tannin tests were positive in some leachates (Table 7.18). In fresh leaves of the trees, all tests were positive. In the second trial soil profile of Pinus wallichiana (Blue Pine) tree was taken. In this trial 3-4 times collected leachate was run from the same soil-litter profile assembly in lysimeter and qualitative assessment of phytochemicals was carried out. The results are presented in Table 7.19.

Table 7.19. Qualitative assessment of secondary metabolites from Pinus wallichiana (Blue Pine) tree soil (Harsil) profile from multiple run leachate

Sl. No	Phyto-chemicals	Litter Leachate (Distilled Water)	Litter Leachate (Tap Water)	Soil Leachate (Distilled Water)	Soil Leachate (Tap water)	Litter+Soil Leachate (Distilled water)	Litter+ Soil Leachate (Tap water)
1.	Flavonoids	-	-	-	-	-	-
2.	Terpenoids	+	+	+	+	+	+
3.	Tanins	+	+	+	+	+	+
4.	Carbohydrates	-	-	-	-	-	-
5.	Steroids	+	+	+	+	+	+

6.	Saponins	-	-	-	-	-	-

In the second trial, Pinus wallichina tree (blue pine) litter was used along with the collected soil samples. Terpenoid, tannin and steroid tests were positive (Table 7.19). In II trial we collected concentrated amount of leachate, hence more secondary metabolites were positive during the qualitative estimation (Table 7.19). In III trial Cedrus deodara and Pinus wallichina litter was taken to collect the leachate. The results are presented in Table 7.20

Table 7.20: Qualitative assessment of secondary metabolites from Cedrus deodara (Deodar) and Pinus wallichina tree (blue pine) tree soil (Harsil) profile from multiple run leachate

Sl. No.	Phyto-chemicals	Litter Leachate (Distilled Water)	Litter Leachate (Tap Water)	Soil Leachate (Distilled Water)	Soil Leachate (Tap water)	Litter+Soil Leachate (Distilled water)	Litter+Soil Leachate (Tap water)
1.	Flavonoids	-	-	-	-	-	-
2.	Terpenoids	+	+	+	+	+	+
3.	Tanins	+	+	+	+	+	+
4.	Carbohydrates	-	-	-	-	-	-
5.	Steroids	+	+	+	+	+	+
6.	Saponins	-	-	-	-	-	-

Terpenoid, tannin and steroid were observed positive in the qualitative estimation of leachate for secondary metabolites. During overall qualitative estimation of secondary metabolites in all the trial runs using different litter combinations in Lysimeter for the leachate samples, carbohydrate and saponin tests were negative.

7.2.4 Antibacterial properties of plant-leaf litter-soil leachate from Lysimeter study

Agar Disc Diffusion method (Bauer et al., 1966) and Agar Well method (Magaldi et al., 2004) were used for understanding the Antibacterial properties of plant-leaf litter-soil leachate from Lysimeter study. After assessing the presence of qualitative secondary metabolites in the leachates, antibacterial test against E. coli and S.aureus using disc diffusion and agar well diffusion methods was carried out. No inhibition zone was observed in the leachates collected from Cedrus deodara (Deodar) and Pinus wallichina tree (blue pine) tree soil (Harsil) profile from multiple run leachate (Fig. 7.24).

Results for Agar Well Diffusion Method | **Results for Agar Disc Diffusion Method**

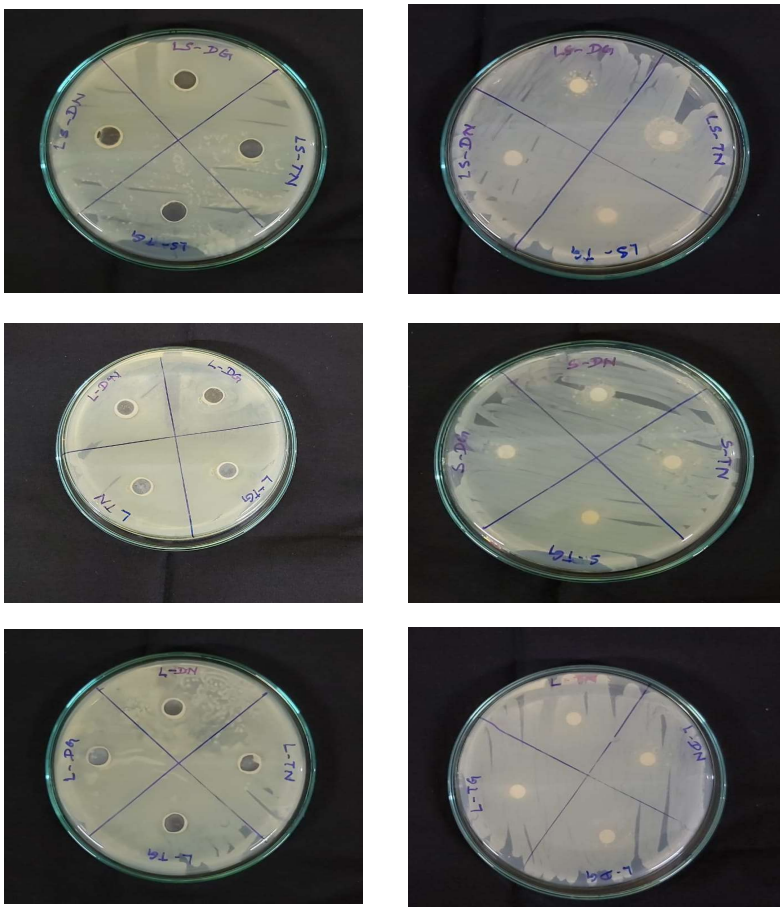

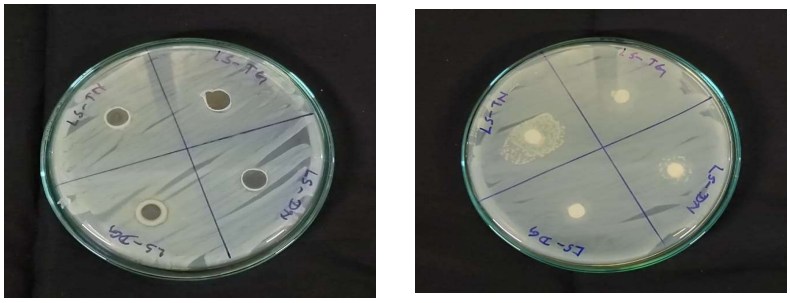

Fig.7.24: Antibacterial test of leachates using Agar Disc Diffussion Agar Well Diffusion method showing no inhibition zone

CHAPTER – 7C

SALIENT FINDINGS

The study undertaken has three main components, viz., chemical, biological, and health aspects, and nine sub-components to understand the specific characteristics of the River Ganga. A systematic attempt has been made to understand the physio-chemical aspects along the entire length of the River Ganga. In total, thirteen locations were selected for the water sampling, which was divided into the following two stretches:

- Stretch I – Upper stretch (Gomukh, Gangotri, Harshil, Maneri, Tehri, Devprayag, Rishikesh/ Haridwar)
- Stretch II – Lower Stretch (Bijnor, Kanpur, Allahabad, Varanasi, Patna, and Bhagalpur).

The water quality of River Ganga was monitored during the pre-monsoon and post-monsoon seasons. The high-density population and industrialization centers situated on the bank of the River Ganga in the lower stretch have adversely affected the River's water quality. Hence, compared to the upper stretch, the EC, alkalinity, hardness, COD, and BOD of the River were high in the lower stretch.

To study the diurnal variation of dissolved oxygen in the River Ganga, three main cities Kanpur, Prayagraj, and Varanasi, were selected. It was observed that there are no significant diurnal variations in DO levels at the surface and 1.5 m depth. The results of the diurnal variation experiments showed that the average DO value was 7-8mg/l day and night over 48 hours. The DO at the surface decreased to < 2mg/l during the sewage mixing but did not show a significant decrease at 2m and 4m depths. This may be attributed to factors such as reduction in organic load, shallow depth of the River, high velocity of water (> 0.3m/s), and the river profile. The DO was restored to 7-8mg/l within a distance of 1.6 km from the mixing point of sewage and the River during the post-monsoon period compared to the pre-monsoon period.

The Quantitative Microbial Risk Assessment (QMRA) of the River Ganga concludes that the microbial risk associated with the ingestion is far more than the dermal contact, inhalation, and exposure via vector breeding. Pathogenic strain *E. coli O157:H7* was considered in QMRA. The results of the QMRA also confirmed the poor quality of the Ganga River for irrigation at specific locations.

Further, a comprehensive study of geochemical partitioning of metals at trace level reveals that several metals are present at Gomukh and Gangotri in high concentration ranges, which

may be due to heavy sediment load and geogenic origin. The suspended fractions sampled at the surface of the water body decrease post-Tehri. The depth sampling and spatial trend of all the metals show substantial settling of metals bound to suspended fractions in the Tehri reservoir. The maximum occurrence of metals such as As, Cu, Cr, Mn, and Pb is in suspended form, whereas Zn is predominantly present in dissolved fractions in both seasons. The religious activities at Har ki Pauri might contribute to the elevated level of Ag at this location. It was also observed that many metals show higher levels in the pre-monsoon season, which could be due to the low dilution in the monsoon season. The anthropogenic activities contributed to the elevated levels of metals at Rishikesh and Haridwar.

For the comprehensive analysis of sediment and water of River Ganga, the samples were collected from 14 locations of the Indo-Gangetic plain, starting from Gomukh to Bhagalpur. The physicochemical characteristics can be correlated to reported non-putrefying properties. The sediments were sieved mechanically into various fractions, and it was found that the sediments are highly heterogamous, having a size of 250 µm.

However, the sediments collected from Koteshwar- and Tehri- reservoirs show midget particle size distribution due to the inflow of silts and gradual accumulation at the bottom of the river/reservoir over time. From the depth analysis of the sediments at Chinyalisaur, the sediment fraction of the size > 500 µm was observed predominantly at the bottom of the river/reservoir due to the removal of finer sediments upon contact with the river water.

From the laser light scattering experiments, it was found that the suspended sediments are present in the samples. Dynamic light scattering studies showed the average size of the suspended sediments in the range of 300 and 600 nm. The sediment size of the samples collected in most locations decreases with the increase of centrifugation up to 2500 rpm; however, it increases again with the increase of centrifugation (3500 and 4500 rpm). Although the possible attributes are not explicit at present for this observed anomaly, the presence of amorphous and organic components along with the inorganic fractions in the SS samples may show this unusual behaviour.

To determine the surface charge of the colloidal particles present in suspension, zeta potential analysis-based studies were carried out, which were in the range of +5 to -15 mV. Although the surface charge of the particles is relatively lower, the continuous flow of water in the

River allows most fine particles to remain in suspension, which may influence the microorganisms in the water. It was observed that the suspended sediments contained nano-ordered single and polycrystalline structures, which were highly dispersed, containing rod-like sediments and organic matter/ moieties. Interestingly, dispersed nano sediments and embedded microbial-like structures are also found in suspended sediments, which are amorphous. Suspended sediments from Koteshwar showed fiber- and needle-like structures. Long-range amorphous tubes, as well as rods, were observed in the Suspended sediments samples after centrifugation. Also, nanoparticles (5-10 nm) embedded microbial systems were observed when the suspended sediment samples were collected at 50 m depth in the Tehri reservoir. Long-range interconnected spherical-shaped organic moieties were observed in the suspended sediments samples collected at 70 m depth in the Tehri reservoir. The presence of nano-ordered crystalline/amorphous sediments from the first stretch of River Ganga may be involved in the antimicrobial activity, which can be corroborated by the non-putrefying property of River Ganga.

From the XRD analysis, silicon-based minerals/phases, aluminum-, calcium-, sodium-, potassium- and magnesium-based minerals are very commonly found in the river sediments. In addition to the commonly found minerals, Fe-, Ti- and manganese (Mn) based minerals were also found, which have variable oxidation states that may influence microbial activity.

The elemental analysis of sediments was performed by XRF and ICP-MS techniques. Although several elements are present in the sediment samples, Si, Al, Ca, Mg, K, and Na are the most abundant, few transition metals were found (e.g., Zn, Cu, Ni, Zr, etc.). Apart from these elements, Fe is found with the highest concentration at various locations in the river basin, followed by Ti. Magnesium is also found at a relatively higher concentration of 27000 mg/l.

The occurrence of a high concentration of metals at Tehri and Koteshwar could be due to the accumulation of incoming silts/mineral deposits from the streams discharging in the reservoirs as the velocity in these streams is close to the reservoirs is low. The gradual deposition of minerals that are very fine at Tehri- and Koteshwar- reservoirs are responsible for a very high concentration of metals. The minerals containing Fe, Al, Mg, Ti, etc., may be involved in the antibacterial activity of the sediment samples collected from various locations in River Ganga.

The antimicrobial activity experiments by utilizing water of the first stretch of River Ganga showed that samples collected from Tehri exhibited the highest antibacterial potential. In contrast, Harsil, Gangotri, and Mana also showed antibacterial potential to some extent. From the metal analysis of these samples, it was found that the Fe and Ti content in the water of the Tehri reservoir is much higher compared with that of the other locations. This may be due to the accumulation of silt over time in the Tehri reservoir. From the detailed investigations of the sediment samples collected from the River Ganga, it was observed that the sediment samples collected from the first stretch showed antimicrobial activity, which may also be contributing to the non-putrefying property of the River.

A systematic attempt is made to identify the presence of phytochemicals in Ganga water to understand if they impart any special property to river Ganga water. Considering the complexity of river water composition, the study area was restricted to the upper stretch of the River. To narrow down the list of probable compounds, the dominant vegetation parts of medicinally important trees were collected from the catchment areas, and simulated experiments were performed to identify the presence of such compounds through leaching experiments. These compounds and other phytochemicals in vegetation around the catchment area were then targeted for the possible presence in river water using advanced analytical techniques. Riparian and upland vegetation likely introduces secondary metabolites to adjacent lateral streams flowing through forests and finally discharging into Bhagirathi and Alaknanda rivers.

Simulated experiments inferred the presence and qualitative confirmation of organics/terpenes and related compounds/phytochemical/secondary metabolites in the leachates. This also relates to the phytochemicals present in the plant species in riparian buffers.

Results of Ganga River water analysis confirmed organic fingerprinting leading to the presence of terpenes and related compounds/phytochemical/secondary metabolites. Interestingly some of the probable compounds in the river water samples were also observed in leachates of simulated experiments, thus strengthening the hypothesis of their origin from surrounding vegetation in the catchment area. The possible sources of these phytochemical signatures can be attributed to rich and biodiverse mega watersheds, landscapes of this stretch, and anthropogenic activities. Dilution plays a crucial role in the effective concentrations of these phytochemicals at different locations of the River. It ultimately determines the potential of possible contributions to impart any significant medicinal or special properties to river

water. The concentrations of these metabolites in Ganga water, however, were mostly deficient, to be able to impart any significant medicinal or non-putrefying properties individually. Additionally, the complexity of the intra-ecosystem interactions, which requires an in-depth assessment of the scenarios and drivers controlling the leaching and persistence of these phytochemicals in the Ganga water, must also be considered in future studies. However, these initial findings strongly suggest a detailed related investigation in the future.

CHAPTER -8

Biological and Health Component

Final Report

A Detail Study to Understand the Non-Putrefying Property of River Ganga in both Water and Sediment

Sponsored by:
Ministry of Water Resources, River Development & Ganga Rejuvenation, New Delhi

CSIR- National Chemical Laboratory,

Pashan, Pune-411008

CSIR-National Environmental Engineering Research Institute Nehru Marg, Nagpur – 440 020

March, 2018 – December 2020

Metaviromics approach for understanding viral diversity, taxonomy and functional analysis

Project Investigators:

1. *Dr. Mahesh Dharne*
Principal Scientist,
NCIM Resource Centre,
CSIR-National Chemical Laboratory (NCL),
Pune, Maharashtra.
Email: ms.dharne@ncl.res.in ; msdharne@gmail.com
Ph: 020-25902456

2. *Dr. Syed Dastager*
Senior Scientist,
NCIM Resource Centre,
CSIR-National Chemical Laboratory (NCL),
Pune, Maharashtra.
Email: sg.dastager@ncl.res.in; syedmicro@gmail.com
Ph: 020-25902505

OBJECTIVES and Proposed activities:

Objectives

- To deduce diversity, community and metabolic potential of uncultured bacteriophages in Ganga water and sediments using metavirome approach
- Assessment for distribution of bacteriophage communities with respect to their hosts and seasonal factors

Proposed activities

- Isolation of total viral/bacteriophage and microbial nucleic acids extraction from river sediments
- High throughput metagenome sequencing on NGS platform
- Comprehensive analysis of viral/ bacteriophage taxonomic and functional diversity and their bacterial hosts

Proposed milestones

Sr. No	Milestones	Months						
		3	6	9	12	15	18	24
1.	Sampling from selected locations, transportation to lab							
2.	Isolation of metavirome DNA, pre-processing							
3.	Metavirome sequencing by Nanopore technology							
4.	Data mining, QC, filtration, Community analysis							
5.	Statistical analysis to determine abundance of viral taxa, interpretation of results							
6.	Correlation with environmental parameters (pre- and post-monsoon)							
7.	Compilation, report making, publication, report submission							

Index

Sr. No	Contents	Page No
1.	**Total viral/ bacteriophage diversity (TVD) in sediments of River Ganga and comparison with pre- and post-monsoon**	**5-31**
1.1	Total viral/ bacteriophage diversity (TVD) in the sediments of **upper stretch** of River Ganga	5-16
1.2	Total viral/ bacteriophage diversity (TVD) in the sediments of **lower stretch** of River Ganga	17-26
1.3	Comparative viral/bacteriophage diversity and host-phage relationship across the **entire stretch** of River Ganga	27-31
2.	**Total microbial diversity (TMD) in the sediments of River Ganga and comparison with pre- and post-monsoon**	**32-68**
2.1	Total microbial diversity (TMD) in the sediments of **upper stretch** of River Ganga	32-35
2.2	Total microbial diversity (TMD) in the sediments of **lower stretch** of River Ganga	36-45
2.3	Functional analysis of metagenomic data across **entire stretch** of River Ganga	46-68
3.	**Total microbial (TMD) and viral/phage (TVD) diversity of control rivers (Yamuna and Narmada) and comparison with Ganga river**	**69-75**
3.1	Total microbial (TMD) and viral/phage (TVD) diversity of River Yamuna	69-71
3.2	Total microbial (TMD) and viral/phage (TVD) diversity of River Narmada	72-74
3.3	Comparison of microbial (TMD) and viral/ phage (TVD) diversity of **Ganga river with the control rivers**	75
4.	**Summary and Conclusion**	**76-77**
5.	**Publications, Patents etc**	**78**

1. Total viral/ bacteriophage diversity (TVD) in sediments of River Ganga and comparison with pre- and post-monsoon

1.1. *Total viral/ bacteriophage (TVD) in the sediments of upper stretch of River Ganga*

1.1.A. Methodology:

Extraction of metagenomic DNA

All the sediment samples collected were processed downstream for metaviromic analysis, details of which have been condensed in (Table.1) Total DNA was extracted from the 10 gm of sediment samples using DNeasy PowerMax Soil Kit (Qiagen) as per the manufacturer's protocol. The quality and concentration of DNA for each sample was assessed by Nanodrop Lite spectrophotometer (Thermo Fisher Scientific) and qubit fluorometer (Thermo Fisher Scientific) quantification using qubit BR assay kit (Thermo Fisher Scientific, Q32853) and the extracted DNA were stored at -20°C.

In-situ DNA amplification using Repli-G, MALBAC and Long Amp method

Regular DNA extraction kits failed to give DNA from upper stretch samples (may be due to low microbial load). The sediments from the upper stretch of Ganga River were subjected to amplification methods so as to meet the required quantity (900 ng) for nanopore sequencing. Repli-G (Qiagen), MALBAC (Yikon Genomics, China) were used for exponential amplification as per manufacturers' protocol.

Nanopore Sequencing

The extracted DNA were subjected to Nanopore Sequencing, using 1D Native barcoding genomic DNA (with EXP-NBD103 and SQK-LSK108) protocol as prescribed by the (Oxford Nanopore Technologies, Oxford, UK) with certain modifications. In brief, 900 nanogram-1 microgram of DNA samples were subjected to end repair step and the resulting DNA were quantified using Qubit fluorimeter (Thermo Fischer Scientific). Further, 500 ng of End prepped DNA fragments were used for library preparation wherein the tether and the

adapter were added using their respective kits like- Native Barcoding Kit 1D (EXP-NBD103) and Ligation Sequencing Kit 1D (SQK-LSK108) (Oxford Nanopore Technologies, Oxford, UK). The library was then prepared for loading using Library Loading Bead Kit (EXP-LLA001), (Oxford Nanopore Technologies, Oxford, UK). The MinION sequencing was carried using MinION sequencer. Prior to the sequencing run, the flow cell (FLO-MIN 106 R9, Oxford Nanopore Technologies, Oxford, UK) was primed with an initial volume of 800 µL of priming mix followed by 5 mins of incubation at room temperature followed by consequent addition of 200 µL of priming mix. Subsequently, 75 µL of the library sample was added to the Spot-On sample port of the MinION flow cell and the sequencing run was carried for 48 hours.

Data analysis

The raw reads obtained after the run were converted to fastq using Albacore (v2.2.7). Additionally, base-calling, pre-processing of reads and demultiplexing was also performed by Albacore. All of the low-quality sequences were discarded. Further, Poretools was used to carry out another round of Quality Check (QC). Error correction of the reads was carried out using Canu, which has a MHAP based error-correction module, to give good quality long reads.

The resultant fastq files were subjected to WIMP analysis on Metrichor EPI2ME platform (Oxford Nanopore Technologies, Oxford, UK). EPI2ME works on support centrifuge engine which allows quick taxonomic assignments of supplied reads against EPI2ME's own custom genome databases of Bacteria, Archaea, Eukarya, and Viruses and thus, can also be used for real time analysis. The results of WIMP were converted into taxonomic profiles using in-house scripts written in Perl which can create tables of assignment using the read level data at super-kingdom, phylum, class, order, family and genus level. Additionally, the reads were annotated and statistically analysed for taxonomic and functional and diversity using MG-RAST.

Sample code	Sample Locations	Sampling year
GA1/G01DR	Gomukh	2017/2018,2019,2020
GB2/G02UR	Gangotri Upstream	2017/2018,2019,2020

GB3/G02DR	Gangotri downstream	2017/2018,2019,2020
GB4/G03UR	Harshil	2017/2018,2019,2020
GB5/G03DR	Harshil	2017/2018,2019,2020
GB6/G04UR	Maneri	2017/2018,2019,2020
GB7/G04DR	Maneri	2017/2018,2019,2020
GC8	Mana	2017
GC9	Badrinath (DS)	2017
GC10	Karnprayag (Pinder)	2017
GC11	Karnprayag (Alaknanda)	2017
GC12	Karnprayag (Confluence)	2017
GC13	Devprayag (Bhagirathi)	2017
GC14	Devprayag (Alaknanda)	2017
GC15	Devprayag (Confluence)	2017
G6C	Chiyali Saur	2017
G8/G07UR	Tehri reservoir Bhagirathi	2017/2018,2019,2020
G9G07DR	Tehri reservoir Bhagirathi	2017/2018,2019,2020
G10	Koteshwar	2017
G12US	Rishikesh upstream	2017/2018,2019,2020

1.1.B. Results

Viral diversity across 2017 samples

Kaiju database was used for analyses of upper-stretch viral diversity for Oct'2017 samples. Analyses revealed dominance of Siphoviridae (50-60%) followed by Myoviridae (7-15%) in all the locations. However, at Tehri, Baculovirirdae was observed to be predominant comprising 25% of its total viral diversity (Fig.1).

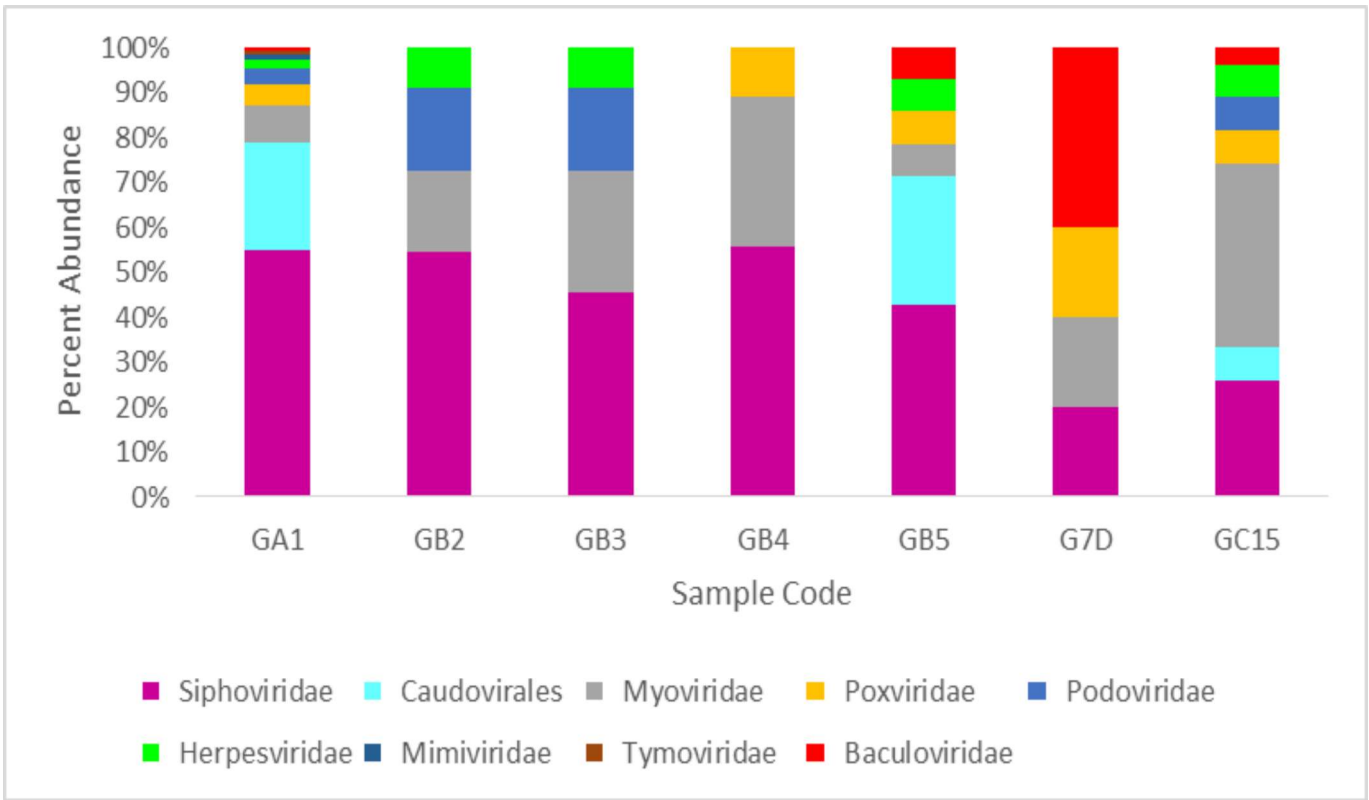

Fig.1: Viral diversity across the upper-stretch of River Ganga from Gomukh to Devprayag (Oct'2017).

Further for analysis of bacteriophage diversity, MG-RAST platform was used and the output of phage diversity for upper-stretch was seen in form of a Krona plot (Fig.2A; Fig.2B)

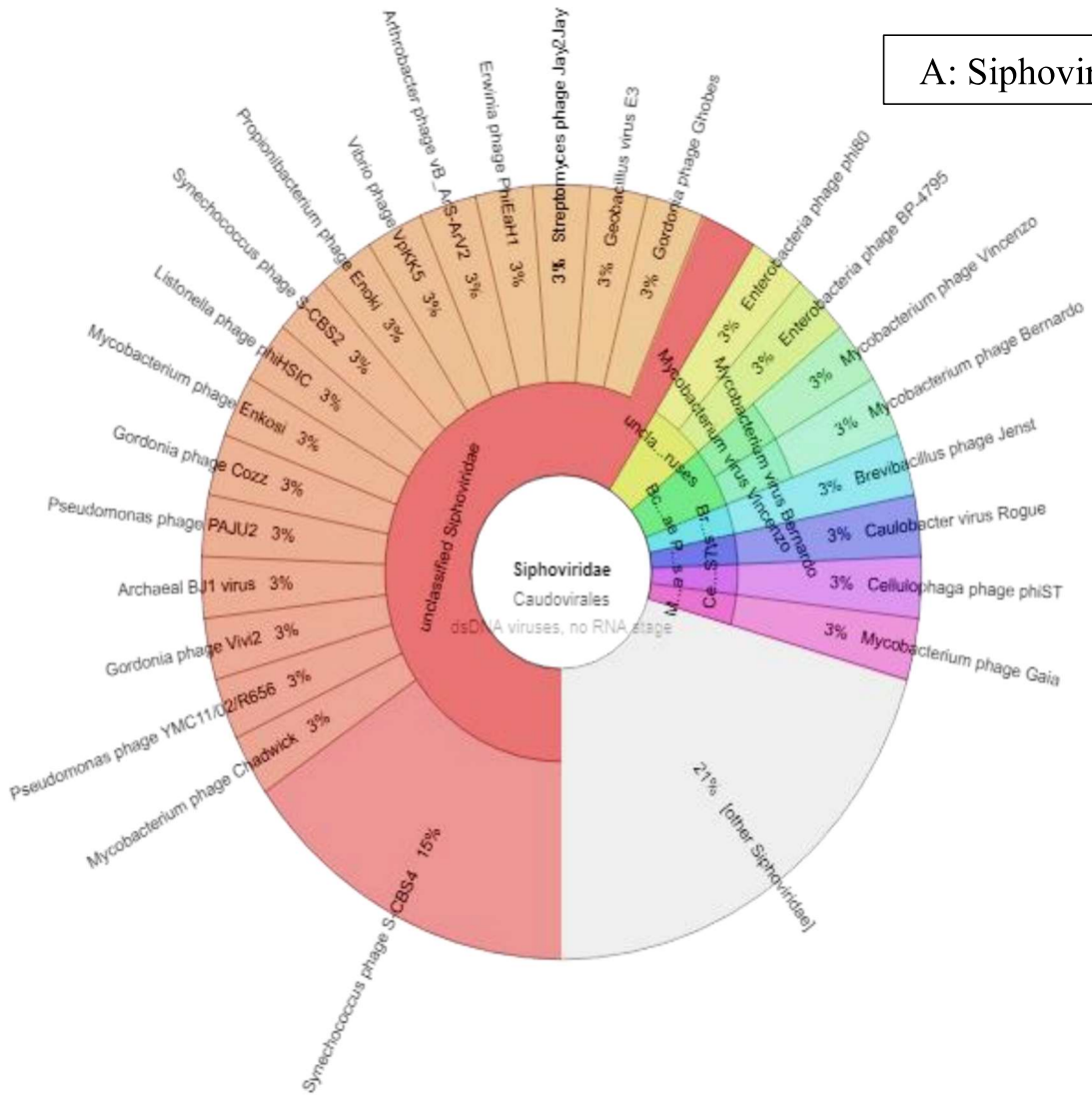

Fig 2A: Krona plot of phage families of upper stretch samples from Oct'17 samples: Siphoviridae (A).

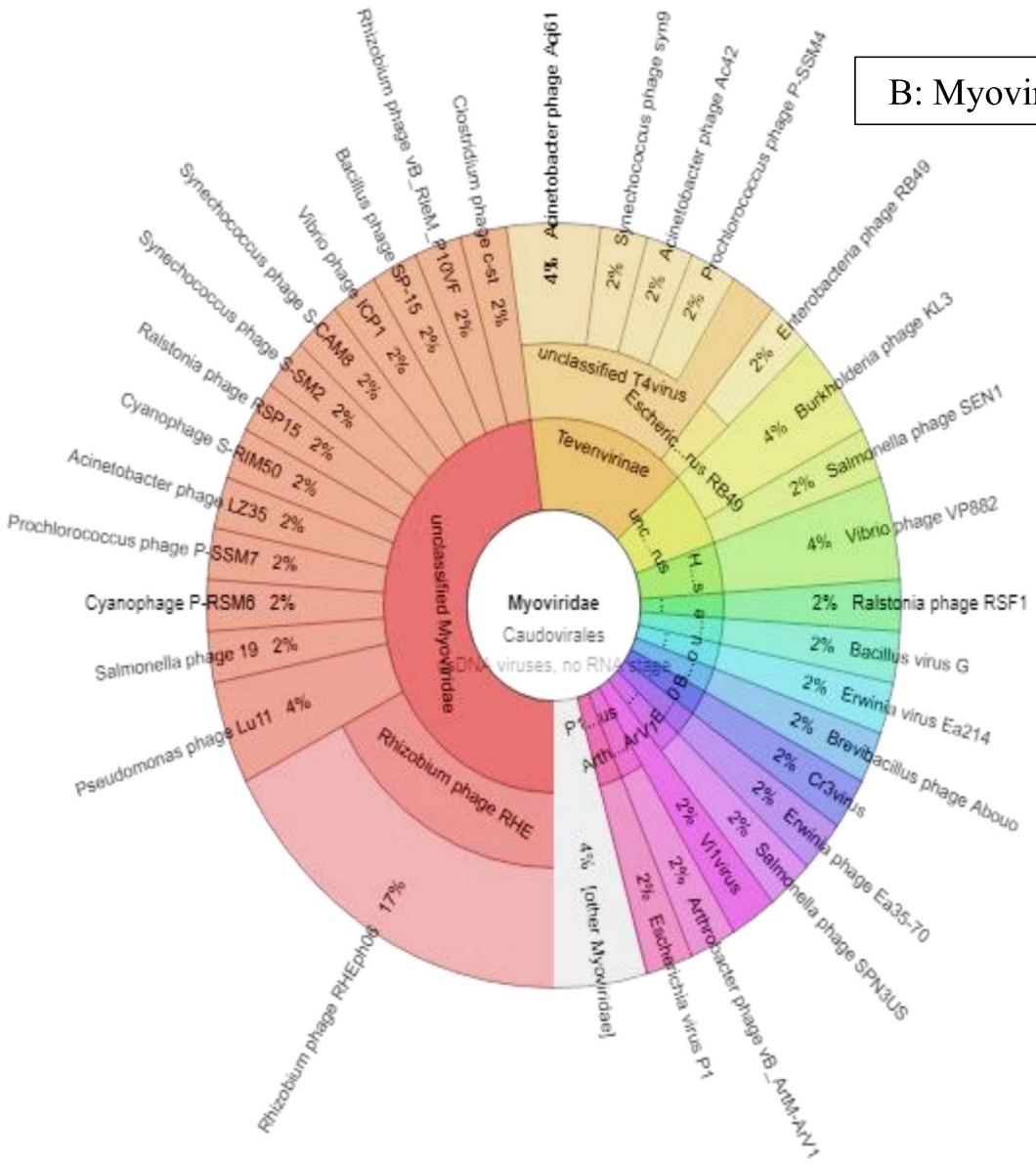

Fig 2B: Krona plot of phage families of upper stretch samples from Oct'17 samples: Myoviridae (B).

Viral diversity across 2018 samples

EPI2ME analysis of the upper stretch samples revealed presence of several bacteriophages such as Bacillus phage; Pseudomonas phage; Cronobacter phage; Escherichia phage; Mycobacterium phage, etc. (Fig.3).

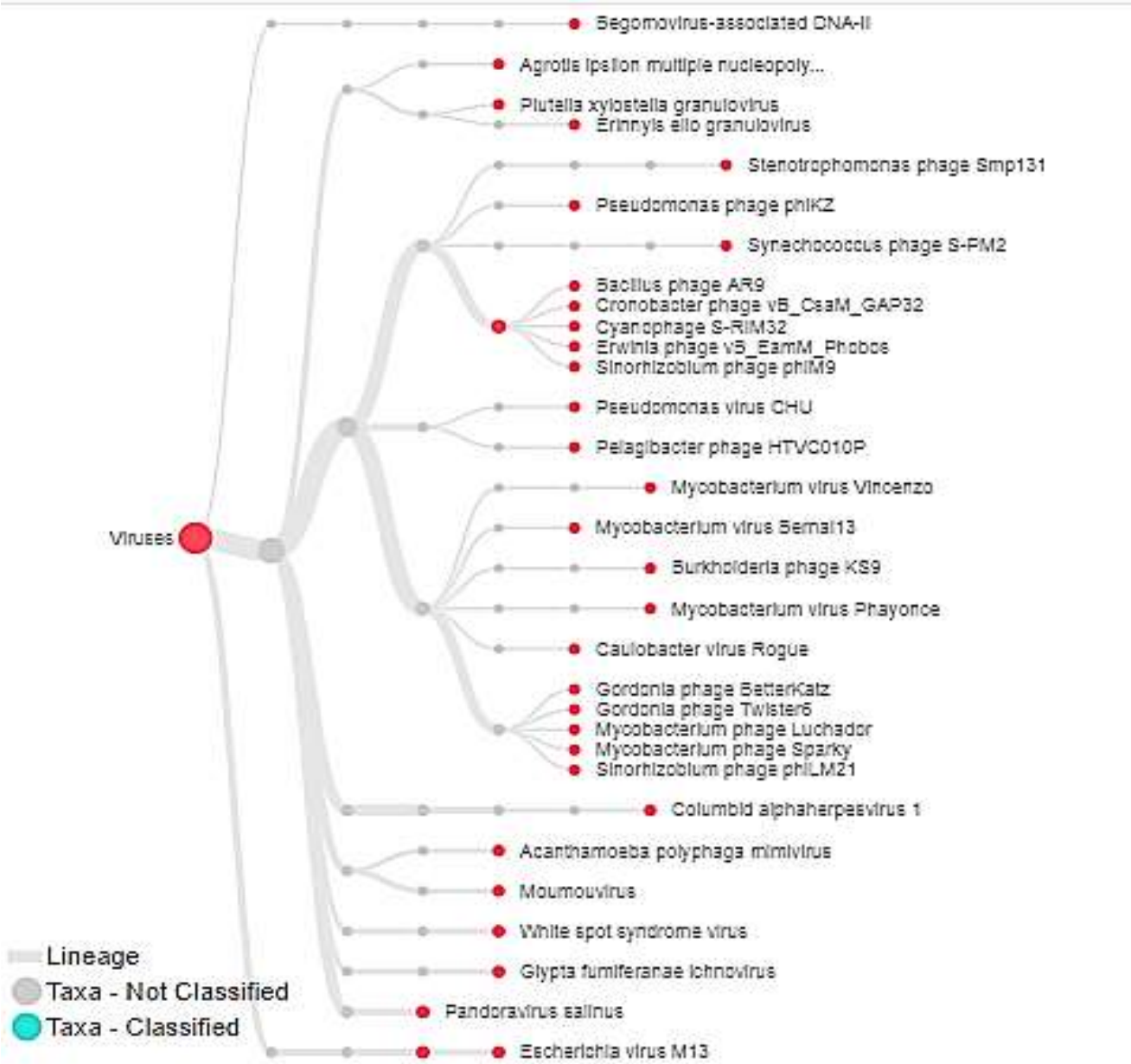

Fig .3: Taxonomic tree showing presence of viral genera along the upper stretch samples of River Ganga spanning from Gomukh to Rishikesh (2018 samples).

Viral diversity across 2019 samples

Further, MG-RAST analysis of the upper stretch samples for the year 2019, revealed presence of several bacteriophages with a maximum abundance of Bacillus phage (55-60%); Pseudomonas phage (20-25%) and Mycobacterium phage (10-15%) (Fig.4).

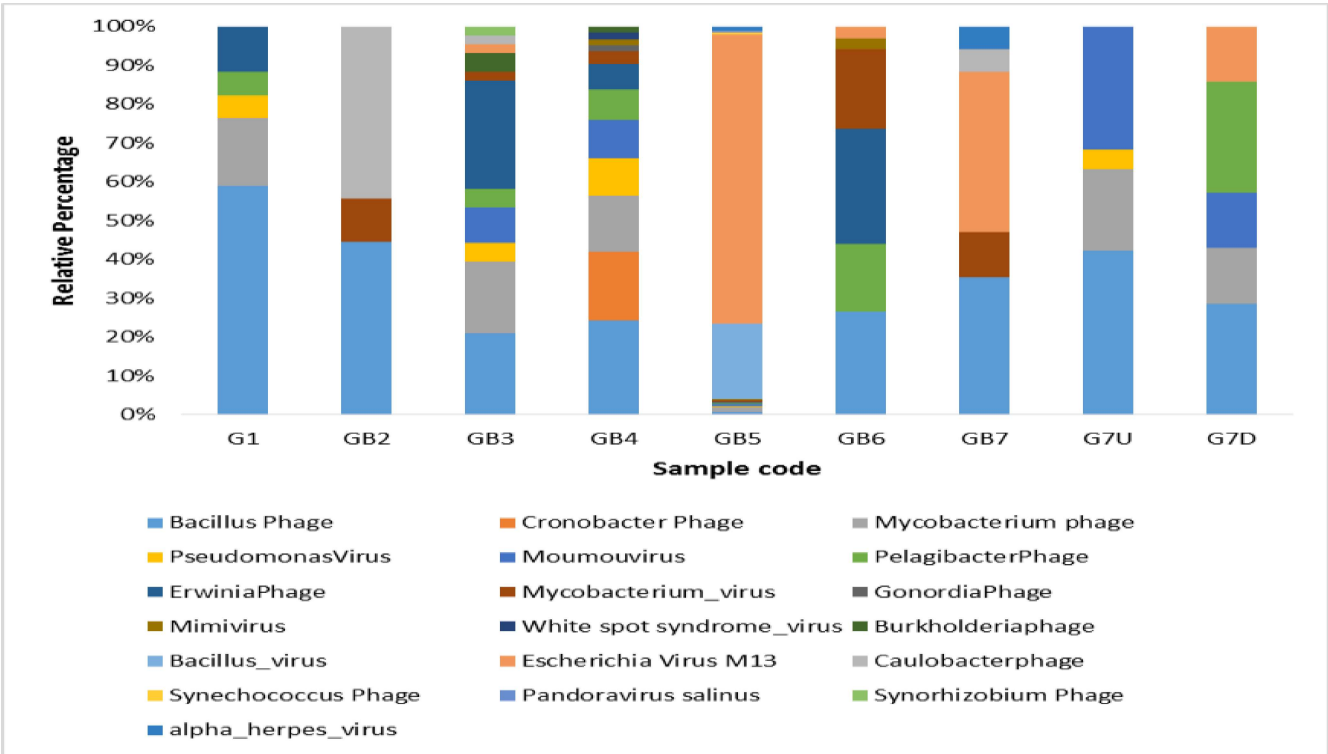

Fig .4: Graph showing presence of viral genera along the upper stretch samples of River Ganga spanning from Gomukh to Tehri (2019 samples) (Only Top 20 genera are highlighted).

Viral diversity across 2020 samples

MG-RAST analyses of the upper stretch samples revealed a plethora of viral diversity, with the highest relative abundance of 67% for the family of bacteriophages (Caudovirales) (Fig.5). After delineating the phage diversity in the samples corresponding to each location, a predominance of Siphoviridae was observed at all locations (60-90%) except for Tehri, where Myoviridae was found to be dominating with a relative abundance of 50% (Fig.6).

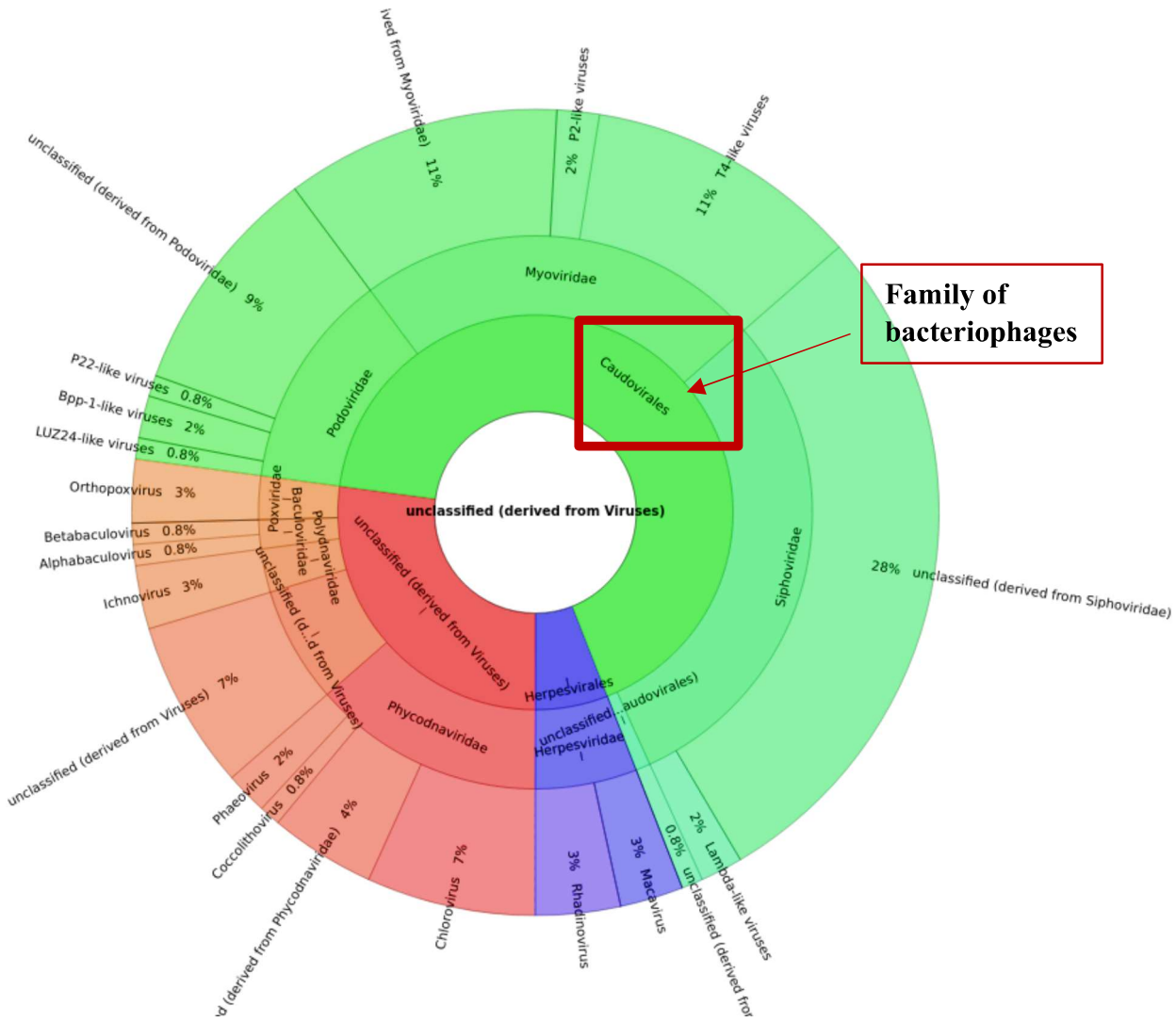

Fig.5: Krona plot showing total viral diversity along the upper stretch of River Ganga (2020 samples).

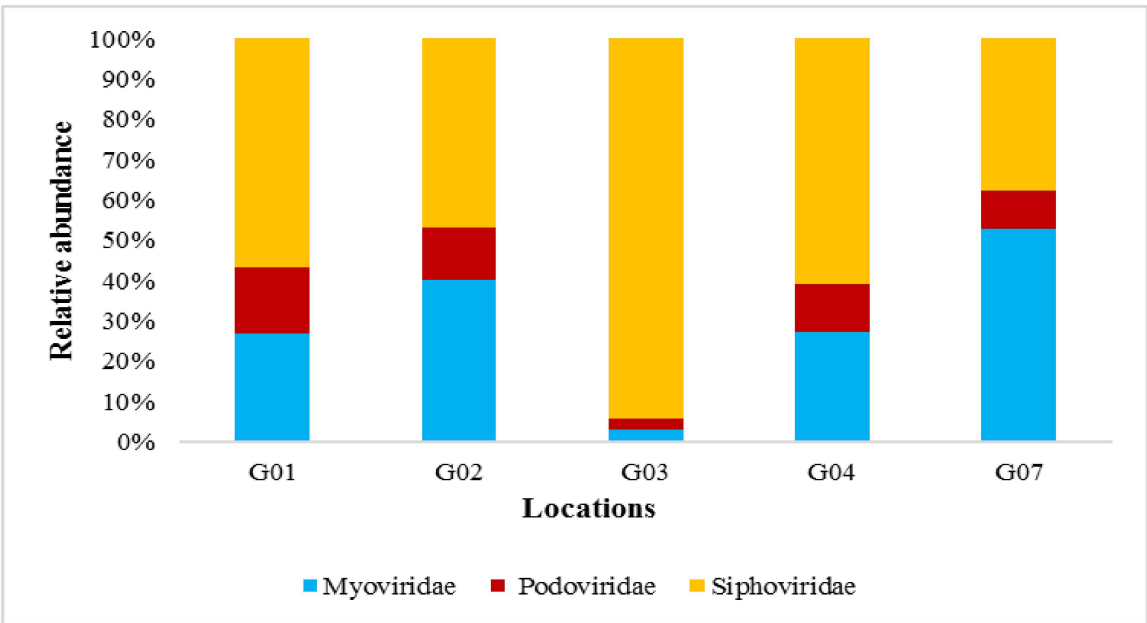

Fig.6: Graph showing total phage diversity (2020 samples) along the upper stretch of River Ganga

Further, to understand the phage diversity at genus level, the data was normalized and phage reads were combined and only those that passed the minimum cutoff value (excluding singletons) were mapped with krona plot for genus level phage diversity from Siphoviridae and Myoviridae families of bacteriophages. The plot showed presence of several bacteriophages such as Bacillus phage; Pseudomonas phage; Cronobacter phage; Escherichia phage; Mycobacterium phage, against pathogenic microbes. Additionally, it was observed that several phage reads (29% of Siphoviridae; 15%Myoviridae) were categorized as unclassified/other, indicating possibility of presence of novel phages therein (Fig.7).

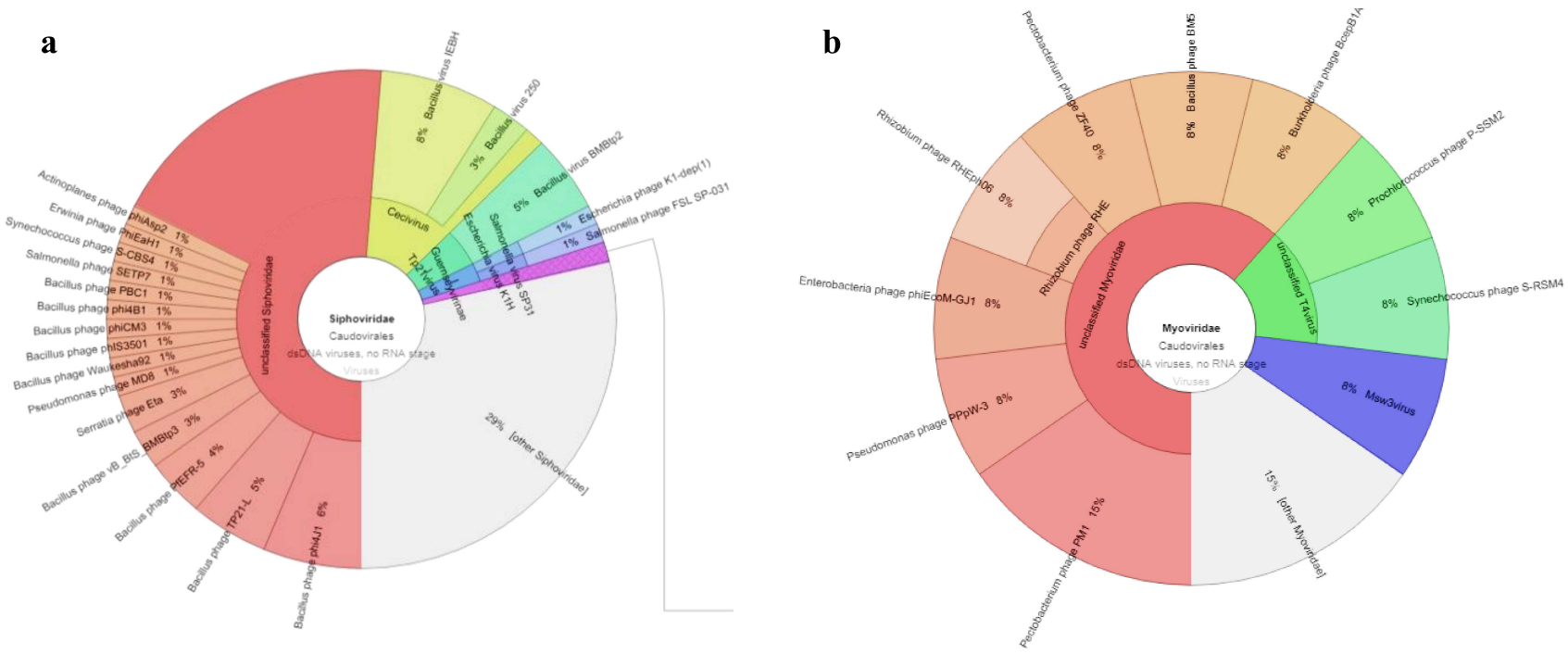

Fig.7: Krona plot of phage families: Siphoviridae (a) and Myoviridae (b).

Seasonal comparison of the viral diversity

A comparative analysis for viral diversity for lower stretch samples was performed based on seasons. The data was normalized and phage reads were combined and only those that passed the minimum cutoff value (excluding singletons) were mapped with krona plot for genus level phage diversity from Siphoviridae and Myoviridae families of bacteriophages. The plot showed presence of several bacteriophages such as Bacillus phage; Pseudomonas phage; Cronobacter phage; Escherichia phage; Mycobacterium phage, against pathogenic microbes.

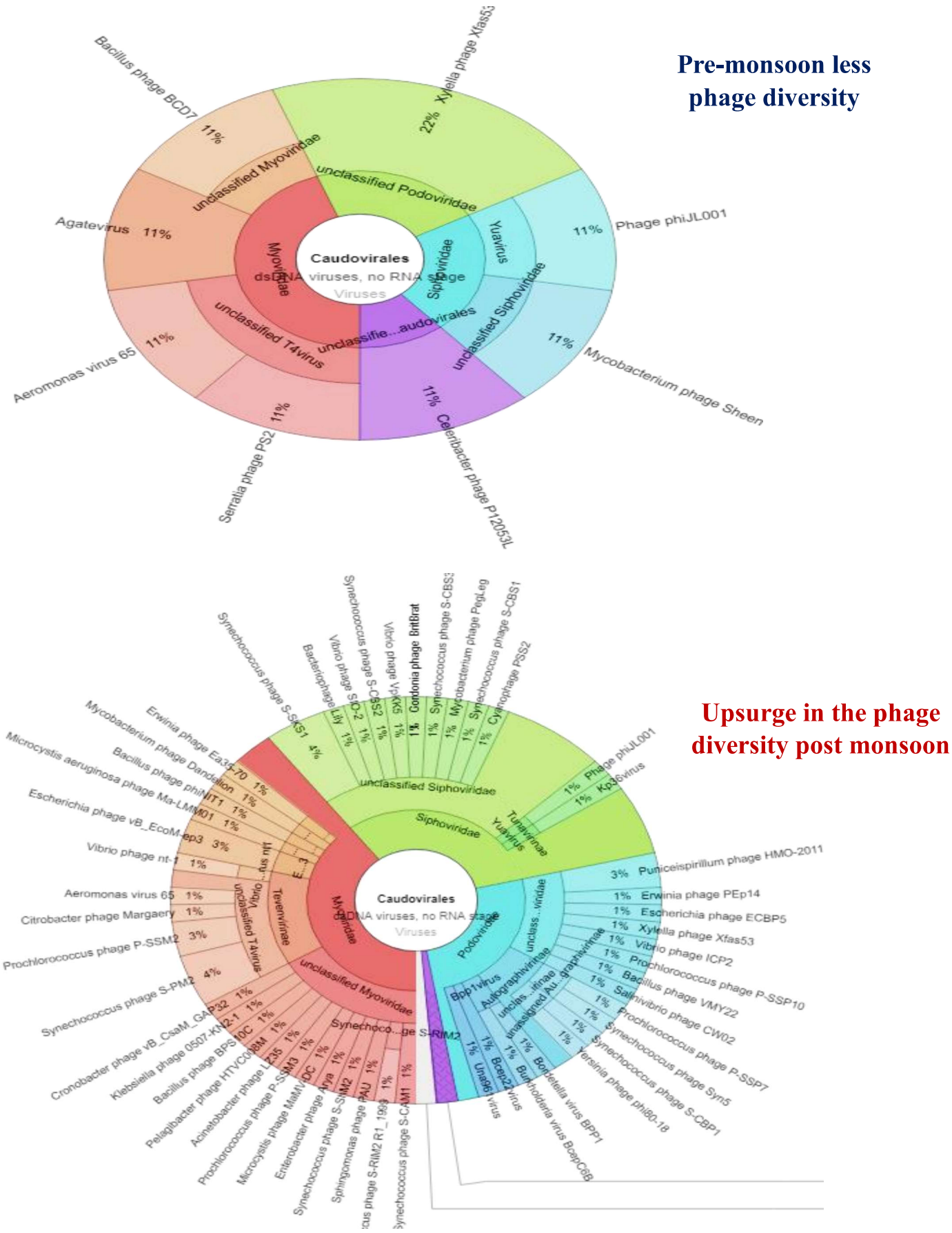

Fig.8: Analysis from Metavirome sequencing revealed an upsurge in the phage diversity post-monsoon as compared to that of the pre-monsoon samples.

Delving ahead of phage diversity, functional annotation of the upper stretch samples was carried out using Subsystems and KEGG tool of MG-RAST to understand the phage related functions (Fig.9). Presence of hits against phage related proteins indicate a strong presence of host-phage relationship.

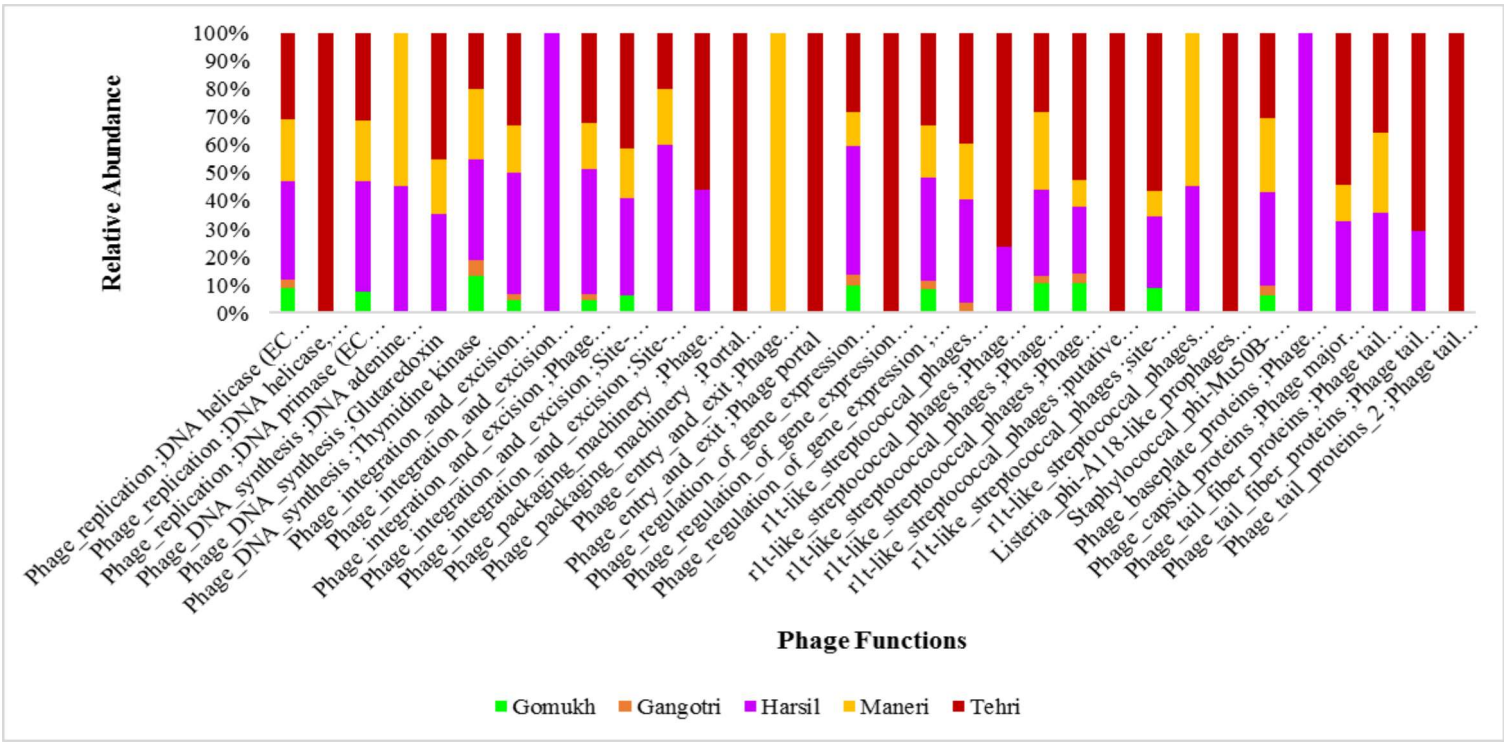

Fig.9: Graph showing functional hits of phage related proteins across the upper stretch samples.

1.2 Total viral/ bacteriophage diversity (TVD) in the sediments of lower stretch of River Ganga

1.2.A Methodology

Sampling details

Sediment samples were collected in triplicates from 15 sites, in the year 2017 and 2018. Details of the samples have been enlisted in Table.2

Sample code	Location	Sampling Year
G12DS	Rishikesh downstream	2017/2018
G13US	Bijnor upstream	2017/2018
G13DS	Bijnor downstream	2017/2018
G14US	Kanpur upstream	2017/2018
G14DS	Kanpur downstream	2017/2018
G15US	Allahabad upstream	2017/2018
G15(S)	Allahabad Sangam	2017/2018
G15(Y)	Allahabad Yamuna	2017/2018
G15DS	Allahabad Downstream	2017/2018
G16US	Varanasi upstream	2017/2018
G16DS	Varanasi downstream	2017/2018
G17US	Patna upstream	2017/2018
G17DS	Patna downstream	2017/2018
G18US	Bhagalpur Upstream	2017/2018
G18DS	Bhagalpur Downstream	2017/2018

Table. 2: Details of the Lower stretch samples processed in the study.

Extraction of metagenomic DNA from lower stretch samples of Ganga River

Total DNA was extracted from the samples using RNeasy PowerSoil Total RNA Isolation Kit (Qiagen) and RNeasy PowerSoil DNA Elution Kit (Qiagen). The DNA quality and concentration for each sample was assessed by Nanodrop Lite Spectrophotometer (Thermo Fisher Scientific) and Qubit fluorometer (Thermo Fisher Scientific) quantification using qubit BR assay kit (Thermo Fisher Scientific, Q32853).Nanopore sequencing and data analysis was carried out as mentioned above (Pg.5-6).

1.2.B Results

Viral diversity and funcional annotation of the lower stretch samples

The metavirome analysis showed that River Ganga has a unique viral diversity. The most dominant viral families include *Siphoviridae>Myoviridae>Herpesviridae>Podovirdae>Poxviridae* (Fig.10a). The Virome encompass a plethora of bacteriophages against several pathogenic and putrefying bacteria such as *Vibrio; Campylobacter; Salmonella; Shigella; Klebsiella; Enterobacter; Clostridium and Bacillus.* The existence of bacteriophages against these microbes could be correlated with one of the "non-putrefying" property of River Ganga. In addition, bacteriophages against other pathogenic bacteria like *Aeromonas; Acinetobacter; Pseudomonas; Escherichia; Staphylococcus; Listeria; Bordetella; Stenotrophomonas;* and *Mycobacterium* were also detected.

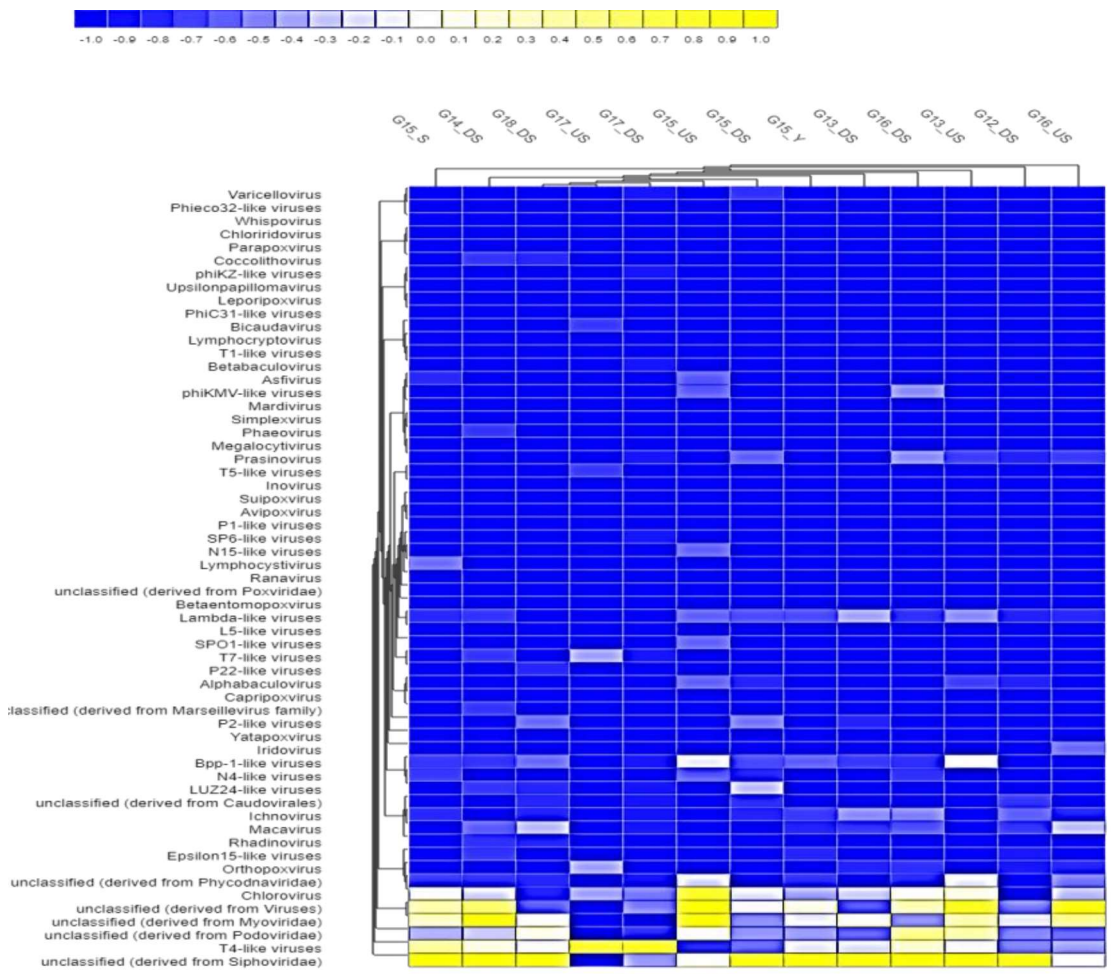

Fig. 10a: Heatmap showing abundance of viruses in the lower stretch of River Ganga. The yellow color indicates maximum abundance while the blue depicts lower abundance.

From the MG-RAST analysis, a total of 7 viral orders namely, Bunyavirales; Caudovirales; Tymovirales; Picornavirales; Ligamenvirales; Herpesvirales and Mononegavirales were observed. Additionally, a total of 40 viral families belonging to these orders were classified which includes families of tailed bacteriohages (Myoviridae and Siphoviridae), families of giant viruses (Mimiviridae; Phycodnaviridae and Pandoraviridae) followed by several families of human pathogenic viruses (Togaviridae; Herpesviridae; Alloherpesviridae; Poxviridae; Paramyxoviridae; Adenoviridae; Polyomaviridae and Parvoviridae) were observed in Dec' 2017 samples spanning 1200 km. of River Ganga from Rishikesh (G12) to Bhagalpur (G18) **(Fig.10b)**.

Fig .10b: MG-RAST Classification of Viral reads portraying presence of viral order and families from Haridwar to Bhagalpur

Functional annotation of the lower stretch samples was carried out using Subsystems and KEGG tool of MG-RAST to understand the phage related functions (Fig.10c). Presence of hits against phage related proteins indicate a strong presence of host-phage relationship.

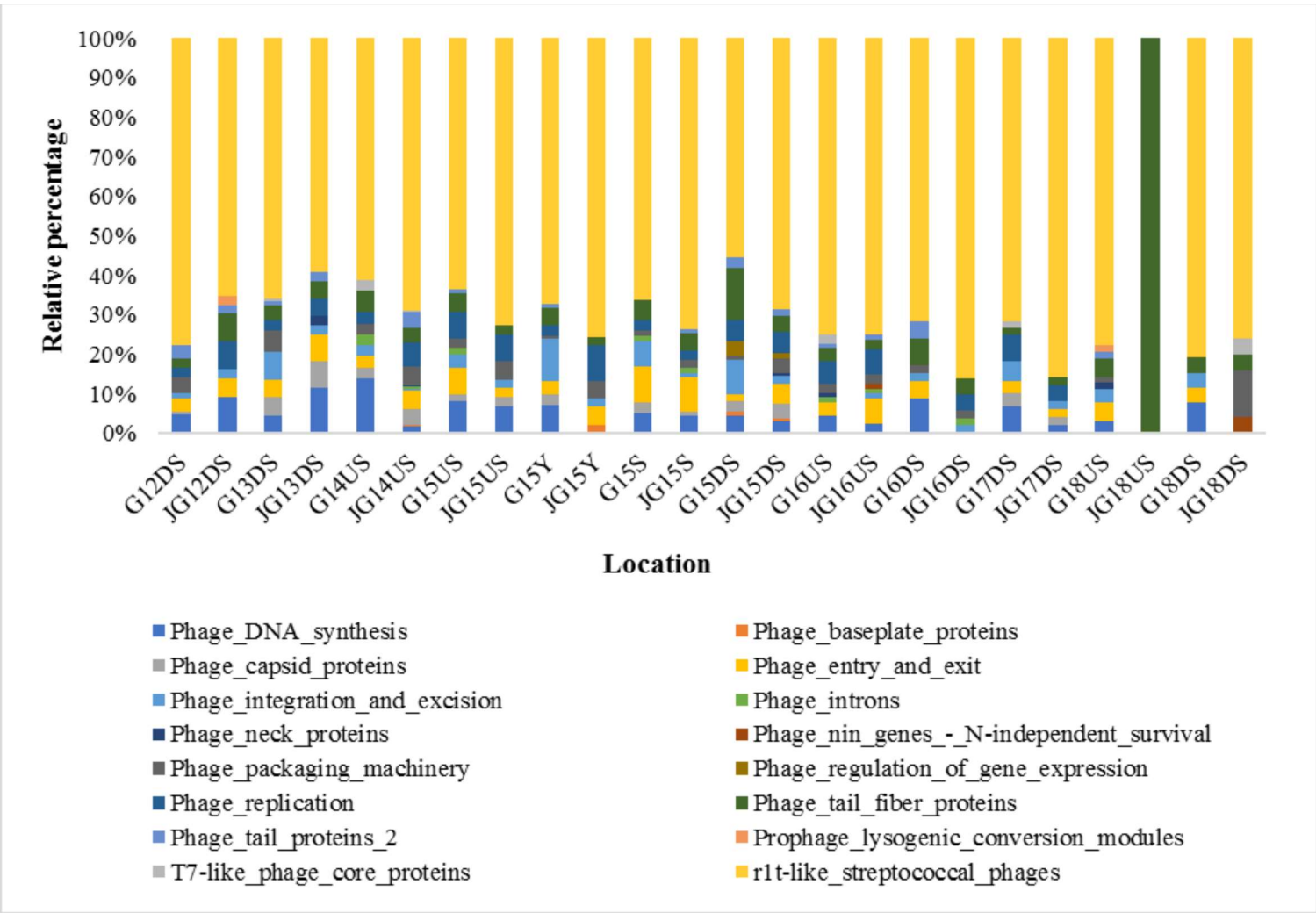

Fig.10c: Graph showing functional hits of phage related proteins across the lower stretch samples.

Viral Taxonomic and functional distribution of confluence samples

The most dominant viral families in the confluence microbiome include the *Siphoviridae>Myoviridae>Herpesviridae>Podovirdae>Poxviridae.* Also, several giant virus families were observed which includes *Mimiviridae; Phycodnaviridae; Ascoviridae; Iridoviridae and Pandoraviridae* (Fig. 11a and 11b)

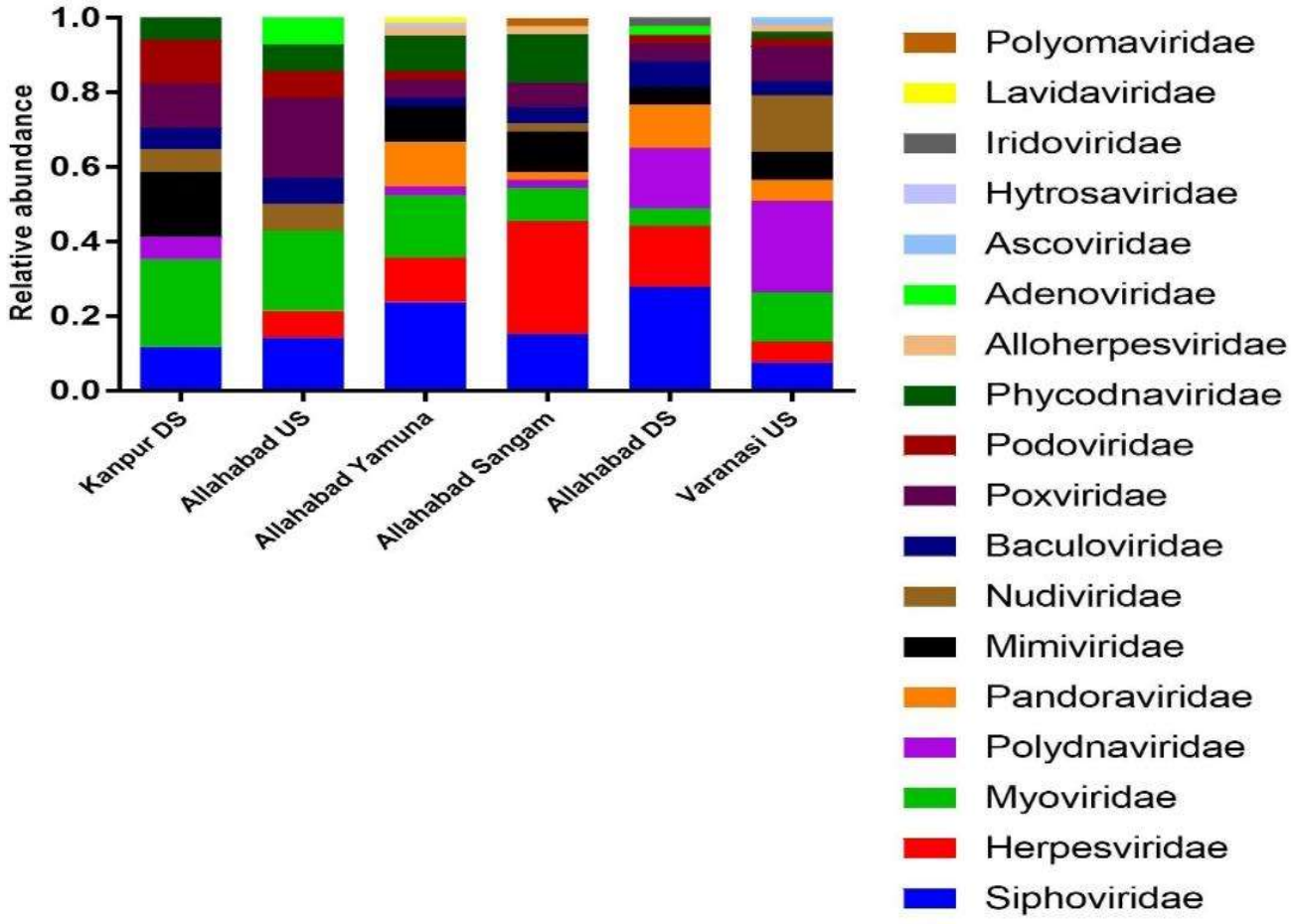

Fig.11a: Viral Diversity at family level of confluence samples (Sediment)

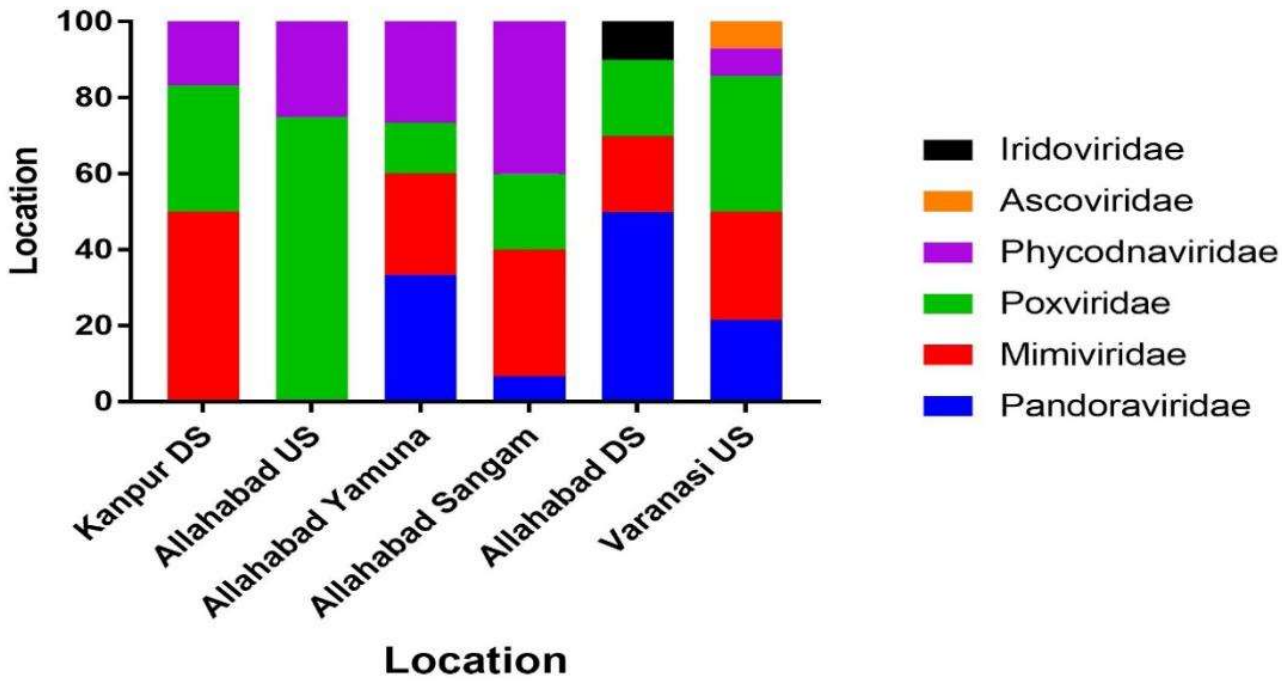

Fig.11b: Diversity of giant viruses at family level of confluence samples (Sediment)

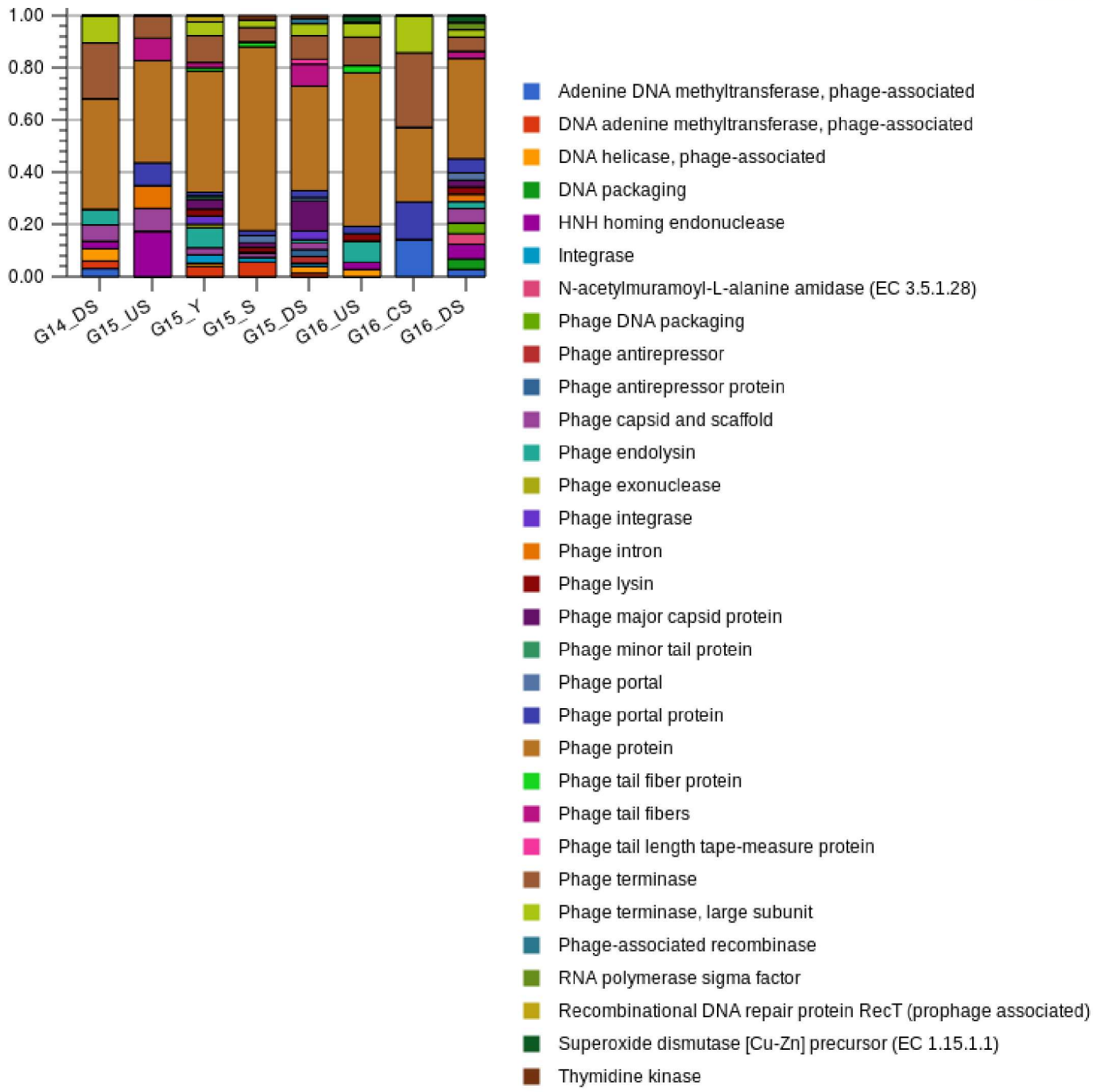

Fig. 12: Functional analysis of phage related proteins present across the confluence samples

Seasonal comparison of viral diversity across lower stretch

The taxonomic comparison with respect to temporal variation of the lower stretch samples showed relative proportions of Viral and Prokaryotic communities. Viral diversity at the phylum level appeared to be similar in both the seasons. However; in-depth metavirome analysis at the species level revealed an upsurge in the viral community composition post-monsoon (Fig.13). The *Caudovirales* taxon dominated all metaviromes. In particular, members of the family *Siphoviridae* were dominant in most metaviromes. Within the dsDNA viruses, members of

rare taxonomic groupings such as the families *Mimiviridae; Iridoviriae; Nudiviridae; Poxviridae; Baculoviridae* and the order *Herpesvirales* were detected.

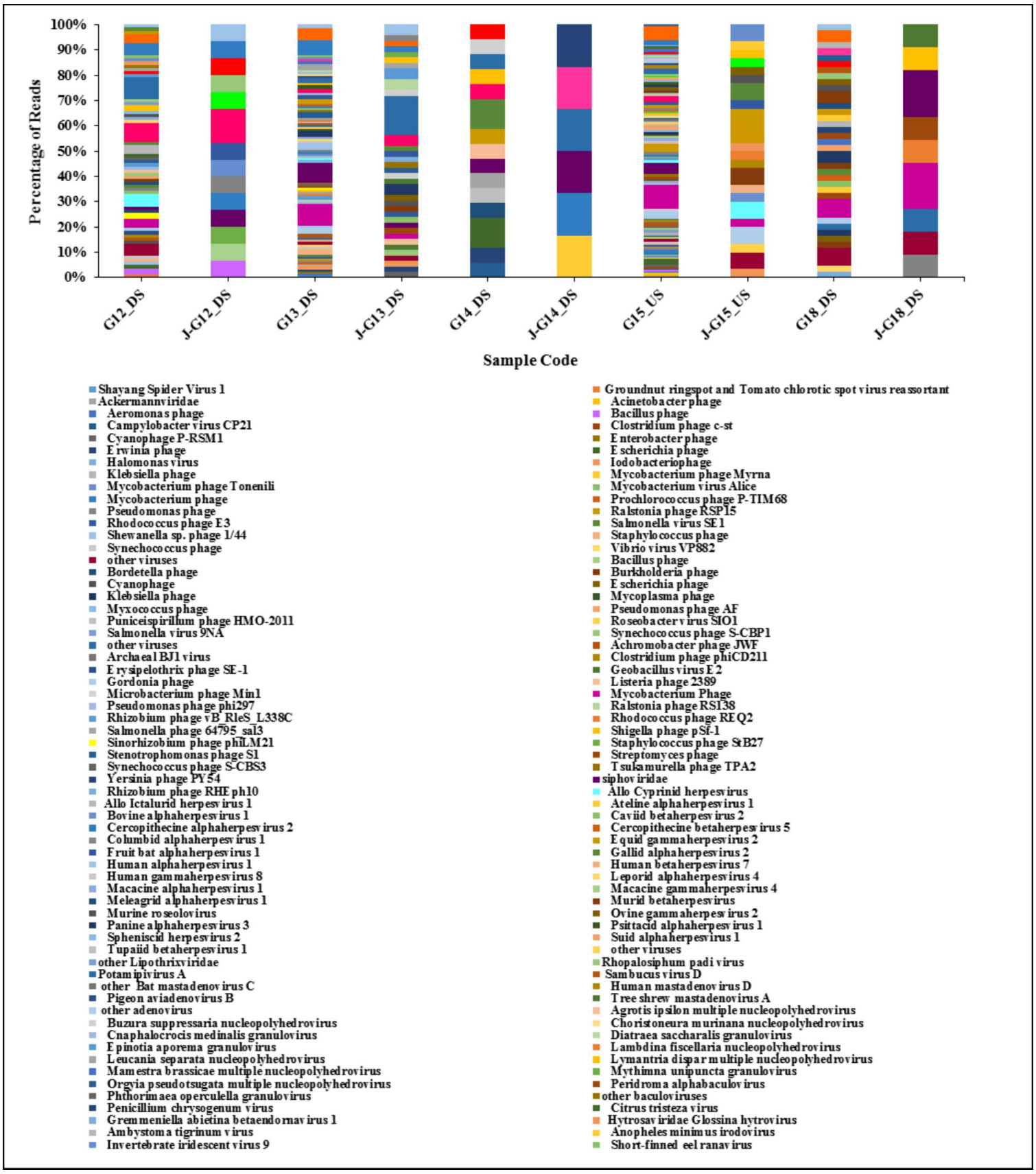

Fig.13 Comparison of Viral diversity of the lower stretch samples of River Ganga

Further analysis of the virome data showed existence of several "giant viruses" in River Ganga, which flourished with respect to their occurrence in the post-monsoon samples (Fig.5). There are several reports on presence of Giant viruses in distinct locations and in different habitat ranging from permafrost to the rivers (Yoosuf et al., 2012, Legendre et al., 2015). Till date, none of the Indian rivers have been documented for the presence of giant viruses.

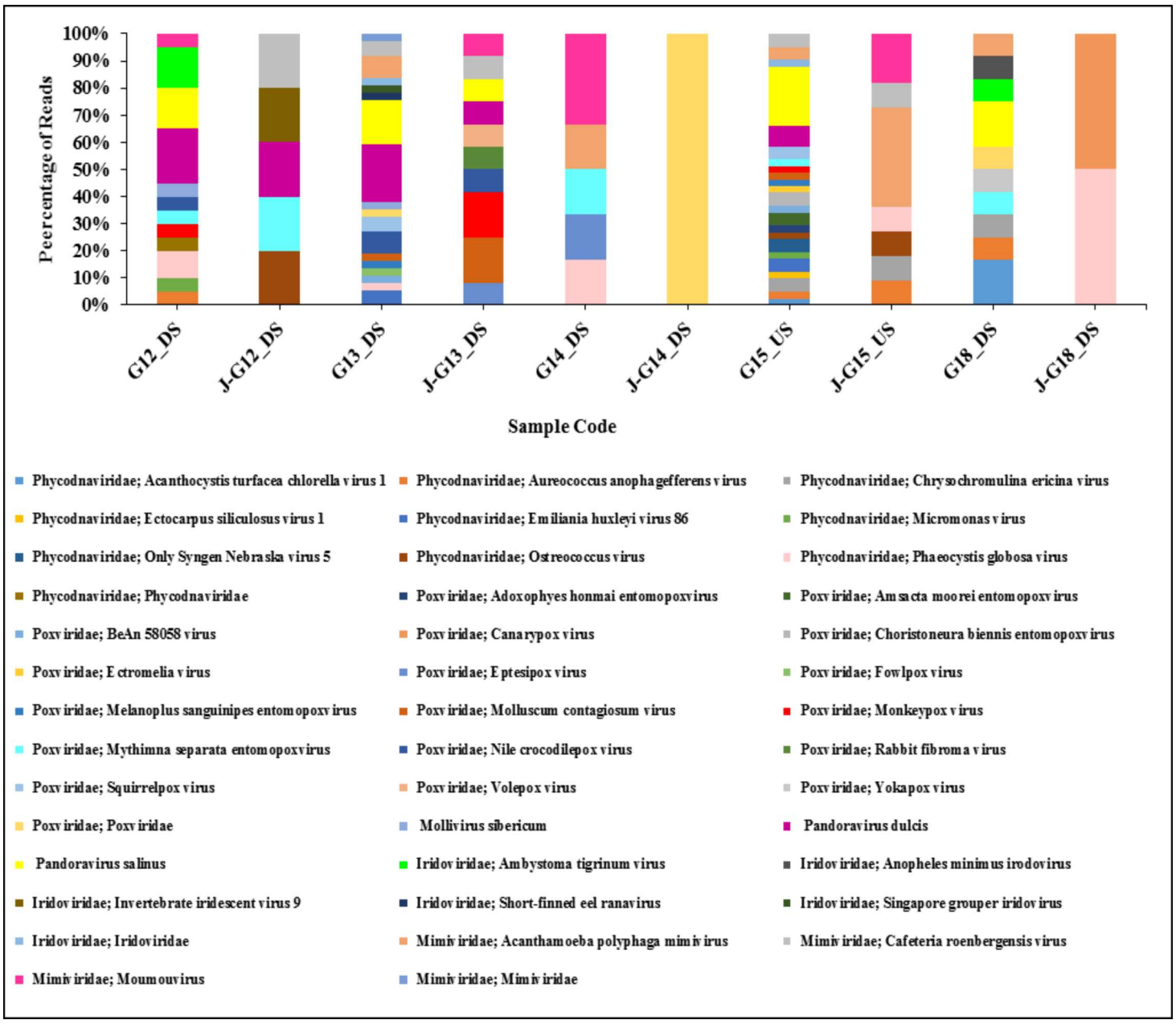

Fig.14 Comparison of giant viruses' diversity of the lower stretch samples of River Ganga

It should be noted that resulting number of reads associated with viruses might seem relatively low, as the steps involved in sequencing were selective for DNA viruses. The ensuing analysis is therefore restricted to only part of the total viral diversity.

Additional comparative analysis for viral diversity was done using Krona plots. It was observed that during post-monsoon season (oct'17), there is almost equal presence (50%) of phage

related family- Caudovirales and other viral families which together account for 50%). On the other hand, the pre-monsoon samples (Jun'18) showed an upsurge in the relative abundance of Caudovirales (71%). Additionally, it was observed that in the lower stretch there is a predominance of Myoviridae as opposed to that of upper stretch with a predominance of Siphoviridae (Fig.15).

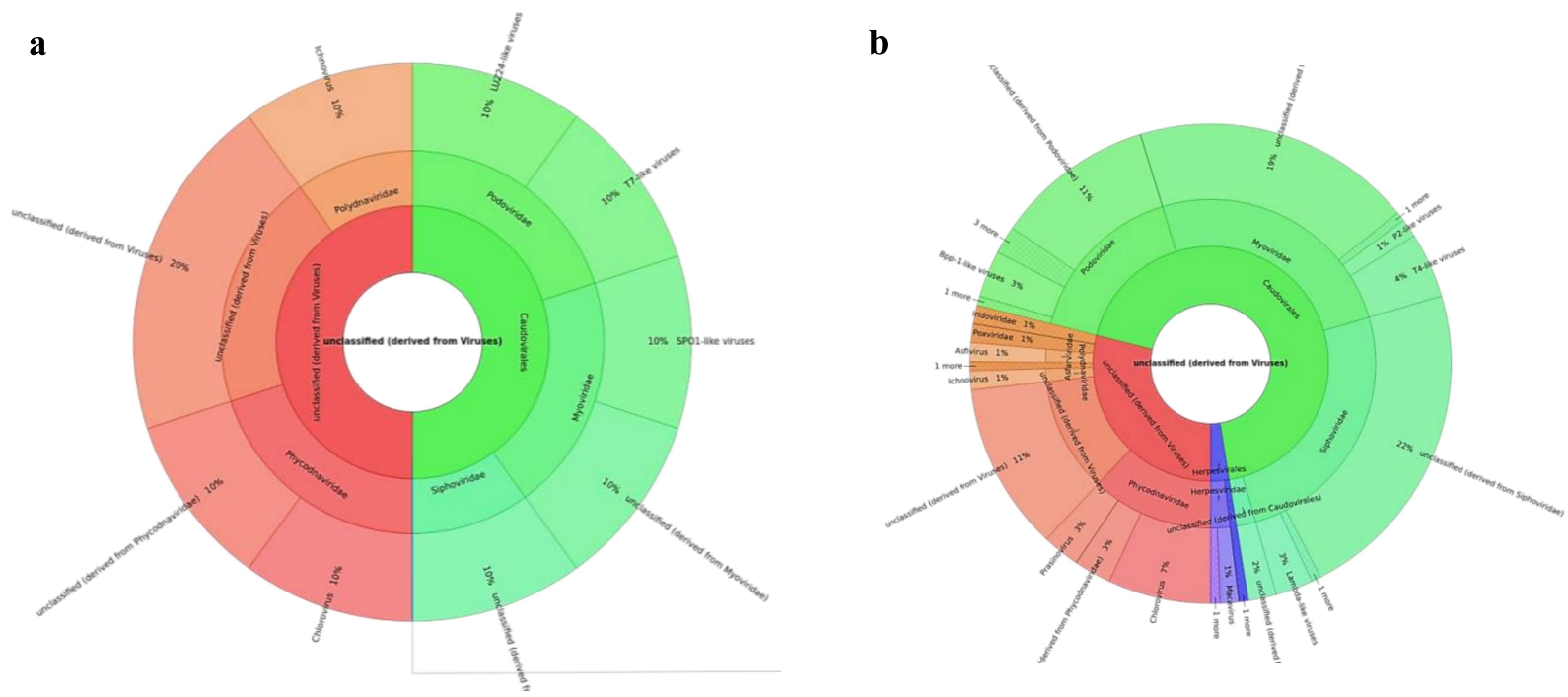

Fig.15: Krona plot of Viral diversity across lower stretch (post monsoon: Oct'17 (a) and pre-monsoon: Jun 2018 (b) samples).

To understand the phage diversity at genus level, the data was normalized and phage reads were combined and only those that passed the minimum cutoff value (excluding singletons) were mapped with krona plot for genus level phage diversity from Siphoviridae and Myoviridae families of bacteriophages. The plot showed presence of several bacteriophages such as Bacillus phage; Pseudomonas phage; Cronobacter phage; Escherichia phage; Mycobacterium phage, against pathogenic microbes.

a **b**

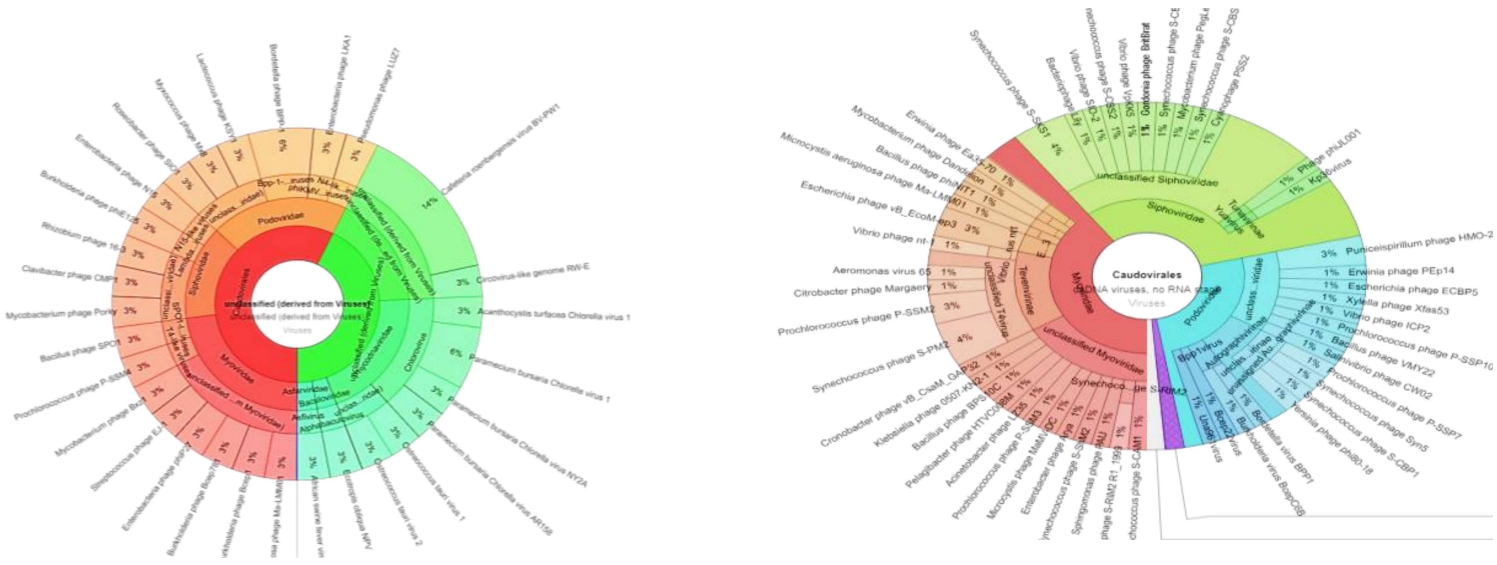
Caudovirales
Podoviridae
Siphoviridae
unclassified Siphoviridae
Myoviridae
unclassified Myoviridae
Phage phiJL001
Kplovirus
Puniceispirillum phage HMO-2
Erwinia phage PEp14
Escherichia phage ECBP5
Xylella phage Xfas53
Vibrio phage ICP2
Prochlorococcus phage P-SSP10
Bacillus phage VMY22
Salinivibrio phage CW02
Prochlorococcus phage P-SSP7
Synechococcus phage Syn5
Synechococcus phage S-CBP1
Bacillus virus BPP1
Bacillus virus BeachCity
Aeromonas virus 65
Citrobacter phage Margaery
Prochlorococcus phage P-SSM2
Synechococcus phage S-PM2
Cronobacter phage vB_CsaM_GAP32
Klebsiella phage BPS
Bacillus phage BPS
Pelagibacter phage HTVC008M
Acinetobacter phage
Prochlorococcus phage P-SSM3
Macrocystis phage MAV1
Enterobacter phage
Synechococcus phage S-RIM2
Synechococcus phage S-RIM8
Synechococcus phage S-CAM1
Synechococcus phage S-SM1
Vibrio phage S-CB2
Bacillus phage
Erwinia phage Ea35-70
Mycobacterium phage Dandelion
Bacillus phage
Microcystis aeruginosa phage Ma-LMM01
Escherichia phage vB_EcoM-ep3
Vibrio phage nt-1
Synechococcus phage S-CBS2
Synechococcus phage S-CBS1
Synechococcus phage S-CBS
Cyanophage PSS2
Mycobacterium phage Pegi
Synechococcus phage S-CBS
Vibrio phage VpV262
Gordonia phage Bethlehem
Synechococcus phage S-CBS
Mycobacterium phage Pegi
Synechococcus phage S-CBS
Cyanophage PSS2
Synechococcus phage S-CBS
Synechococcus phage S-CBS
Synechococcus phage S-CBS

1.3 Comparative viral/bacteriophage diversity and host-phage relationship across the entire stretch of River Ganga.

Results

Comparative viral diversity of upper and lower stretch samples

WIMP classification of the metavirome data obtained after nanopore sequencing, identified 14 virus families, in which prokaryotic viruses were the most abundant and dominated by the order *Caudovirales*. The relative abundance ranking of the different families was as follows: tailed bacteriophage families *Myoviridae* > *Siphoviridae* > *Podoviridae*, followed by the algae-infecting family *Phycodnaviridae*, the animals and humans infecting family *Herpesviridae,* the insect- infecting family *Iridoviridae* and the amoeba-infecting family *Mimiviridae* (Fig.17). Interestingly, large viruses belonging to the families *Phycodnaviridae* and *Mimiviridae* were detected, which should have been removed during the filtration process due to the use of a 0.22-µm filtration step to remove bacterial cells. The presence of these giant viruses' families suggest that this filtration process allowed partial mimivirus, pandoravirus, particles or their free-floating DNA to pass through the membrane. *Mimivirus; Pandoravirus; Mollivirus; Moumouvirus; Phaeocystisglobosa virus* appear to infect amoeba, which are ubiquitous in nature and have been isolated from diverse environments including freshwater lakes, river waters, salt water lakes, sea waters, soils and the atmosphere; supporting the existence of these giant viruses in River Ganga.

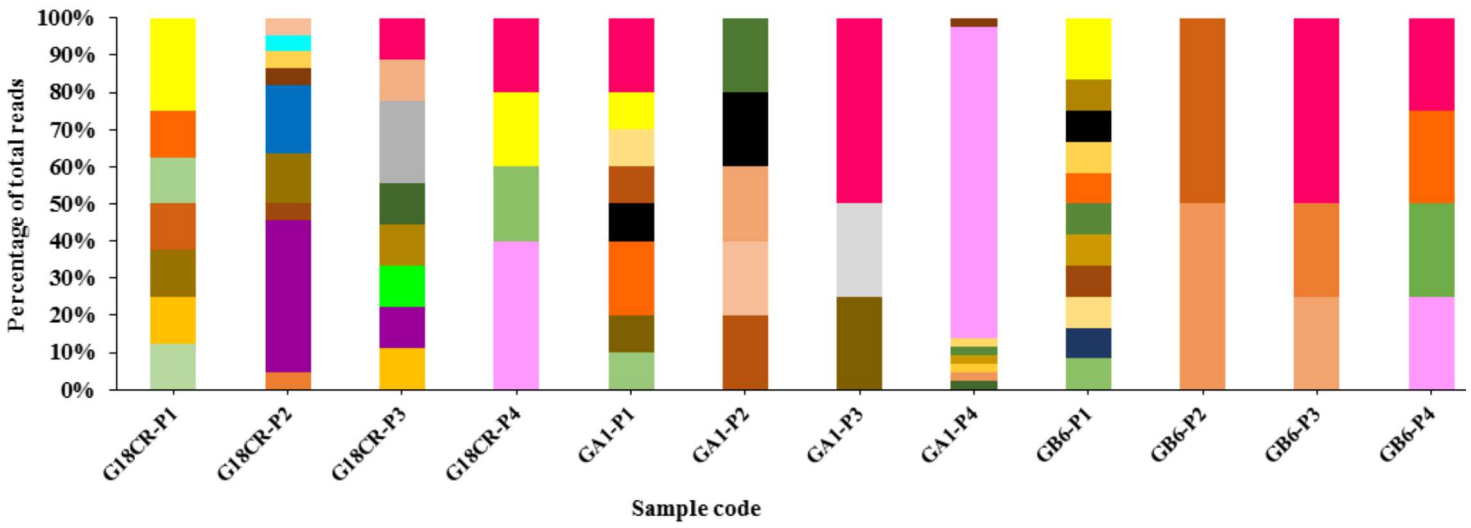

- Viruses; other_Viruses; other_other_Viruses; Pandoravirus salinus
- Viruses; other_Viruses; other_other_Viruses; Pandoravirus dulcis
- Viruses; other_Viruses; other_other_Viruses; Mollivirus sibericum
- Viruses; other_Viruses; other_other_Viruses; Halovirus VNH-1
- Viruses; other_Viruses; other_other_Viruses; Aspergillus foetidus dsRNA mycovirus
- Viruses; other_Viruses; Poxviridae; Rabbit fibroma virus
- Viruses; other_Viruses; Poxviridae; Molluscum contagiosum virus
- Viruses; other_Viruses; Poxviridae; Ectromelia virus
- Viruses; other_Viruses; Poxviridae; Cowpox virus
- Viruses; other_Viruses; Polydnaviridae; Glypta fumiferanae ichnovirus
- Viruses; other_Viruses; Polydnaviridae; Cotesia congregata bracovirus
- Viruses; other_Viruses; Phycodnaviridae; Phaeocystis globosa virus
- Viruses; other_Viruses; Phycodnaviridae; Paramecium bursaria Chlorella virus AR158
- Viruses; other_Viruses; Nudiviridae; Kallithea virus
- Viruses; other_Viruses; Nudiviridae; Gryllus bimaculatus nudivirus
- Viruses; other_Viruses; Mimiviridae; Moumouvirus
- Viruses; other_Viruses; Mimiviridae; Acanthamoeba polyphaga mimivirus
- Viruses; other_Viruses; Iridoviridae; Frog virus 3
- Viruses; other_Viruses; Hytrosaviridae; Glossina hytrovirus
- Viruses; other_Viruses; Flaviviridae; Hepacivirus C
- Viruses; other_Viruses; Chrysoviridae; Penicillium chrysogenum virus
- Viruses; other_Viruses; Baculoviridae; Peridroma alphabaculovirus
- Viruses; other_Viruses; Baculoviridae; Orgyia pseudotsugata multiple nucleopolyhedrovirus
- Viruses; other_Viruses; Baculoviridae; Mythimna unipuncta granulovirus
- Viruses; other_Viruses; Baculoviridae; Mamestra configurata nucleopolyhedrovirus A
- Viruses; other_Viruses; Baculoviridae; Leucania separata nucleopolyhedrovirus
- Viruses; other_Viruses; Baculoviridae; Hyphantria cunea nucleopolyhedrovirus
- Viruses; other_Viruses; Baculoviridae; Diatraea saccharalis granulovirus
- Viruses; other_Viruses; Baculoviridae; Chrysodeixis chalcites nucleopolyhedrovirus
- Viruses; other_Viruses; Baculoviridae; Agrotis ipsilon multiple nucleopolyhedrovirus
- Viruses; other_Viruses; Ascoviridae; Trichoplusia ni ascovirus 2c
- Viruses; Picornavirales; Secoviridae; Rice tungro spherical virus
- Viruses; Picornavirales; Picornaviridae; Aichivirus C
- Viruses; Nidovirales; Mesoniviridae; Alphamesonivirus 5
- Viruses; Mononegavirales; Nyamiviridae; Nyamanini nyavirus
- Viruses; Herpesvirales; Herpesviridae; Human alphaherpesvirus 3
- Viruses; Herpesvirales; Herpesviridae; Equid gammaherpesvirus 5
- Viruses; Herpesvirales; Alloherpesviridae; Cyprinid herpesvirus 3
- Viruses; Herpesvirales; Alloherpesviridae; Cyprinid herpesvirus 1
- Viruses; Herpesvirales; Alloherpesviridae; Anguillid herpesvirus 1
- Viruses; Caudovirales; other_Caudovirales; Providencia phage Redjac
- Viruses; Caudovirales; Siphoviridae; other_Siphoviridae
- Viruses; Caudovirales; Siphoviridae; Synechococcus phage S-SKS1
- Viruses; Caudovirales; Siphoviridae; Streptomyces phage SV1
- Viruses; Caudovirales; Siphoviridae; Pseudomonas phage PS-1
- Viruses; Caudovirales; Siphoviridae; Propionibacterium phage PHL116
- Viruses; Caudovirales; Siphoviridae; Leuconostoc phage phiLN25
- Viruses; Caudovirales; Siphoviridae; Flavobacterium phage 11b
- Viruses; Caudovirales; Siphoviridae; Bacillus virus TP21
- Viruses; Caudovirales; Podoviridae; Xylella virus Prado
- Viruses; Caudovirales; Myoviridae; other_Myoviridae
- Viruses; Caudovirales; Myoviridae; Vibrio phage 11895-B1
- Viruses; Caudovirales; Myoviridae; Synechococcus phage
- Viruses; Caudovirales; Myoviridae; Shigella virus SP18

Fig.17 Comparison of Virus enrichment Protocols to understand the total viral diversity

To understand the comparative viral diversity for the upper stretch data and the lower stretch data. MG-RAST was done. Analysis of the upper stretch samples revealed a plethora of viral diversity, with the highest relative abundance of 67% for the family of bacteriophages (Caudovirales) with a predominance of Siphoviridae (32%) (Fig.18). For lower stretch a predominance of Myoviridae (28%) was observed, as opposed to that of upper stretch with a predominance of Siphoviridae (Fig.19).

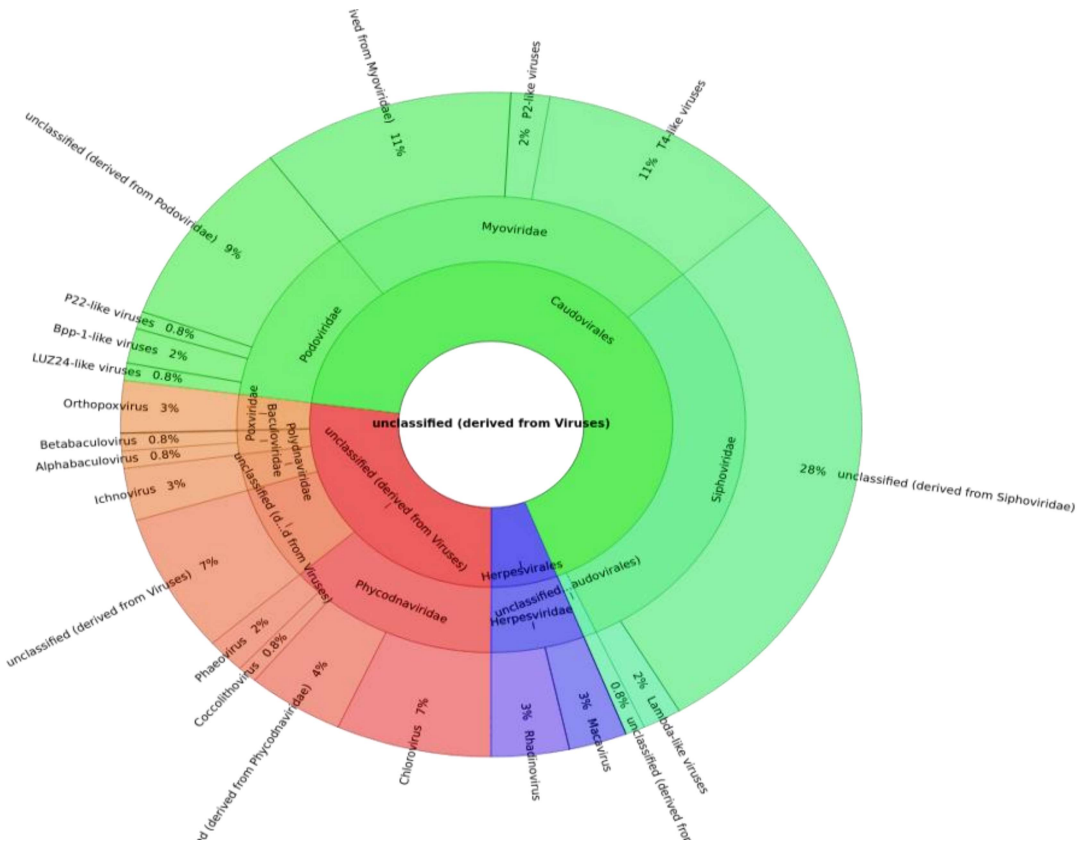

Fig.18: Krona plot of phage families of upper stretch

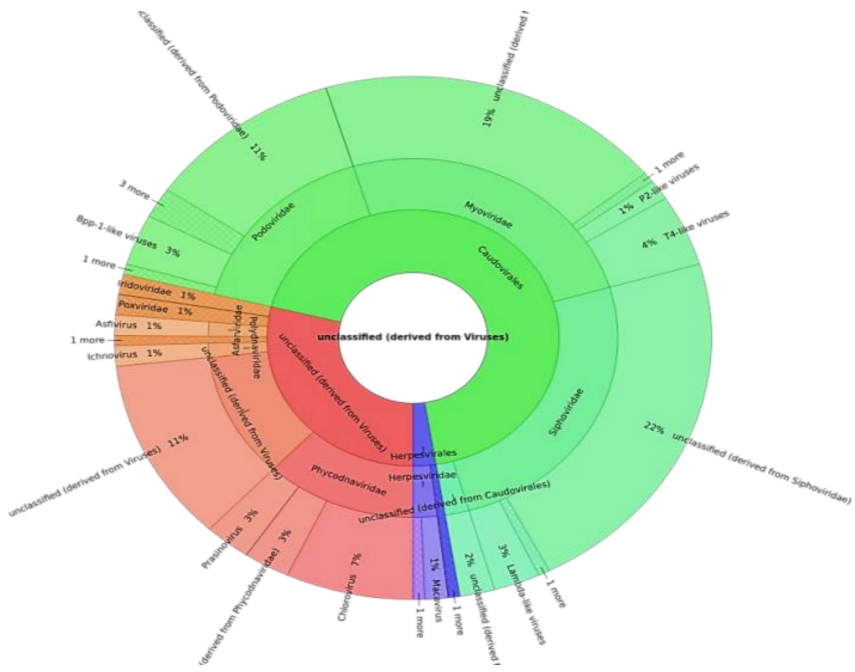

Fig.19: Krona plot of phage families of lower stretch

Host-phage presence in the entire stretch

Host-phage presence across the entire stretch of River Ganga was established and tabulated on the basis of the relative abundance of bacteriophages and presence of their cognate host. Analysis revealed presence of plethora of phages and their corresponding hosts which were then divided into groups. The grouped data consists of putrefying bacteria, human pathogens, plant pathogens, photosynthetic microbes, plant growth promoting rhizobacteria (PGPR), and others.

HOST	PHAGE
Putrefying bacteria	
Vibrio cholerae	Vibrio phage
Shigella sp.	Shigella phage
Enterobacter cloacae	Enterobacteria phage
Klebsiella pneumoniae, K. oxytoca	Klebsiella phage
Salmonella sp, *S. enterica, S. typhimurium*	Salmonella phage
Clostridium sp.	Clostridium phage
Bacillus sp.	Bacillus phage
Campylobacter jejuni, Campylobacter sp.	Campylobacter phage
Human Pathogens	
Escherichia coli, Escherichia sp.	Escherichia phage
Aeromonas sp.	Aeromonas phage
Acinetobacter baumannii, Acinetobacter sp.	Acinetobacter phage
Pseudomonas aerogenes, Pseudomonas putida, Pseudomonas sp.	Pseudomonas phage
Staphylococcus aureus	Staphylococcus phage
Streptococcus sp.	Streptococcus phage
Corynebacterium sp.	Corynebacterium phage
Listeria sp.	Listeria phage
Bordetella sp.	Bordetella phage
Burkholderia	Burkholderia phage
Stenotrophomonas maltophilia	Stenotrophomonas phage
Mycobacterium sp.	Mycobacterium phage
Haemophilus sp.	Haemophilus phage
Aggregatibacter sp.	Aggregatibacter phage
Gordonia sp.	Gordonia phage
Cronobacter sp.	Cronobacter phage
Yersinia sp.	Yersinia phage
Plant Pathogens	
Xanthomonas oryzae, X. campestris	Xanthomonas phage
Xylella sp.	Xylella phage
Pseudomonas syringae	Pseudomonas phage
Ralstonia solanacearum	Rasltonia phage
Erwinia sp.	Erwinia phage

Clavibacter sp.	Clavibacter phage
Photosynthetic microbes	
Synechococcus sp.	Synechococcus phage
Prochlorococcus sp.	Prochlorococcus phage
Microcystis sp.	Microcystis phage
PGPR	
Azospirillum sp.	Azospirillum phage
Rhizobium sp.	Rhizobium phage
Bradyrhizobium sp.	Bradyrhizobium phage
Other bacteria	
Thalassomonas sp.	Thalassomonas phage
Roseobacter sp.	Roseobacter phage
Flavobacterium sp.	Flavobacterium phage
Streptomyces sp.	Streptomyces phage
Lactococcus sp.	Lactococcus phage
Lactobacillus sp.	Lactobacillus phage

2. Total microbial diversity (TMD) in the sediments of River Ganga and comparison with pre- and post-monsoon

2.1. Total microbial diversity (taxonomic and functional) (TMD) in the sediments of upper stretch of River Ganga

2.1.A Methodology:

Extraction of metagenomic DNA, targeted amplification and nanopore sequencing was performed as mentioned above (Pg 4-5). The taxonomic data analysis was carried out using EPI2ME software, Kaiju database and MG-RAST. For functional annotation, MG-RAST was used with subsystems and KO databases.

2.1.B Results:

Taxonomic diversity of bacteria and archaea.

EPI2ME analysis of the upper stretch samples revealed presence of several extremophilic bacteria such as *Sulfuritalea; Thiobacillus; Sulfuricaulis; Sideroxydans; Polaromonas,* etc. (Fig.20). Additionally, we classified the archaeal reads which revealed presence of halophilic and methanogenic archaea (Fig.21).

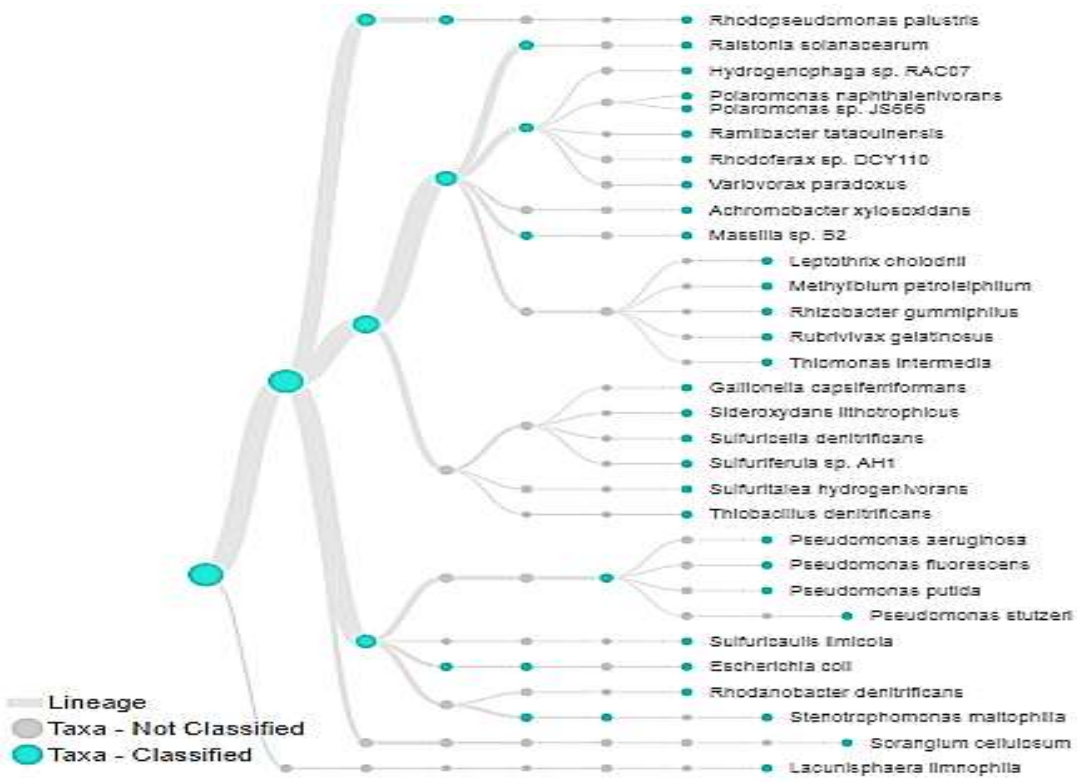

Fig .20: Taxonomic tree showing presence of Bacterial genera along the upper stretch samples of River Ganga spanning from Gomukh to Rishikesh.

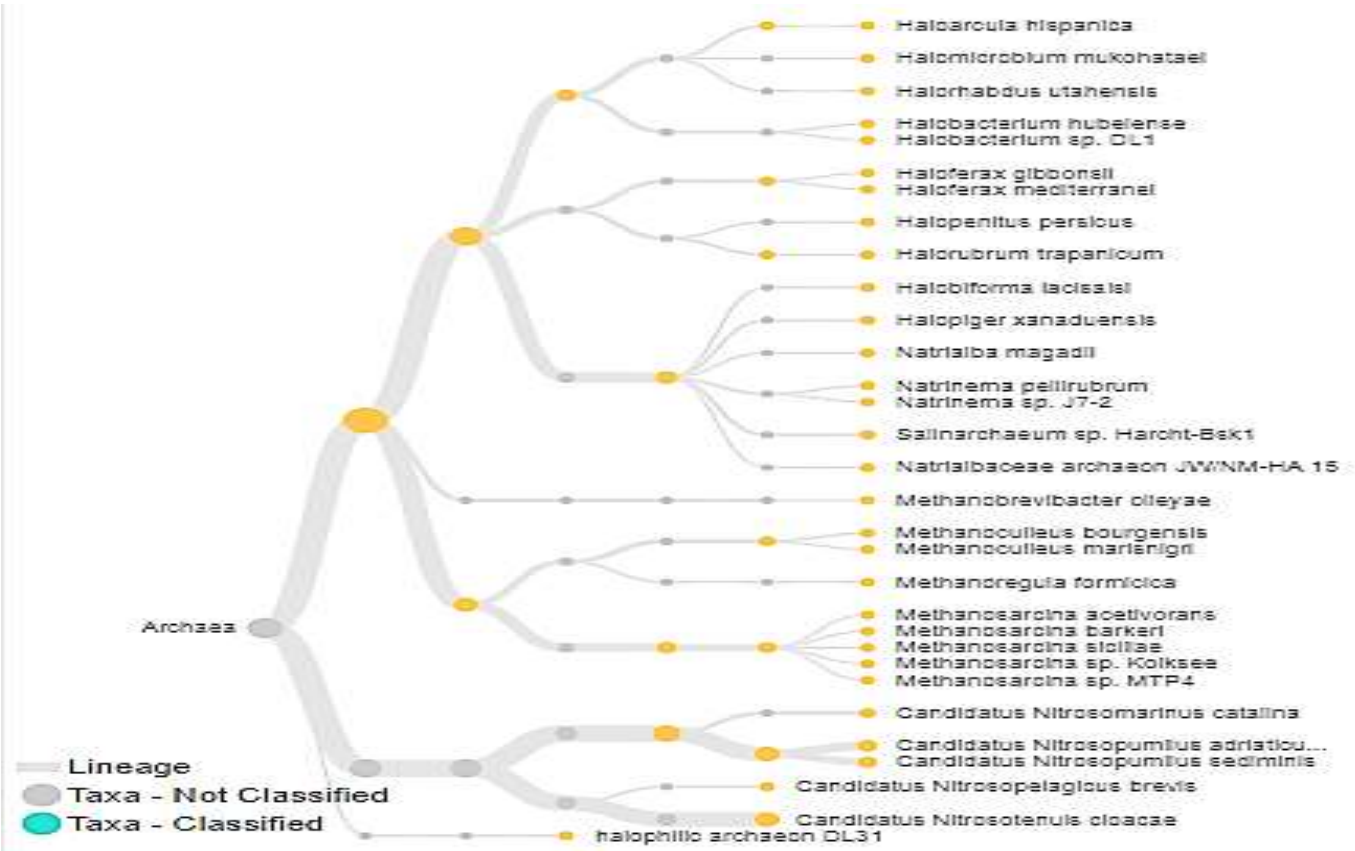

Fig .21: Taxonomic tree showing presence of Archaeal genera along the upper stretch samples of River Ganga spanning from Gomukh to Rishikesh.

Further, MG-RAST was used to map the bacterial and archeal diversity location-wise. Bacterial classification of the reads showed a predominance of Proteobacteria (70-80%) followed by Firmicutes (10-15%) and Actinobacteria (7-10%). (Fig.22).

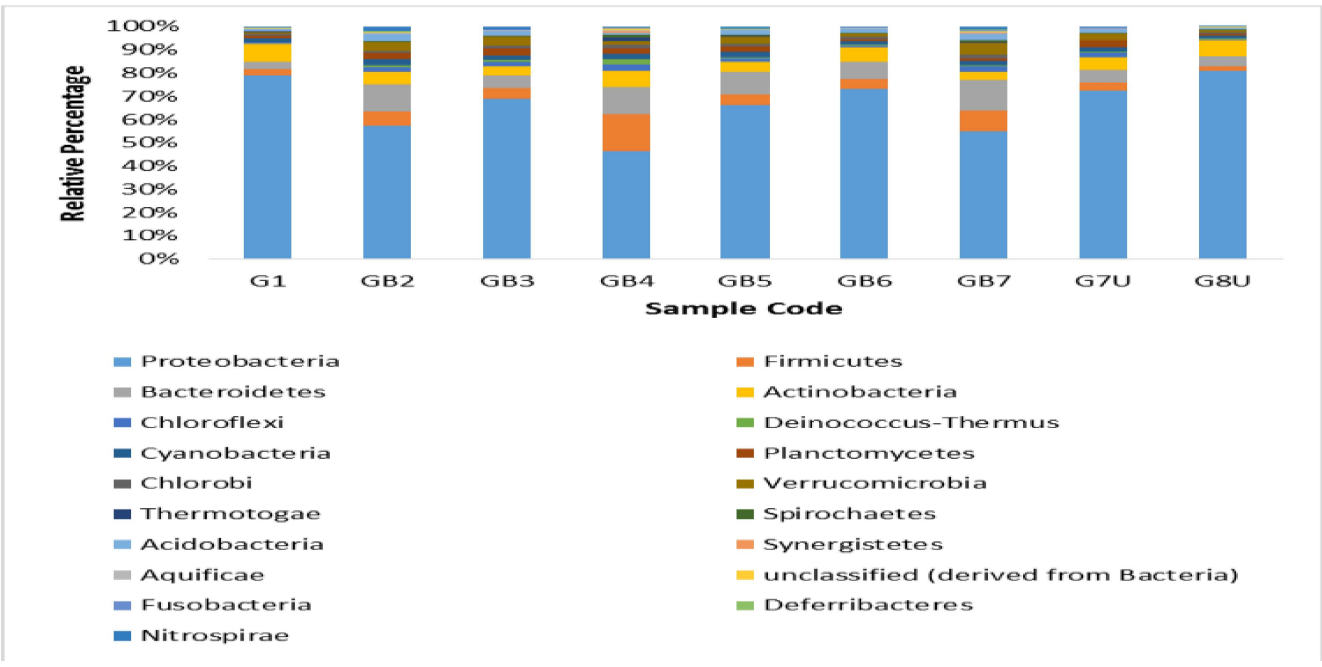

Fig .22: Graph showing presence of Bacterial Phyla along the upper stretch samples of River Ganga spanning from Gomukh to Tehri. (Only Top 20 phyla are highlighted)

Further classification of the bacterial reads up to genus level revealed a predominance of bacteria such as *Burkholderia (30-35%); Pseudomonas (24-28%); Shewanella (18-23%)* and *Nitrosococcus (12-14%)* and *Thioalkalivibrio (10-14%)* (Fig. 23).

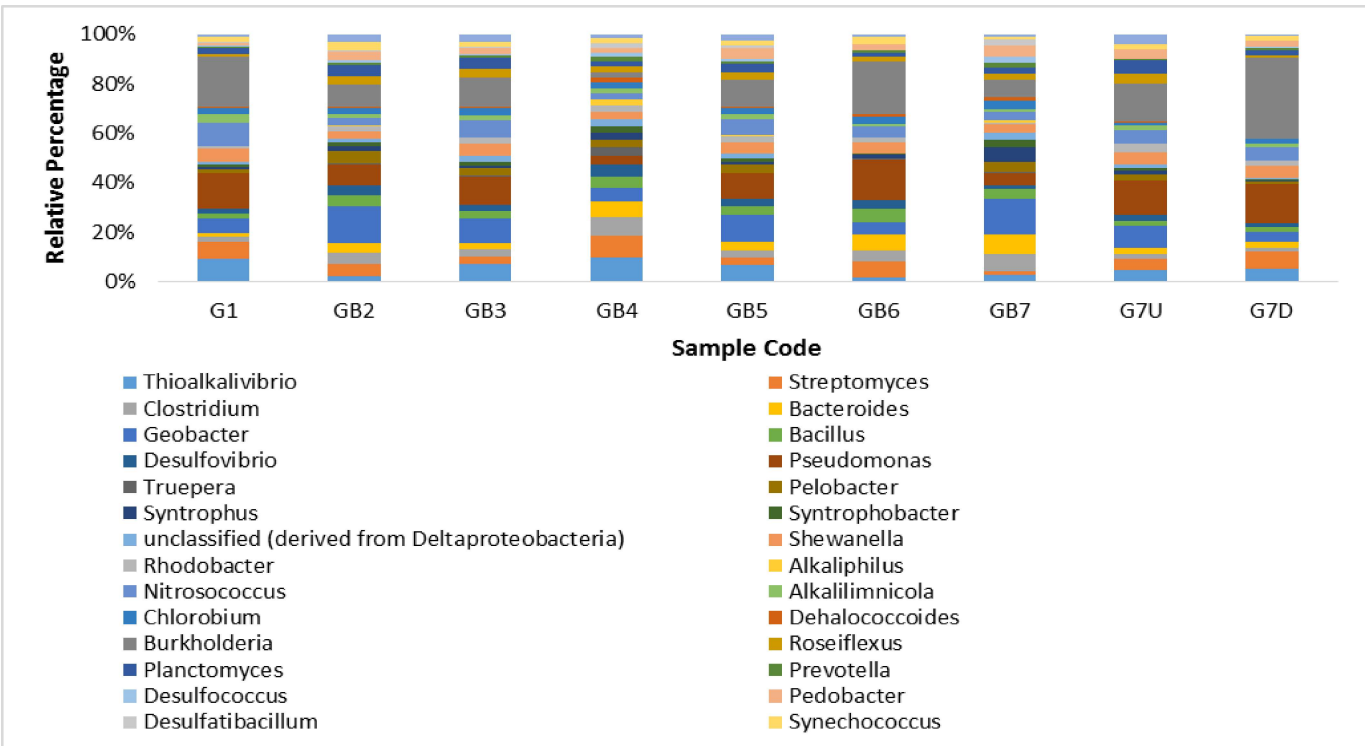

Fig .23: Graph showing presence of Bacterial genera along the upper stretch samples of River Ganga spanning from Gomukh to Tehri. (Top 30 genera are highlighted).

Archaeal classification of the reads showed a predominance *of Euryarchaeota* (70-80%) followed by *Tahumarchaeota (12-18%) and Crenarchaeota (7-9%)*. (Fig.24).

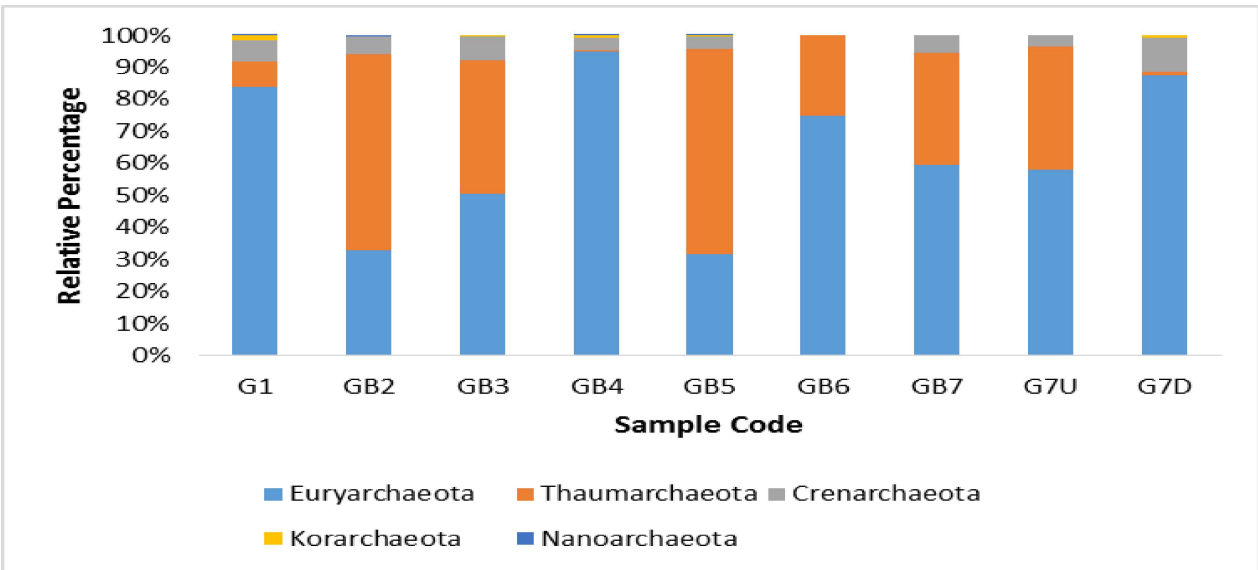

Fig .24: Graph showing presence of Archaeal phyla along the upper stretch samples of River Ganga spanning from Gomukh to Tehri.

Further, the genus level classification of archaeal reads showed a predominance of Methanogenic Archaea such as *Methanosarcina (40-50%); Methanoaseta (25-30%); Methanoculleus (21-24%); and Methanospirillum* (15-20%). (Fig.25).

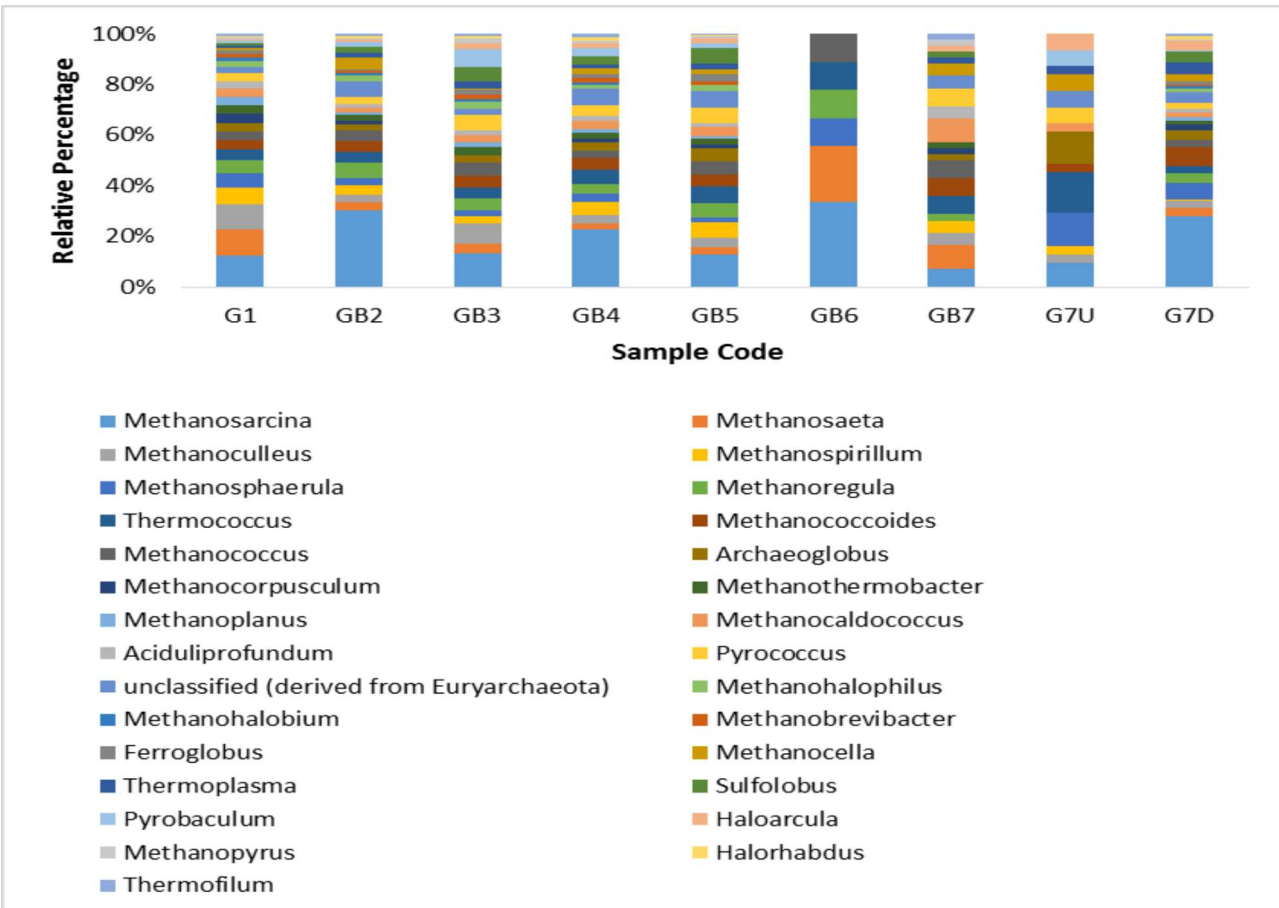

Fig .25: Graph showing presence of Archaeal genera along the upper stretch samples of River Ganga spanning from Gomukh to Tehri. (Top 30 genera are highlighted).

Functional aspects of the upper stretch diversity.

The functional profile of the samples was deduced using MG-RAST. From the initial analysis it was evident that the microbes belonging to this stretch has genes spanning a diverse range of metabolism which includes Protein Metabolism (60-63%); Amino Acids Derivatives (30-34%); Carbohydrate metabolism (12-15%) and Respiration (10-12%). (Fig 26).

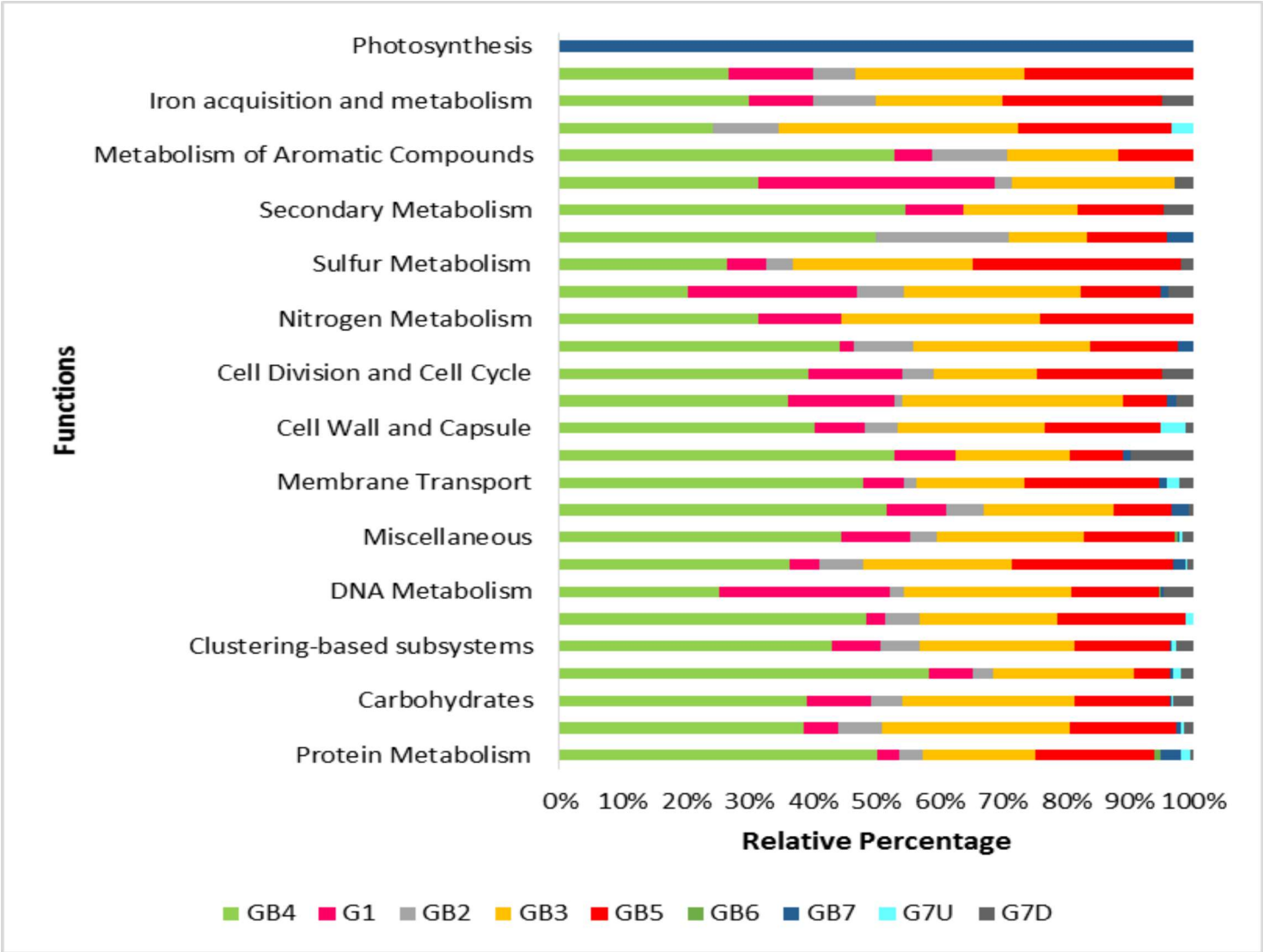

Fig .26: Graph showing presence of functional genes along the upper stretch samples of River Ganga spanning from Gomukh to Tehri.

2.2. Total microbial diversity (TMD) in the sediments of lower stretch of River Ganga

Taxonomic and functional distribution of Triveni sangam confluence samples

In the upstream of the confluence and the confluence (G14DS; G15US and G15S), Proteobacteria (59.2%; 58.3% and 59.4%) was predominant followed by Bacteroidetes (7.6%;7.4% and 6.5%) and Firmicutes (6.7%; 6.9% and 6.1%) respectively. Similar observations were noted in the Yamuna River sample (G15Y), with a higher abundance of Proteobacteria (64.1%), Bacteroidetes (4.6%) and Firmicutes (5.2%). Further, the immediate downstream of the confluence (G15DS) observed an increase of Proteobacteria to 74%, while the percentage of Bacteroidetes and Firmicutes decreased to 3.4-3.5% respectively. However, the alteration in the bacterial community structure seems to be a transient, as the farther downstream samples (G16US; G16DS), showed a lower relative abundance of Proteobacteria (60%; 55%), Bacteroidetes (8%; 6%) and Firmicutes (6.2%; 6.5%) (Fig 27) (Samson et. al, 2019).

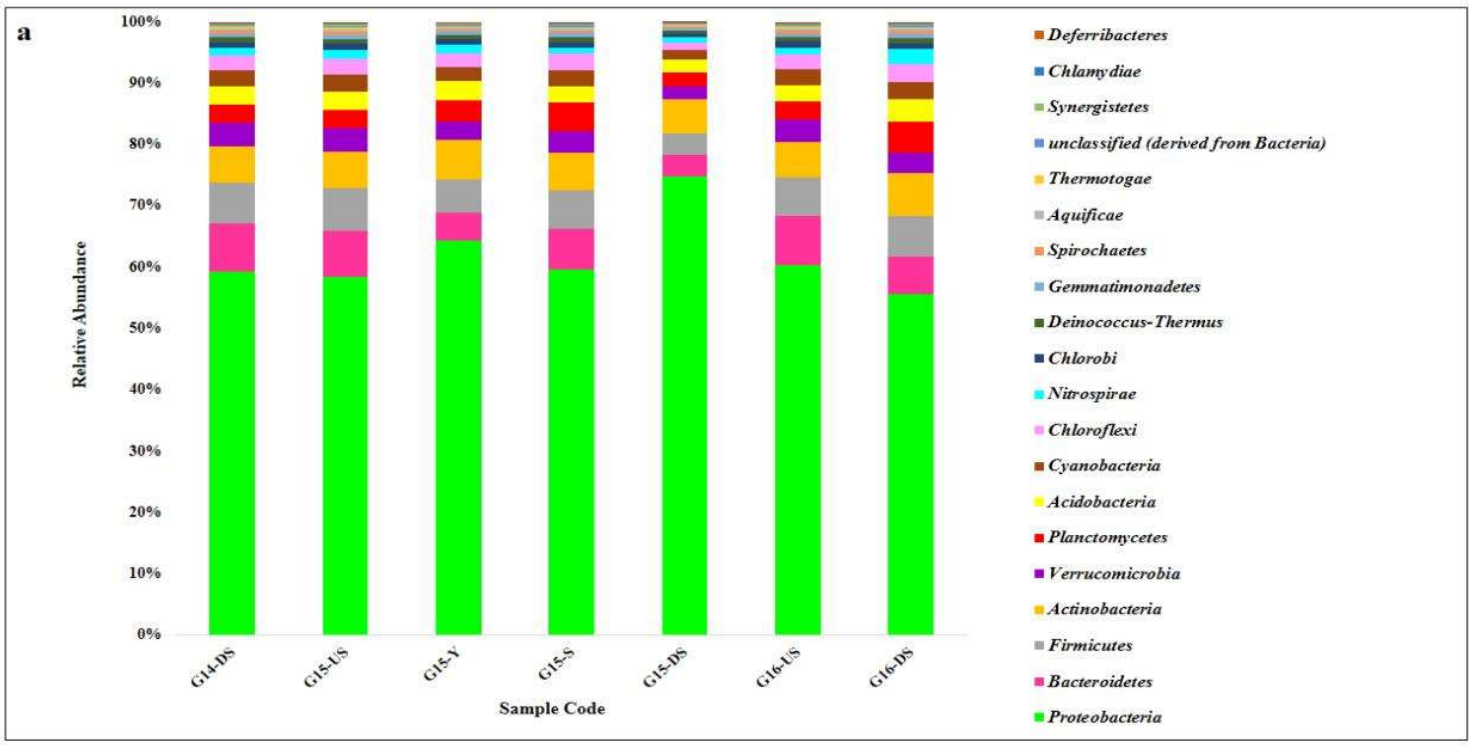

Fig. 27: Bacterial Diversity at phylum level of confluence samples (Sediment). Top 20 Genera are shown (Samson et. al, 2019).

Classification of the reads assigned to the Archaeal domain showed a predominance of Thaumarchaeota in G14DS; G15US; G15S, G16US and G16DS with a relative abundance of 65.7%; 65.6%; 65.1%; 58.3%; 68.3% respectively. However, in G15Y and G15DS, the percentage of archaeal phyla varied significantly. A higher relative abundance of phylum Euryarchaeota (44% and 40%) was observed in G15Y and G16US respectively. Moreover, for G15DS a distinct archeal diversity was observed with Euryarchaeota (61%), followed by Thaumarchaeota (33.4%) (Fig 28) (Samson et. al, 2019).

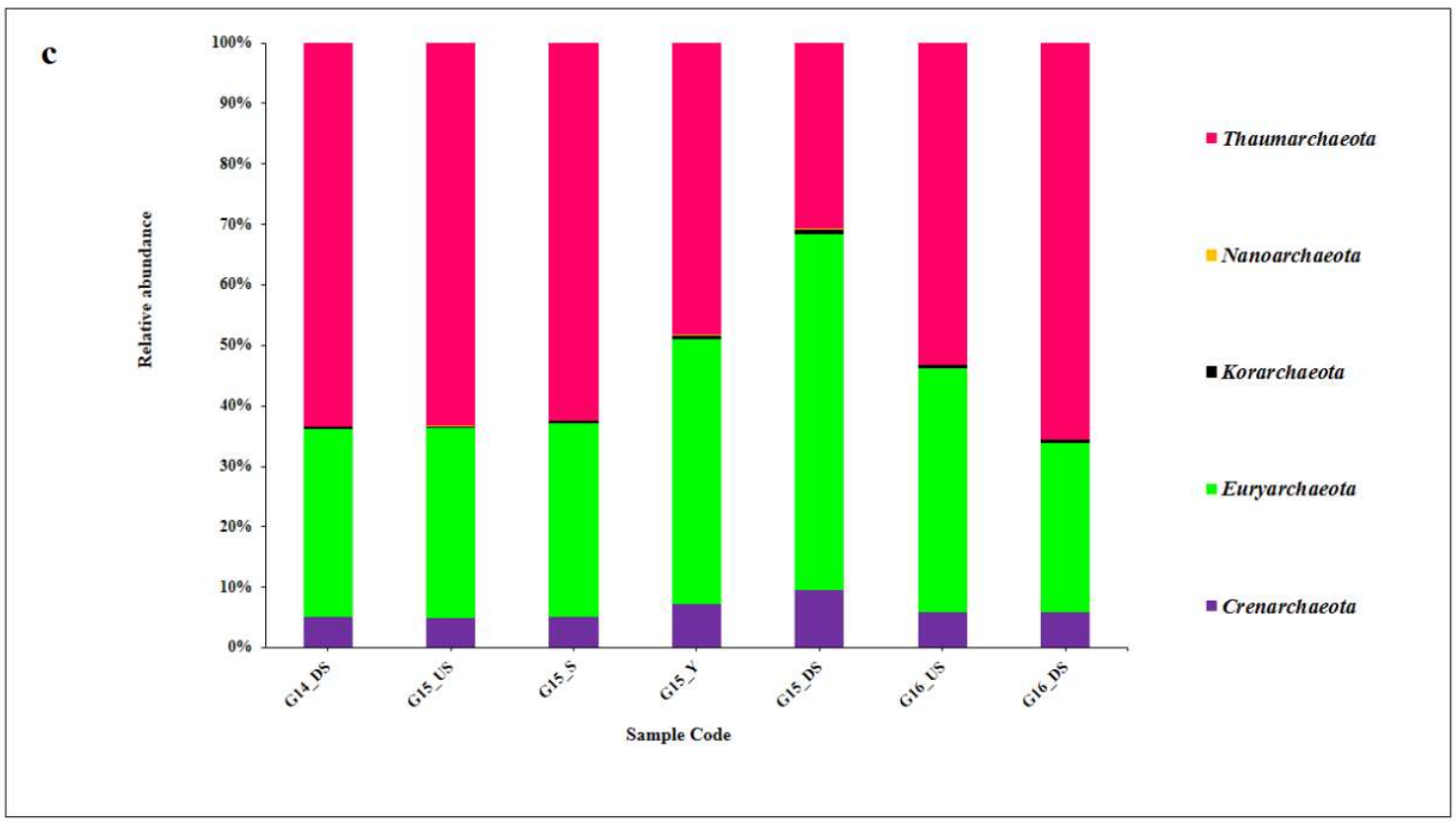

Fig. 28: Archaeal Diversity at phylum level of the confluence samples (Sediment). (Samson et. al, 2019).

Functional gene analysis of the confluence samples.

KEGG analysis was performed to decipher the metabolic potentials of each sequence by assigning KEGG Orthology (KO) numbers obtained from known reference hits and annotation of the metabolic pathways was done using KEGG pathway analysis. Amongst all the functions, 60% of the sequences were assigned to metabolism which encompasses amino acid metabolism, biosynthesis of secondary metabolites, carbohydrate metabolism, cofactors and vitamins metabolism, energy metabolism, glycan synthesis and metabolism, lipid metabolism, metabolism of terpenoids and polyketides, nucleotide metabolism and xenobiotic biodegradation and metabolism

(Fig. 29a and 29b). Annotated pathways for metabolism of xenobiotic compounds such as Chlorocyclohexane and Chlorobenzene, Benzoate, Aminobenzoate and Nitrotoluenes were present in all samples except G15US. Additionally, the potential for degradation of steroid, drugs and herbicides such as dioxin, caprolactum, and atrazine was observed in G15Y. These additional metabolic features except for steroid and dioxin metabolism, (exclusive of G15Y) were also present in the confluence and the immediate downstream i.e., G15S and G15DS. However, the farther downstream locations G16US and G16DS showed xenobiotic degradation profile comparable to that of the upstream of the confluence (Fig. 29c).

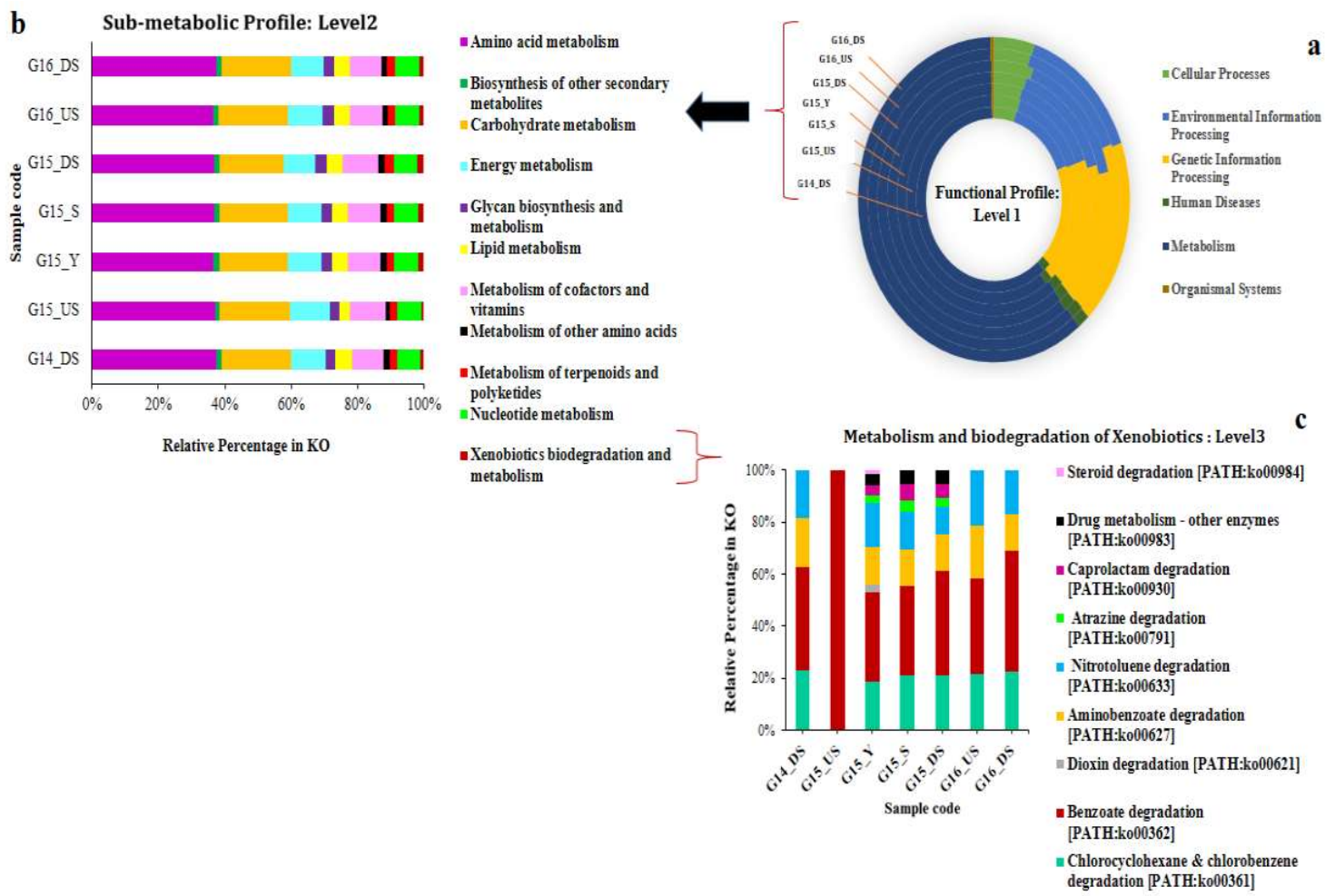

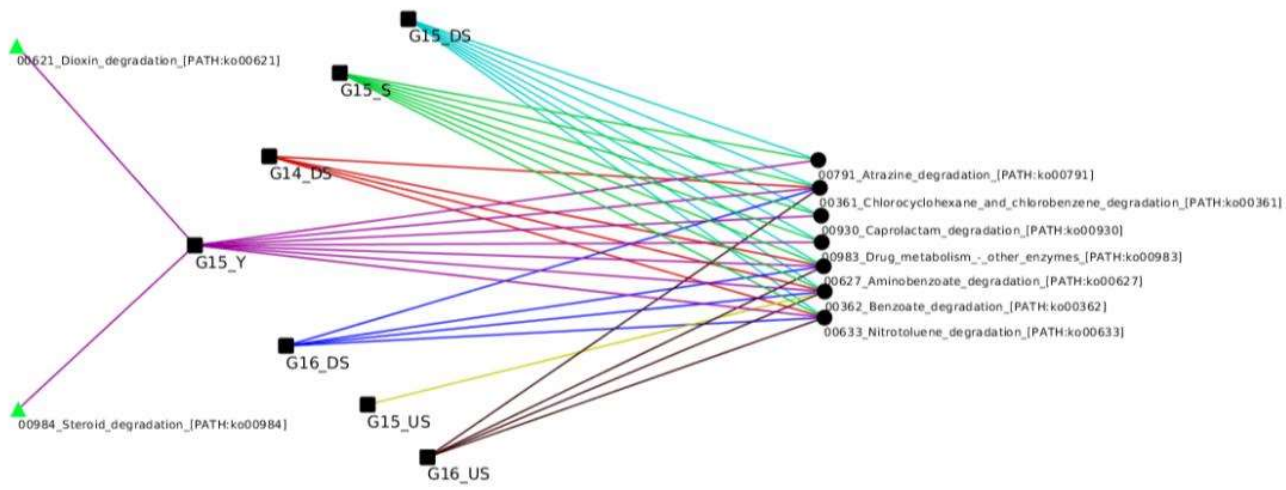

Fig. 29. Classification of reads assigned to metabolism according to KEGG database **a)** Relative Percentage of reads assigned to all functions; **b)** Sub-metabolic profile; **c)** Biodegradation of xenobiotic compounds; **d)** Network plot elucidating the potentials for xenobiotic degradation shared by the microbes of each location (black dots) and those unique to the microbes (arrows pointing outwards).

SEED database was used to decipher the genes conferring resistance to toxic compounds such as heavy metals and antibiotics. Resistance to heavy metals such as zinc, mercury, copper, cobalt, cadmium, arsenic and antibiotics such as fluoroquinolones and beta-lactams was observed in all the samples. Apart from this, genes conferring Multiple Drug Resistance (MDR) due to presence of efflux pumps was seen in all the samples. In addition to these genes, G15Y encompassed an additional set of genes supplementing diverse functionality. These genes include resistance to chromium compounds, copper homeostasis, presence of mercuric reductase, a separate MDR cluster, tolerance to Colicin E2 and Methicillin Resistance Staphylococci (MRSA). Interestingly, concomitant presence of these genes was observed at the confluence (G15S) and the immediate downstream (G15DS) sample (Fig. 30).

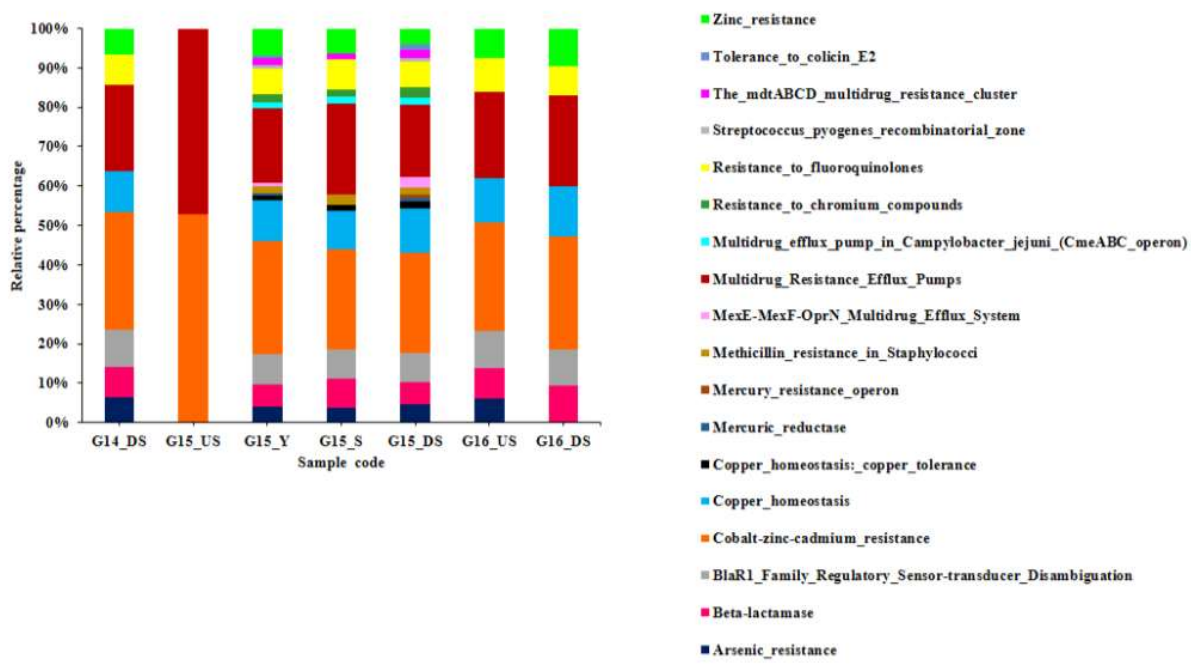

Fig. 30. Grouping of the reads mapping to resistance to toxic compounds and antibiotics according to KEGG database.

To delineate further and understand the antimicrobial resistance (AMR), MegaRES was used to annotate the metagenomic samples, classifying them on the basis of genes imparting resistance to a particular class of antibiotics and also revealing the mechanism of resistance lying underneath (Fig. 31a). From the categorization, a unique pattern of distribution of AMR genes with respect to resistance to different classes of antibiotics such as aminocoumarins, aminoglycosides, betalactams, elfamycins, lipopeptides, Macrolides-Lincosamide-Streptogramines (MLS), MDR, phenicol, rifampin and sulfonamide was observed. The relative percentage of aminocoumarins, rifampin resistance was higher in G14DS (10.78%, 23.52%); G15US (11.27%, 41.81%); G16DS (8%, 36%) as compared to that of G15Y (0.47%, 0.47%); G15DS (0.14%, 0.84%); G16US (1.31%, 1.31%). Resistance to aminoglycosides and sulfonamides was maximum at G15Y (24.88%, 14.92%) which appeared to be carried downwards at G15S (21.98%, 0.86%), G15DS (20.53%, 0.28%). Strikingly, confluence G15S also harbored certain distinct mechanisms such as a higher resistance to beta-lactamases (50.86%) and lipopeptides (2.5%), respectively that were possibly passed downstream to G15DS (33.6%, 0.421%), while started diminishing from G16US (1.31%) and were absent in G16DS (Fig. 31b). Further, to comprehend the shared and the unique mechanism of antibiotic resistance, a

networking plot was constructed using Cytoscape v3.2.7 (Vey and Moreno-Hagelsieb, 2012) (Fig. 31c).

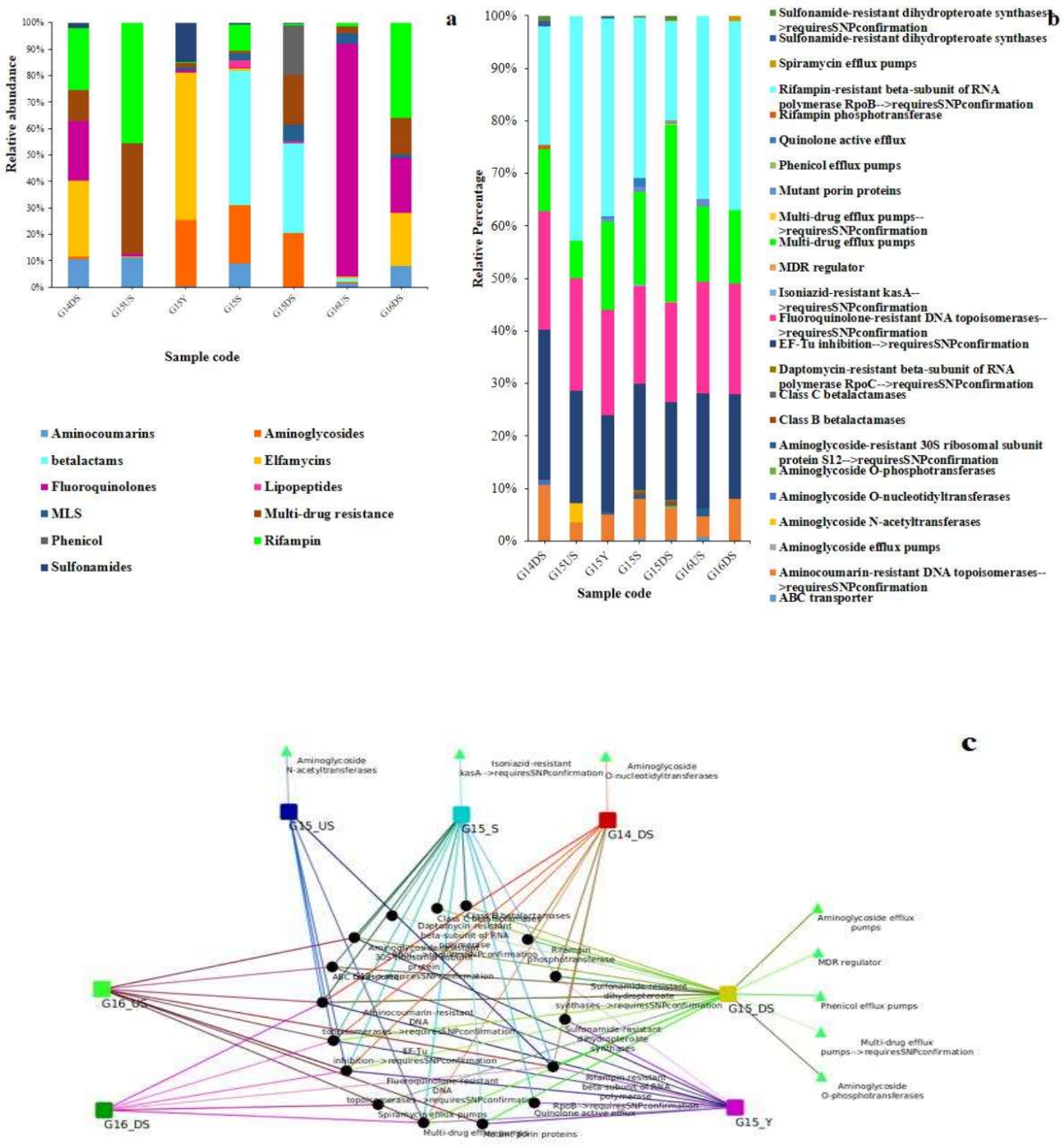

Fig. 31. Antibiotic Resistance profiling of the metagenomic samples using MegaRES **a)** Resistance to the class of antibiotics; **b)** Mechanism of Resistance against different classes of antibiotics; **c)** Network plot showing resistance mechanisms unique to a particular location

Bacterial and archaeal diversity of the entire lower stretch samples

Amongst the bacterial phyla, the most dominating phyla were the *Proteobacteria* (70%) followed by the *Actinobacteria* (20%) and the *Bacteroidetes* (6%). Further analysis of the bacterial phyla revealed the presence of certain rare phyla such as *Calditriarchaeota; Kritimtiellaeota; Coprothermobacterota; Elusimicrobia; Armantimonadates; Cladiserica; Ignavibacteriae; Deferribacters; Dictyoglomi; Nirospirae* and *Synergistestes* (Fig.32). Strikingly, certain bacterial phyla such as *Aquificae; Deinococcus-Thermus; Thermotogae; Thermodesulfobacteria; Chloroflexi* etc. having a wide distribution at high temperatures and hydrothermal environments were observed along the entire stretch of River Ganga.

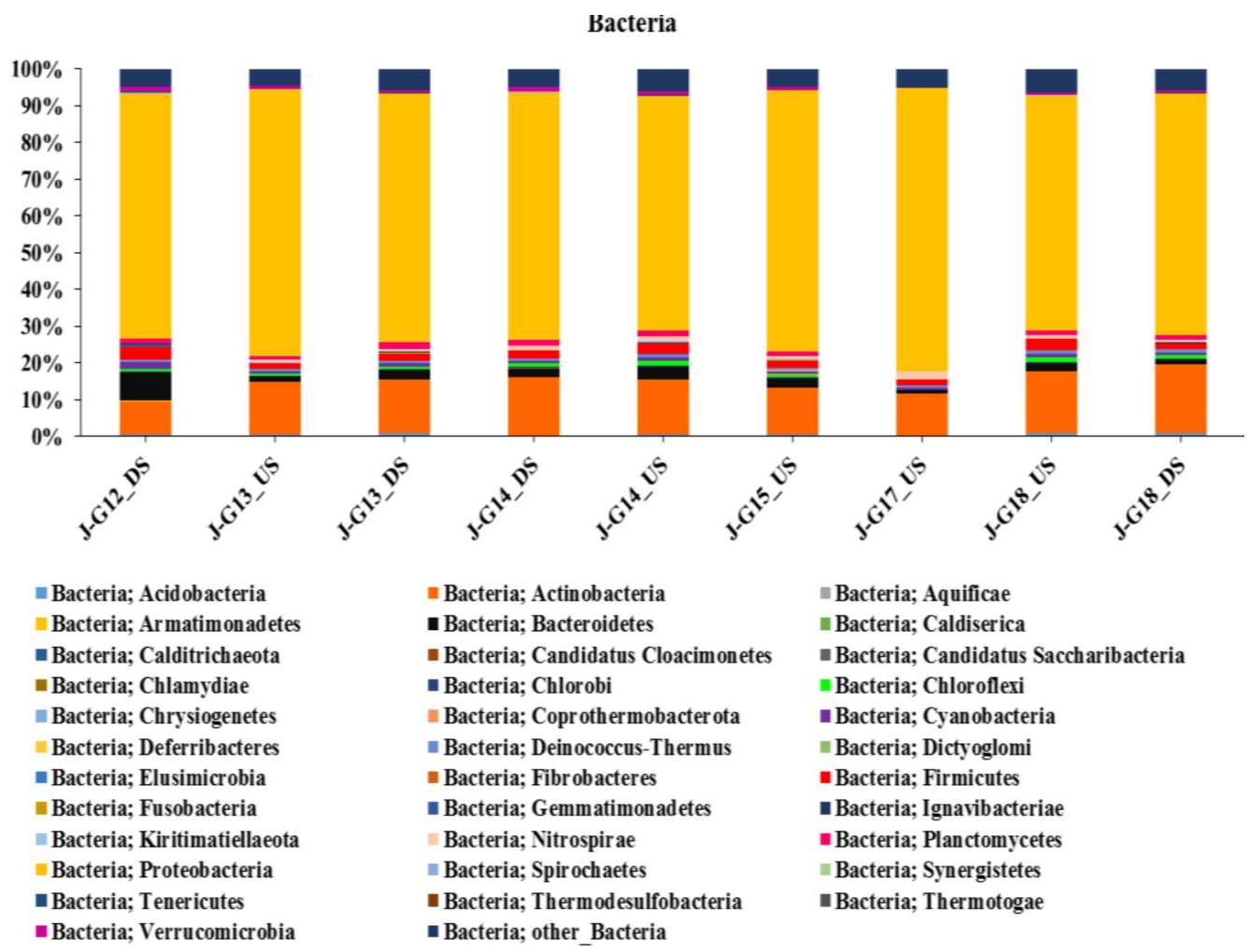

Fig32. Bacterial diversity of the lower stretch samples of River Ganga June 2018 sampling expedition.

From the archaeal phyla, unique phyla such as *Candidatus Korarcheota* and *Candidatus Micrarchaeota* were observed (Fig.33).

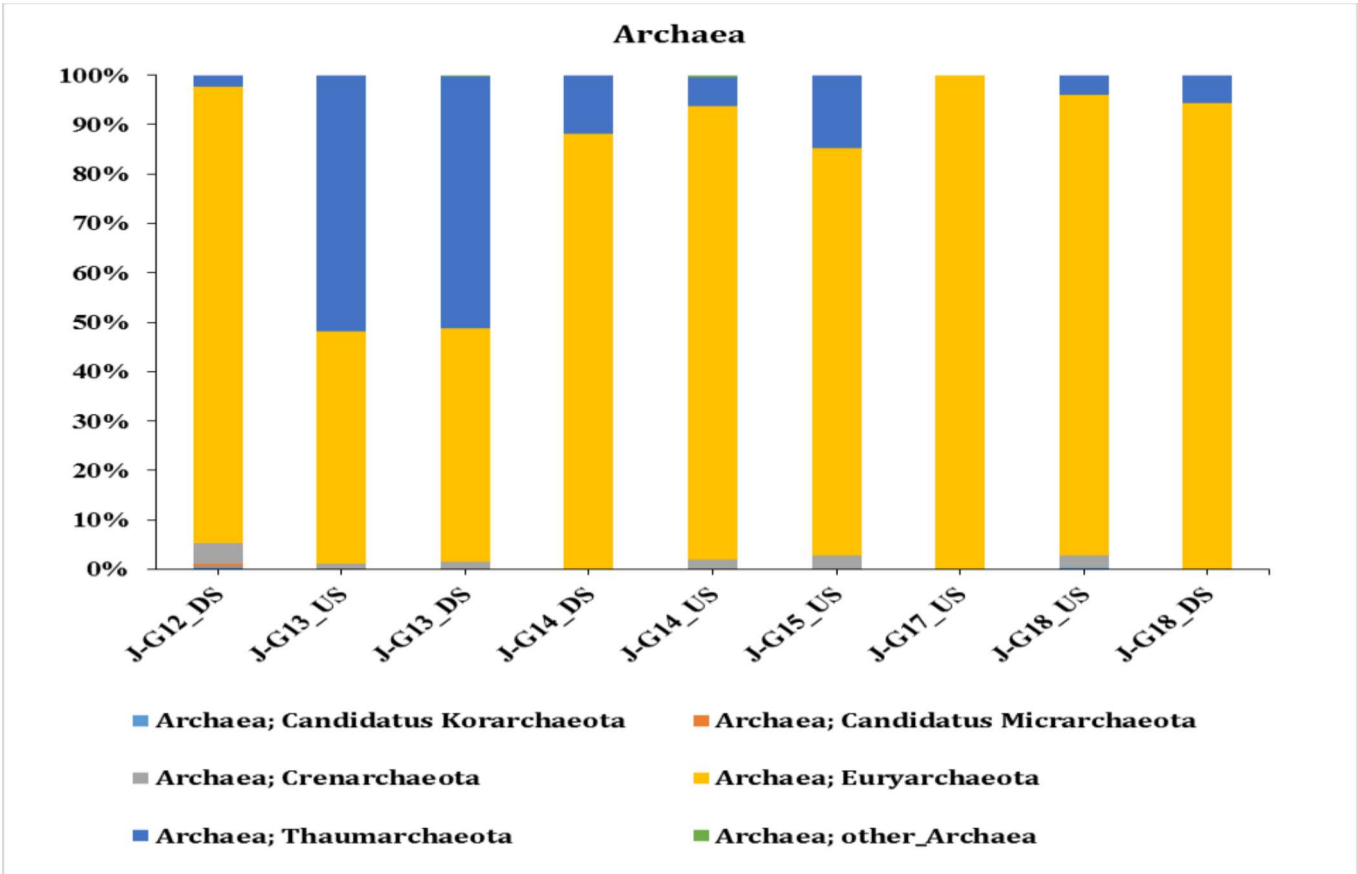

Fig.33: Archaeal diversity of the lower stretch samples of River Ganga June 2018 sampling expedition.

The overall structure of the bacterial community appears to be similar with *Proteobacteria* as the predominant phylum followed by *Actinobacteria* and *Bacteroidetes*. However, a meticulous observation shows that after *Protebacteria* group, the *Actinobacteria* and *Bacteroidetes* phyla dominate in the post monsoon season. River Ganga at Rishikesh shows a distinct set of microbial communities having the phyla *Firmicutes* and *Cyanobacteria* in a moderate abundance as opposed to the other downstream locations wherein these phyla are present in a lower abundance (Fig 34).

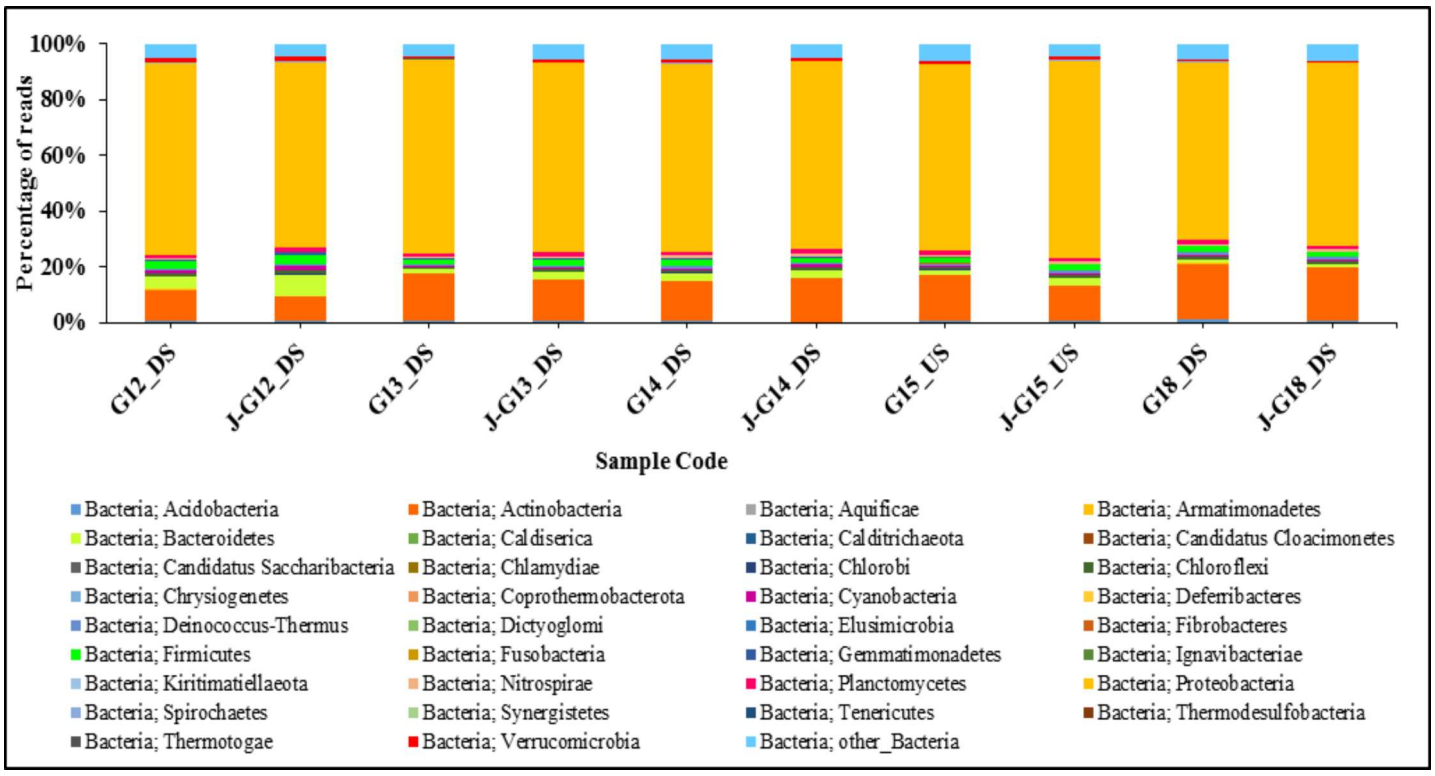

Fig.34 Comparison of bacterial diversity of the lower stretch samples of River Ganga

A substantial difference was observed in the archaeal diversity at the phylum level as an attribute of the seasonal variation. The members of phylum *Euryarchaeota* showed a significant escalation in the pre-monsoon samples as opposed to the members of phylum *Thaumarchaeota* which dominated the post-monsoon samples (Fig 35).

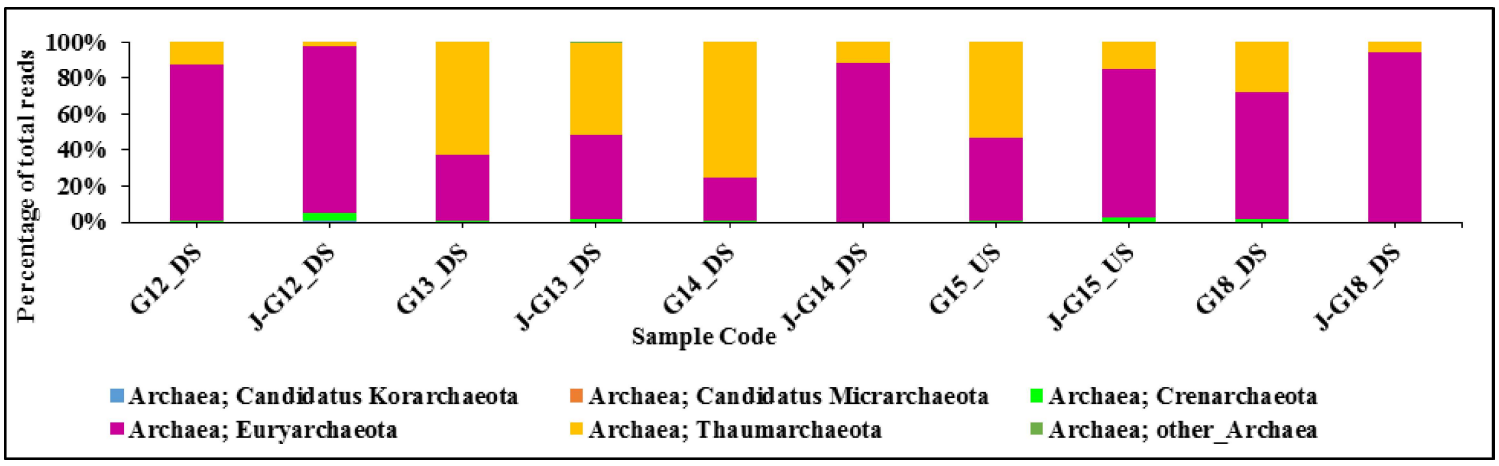

Fig.35 Comparison of archaeal diversity of the lower stretch samples of River Ganga

2.3 Functional analysis of metagenomic data across entire stretch of River Ganga

Results

Metagenomic mining for basic metabolic pathways

KEEG profiling and mining of the entire metagenomic data for functional annotation revelaed several metabolic pathways in the native microbes responsible for sustaining the bio-geochemcical cycling in the ecological niche of Ganga. (glycolysis; tricarboxylate cycle; starch and sucrose metabolism; carbon fixation; nitrogen metabolism; sulfur metabolism and methane metabolism) (Fig. 36-42).

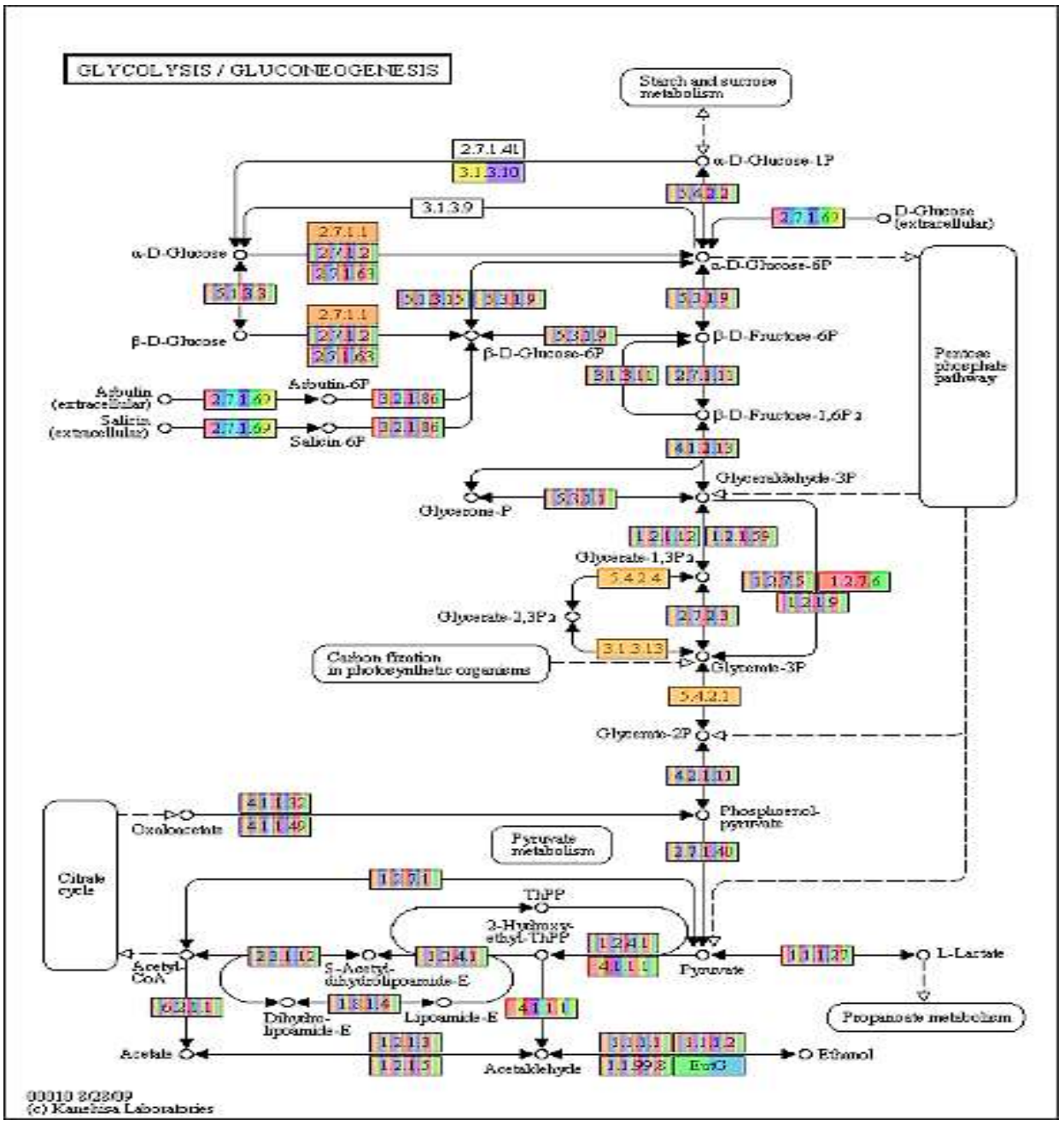

Fig.36: Presence of glycolytic and gluconeogenesis pathway in the microbes across the entire stretch of Ganga River.

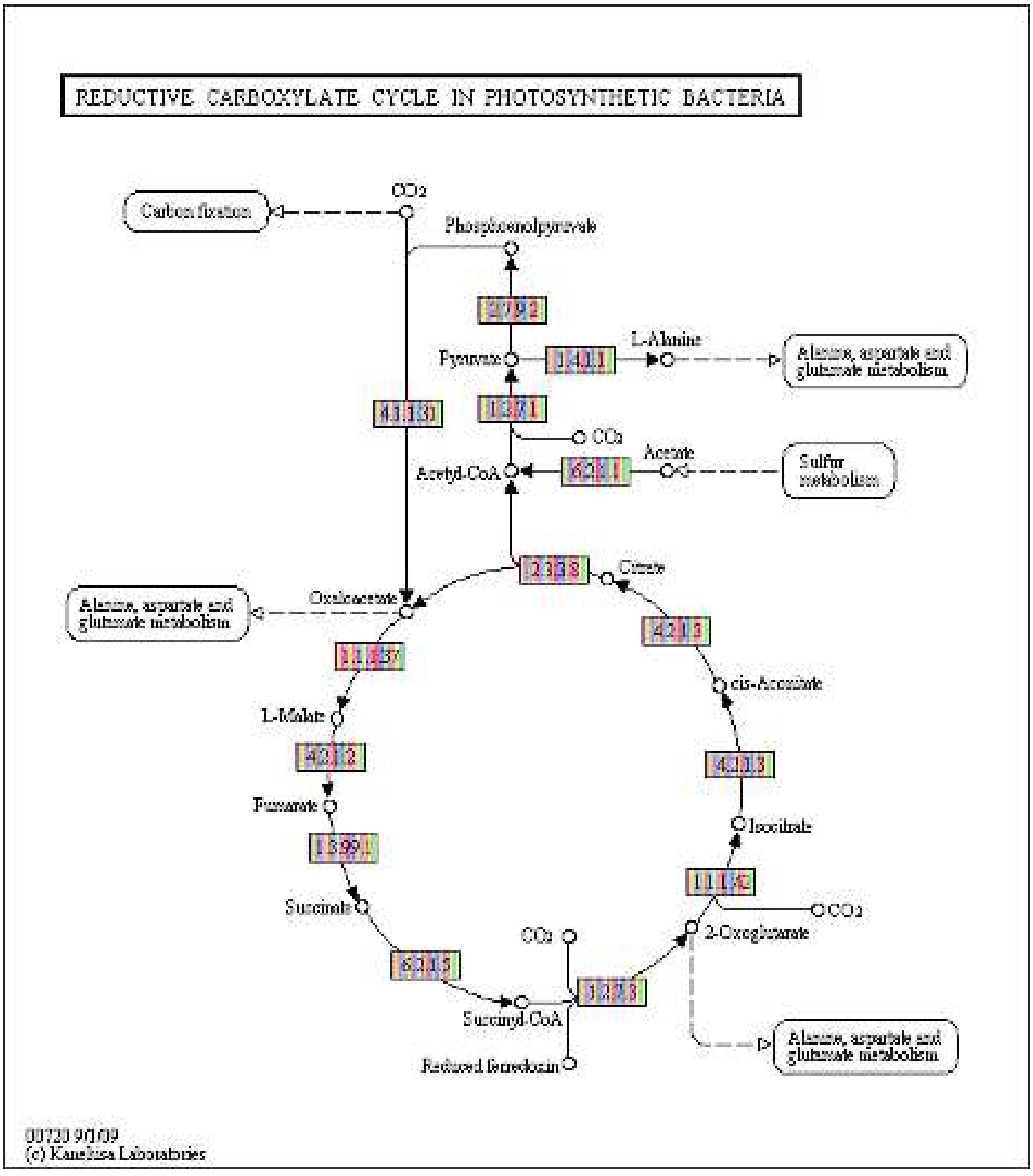

Fig.37: Presence of reductive carboxylate pathway in the photosynthetic microbes across the entire stretch.

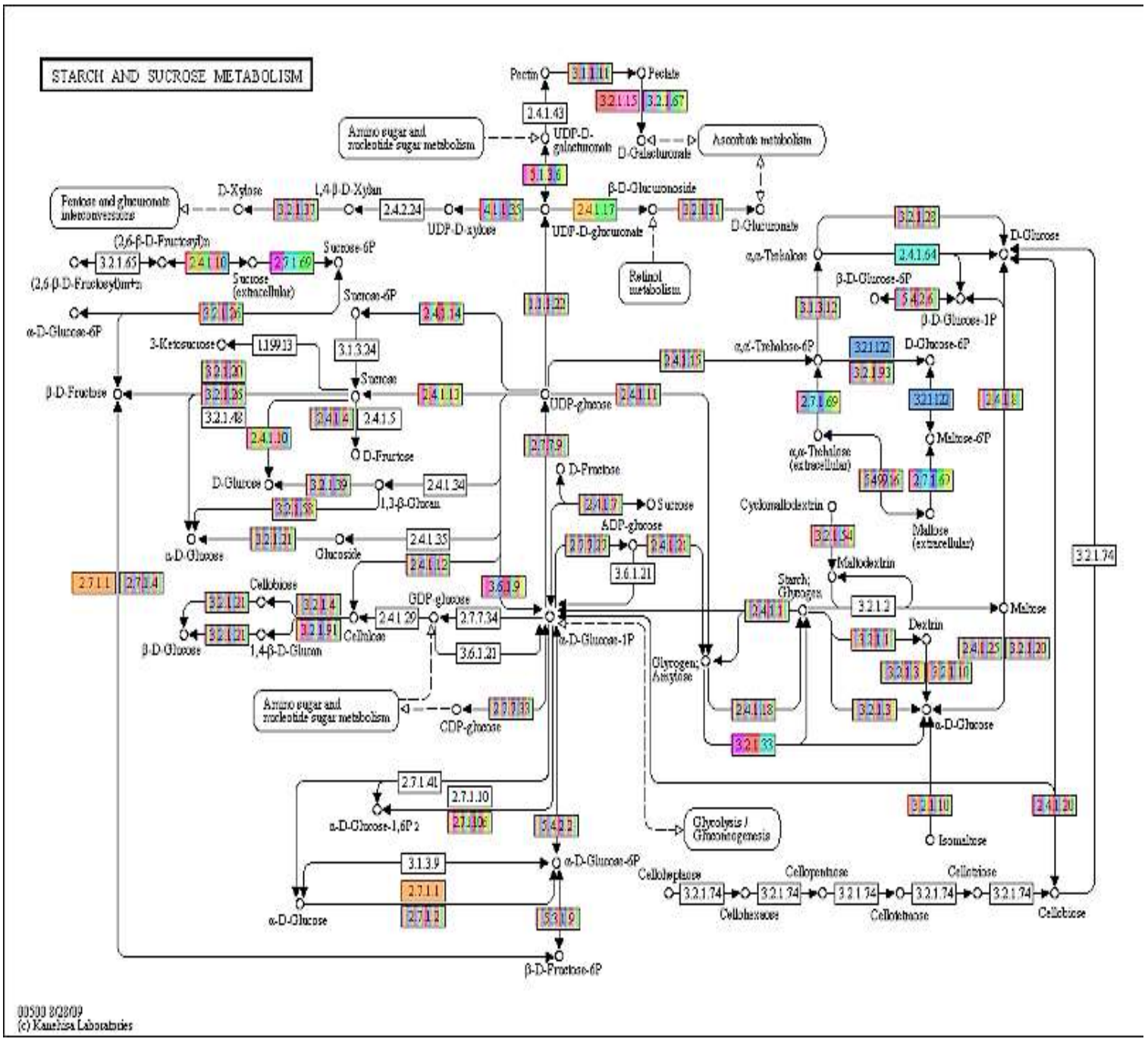

Fig.38: Presence of starch and sucrose metabolic pathway in the microbes across the entire stretch.

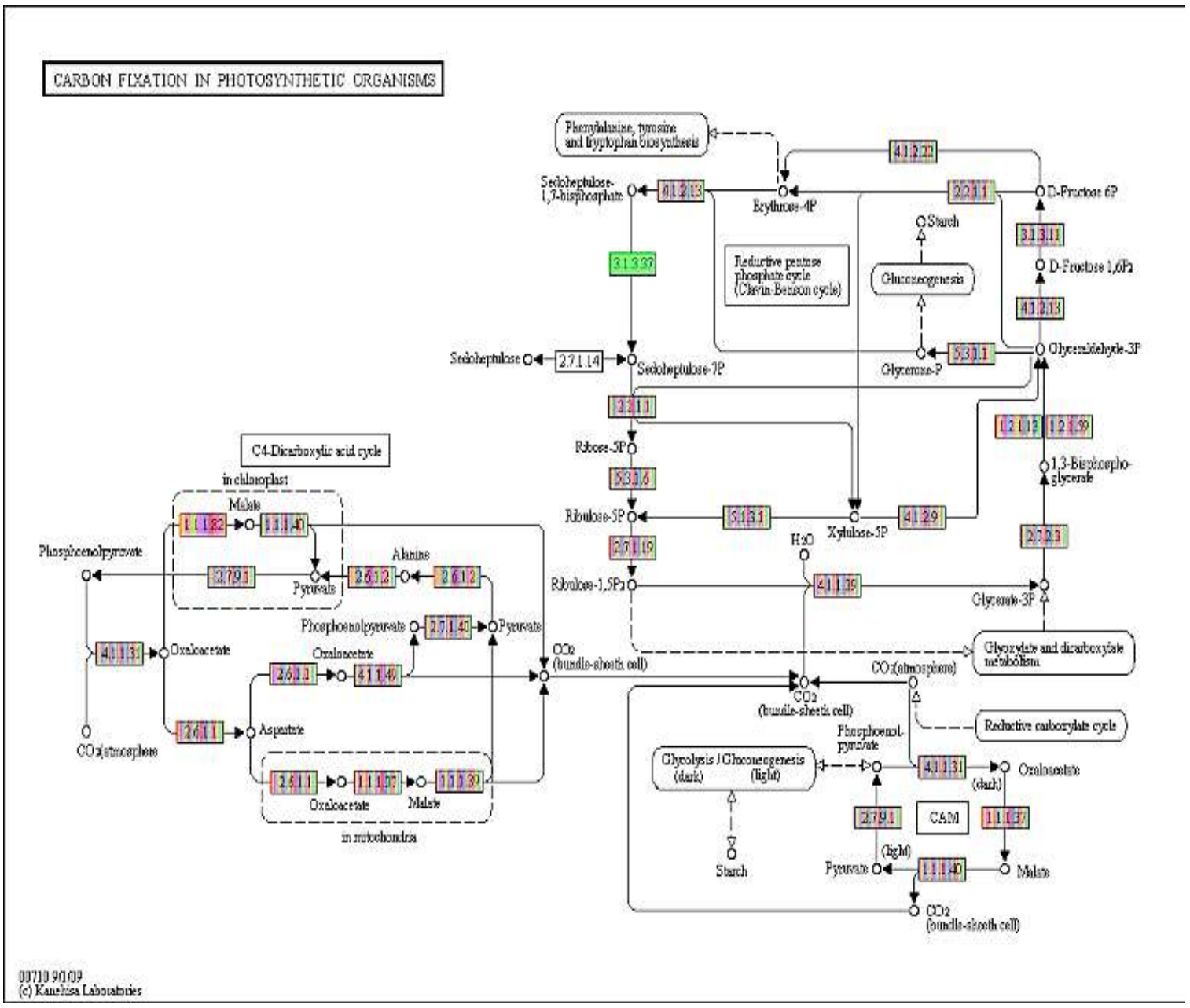

Fig.39: Presence of carbon fixation pathway in the photosynthetic microbes across the entire stretch.

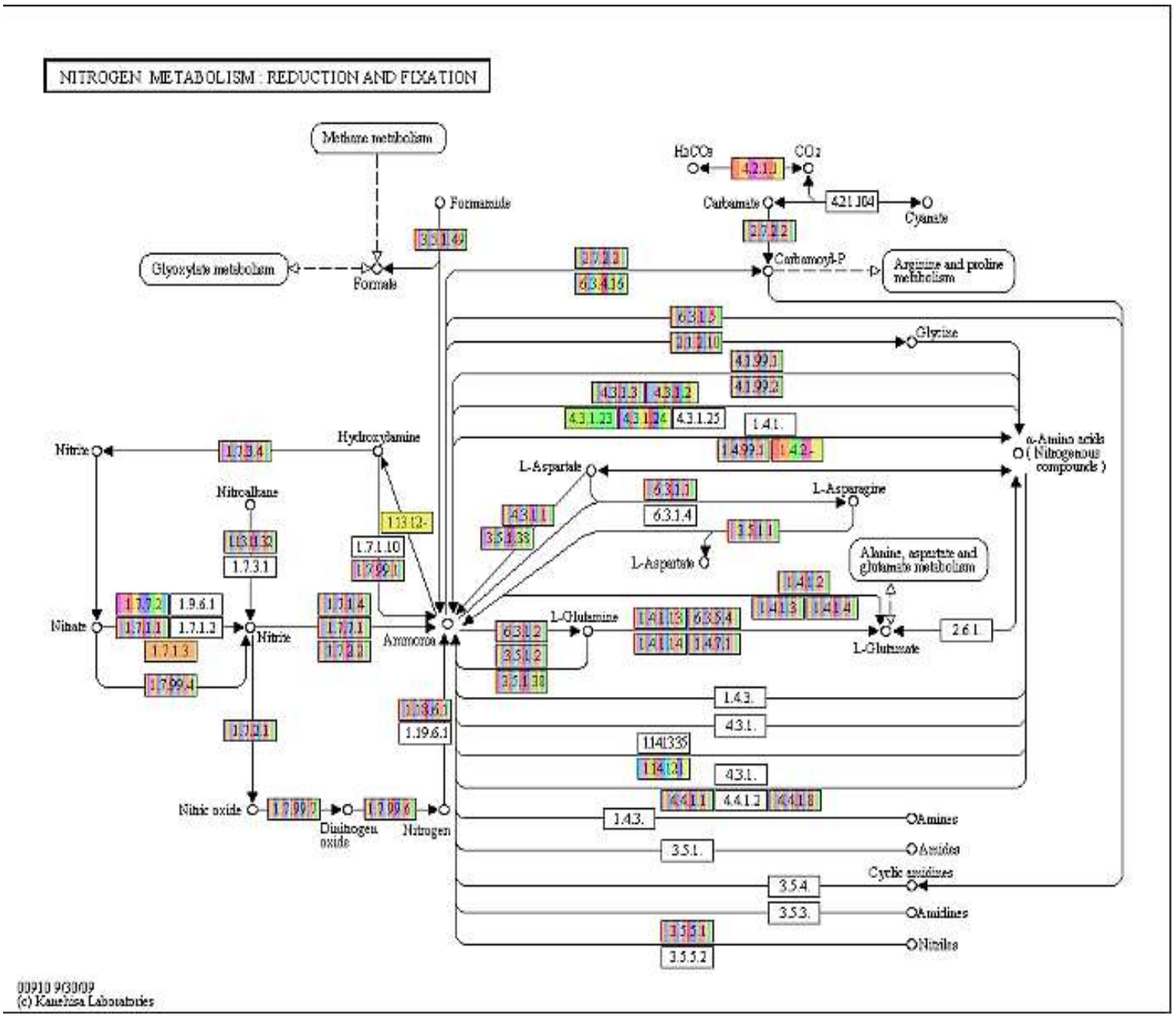

Fig.40: Presence of nitrogen metabolism, reduction and fixation pathway in the nitrifying, denitrifying microbes across the entire stretch.

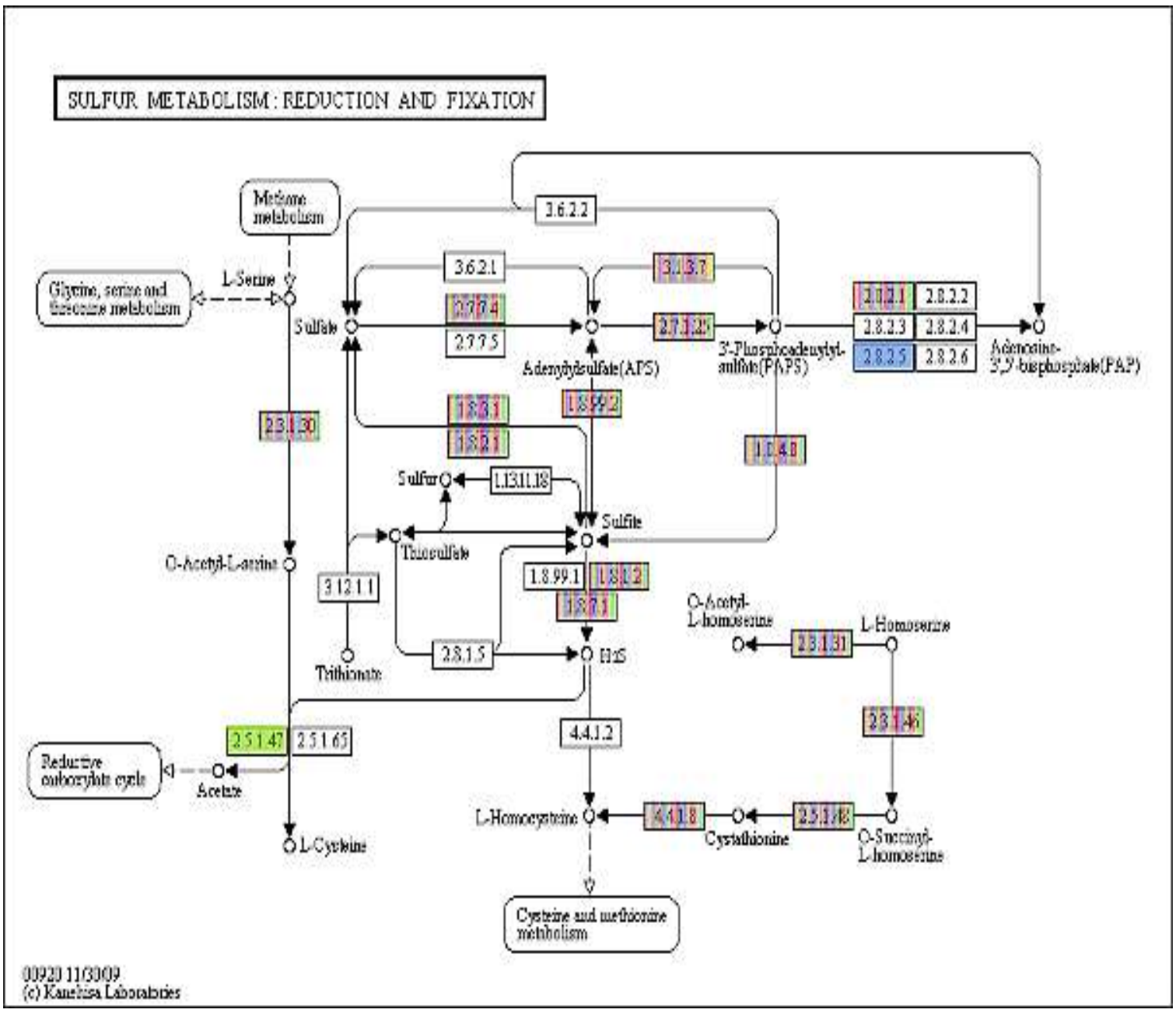

Fig.41: Presence of sulfur metabolism, reduction and fixation pathway in the sulfur reducing bacteria and archaea (SRB/A) and sulfur oxidizing microbes (SOB/A) across the entire stretch.

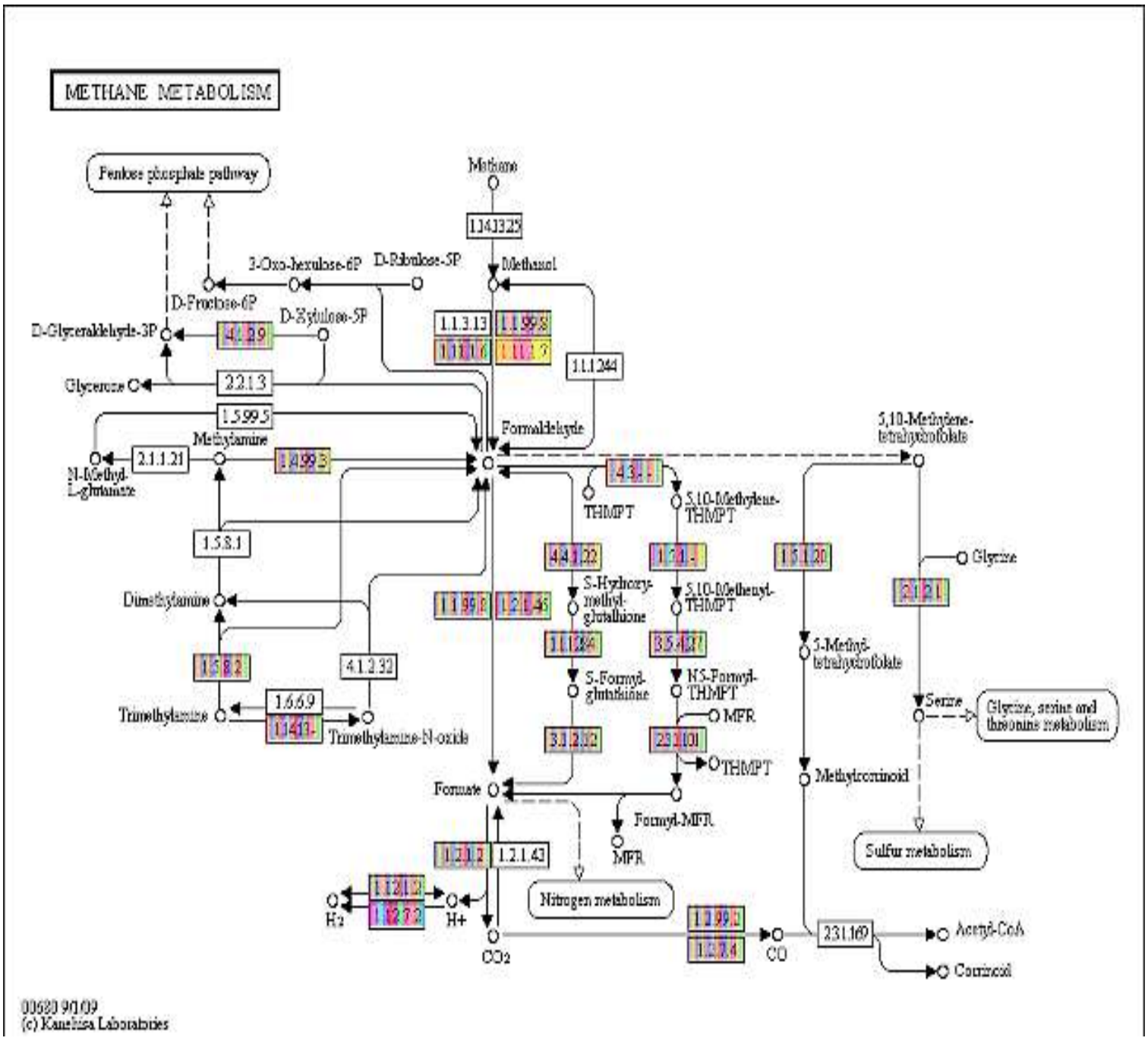

Fig.42: Presence of methane metabolism pathway in the methanotrophs and methanogens across the entire stretch.

Metagenomic mining for presence of xenobiotic metabolic pathways

Further the metagenomic data was annotated for metabolic pathways pertaining to metabolism of xenobiotic compounds. Analysis revealed presence of potential microbes across the entire stretch with pathways for degradation of polyaromatic hydrocarbons (naphthalene); cyclochlorohexane (CHC); benzoate; biphenyl; ethylbenzene; styrene; xylene; toluene and phenol. Correlating the taxonomic diversity, bacteria such as *Pseudomonas, Serratia, Acinetobacter, Arthrobacter, Sphingomonas, Sphingobacterium, Stenotrophomonas,*

Xanthomonas, Mycobacterium, Burkholderia, Rhodococcus, etc. that are capable of degrading these pollutants were first identified at the confluence sample of *Triveni sangam* (Samson et.al, 2019) and then were found to be present across the entire stretch. Additionally, there are certain fungi such as *Aspergillus, Penicillium, Kluveromyces, Lodderomyces, and Nakaseomyces* are also known to possess these xenobiotic degradation pathways. All these fungi were first identified in the confluence samples (Samson et.al, 2020) and their hits are also present in the metagenomic data set of the entire stretch. (Fig43-Fig.52).

Cyclochlorohexane are alicyclic hydrocarbons that are moderately toxic and are usually present in municipal waste water after terminal chlorination. They are not directly hazardous to humans but severely affect the aquatic life (US-EPA). Presence of microbes with degradation potential of CHC maybe due constant exposure of microbes to such waters or due to horizontal gene transfer (HGT) between the microbes.

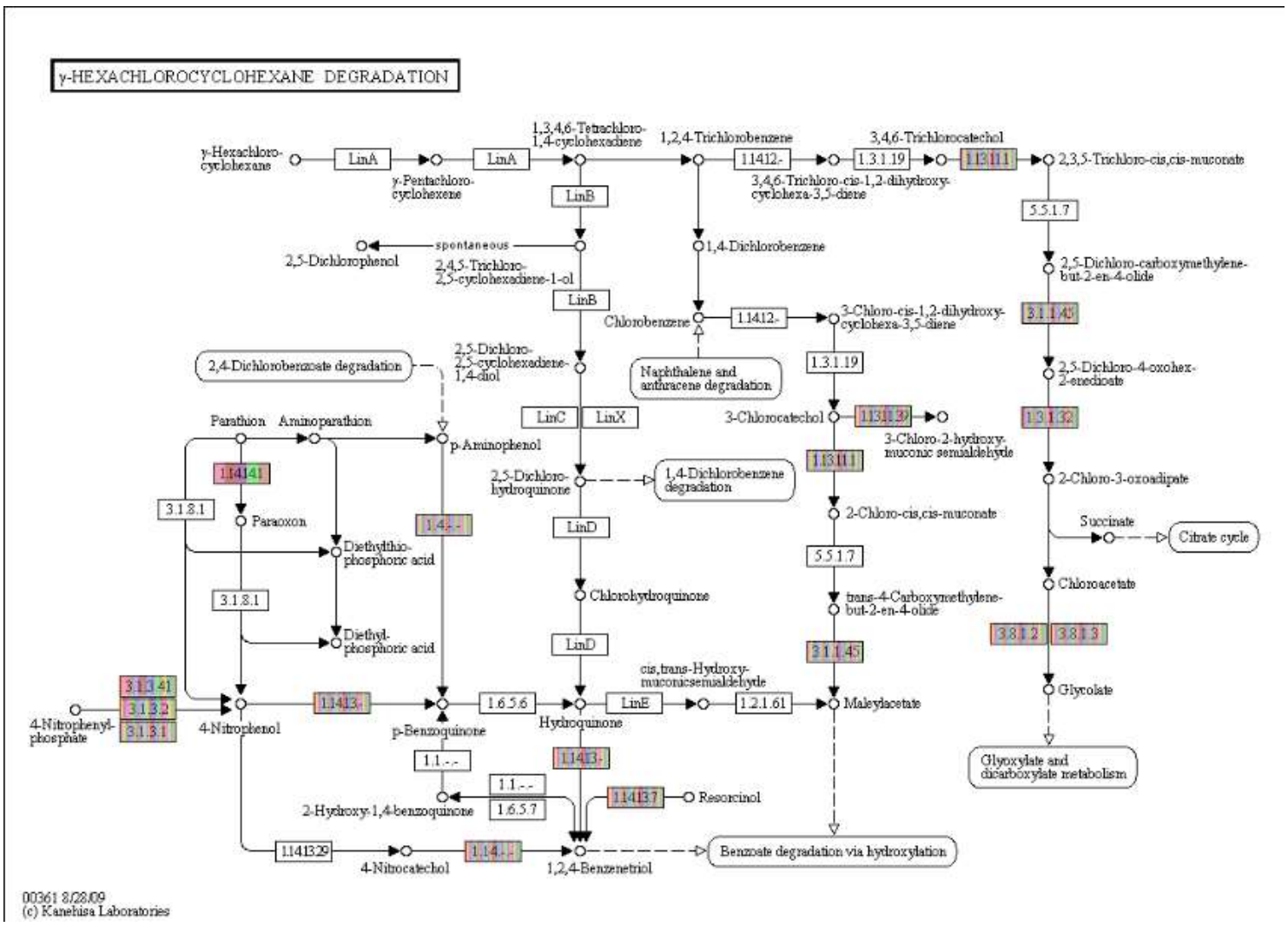

Fig.43: Presence of CHC degradation pathway in the microbes across the entire stretch.

Ethylbenzene is mainly used in the manufacture of styrene. Acute (short-term) exposure to ethylbenzene in humans results in respiratory effects, such as throat irritation and chest constriction, irritation of the eyes, and neurological effects such as dizziness. Chronic (long-term) exposure to ethylbenzene in humans has shown conflicting results regarding its effects on the blood (US-EPA). Biodegradation of ethylbenzene mainly proceeds via anaerobic pathway and the plasmid containing catabolic genes toward this compound are acquired by microbes through HGT.

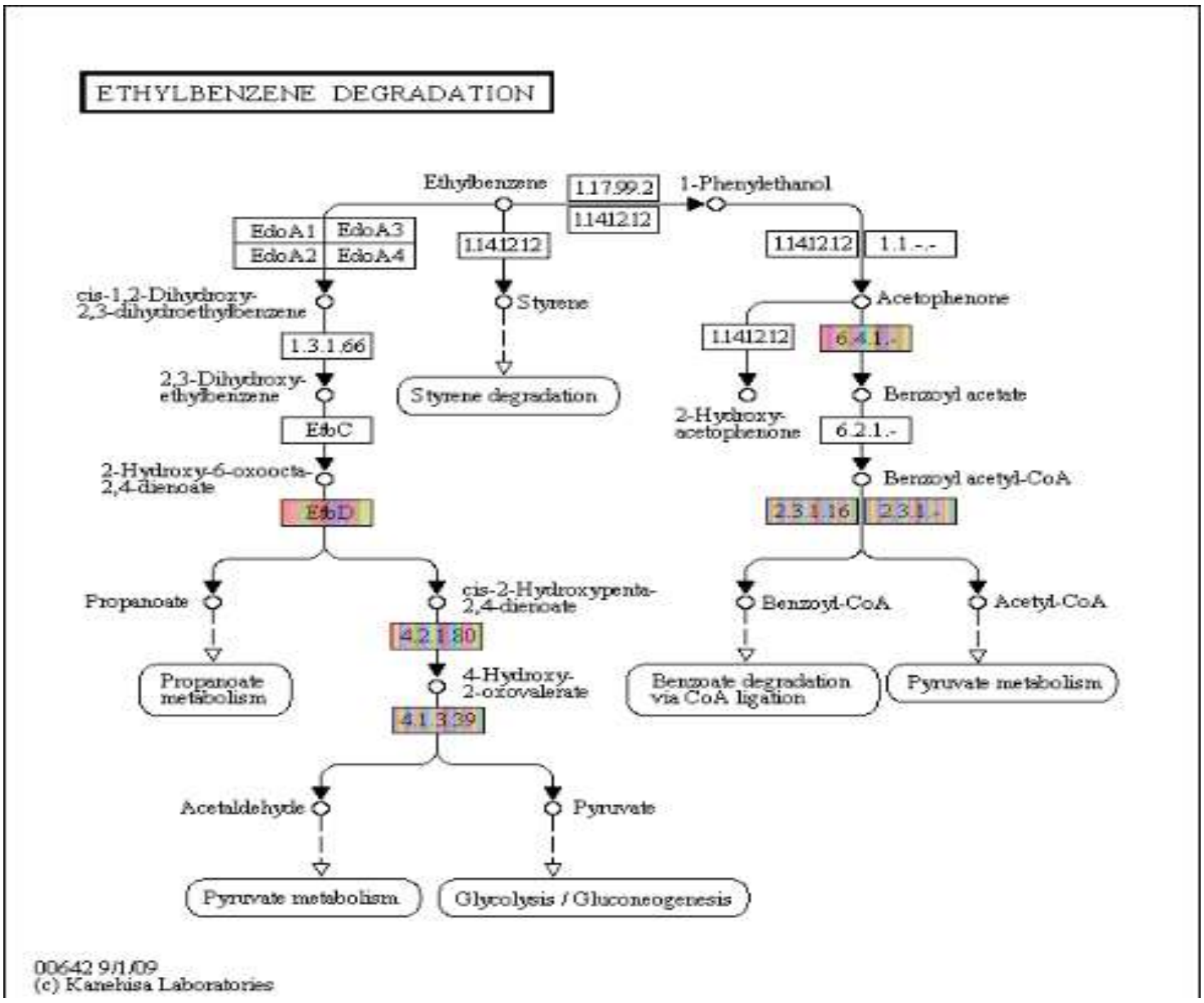

Fig.44: Presence of Ethylbenzene degradation pathway in the microbes across the entire stretch.

Styrene is one of the most important monomers worldwide, and its polymers and copolymers are used in an increasingly wide range of applications. The major uses are in plastics, latex paints and coatings, synthetic rubbers, polyesters and styrene-alkyd coatings. Styrene occurs naturally as a degradation product in cinnamic acid containing plants and as a by-product of fungal and microbial metabolism. Styrene evaporates readily from water to air. However, its presence is usually traceable to an industrial source or to improper disposal. The monomer styrene can be degraded by various microorganisms under aerobic and anaerobic conditions. Therefore, several peripheral pathways are employed yielding few central intermediates as 3-vinylcatechol, phenylacetic acid, benzoic acid, or 2-ethylhexanol (https://www.euro.who.int/__data/assets/pdf_file/0018/123066/AQG2ndEd_5_12Styrene.pdf)

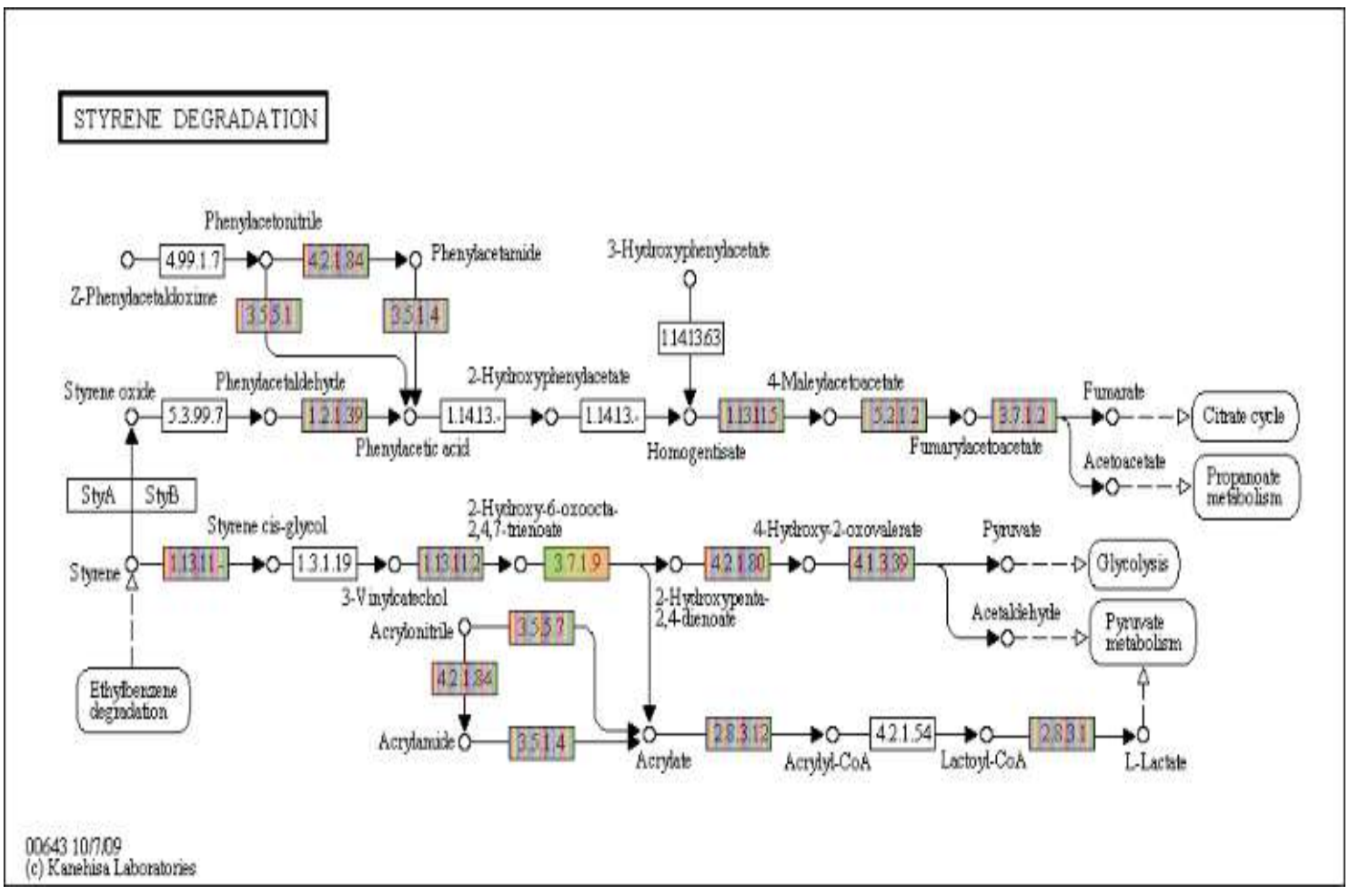

Fig.45: Presence of styrene degradation pathway in the microbes across the entire stretch.

Acute (short- term) exposure of humans to naphthalene/ methyl-naphthalene by inhalation, ingestion, and dermal contact is associated with hemolytic anemia, damage to the liver, and neurological damage. EPA has classified naphthalene and/or methyl-naphthalene as a Group C, possible human carcinogen. Degradation of naphthalene is of great concern and therefore exploring microbes with this potential in Ganga river would be interesting.

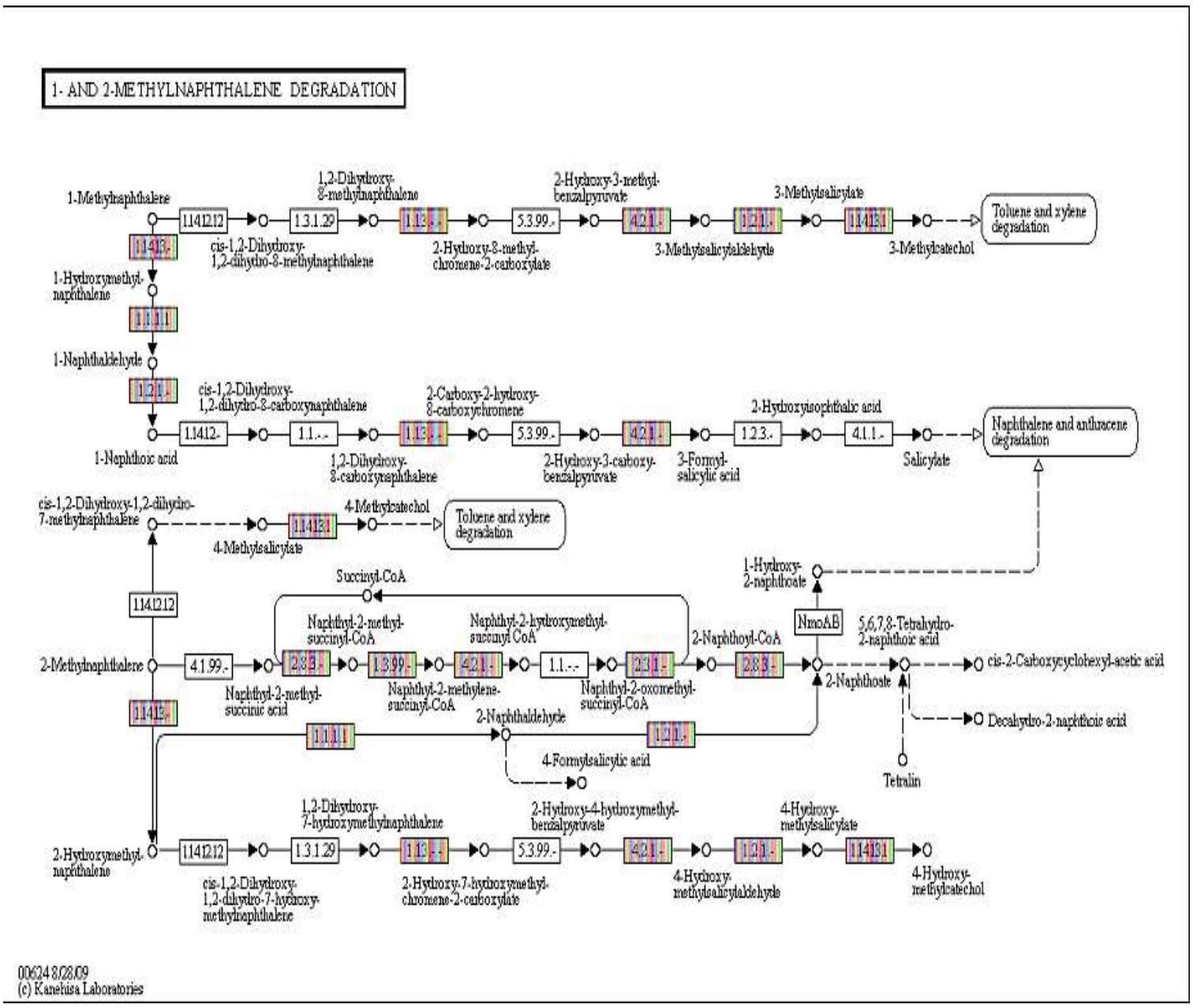

Fig.46: Presence of methyl-naphthalene pathway in the microbes across the entire stretch.

Tetrachloroethene is widely used for dry-cleaning fabrics and metal degreasing operations. Effects resulting from acute (short term) high-level inhalation exposure of humans to tetrachloroethene include irritation of the upper respiratory tract and eyes, kidney dysfunction, and neurological effects such as reversible mood and behavioral changes, impairment of coordination,

dizziness, headache, sleepiness, and unconsciousness. The primary effects from chronic (long term) inhalation exposure are neurological, including impaired cognitive and motor neurobehavioral performance. Tetrachloroethene exposure may also cause adverse effects in the kidney, liver, immune system and hematologic system, and on development and reproduction. Studies of people exposed in the workplace have found associations with several types of cancer including bladder cancer, non-Hodgkin lymphoma, multiple myeloma. EPA has classified tetrachloroethene as likely to be carcinogenic to humans (US-EPA). Microbial degradation of chloroethenes can take place either through anaerobic organohalide respiration, where chloroethenes serve as electron acceptors; anaerobic and aerobic metabolic degradation, where chloroethenes are used as electron donors; or anaerobic and aerobic co-metabolic degradation, with chloroethene degradation occurring as a by-product during microbial metabolism of other growth substrates, without energy or carbon benefit (Sevcu et al, 2017).

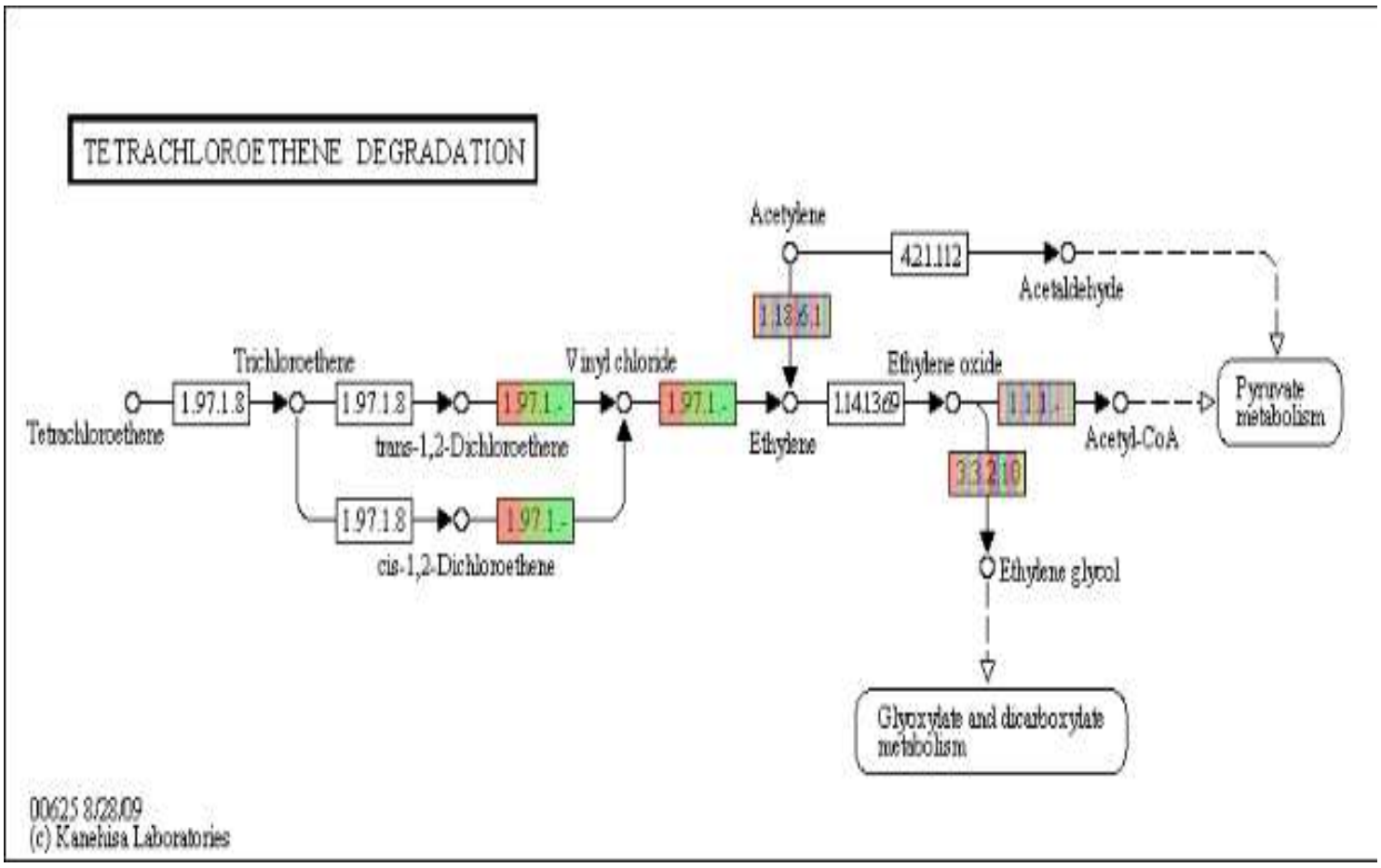

Fig.47: Presence of tetrachloroethene degradation pathway in the microbes across the entire stretch.

Benzene, toluene and xylene isomers (BTX) are the major components of gasoline. Because of their low water solubility and their acute toxicity and genotoxicity, BTX components are classified as priority pollutants by the U.S. Environmental Protection Agency. Due to the sequences of accidental gasoline spills and leakage from service station tanks, they are prime sources of aquifer contamination. It is known that microbes degrading toluene and xylene can also degrade benzene (Oteneo et.al, 2014). Therefore, it is important to explore these microbes for co-metabolic and efficient degradation of these monoaromatic hydrocarbons.

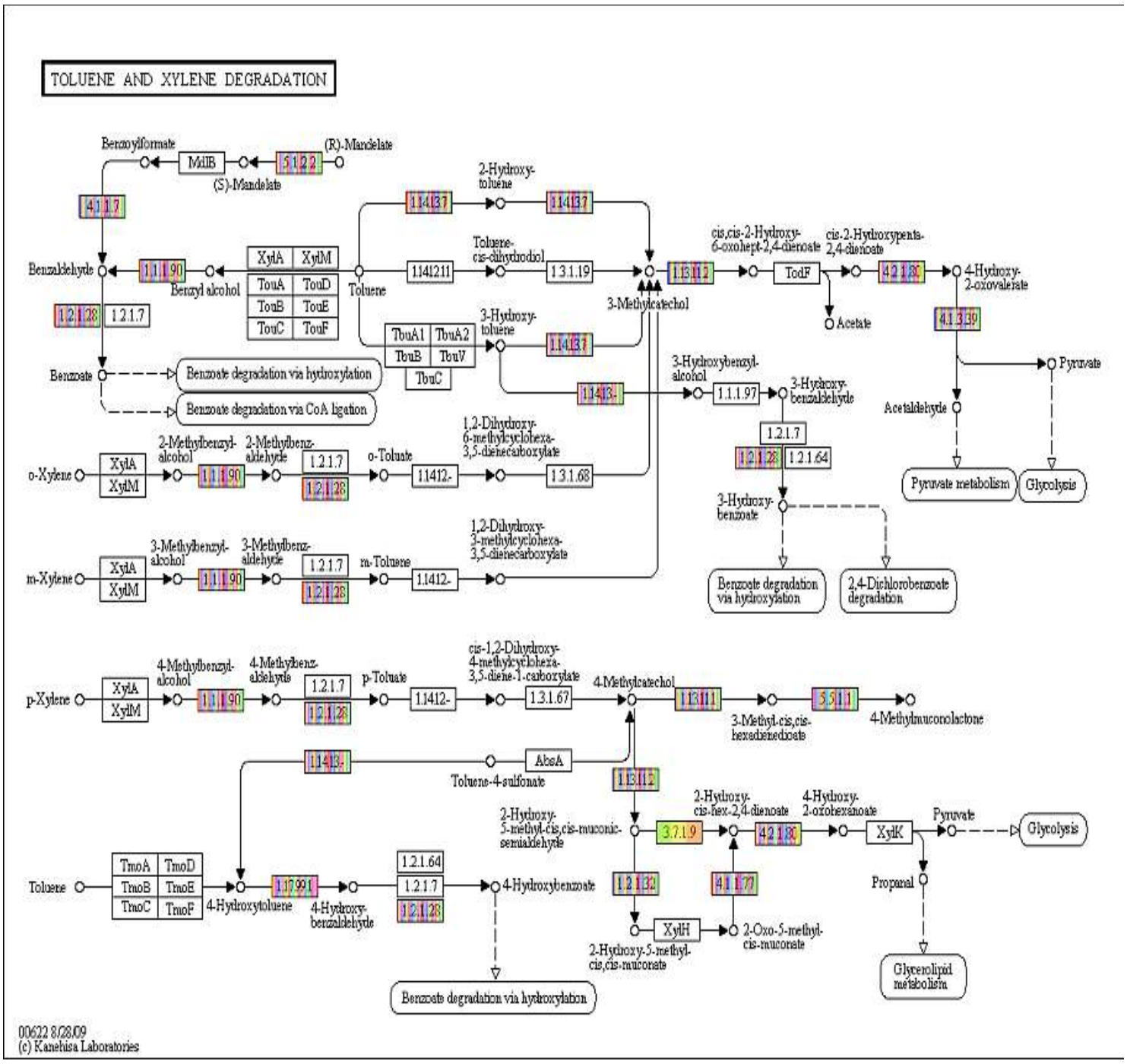

Fig.48: Presence of Toluene and Xylene degradation pathways in the microbes across the entire stretch.

Benzoate and its derivatives such as fluorobenzoate and dichlororbenzoate are used as pesticide and have a high toxicity profile as per US-EPA. Microbes, especially, the de-nitrifying bacteria have been known for co-metabolism of these compounds to their less toxic forms.

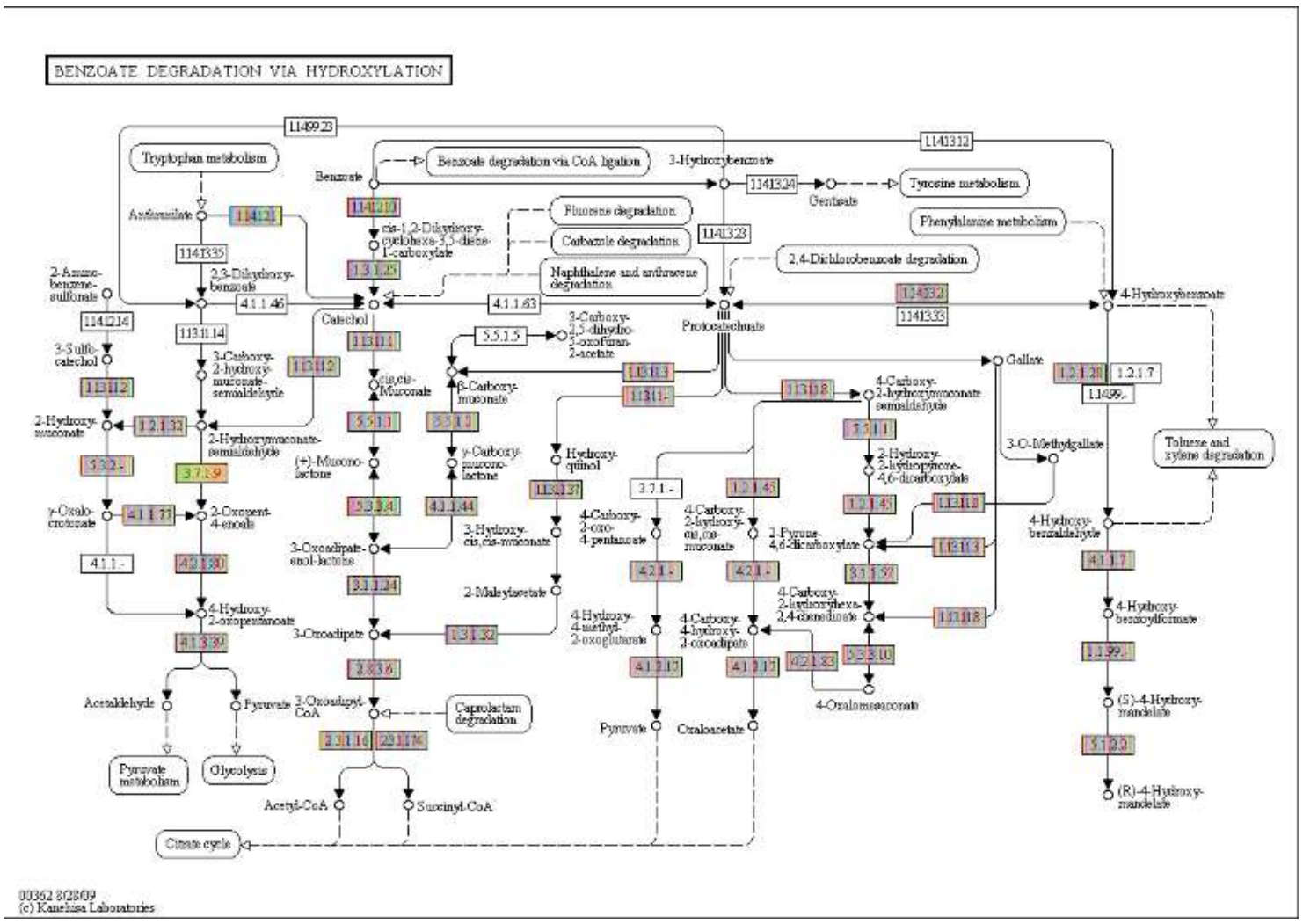

Fig.49: Presence of benzoate degradation pathway in the microbes across the entire stretch.

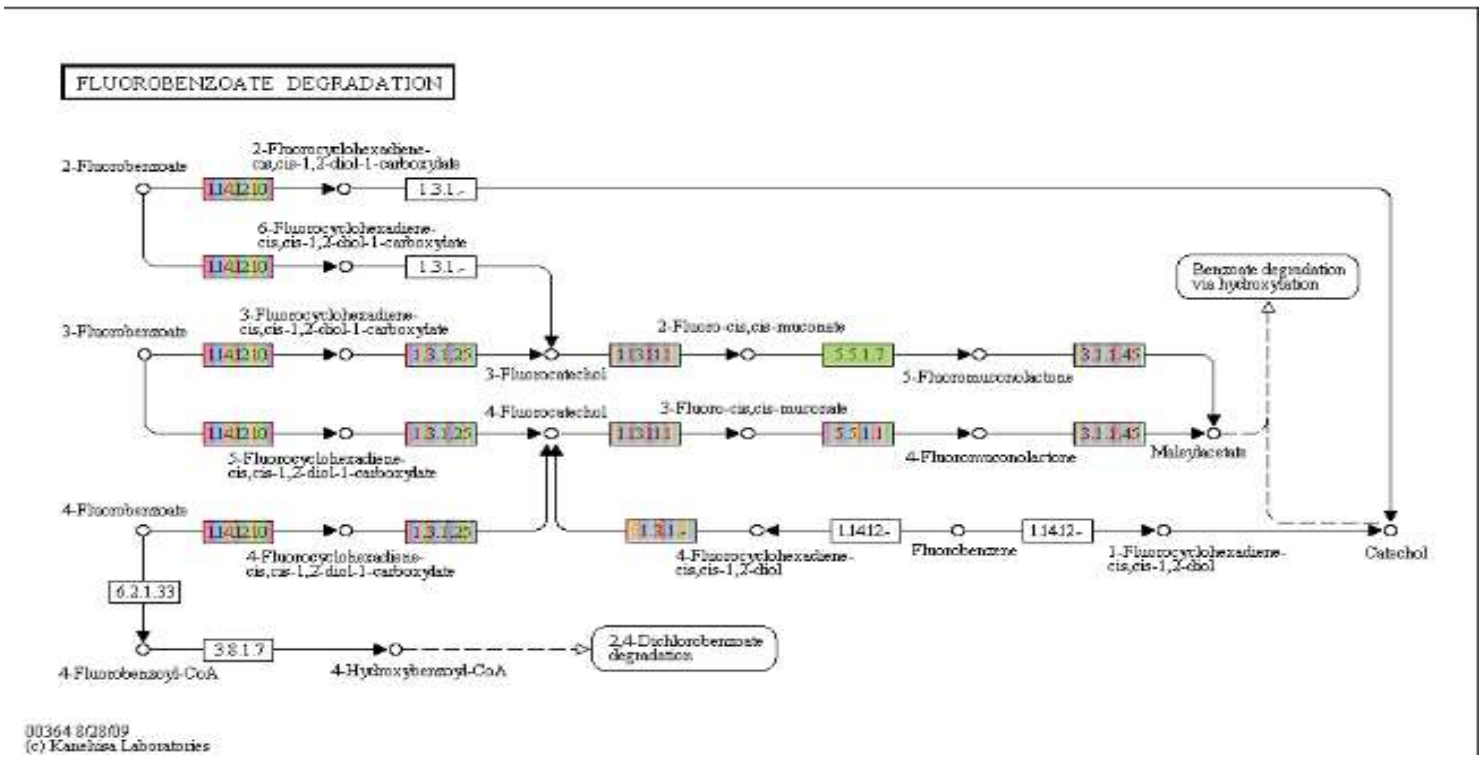

Fig.50: Presence of fluoro-benzoate degradation pathway in the microbes across the entire stretch

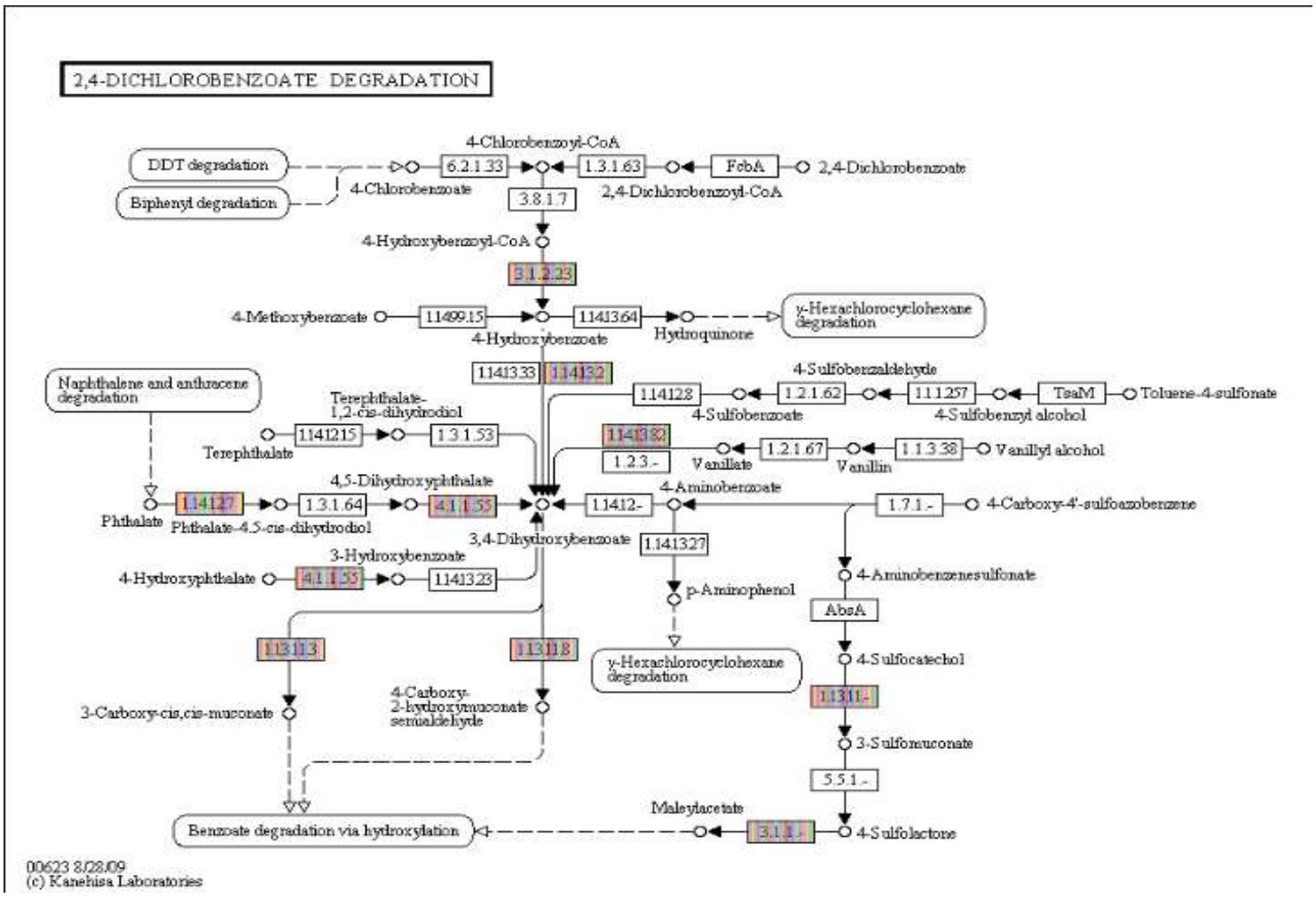

Fig.51: Presence of Dichloro-benzoate degradation pathway in the microbes across the entire stretch

Bisphenol-A (BPA) is a high production volume (HPV) chemical widely used in manufacturing polycarbonate plastics and epoxy resins used in nearly every industry. Moreover, BPA has been identified as an environmental endocrine disruptor for its estrogenic and genotoxic activity. Thus, BPA contamination in the environment is an increasingly worldwide concern, and methods to efficiently remove BPA from the environment are urgently recommended. Presence of metabolic pathways in microbes for BPA degradation in Ganga river could be advantageous to isolate and exploit their potentials in the bioremediation.

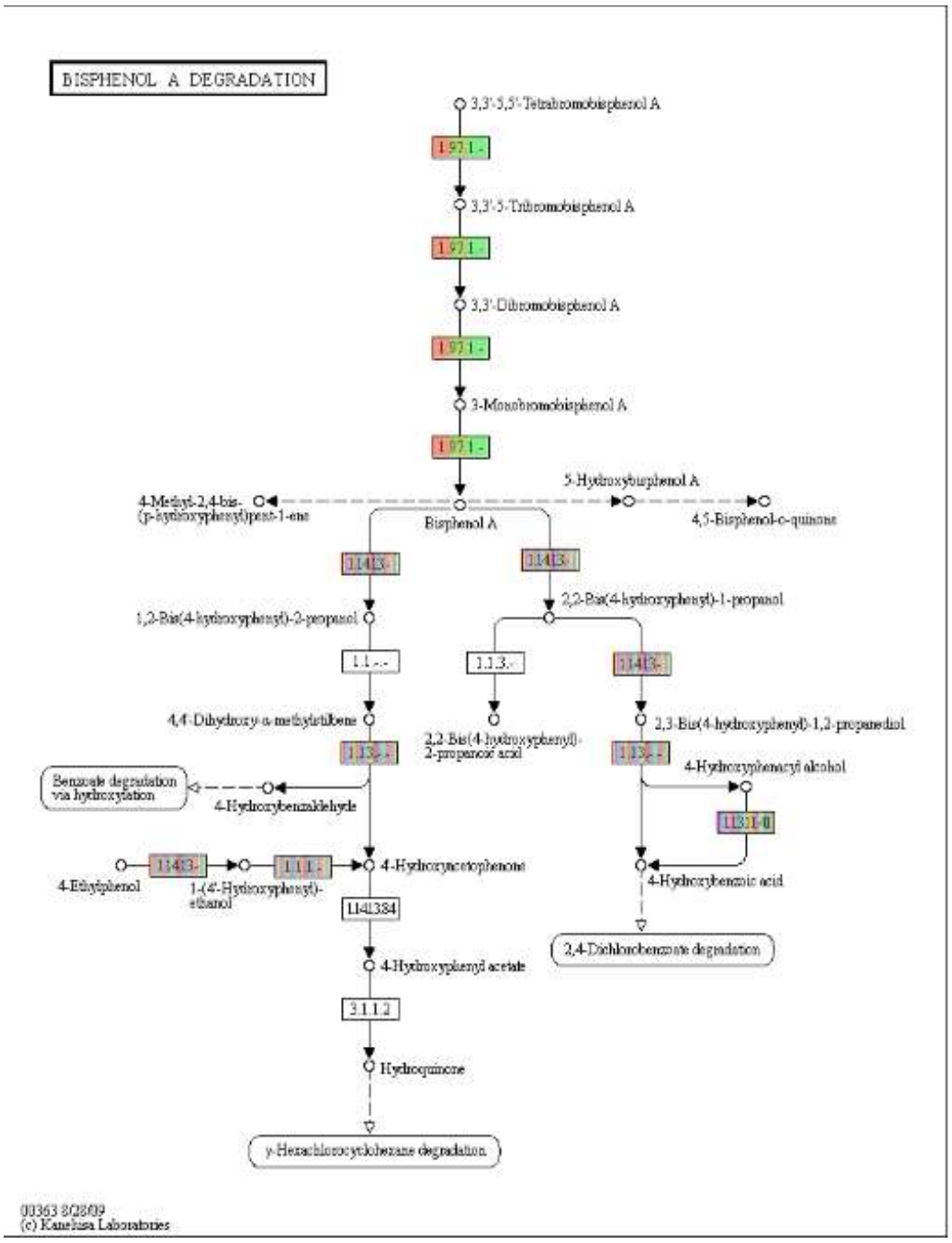

Fig.52: Presence of BPA degradation pathway in the microbes across the entire stretch.

Polychlorinated biphenyls (PCBs) are toxic, persistent pollutants of worldwide concern whose cleanup using conventional methods like incineration or relocation to specialized landfills is often prohibitively expensive. An alternative strategy for in situ PCB removal is biodegradation by microorganisms capable of metabolizing PCBs (Fletcher et. al, 2006). Microbes in Ganga river could be explored for this potential.

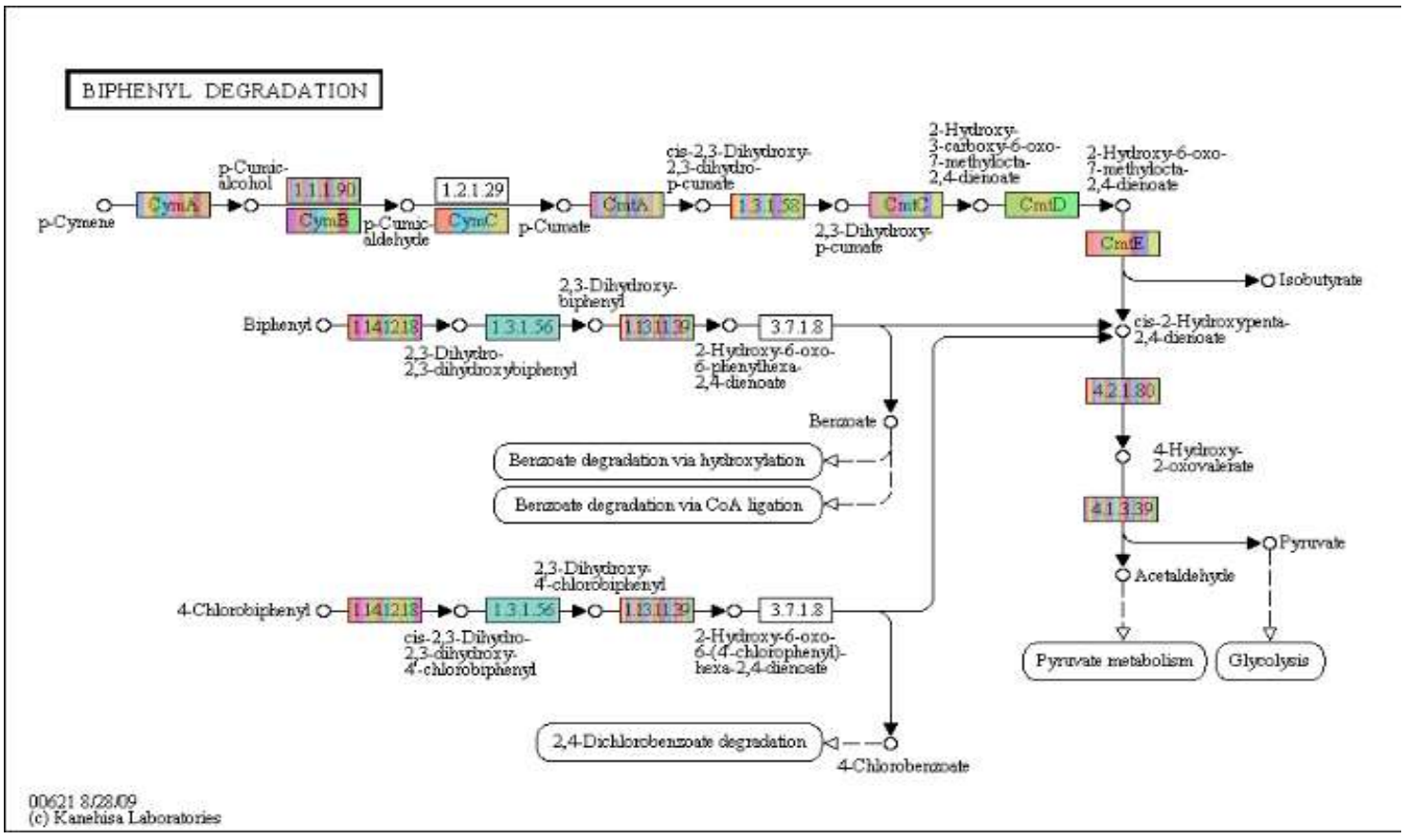

Fig.53: Presence of biphenyl degradation pathway in the microbes across the entire stretch.

Metagenomic mining for tracing virulence and infections

Identifying virulence genes experimentally is one of the cornerstones of bacterial pathogenesis research. Experimental approaches typically include cloning of genes potentially involved in pathogenesis into a laboratory strain, transposon mutagenesis to generate a collection of mutants, or detection of genes essential for survival in the host by *in vivo* expression technology. The advent of metagenomics and its application to the study microbiome and the genes conferring pathogenicity and enhancing virulence has given us a unique opportunity to map the pathobiome and virulome of the ecological niche under study (Mira et. al, 2011; Yadav et al, 2020).

Metagenomic mining of the dataset for virulome revealed presence of six different types of bacterial secretion systems (Fig.54). Many pathogens use dedicated protein secretion systems

to secrete virulence factors from the cytosol of the bacteria into host cells or the host environment. In general, bacterial protein secretion apparatuses can be divided into different classes, based on their structures, functions, and specificity (Mecsas et al., 2015).

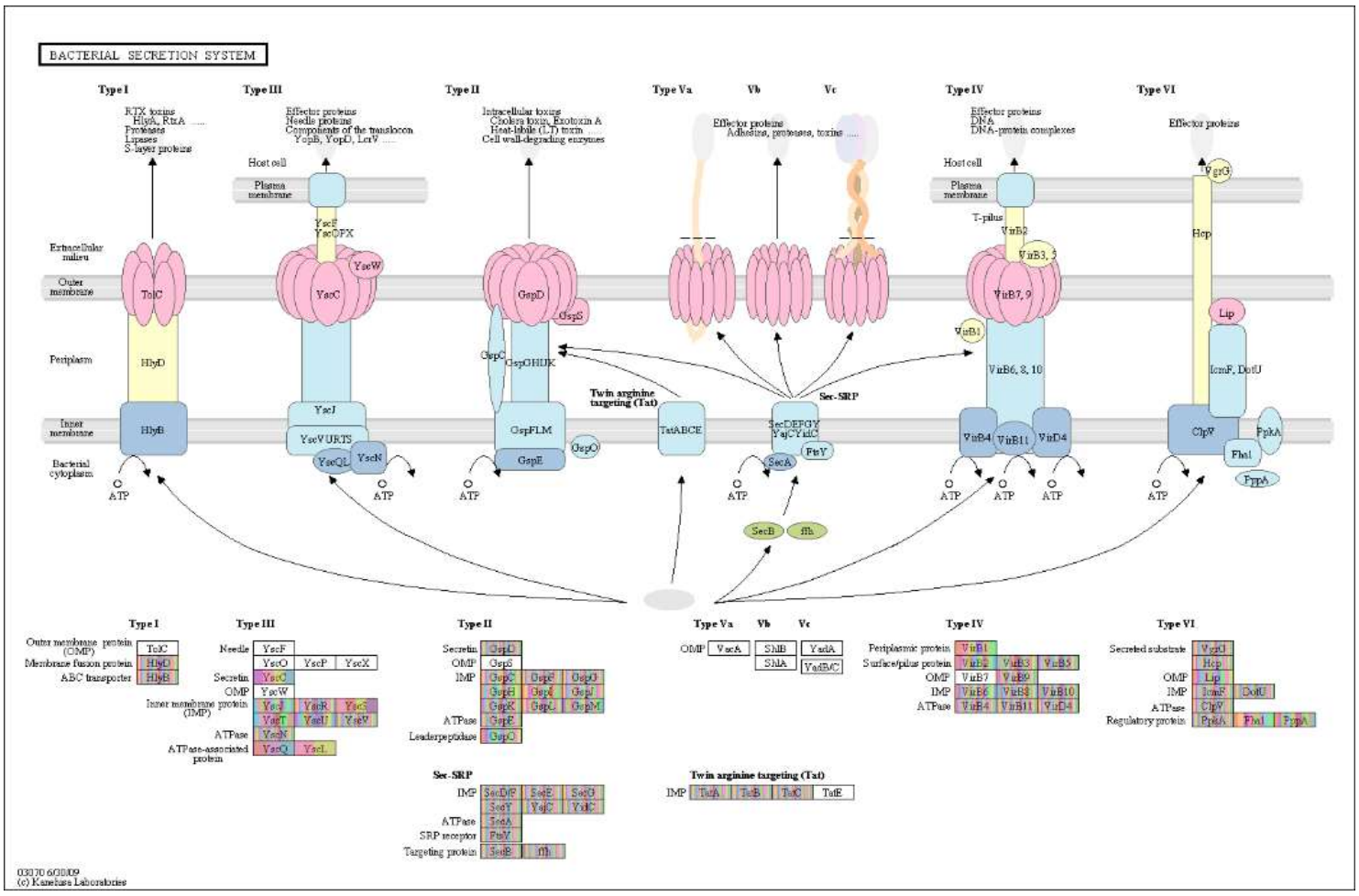

Fig.54: Representative KEGG pathway for bacterial secretion system across the entire stretch.

Further classification of data for gaining insights into infectious cycle of the pathogens revealed presence of infectious pathways of *E. coli, H. pylori and V. cholerae* (**Fig.55-57**).

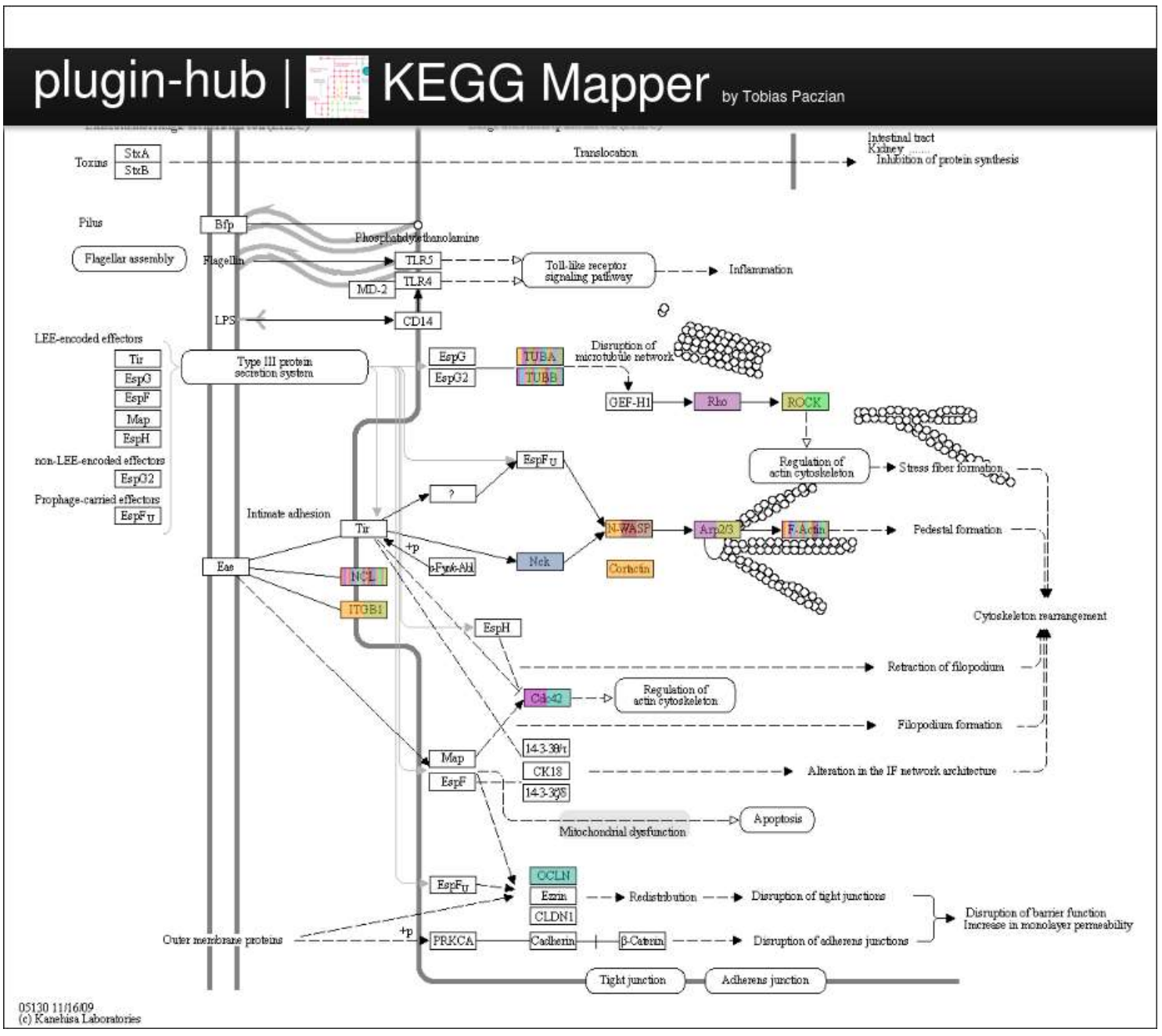

Fig.55: Representative KEGG pathway for *E. coli* infection across the entire stretch.

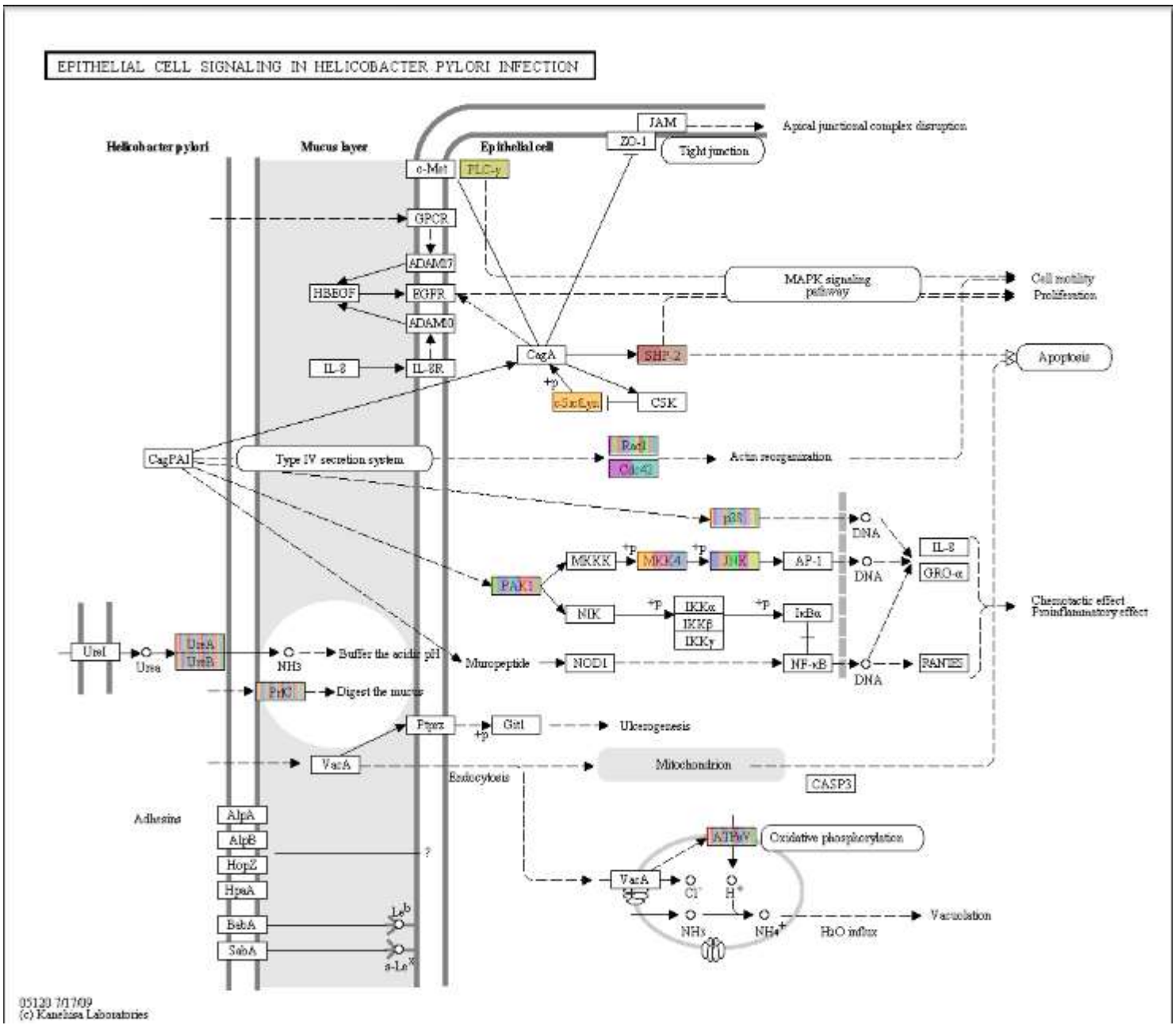

Fig.56: Representative KEGG pathway for *H. pylori* infection across the entire stretch.

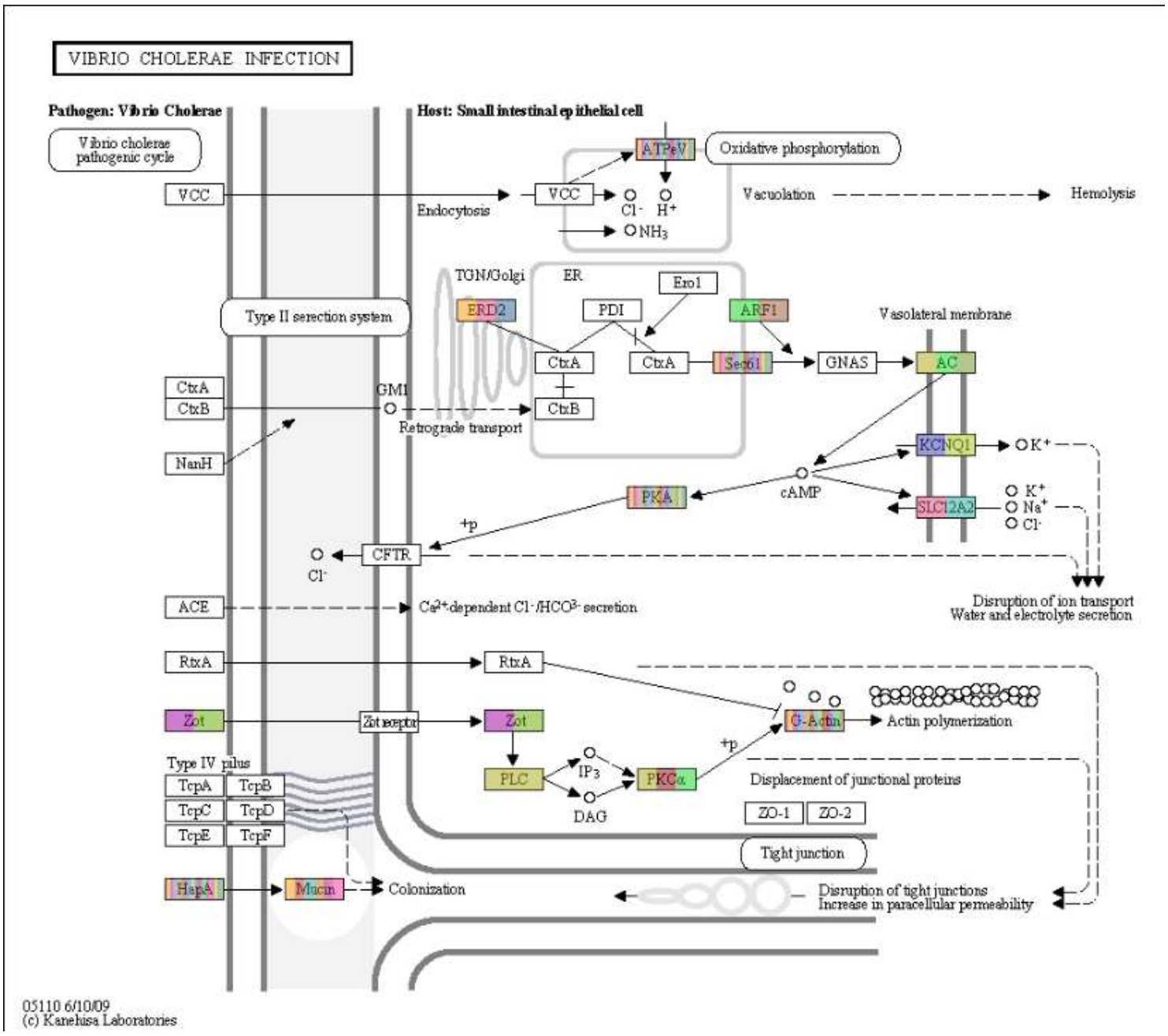

Fig.57a: Representative KEGG pathway for *V. cholerae* infection across the entire stretch.

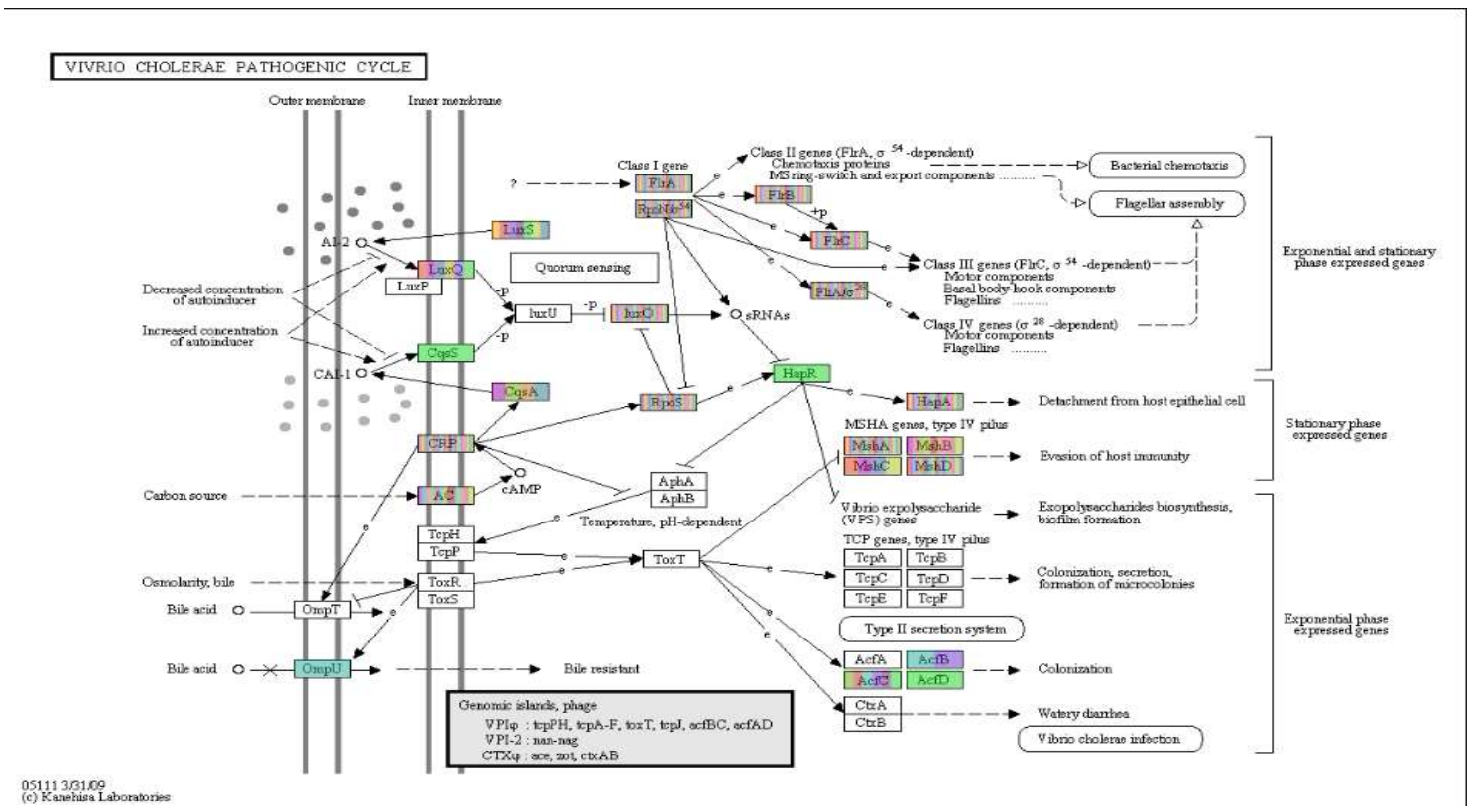

Fig.57b: Representative KEGG pathway for *V. cholerae* pathogenic cycle across the entire stretch.

Biosynthesis of streptomycin

Metagenomic mining of data for antibiotic production revealed potential of *Streptomyces* for production of streptomycin (Fig.58). Streptomycin is an aminoglycoside antibiotic that acts by binding to the 30S ribosomal subunit of susceptible organisms and disrupting the initiation and elongation steps in protein synthesis.

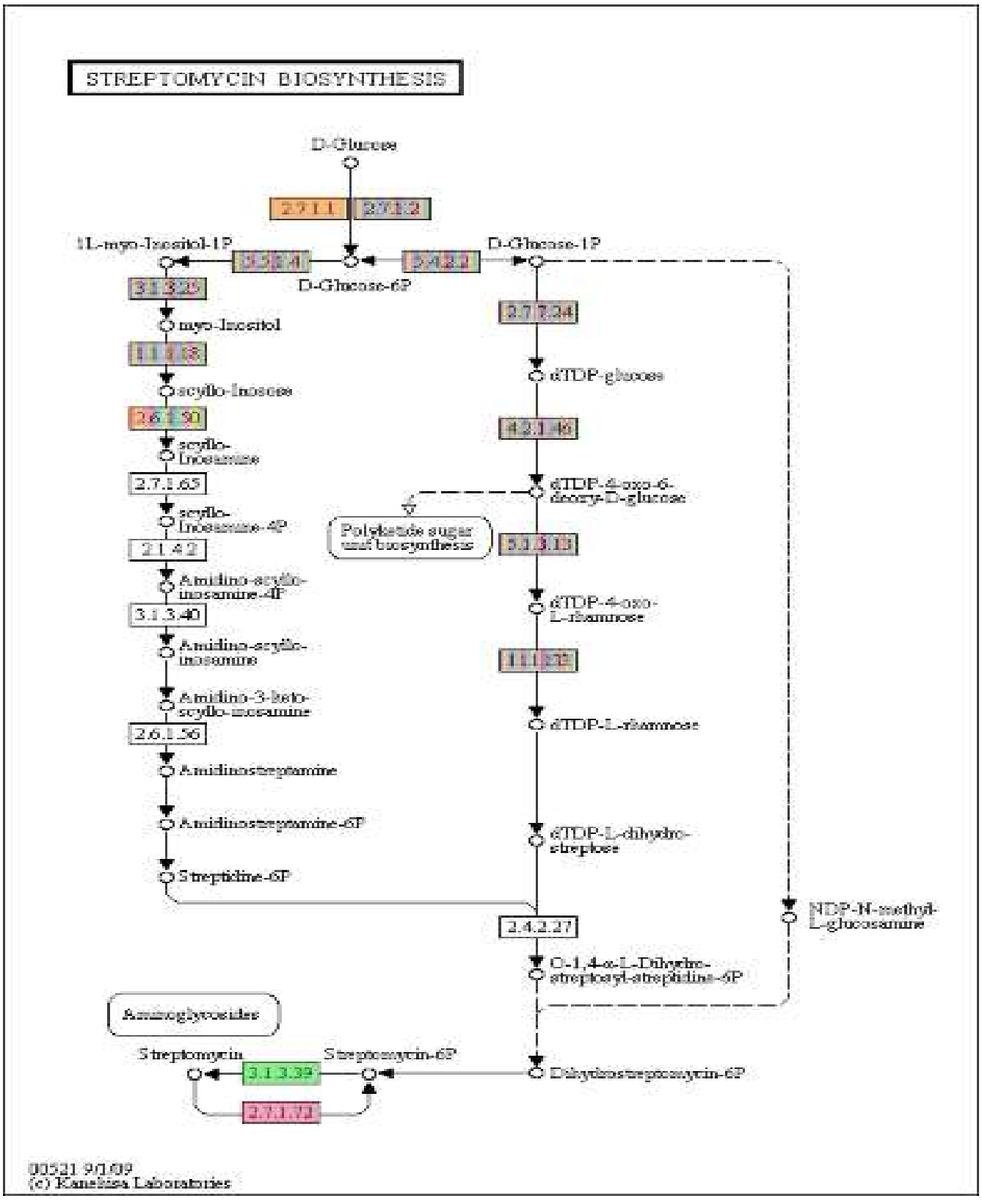

Fig.58: Representative KEGG pathway for biosynthesis of streptomycin across the entire stretch.

3. Total microbial (TMD) and viral/phage (TVD) diversity of control rivers (Yamuna and Narmada) and comparison with Ganga river

Results

Total microbial (TMD) and viral/phage (TVD) diversity of River Yamuna by nanopore sequencing

EPI2ME analysis of the upper stretch samples revealed presence of several bacteriophages such as Pseudomonas phage; Aerococcus phage; Mycobacterium phage, etc. (Fig.59). Bacterial classification of the reads showed presence of extremophilic bacteria such as *Sulfuritalea; Acidobacter; Polaromonas,* etc. (Fig.60). Additionally, we classified the archaeal reads which revealed presence of halophilic and methanogenic archaea (Fig.61).

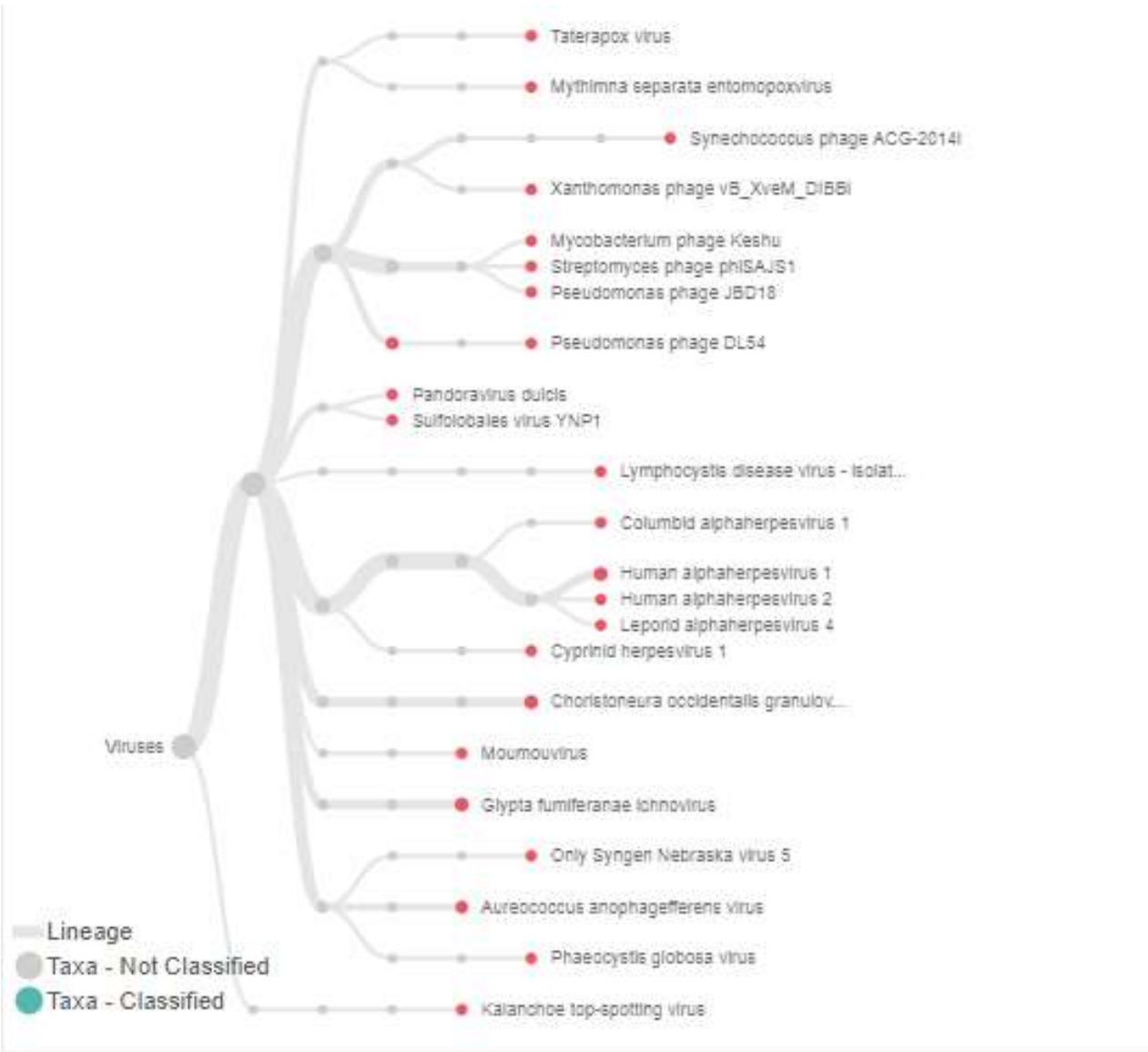

Fig .59: Taxonomic tree showing presence of viral genera along the upper stretch samples of River Yamuna spanning from Yamunotri to Dakpatthar.

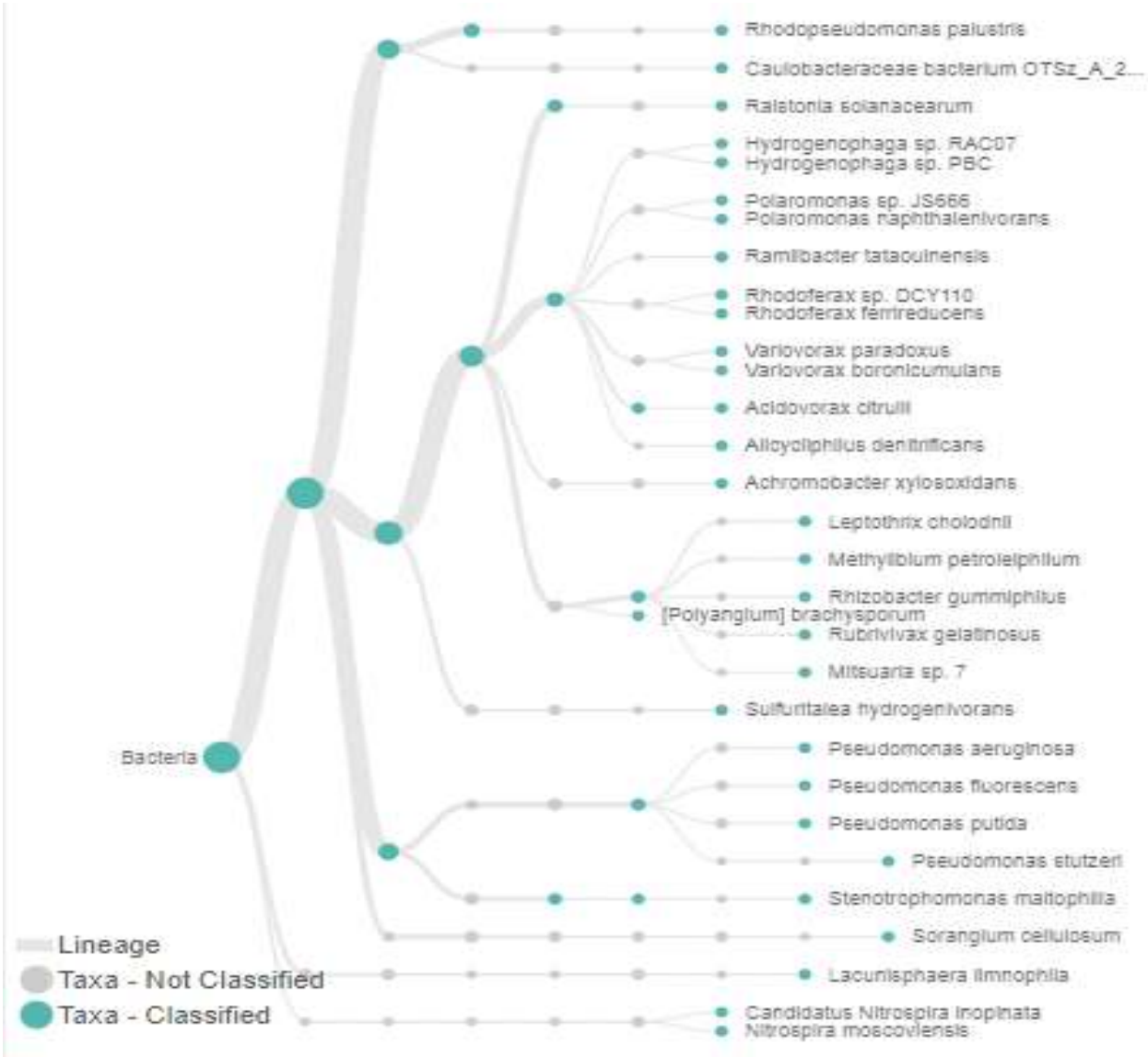

Fig .60: Taxonomic tree showing presence of bacterial genera along the upper stretch samples of River Yamuna spanning from Yamunotri to Dakpatthar.

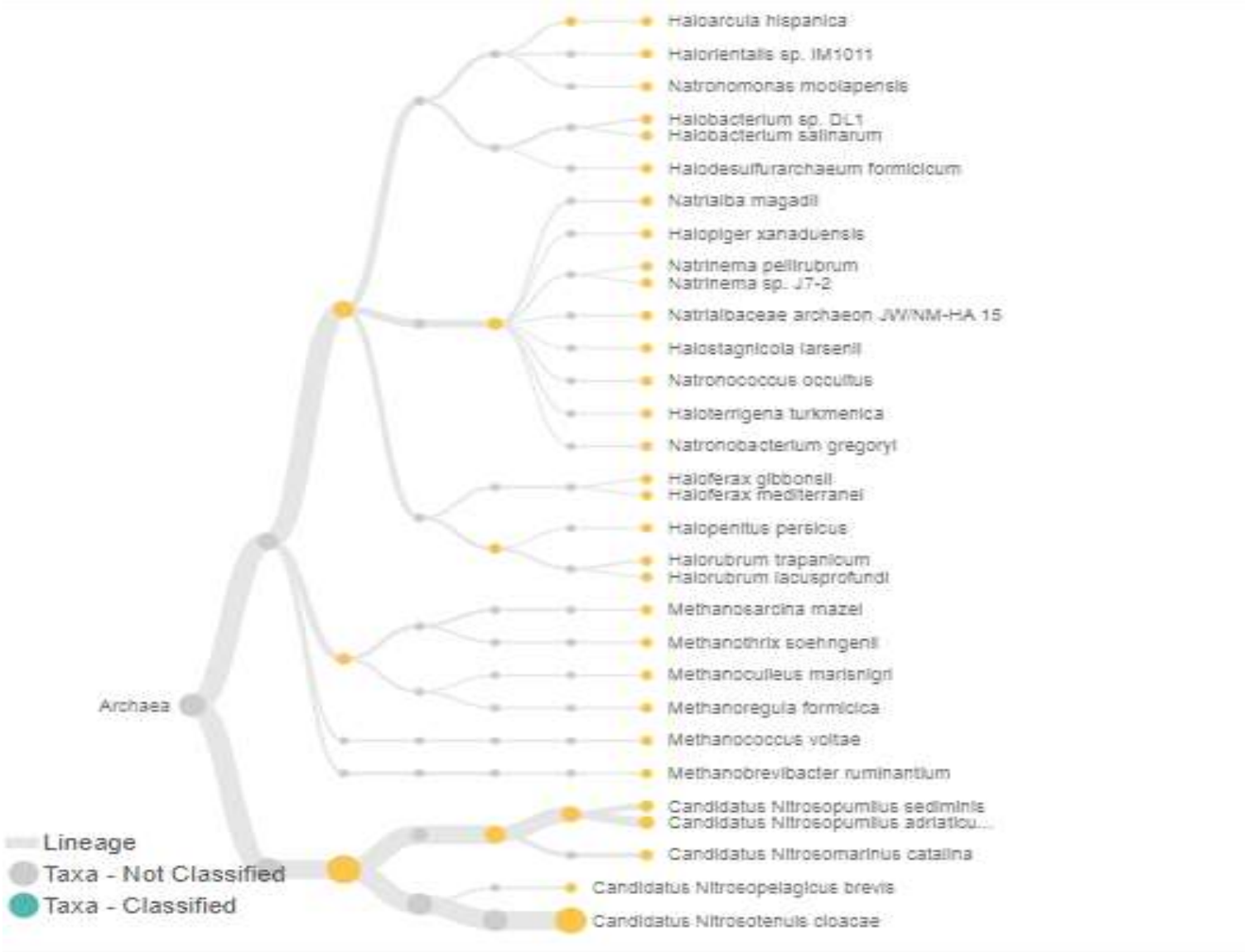

Fig .61: Taxonomic tree showing presence of archaeal genera along the upper stretch samples of River Yamuna spanning from Yamunotri to Dakpatthar.

3.2 Total microbial (TMD) and viral/phage (TVD) diversity of River Narmada

EPI2ME analysis of the upper stretch samples revealed presence of several phages of higher invertebrates followed by giant viruses and a dismal number of bacteriophages (Fig.62). Bacterial classification of the reads showed presence of extremophilic bacteria such as *Sulfuritalea; Acidobacter; Polaromonas,* etc. (Fig.63). Additionally, we classified the archaeal reads which revealed presence of halophilic and methanogenic archaea (Fig.64).

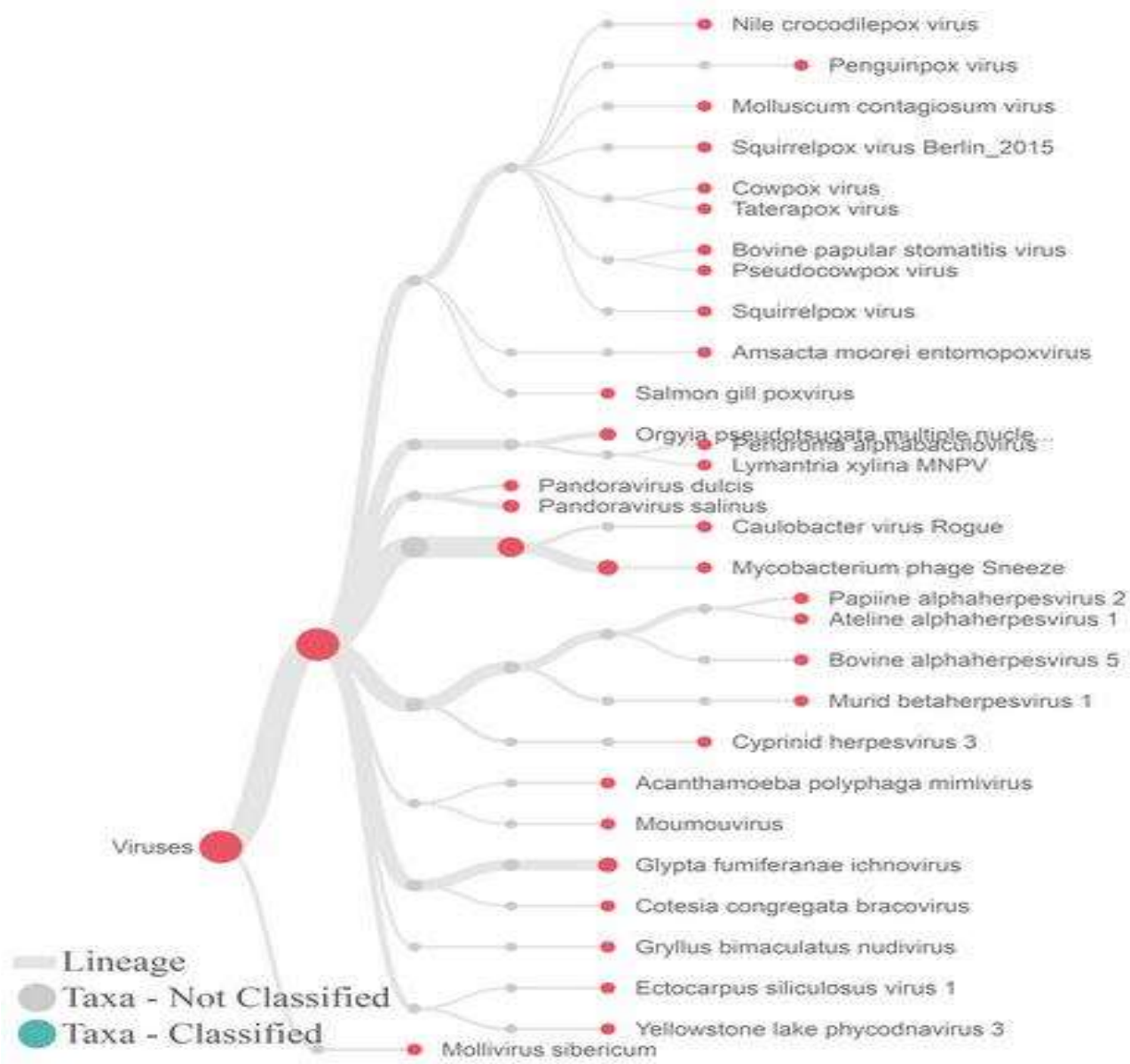

Fig .62: Taxonomic tree showing presence of viral genera along the upper stretch samples of River Narmada spanning from Mandla to Hoshangabad.

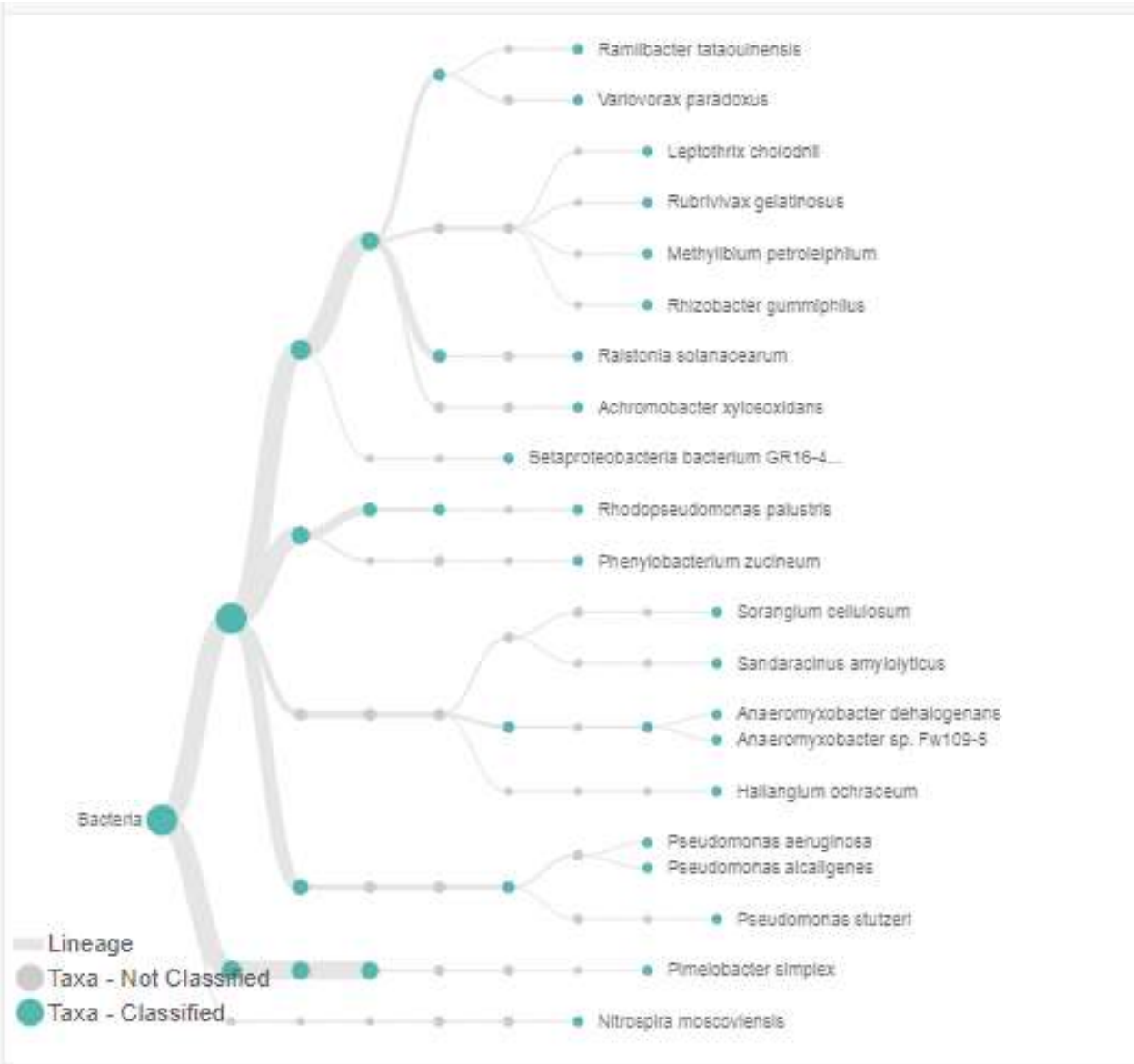

Fig .63: Taxonomic tree showing presence of bacterial genera along the upper stretch samples of River Narmada spanning from Mandla to Hoshangabad.

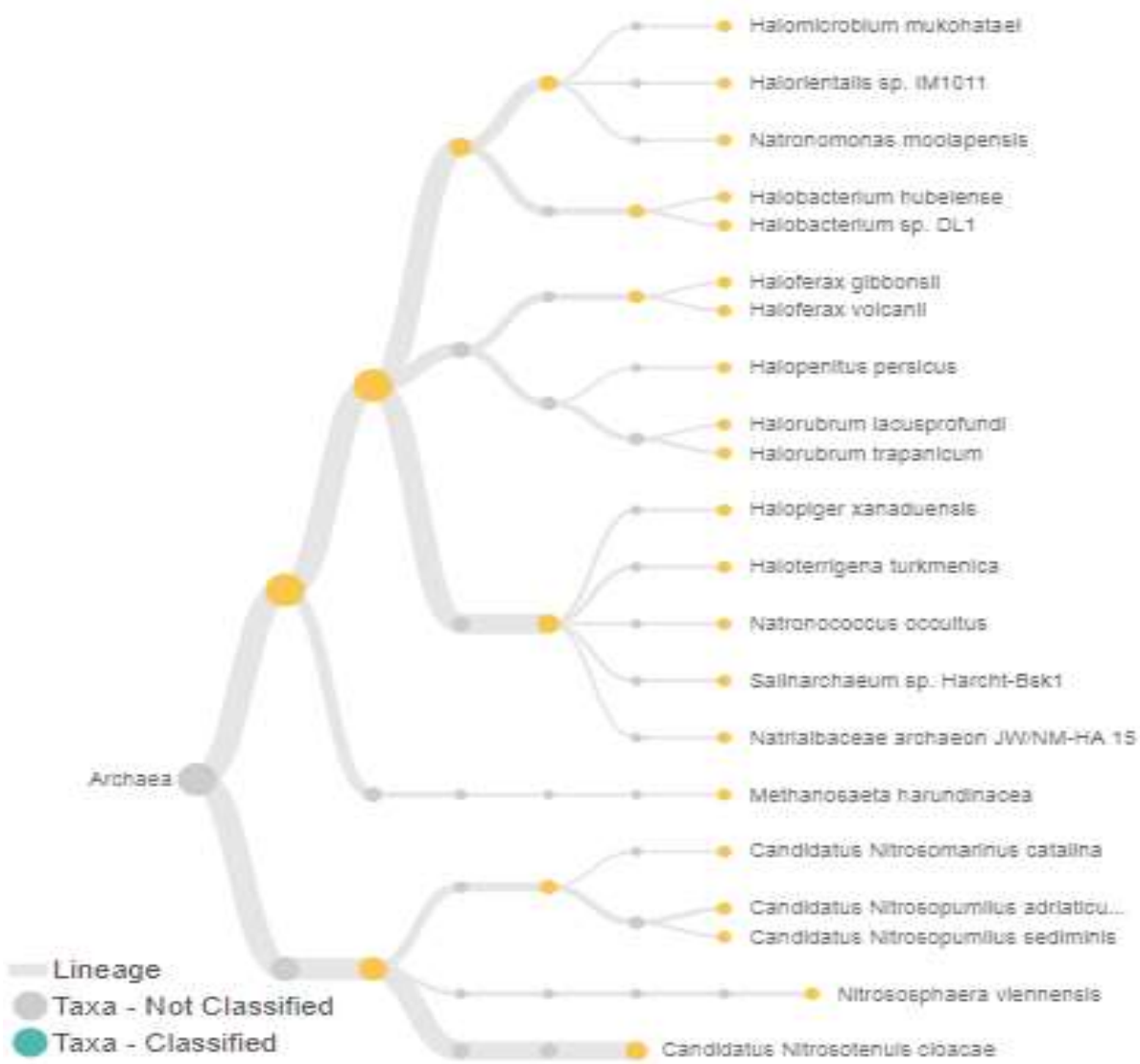

Fig .64: Taxonomic tree showing presence of archaeal genera along the upper stretch samples of River Narmada spanning from Mandla to Hoshangabad.

3.3. Comparison of Taxonomic diversity between Ganga river with the control rivers

- Presence of extremophilic bacteria such as *Sulfuritalea; Thiobacillus; Sulfuricaulis; Sideroxydans; Polaromonas* in all the three rivers.
- Presence of halophilic and methanogenic archaea in all the three rivers.
- River Ganga shows highest bacteriophage diversity as compared to the control rivers.
- Presence of several bacteriophages against pathogenic bacteria like *Pseudomonas Aerococcus Mycobacterium* in River Yamuna.
- Presence of several phages of higher invertebrates followed by giant viruses and a dismal number of bacteriophages in River Narmada.

4. Summary and Conclusion

Overall summary

1. The upper stretch of River Ganga revealed presence of several bacteriophages such as *Bacillus phage; Pseudomonas phage; Cronobacter phage; Escherichia phage; Mycobacterium phage,* against pathogenic bacteria. Additionally, it was observed that several phage reads (29% of Siphoviridae; 15% Myoviridae) were categorized as unclassified/other, indicating possibility of presence of novel phages in river Ganga.
2. For lower stretch of River Ganga samples, post-monsoon season (Oct'2017) showed 50% of Caudovirales and the pre-monsoon samples (Jun'18) showed an upsurge in the relative abundance of Caudovirales (71%). Additionally, it was observed that in the lower stretch there is a predominance of Myoviridae as opposed to that of upper stretch with a predominance of Siphoviridae.
3. Comparison of the viral diversity of River Ganga and the control rivers revealed presence of highest bacteriophage diversity in River Ganga followed by River Yamuna. River Narmada had a rich entemophage as compared to the bacteriophage ones.
4. Presence of hits against phage related proteins (integration, excision, tail fibers, regulation, phage DNA replication, etc) indicate a strong presence of host-phage relationship in both upper and lower stretch samples.
5. Presence of several virulence mechanisms in the lower stretch such as adhesion, bacteriocins, invasion and intracellular resistance, toxins and superantigens and resistance to toxic compounds.
6. Establishment of host-phage presence across the entire stretch of Ganga river, revealed phages and their host for diverse group such as putrefying bacteria, human pathogens, plant pathogens, photosynthetic microbes, plant growth promoting rhizobacteria (PGPR), and others.
7. Metagenomic mining of the entire dataset for functional profiling of the metabolic plasticity, and pathobiome and virulome across the entire stretch of Ganga.

Conclusion

This study underscores metaviromic approach to gain insights into the viral diversity with focus on bacteriophages of River Ganga. Deciphering the taxonomic and functional diversity of River Ganga across its entire stretch through various seasons was carried out for the first time in the present study. The data obtained from the study could be used to isolate novel phages against a diverse bacterial host range. Further presence of *Herpesviridae* and several other human pathogenic viral families were also noted across the sequenced stretch of River Ganga from Rishikesh to Bhagalpur, suggests need of management strategies to prevent the viral load entering in river. The functional annotation of total microbial diversity revealed microbes with diverse range of metabolic potentials, which could be isolated and exploited for bioremediation and other uses. Additionally, resistome profiling revealed presence of several anti-microbial and heavy-metals resistance genes. Overall, metavirome approach could be used as rapid surveillance tool to decipher uncultivable microbial diversity and would aid in guiding specific isolation of bacteriophages that might get missed-out using standard culture based approach. Also, metagenomic approach can be used to understand taxonomic and functional aspects in a faster way and can be used as a guide for isolation of therapeutic microorganisms.

Publications:

1) Samson R., Shah M., Yadav R., Sarode P., Rajput V., Dastager S., Dharne M*., Khairnar K.*, Metagenomic insights to understand transient influence of Yamuna River on taxonomic and functional aspects of bacterial and archaeal communities of River Ganga. 2019. Science of Total Environment. doi.org/10.1016/j.scitotenv.2019.04.166.

2) Samson R., Shah M., Yadav R., Sarode P., Rajput V., Dastager S., Dharne M.*, Khairnar K.*, Deciphering taxonomic and functional diversity of fungi as potential bioindicators within confluence stretch of Ganga and Yamuna Rivers, impacted by anthropogenic activities. 2020. Chemosphere, https://doi.org/10.1016/j.chemosphere.2020.126507.

* Corresponding author

Any patents applied for: Nil

Date: 18.01.201 Signature of PI

(Dr. Mahesh Dharne) (Dr. Syed Dastager)

A Detail Study to Understand the Non-Putrefying Property of River Ganga in both Water and Sediment

Project Report

(August 2017 to December 2020)

Department of Biotechnology
Indian Institute of Technology Roorkee,
Roorkee- 247667

Sponsor:

Ministry of Water Resources, River Development & Ganga Rejuvenation, New Delhi

CSIR-National Environmental Engineering Research Institute, Nehru Marg, Nagpur – 440 020

Project Investigator:

Name: Dr. Krishna Mohan Poluri
Designation: Associate Professor
Organization: India Institute of Technology Roorkee, Roorkee
Address: Department of Biotechnology, India Institute of Technology Roorkee, Roorkee- 247667, Uttrakhand
Telephone: +91-1332-284779
E-mail: mohanpmk@gmail.com, krishfbt@iitr.ac.in

Specific Objectives:

(A) Transmission electron microscopy (TEM) analysis of bacteriophages isolated from Ganga waters

(B) Structural and functional characterization of Pseudomonas phage endolysin detected by NEERI from Ganga bacteriophages

(C) NMR based metabolic analysis of bacteriophage endolysin producing bacteria

(D) Heavy metal remediation characteristics of microalgal species detected from Ganga waters near Haridwar

Milestones:

Sr. No.	Work Details	Bar Chart Months									
	Start Month Aug 2017	**0-3**	**4-6**	**7-9**	**10-12**	**13-15**	**16-18**	**19-21**	**22-24**	**25-27**	**28-30**
Morphological, Structural, biochemical and metabolic analysis of bacteriophages, phage proteins, and algae isolated from Ganga											
(A) Transmission electron microscopy (TEM) analysis of bacteriophages isolated from Ganga waters											
(B) Structural and functional characterization of Pseudomonas phage endolysin detected by NEERI from Ganga bacteriophages											
(C) NMR based metabolic analysis of bacteriophage endolysin producing bacteria											
(D) Heavy metal remediation characteristics of microalgal species detected from Ganga waters near Haridwar											
Data analysis and reporting of the structural, morphological and metabolic profiling of all the samples											
Report/Recommendation/Publication											

Ganga and Yamuna water sampling during the project

1. Ganga water sampling during August to October 2017:

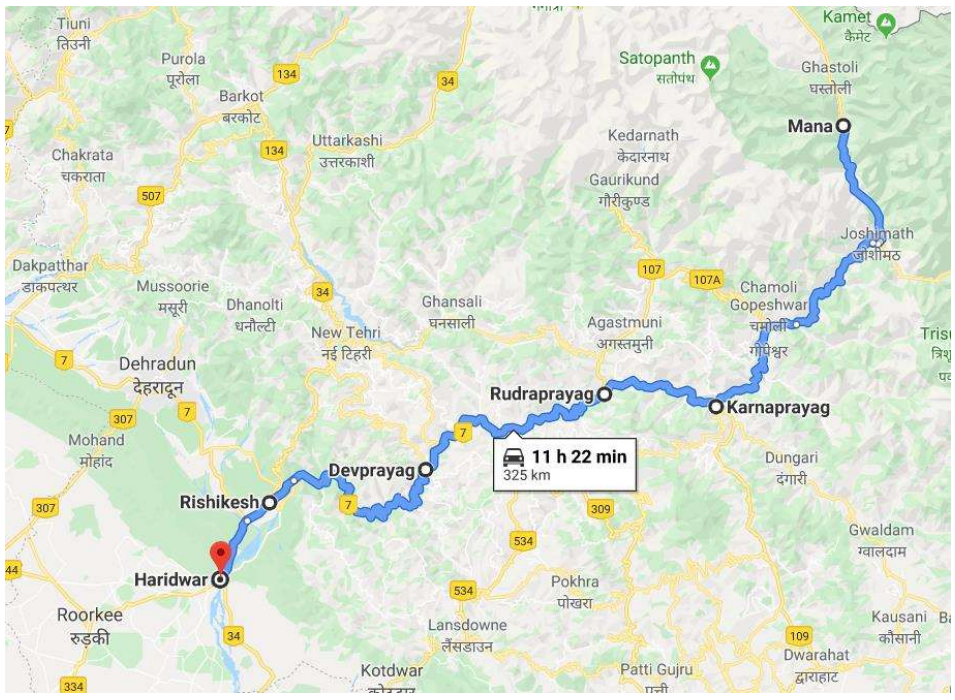

Sampling Locations: Mana, Badrinath, Karnaprayag, Rudraorayag, Devprayag, Rishikesh, Haridwar

2. Ganga water sampling during November 2017 to January 2018:

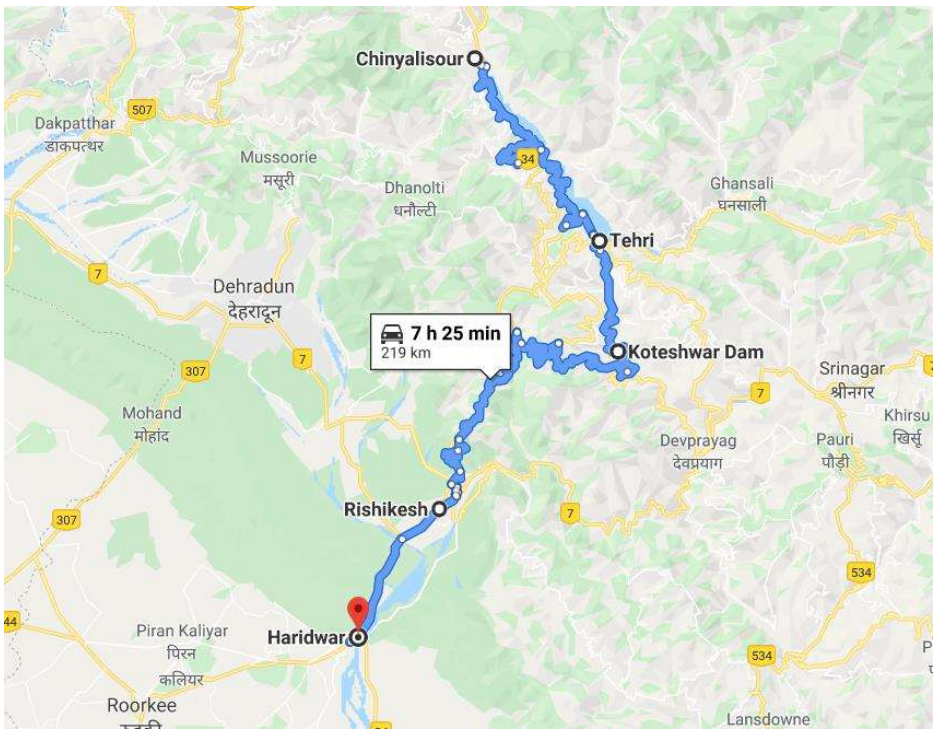

Sampling Locations: Chiniyalisour, Tehri Dam, Koteshwar Dam, Rishikesh, Haridwar

3. Ganga water sampling during the May to July 2018

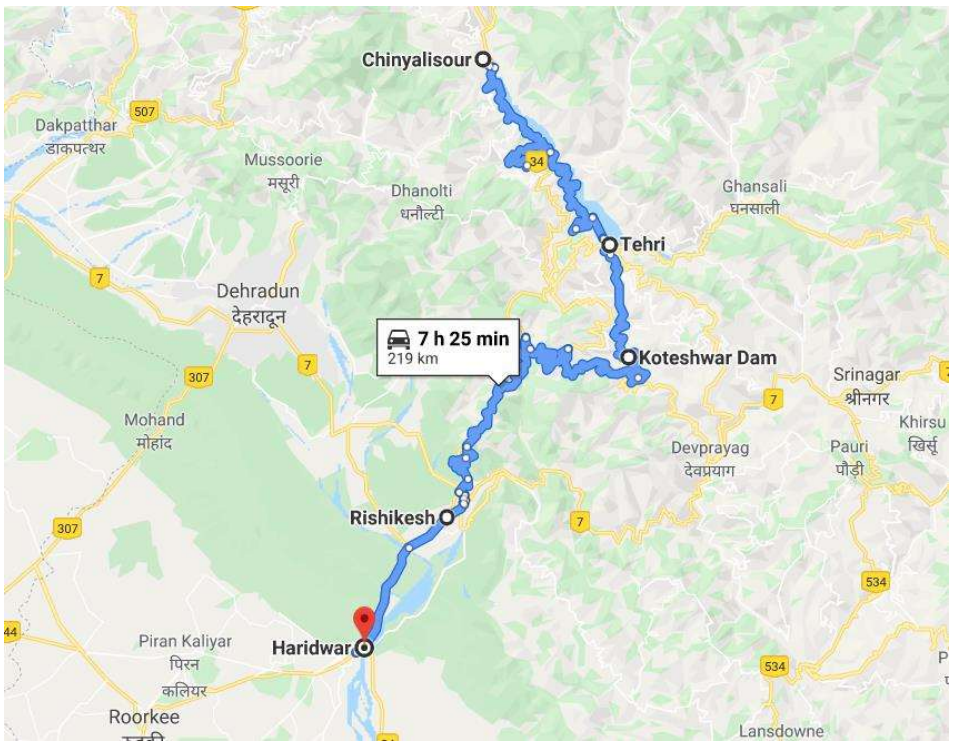

Sampling Locations: Chiniyalisour, Tehri Dam, Koteshwar Dam, Rishikesh, Haridwar

4. Yamuna water sampling during the May to July 2018

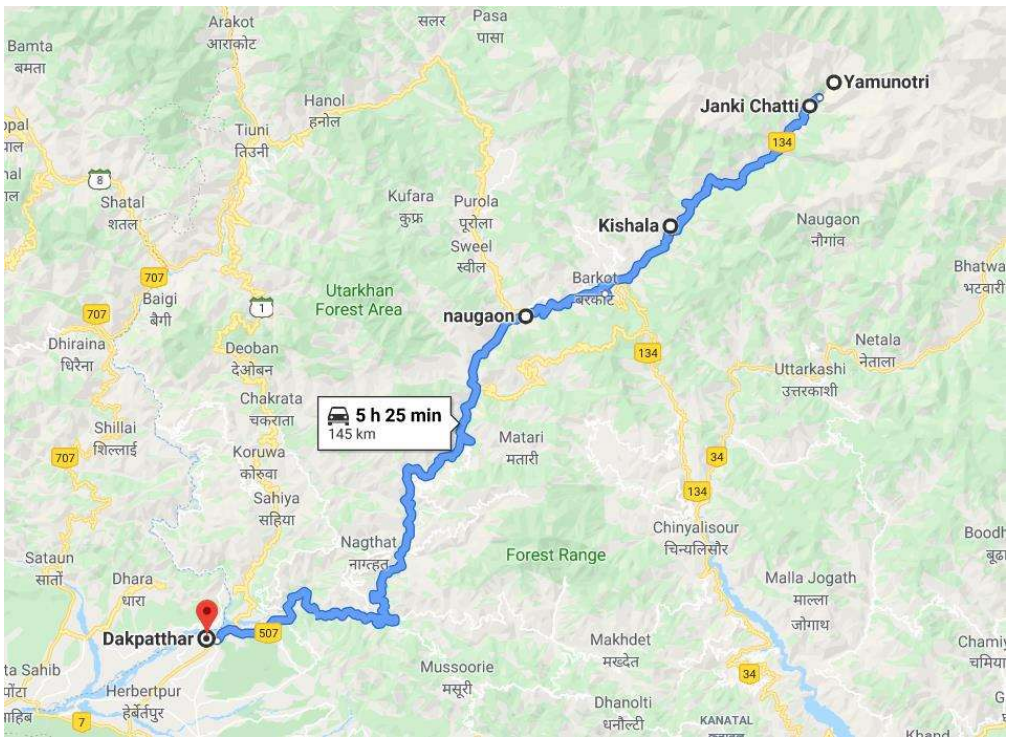

Sampling Locations: Yamunotri, Janki chatti, Kishala bridge, Naugoan, Dakpatthar

5. Ganga water sampling during the November 2018 to January 2019

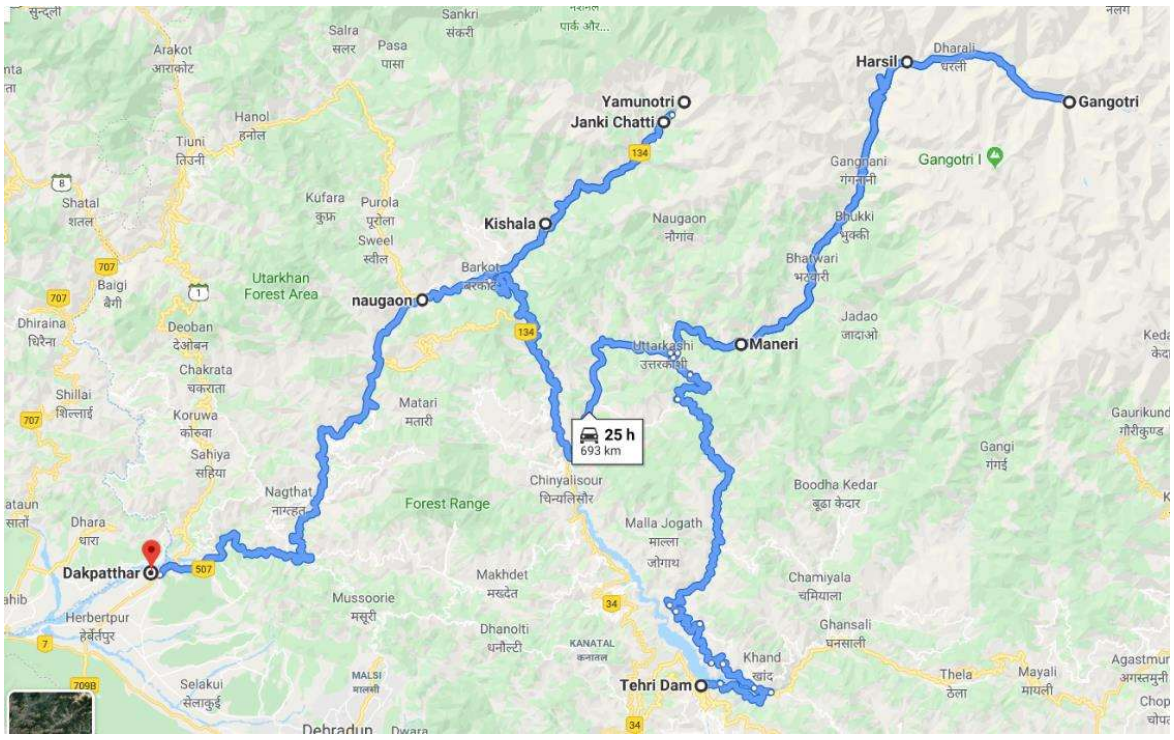

Sampling Locations: Tehri Dam, Maneri, Harshil, Gangotri, Janki chatti, Kishala, Naugaon, Dakpatthar

6. Ganga water sampling during the May to July 2019

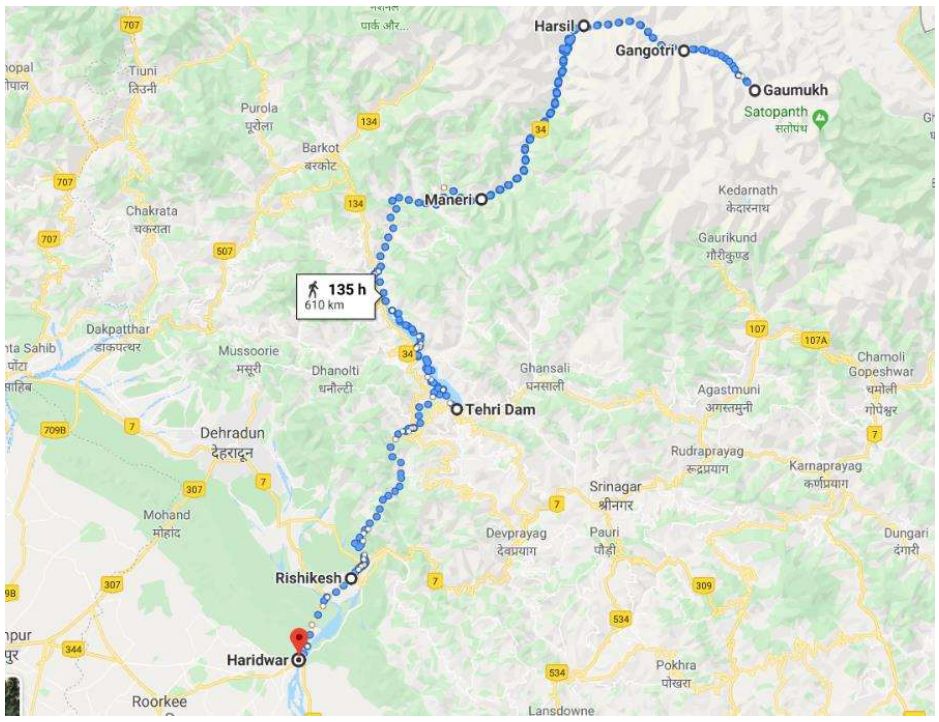

Sampling Locations: Gomukh, Gangotri, Harshil, Maneri, Tehri Dam, Rishikesh, Haridwar

Water sample collection procedures:

- Water samples were collected from each location along with upstream and downstream location point.
- Water samples were collected from about 30 cm depth in 1000 ml pre-sterilized bottles using grab sampling approach.
- Collected samples were immediately kept on ice (4˚C) and transported until used in the laboratory.
- Laboratory experiments were performed within 24-48 hours of sample collection by membrane filtration technique (MFT).

Transmission electron microscopy (TEM) analysis of bacteriophages isolated from Ganga waters

TEM analysis of bacteriophage:

Transmission electron microscopy (TEM) became a popular technique for the identifications, classifications of bacteriophages and comparative virology. In general, electron microscope comprises high beam electron illumination source, series of lenses (i.e. condenser lens, objective lens and projection lens), specimen holder and huge camera. In TEM, the electron micrographs are generated from the transmitted and scattered electrons by the samples. So the bacteriophage samples need a good negative staining agent for clear imaging. The principle of negative staining is to mix the bacteriophages with an electron-dense staining solution of a metal salt of high molecular weight and small molecular size, by which the bacteriophages were appear white in a dark background. The negative stain used in this current study is 2% uranyl acetate. It is dissolved slowly in distilled water.

Material and Methods:

Sample collection: The given bacteriophages samples were procured and purified by Dr. Khairnar research group at NEERI, Nagpur.

Bacteriophage samples that are analyzed are given below:

S. No.	Phage Name	Source	Purified method
1	PB1 – N5822	Ganga	Filtered
2	ϕ crude lysate	Ganga	Filtered
3	ϕM PEG precipitated	Ganga	PEG precipitated
4	Gau 1:1000	Ganga	Filtered

Images of bacteriophages were recorded with a Tecnai G2 20 S-TWIN Transmission Electron Microscope (TEM) (FEI Netherlands) operated at 200 kV. Samples were prepared by depositing two to three droplets of samples onto a Carbon coated copper grids (Icon Analytical Equipment Pvt. Lt).

Carbon coated copper grid details:

Carbon grid is a small circular chip-like thing with two sides – copper coated and carbon coated side. Sample is loaded onto the carbon side of this grid. The grid used by us was 4-5mm diameter with 200 mesh size.

Sample preparation protocol for TEM imaging of bacteriophages:

- Place carbon coated copper grid on a filter paper
- 10 µl of phage sample (2.5 x 10^8 PFU/ml titre) is loaded onto the carbon coated copper grid and let it settle for 2 minutes.
- Remove the water content by tissue paper.
- For drying, keep the sample loaded copper grid under red light lamp about 5 minutes.
- Add 10 µl staining solution (1:1 ratio) 2% Uranyl acetate + 4mM $MgCl_2$. **Note**: Uranyl acetate is toxic and must be handled with care.
- Dry under red light or normal air dry, for about 10-15 minutes. **Note**: When doing TEM, sample must be absolutely dry.
- Place the carbon coated copper grid on the holder of TEM and insert into the TEM machine.
- Wait for vacuum generation for 2 min till cut off sound is heard.
- Imaging is done at around 34,000 X magnification and 200kV.

Results:

<u>Observation-I</u>

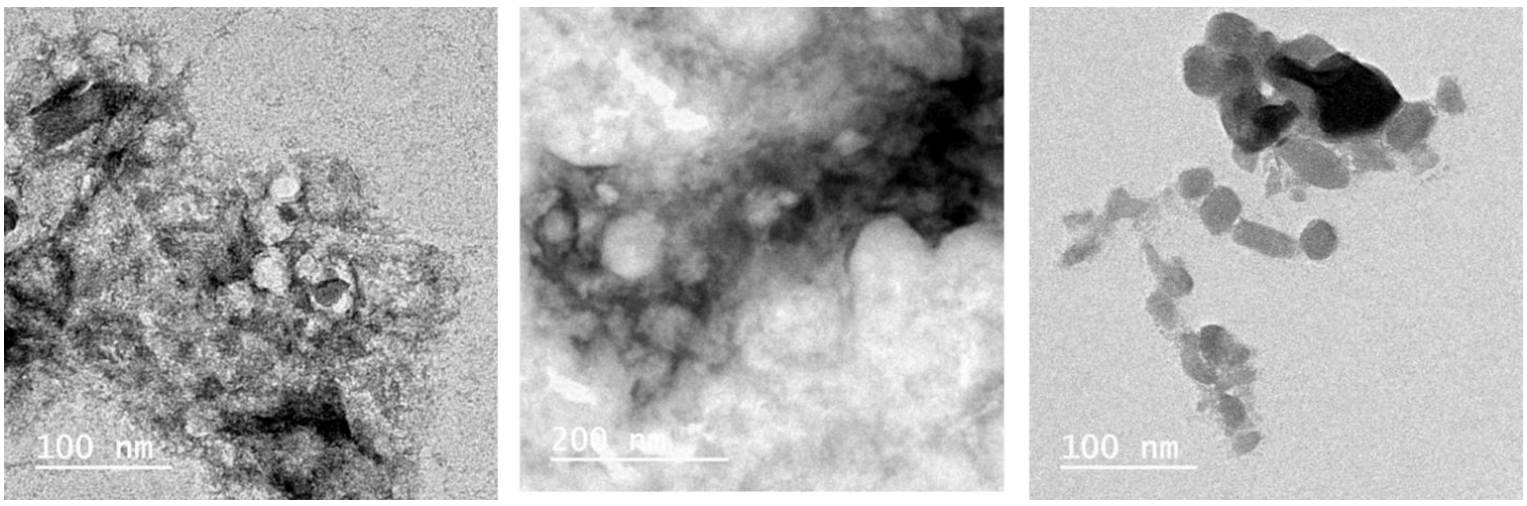

Figure 1: TEM micrographs of bacteriophages in 100nm and 200nm scale.

The aggregation of bacteriophages is observed in TEM at 200nm and 100nm scale. Aggregation of phage by salts have to optimized by filtration for the subsequent elimination of PEG. Along with bacteriophages, Clumps like structured were seen all over the grids.

Observation-II

Sample: PB1

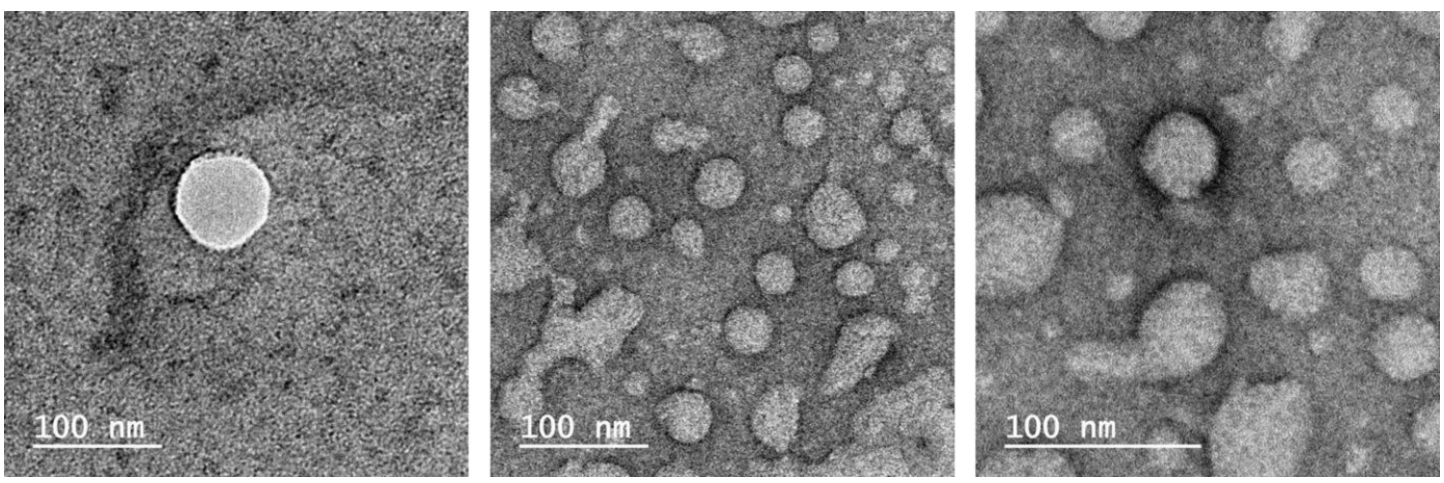

Figure 2: TEM micrograph of PB1 in 100nm scale.

Sample: ϕM

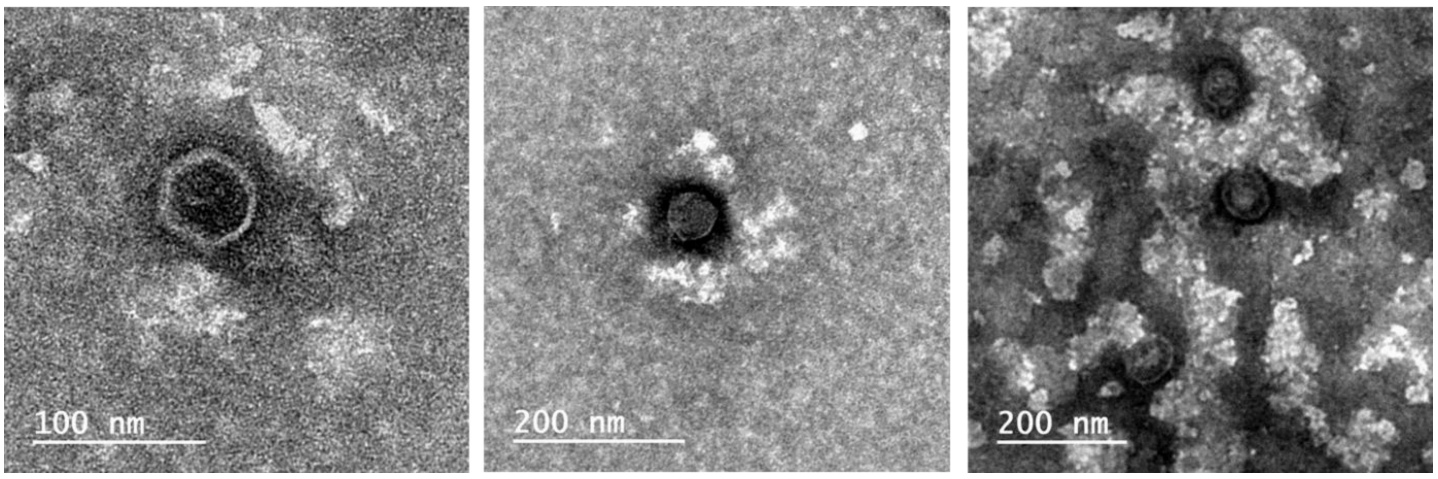

Figure 3: TEM micrograph of PB1 in 100nm and 200nm scale.

PB1 Phages was visualized better in 100nm scale. The TEM micrographs were taken in 100nm scale for the better visualization of bacteriophages. ϕM Phages was visualized in 100nm and 200nm scale. It is clearly seen that phages are ϕM icosahedral with a lighter outline and darker inside. PB1 and ϕM phage samples were observed in tailless phage structure. The hexagonal capsid structure signifies the presence of bacteriophages in the sample. The average diameter of the phage outer capsids is 80nm.

Observation-III

Sample: PB1

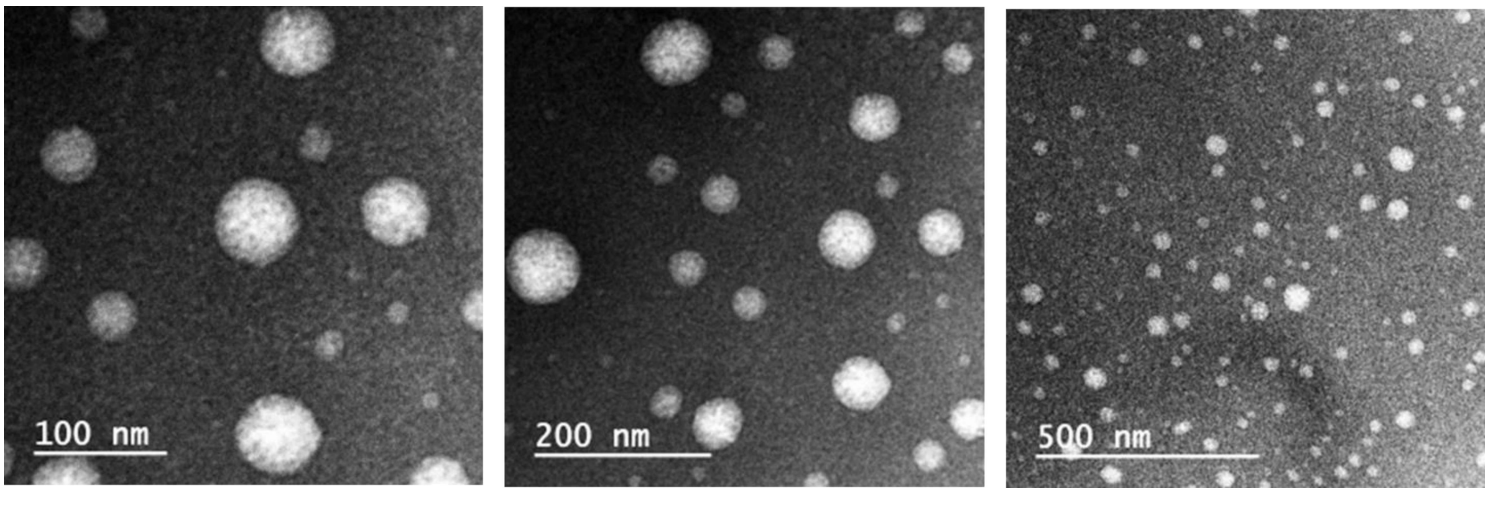

Figure 4: TEM micrograph of PB1 in 100nm, 200nm and 500nm scale.

Sample: Centrifuged PB1

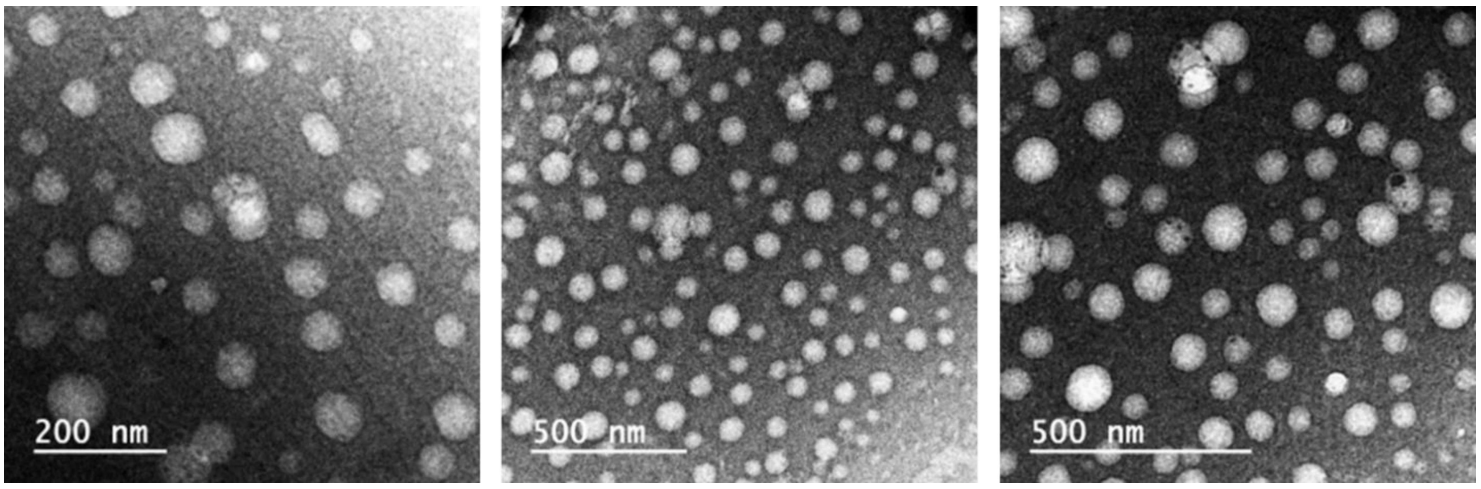

Figure 5: TEM micrograph of centrifuged PB1 in 100nm, 200nm and 500nm scale.

The TEM micrographs were taken in 100nm, 200nm and 500nm scale for the better visualization of bacteriophages. Centrifuged PB1 Phages were visualized in 200nm and 500nm scale resolutions. Icosahedral and high number of phages were seen after centrifugation. PB1 and ϕM phage samples were observed in tailless phage structure. The hexagonal capsid structure signifies the presence of bacteriophages in the sample. The average diameter of the phage outer capsids is 80nm. Icosahedral PB1 Phages were visualized in 100nm, 200nm and 500nm scale resolutions.

Concluding Remarks:

- From the preliminary standardization experiment, clear phages were not observed. Thread-like and clumps were seen. it was observed that phages of high titre in the range of $10^5 – 10^8$ are preferred for TEM analysis.
- Pb1 phages were looked opaque and icosahedral. ϕM were also looked icosahedral with a lighter outline and darker inside. Tail was not visible in both samples.
- High speed centrifugation is required before TEM analysis for the sufficient amount of cells deposition over the grids.
- It was concluded that Phages of high titre in the range of $10^5 – 10^8$ are preferred for TEM analysis. Phage lysates filtered with 0.22μm syringe filter will help to eliminate PEG and reduce the clump formations in TEM micrographs. Icosahedral and high number of phages were undoubtedly visualized.

(B) Structural and functional characterization of Pseudomonas phage endolysin detected by NEERI from Ganga bacteriophages

A *Pseudomonas* phage and its endolysin from Ganga water has been isolated by Dr. Khairnar's research gorup at NEERI, Nagpur. The complete genome sequence analysis reveals that *Pseudomonas* phage encodes for an endolysin that can act as a therapeutic solution for the multidrug resistance (MDR) infections.

In order to find out the evolutionarily closest proteins to the endolysin a database search algorithm such as Basic Local Alignment Search Tool (BLAST) was used. BLAST performs the sequence alignment of the target sequence against the database (like PDB) of proteins sequences. The sequence alignment results suggested that *Pseudomonas* phage endolysin shows maximum similarity with muramidase from *Acinetobacter baumannii* AB 5075UW prophage. After finding a template, sequence alignment was done by using Clustal Omega online tool. This gives an overview of the general features of the protein family such as the degree of conservation, the presence and location of consensus sequence motifs, etc.

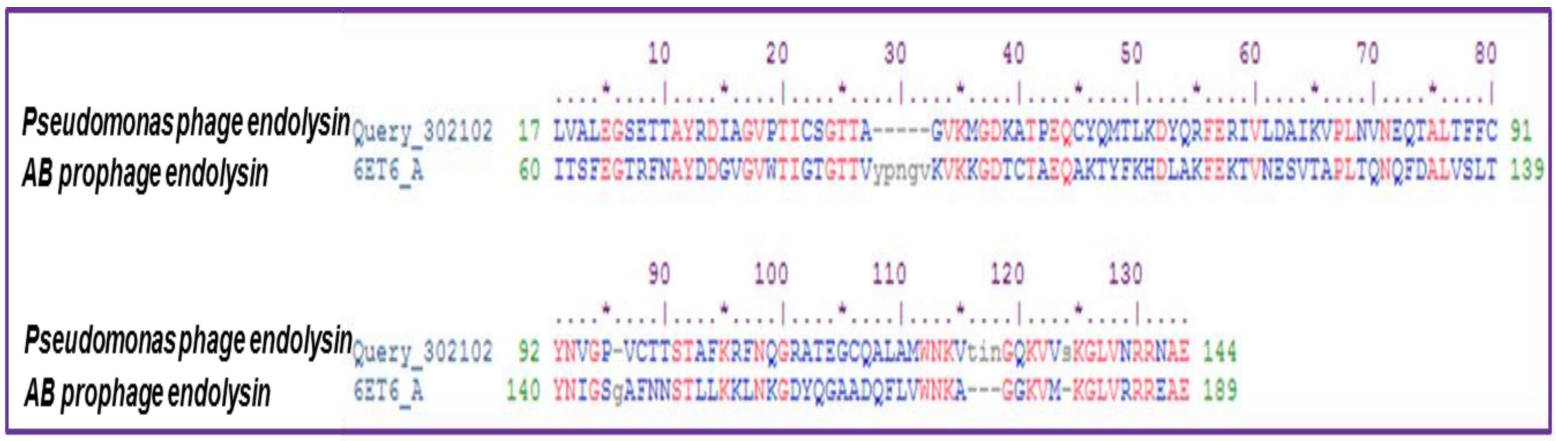

Figure 1: The sequence-specific alignment of *Pseudomonas* phage endolysin and *Acinetobacter baumannii* AB 5075UW prophage muramidase.

The isolated protein is also known as phage endolysin/lysozyme or N-acetylmuramidase and belong to the family of glycosyl hydrolytic enzymes. Muramidases are the most commonly found endolysins that target highly conserved bonds present in peptidoglycan layer of bacteria. Peptidoglycan is a very complex structure and consists of a sugar backbone made up of alternating units of N-acetyl glucosamine (NAG) and N-acetyl muramic acid (NAM). These sugar polymers are cross-linked by species-specific oligopeptide attachments at NAM sugar moiety. Bacteriophage muramidases have evolved to deal with this complexity of the peptidoglycan layer. They hydrolyse the β-1,4 glycosidic linkage between the N-acetylglucosamine (NAG) and N-acetylmuramic acid (NAM), thereby reduces the glycan chain into disaccharide units as shown in the following figure 2.

These phage-encoded enzymes favor the release of virions by lysis the host bacterium during their maturation. In literature, a number of muramidases have been reported that target various Gram-positive as well as Gram-negative bacteria. A small quantity of purified

recombinant muramidase can result in the immediate killing of the target bacterium when applied externally. They have been used successfully in a variety of animal models to control pathogenic antibiotic-resistant bacteria associated with various infections and life-threatening diseases. Their species-specific nature for the pathogen without disturbing the normal flora and the low chance of bacterial resistance makes them an ideal antibacterial agent.

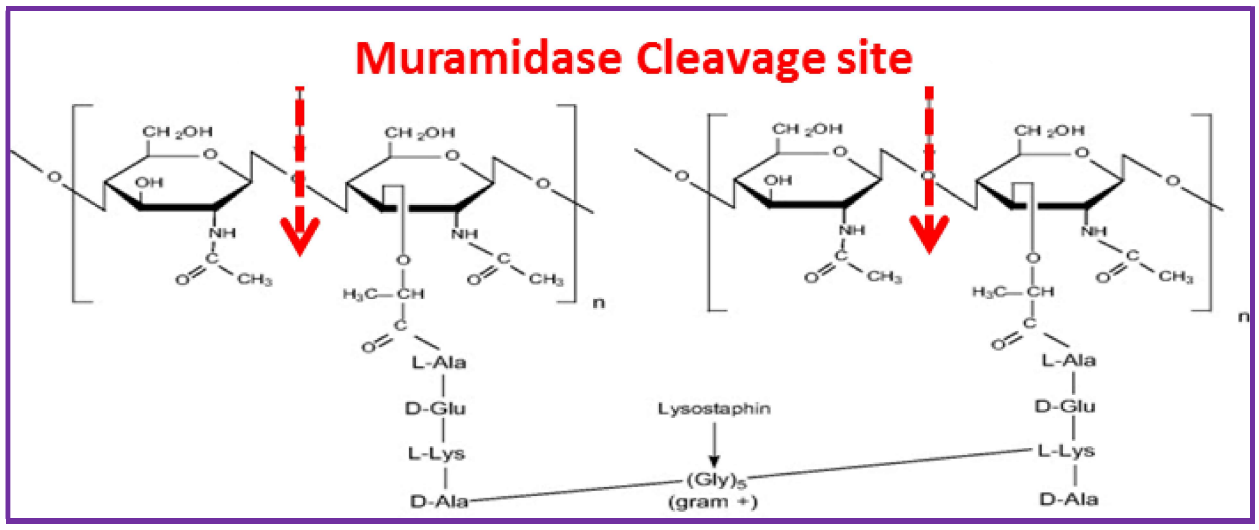

Figure 2: The cross-linking in peptidoglycan layer of Gram-positive bacteria and mode of the action of muramidase.

Sequence analysis and 3D structure prediction of *Pseudomonas* phage endolysin:

In order to elucidate the structure-function relationship of this phage endolysin first we have generated the structure by using homology modelling approach which is also called as comparative modelling or template-based modelling. In this approach modelling of a protein 3D structure is done using an experimental known structure of a homologous protein i.e. the template. The steps required for homology modelling are shown below.

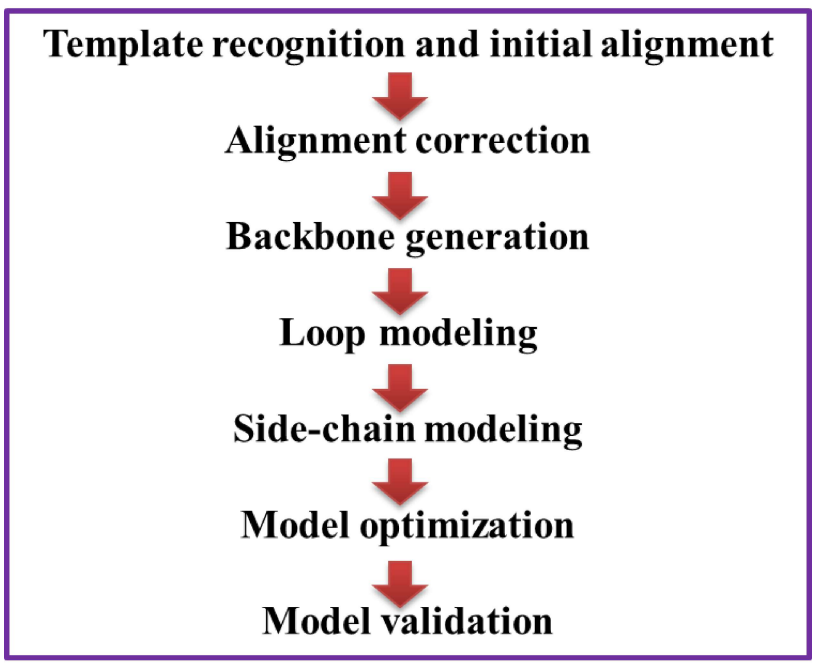

Figure 3: The scheme of protein 3D structure determination using homology modelling.

The isolated phage endolysin/lysozyme protein has highest sequence alignment results with *Pseudomonas* phage endolysin shows maximum similarity with muramidase from *Acinetobacter baumannii* AB 5075UW prophage. This AB prophage endolysin protein structure can be used as a template structure for the 3D structure modelling of *Pseudomonas* phage endolysin.

Homology Modelling of *Pseudomonas* phage endolysin:

- Homology modeling methods uses evolutionary related proteins that share a similar structure to predict 3D structure of a protein.
- The method is based on the fact that structural conformation of a protein is more highly conserved than its amino acid sequence, and that small or medium changes in sequence normally result in little variation in the 3D structure.
- Homology modeling is helpful in molecular biology, such as hypotheses about the drug design, ligand binding site, substrate specificity, and function annotation. It can also provide starting models for solving structures from X-ray crystallography, NMR and electron microscopy.
- Quality of model is directly linked with the identity between template and target sequences, as a rule that, models built over 50% sequence similarities are accurate enough for drug discovery applications, those between 25 and 50% identities can be helpful in designing of mutagenesis experiments and those in between 10 and 25% are tentative at superlative

<u>Steps of development of homology model is as follows:</u>

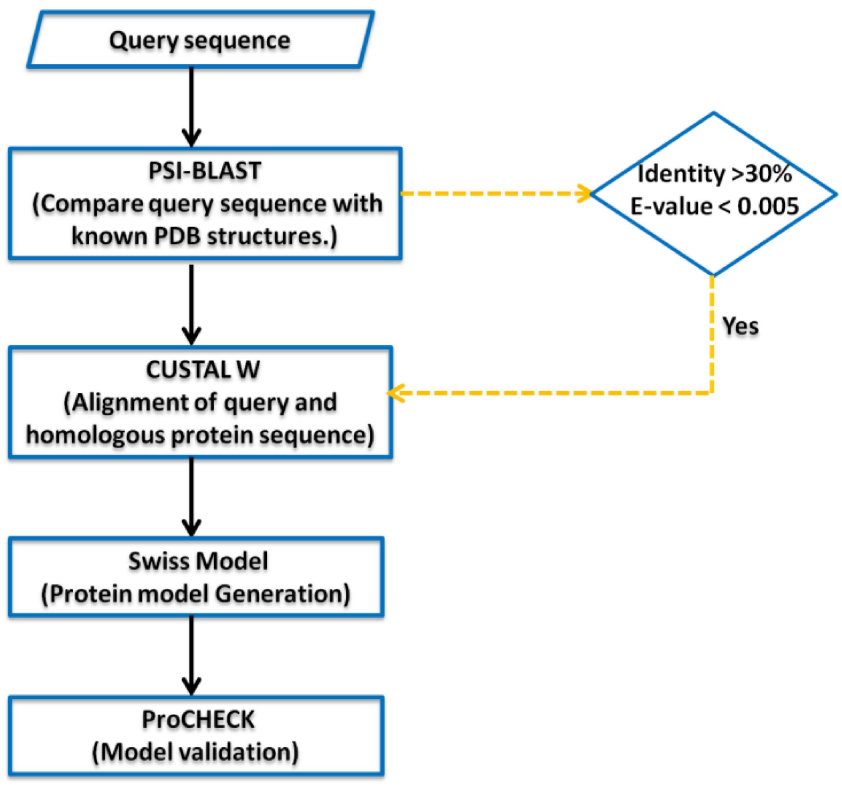

Figure 4: Steps of homology modeling.

- **Identification of template:** Template sequence was identified by PSI-BLAST (NCBI) using *Pseudomonas* phage endolysin sequence as query and PDB structures database as reference dataset. PDB structure having more that 40% identity and minimum E-value was selected as template.
- **Single or multiple sequence alignments:** CLUSTAL W was used for alignment of query and template sequence.
- **Model building for the target based on the 3D structure of the template:** Homology model was generated by SWISS-MODEL using PDB ID 6ET6 (*Acinetobacter baumanii* endolysin) as template.
- **Model refinement, analysis of alignments, gap deletions and additions**
- **Model validation**

Results:

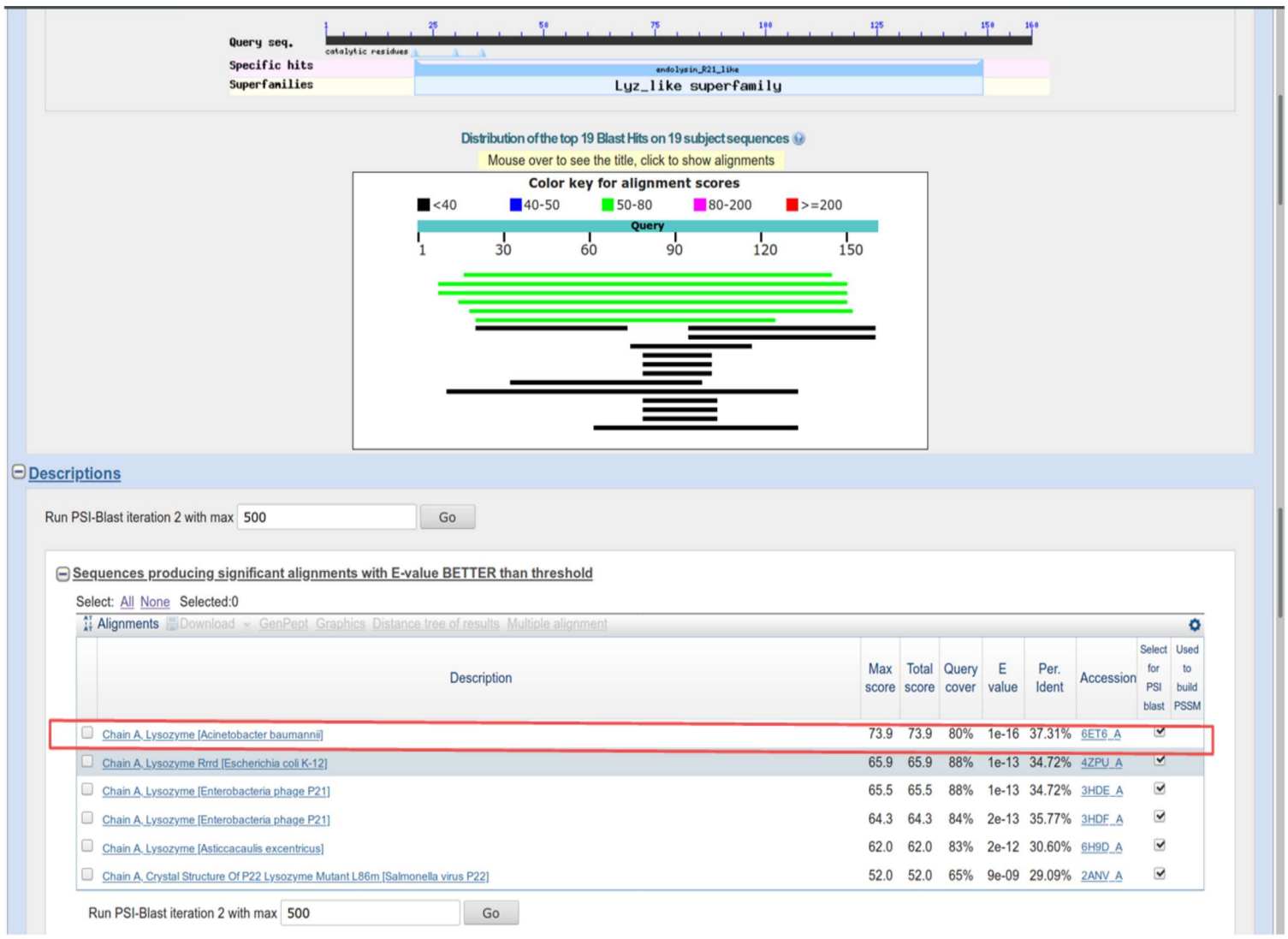

Figure 5: PSI-BLAST result for *Pesudomonas* phage endolysin.

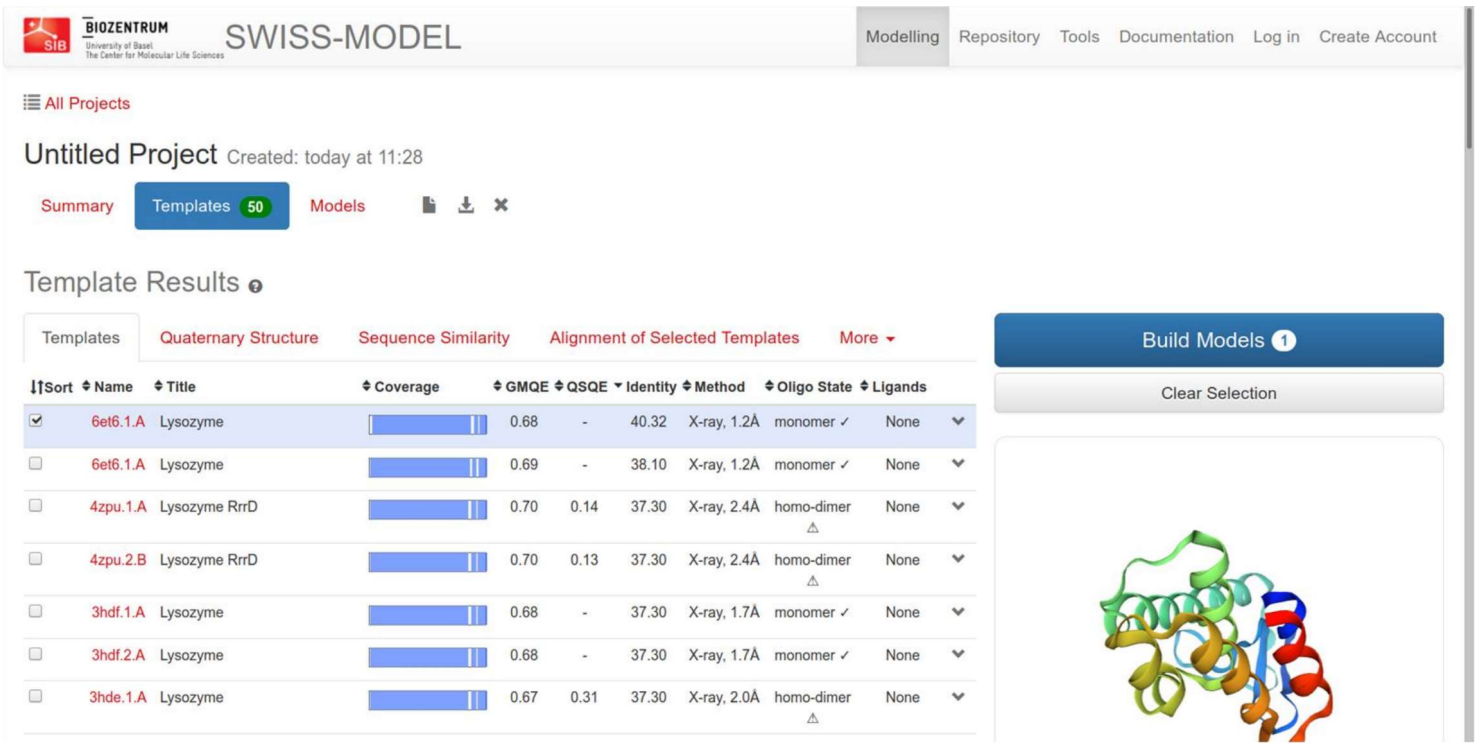

Figure 6: Template selection using SWISS-MODEL.

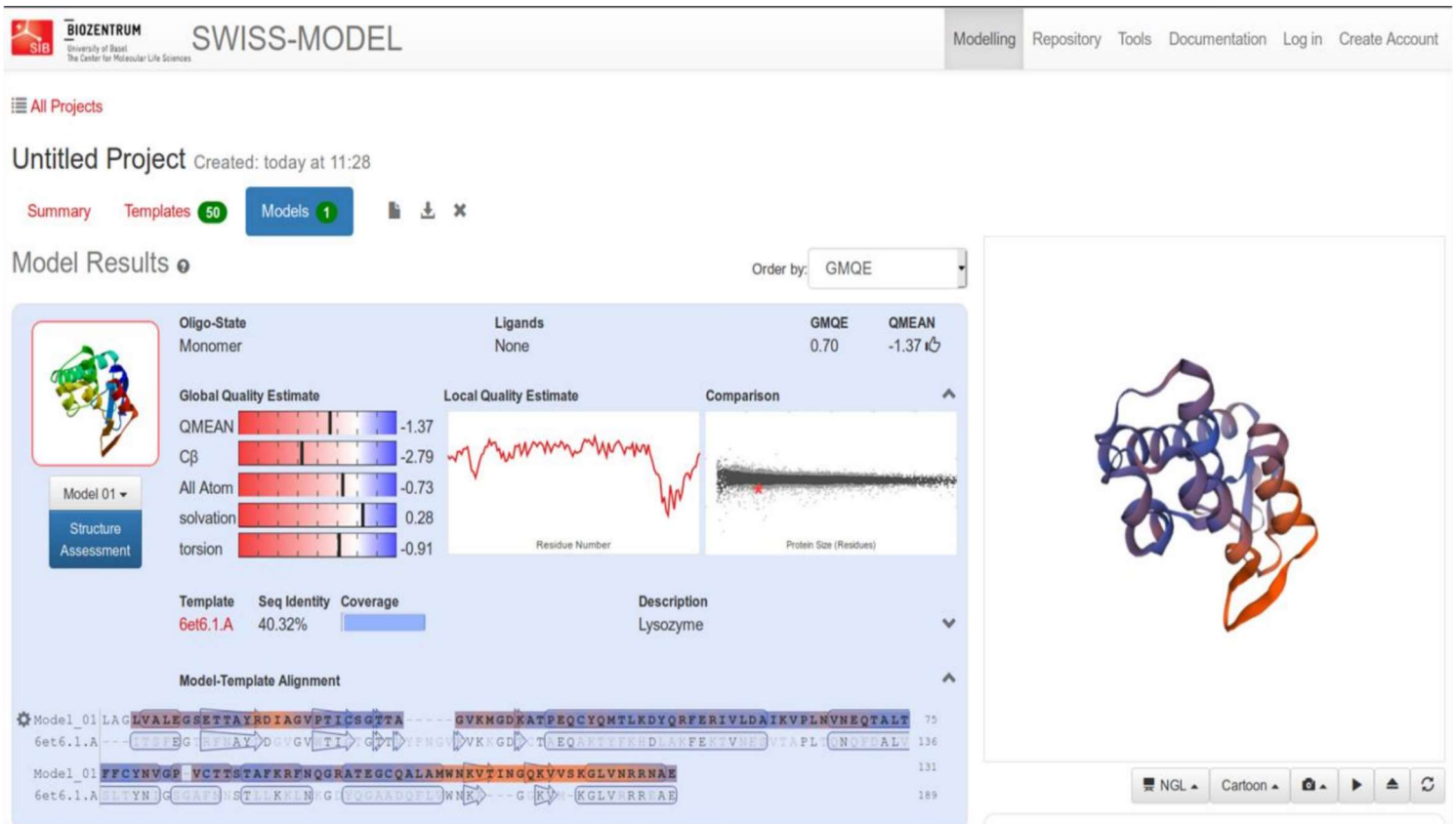

Figure 7: Homology model generation by SWISS-MODEL.

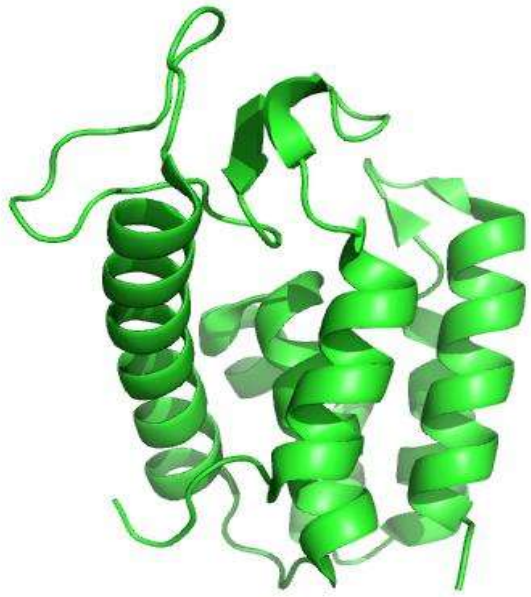

Figure 8: 3D structure of *Pseudomonas* phage endolysin generated by SWISS-MODEL.

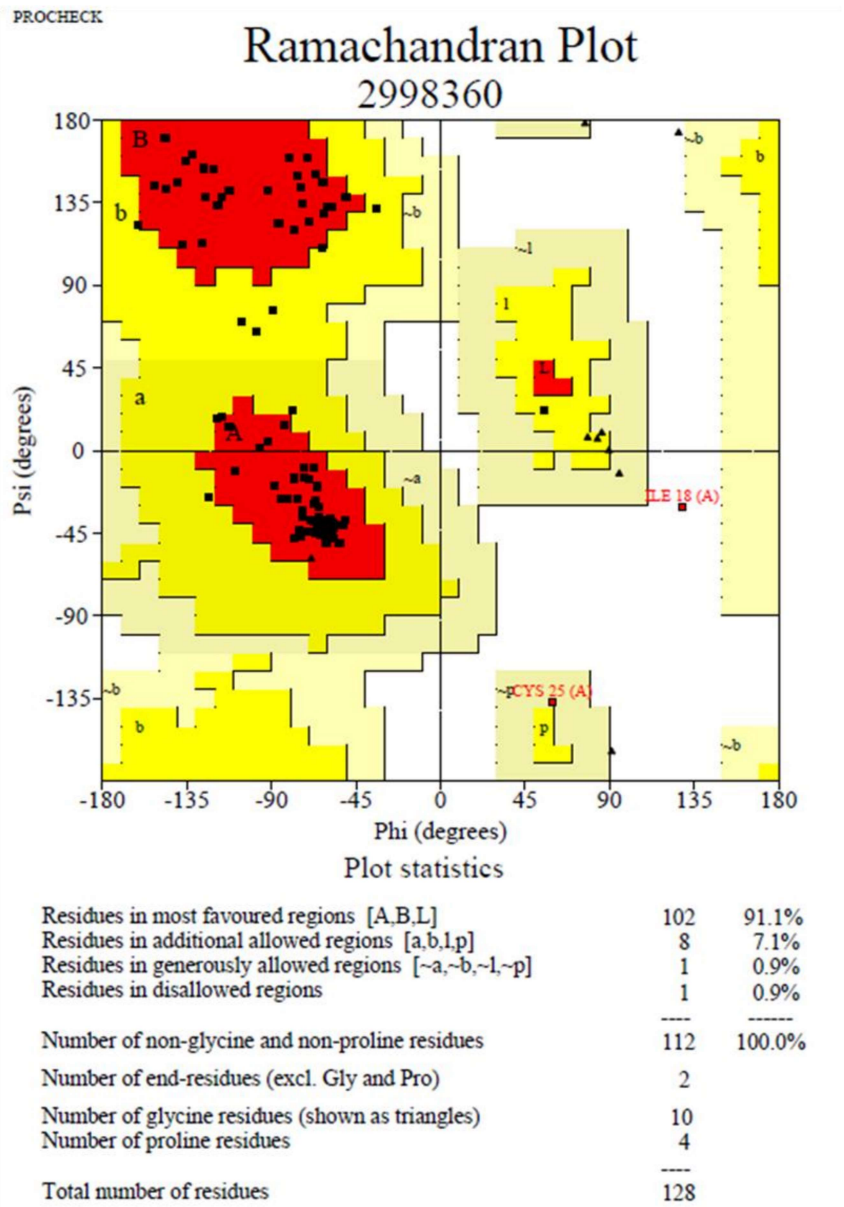

Figure 9: Procheck results of generated 3D structure *Pseudomonas* phage endolysin protein.

3D Structure determination of *Pseudomonas* phage endolysin protein was produced by SWISS-MODEL and validated by Procheck online tool. The procheck results of modelled 3D structure shows almost 99% amino acids are in favorable and allowed region of Ramachandran plot.

Endolysin:

Endolysin are encoded by double stranded DNA bacteriophage during the late phase of gene expression in the lytic cycle to degrade the host peptidoglycan. First phage encoded endolysin was found from *S. aureus* infecting phage. Endolysins are also effective in rapid lysis of bacterial cell when applied externally as a purified recombinant protein. Hence, they can serve as alternative of current antibiotics Endolysins have a broader host range that's makes them preferable for treatment of various bacterial infections. Phage endolysins exert their uniqueness on the basis of three factors namely, a) enzyme activation by specific components present in host cell wall, b) specificity in substrate recognition and cell wall binding, c) Cleave unique linkages.

Endolysins can cleave peptide or amide, glyosidic bonds present in bacterial peptidoglycan. On the basis of specific linkage endolysins cab be classified into following categories: (a) N-acetylmuramidases; (b) endo-β-N-acetylglucosaminidase; (c) endopeptidase; (d) trans glycosylase; and (e) N-acetylmuramoyl-L-alanine. Among several classes of endolysins, amidases (also called N-acetylmuramoyl-L-alanine amidases) are known for their rapid lysis activity. Majority of endolysins infecting gram -negative bacteria are 15-20 kDa single domain globular proteins consisting of single catalytic domain.

Purification of endolysin proteins:

- *E. coli* BL21 cells were transformed with a plasmid containing gene for endolysin.
- The large culture (500ml) was grown at 37^0C and 220 rpm to an OD of 0.4-0.5 using saturated overnight 10 ml seed culture, induced with 0.5mM isopropyl β-D-1-thiogalactopyranoside (IPTG), and incubated at 37^0C and 220 rpm for an additional 4 hrs.
- Cells were harvested by centrifugation at 6000 rpm for 10 min, resuspended in 50 ml of phosphate buffer (pH 8) and treated with PMSF(100mM) and BME(1mM).
- Cells were sonicated and then centrifuged at 14000rpm for 1 hour at 4^0C.
- Proteins were purified separately by a combination of ion-exchange chromatography using DEAE (Bio-Rad) and size exclusion chromatography. After sonication and centrifugation, the cell supernatant was applied onto DEAE column pre-equilibrated with phosphate buffer [20 mM phosphate (pH 8), 1 mM EDTA, 4 % glycerol and 10 mM NH_4Cl].
- The flow-through (FT) was collected after passing the supernatant for three to four times through the column.
- The column was then washed with equilibration buffer, and equilibration buffer + 0.5 M NaCl (W2).
- Protein fractions were then dialyzed overnight phosphate buffer [20 mM phosphate (pH 7.0), 0.1 M NaCl and 5 mM EDTA pH 7.0].

- Protein fraction was further passed through size exclusion chromatography (SEC) using Superdex 200 prep grade column in 20 mM phosphate buffer containing 0.1 M NaCl, 5 mM EDTA and 1 % glycerol (pH 7).
- The pure protein fractions were collected and concentrated using Centricon tubes (10 kDa cut off membrane-Millipore).
- The purity of endolysin protein was assessed using a 12 % SDS-PAGE gel, and the exact concentrations of endolysin protein was obtained spectrophotometrically using molar extinction coefficient's of 26470 M^{-1} cm^{-1}.

Results:

Pure Phage endolysin of molecular weight 17 KDa was overexpressed and purified using ion-exchange chromatography using DEAE (Bio-Rad) and size exclusion chromatography**.**

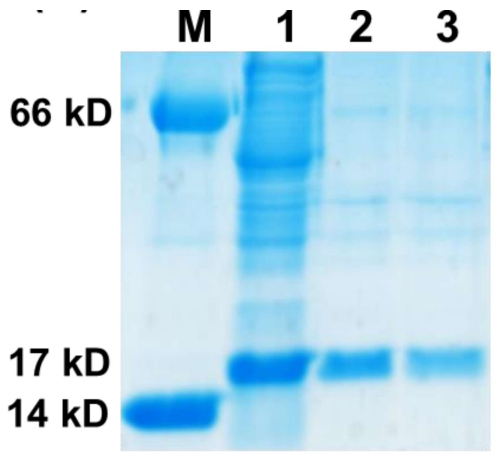

Figure 10: 12 % SDS-PAGE gel analysis of endolysin (17 kD) purification using DEAE ion-exchange chromatography. Lane M represents the marker (BSA=66 kDa, and HEL=14 kDa), Lane 1: cell lysate; Lane 2: flow through, and Lane 3: wash with equilibration buffer; Both Lane 2 and Lane 3 containing the proteins of interest.

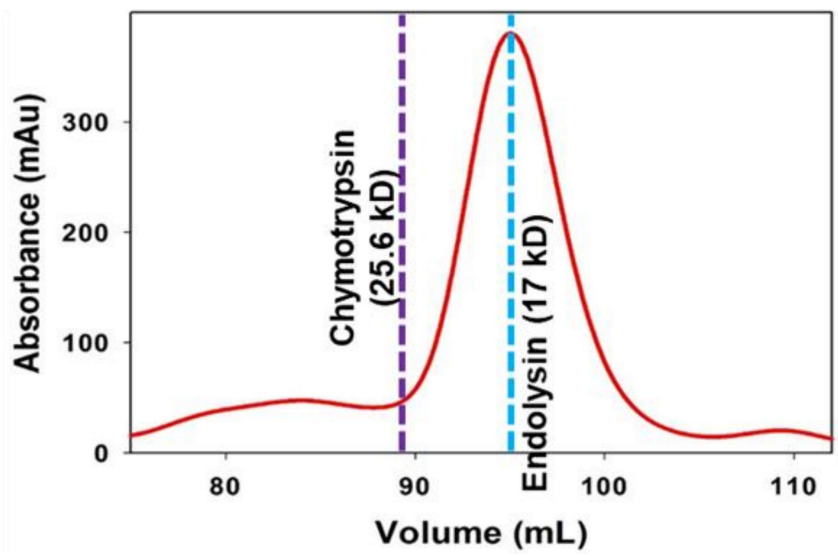

Figure 11: Size exclusion chromatography (SEC) based purification of endolysin.

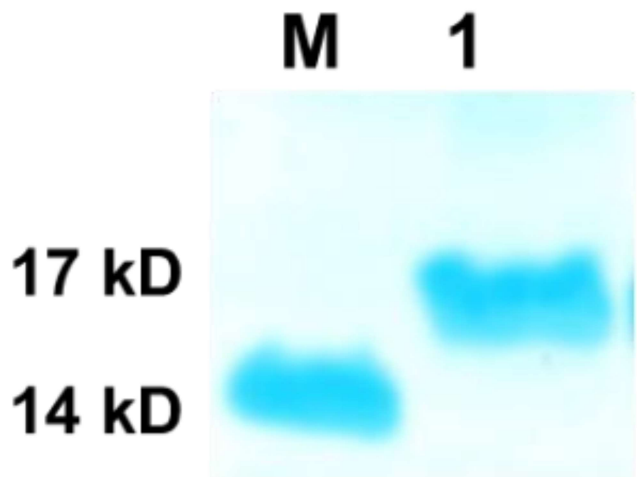

Figure 12: SDS-PAGE gel of pure endolysin protein (Lane 1) obtained after SEC.

Phage endolysin of molecular weight was overexpressed and purified using ion-exchange chromatography using DEAE (Bio-Rad) and size exclusion chromatography for functional (Antimicrobial) study.

The therapeutic use of phage -encoded endolysins have increased in the last decade due to enhanced difficulties in the treatment of antibiotic-resistant strains of bacteria and due to the urgent need of alternative antimicrobial compounds that can combat emerging multidrug – resistant bacterial pathogens. Endolysins are regarded as the potential antibacterial agents in food science (Bio preservatives), bio control agents (disinfectants).

The susceptibility of the microbial cells to the endolysin was determined by micro broth dilution assays of endolysin protein with inoculations of approximately 10^5 colony forming units per milliliter (CFU/mL) of the respective organisms. Further to validate the bacterial lysis of the *Pseudomonas* bacteria, the endolysin activity and the cell lysis behavior was monitored against *Pseudomonas aeruginosa* bacterial cells (MTCC 1688) using Scanning electron microscope (SEM) and Atomic force microscope (AFM) techniques. The bacterial samples were prepared stepwise, followed by their deposition on glass slides. The samples for SEM were pre-coated with gold film. For AFM sample preparation, drop coating method was used; a drop of bacterial sample (treated or untreated) was spread on a glass slide, dried at room temperature and visualized under the atomic force microscope.

Endolysins infecting Gram-Negative bacteria:

They possess single -domain structure of an EAD/ or Catalytic domain. They are shorter in length with 15-20 kDa in weight and are globular proteins. PG of gram negative located between OM and periplasmic space so it is devoid of surface protein and carbohydrate which limits the access to PG from outside and might be the reason of having single domain. Few Gram negative endolysins are reported to have modular domain structure e.g.: Endolysin KZ144 (P. aeruginosa phage ϕ KZ), EL188 (P. aeruginosa phage EL) composed of N-terminal CWD and C-terminal EAD. (Whereas another P. aeruginosa Lu 11 endolysin has N-terminal

EAD and C-terminal CBD. The possible reason for such modular structure could be explained by the early phage evolution phenomenon which suggests that different domain coding genes modules were exchanged between phages during era of early phage evolution and further rearrangement of gene fragments gave rise to new protein with diverse combination.

Determination of MIC:

- MIC tests were performed by a standard broth microdilution assay in microtiter plates to find out which sub- and supra-MICs should be used to treat the bacteria for the lysis studies.
- Serial dilutions of the lysozyme were made in salt-free Luria broth (LB) medium, containing 10 g/liter tryptone and 5 g/liter yeast extract, but no salts, Test cultures, inoculated with cells grown overnight, were obtained in standard LB medium with 10 g/liter sodium chloride by cultivation up to mid-exponential growth phase.
- The cells were then resuspended in salt-free LB medium for inoculation of microtiter plates.
- The wells of the microtiter plates, filled with lysozyme dilutions in salt-free LB medium, were then inoculated with 200µL of the test organism up to the desired inoculation density.
- After incubation at 37°C for 20 h, the MIC was taken as the lowest concentration at which no growth was observed.

Results: MIC value for *Pseudomonas aeruginosa* strain was determined to be in range of 50 -100 µg/mL.

pH based Cell Lysis Turbidity Assay of Endolysin:

- To perform the assay, bacterial cells were cultivated in 10 ml of LB medium and allowed to grow at 37·C until (OD 0.6-0.8).
- The cells were treated with 0.1M EDTA for 5 min at room temperature and divided into 1ml aliquots, pelleted by a brief centrifugation and resuspended in 1 ml of buffer (10mM potassium phosphate buffer and 10µM $ZnSO_4$.
- pH dependent amidase activity was measured with 500µL of cell suspension(OD~0.7) by adding 50µg of endolysin.
- For all the samples absorbance was measured at 600nmin 1 min interval at room temperature with regular mixing with a micropipette after each reading.
- The experiments were performed in triplicates and for control no enzyme was added and cells were monitored for the total experimental period of 10-15 min.

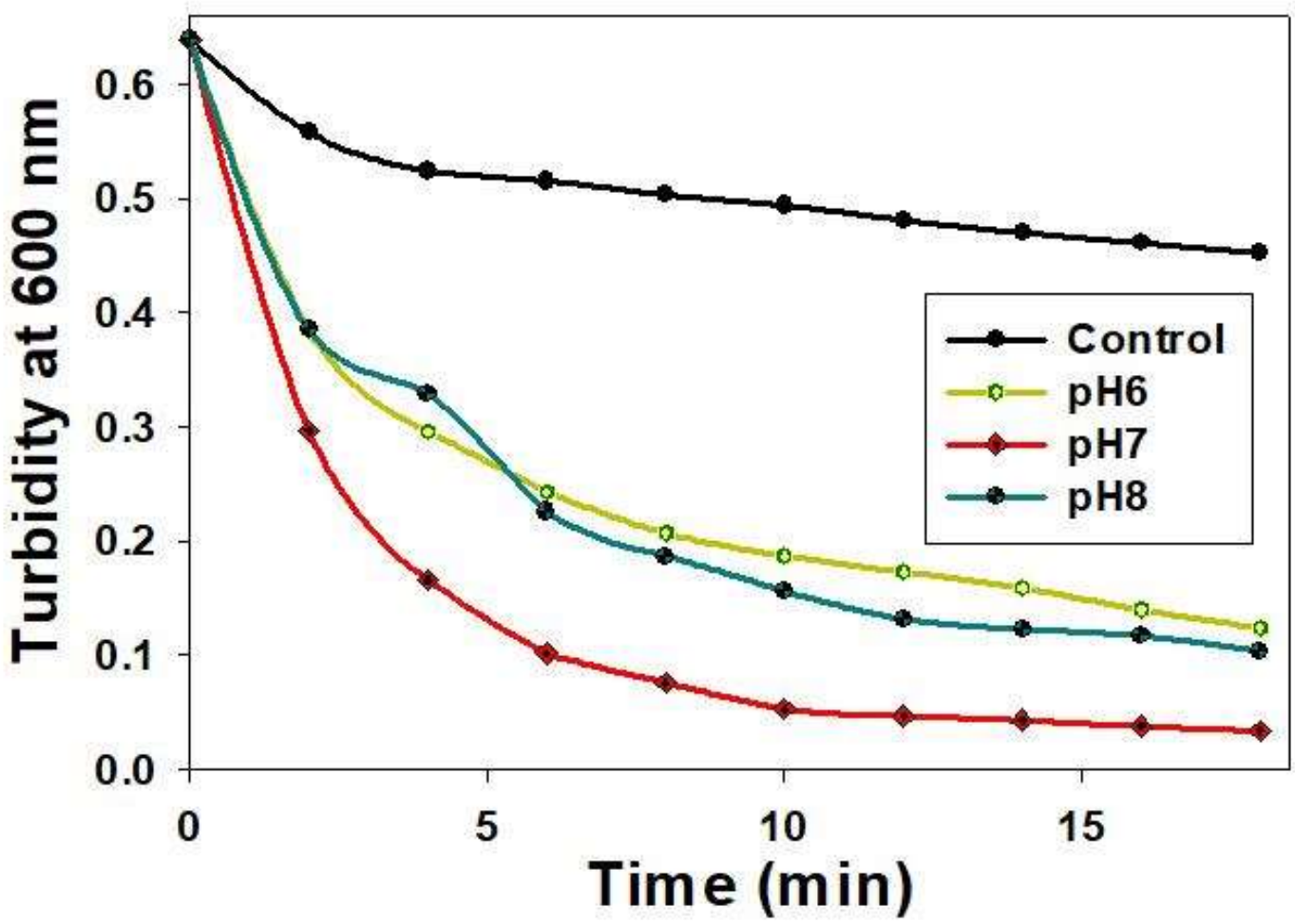

Figure 13: Turbidimetric assay depicting the lysis of *P.aeruginosa* bacterial cells treated with endolysin at different pH.

Cell Lysis Turbidity Assay against different bacteria:

- To perform the cell lysis assay, *P.aeruginosa* bacterial cell were cultivated in 10 ml of LB medium and allowed to grow at 37˚C until (OD 0.6-0.8).
- The cells were treated with 0.1M EDTA for 5 min at room temperature and divided into 1ml aliquots, pelleted by a brief centrifugation and re suspended in 1 ml of buffer (10mM potassium phosphate buffer and 10µM $ZnSO_4$.
- pH dependent amidase activity was measured with 500µL of cell suspension(OD~0.7) by adding 50µg of endolysin.
- For all the samples absorbance was measured at 600nmin 1 min interval at room temperature with regular mixing with a micropipette after each reading.
- The experiments were performed in triplicates and for control no enzyme was added and cells were monitored for the total experimental period of 10-15 min.

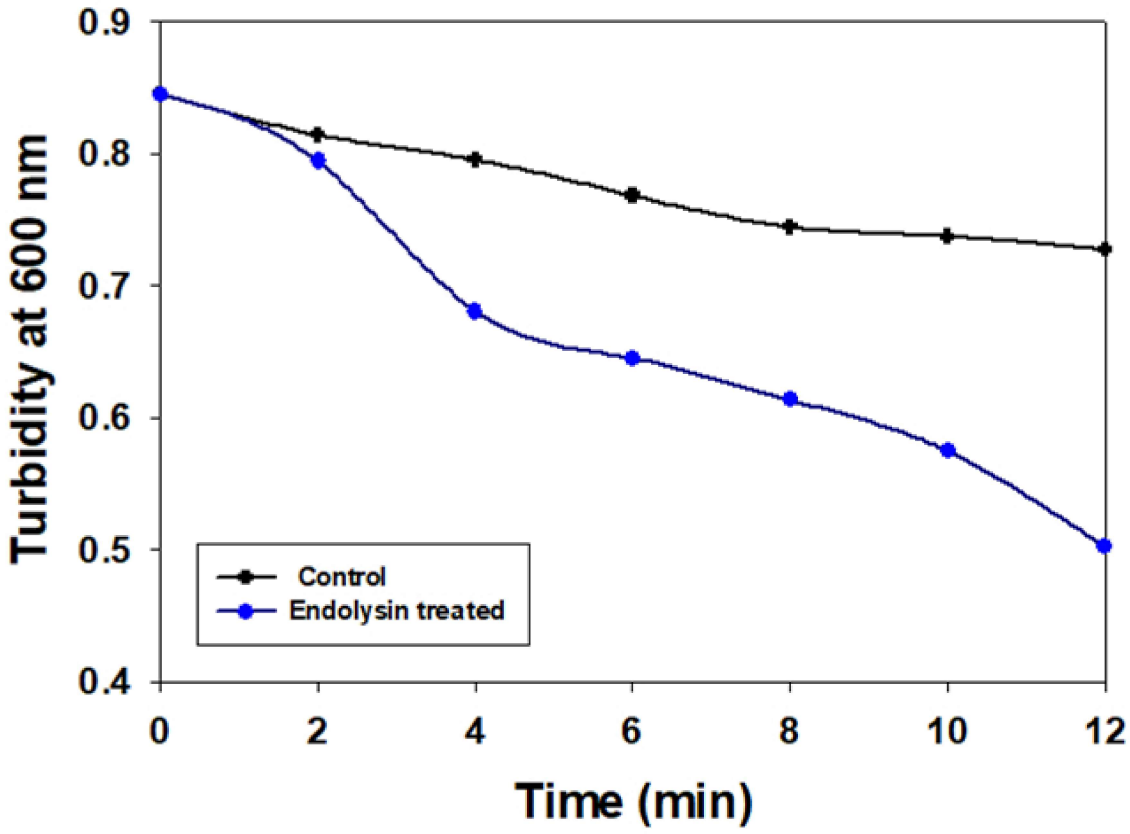

Figure 14: Turbidimetric assay depicting the lysis of bacterial cells treated with endolysin at pH7 against *E. coli* bacterial cells.

The MIC value of endolysin against *Pseudomonas aeruginosa* bacterial strain was obtained in the range of 50 -100 µg/mL. The antibacterial efficiency of phage endolysin was successfully established by turbidimetric assay depicting the lysis of bacterial cells treated with endolysin at different pH (pH 6, pH 7, pH 8).

Bacterial cell microscopy:

Versatile types of microscopic techniques have been employed in various biomedical fields such as microbiology, biochemistry which have enabled the researchers to study the detailed morphology dependent functional features of biomaterials. Scanning electron microscopy (SEM) and atomic force microscopy (AFM) of *P.aeruginosa* bacterial strain was carried out to observe changes in surface morphologies of the bacterial cells after treatments with the antibacterial agents. The bacterial samples were prepared stepwise, followed by their deposition on glass slides. The samples for SEM were precoated with gold film.

SEM is one of the electron microscopic technique which utilizes high intensity electron beam to record images by targeting focused electron beam onto their surface. When this electron beam interacts with simple they reflect secondary and backscattered electrons with different kinectic energies that are detected by befitting detector. AFM is a very high –resolution type of scanning probe microscopy with resolution upto nanometer range. AFM have application in

various disciplines of sciences including molecular and cellular biology, and medicines. In cellular biology, AFM can be used to distinguish infected cells and normal cells based on hardness of cells.it can be used to indent cells o study how they regulate the stiffness of the cell wall or cell membrane. For AFM sample preparation, drop coating method was used; a drop of bacterial sample (treated or untreated) was spread on a glass slide, dried at room temperature and visualized under the atomic force microscope.

Preparation of bacterial cell sample for SEM:

- Carl Zeiss Gemini FE-SEM was used to study the morphological changes in control and lysozyme treated bacteria.
- Bacterial cells at mid exponential phase were treated with lysozyme for 10 min, followed by centrifugation for 5 min at 6000rpm.
- The pellet was washed thrice with 200 µl Mili Q water and finally suspended in 20µl Mili Q water.
- 10 µl of this was smeared on fresh glass slide and fixed with 2.5% glutaraldehyde followed by gradient washing with ethanol and finally re-suspended in water, and then deposited onto glass slide as a droplet.
- Untreated controls were prepared in buffer only.
- The smear was air dried at room temperature and then sputtered with gold to ensure appropriate conductivity of the sample for analysis.

Preparation of bacterial cell sample for AFM:

- AFM was used to study the roughness, rigidity in control and lysozyme treated bacteria.
- Bacterial cells at mid exponential phase were treated with lysozyme for 10 min, followed by centrifugation for 5 min at 6000rpm.
- Untreated controls were prepared in buffer only. For sample preparation, the pellet was washed thrice with 200 µl Mili Q water and finally suspended in 20 µl Mili Q water.
- 10 µl of this was smeared on fresh glass slide and fixed with 2.5% glutaraldehyde followed by gradient washing with ethanol and finally re-suspended the cells in water, and then deposited onto glass slide as a droplet.

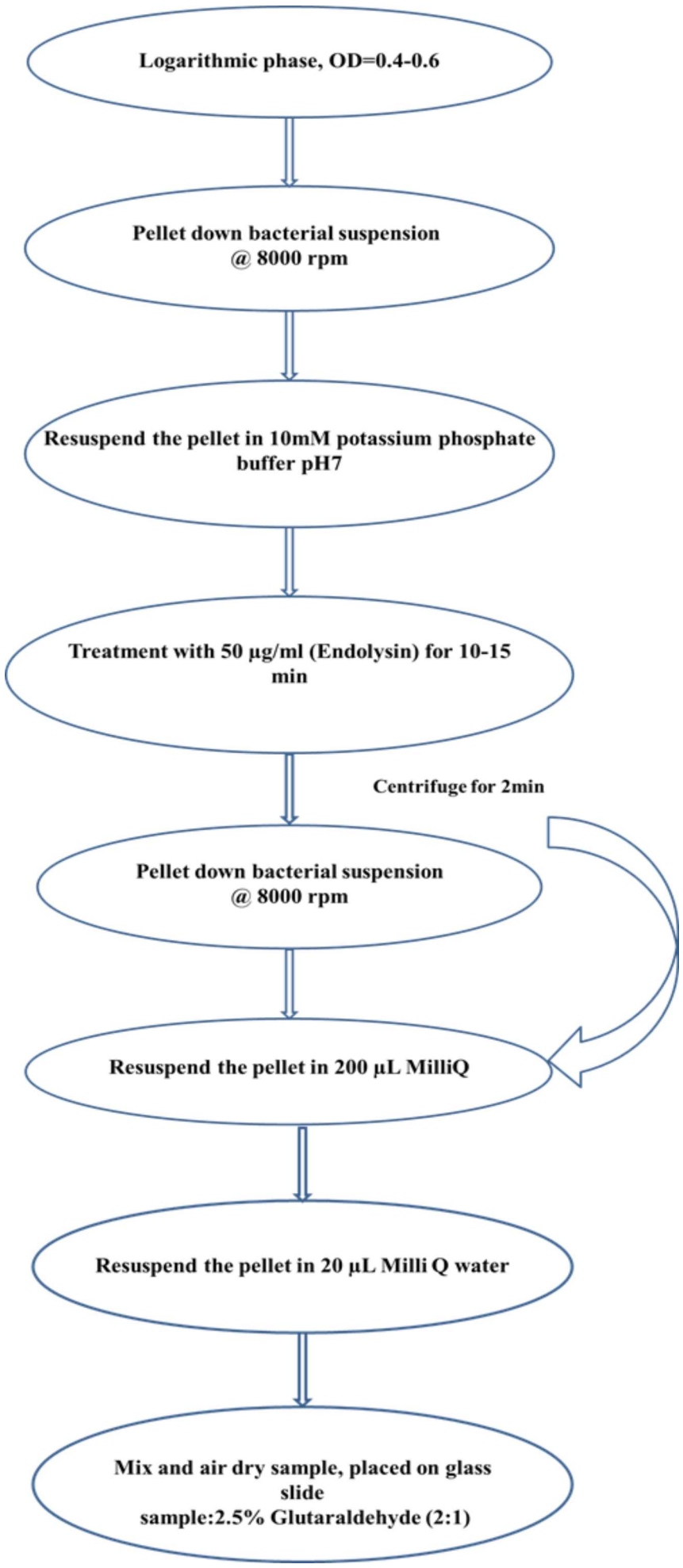

Figure 15: Schematic showing protocol for preparation of bacterial cells for SEM analysis.

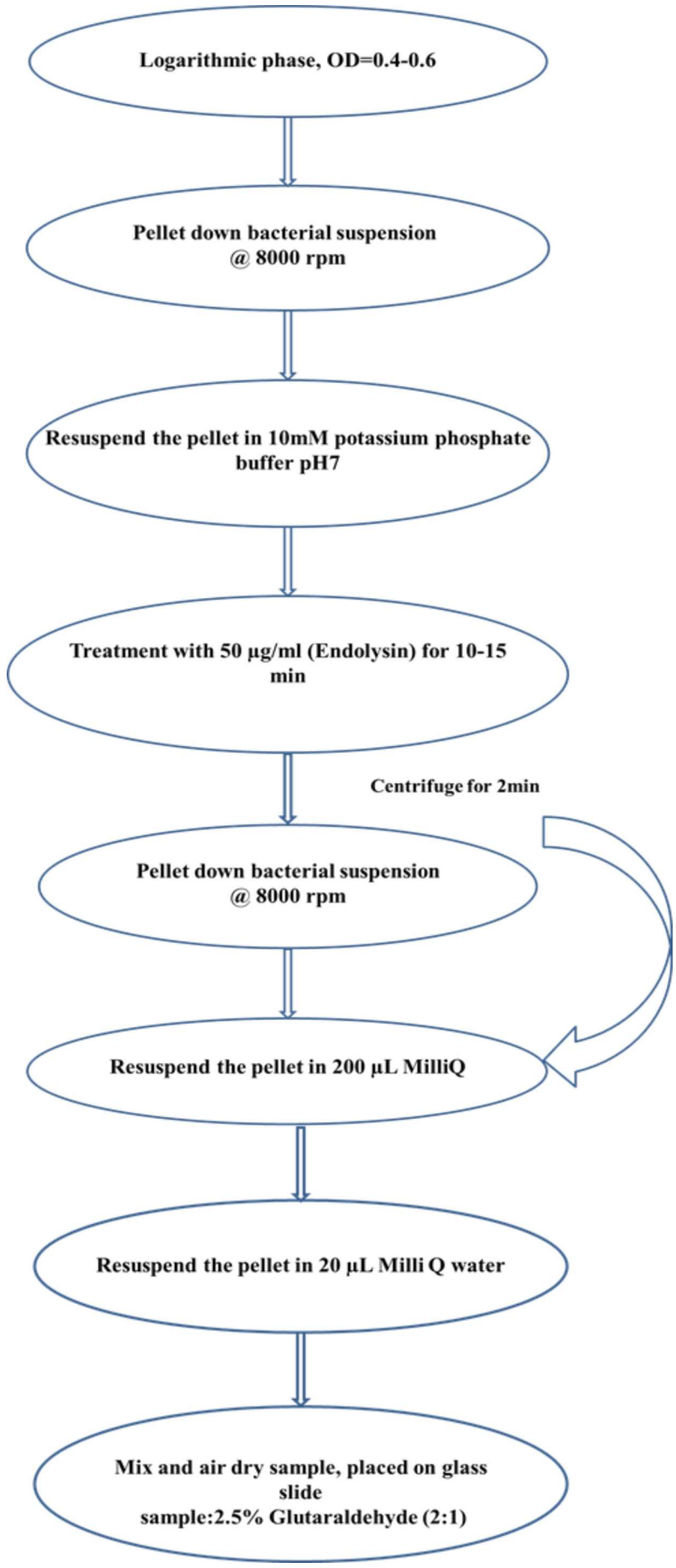

Figure 16: Schematic showing protocol for preparation of bacterial cells for AFM analysis

Results:

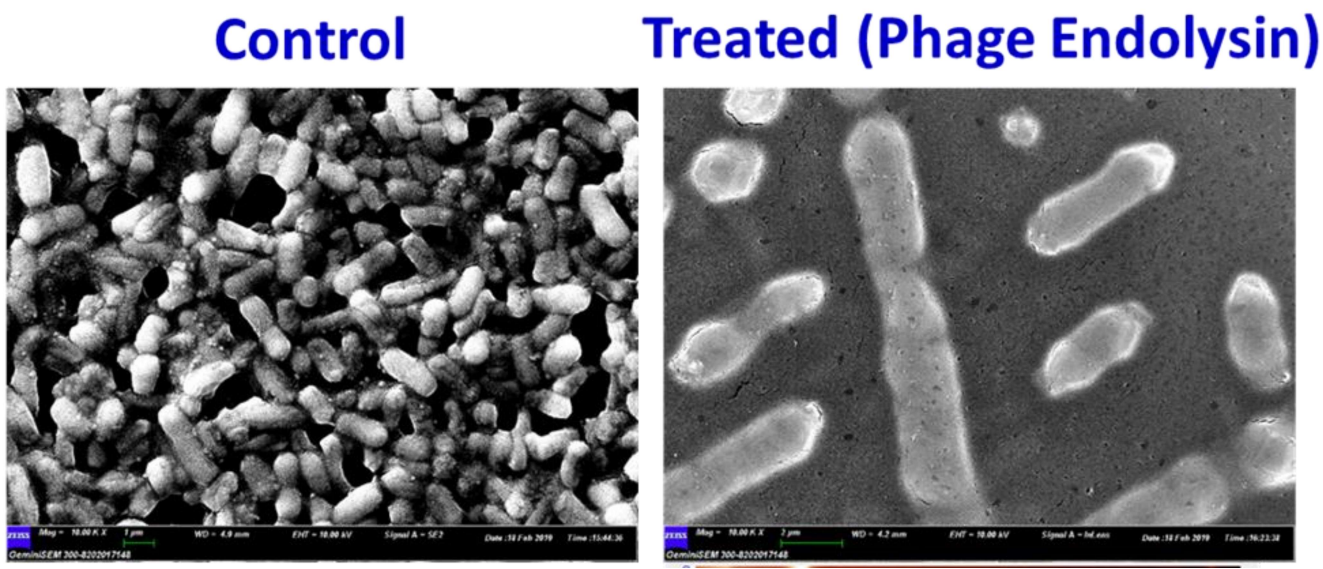

Figure 16: SEM microscopic images showing control (left) and phage endolysin treated (right) *P.aeruginosa* bacterial cells.

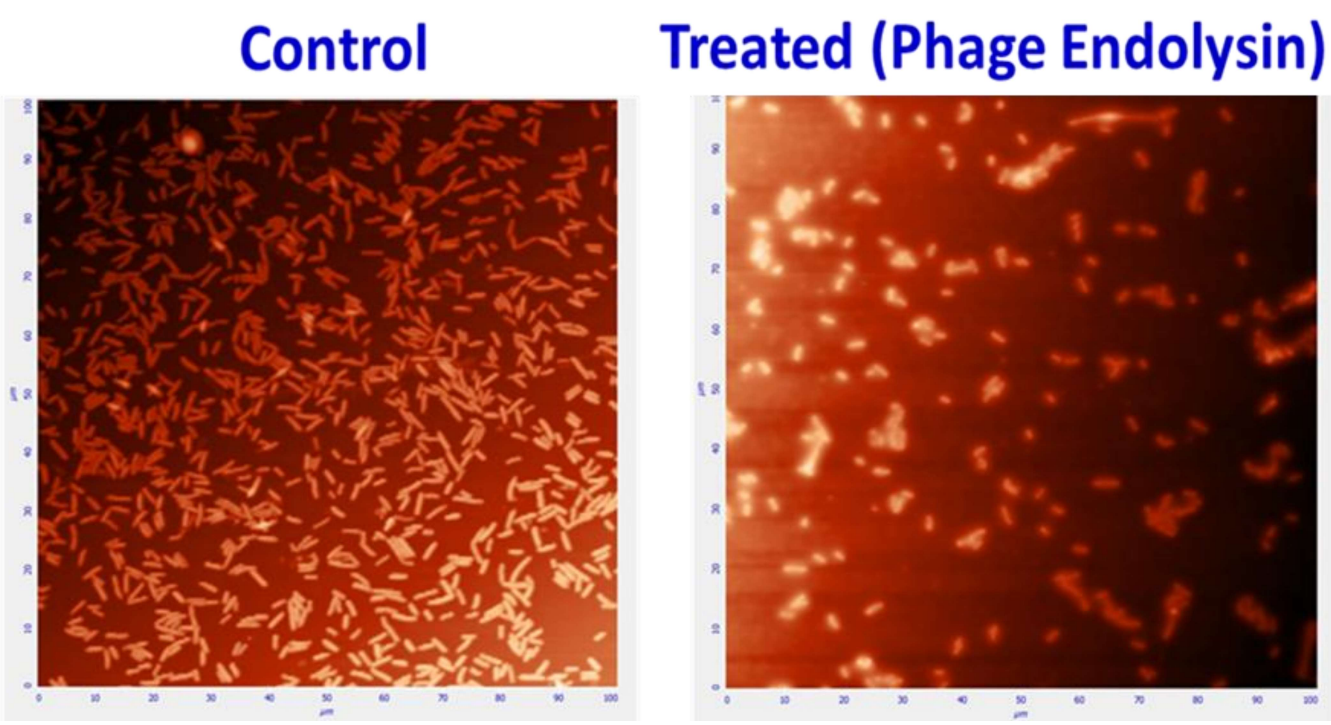

Figure 17: AFM images showing control (left) and phage endolysin treated (right) *P.aeruginosa* bacterial cells.

The antimicrobial efficiency of phage endolysin against *P. aeruginosa* bacterial strain was positively verified with two different microscopic techniques such as SEM and AFM. The bacterial cell count was reduced after the treatment of endolysin which can be visualized in SEM and AFM.

Quantifying bacterial cell lysis using GFP based fluorimetric assay:

Quantitative elucidation of antimicrobial or cell lysis properties of a given protein, peptide, nanomaterial or a small molecule is essential to compare and contrast their potencies. Antimicrobial potencies of such molecules are very sensitive to the given physiological/environmental conditions such as membrane/peptidoglycan composition, pH, temperature, salt concentrations and presence of different metal ions. Turbidimetric assay and flow cytometry are the most routinely used techniques to determine/quantitate cell viability or lysis. Turbidimetric assay, which is performed using an absorption spectrometer quantifies the cell lysis based on the decrease in turbidity (optical density) or cell density at around 600 nm wavelength. On the other hand, flow cytometry is a cell counting technique that sorts the heterogeneous mixture of cell populations and quantifies the individual populations based on the intensity of fluorescence markers. Although these techniques are robust, they do have some practical limitations. For example, the turbidimetric assay stands in need of high density of cells to accomplish significant signals, whereas flow cytometry is a very complex and expensive method that requires a high level of maintenance and training.

Henceforth, an alternative, quick and economical method to detect and quantify the antimicrobial activity of endolysins and other antimicrobial agents is indeed beneficial. Steady-state fluorescence spectroscopy is a very robust quantitative technique that has been commonly used to quantitate the parameters related to protein denaturation, DNA melting, ligand binding, and biomolecular interactions, etc. It is well established that fluorescence property of green fluorescent protein (GFP) has been used as a marker for different cell type death as well as to track various biological processes such as cancer, organogenesis, tissue remodeling, protein localization and cellular dynamic, etc. Owing to this remarkable fluorescence property, GFP encoding gene was expressed specifically along with the target gene or genetically incorporated in the genome of host cells in order to make them fluorescent.

Measurement of supernatant GFP fluorescence (peak intensity) under a given environmental condition or an antimicrobial agent (bacteriophage endolysins in the present study) is proportional to the extent of cell lysis. This also infers that once the background fluorescence is subtracted from control cells, only lysed cells results in GFP emission peak. Normalization of intensity profiles with respect to completely lysed cells will provide the percentage of lysis or the antimicrobial efficiency. Over the other techniques, fluorescence spectroscopy has several advantages such as 1) Rapid measurement and precise quantification; 2) Specific signal pattern from known fluorophore; 3) Low cell/sample concentration; 4) Ease of working with different antimicrobial agents/cell types at various environmental conditions.

Two different bacteriophage endolysin family members namely T7 endolysin (T7L) and T4 endolysin (T4L) that are known to lyse *E. coli* cells were chosen to analyze the antimicrobial activity using this GFP-based fluorescence approach. These two endolysins are not only differing

at the cleavage site of the peptidoglycan layer but also vary in their mode of actions due to their distinct 3D structural organizations and catalytic sites. Henceforth, T7L and T4L represent diverse phage endolysin protein family members to elucidate cell lysis phenomenon using the GFP-based quantitative fluorescence detection method.

Methods:

Protein expression and purification:

The pAR4593 plasmid containing T7L gene was used for the expression of wild type T7L. For T4L expression, plasmid pHS1403 (Addgene #18110) containing T4L gene sequence was used. Bacteriophage-encoded endolysins, T7L and T4L were grown and expressed in *E. coli* at 37 ºC. Proteins were purified separately by a combination of ion-exchange chromatography using DEAE (Bio-Rad) and size exclusion chromatography. After sonication and centrifugation, the cell supernatant was applied onto DEAE column pre-equilibrated with phosphate buffer [20 mM phosphate (pH 8), 1 mM EDTA, 4 % glycerol and 10 mM NH_4Cl]. The flow-through (FT) was collected after passing the supernatant for three to four times through the column. The column was then washed with equilibration buffer, and equilibration buffer + 0.5 M NaCl (W2). Protein fractions were then dialyzed overnight phosphate buffer [20 mM phosphate (pH 7.0), 0.1 M NaCl and 5 mM EDTA pH 7.0]. T7L and T4L were further passed through size exclusion chromatography (SEC) using Superdex 200 prep grade column in 20 mM phosphate buffer containing 0.1 M NaCl, 5 mM EDTA and 1 % glycerol (pH 7). The pure protein fractions were collected and concentrated using Centricon tubes (10 kDa cut off membrane-Millipore).The purity of T7L and T4L were assessed using a 12 % SDS-PAGE gel, and the exact concentrations of T7L and T4L were obtained spectrophotometrically using molar extinction coefficient's of 26470 M^{-1} cm^{-1} and 25440 M^{-1} cm^{-1} respectively.

Preparation of GFP expressing *E. coli* cells:

The plasmid (Addgene #29663) encoding mEGFP gene was transformed in *E. coli* BL21 (DE3) cells. mEGFP expressing cells were then grown at 37 °C in LB broth containing kanamycin (50 µg/mL). The bacterial cells were allowed to grown until it reached its exponential phase (0.5-0.6 OD_{600}). Expression of the GFP was induced using 0.5 mM IPTG, and further grown for 3 h at 37 °C. Cells were sensitized with 0.1 M EDTA for 5 min at 25 °C. Aliquots (2 mL) of cell culture were transferred to microcentrifuge tubes and pelleted by centrifugation at 6000 rpm for 10 min at 4 °C. The pellets were gently washed twice with 200 µL of 0.9 % saline, resuspended in 1 mL of 10 mM potassium phosphate buffer and stored at -20 °C. To assess the antimicrobial activity 50 µg of proteins (T4L / T7L) were added into the *E. coli* cell suspensions and incubated for 15 min at room temperature. The cell suspensions were immediately centrifuged (6000 rpm) for 10 min at 4 °C. The supernatants were recovered for the fluorescence spectroscopic analysis and pellets were used for fluorescence-based microscopic analysis.

Sample preparation:

To perform the pH dependent experiments, cell pellets were resuspended in 1 mL of 10 mM potassium phosphate-acetate buffer (pH 5-8). The influence of salt on the enzyme activity was studied by incubating the cells in a buffer (pH 7) containing NaCl concentrations of 50 mM, 100 mM, 500 mM, 1 M, and 2 M. For T7L protein based pH dependent and salt-dependent lysis studies, additionally 1 mM $ZnSO_4$ was also added into the samples. All the experiments were conducted thrice at room temperature with independent cultures.

GFP based Fluorescence spectroscopy:

GFP fluorescence at different pH (pH 5-8) and NaCl concentrations was quantified using a Hitachi F-4600 fluorescence spectrophotometer with excitation at 480 nm and the emission was collected from 490 - 600 nm using of 2.5 nm excitation/emission slit widths. The fluorescence emission of untreated bacterial cell suspensions at 509 nm (λ_{max}) was used to subtract the background fluorescence from the emission profiles of T7L and T4L treated samples. To investigate the reproducibility of GFP emission levels, fluorescence measurements were repeated thrice using cell suspensions prepared from independently grown cultures. For all the cell lysis assays (pH and salt dependent) using fluorescence spectroscopy measurements, the pH of the cell supernatants were measured using micro electrode, and were adjusted to the reported pH value, as both GFP and the endolysins (T4L and T7L) are highly sensitive to pH. Further, the observed fluorescence intensities were corrected/normalized by using the fluorescence emission profiles of GFP in the absence of enzyme (endolysin) under these conditions. The percentage relative enzyme activity was calculated compared to the untreated sample using Sigma Plot 12.0 software.

Fluorescence microscopy:

Fluorescence imaging of GFP containing living cells was done by using Axio Scope A1 (Carl Zeiss) fluorescence microscope under various conditions (such as pH, salt, and metal ions). Pellets were washed twice with 200 µL of 0.9 % saline and finally resuspended in 200 µL of saline. 10 µL was taken from each homogenous suspension, placed and air-dried over the microscope slides for microscopic analysis. Images were captured under a 100x oil immersion objective lens using a GFP observation filter and reconstructed/analyzed with Zen software (Zeiss).

Turbidimetric assay:

For the turbidimetric assay, *E. coli* cell suspensions were treated with 50 µg of T7L /T4L proteins. This assay was performed as described elsewhere. All the experiments were repeated at least thrice, and the pH of all the samples was corrected before performing cell lysis assays. The percentage relative enzyme activity was calculated compared to the untreated sample using Sigma Plot 12.0 software.

Results:

The GFP based fluorescence approach is broadly comprised of two steps: (a) generating a GFP based cell system and (b) monitoring the lysis behavior in the presence of antimicrobial agents (T4L / T7L) by measuring the GFP fluorescence. The overall protocol with step-wise details has been presented as a schematic in Fig. 18. The first step of generating a particular type of GFP expressing bacterial cells is a onetime process, and can be achieved by transforming GFP containing plasmid into the cells or by genetic modification.

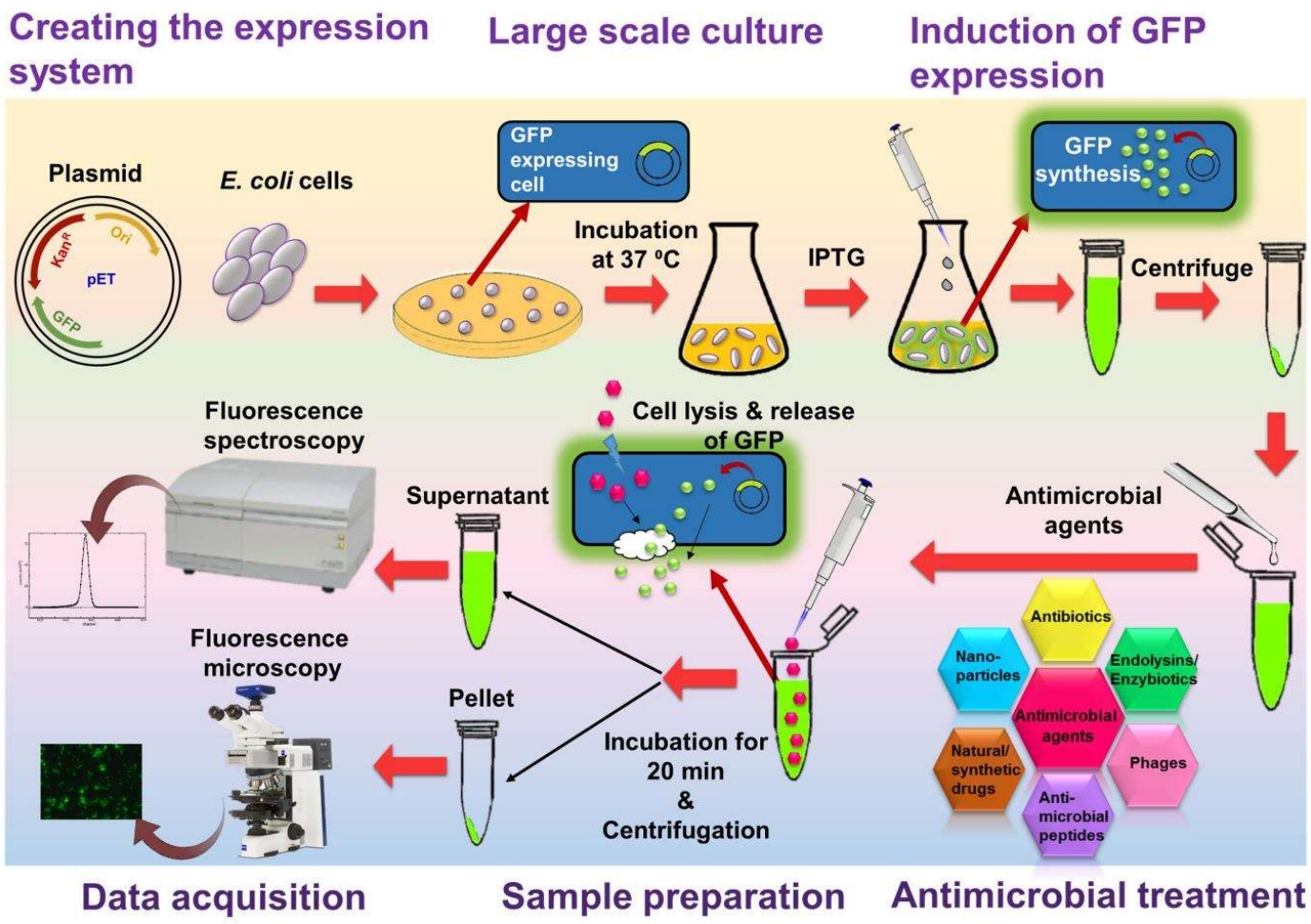

Figure 18: Schematic representation of the steps involved in the proposed method for the quantification of cell lysis using GFP-based fluorescence detection.

A pET vector containing GFP has been incorporated into the host E. coli BL21 (DE3) cells using a standard heat shock transformation protocol. These cells were cultured and induced using IPTG to generate cells expressing GFP. A single colony was picked to culture the cells to minimize the heterogeneity of GFP expression due to the variable count of plasmids in bacterial cell populations. Once the GFP expressing cells are ready, they can be stored in batches for different experiments or else the glycerol stocks can be maintained to achieve uniform results and population of GFP expressing cells.

Elucidating the role of pH on T7L and T4L lysis activity:

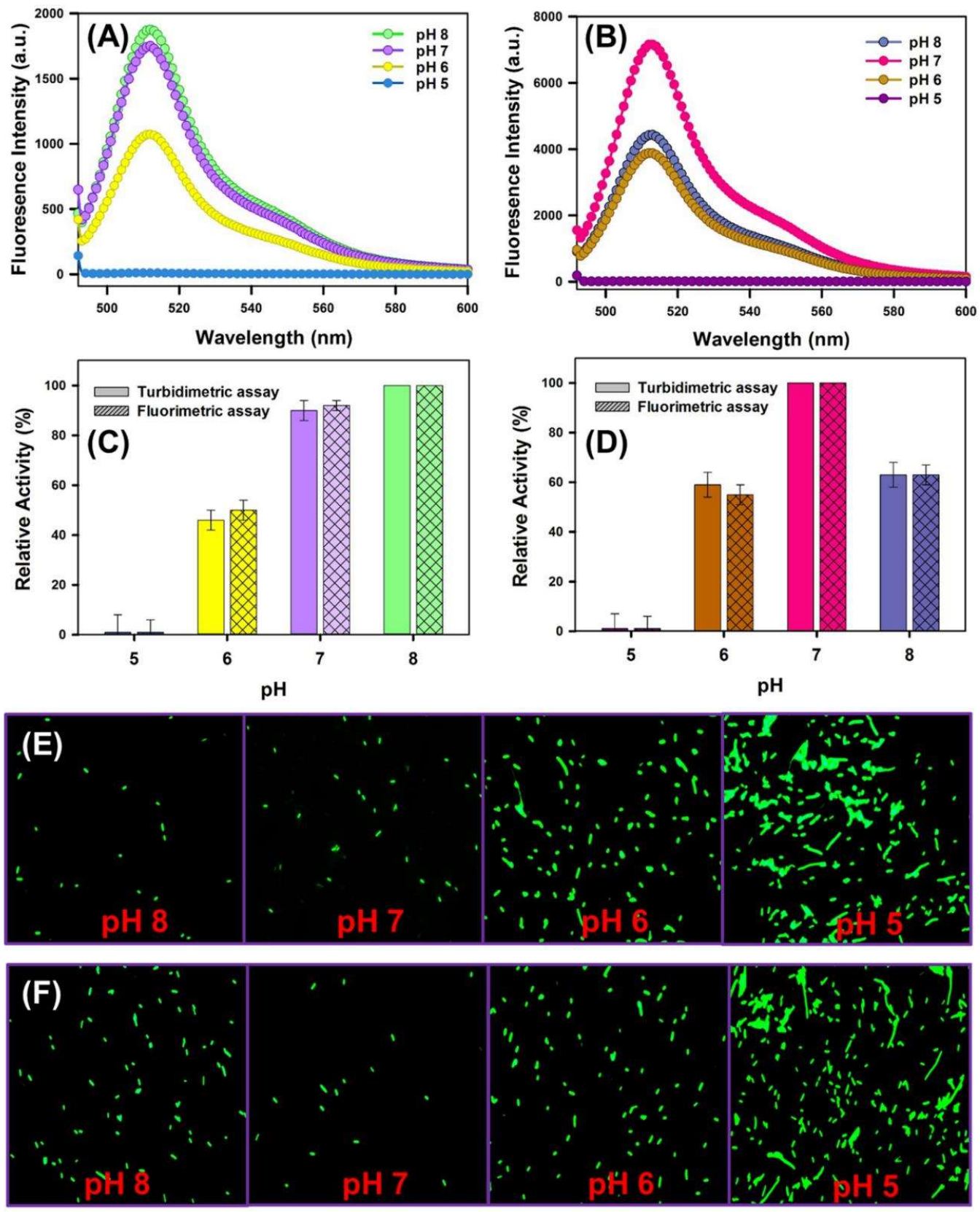

Figure 19: Effect of pH (pH 5-8) on the antibacterial activities of T7L and T4L. GFP fluorescence emission profiles of (A) T7L and (B) T4L in the wavelength range of 490–600 nm; Histogram representation of relative percentage activities of (C) T7L and (D) T4L calculated by data obtained from turbidimetric assay and GFP based fluorescence spectroscopy. Fluorescence microscopy images of GFP expressing E. coli cells treated with (E) T7L and (F) T4L.

It is well established that both T7L and T4L show pH-dependent activity profiles. T7L exhibits maximum antibacterial activity around pH 7-8 and gradually decreases below pH 7. Similarly, the optimum pH for the antimicrobial activity of the T4L is around 7.0. The GFP-based fluorimetric assay was performed in the pH range 5-8 to quantify the pH-dependent activities of both the endolysins . The GFP emission profiles in **Fig. 19A** demonstrate that in case of T7L, pH 8 and 7 supernatants show a maximum increase in GFP emission, which arises due to the maximum cell lysis at these pH values. The decrease in the fluorescence intensity at pH 6 correlated well with the reduction in cell lysis ability. Further, the complete loss of the GFP fluorescence i.e., almost equal to that of the control (untreated) cells suggests that at pH 5, T7L is completely inactive. For T4L, maximum GFP fluorescence is observed at pH 7 suggesting the maximum activity at this pH. The fluorescence intensities at pH 6 and 8 are substantially decreased, correlating to its decreased activity at these pH values. Complete loss of GFP fluorescence intensity at pH 5 establishes the fact that T4L is also completely inactive at this pH value.

Using the normalized fluorescence intensities at different pH values, relative activities of T7L and T4L were calculated **(Fig. 19 C-D)**. T7L exhibited maximum activity at pH 8, retained ~ 92 % and ~ 50 % activity at pH 7 and pH6, respectively (**Fig. 19C)**. T4L exhibited maximum activity at pH 7; and retained ~ 55 - 60 % activity at pH 6 / pH 8 **(Fig. 19D)**. No significant activity was found at pH 5 for either of the endolysins. To substantiate the quantitative analysis of the GFP-based measurements, we have performed the turbidimetric assay at all pH values under identical conditions. The results of the pH-dependent turbidimetric studies were also presented in **Fig. 19 C-D** for comparison. Comparative analysis suggested that the GFP-based fluorescence quantification results are in line with the absorbance based turbidimetric results, thus establishing that the designed GFP-based fluorimetric assay has precisely quantitated the cell lysis or percentage activity.

To further confirm the cell lysis behavior, the T7L and T4L treated *E. coli* cell pellets (residual cells after lysis) at different pH values were subjected to fluorescence microscopy analysis to ensure the cell lysis behavior, and also to enumerate that the residual GFP-tagged bacterial cells (live) remain intact in the sample **(Fig. 19 E-F)**. GFP-based fluorescence microscopic images revealed that very fewer populations of GFP-tagged bacterial cells are present at pH 7/8 in case of T7L and at pH 7 in case of T4L thus echoing the fact that maximum lysis activity of these enzymes is taking place at these pH values. At pH 6 for T7L and pH 6/8 for T4L comparatively more number of cells was found to be survived. At pH 5, the cell images almost match with those of the control cells, suggesting for negligible lysis activity.

Effect of salt concentration on the role of pH on T7L and T4L lysis activity:

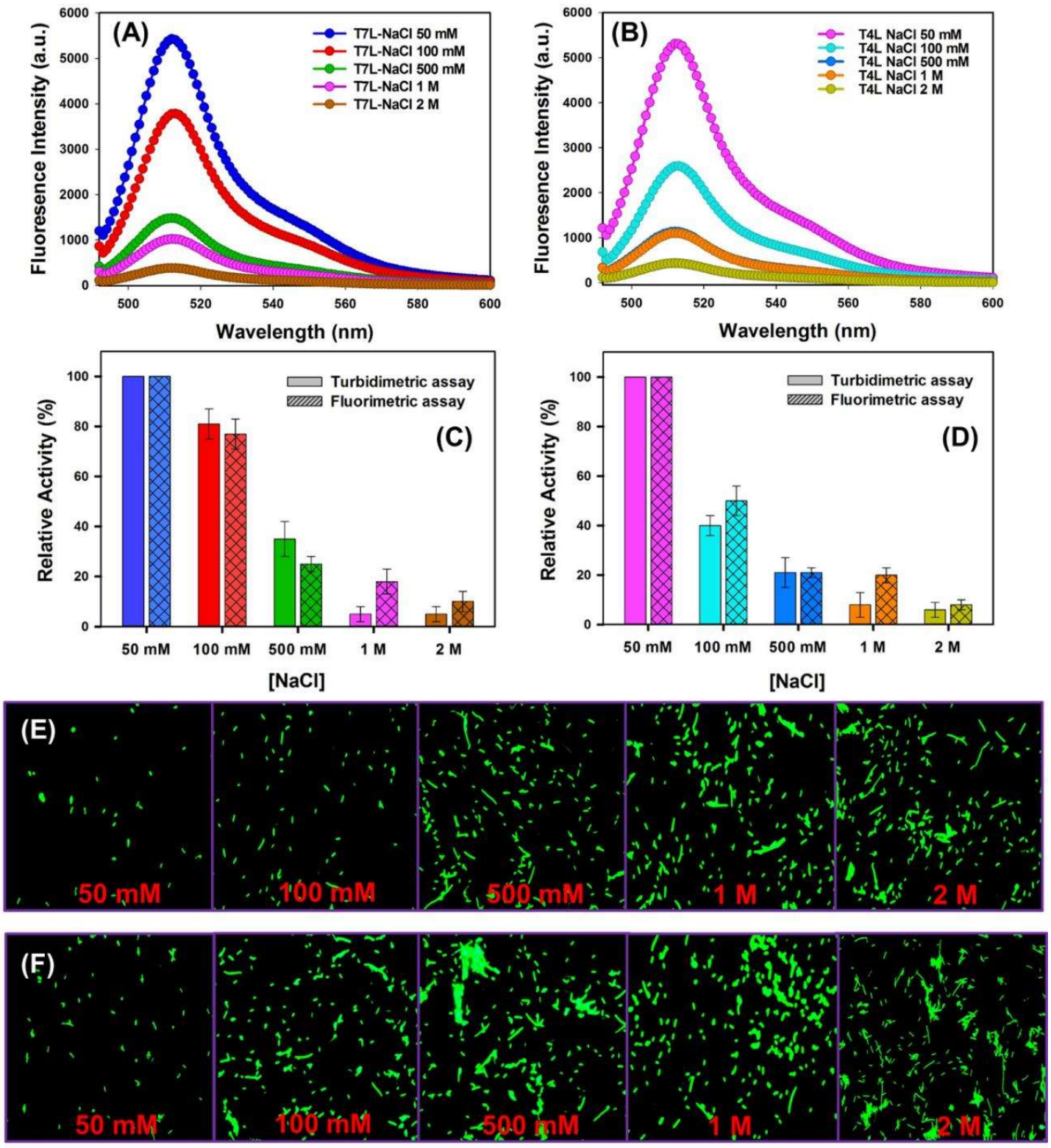

Figure 20: Effect of salt concentrations (50 mM, 100 mM, 500 mM, 1 M, and 2 M NaCl) on the antibacterial activities of T7L and T4L. GFP fluorescence emission profiles of (A) T7L and (B) T4L in the wavelength range of 490–600 nm; Histogram representation of relative percentage activities of (C) T7L and (D) T4L calculated by data obtained from turbidimetric assay and fluorescence spectroscopy. Fluorescence microscopy images of GFP expressing E. coli cells treated with (E) T7L and (F) T4L.

In order to obtain a quantitative measure of GFP fluorescence data at differential salt concentrations, and the effect of NaCl on the antimicrobial activities of T7L and T4L enzymes, the assay was performed at different concentrations of NaCl (50 mM, 100 mM, 500 mM, 1 M, and 2 M). Both the proteins exhibited maximum GFP fluorescence intensity at 50 mM NaCl, and the intensity gradually decreased with increasing salt concentrations **(Fig. 20 A-B)**. The calculation of relative activity using fluorescence spectroscopy propose that 50 mM NaCl is the optimum concentration at which both the proteins could obtain maximum activity **(Fig. 20 C-D)**. In the case of T7L, increasing the amount of NaCl to 100 mM shows ~ 77 % of activity, which decreases to ~ 25 % at 500 mM. Concentrations of NaCl above 500 mM significantly inhibited the lysis reaction. At 1 M and 2 M NaCl, the system was almost inactive and retained only 10-20 % of its original activity **(Fig. 20 C)**. In the case of T4L, the activity was decreased to ~ 50 % at 100 mm NaCl concentration, and to ~ 20 % at 500 mm and 1 M and finally ~ 10 % activity at 2 M NaCl **(Fig. 20 D)**. Relative activity calculations from turbidimetric data presented a similar pattern of activity profiles as shown by fluorescence spectroscopy **(Fig. 20 C-D)**. A similar response pattern of activity against NaCl concentrations was observed in the GFP-based fluorescence microscopy analysis obtained from the residual cell pellets **(Fig. 20 E-F)**. At 50 mM NaCl, where the activity is maximum, a minimum number of intact bacterial cells were observed for both T7L and T4L, and the cell count gradually increased upon the increase of salt concentration.

Concluding Remarks

- Phage endolysin of molecular weight was overexpressed and purified using ion-exchange chromatography using DEAE (Bio-Rad) and size exclusion chromatography for functional (Antimicrobial) study.
- The MIC value of endolysin against *Pseudomonas aeruginosa* bacterial strain was obtained in the range of 50 -100 µg/mL.
- The antibacterial efficiency of phage endolysin was successfully established by turbidimetric assay depicting the lysis of bacterial cells treated with endolysin at different pH (pH 6, pH 7, pH 8).
- The antimicrobial efficiency of phage endolysin against *P. aeruginosa* bacterial strain was positively verified with two different microscopic techniques such as SEM and AFM. The bacterial cell count was reduced after the treatment of endolysin which can be visualized in SEM and AFM.
- A novel method has been established by using GFP fluorescent bacteria to quantify the antibacterial efficacy of proteins. A strong correlation between the fluorescence intensity and the enzyme activity for both the chosen phage endolysins (T4L and T7L) was observed using the proposed fluorescence method. The lysis results were performed at different environmental conditions such as different pH and salt concentrations in order to validate the robustness of this fluorimetric approach.

(C) NMR based metabolic analysis of bacteriophage endolysin producing bacteria

The NMR based metabolic study was designed to understand the molecular mechanism used by bacteriophages isolated from Ganga waters to lyse the host bacterial species. The NMR based metabolomics analysis aids in understanding the overall metabolic changes while expressing phage endolysin in its host bacterial species along with lytic activity. After entering into host cells the bacteriophages alert the bacterial overall metabolism and make the cellular environment favorable for the endolysin expression. Studying the metabolic changes in bacterial cells helps in understanding effects of endolysin expression and the metabolic profiles of host cells.

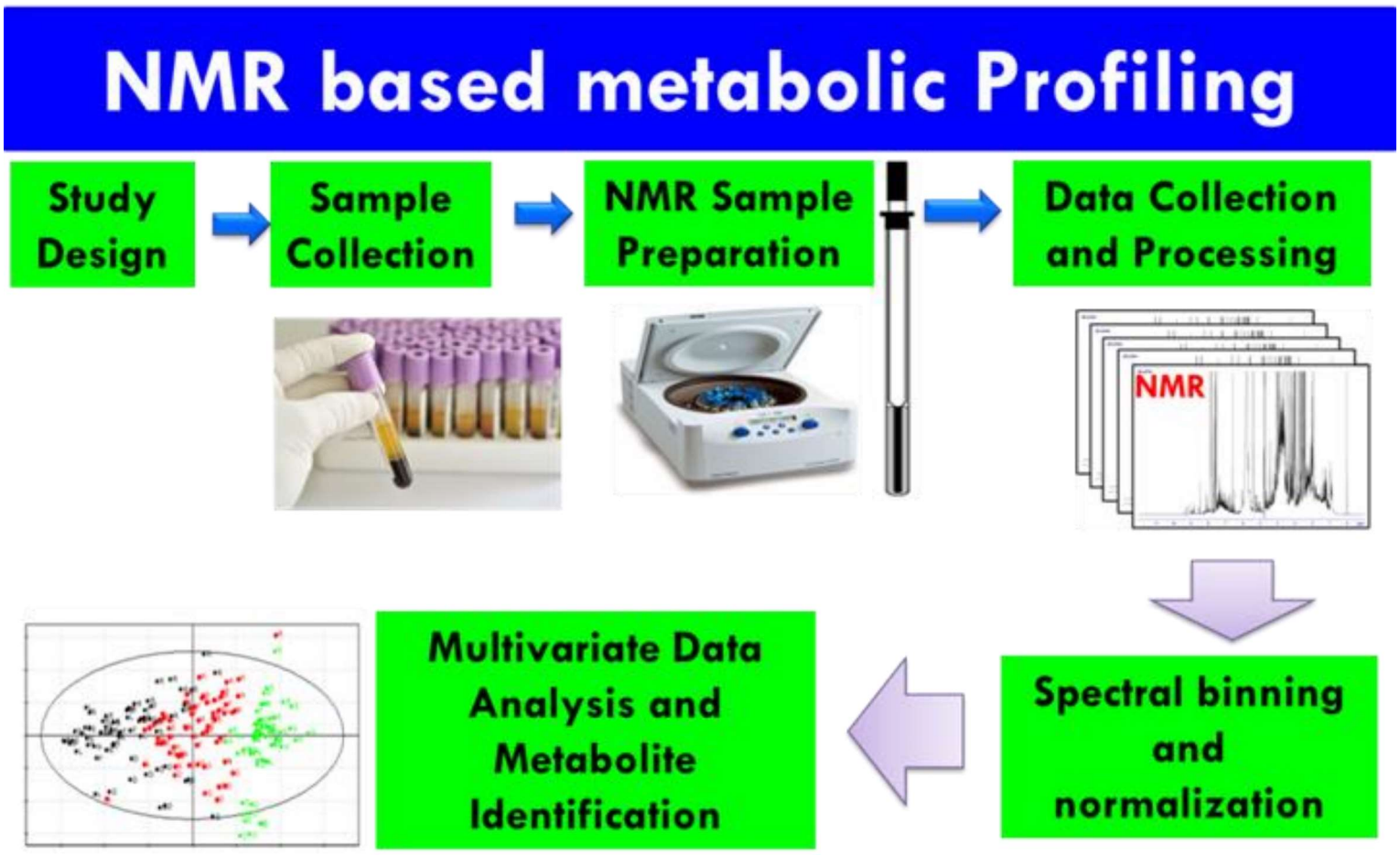

Figure 1: Flowchart showing methods for NMR based metabolic profiling of bacteriophage endolysin producing bacteria.

Sample preparation:

In this study, four different sets of bacterial samples were used to extract metabolites, which include IPTG treated *E. coli* cells, *E. coli* phage polymerase (phage RNAP) and phage endolysin T4 and phage endolysin T7 expressing cells. All *E. coli* BL21 (DE3) cells were cultured in M9 minimal medium. An initial 50 ml culture was grown overnight at 37 °C and then 5ml inoculum transferred to 8 conical flasks containing 250 ml fresh medium and grown at 37 °C and 180 rpm. The cells were grown until an OD 600 of 0.6 and treated with 0.5 mM IPTG. To express phage RNAP and phage endolysin proteins (T4 and T7) cells were transformed with

plasmids containing inducible genes. Cells were then expressed in minimal medium by growing them at 37 °C until it reached its exponential phase (OD600 of ~ 0.6) followed by 0.5 mM IPTG induction and incubated at 37 °C for 3 h. All cultures were grown to a final OD 600 of 2.0 and finally stopped by incubating on ice for 10 min. The control IPTG treated and expressed protein were run on SDS-PAGE gel for visualization (Fig. 2).

Cells were harvested by gentle centrifugation at 4000 rpm, 4 °C, for 5 min. and supernatants were discarded. The pellets were flash-frozen in Liquid N2 and incubated on ice for 10min. The pellets were washed thrice with phosphate-buffered saline (PBS) followed by the same centrifugation procedure. The supernatants were discarded and the pellets were re-suspended in freshly prepared 6ml of quenching solution containing 1:1 ratio of 60 % methanol (- 40 °C) and water and stored at -80 °C. All the frozen samples were thawed on ice. Samples were further sonicated in an ice water bath for 30 min until a clear solution formed, with each cycle consisting of 3-s pulse on and 15-s pulse off. Supernatants were collected by centrifugation for 30 min at 14000 rpm and 4 °C and filtered with Millipore centricon tubes (2 kDa cut off ;). Samples were then condensed by vacuum to remove ethanol. All the samples were divided into aliquots of 500 µl, frozen in liquid nitrogen and lyophilized completely. Further, samples were stored at -80 °C until NMR analysis.

The lyophilized samples were dissolved in 550 µl of D2O, centrifuged (10000 rpm, 5 min), and transferred to a 5 mm NMR tube, 0.0003 mM TSP added as Chemical Shift Indicator.

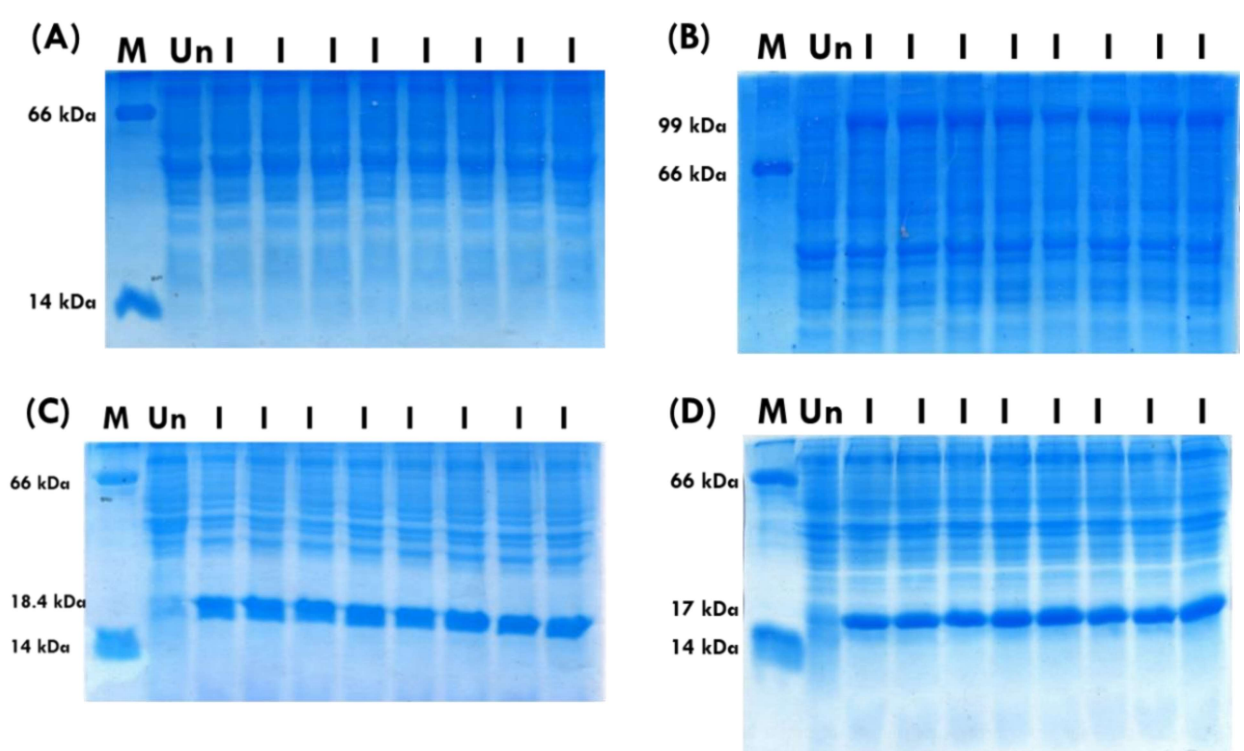

Figure 2: SDS-PAGE (15 %: (A), (C), (D); 12%: (B)) gel analysis of from (A) IPTG treated (B) phage polymerase (RNAP) expressing (C) phage endolysin T4 expressing cells and (D) phage endolysin T7 expressing cells. M=Marker, Un=Un-induced, I=induced.

Data acquisition:

All the ^{1}H NMR spectra were acquired on Bruker 500 MHz NMR spectrometer using Carr-Purcell-Meiboom-Gill (CPMG) pulse sequence (cpmgpr1d) with water pre-saturation (relaxation delay of 4 s). Carr-Purcell-Meiboom-Gill (CPMG) filter reduce broad resonances related to back ground or macromolecules All the data were collected at a temperature of 298 K. Experiments were run with an 832 acquisition scan, 65 K data points and spectral width of 19 ppm.

Processing and metabolite profiling:

Each spectrum was manually Fourier transformed, phased and baseline-corrected using TopSpin 4.0.6 software. Profiling of compounds was done using the Chenomx NMR Suite 8.4 using 500MHz chemical shift database, existing literature, and publicly available *E. coli* Metabolome Database (ECMDB). The spectral data were reduced into spectral bins of 0.01 ppm width for statistical analysis.

Statistical Analysis:

Six replicates of spectral bins of 0.01 ppm width were used in all of four different expressing conditions. The data imported into the web-based Metaboanalyst (v5.0) tool suite, Interquantile range (IQR) data filtering method, and Pareto scaling normalization were chosen.

Univariate data analysis:

For each variable, ANOVA tests whether there are any statistically significant differences between the means of three or more groups. The post-hoc analysis is used in conjunction with ANOVA to further test which means are significantly different from one another A positive result indicates that at least two of the groups differ significantly. The post-hoc analysis is used in conjunction with ANOVA One-way Analysis of Variance (ANOVA) with Post-hoc analysis using Tukey's HSD method performed to identify the significant compounds (Peaks ppm) selected based on the p-value threshold (0.001). Fold changes were calculated for significant metabolite peaks. The peak ppm list and fold changes for the respective groups were mentioned in the **Table 1**.

Multivariate data analysis:

For discriminatory analysis, the principal component analysis (PCA) performed for initial overview of the grouping trend within the data set and outlier detection. For the four different expressing conditions six replicates chosen for each group. Principal component analysis (PCA) is an unsupervised clustering or dimensionality-reduction method, which projects the data into a new coordinate system such that most of the data variance lies in the first few principal components or PCs. The default 2D Scores Plot between PC1 and PC2, draws 95% confidence regions for each group. PCA was performed and 2D score plot shows the significant clustering of the six replicates and distinct differences among four groups.

Next, the data were modeled with the supervised method of partial least squares discriminant analysis (PLS-DA) to reveal class separations between the groups and to further identify the metabolites responsible for class separation. Partial least squares discriminant analysis (PLS-DA) is a supervised method in which the separation is calculated by maximizing the covariance between the data matrix (X) and the class labels (Y). As PLS-DA inclines to overfit the data, therefore, the model needs to be strictly validated to see whether the separation is statistically significant or is due to random noise. To avoid the overfitting of the PLS-DA model, 10-fold cross-validation algorithm, which helps to evaluate 100% classification accuracy using the top 5 latent variables, was used. Cross validation testing performed to determine the optimal number of components needed to build the PLS-DA model. There are three common performance measures—the sum of squares captured by the model (R2), the cross-validated R2(also known as Q2), and the prediction accuracy (Accuracy). The default criterion Q2, used to choose a minimum number of component model is the best. The PLS-DA model was further used to identify the metabolites responsible for the discrimination based on the criterion, that is, variables with variable importance on projection (VIP) value of >1.0 considered as candidate biomarkers.

The box and whisker plots of most important or informative compounds were generated using Important features using variable importance in projection (VIP) score with the best component model given by Q2 value. The bottom and top of the box are always the 25th and 75th percentile (the lower and upper quartiles, or Q1 and Q3, respectively), and the band near the middle of the box is always the 50th percentile (the median or Q2). The upper whisker is located at the smaller of the maximum x value and Q3 + 1.5*IQR (Interquantile Range), whereas the lower whisker is located at the larger of the smallest x value and Q1 - 1.5*IQR. The yellow dot is the average normalized concentration.

Results:

Study 1: Metabolic profile of phage endolysin T7

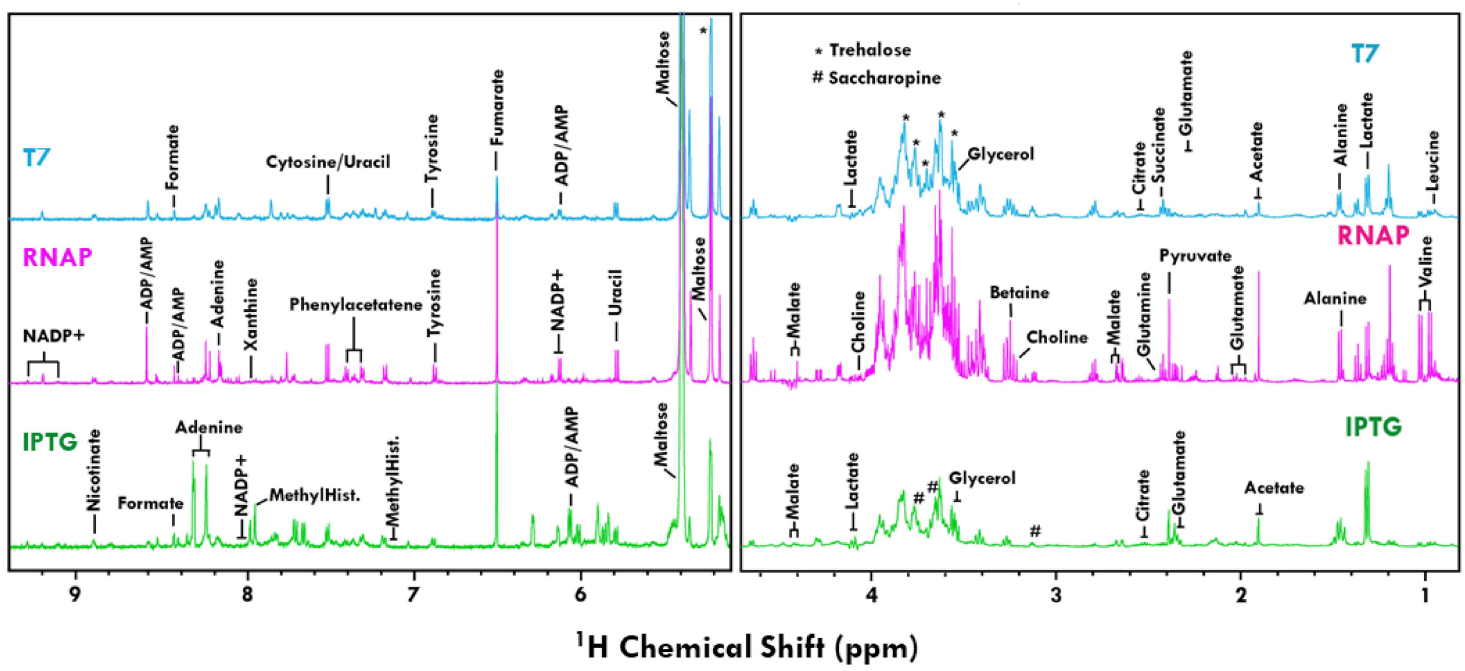

Figure 3: Representative ^{1}H-NMR spectra of *E. coli* metabolites extracted from IPTG treated (Green), phage polymerase (RNAP) expressing (Pink) and phage endolysin T7 expressing cells (Cyan).

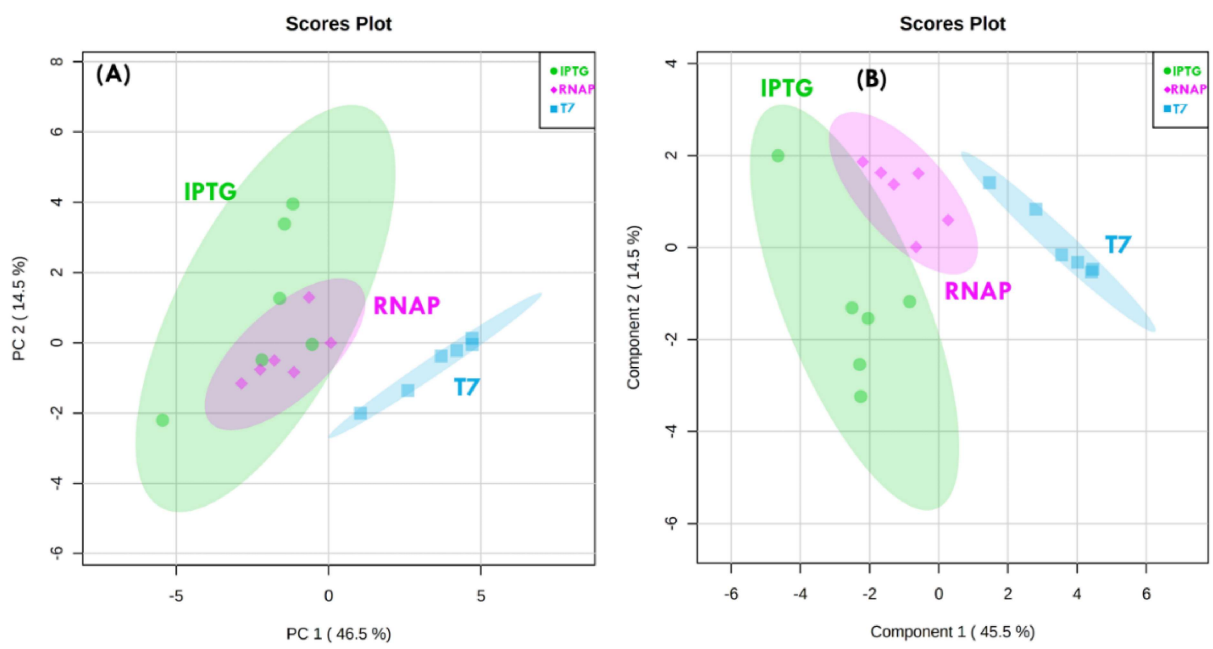

Figure 4: (A)The combined principal component analysis (PCA) 2D score plot and (B) partial least squares discriminant analysis (PLS-DA) resulted from the analysis of 1D ^{1}H Carr–Purcell–Meiboom–Gill (CPMG) spectra of from IPTG treated (Green), phage polymerase (RNAP) expressing cells (Pink) and phage endolysin T7 expressing cells (Cyan). The semitransparent ovals represent the 95% confidence interval.

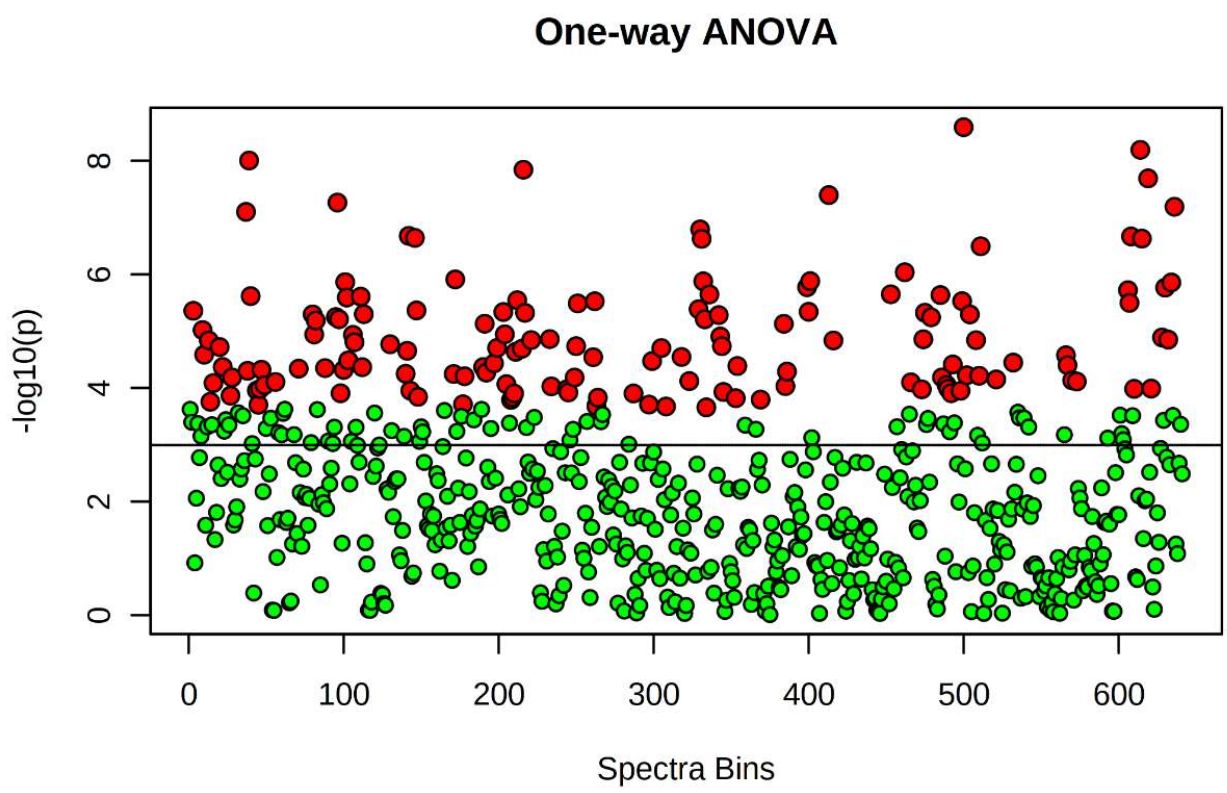

Figure 5: One-way Analysis of Variance (ANOVA) and Post-hoc analysis using Tukey's HSD method performed to identify the significant compounds (Peaks ppm) selected based on the p-value threshold (0.001). The red color dots show the significant metabolites (Peaks) selected based on the p-value threshold (0.001) and the green dots are insignificant peaks.

The metabolomics profiles obtained from IPTG treated, phage polymerase (RNAP) and phage endolysin T7 expressing bacterial cells are shown in **Fig. 3**. 2D scores plot of PCA (**Fig. 4A),** PLS-DA (**Fig. 4B**), showed close group clustering among IPTG treated bacterial cells, and phage polymerase (RNAP) compared to endolysin T7 expressing bacterial cells. PCA scores plot shown overlap in confident interval between IPTG treated bacterial cells, and phage polymerase (RNAP) and distinct phage endolysin T7, whereas slight overlap observed in PLS-DA score plot. One-way Analysis of Variance (ANOVA) and Post-hoc analysis using Tukey's HSD method performed to identify the significant compounds (Peaks ppm) selected based on the p-value threshold (0.001) shown in **Fig.5**. The red color dots show the 147 significant features (Peaks) selected based on the p-value threshold (0.001) and the green dots are 494 insignificant peaks. From the overlay (**Fig. 3**) of ^{1}H CPMG spectra which contain multiple signals from various metabolites like the spectral regions δ (3.21–6.61) contain resonances mainly from glucose and other carbohydrates. If there is significant difference in the quantitative profiles of Carbohydrates, it may understate the discriminatory importance of other metabolites exhibiting relatively small change in their metabolic profiles. Therefore, the CPMG data matrix truncated into total 3 spectral regions: 1. Carbohydrate region δ(3.21–6.61), δ(1.05-1.32) and δ(1.88-1.92) ppm 2. Amino acid region δ(0.6-3.21) ppm and 3. Aromatic compound region δ(5.82-9.35) ppm.

By truncating such spectral regions would allow more reliable analysis for a range of metabolic profiles and would further surmount their discriminatory importance (in terms of VIP scores).

Truncated region wise PLS-DA discriminant analysis:

A. Carbohydrate/Sugar region

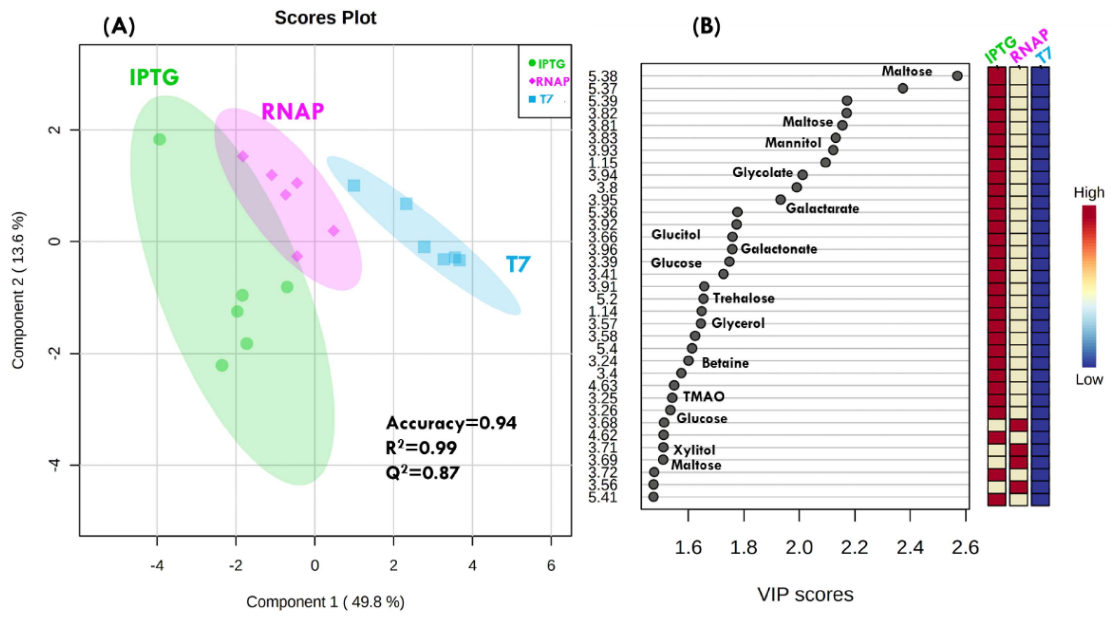

Figure 6: (A) partial least squares discriminant analysis (PLS-DA) resulted from the analysis of truncated Carbohydrate region of 1D ^{1}H Carr–Purcell–Meiboom–Gill (CPMG) spectra of IPTG treated (Green), phage polymerase (RNAP) expressing cells (Pink) and phage endolysin T7 expressing cells (Cyan). (B) The VIP score plots used to identify metabolite entities of discriminatory significance.

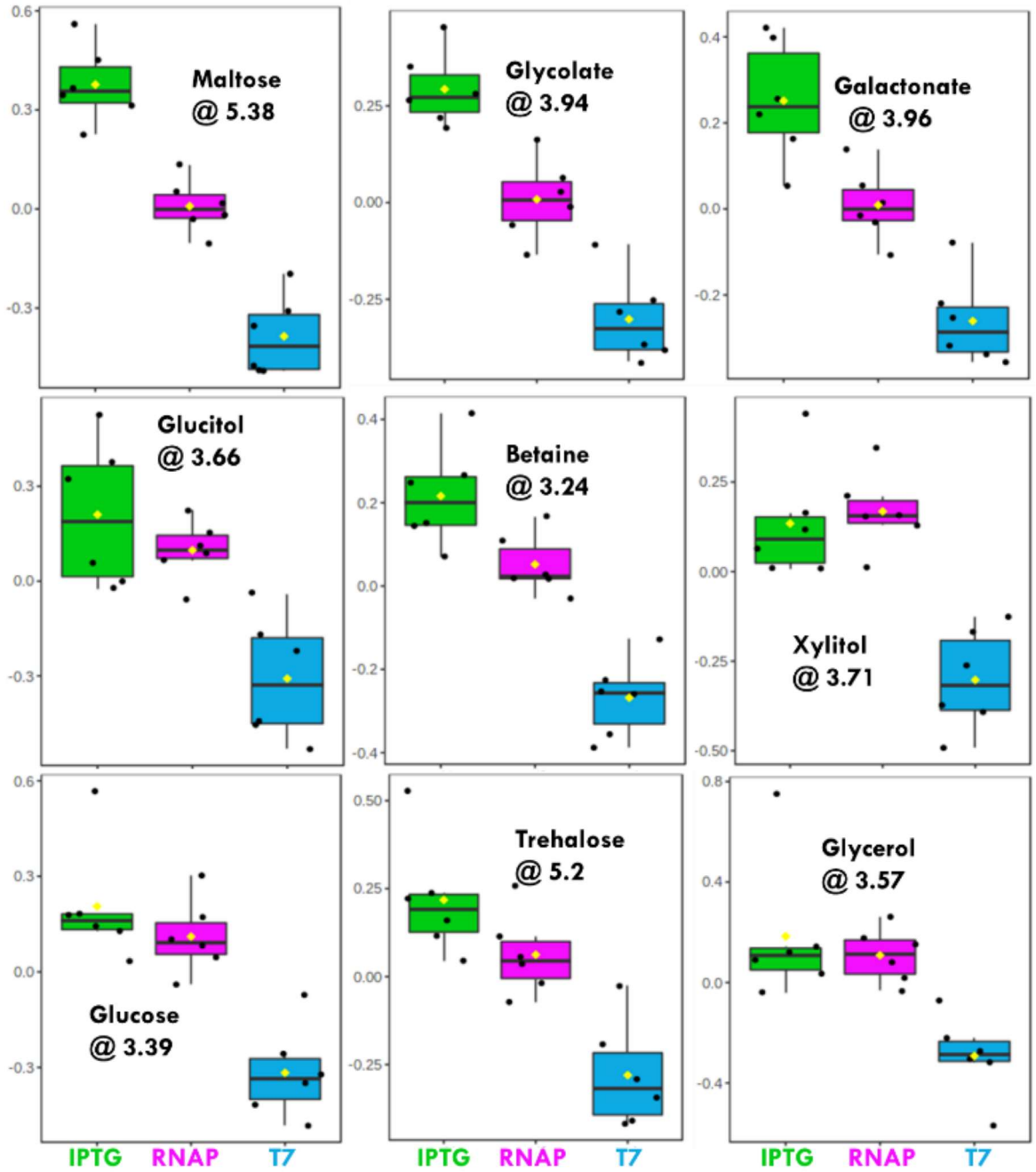

Figure 7: The box and whisker plots showing relative abundance of some of the metabolites showing significant variation among from IPTG treated (Green), phage polymerase (RNAP) expressing cells (Pink), phage endolysin T7 expressing cells (Cyan).

The PLS-DA performed on truncated Carbohydrate/Sugar region δ(3.21–6.61), δ(1.05-1.32) and δ(1.88-1.92) ppm shown 2D score plot (**Fig. 6A**) and cross validated parameters are displayed for the model. The VIP score plot shown for top 35 bins (**Fig. 6B**). The metabolites responsible for the discrimination based on the criterion, that is, variables with variable importance on projection (VIP) value of >1.0 considered as candidate biomarkers. The representative box-cum whisker plots of the relative signal intensity for these potential metabolic markers are shown in Figure 7. Sugars like Maltose, Mannitol, Trehalose and other metabolites detected with high variance for the group discrimination and as biomarkers for the expression of phage endolysin T7 in bacterial cells.

B. Amino acid spectral region

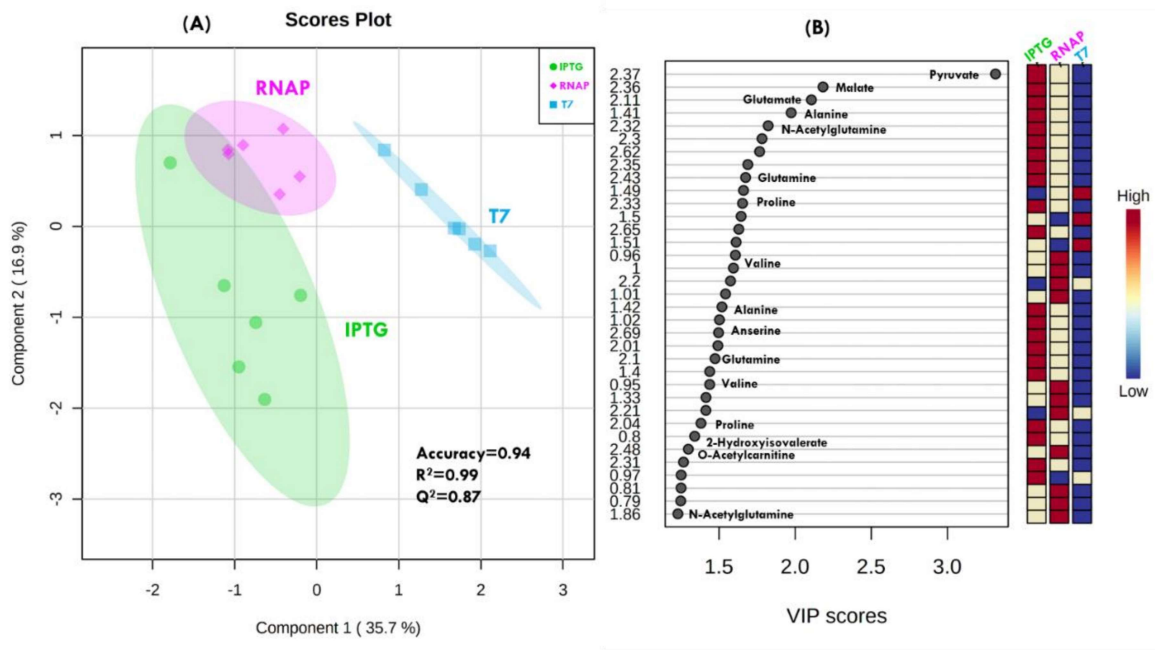

Figure 8: (A) partial least squares discriminant analysis (PLS-DA) resulted from the analysis of truncated Amino acid region of 1D ^{1}H Carr–Purcell–Meiboom–Gill (CPMG) spectra of IPTG treated (Green), phage polymerase (RNAP) expressing cells (Pink) and phage endolysin T7 expressing cells (Cyan). (B) The VIP score plots used to identify metabolite entities of discriminatory significance.

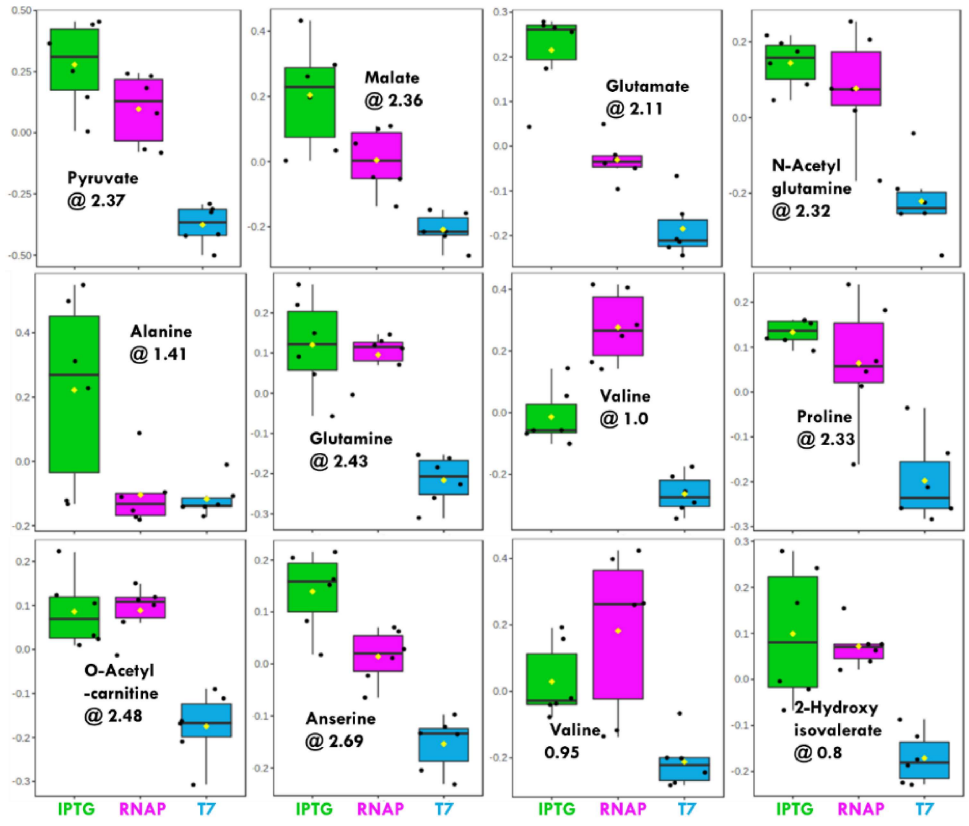

Figure 9: The box and whisker plots showing relative abundance of some of the metabolites showing significant variation among from IPTG treated (Green), phage polymerase (RNAP) expressing cells (Pink), phage endolysin T7 expressing cells (Cyan).

The PLS-DA performed on truncated Amino acid region δ(0.6-3.21) ppm shown 2D score plot(Fig. 7 A) and cross validated parameters are displayed for the model. The VIP score plot shown for top 35 bins (**Fig. 8B**). The metabolites responsible for the discrimination based on the criterion, that is, variables with variable importance on projection (VIP) value of >1.0 considered as candidate biomarkers. The representative box-cum whisker plots of the relative signal intensity for these potential metabolic markers are shown in **Figure 9**. Metabolites like Pyruvate, Malate, Glutamate and other metabolites detected with high variance for the group discrimination and as biomarkers for the expression of phage endolysin T7 in bacterial cells.

C. Aromatic spectral region

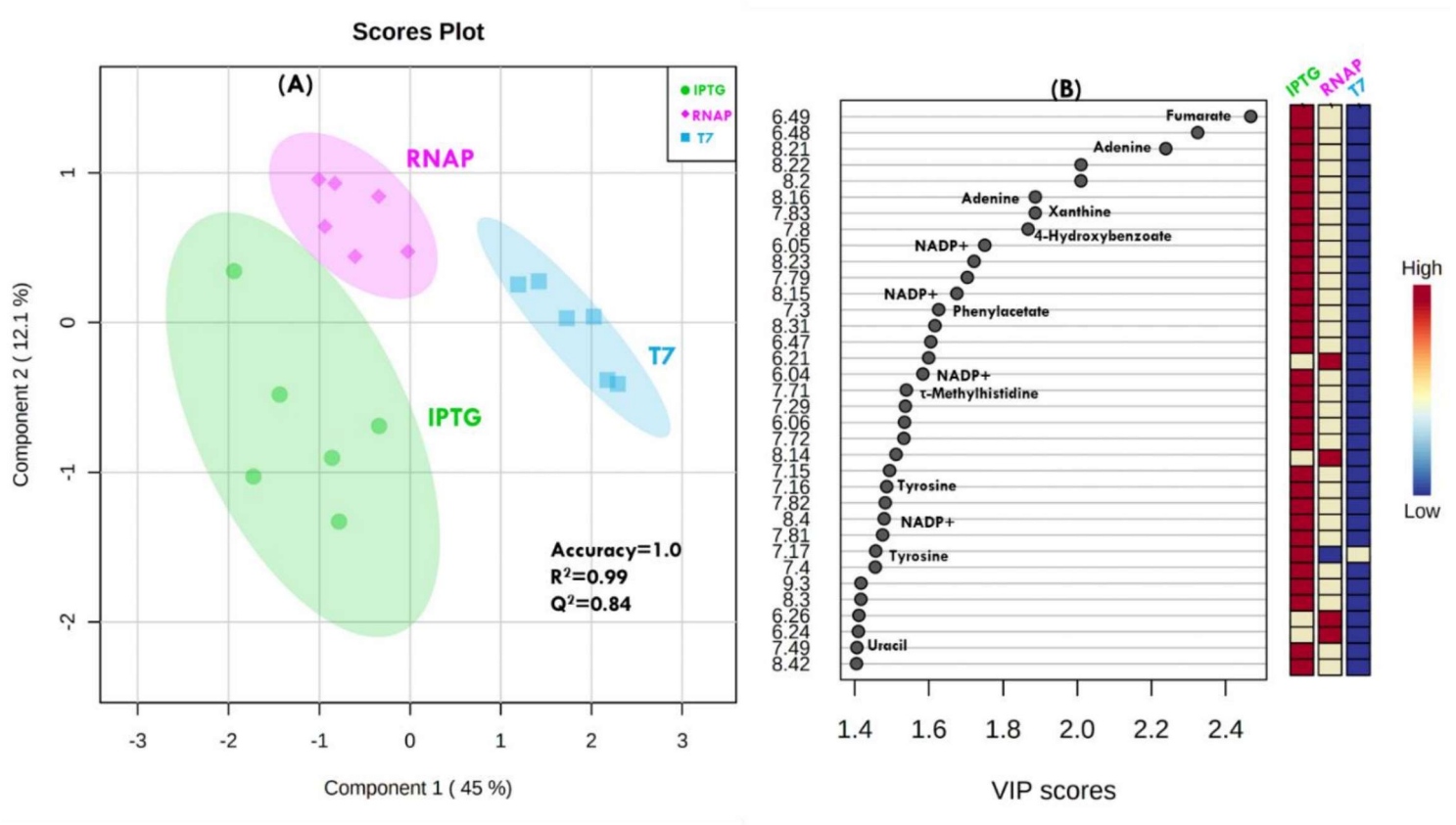

Figure 10: (A) partial least squares discriminant analysis (PLS-DA) resulted from the analysis of truncated Aromatic compounds region of 1D ^{1}H Carr−Purcell−Meiboom−Gill (CPMG) spectra of IPTG treated (Green), phage polymerase (RNAP) expressing cells (Pink) and phage endolysin T7 expressing cells (Cyan). (B) The VIP score plots used to identify metabolite entities of discriminatory significance.

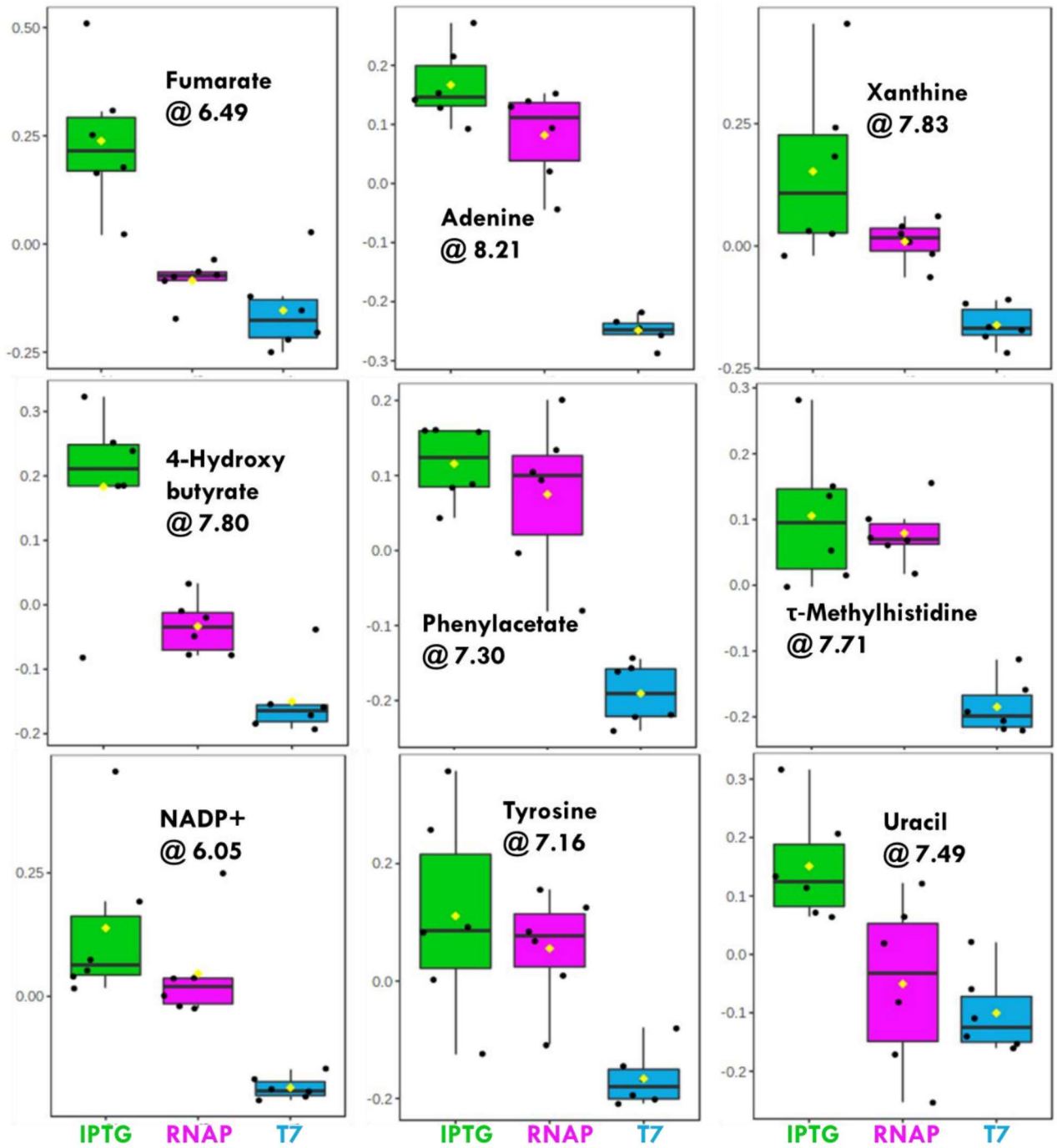

Figure 11: The box and whisker plots showing relative abundance of some of the metabolites showing significant variation among from IPTG treated (Green), phage polymerase (RNAP) expressing cells (Pink), phage endolysin T7 expressing cells (Cyan).

The PLS-DA performed on truncated aromatic spectral region δ(5.82-9.35) ppm shown 2D score plot(**Fig. 10A**) and cross validated parameters are displayed for the model. The VIP score plot shown for top 35 bins (**Fig. 9 B**). The metabolites responsible for the discrimination based on the criterion, that is, variables with variable importance on projection (VIP) value of >1.0 considered as candidate biomarkers. The representative box-cum whisker plots of the relative signal intensity for these potential metabolic markers are shown in **Figure 11**. Metabolites like Fumarate, Adenine, NADP+ and other metabolites detected with high variance for the group discrimination and as biomarkers for the expression of phage endolysin T7 in bacterial cells.

Study 2: Metabolic profile of phage endolysin T4

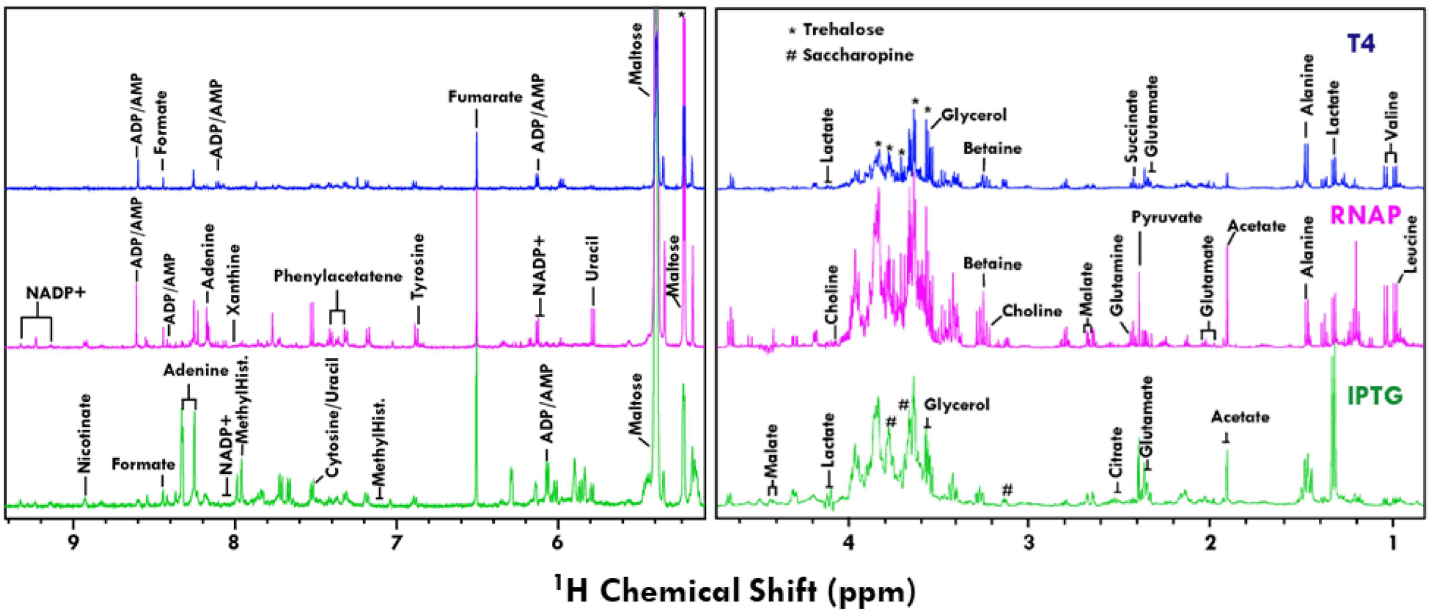

Figure 12: Representative ^{1}H-NMR spectra of *E.coli* metabolites extracted from IPTG treated (Green), phage polymerase (RNAP) expressing (Pink) and phage endolysin T4 expressing cells (Blue)

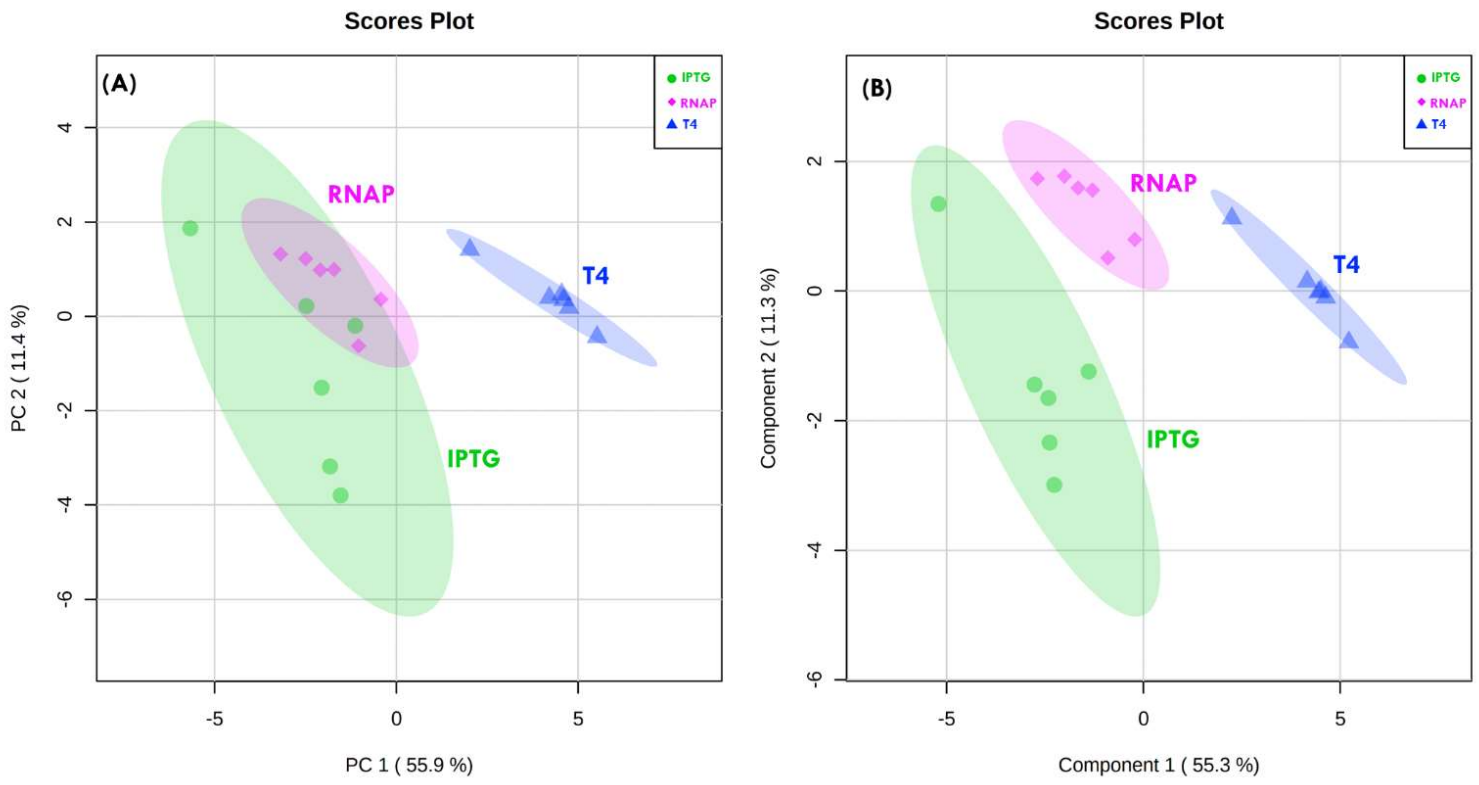

Figure 13: (A)The combined principal component analysis (PCA) 2D score plot and (B) partial least squares discriminant analysis (PLS-DA) resulted from the analysis of 1D ^{1}H Carr−Purcell−Meiboom−Gill (CPMG) spectra of from IPTG treated (Green), phage polymerase (RNAP) expressing cells (Pink) and phage endolysin T4 expressing cells (Blue). The semitransparent ovals represent the 95% confidence interval.

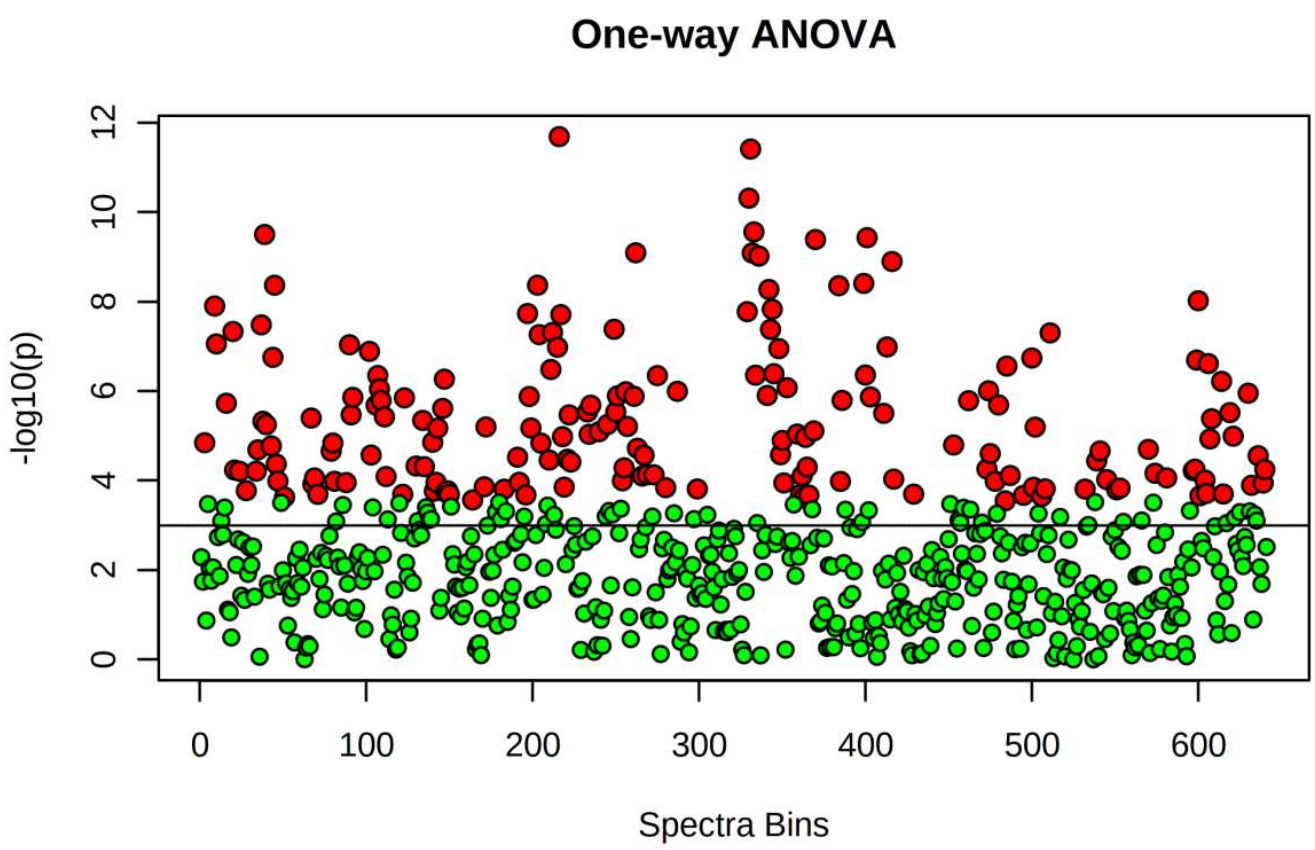

Figure 14: One-way Analysis of Variance (ANOVA) and Post-hoc analysis using Tukey's HSD method performed to identify the significant compounds (Peaks ppm) selected based on the p-value threshold (0.001). The red color dots show the significant metabolites (Peaks) selected based on the p-value threshold (0.001) and the green dots are insignificant peaks.

The metabolomics profiles obtained from IPTG treated phage polymerase (RNAP) and phage endolysin T4 expressing bacterial cells shown in **Fig. 12**. 2D scores plot of PCA (**Fig. 13 A**), PLS-DA (**Fig. 13 B**), showed close group clustering among IPTG treated bacterial cells, and phage polymerase (RNAP) compared to endolysin T4 expressing bacterial cells. PCA scores plot shown overlap in confident interval between IPTG treated bacterial cells, and phage polymerase (RNAP) and distinct phage endolysin T4, whereas distinct separation observed in PLS-DA score plot. One-way Analysis of Variance (ANOVA) and Post-hoc analysis using Tukey's HSD method performed to identify the significant compounds (Peaks ppm) selected based on the p-value threshold (0.001) shown in **Fig. 14**. The red color dots show 183 significant features (Peaks) selected based on the p-value threshold (0.001) and the green dots are 458 insignificant peaks.

Truncated region wise PLS-DA discriminant analysis:

A. Carbohydrate/Sugar region

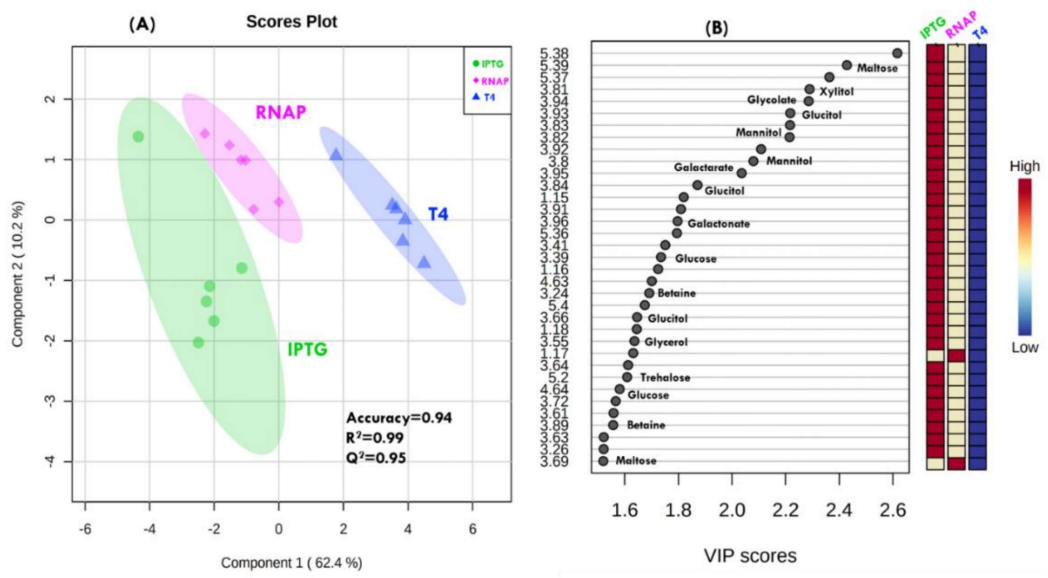

Figure 15: (A) partial least squares discriminant analysis (PLS-DA) resulted from the analysis of truncated Carbohydrate/Sugar region of 1D ^{1}H Carr−Purcell−Meiboom−Gill (CPMG) spectra of IPTG treated (Green), phage polymerase (RNAP) expressing cells (Pink) and phage endolysin T4 expressing cells (Blue). (B) The VIP score plots used to identify metabolite entities of discriminatory significance.

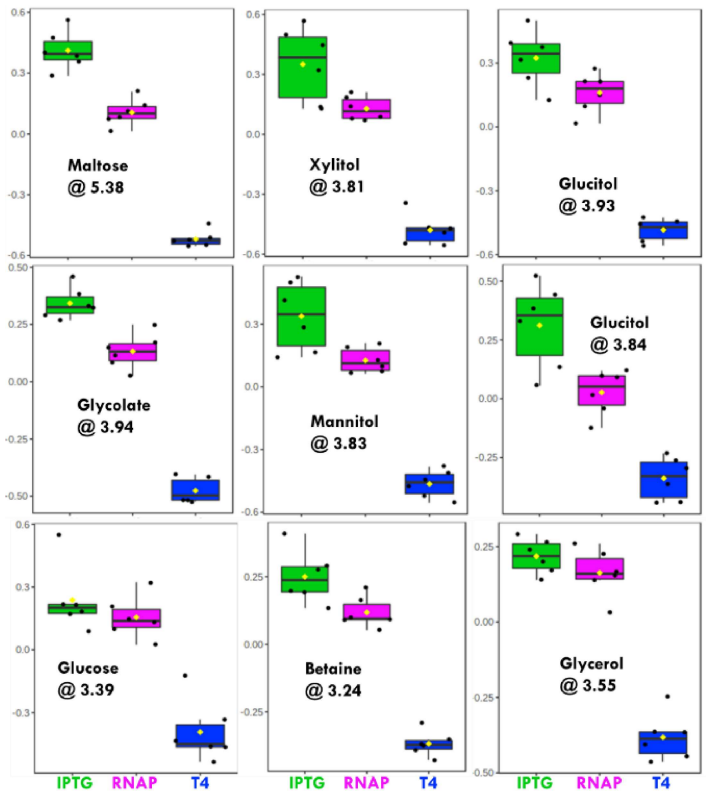

Figure 16: The box and whisker plots showing relative abundance of some of the metabolites showing significant variation among from IPTG treated (Green), phage polymerase (RNAP) expressing cells (Pink), phage endolysin T4 expressing cells (Blue).

The PLS-DA performed on truncated Carbohydrate/Sugar region δ(3.21–6.61), δ(1.05-1.32) and δ(1.88-1.92) ppm shown 2D score plot(**Fig. 15A**) and cross validated parameters are displayed for the model. The VIP score plot shown for top 35 bins (**Fig. 15B**). The metabolites responsible for the discrimination based on the criterion, that is, variables with variable importance on projection (VIP) value of >1.0 considered as candidate biomarkers. The representative box-cum whisker plots of the relative signal intensity for these potential metabolic markers shown in **Fig. 16**. Sugars like Maltose, Xylitol, Glucitol and other metabolites detected with high variance for the group discrimination and as biomarkers for the expression of phage endolysin T4 in bacterial cells.

B. Amino acid spectral region

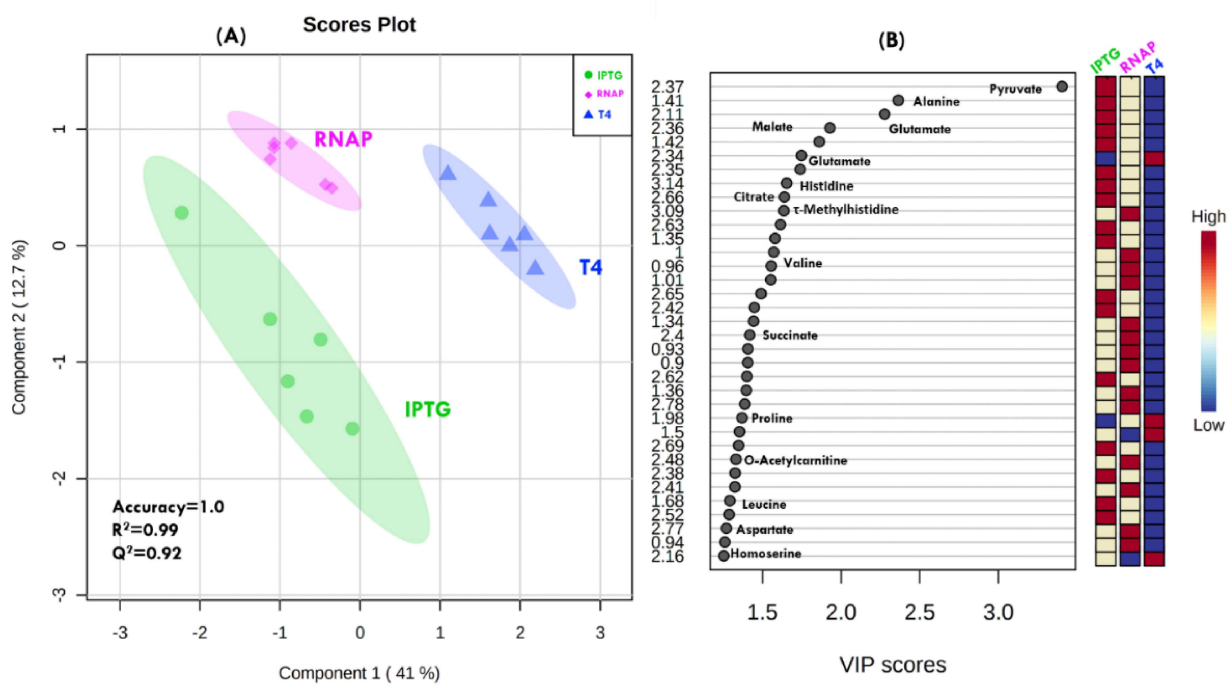

Figure 17: (A) partial least squares discriminant analysis (PLS-DA) resulted from the analysis of truncated Amino acid region of 1D ^{1}H Carr–Purcell–Meiboom–Gill (CPMG) spectra of IPTG treated (Green), phage polymerase (RNAP) expressing cells (Pink) and phage endolysin T4 expressing cells (Blue). (B) The VIP score plots used to identify metabolite entities of discriminatory significance.

The PLS-DA performed on truncated Amino acid region δ(0.6-3.21) ppm shown 2D score plot(**Fig. 17A**) and cross validated parameters are displayed for the model. The VIP score plot shown for top 35 bins (**Fig. 17B**). The metabolites responsible for the discrimination based on the criterion, that is, variables with variable importance on projection (VIP) value of >1.0 considered as candidate biomarkers. The representative box-cum whisker plots of the relative signal intensity for these potential metabolic markers shown in **Fig. 18**. Metabolites like Pyruvate, Alanine, Glutamate and other metabolites identified with high variance for the group discrimination and as biomarkers for the expression of phage endolysin T4 in bacterial cells.

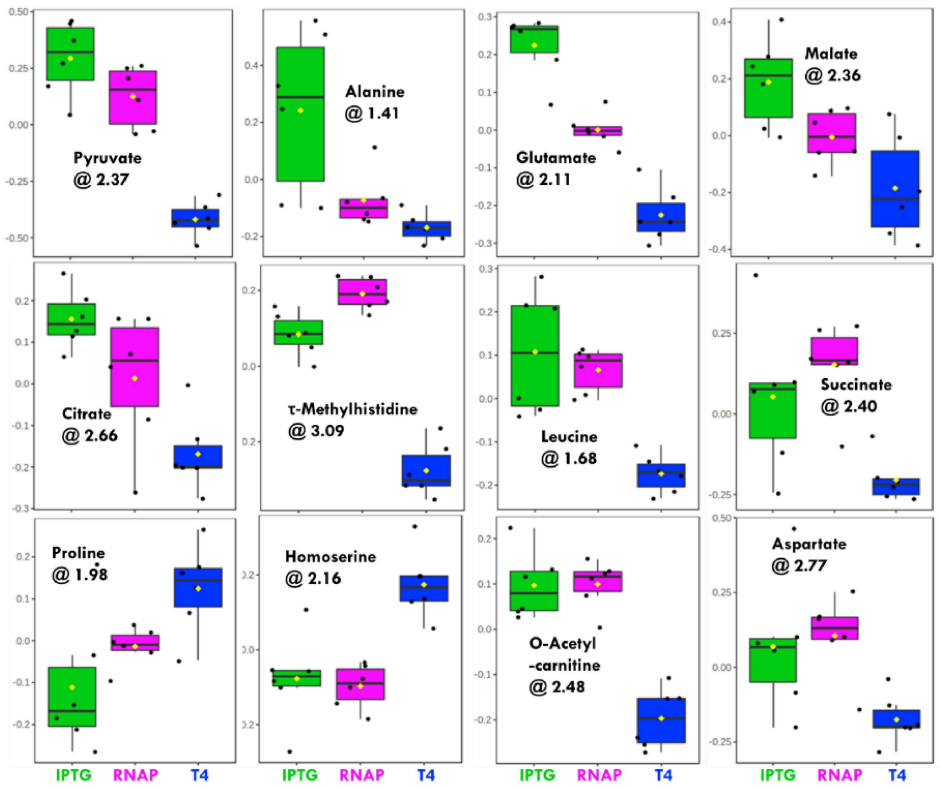

Figure 18: The box and whisker plots showing relative abundance of some of the metabolites showing significant variation among from IPTG treated (Green), phage polymerase (RNAP) expressing cells (Pink), phage endolysin T4 expressing cells (Blue).

C. Aromatic spectral region

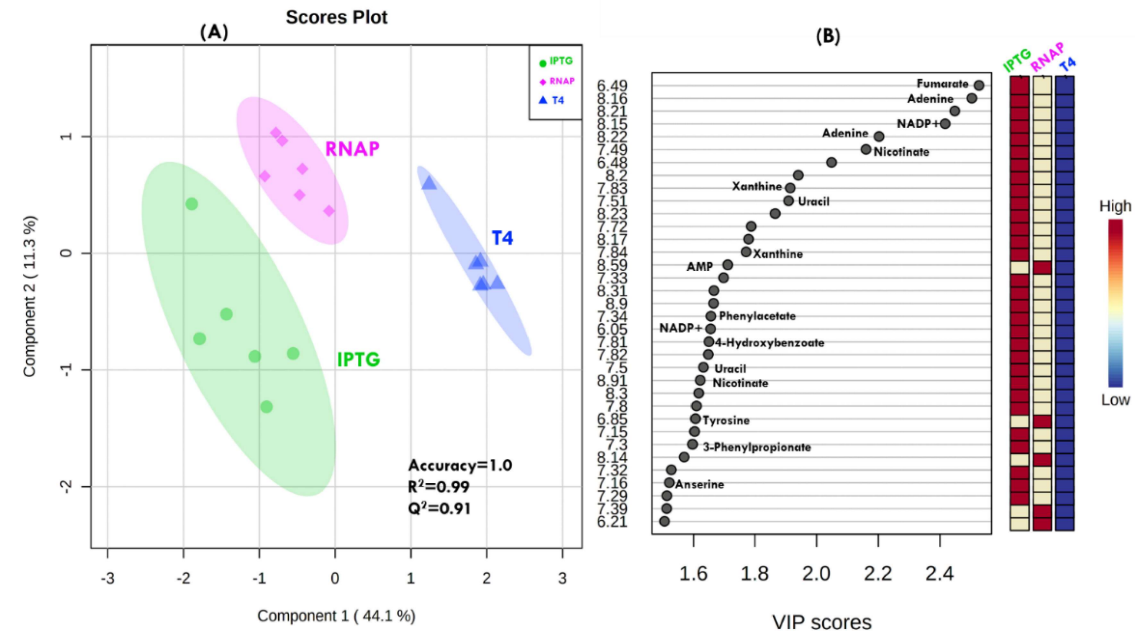

Figure 19: (A) partial least squares discriminant analysis (PLS-DA) resulted from the analysis of truncated Aromatic compounds region of 1D ^{1}H Carr−Purcell−Meiboom−Gill (CPMG) spectra of IPTG treated (Green), phage polymerase (RNAP) expressing cells (Pink) and phage endolysin T4 expressing cells (Blue). (B) The VIP score plots used to identify metabolite entities of discriminatory significance.

The PLS-DA performed on truncated aromatic spectral region δ(5.82-9.35) ppm shown 2D score plot(**Fig. 19A**) and cross validated parameters are displayed for the model. The VIP score plot shown for top 35 bins (**Fig. 19B**). The metabolites responsible for the discrimination based on the criterion, that is, variables with variable importance on projection (VIP) value of >1.0 considered as candidate biomarkers. The representative box-cum whisker plots of the relative signal intensity for these potential metabolic markers are shown in **Fig. 20**. Metabolites like Fumarate, Adenine, NADP+ and other metabolites detected with high variance for the group discrimination and as biomarkers for the expression of phage endolysin T4 in bacterial cells.

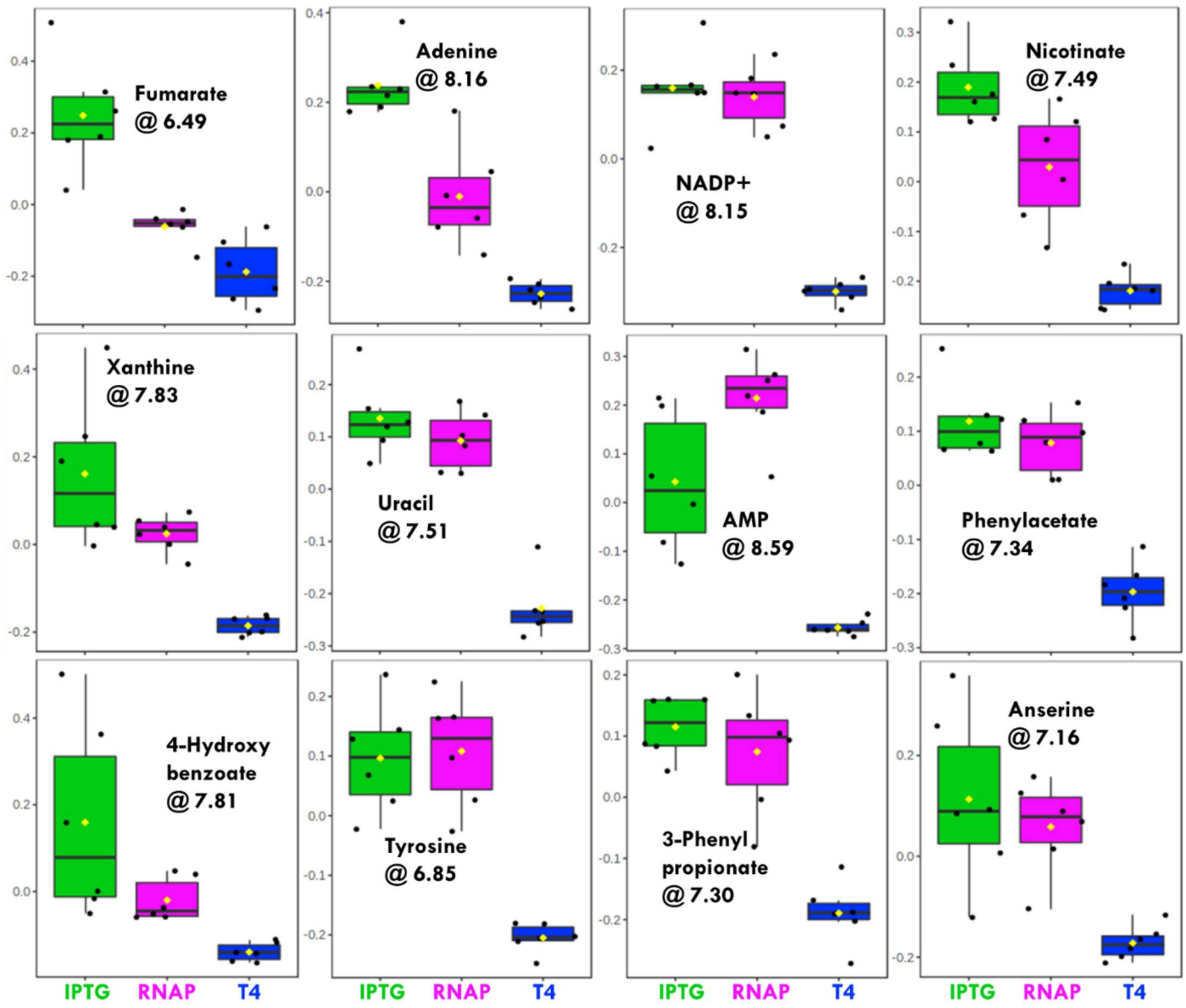

Figure 20: The box and whisker plots showing relative abundance of some of the metabolites showing significant variation among from IPTG treated (Green), phage polymerase (RNAP) expressing cells (Pink), phage endolysin T4 expressing cells (Blue).

Study 3 :Metabolic profile of phage endolysin T7 and phage endolysin T4

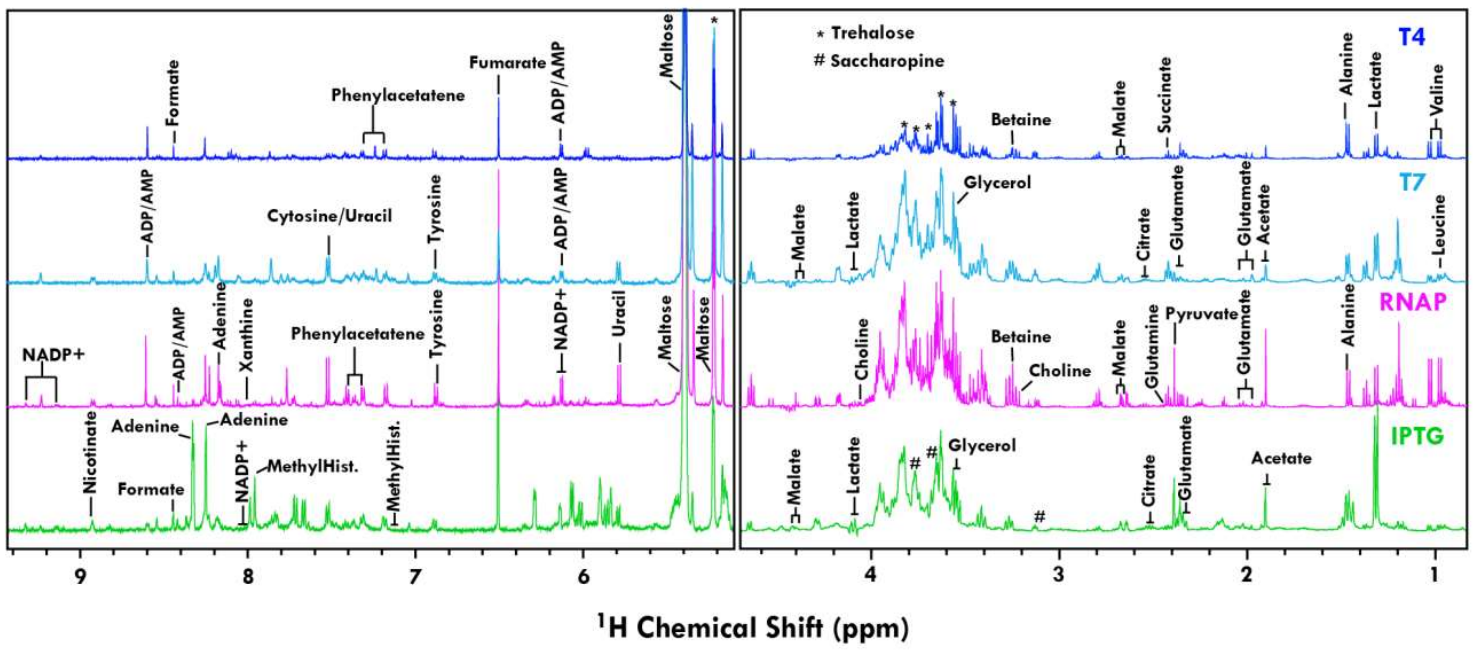

Figure 21: Representative ^{1}H-NMR Carr–Purcell–Meiboom–Gill (CPMG) spectra of *E. coli* metabolites extracted from IPTG treated (Green), phage polymerase (RNAP) expressing (Pink), phage endolysin T7 expressing cells (Cyan) and phage endolysin T4 expressing cells (Blue)

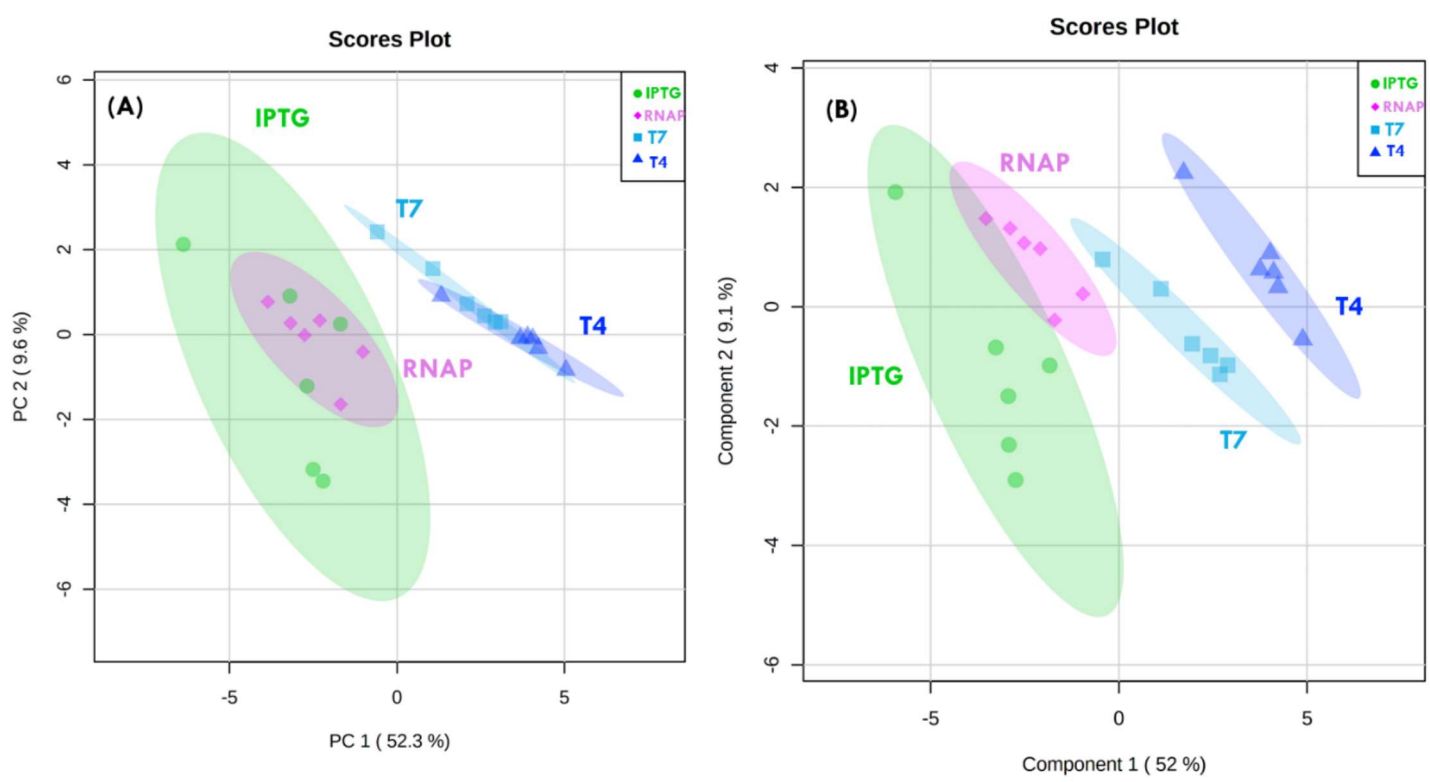

Figure 22: (A)The combined principal component analysis (PCA) 2D score plot and (B) partial least squares discriminant analysis (PLS-DA) resulted from the analysis of 1D ^{1}H Carr–Purcell–Meiboom–Gill (CPMG) spectra of from IPTG treated (Green), phage polymerase (RNAP) expressing cells (Pink), phage endolysin T7 expressing cells (Cyan) and phage

endolysin T4 expressing cells (Blue). The semitransparent ovals represent the 95% confidence interval.

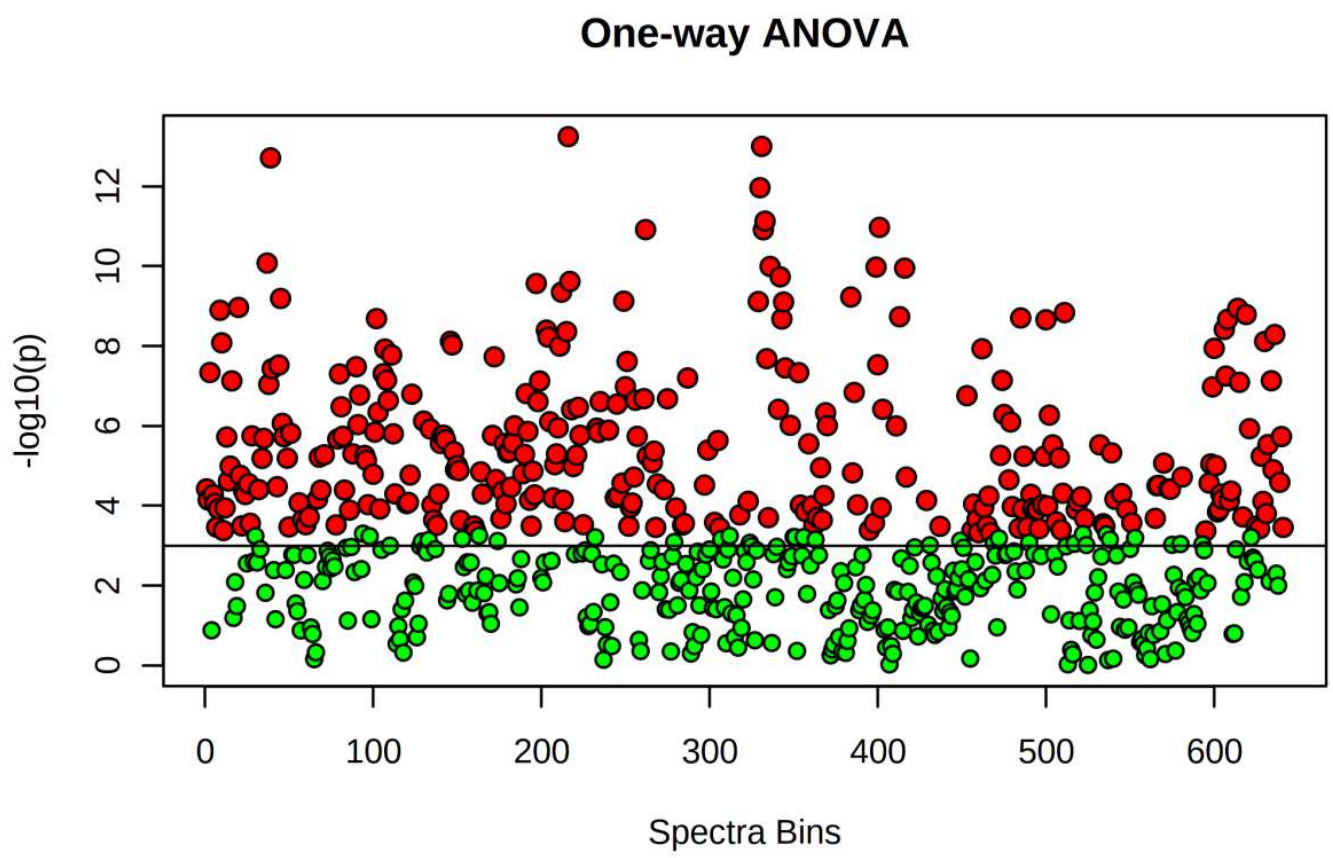

Figure 23: One-way Analysis of Variance (ANOVA) and Post-hoc analysis using Tukey's HSD method performed to identify the significant compounds (Peaks ppm) selected based on the p-value threshold (0.001). The red color dots show the significant metabolites (Peaks) selected based on the p-value threshold (0.001) and the green dots are insignificant peaks.

The metabolomics profiles obtained from IPTG treated phage polymerase (RNAP),phage endolysin T7 and phage endolysin T4 expressing bacterial cells are shown in **Fig. 21**. 2D scores plot of PCA (**Fig. 22A),** PLS-DA (**Fig. 22B**), showed close group clustering among IPTG treated bacterial cells, and phage polymerase (RNAP) and closeness between phage endolysin T7 and phage endolysin T4 expressing bacterial cells in PCA. PLS-DA scores plot shown overlap in confident interval between IPTG treated bacterial cells, and phage polymerase (RNAP) and distinct phage endolysin T7 and phage endolysin T4 groups. One-way Analysis of Variance (ANOVA) and Post-hoc analysis using Tukey's HSD method performed to identify the significant compounds (Peaks ppm) selected based on the p-value threshold (0.001) shown in **Fig. 23**. The red color dots show 309 significant metabolites (Peaks) selected based on the p-value threshold (0.001) and the green dots are 332 insignificant peaks.

Truncated region wise PLS-DA discriminant analysis:

A. Carbohydrate/Sugar region

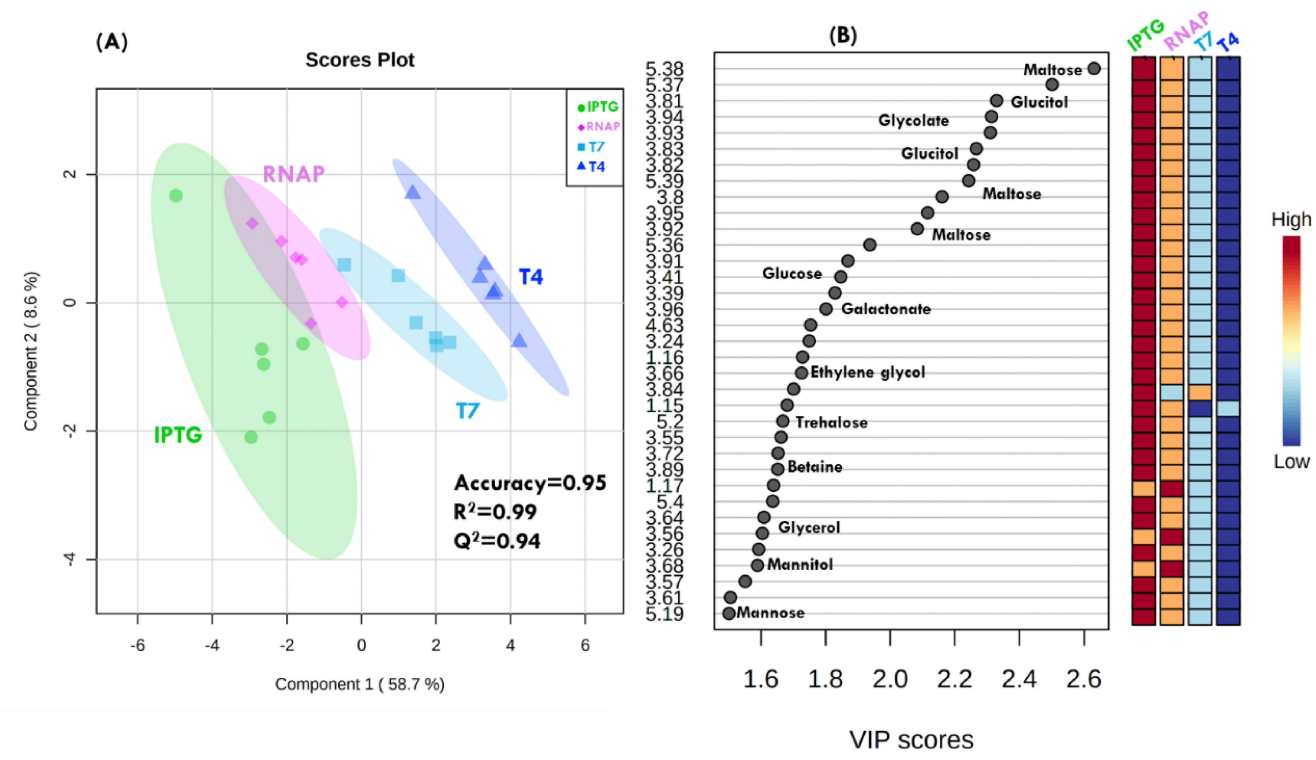

Figure 24: (A) partial least squares discriminant analysis (PLS-DA) resulted from the analysis of truncated Carbohydrate/Sugar region of 1D ^{1}H Carr−Purcell−Meiboom−Gill (CPMG) spectra of IPTG treated (Green), phage polymerase (RNAP) expressing cells (Pink), phage endolysin T7 expressing cells (Cyan) and phage endolysin T4 expressing cells (Blue). (B) The VIP score plots used to identify metabolite entities of discriminatory significance.

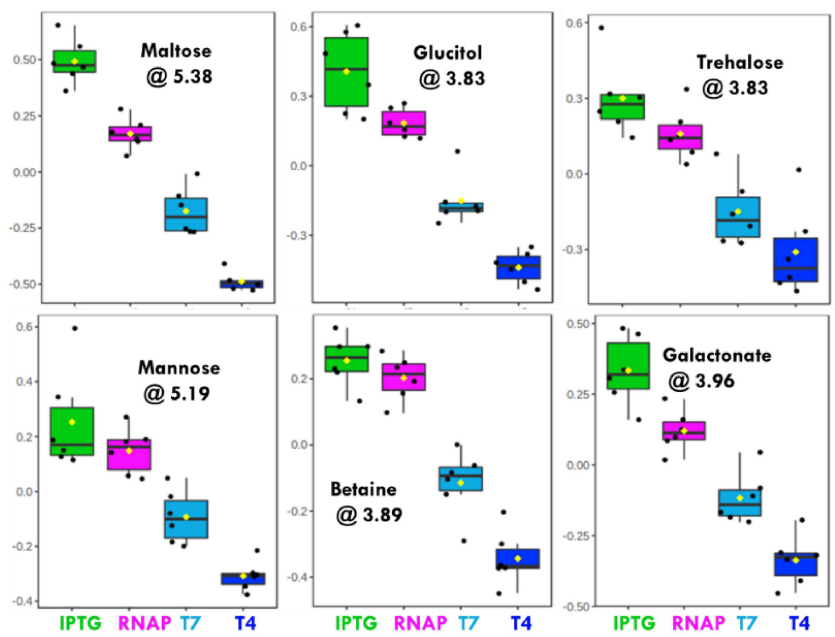

Figure 25: The box and whisker plots showing relative abundance of some of the metabolites showing significant variation among from IPTG treated (Green), phage polymerase (RNAP)

expressing cells (Pink), phage endolysin T7 expressing cells (Cyan) and and phage endolysin T4 expressing cells (Blue).

The PLS-DA performed on truncated Carbohydrate/Sugar region δ(3.21–6.61), δ(1.05-1.32) and δ(1.88-1.92) ppm shown 2D score plot (**Fig. 24A**) and cross validated parameters are displayed for the model. The VIP score plot shown for top 35 bins (**Fig. 24B**). The metabolites responsible for the discrimination based on the criterion, that is, variables with variable importance on projection (VIP) value of >1.0 considered as candidate biomarkers. The representative box-cum whisker plots of the relative signal intensity for these potential metabolic markers are shown in **Fig. 25**. Sugars like Maltose, Glucitol, Trehalose and other metabolites detected with high variance for the group discrimination and as biomarkers for the expression of phage endolysin T7 and phage endolysin T4 expressing bacterial cells.

B. Amino acid spectral region

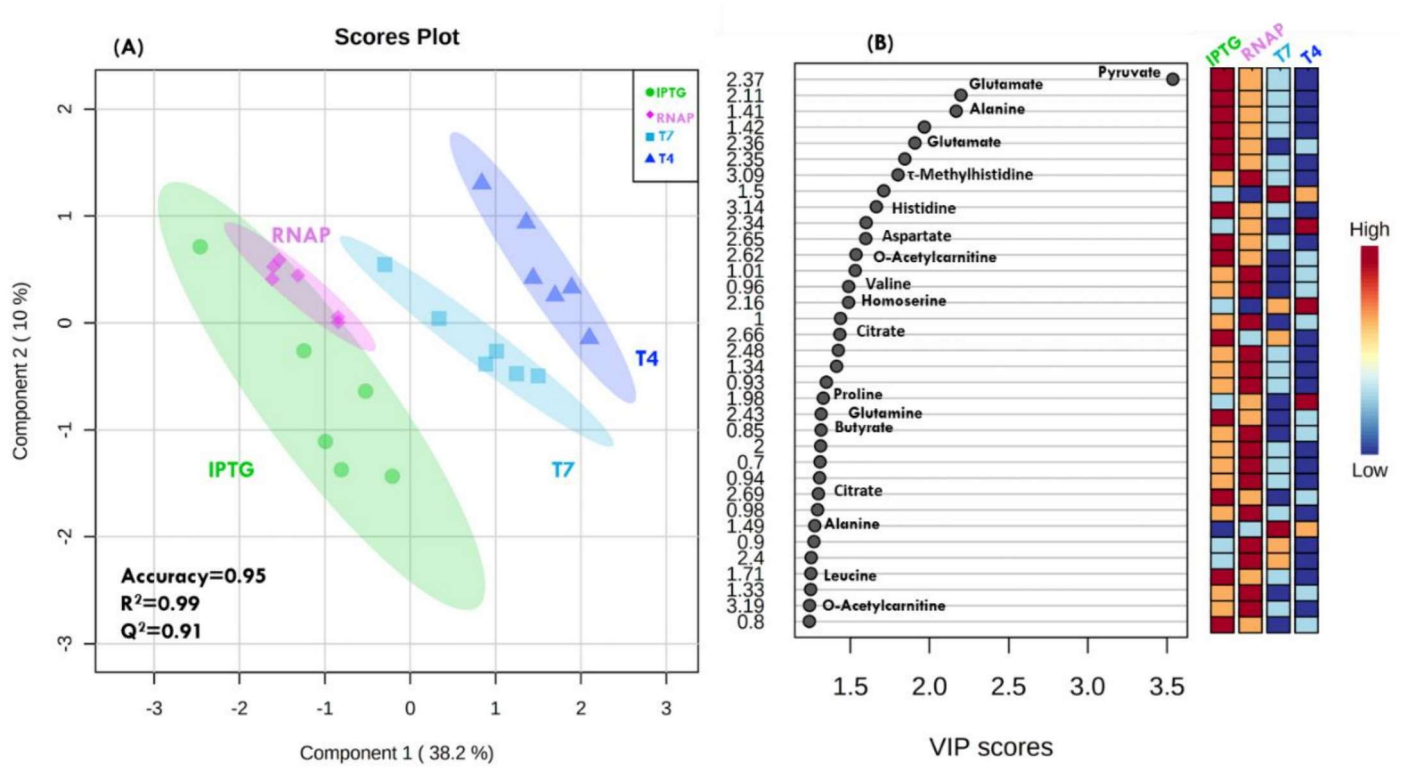

Figure 26: (A) partial least squares discriminant analysis (PLS-DA) resulted from the analysis of truncated Amino acid region of 1D ^{1}H Carr–Purcell–Meiboom–Gill (CPMG) spectra of IPTG treated (Green), phage polymerase (RNAP) expressing cells (Pink), phage endolysin T7 expressing cells (Cyan) and phage endolysin T4 expressing cells (Blue). (B) The VIP score plots used to identify metabolite entities of discriminatory significance.

The PLS-DA performed on truncated Amino acid region δ(0.6-3.21) ppm shown 2D score plot(**Fig. 26A**) and cross validated parameters are displayed for the model. The VIP score plot shown for top 35 bins (**Fig. 26B**). The metabolites responsible for the discrimination based on the criterion, that is, variables with variable importance on projection (VIP) value of >1.0 considered as candidate biomarkers. The representative box-cum whisker plots of the relative

signal intensity for these potential metabolic markers are shown in **Fig. 27**. Metabolites like Pyruvate, Glutamate, Alanine and other metabolites were identified with high variance for the group discrimination and as biomarkers for the expression of phage endolysin T7 and phage endolysin T4 expression in bacterial cells in comparison with phage polymerase.

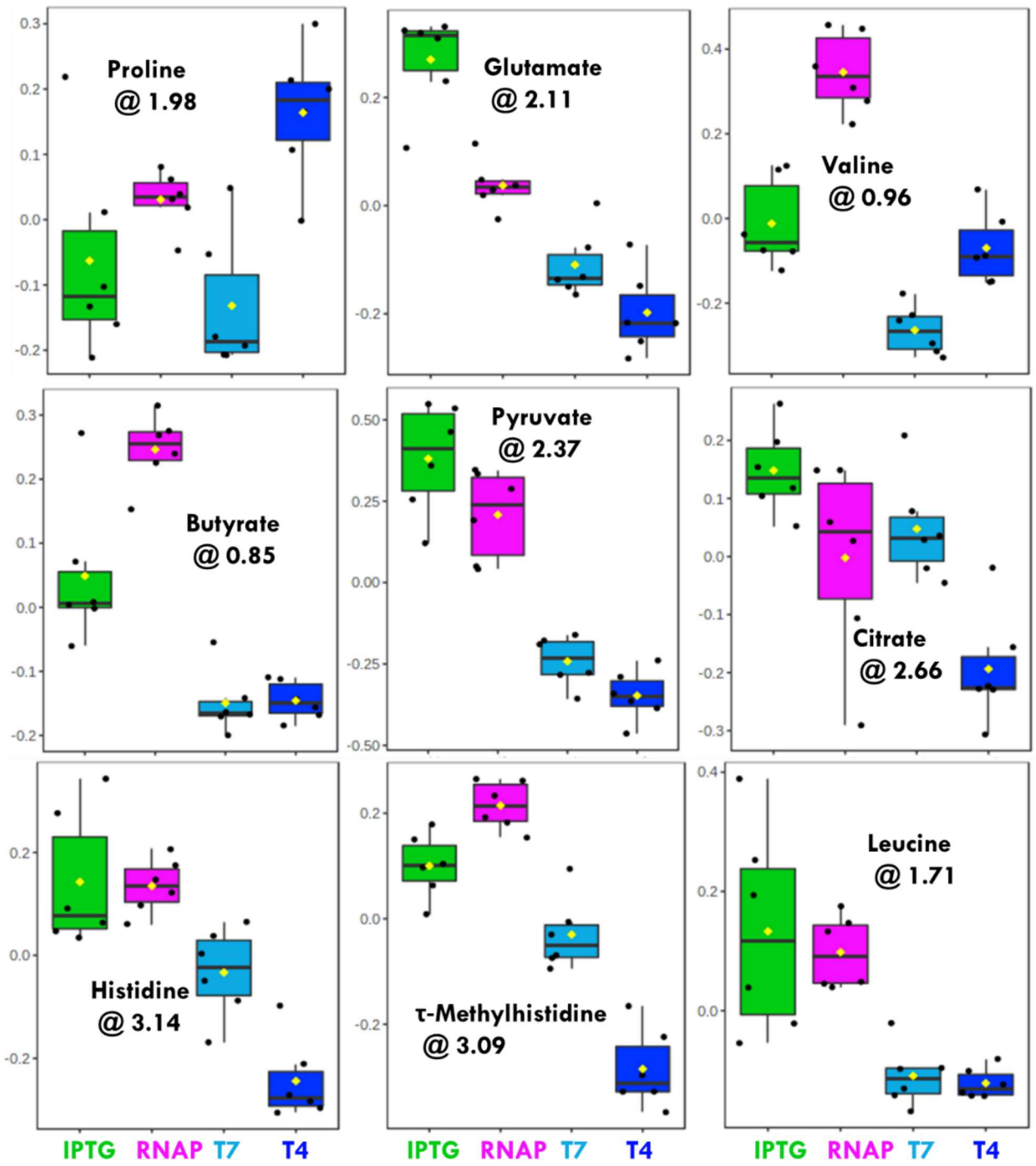

Figure 27: The box and whisker plots showing relative abundance of some of the metabolites showing significant variation among from IPTG treated (Green), phage polymerase (RNAP) expressing cells (Pink), phage endolysin T7 expressing cells (Cyan) and and phage endolysin T4 expressing cells (Blue).

C. Aromatic spectral region

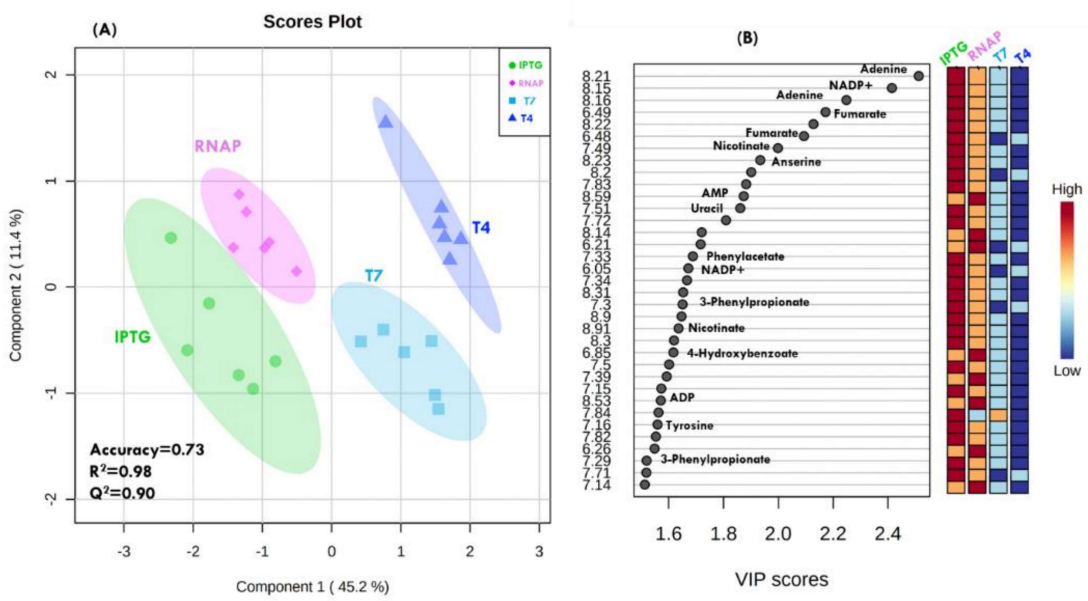

Figure 28: (A) partial least squares discriminant analysis (PLS-DA) resulted from the analysis of truncated Aromatic compounds region of 1D ^{1}H Carr−Purcell−Meiboom−Gill (CPMG) spectra of IPTG treated (Green), phage polymerase (RNAP) expressing cells (Pink), phage endolysin T7 expressing cells (Cyan) and phage endolysin T4 expressing cells (Blue) . (B) The VIP score plots used to identify metabolite entities of discriminatory significance.

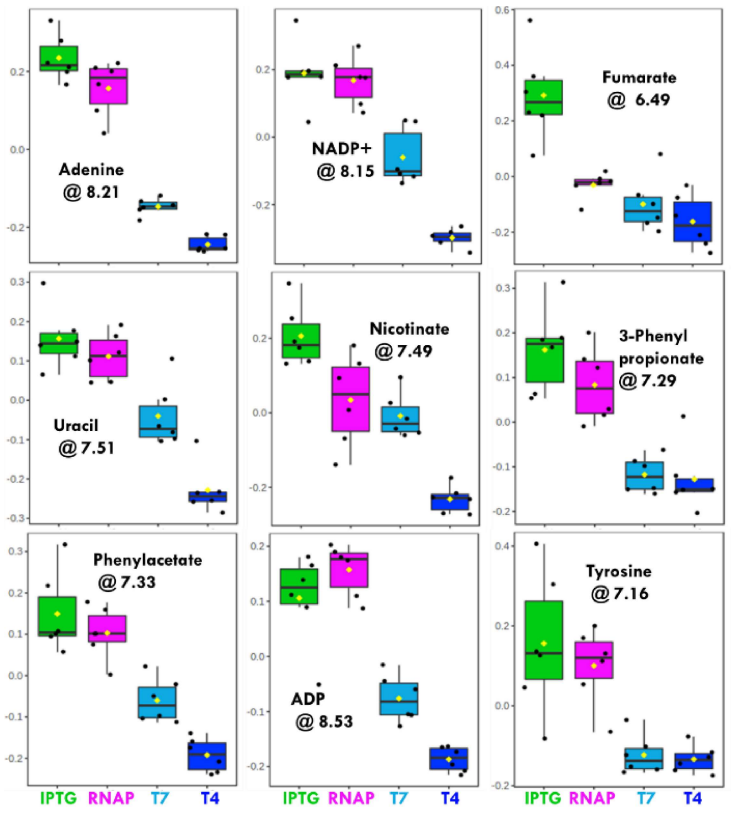

Figure 28: The box and whisker plots showing relative abundance of some of the metabolites showing significant variation among from IPTG treated (Green), phage polymerase (RNAP) expressing cells (Pink), phage endolysin T7 expressing cells (Cyan) and and phage endolysin T4 expressing cells (Blue).

The PLS-DA performed on truncated aromatic spectral region δ(5.82-9.35) ppm shown 2D score plot(**Fig. 28A)** and cross validated parameters are displayed for the model. The VIP score plot shown for top 35 bins (**Fig. 28B**). The metabolites responsible for the discrimination based on the criterion, that is, variables with variable importance on projection (VIP) value of >1.0 considered as candidate biomarkers. The representative box-cum whisker plots of the relative signal intensity for these potential metabolic markers are shown in **Fig. 29**. Metabolites like Fumarate, Adenine, NADP+ and other metabolites detected with high variance for the group discrimination and as biomarkers for the expression of phage endolysin T7 and phage endolysin T4 in bacterial cells.

Table 1: List of metabolites along with their respective chemical shifts and their respective metabolic fold change value w.r.t IPTG treated cells. One-way ANOVA conducted to determine the significant ($p<0.001$) metabolic changes.

S.No	**Metabolite Name**	**Assignment**	**Chemical shifts (δ) in ppm**	**Fold Changes observed**		
				RNAP	**T7**	**T4**
Amino Acids						
1.	Valine	γ^1-CH_3	0.95(d)	1.76	0.38	1.04
2.	Serine	α-CH	3.83(dd)	0.60	0.24	0.08
3.	Proline	$C4H_2$	1.98 (m)	1.31	0.66	2.23
4.	Tyrosine	C3H & C5H	7.16(m)	0.72	0.21	0.20
5.	Histidine	$C6H_2$	3.14(dd)	0.88	0.38	0.07
6.	Glutamate	β-CH_2	2.11(m)	0.46	0.25	0.17
7.	Glutamine	α -NH_2	6.85(s)	1.06	0.38	0.13
8.	Cystine	$C3H_2$&$C6H_2$	3.37(dd)	0.93	0.35	0.26
9.	Alanine	β-CH_3	1.45(d)	2.15	0.19	0.04
10.	Aspartate	C4H	3.89(dd)	0.85	0.26	0.07
11.	S-Sulfo-L-cysteine	$C4H_2$	3.67(dd)	1.43	0.52	0.36
12.	Homoserine	β-CH2	1.99(m)	0.97	0.58	1.70
13.	Glycine	α-CH2	3.53(s)	1.01	1.03	0.67
14.	N-Acetylglutamine	$C5NH_2$	6.81 (s)	1.08	0.44	0.23
15.	Leucine	*β,β'*-CH_2	1.71(m)	0.68	0.15	0.13
Carbohydrates/Sugars						

16.	Xylitol	C1H2	3.73(d)	0.85	1.37	0.80
17.	Xylose	C4H	3.41(t)	0.76	0.23	0.08
18.	Trehalose	C12H	3.83(m)	0.60	0.24	0.08
19.	Maltose	C2H	5.38(d)	0.50	0.19	0.05
20.	Mannitol	C5H&C7H	3.81(d)	0.59	0.26	0.08
21.	Mannose	C1H	5.19 (d)	0.72	0.34	0.14
22.	Glucitol(Sorbitol)	C5H	3.83(m)	0.60	0.24	0.08
23.	Gluconate	$C2H_2$	3.81(m)	0.59	0.26	0.08
24.	Glucose	C2H	4.63(d)	0.65	0.26	0.06
Nucleotides						
25.	Thymidine	C6H	7.62(q)	0.37	0.38	0.18
26.	Cytosine	C4H	7.51(d)	0.84	0.46	0.17
27.	dTTP	C2H	6.33(t)	0.59	0.28	0.23
28.	ADP	C7H	8.53(s)	1.25	0.31	0.11
29.	Adenine	C2H	8.21(s)	0.72	0.11	0.04
30.	AMP	C7H	8.59(s)	1.28	0.45	0.15
31.	Xanthine	C2H	7.93(s)	1.57	0.53	0.60
32.	Uracil	C6H	7.51(d)	0.84	0.46	0.17
33.	$NADP^+$	C41H	9.12(d)	0.61	0.16	0.27
Organic acids						
34.	Acetate	$C4H_3$	1.89(s)	0.39	0.31	0.24
35.	Galactarate	C6H&C8H	3.95(s)	0.65	0.21	0.04
36.	Galactonate	C3H&C7H	3.95(m)	0.65	0.21	0.04
37.	Glucuronate	C5H&C3H	3.73(m)	0.85	1.37	0.80
38.	Pyruvate	$C6H_3$	2.37(s)	0.60	0.08	0.04
39.	Levulinate	$C4H_3$	2.225(s)	3.49	0.60	0.75
40.	Malate	$C5H_2$	2.37(dd)	0.60	0.08	0.04
41.	Malonate	CH2	3.10 (s)	0.72	0.78	0.56
42.	cis-Aconitate	C8H	5.77(s)	0.92	0.30	0.06
43.	Citrate	$C2H_2$	2.67(d)	0.78	1.09	1.03
44.	Glycolate	α-CH2	3.94 (s)	0.56	0.25	0.03
45.	Succinate	$C2H_2$&$C3H_2$	2.40 (s)	1.21	1.06	0.36
46.	Lactate	β -CH_3	1.30(d)	1.18	0.90	0.63
47.	Formate	C2H	8.42(s)	0.63	0.27	0.41
48.	Fumarate	C4H&C5H	6.49(s)	0.23	0.17	0.11
49.	Butyrate	$C4H_3$	0.85(t)	2.47	0.19	0.18
Others						

50.	1 - Methyl Histidine	C2H	7.71(s)	0.85	0.20	0.24
51.	1,3-Dihydroxyacetone	$C2H_2$	3.57(s)	0.69	0.17	0.13
52.	2-Hydroxyisovalerate	$C6H_3$	0.81(d)	2.67	0.11	0.71
53.	3-Hydroxybutyrate	$C5H_3$	1.20(d)	0.81	0.61	0.08
54.	3-Phenylpropionate	C2H&C6H	7.29(m)	0.75	0.31	0.30
55.	4-Hydroxybenzoate	C2H&C6H	6.85(d)	1.06	0.38	0.13
56.	Acetoin	$C6H_3$	2.23(s)	2.59	0.30	1.06
57.	Anserine	C2H	8.23(d)	0.93	0.28	0.21
58.	Betaine	$C3H_2$	3.89(s)	0.85	0.26	0.07
59.	Cadaverine	$C3H_2$&$C5H_2$	1.43(q)	2.30	0.58	0.64
60.	Choline	$C5H_3$&$C6H_3$&$C7H_3$	3.19(s)	0.94	0.51	0.51
61.	Ethylene glycol	$C1H_2$&$C2H_2$	3.67(m)	1.43	0.52	0.36
62.	Glycerol	β-CH	3.81(m)	0.59	0.26	0.08
63.	Myo-Inositol	C2H	3.25(t)	0.60	0.26	0.20
64.	Nicotinic acid	C2H	8.91(d)	0.86	0.33	0.17
65.	O-Acetylcarnitine	$C9H_2$	3.81(dd)	0.59	0.26	0.08
66.	Phenylacetic acid	C5H&C3H	7.33(m)	0.79	0.34	0.13
67.	Saccharopine	C11H	3.57(t)	0.69	0.17	0.13
68.	Trimethylamine N-oxide	$C1H_3$&$C3H_3$&$C4H_3$	3.25(s)	0.60	0.26	0.20

Metabolic pathway analysis and biological significance interpretation:

68 compounds further assigned then annotated with KEGG and HMDB databases which showed significant metabolic profiles in endolysin T7 and endolysin T4 expressing cells in comparison to phage polymerase (RNAP) expressing cells, these compound list used to interpret the different metabolic pathways involved (E.coli metabolic database) using "Pathway Analysis" module in Metabo Analyst 5.0 .The module uses Hypergeometric Test for pathway enrichment and the topology analysis by Relative-betweeness Centrality of the pathways involved.

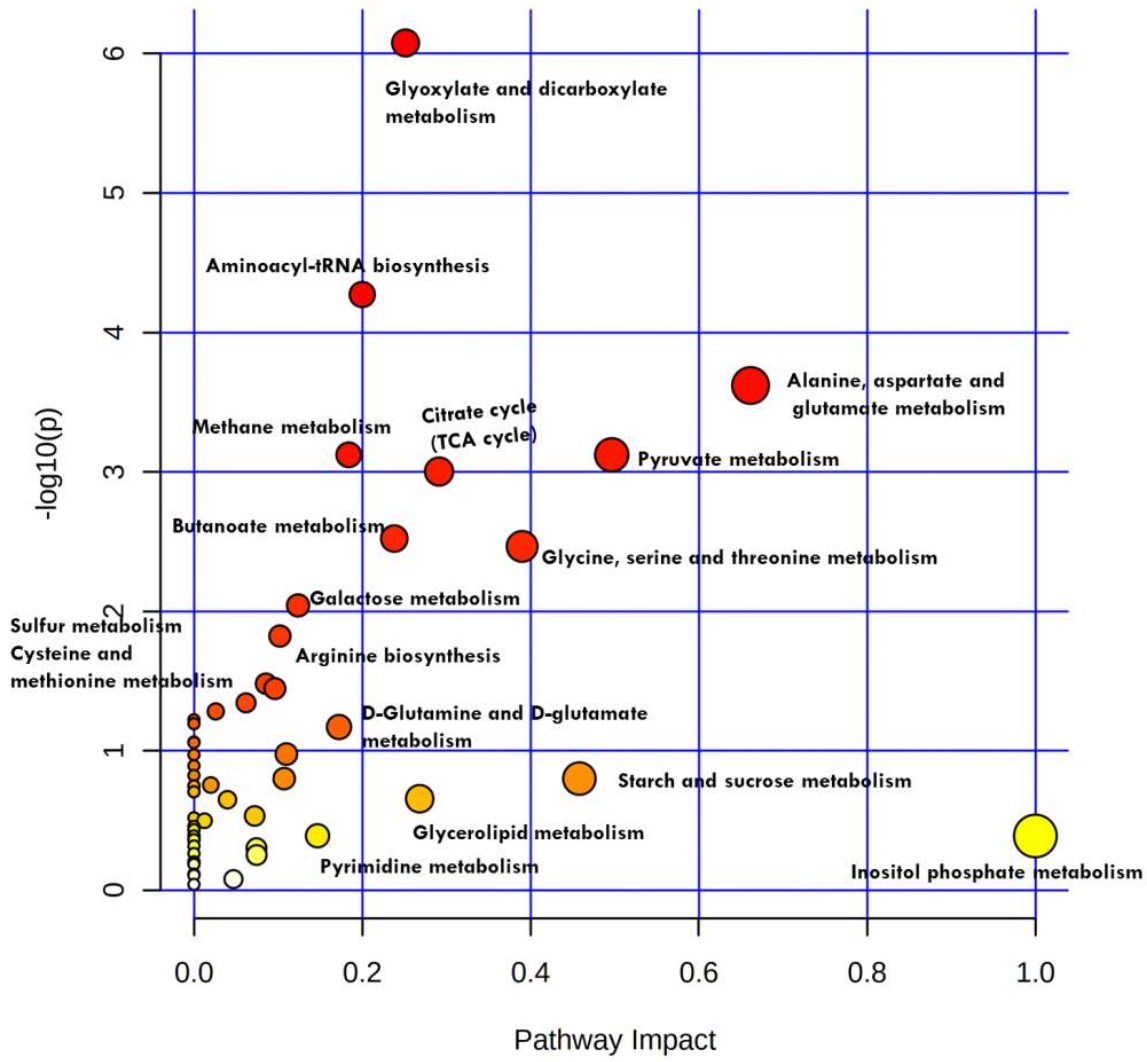

Figure 30: Summary of Pathway Analysis.

The **Fig. 30** shows all matched pathways according to the p values from the pathway enrichment analysis and pathway impact values from the pathway topology analysis. Around 50 metabolic pathways identified for given list of compounds. Among which pathways involved in Amino acids and Carbohydrate metabolism showed high impact.

Concluding remarks:

- The present work demonstrated the differential metabolic profiles in bacterial cells upon expression with phage endolysin T7 and phage endolysin T4.
- 2D Score plots of PLS-DA models showed distinct discriminant clustering among IPTG treated, phage endolysin T7, phage endolysin T4 and phage polymerase (RNAP) expressing bacterial cells
- The metabolic profiles of phage endolysin expressing cells were compared with phage polymerase (RNAP) expressing cells, where endolysin metabolic profiles showed major decrease in concentrations, whereas phage polymerase (RNAP) expressing cells showed similar trends as compared to control IPTG treated bacterial cells.
- Between phage endolysin T7 and phage endolysin T4, phage endolysin T4 showed high impact on most of the metabolic concentrations
- Pathway impact analysis showed that amino acid and carbohydrate/sugar metabolic pathways affected at a greater extent compared to other pathways.

(D) Heavy metal remediation characteristics of microalgal species detected from Ganga waters near Haridwar

The holy river Ganga is one of the scared rivers in India. It provides life sustenance to environment and ecology. Moreover, due to the copious availability of water throughout the year, it plays a major role in economy and civilization of human. Unfortunately, the advancement in human civilization also arises a question of safe potable water. Ungenerous release of pollutants, especially from heavy industries are major concern in developing countries. Intensification in industrial activities to meet the inexorable need of humans in the past few decades have also caused a long-term adverse impact on the environment. More often, the natural aquatic bodies are considered as the sink for the chemical wastes released from the industries. Industrial activities including smelting, mining, ore processing, electroplating, pigment manufacturing, battery production, disposal, textile, dye and chemical fertilizer production etc. are the prime contributor of chemical wastes. The released wastes from aforementioned industries contain hazardous pollutants like heavy metals, metalloids, organic and inorganic pollutants along with radionuclides. Among all, the persistent nature of heavy metals in aquatic bodies lead to its aggravation in the food chain causing severe threat to human life. There are numerous studies that highlight the status of heavy metals in Ganga water. Toxic elements such as arsenic (As), cadmium (Cd), cobalt (Co), chromium (Cr), copper (Cu), iron (Fe), manganese (Mn), zinc (Zn), and lead (Pb) are present in sediments and water of river Ganga, in varying concentrations ranging from substation to substation. The river Ganga originating from Gomukh in Uttar Kashi (Uttarakhand), passes through Haridwar Ghats, touches the banks of Kanpur, Varanasi in Uttar Pradesh, entering Bihar flowing to West Bengal and then enters to Bangladesh. Through this journey, it sustains more than 300 million people in India, Nepal and Bangladesh. The basins of Ganga in India cover the most populated and industrial areas. This arises the main concern as the industrial effluents released in the nearby areas carry significant quantities if heavy metals. The non-biodegradable and recalcitrant nature of these toxic heavy metals present in the river is potential risk to aquatic ecosystem, animals and humans.

Indeed, self-cleansing and healing nature of the sacred river Ganga is gaining attention throughout the globe. The mystery of the sacred water lies in the microbiome of the water which mainly involves the bacteriophages, algae and aquatic macrophytes. Microorganisms that inhabit extreme ecological niches have evolved and prospered as a consequence of persistence, adaptation, and specialization, serving as reservoirs of genotypes and specialized phenotypes. This phenotypic and genotypic plasticity makes extremophile microorganisms promising from the biotechnological perspective because they are adapted to unfavorable environments and provide efficient cells, enzymes, and catalytic systems under extreme conditions. Due to their unique physiological and enzymatic characteristics, these microorganisms provide potential applications for the bioremediation of soils, sediments and water contaminated with toxic pollutants.

Among all, microalgae have recently emerged as the potential candidate for removal of toxic pollutants. Its underlying mechanism of dealing with toxicity attracts attention of various scientific community. Microalgae are noteworthy photosynthetic microorganisms, yet simple and single celled but exhibit an intrinsic property to adapt and survive in harsh conditions and stressed environment. To understand the adaptive behavior of such microalgae we need to isolate tolerant strains and unravel the mechanism of the same. Keeping the above points in mind, we have categorized our whole work in four major studies: They are as following:

1. Isolation and screening of heavy metal tolerant oleaginous microalgae species from area near Haridwar Ghat.

2. Morphological and Molecular characterization of the isolated strains by 18 rRNA sequencing technology

3. NMR-based metabolomics to get insights into the molecular pathway responsible for heavy metal tolerance.

Study 1: Isolation and screening of heavy metal tolerant oleaginous microalgae species from area near Haridwar Ghat.

Isolation: In the first objective, water and soil samples were collected from contaminated area near Haridwar Ghat. The samples were serially diluted and spread over BBM (bold's basal media) agar plates. Those plates were incubated at room temperature under continuous illumination (300 µmol m^{-2}/s) for 15-20 days. After incubation, single colonies were picked with the help of sterilized needle, observed under microscope and streaked over another BBM agar plates. This step is repeated till single colonies are obtained. The obtained single cells are inoculated in BBM and allowed to grow for 10-15 days to get a well grown microalgae culture.

Materials and equipment required for isolation of microalgae:

- 50 ml falcons
- Strainer
- Sterilized BBM agar petri plates
- Inoculation loop
- Ampicillin stock (100 mg/ml)
- Amphotericin stock (1 mg/ml)
- Laminar air flow
- Fluorescence microscope
- Incubator @ 25 °C
- White light illumination (300 µmol m^{-2}/s)

Table1: Composition of modified BBM (purchased from Himedia, India)

Chemical name	Quantity (g/L)
Sodium nitrate ($NaNO_3$)	0.25
Potassium dihydrogen phosphate (KH_2PO_4)	0.175
Potassium hydrogen phosphate(K_2HPO_4)	0.075
Magnesium sulphate heptahydrate ($MgSO_4 \cdot 7H_2O$)	0.075
Sodium chloride (NaCl)	0.025
Calcium chloride dihydrate ($CaCl_2.2H_2O$	0.025
Iron sulphate heptahydrate ($FeSO_4 \cdot 7H_2O$)	0.005
Disodium ethylenediaminetetraacetic acid, Na_2-(EDTA)	0.005
Micronutrient solution	1 ml
pH	7.2-7.4

Table 2: Composition of micronutrient solution (purchased from Himedia India)

Chemical name	Quantity (g/L)
Boric acid (H_3BO_3)	2.86
Zinc sulphate heptahydrate ($ZnSO_4 \cdot 7H_2O$)	0.222
Copper sulphate pentahydrate ($CuSO_4 \cdot 5H_2O$)	0.079
Manganese chloride tetrahydrate ($MnCl_2 \cdot 4H_2O$)	1.81
Cobalt nitrate hexahydrate ($Co(NO_3)_2 \cdot 6H_2O$)	0.041
Sodium molybdate dehydrate ($Na_2MoO_4.2H_2O$)	0.390

Methods:

- In detail, the collected soil sample was first diluted with autoclaved distilled water and was observed under light microscope to confirm the presence of green microalgal species.
- After monitoring the presence of microalgal species, the sample was further diluted with distilled water and the highest dilution was plated on BBM agar plate.
- The plates were irradiated under white cool fluorescent tubes (300 µmol m^{-2} s^{-1}) at 25°C for 15-20 days under observation.
- The points having green colonies were marked and streaked on different BBM agar plates for further experiments.
- After various rounds of streaking, clear colonies on different plates were obtained and confirmed by microscopic analysis.

- Furthermore, the single green colonies were picked with sterilized tips and were inoculated in 20 ml BBM media.
- The cultures were allowed to grow properly for 15-20 days and the cultures were monitored after every 3 days under microscope to avoid any contamination.
- After complete growth of cell culture, glycerol sock was made and preserved under -80ºC.

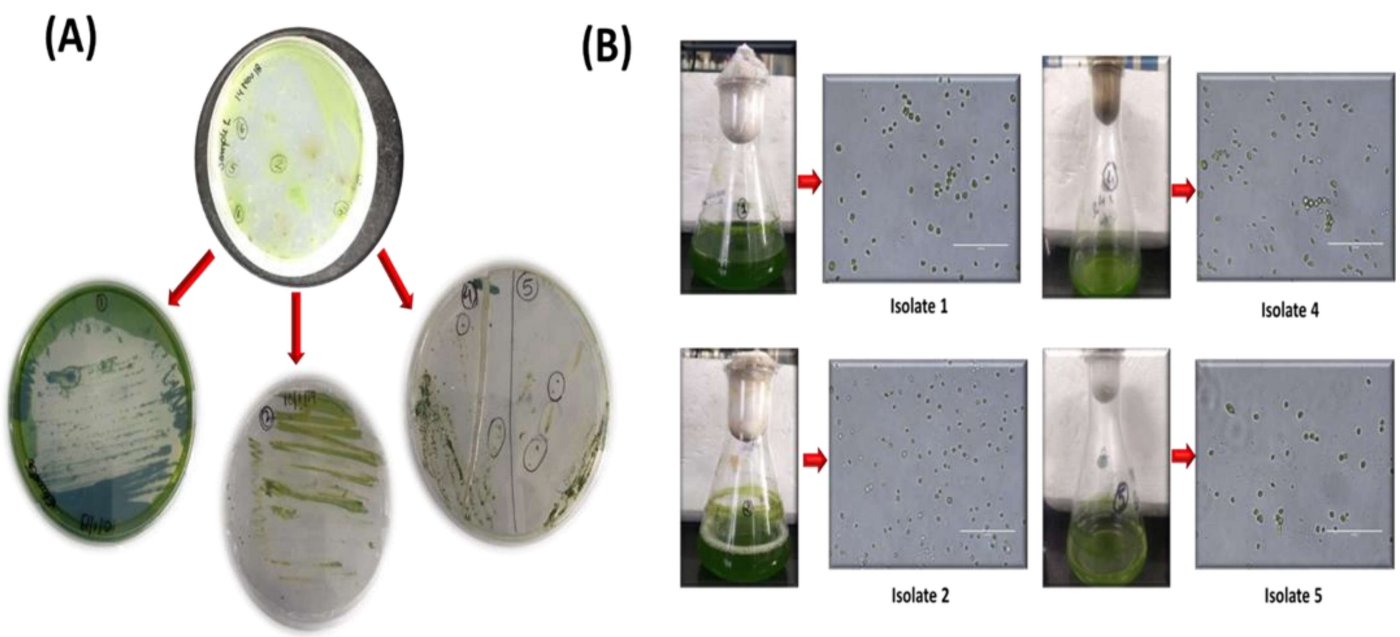

Figure 1: (A) Isolation of four new microalgae isolates and **(B)** cultivation of microalgae and microscopy images.

(B) Screening and selection of potent species for removal of heavy metals such as arsenic, cadmium and lead:

Heavy metal uptake by microalgae is not a single step process; it comprises of different mechanisms including physical adsorption, electrostatic interactions, complexation, ion exchange, oxidation, reduction and precipitation etc. However, the principal mechanism can be divided into two basic steps (1) the fast adsorption of heavy metal ions onto the functional groups available on the cell wall of the microalgae also termed as biosorption and (2) the slow internalization of the metallic ions inside the cell or bioaccumulation.

Biosorption

Biosorption is a surface phenomenon, which is rapid, reversible, and independent of the metabolism of the cell. The cell wall of microalgae is made up of proteins, polymeric chain of different sugar molecules such as starch, cellulose, hemicellulose and lipid constituting different functional groups [-COOH (carboxyl), -OH (hydroxyl), $-PO_3$ (phosphate), $-SH_2$ (sulfyhydryl) and $-NH_2$ (amino) etc. These functional groups lead to the efficient binding of different heavy metals

making microalgae an excellent biosorption surface. Biosorption can be categorized in two processes: physical adsorption and chemical adsorption. Physical adsorption can be defined as the retention of metal ions on the biosorbent i.e. algae biomass by virtue of Vander Waals force and electrostatic interaction, whereas chemical biosorption involves a chemical reaction such as ion exchange.

Bioaccumulation:

Bioaccumulation is an active metal uptake process and irreversible in nature comprising both adsorption and absorption. It is a comparatively slow process as to biosorption as there exist transfer of the metal ions through the cell membrane barrier and their consequent sequestration inside the cells organelles. Membrane transporters play a pivotal role in the interaction of the microalga with the heavy metal ions. Once the metal reaches inside the cell, detoxification can occur by either binding to specific peptides or their compartmentalization in cell organelles or by fluxing out the metal again outside the cell. The most common phenomenon is production of phytochelatins or metallothionien peptides which bind to metal ions and form organometallic compounds which prevent the toxicity to cells. Phytochelatins are basically low molecular weight (2 to 10 kDa) cysteine rich peptides. Synthesis of phytochelatin in microalgae is reported to be induced by bioaccumulation of heavy metals such as Ag, Au, Co, Cd, Hg, Pb, Zn and As. The underlying mechanism of metal detoxification can be understood by **Fig 4**.

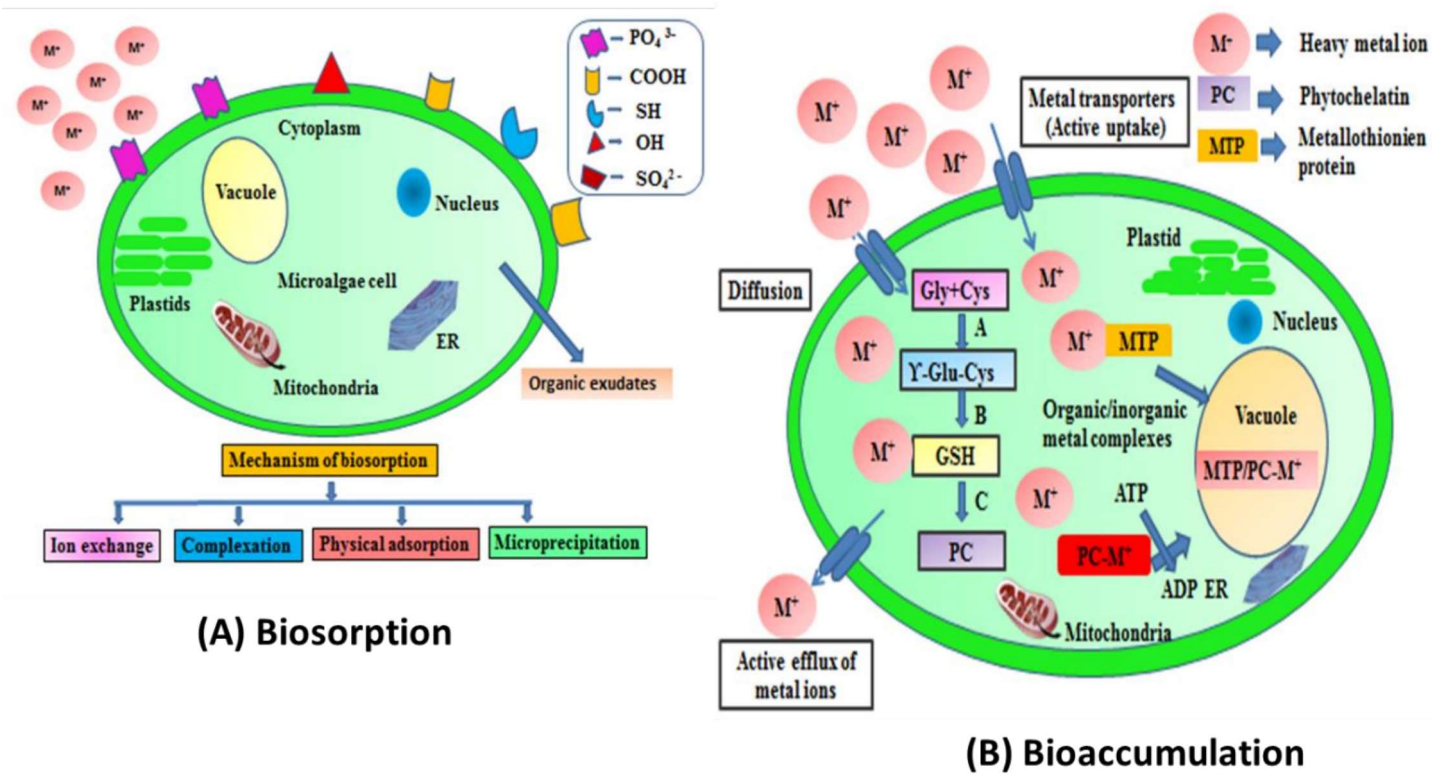

Figure 2: Mechanism of heavy metal removal by microalgae **(A)** Biosorption and **(B)** Bioaccumulation**.**

Few previously isolated and sequenced microalgae strains from contaminated Haridwar Ghats, (three *Scenedesmus* sps., *one Chlamydomonas*, and two *Chlorella* sps.), were studied for their ability to grow and remove heavy metals such as arsenic, cadmium and lead separately in BBM supplemented with different concentrations of these metals. After several investigations, and on the basis of microscopic analysis and viability of microalgae species in heavy metal supplemented BBM, concentration of arsenic, cadmium and lead was fixed to 5 and 10 ppm.

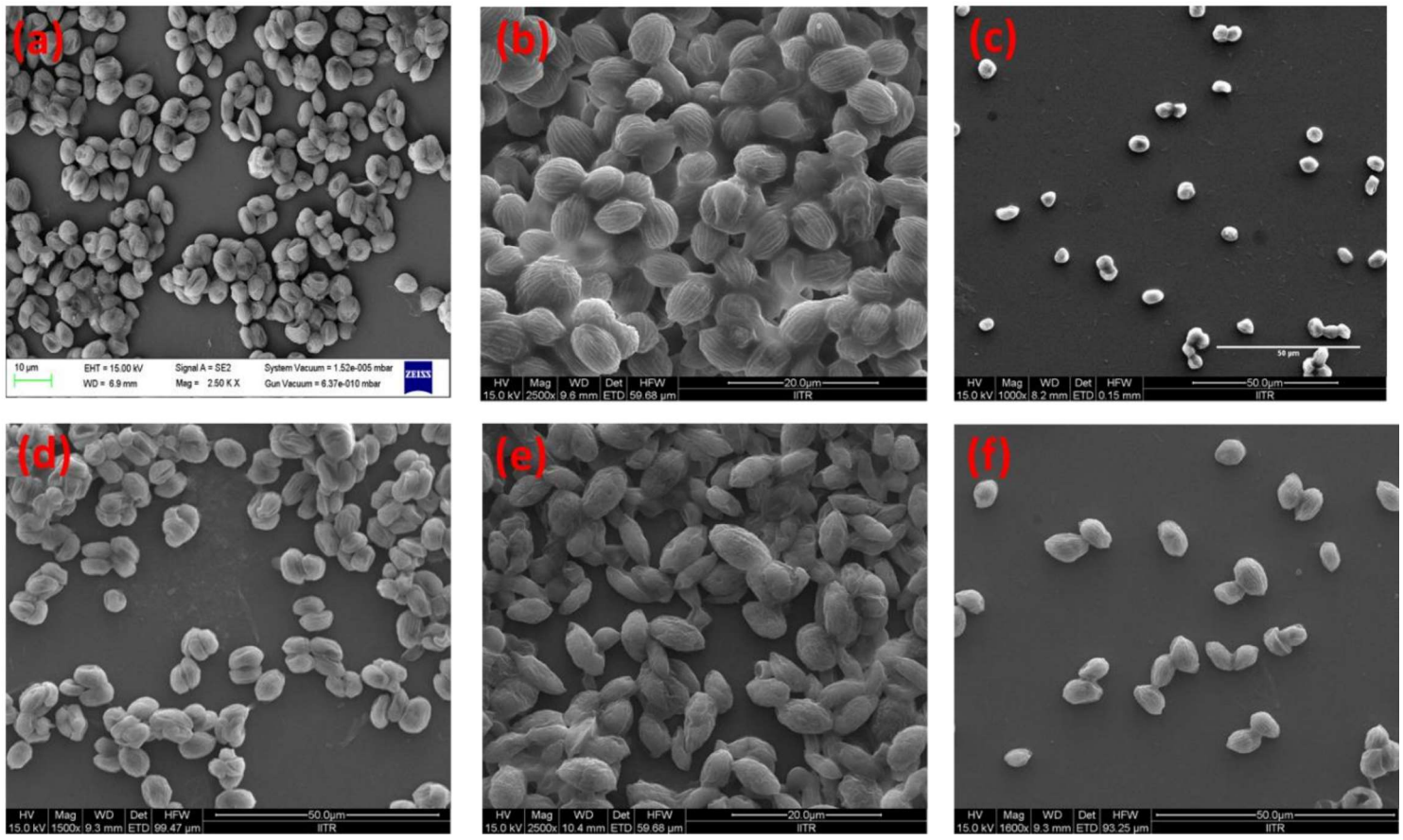

Figure 3: Scanning electron microscopy (SEM) images **a)** *Scenedesmus* sp. 1 **b)** *Scenedesmus* sp. 2 **c)** *Chlorella* sp.1 **d)** *Chlamydomonas* sp**. e)** Scenedesmus *sp.* 3 **f)** *Chlorella sp.*2

Materials required for studying detoxification of heavy metals by microalgae:

- Milli Q water
- Concentrated Nitric acid (HNO_3)
- Glass test tubes
- Lead nitrate ($PbNO_3$)
- Cadmium chloride ($CdCl_2$)
- Sodium arsenate ($Na3AsO_4$)
- Sodium arsenite ($NaAsO_2$)
- Well grown microalgae culture

- ICP-MS (Inductively coupled plasma membrane mass spectroscopy)
- Syringe filters (0.45 µm)

Method:

- In detail, different microalgae species were exposed to (5, 10, 25, 50, 100, 200, 300, 400, 500, 600, 700, 800, 900 and 1000 mg L^{-1}) of As (III), As (V), Cd (II), and Pb (II) by dissolving sodium arsenite, sodium arsenate, cadmium chloride and lead nitrate salts respectively in MilliQ water.
- On the basis of viability studies, different microalgae species were selected as per their potential to grow in toxic concentrations of different heavy metals.
- Further, the potent species were grown in selected concentration for a period of 15 days and were microscopically examined after incubation.
- To examine the stress induced lipid production in microalgae species, Nile red staining was done to stain the neutral lipid bodies in the cells.
- Simultaneously, the supernatant was collected to examine the residual heavy metal concentration in the media.

Preparation of samples for quantitative analysis of heavy metals after treatment by microalgae:

- Before, measuring the residual heavy metal content in supernatant, standards of each salt were made in MilliQ water with different concentrations ranging from 5 to 50 ppb.
- In order, to perform the analysis, the samples were diluted appropriately to bring the concentration in ppb range.
- Before dilution, the samples were filtered with 0.45 µm syringe filter and all the glass wares used were soaked in 0.1 M HNO_3 to avoid any prior metal contamination.

Preparation of samples for Nile red staining:

- Nile Red stain (9-diethylamino-5H-benzo[a]-phenoxazine-5-one) was purchased from Invitrogen (Life Technologies, USA).
- Nile red stock (1 mg/ml) was made in DMSO (Dimethyl sulfoxide) and was further diluted 100 times with same solvent.
- Well grown cultures after 10-15 days of incubation were used for Nile red staining.
- 200 µl of microalgae suspension was mixed with 10 µl of Nile red solution and incubated for 15 minutes in dark at room temperature.
- After incubation, cells were washed thrice with 0.9% NaCl in order to wash any remaining dye.
- After appropriate washing, the cells were microscopically analyzed for yellow color florescence under RFP filter.

Results:

Arsenic detoxification studies:

- Exposure of different microalgae species to various concentration of arsenic showed that *Chlorella* sp.2 and *Scenedesmus* sp. 1 were able to grow properly in 500 ppm of both forms of arsenic but 10 ppm was fixed for all the studies.
- Microscopy analysis and Nile red staining showed that underlying mechanism to cope with metal toxicity is lipid production.
- Percentage removal of both forms of arsenic was observed after 10 days of incubation by using supernatant and analyzing it with ICP MS (Inductively coupled plasma mass spectrometry).

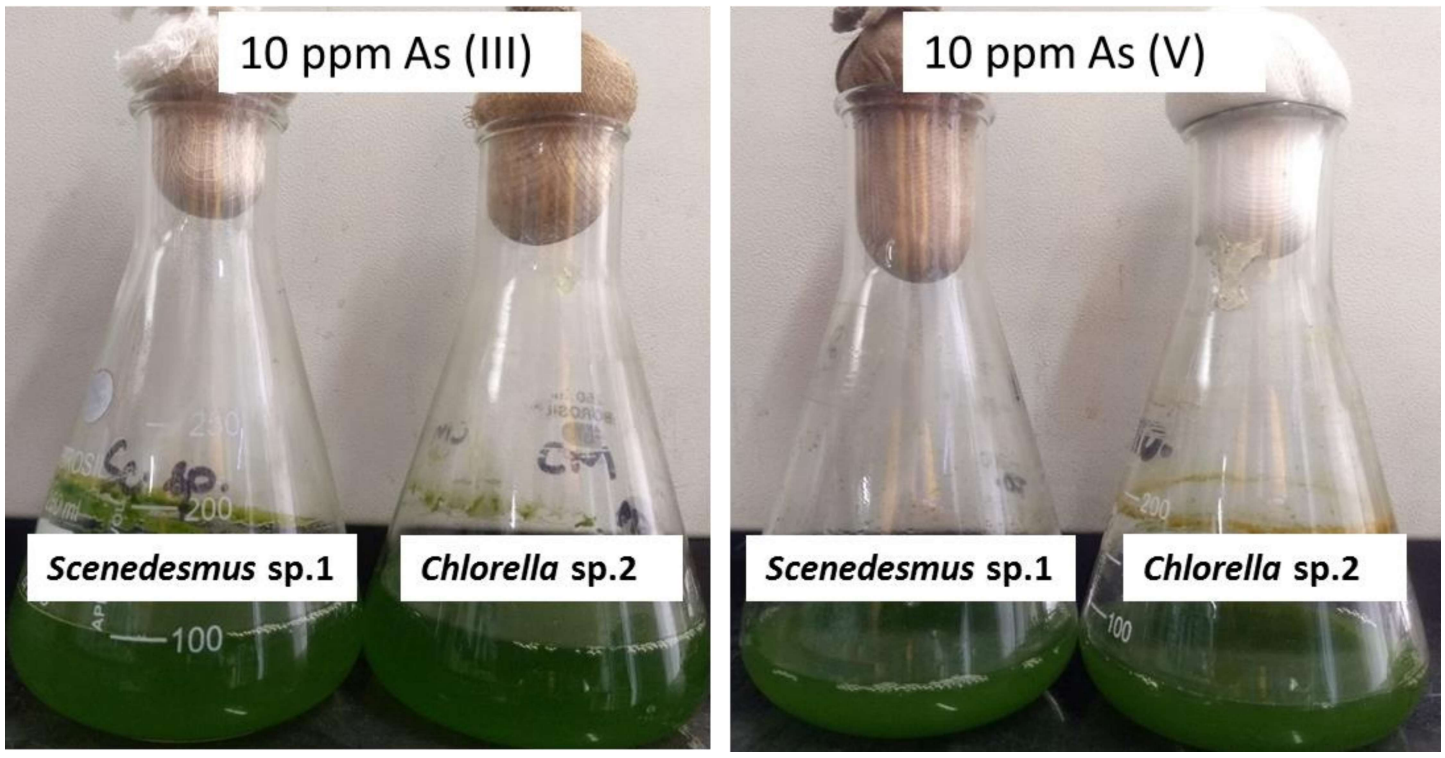

Figure 4: Cultures of *Scenedesmus* sp.1 and *Chlorella* sp.2 grown in BBM spiked with 10 ppm of As (III) and As (V).

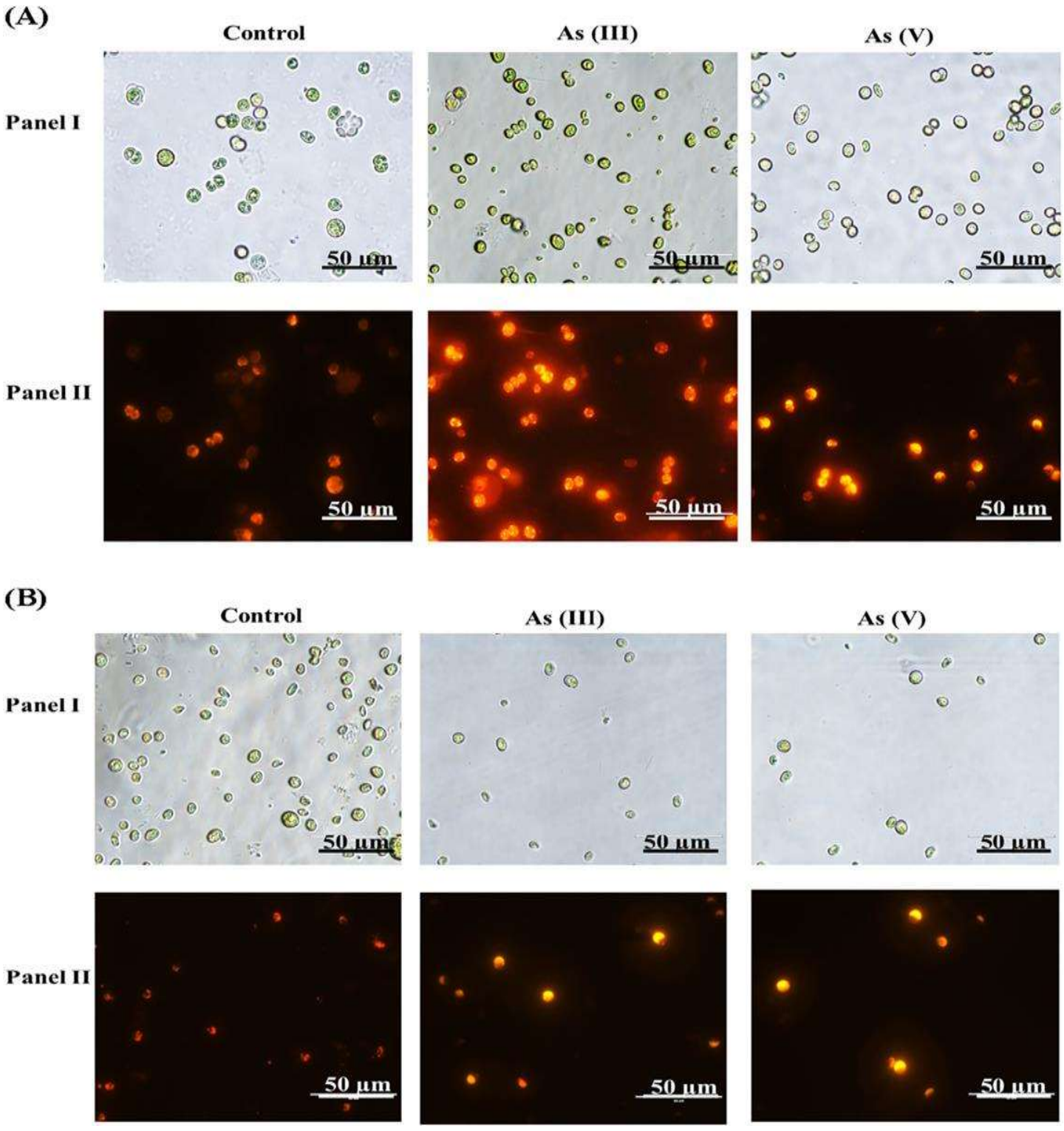

Figure 5: Microscopy images of arsenic spiked microalgae (A) *Chlorella* sp. 2 (B) *Scenedesmus* sp.1.

Cadmium detoxification studies:

- Different microalgae species were grown in cadmium supplemented with concentration ranging from 5-1000 mg/L of cadmium, and on the basis of viability studies, two concentrations 5 and 10 ppm were selected.
- Microscopy and Nile red staining was done to observe lipid induction in cells.
- Removal of cadmium form media was analyzed in supernatant by ICP-MS.

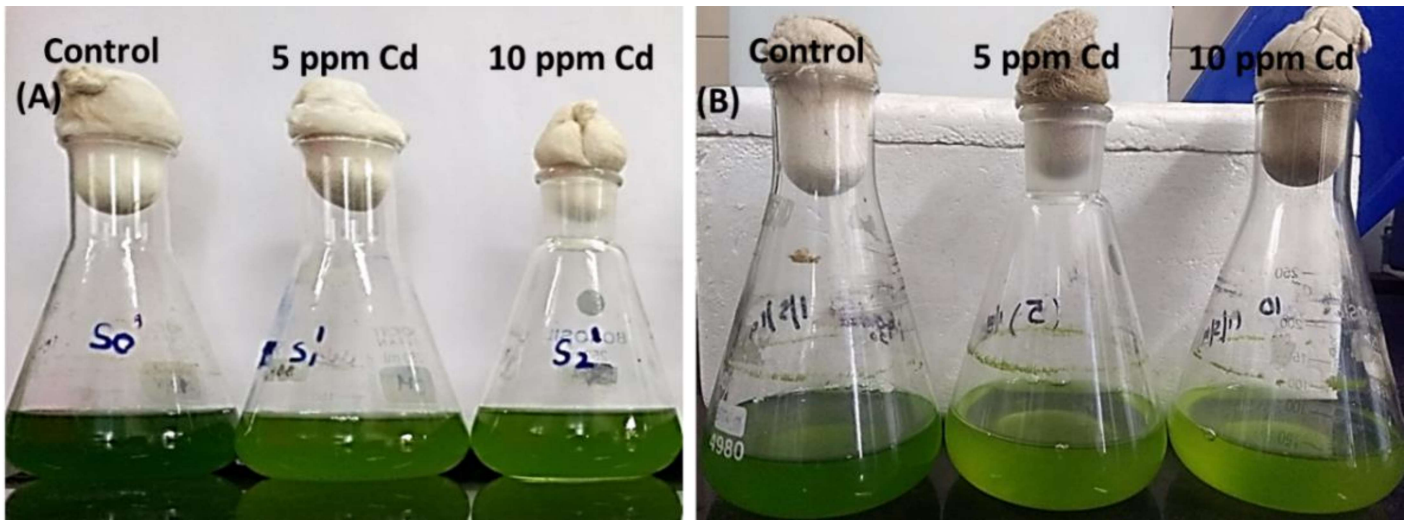

Figure 6: Cultures of (A) *Scenedesmus* sp.1 (B) *Scenedesmus* sp. 2 grown in BBM spiked with 5 and 10 ppm of Cd (II).

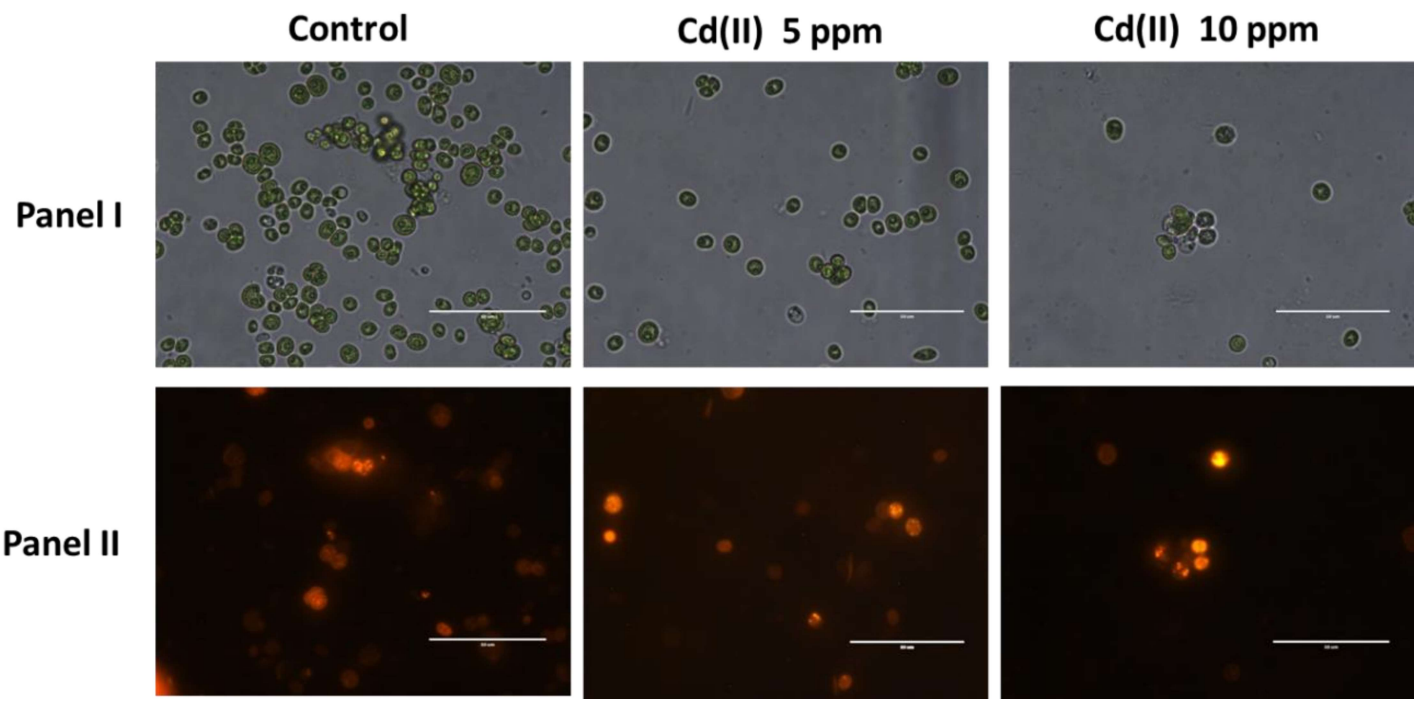

Figure 7: Microscopy and Nile red staining images of *Scenedesmus* sp.1 on exposure of cadmium chloride.

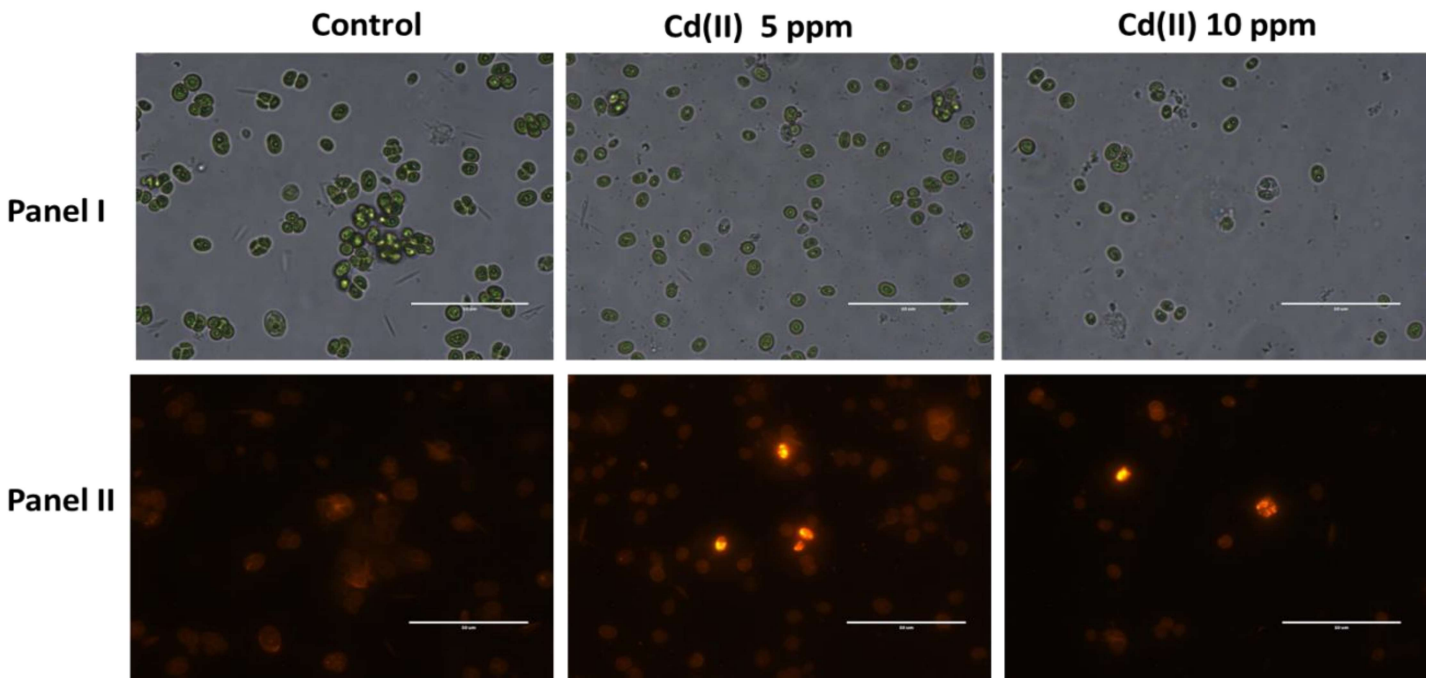

Figure 8: Microscopy and Nile red staining images of *Scenedesmus* sp. 2 on exposure of cadmium chloride.

Lead detoxification studies:

- For lead removal lead nitrate was supplemented in BBM at concentration of 5 and 10 ppm and different microalgae species were cultivated for 15 days.
- Microscopy and Nile red staining was done to observe induction of lipid bodies in the cell.
- Removal of lead in the medium was studied by using the supernatant and analyzing it with ICPMS.

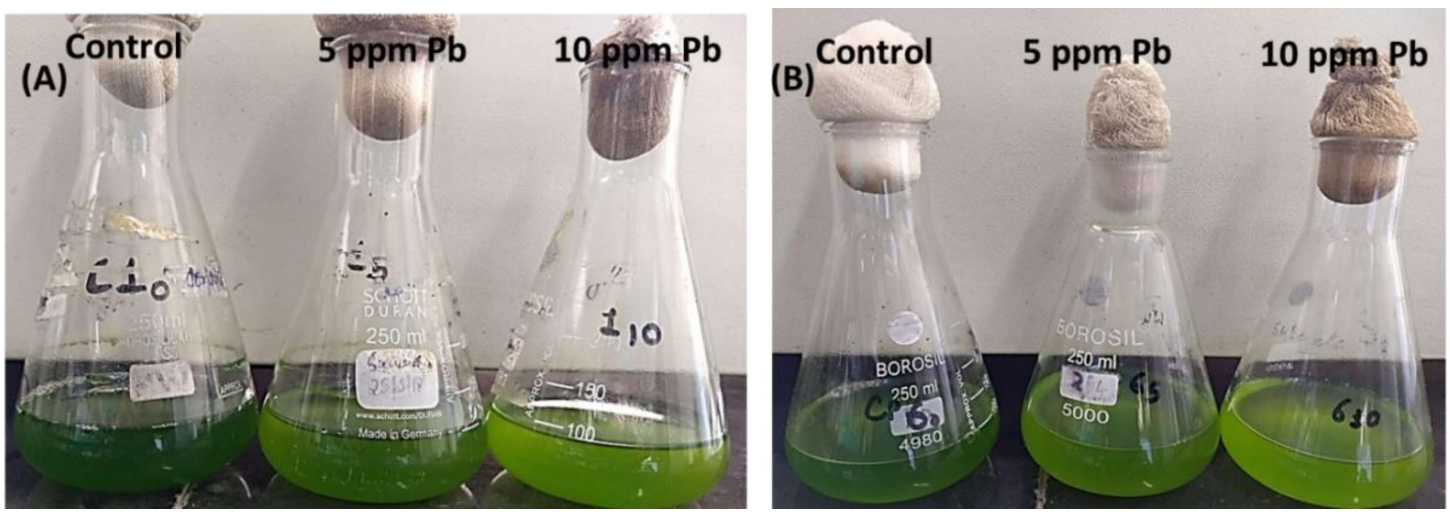

Figure 9: Cultures of (A) *Scenedesmus sp.* 1 (B) *Chlorella* sp.1 grown in BBM spiked with 5 and 10 ppm of Pb (II).

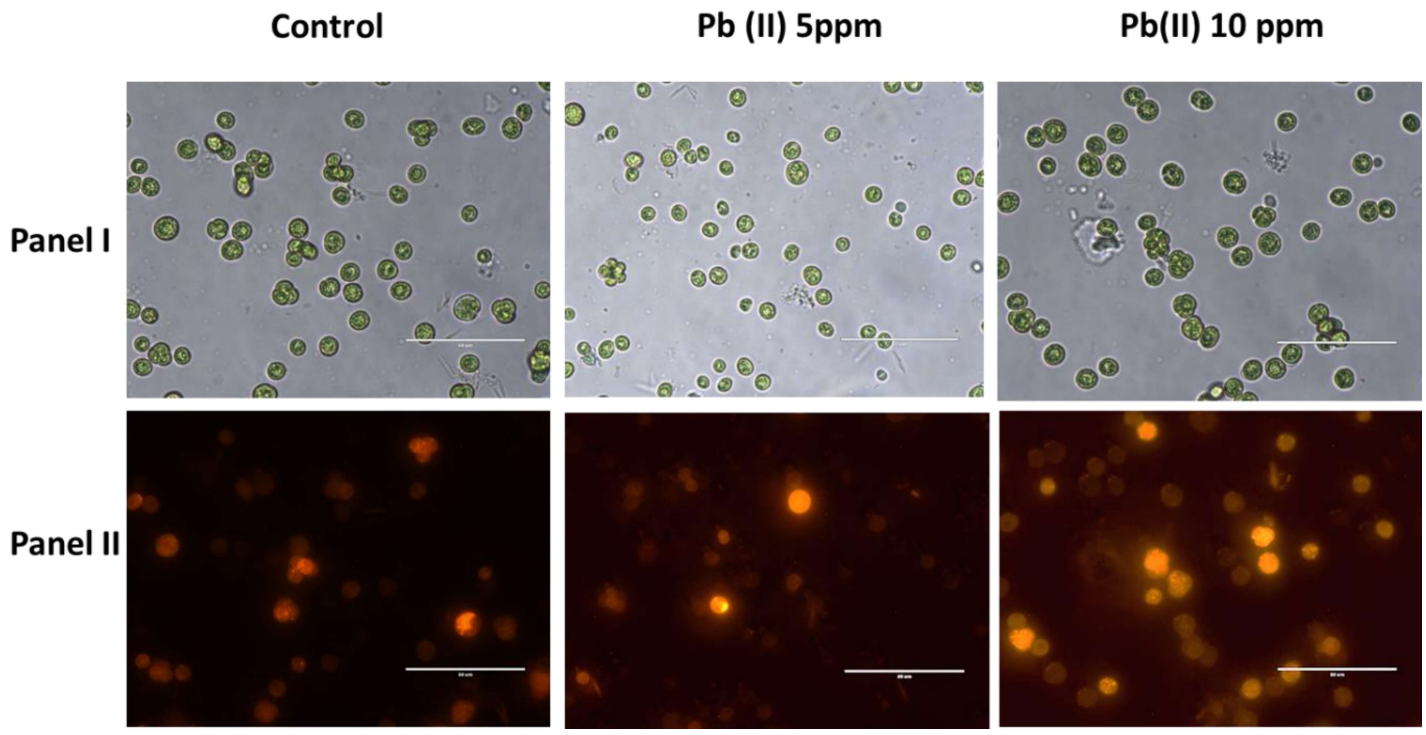

Figure 10: Microscopy and Nile red staining images of *Scenedesmus* sp. 1 on exposure of lead nitrate.

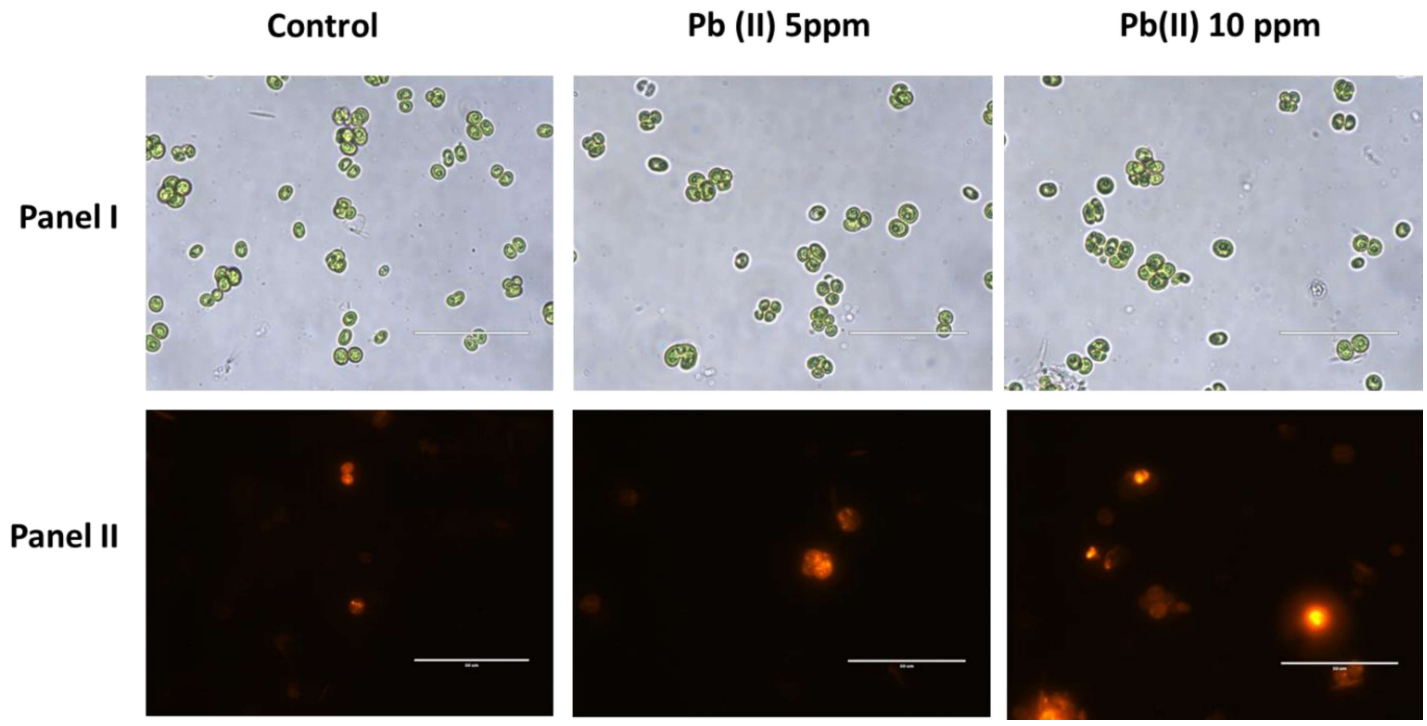

Figure 11: Microscopy and Nile red staining images of *Chlorella* sp. 1 on exposure of lead nitrate.

Conclusions:

- In conclusion, this study shows the potential of different microalgae species to grow and tolerate heavy metal ions such as Arsenic, both As (III) and (V), Cadmium Cd (II), and Lead Pb (II).
- Among all the screened microalgae strain, *Scenedesmus* sps. and *Chlorella* sps. showed high tolerance against As (III), As (V), Cd (II), and Pb (II).
- Further, the excellent removal efficiency of the microalgae species opens the possibility of utilizing these microalgae strains as candidate for bioremediation. The removal profile of all the used stain in presence of different heavy metal ions has been represented in **Table 3**.
- Overall, this study proposes an eco-friendly approach for wastewater bioremediation in a cost-effective manner.

Table 3: Removal efficiency of the selected microalgae strains in different heavy metals

Microalgae species	**Arsenic (10 ppm)**		**Cadmium**		**Lead**	
	As (III)	**As (V)**	**5 ppm**	**10 ppm**	**5 ppm**	**10 ppm**
Scenedesmus sp.1	**98%**	**97%**	**89%**	**93.56%**	**88.6%**	**91.4%**
Chlorella sp.1	**89%**	**86%**	**-**		**-**	
Chlorella sp.2	**-**		**-**		**91.6%**	**94.5%**
Scenedesmus sp.2	**-**		**80%**	**85%**	**-**	
Coccomyxa sp.	**-**		**95%**	**94%**	**98.4%**	

Study 2: Morphological and molecular characterization of the isolated strains by 18 rRNA sequencing technology

Morphological characterization: Microscopic observation under light microscope help to understand the shape and size of the isolated strains. It also helps to understand the overall properties based on classical taxonomy. Further confirmation of the cells size and structural information, scanning electron microscopy is used. FE-SEM helps to understand the surface detailing of the cells, gets the accurate size, shape, presence or absence of coenobium with details of the edges. In brief, algal cell suspension was fixed with 2.5 % glutaraldehyde and incubated overnight in dark at 4°C. Before examination, the samples were dehydrated in 10-90% ethanol and sputtered with gold to ensure the electrical conductivity of the samples during FE-SEM analysis. In case of heavy metal treatment, FE-SEM also help to understand the underlying mechanism of biosorption, through which metals get attached to cell surface of the microalgae. The aberration and disorganization in the cell wall are also clearly visible under such heavy metal toxicity.

Molecular characterization: The uncontaminated and single cell culture is treated appropriately to isolate the genomic DNA. The genomic DNA is amplified by using ITS fragments in PCR

(polymerase chain reaction) machine. The nucleotide sequence is obtained and compared with the available sets in the NCBI database. In result, a phylogenetic tree is drawn with MEGA7 software to get the closest member to the unknown segment. Based on the similarity index the unknown set is assigned a genus name.

Material and methods:

- After several rounds of streaking, single colonies of isolate 1 and 2 were cultivated in flasks and 50 ml culture suspension of each was collected for genomic DNA isolation.
- Genomic DNA for both samples was amplified using the ITS 1 "TCCGTAGGTGAACCTGCGG" and ITS2: GCTGCGTTCTTCATCGATGC and were sequenced using ABI 3130XL Genetic Analyzer machine.
- Amplification Strategy: Sample:1µl (10 times dilution of genomic DNA), Primer(10pmol/µl): 0.25/0.25µl (ITS1/ITS2), TaqMaster mix(G9 Taq): 12.5µl Distilled water: 11µl, Total volume: 25µl.
- PCR program used for above amplification was as follows: 95°C for 5min , (95°C for 30 sec, 55°C for 30sec and 72°C for 30sec) 30 cycles and 72 °C for 10min
- The FASTA sequences obtained were compared with the sequences available at NBCI database (http://www.ncbi.nlm. nih.gov/), using BLAST programme.
- To determine the relationships of novel microalgae isolates, phylogenetic tree was constructed using MEGA 7 software.
- The evolutionary history was inferred using the Neighbor-Joining method. The optimal tree with the sum of branch length = 0.60081441 is shown.
- The tree is drawn to scale, with branch lengths in the same units as those of the evolutionary distances used to infer the phylogenetic tree. The evolutionary distances were computed using the Maximum Composite Likelihood method and are in the units of the number of base substitutions per site.

Results:

<u>Genomic DNA amplification results:</u>

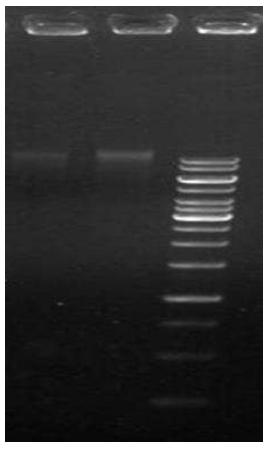

Figure 12: Lane 1 (isolate 1), Lane 2 (isolate 2) and Lane 3,1 kb DNA ladder.

Table 4: FASTA sequence of isolate 1 obtained after sequencing

ITS sequence	Raw FASTA sequence of isolate 1 obtained after sequencing
>Algae1-ITS1	TTTTTAAACACAAACCGCGGACCAACGTATCCCGCGGACGG CTTCTTCTTCGTGAAAGAAAGCCGGCTGTGCGCTTGTCCCTG TCCGGCGCCTCTTCGGGGGAGCCGGCAGGTCTGGCGGGCTG GGGAGGACGCTCTCCTCTAACCGGGAGAGGGGCCAACCCCG GCTGGCAAAACCCCTATTCAATCCCCAACAGCAATCCATCTG AAGATCTGGACGGCCGCTTGAGTGCGGTCGTCTCCAACCGA AGACAACTCTCAACAACGGATATCTTGGCTCCCGCATCGATG AAGAACGCAGCAA
>Algae1-ITS2	TGTTAGTTGGTTGGGAGTGTCTTCGGTGGAGACGACCGCACT CAAGCGGCCGTCCAGATCTTCAGATGGATTGCTGTTGGGGAT TGAATAGGGGTTTTGCCAGCCGGGGTTGGCCCCTCTCCCGGT TAGAGGAGAGCGTCCTCCCCAGCCCGCCAGACCTGCCGGCTC CCCCGAAGAGGCGCCGGACAGGGACAAGCGCACAGCCGGCT TTCTTTCACGAAGAAGAAGCCGTCCGCGGGGATACGTTGGTT CGCGGTTTGTGTTTGATCGATGCAATGATCCTTCCGCAGGTT CACCTACGGAA

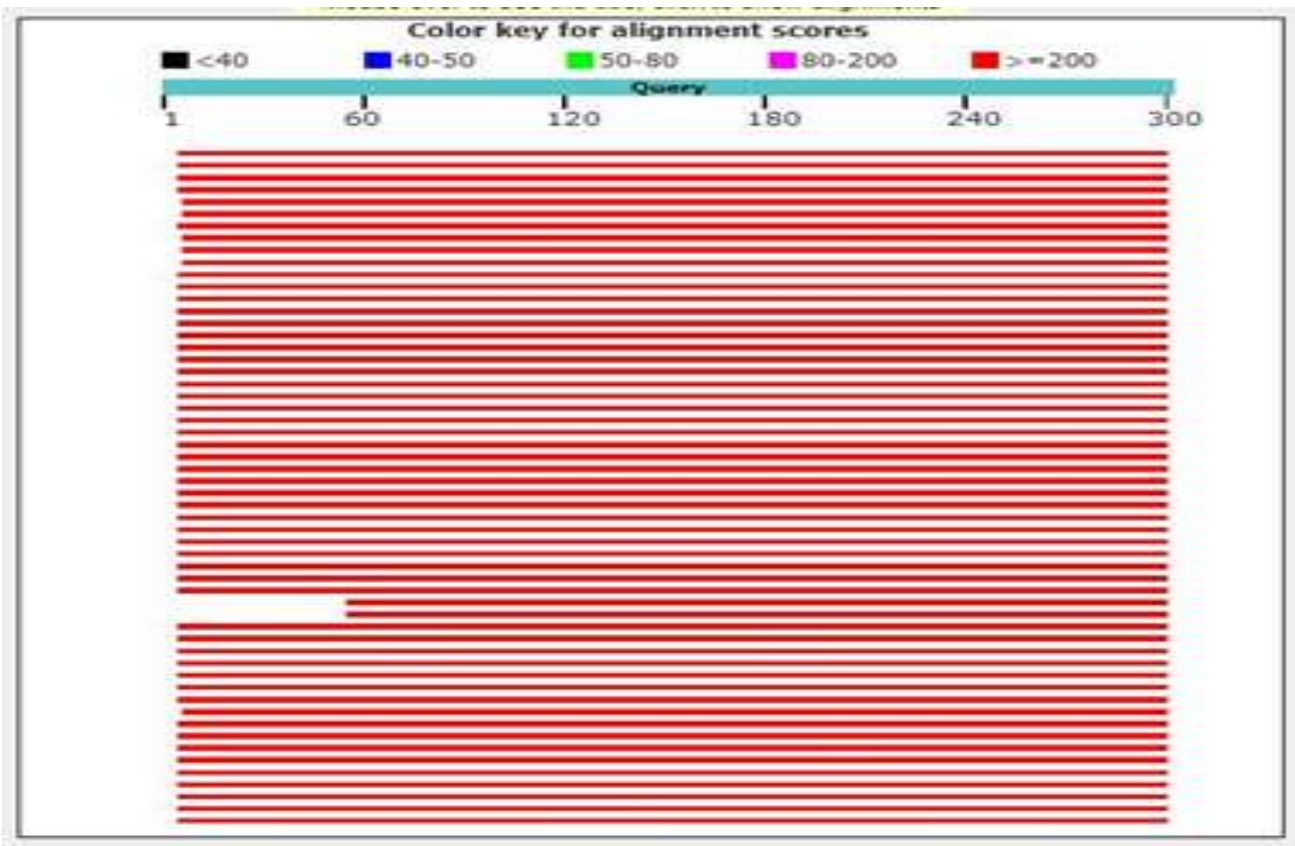

Figure 13: NCBI Blast report for isolate 1

Table 5: Sequences similarity results of FASTA sequence of algal isolate 1 with nucleotide sequences present in NCBI database

Sequences producing significant alignments:	**Score (Bits)**	**E-value**	**Maximum identity**
Coccomyxa melkonianii strain SCCA048 18S ribosomal RNA	520	$2e^{-143}$	98%
Coccomyxa sp. Obi small subunit ribosomal RNA	412	$3e^{-111}$	92%
Coccomyxa sp. KJ small subunit ribosomal RNA	412	$3e^{-111}$	92%
Coccomyxa simplex strain KZ-5-4-4 internal transcribed sequence	318	$6e^{-83}$	86%
Coccomyxa sp. GA5a genes for 18S rRNA, ITS1, 5.8S rRNA	303	$2e^{-78}$	86%
Choricystis sp. GSE4G genomic DNA containing 18S rRNA	303	$2e^{-78}$	86%
Coccomyxa sp. LXD 18S ribosomal RNA gene, partial	302	$6e^{-78}$	85%
Coccomyxa simplex genomic DNA containing 18S rRNA	281	$8e^{-72}$	84%
Coccomyxa sp. CCAP 216/24 18S rRNA gene (partial)	279	$3e^{-71}$	84%

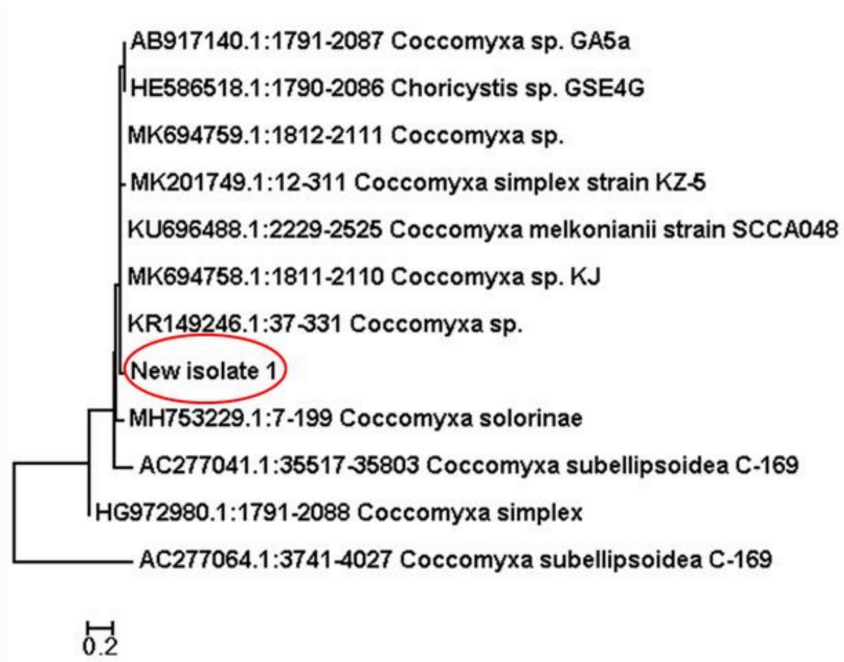

Figure 14: Phylogenetic tree showing relationship among isolate 1 and different closely related *Coccomyxa* sp. retrieved from NCBI

Table 6: FASTA sequence of algae isolate 2

ITS sequence	Raw FASTA sequence of isolate 2 obtained after sequencing
>Algae2-ITS1	TATCGAAAGATCACCCTGTGCACCAAACCGTCCCTCGTGCGG CGCTCCACCTCGCCATCCCGGCGGGTGGGGGGCGGCGAGCG CCGTGTTCCTGGGCGGGGGCTCCTCGGAGCGCCGTCAAGGTC CGGCGGGCGCCCCTCCACATGCGCGGCTTCGGTCGCCTTGGG AGGACACGCGTCGGCAAAAACACCCCATATCCAACCCTTTTT CACCCCAAACCTGAACTTCATCTGAAGCATTTTGCGTCTCGA GCTTGCCTCGACCGCAGCCAAACCAATGACAACTCTCAACAA CGGATATCTTGGCTCCCGCATCGATGAAAAACGCAAAAAAA CTGGAGGGGTGATTCACGGGGAAAAAAACCGTCCTAGAGGG GGGCTCCCCCAAACGAGGGGGGGGGGGGGCGGCAACCCTT TTTTCTGGTGTGTGGTTCTCCCAAAACACCTTAATGTCGGGG GGGGCCCCCTCCATGCGCCGTTGTAGTGGCGGGGGGGGGA AAGATTCACACAACCCCCCTTA
>Algae2-ITS2	AATTCGGTGCTGAGATTGTCATTGGTTTGGCTGCGGTCGAGG CAGCTCGAGACGCAAATGCTTCAGATGAAGTTCAGGTTTGGG GTGAAAAAGGGTTGGATATGGGGTGTTTTTGCCGACGCGTGT CCTCCCAAGGCGACCGAAGCCGCGCATGTGGAGGGGCGCCC GCCGGACCTCGACGGCGCTCCGAGGAGCCCCCGCCCAGGAA CACGGCGCTCGCCGCCCCCCACCCGCCGGGATGGCGAGGTG GAGCGCCGCACGAGGGGACGGTTTGGTTGCCAGGGTGGATT CAATCGATTCAATGATCCTTCCGCAGGTTCACCTACAGAAAA TTGAACCATGAATCACCGGGAAACAAACCGTCTCTCGAGGG GTTCCCTCCCCCCTGGGGGGGGGGGGGGGGGGGACCCCGTG TTTCGGGGGGGGGGCTCCCGGAGCCCCTTTAAGTTCGGGGGG GCCCCTCAATGCGTGGTTTCTTGGTGGGGGGGGGGAACGTTG AAAAAACCCAATCCTTTTGTTCCA

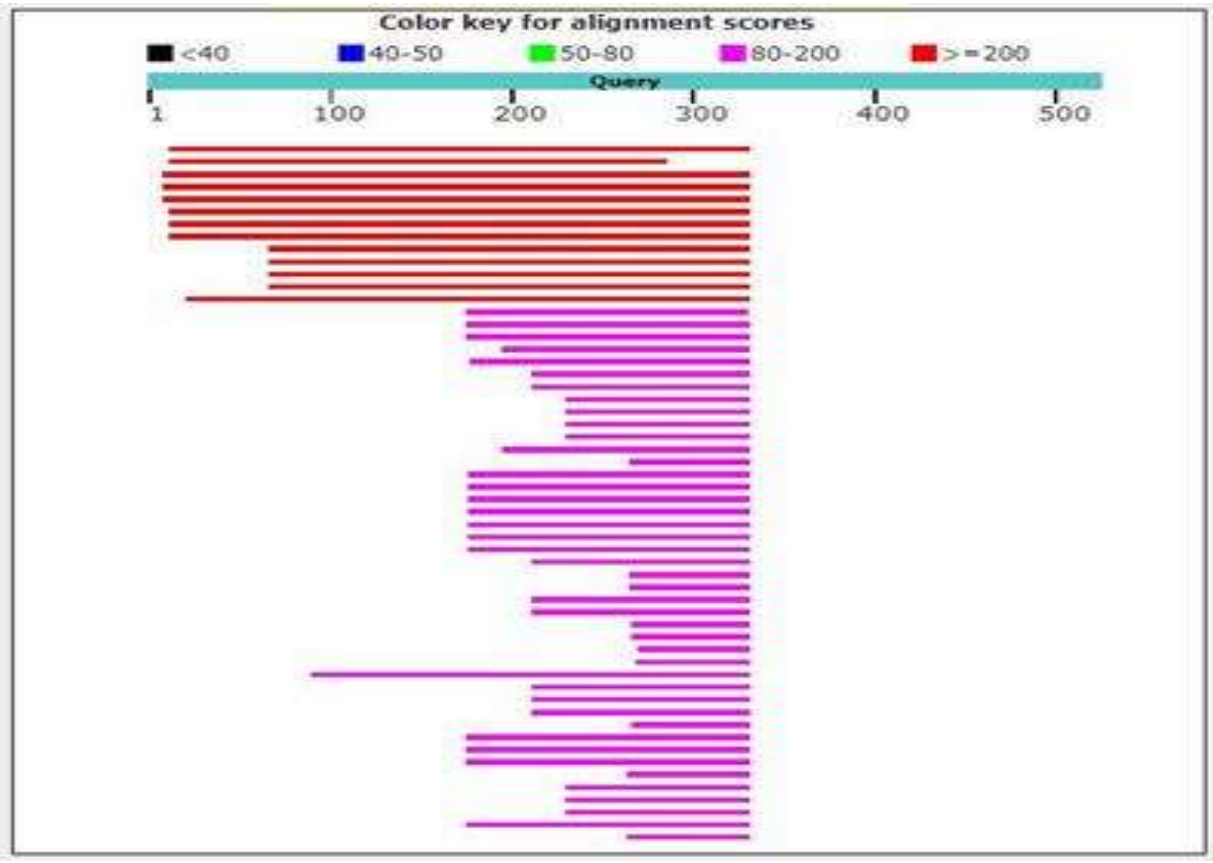

Figure 15: NCBI Blast report for isolate 2

Table 7: Sequences similarity results of FASTA sequence of algal isolate 2 with nucleotide sequences present in NCBI database

Sequences producing significant alignments:	**Score (Bits)**	**E-value**	**Maximum identity**
Chlorella sorokiniana isolate 34-2 18S ribosomal RNA	547	$1e^{-151}$	98%
Chlorella sorokiniana strain UUIND6 small subunit ribosomal rRNA	481	$1e^{-131}$	99%
Chlorella sorokiniana internal transcribed spacer 1	305	9e-79	84%
Chlorella sp. I3 internal transcribed spacer 1, partial	300	4e-77	84%
Chlorella sp. S1 internal transcribed spacer 1, par	294	2e-75	84%
Chlorella sorokiniana isolate CFR 3-05/FW internal	291	3e-74	84%
Chlorella thermophila strain ITBB HTA1-65 18S ribosomal rRNA	285	1e-72	83%
Chlorella sp. TISTR 8990 18S ribosomal RNA, partial gene	285	1e-72	83%

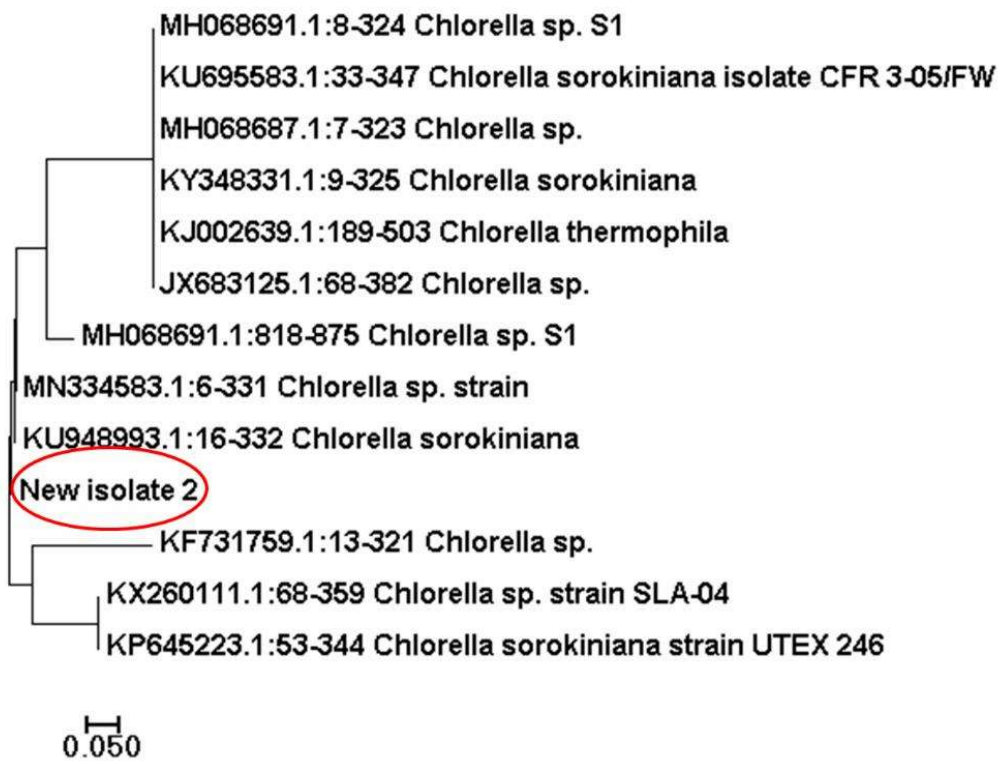

Figure 16: Phylogenetic tree showing relationship among isolate 2 and different closely related *Chlorella* sp. retrieved from NCBI

Molecular characterization for identification of new isolates:

BLAST runs of obtained FASTA sequence of isolate 1 showed its close relation to *Coccomyxa melkoniani* with 98% similarity.
BLAST runs of obtained FASTA sequence of isolate 2 showed its close relation to *Chlorella sorokiniana* with 99% similarity.

Conclusions:

- The two new isolates were sequenced by 18S rRNA technology. Isolate 1 was found to be closely identical to *Coccomyxa* sp., whereas isolate 2 belong to class of *Chlorella* sp. Similarities of these strains to *Coccomyxa* and *Chlorella* sp. also ensures the potential of these algae species as good heavy metal remediating agents.
- The bioremediation potential of one of the isolated strains *Coccomyxa* was shown by its highest removal efficiency of approximately 98% from 10 ppm of removal of Cd (II) and Pb (II).

Study 3: NMR-based metabolomics to get insights into the molecular pathway responsible for arsenic tolerance and removal.

Rapid industrialization and urbanization has led to escalation in levels of heavy metals in aquatic ecosystems, thus posing a greater threat to plant, animal and human life. Among the heavy metals, arsenic (As) has been reported to cause high incidence of arsenicosis in more than 20 countries across the globe, thereby listing it as category 1 and class A carcinogen by the US Environmental Protection Agency (USEPA). Arsenic has a complex physico-chemistry as it exists it two interchangeable forms, anoxic trivalent As (III) and toxic pentavalent As (V) in the aquatic ecosystems.

The conventional techniques deployed for the removal of arsenic from the contaminated water bodies are biased towards one form of arsenic species, pH dependent, require high maintenance and expensive mineral adsorbents making the overall process costly and less efficient. In this regard, microalgae have emerged as budding vectors for green mitigation of arsenic (III, V) from contaminated water sources owing to its (a) inexpensive and copious availability and, (b) high surface to volume ratio providing large contact area for the metal binding, thus increasing the binding, efficacy as well as the removal. Previous studies have demonstrated the effectiveness of both marine and fresh water microalgae as phycoremediators of arsenic. Based on the earlier experiments performed to screen the hyper-tolerant microalgae strain, it was observed that *Scenedesmus* sp. IITRIND2 showed excellent growth characteristics even in higher concentrations of both forms of arsenic (As (III, V) in the media. The microalga adapted to such high arsenic levels by altering its biochemical composition as evidenced by the observed changes in protein, carbohydrate, lipid content and photosynthetic pigment **(Fig 17 A-F)**. These observed results intrigued us to explore the tolerance mechanism adopted by the microalgae at molecular level to survive such toxic concentration.

In the current investigation, ^{1}H NMR based metabolomics approach coupled with various biophysical techniques was used to unravel the differential metabolic profiles and morphological features of *Scenedesmus* sp. IITRIND2 in the presence of As (III) and As (V). Our initial goal is to identify the metabolites associated with arsenic stress and to categorize them according to their biological functions of microalga. Considering the difficulties in the metabolite extraction of algal species due to its firm cell wall structure, till date only 10-12 metabolites have been reported using NMR based approach upon heavy metal stress (cadmium, copper and lead) in microalgae. Using our improvised metabolite extraction protocol for microalgae, we were able to extract and identify a total of ~ 45 metabolites. Furthermore, the current investigation unveiled eighteen differential metabolites that are characteristic to mitigation and alteration of hosts signaling pathways upon uptake of As (III) and As (V). It is worth noting that no such comprehensive NMR metabolic profiling was available on As (III, V) or other heavy metal bioremediation by microalgae.

Materials and Methods:

Microalgae cultivation and Experimental design:

Scenedesmus sp. IITRIND2 (Genebank Accession number KT932960) was isolated from fresh water lake in India and maintained in modified Bold's Basal medium (BBM). Arsenic stock solutions (10 g L^{-1}) were prepared by dissolving salts of $NaAsO_2$ (As-III) and $Na_2HAsO_4.7H_2O$ (As-V) in sterilized distilled water. To perform the experiments, the microalga was adapted and cultivated in synthetic soft water (SSW). The microalga was cultivated in Erlenmeyer flasks (250 mL) containing 75 mL of culture for 96 h (log phase) in SSW at 27 °C, with a photoperiod of 16 h [8 h light- dark cycle irradiated with 6 white fluorescent lights (300 µmol m^{-2} s^{-1})]. The cells were then centrifuged at 6000 x g for 10 min and cell pellet (1 X 10^5 cells/mL) obtained was washed thrice with autoclaved distilled water and then re-suspended for inoculation in SSW, SSW with 500 mg/L of As (III), SSW with 500 mg/L of As (V) respectively. The number of cells were counted using haemocytometer cell counter by staining cells with trypan blue. Briefly, 100 µL of microalgal cells were mixed with 100 µL of trypan blue (0.4 % in PBS; pH 7.2) and incubated for 5 min. The cell suspension (10 µL) was then used to count the cells using a compound microscope. The cell density was then calculated according to the formula:

Cell density (cells/mL) = (Average no. of cells per square * Dilution Factor) / Volume of the square

The toxicity of As (III) and As (V) to the microalga was determined using a 96 h growth inhibition bioassay. Inductive coupled plasma mass spectroscopy (ICP-MS; Perkin Elmer, ELAN DRC-e) was used to estimate the amount of arsenic (III, V) left in the SSW after 10 days of algal growth. The concentration of arsenic was calculated by plotting a standard curve from different concentrations (0, 10, 20, 50, 100, 250, 500 mg/L) of As (III) and As (V) using a mixture of Rh, Ge, Ir (100 mg/L) as internal standard. The metal uptake capacity was evaluated using the following equation:

Metal uptake capacity (%) = (Initial metal concentration in medium- Final metal concentration in medium *100)/ Initial metal concentration in medium

Characterization of arsenic interaction and morphological changes in *Scenedesmus* sp. IITRIND2:

The adsorption of As (III, V) on to the microalga was analyzed by Fourier transform infrared (FT-IR) spectroscopy (Thermo Nicolet NEXUS, Maryland, USA) at 400–4000 cm^{-1} wavenumber range, and with Field emission scanning electron microscopy (FE-SEM) coupled to Energy dispersive X-ray (EDX) spectroscopy (FE-SEM Quanta 200 FEG). Atomic force microscopy (AFM) analysis (NT-MDT-INTEGRA) was performed to visualize the changes in the surface morphology of arsenic spiked microalgal cells. Briefly, the microalgal cells (2 X 10^6) were fixed on poly-L-lysine coated glass slides using 2.5 % glutaraldehyde (24 h in dark at 4°C) followed by dehydration (10-100 % ethanol) and then visualized under the microscope.

NMR based metabolomics :

For the extraction of the metabolites 40 mg of lyophilized microalgal biomass (harvested on 10th day) from the control, As (III) and As (V) cultures, was grounded with liquid N_2 using 1 mL of 20 % methanol, as mixture of methanol: water allows a better separation of polar components from the non-polar components by lowering down the surface tension, polarity of the water and increasing the density. The process was repeated twice; supernatant was pooled together and lyophilized for overnight. Lyophilized samples were reconstituted in phosphate buffer (0.1 M, pH 7.4) and the samples were re-lyophilized again to maintain the uniform pH across all the samples in order to have a spectral overlap of chemical shifts across the samples, and also to facilitate the NMR acquisition in deuterium oxide (D_2O). The lyophilized samples were dissolved in 550 µL of D_2O containing a chemical shift indicator (4,4-dimethyl- 4-silapentane- 1- sulfonic acid (DSS), 0.5 mM). All proton NMR spectra were acquired on an 800 MHz NMR spectrometer equipped with cryoprobe. Each NMR spectrum consisted of 128 scans of 16384 data points in the frequency domain, and the spectra were collected using a Carr–Purcell–Meiboom–Gill (CPMG) pulse sequence consisting of water pre-saturation (during relaxation delay of 4.00 s).

The 1D spectra were Fourier transformed using an exponential window with a line broadening value of 0.5 Hz, phased and baseline corrected using Chenomx NMR suite 8.1 (Chenomx Inc., AB, Canada) prior to chemical shift and intensity measurements. ^{1}H NMR chemical shifts in all the spectra [control and arsenic (III, V) spiked] were referenced with respect to the methyl peak of DSS at 0.00 ppm. Chemical shifts in the 1D ^{1}H NMR spectra were identified and assigned using the 800 MHz chemical shift database in Chenomx Profiler and were validated by comparing it with the other databases and literature report.

The resonance assignments obtained for the microalga samples were further validated using two-dimensional NMR experiments such as homonuclear ^{1}H—^{1}H TOCSY (total correlation spectroscopy), ^{1}H-^{13}C HSQC (single-quantum correlation spectroscopy) and 2D *J*-resolved (JRES) NMR spectra, based on their specific patterns of HH/CH correlations, and ^{1}H-^{1}H scalar coupling constants respectively. HSQC and TOCSY analysis was validated using Metabo-Miner with tolerances of 0.02 ppm (^{1}H) and 0.5 ppm (^{13}C).

NMR Methodology for 2D NMR experiments:

Unambiguous assignments of various metabolites of *Scenedesmus* sp. IITRIND2 were obtained using two-dimensional *J*-resolved (JRES), TOCSY (total proton-proton correlation spectroscopy) and HSQC (heteronuclear single quantum correlation) spectrum. These spectra were recorded for some of the randomly selected normal and arsenic spiked samples.

Homonuclear 2D *J*-resolved spectra (jresgpprqf) were recorded in magnitude mode using quadrature phase (QF) with water pre-saturation during recycle delay (RD) of 2 sec. 16K data

points were collected along direct proton (*F*2) dimension with spectral width of 16 ppm, whereas, along indirect J- Couplings (*F*1) dimension, 80 points (increments) corresponding to spectral width of 78 Hz (~0.0976 ppm) were collected and for each *F*1 increment, 32 transients were acquired. Prior to Fourier transformation (FT), free induction decay (FID) signals were weighted in both dimensions by a sine-bell function and zero-filled in the *F*1 dimension to 256 data points. The spectra were tilted by 45° to provide orthogonality of the chemical shift and coupling constant axes and subsequently symmetrized about the *F*1 axis.

Two-dimensional ^{1}H-^{1}H TOCSY (dipsi2esgpph) and sensitivity enhanced ^{1}H–^{13}C HSQC (hsqcetgp) spectra were acquired in phase sensitive mode using time proportional phase incrementation (TPPI). 2D TOCSY spectrum was recorded using 2048 data points along direct dimension (*F*2) and 512 increments along indirect dimension (*F*1) with 32 transients per increment and a spectral width of 12 ppm in both dimensions. The FIDs were weighted using a sine–bell-squared function in both dimensions and zero filled to 2048 and 4096 data points, respectively, in the *F*1 and *F*2 dimensions prior to FT. For TOCSY experiment a mixing time of 80 ms was used. Spin-lock was achieved by a DIPSI2 pulse sequence during the TOCSY mixing time. The relaxation delay (RD) was 3.0 sec.

2D HSQC spectrum was recorded with inverse ^{13}C detection and using ^{13}C decoupling during acquisition using GARP-1.2. A relaxation delay of 2.0 sec was used between successive pulse sequence cycles and a refocusing delay equal to 1/(4*1*J*C–H =1.75 ms) was employed. 2048 x 256 complex *t*2 (^{1}H) and *t*1(^{13}C) data points with 128 scans per increment were acquired with spectral widths of 12 and 165 ppm, respectively, in the ^{1}H and ^{13}C dimensions. The FIDs were weighted using a sine-bell-squared function in both dimensions and zero filled to 4096 and 2048 data points, respectively, in the *F*2 and *F*1 dimensions prior to FT. After FT, the final spectrum was manually phase corrected and ^{1}H and ^{13}C dimensions were referenced to lactate methyl protons and carbon, respectively, at 1.31 and 22.5 ppm.

Multivariate analysis:

For multivariate data analysis, the NMR spectra were integrated, normalized against internal standard area of DSS, and the data were reduced into spectral bins (0.03 ppm width) using Pathomx. The resultant data was imported into Metaboanalyst (v3.0) software for multivariate data analysis; performed using the principal component analysis (PCA). Metabolites that influenced the differentiation pattern were identified from the loading plot, the greater the distance of a particular variable from the origin (0,0), the greater is its contribution in distinguishing the groups. The relative metabolic changes were assessed using univariate (or box-plot) analysis and statistical significance was determined by one-way analysis of variance (ANOVA) using Metaboanalyst. Unsupervised hierarchical clustering using Ward linkage was further employed to create the heat map consisting of 40 metabolite entities (with $p<0.001$) that had the highest impact on separation of the different treatment groups. The resulted heat map was used to assess, how similar or different the arsenic samples are compared to normal control samples based on their metabolite profiles.

Results:

Arsenic (III, V) is a toxic heavy metalloid whose uptake by the microalga induces stress influencing most of its morphological, physico-chemical, and biochemical characteristics. To investigate the maximum arsenic tolerance and bioremediation efficiency of *Scenedesmus sp*. IITRIND2, the microalga strain was cultivated at different concentrations of As (III, V) ranging from 10-1000 mg/L. *Scenedesmus sp*. IITRIND2 was able to tolerate up to 500 mg/L of both As (III) and As (V) with an IC_{50} value of ~ 779 and 622 mg/L (**Fig. 18A**). The microalga showed ~ 98 % removal of both the arsenic forms at initial metal concentration of 10 mg/L which systematically reduced to ~ 72 % once the initial metal concentration in the growth medium was increased to 500 mg/L (**Fig. 18B**). Further, to understand the holistic effects of arsenic on the morphological features and metabolome of microalga (*Scenedesmus* sp. IITRIND2), we deployed ^{1}H NMR based metabolomics coupled with various biophysical methods.

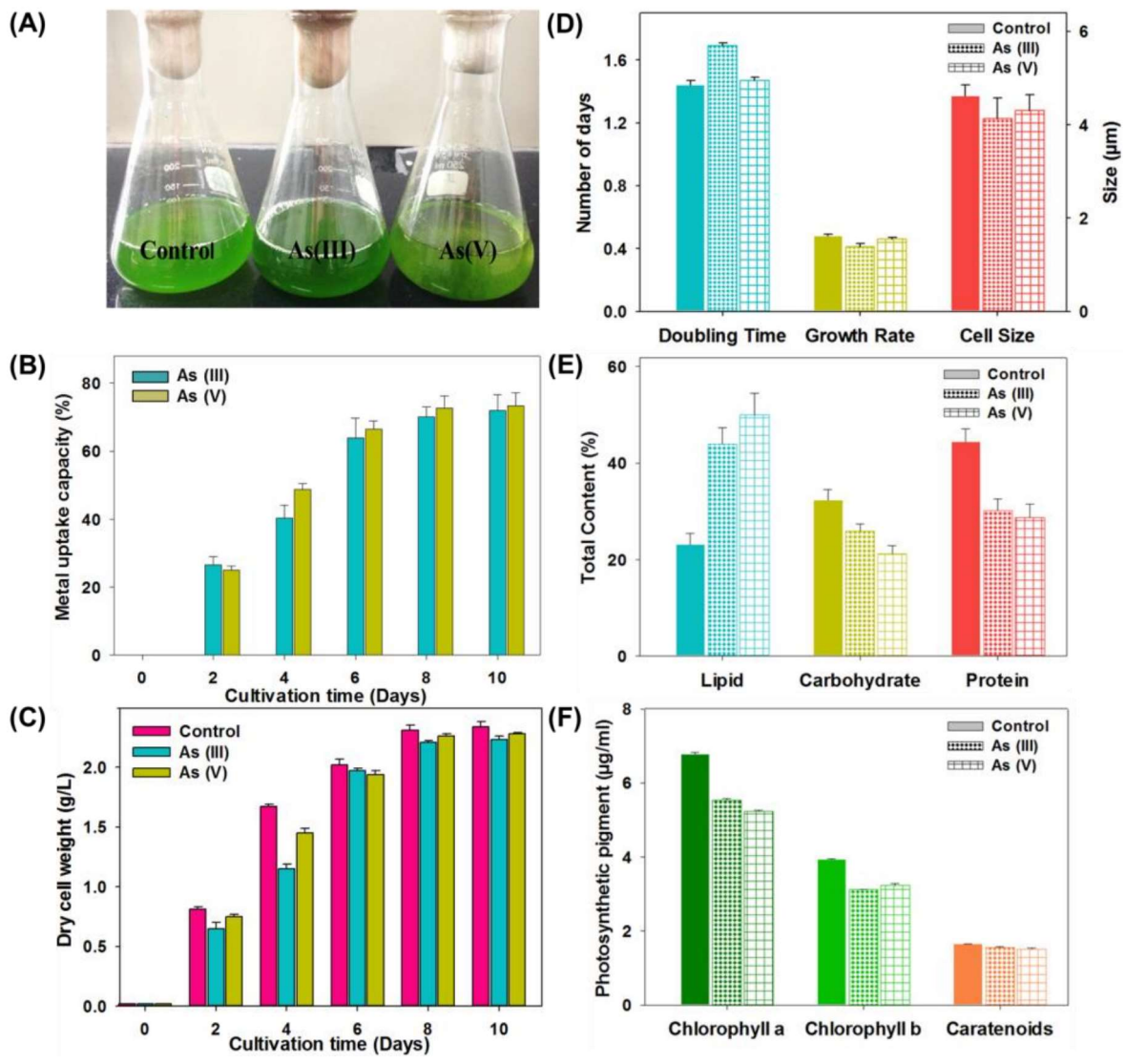

Figure 17: (A) Flask cultures of *Scenedesmus* sp. IITRIND2 cultivated in SSW in the presence of 500 mg/L of As (III) and As (V) respectively at the end of tenth day. Effect of arsenic (III, V) on **(B)** metal uptake capacity; **(C)** growth curve; **(D)** doubling time, specific growth rate and cell size; **(E)** total lipid, carbohydrates and protein content; **(F)** photosynthetic pigments (chlorophyll a, chlorophyll b and carotenoids). All the biochemical analysis for biomolecules and pigments were performed after a growth period of 10 days.

Interaction between As (III, V) and microalgal cell surface:

Arsenic in aquatic ecosystems exists mainly in two forms, anoxic trivalent As (III) and oxic pentavalent As (V). Both the arsenic forms can further exist in different anionic and cationic species depending on the pH. In the present study, the pH of the growth media ranged between pH 7-8 causing As (V) to exists in $HAsO_4^{-2}$ and $HsAsO_4^{-}$ while As (III) majorly (> 90%) exists in its neutral form H_3AsO_3 respectively. The green microalgae cell wall possesses distinct functional groups (O-, N-, S- and P-) that helps in the binding of heavy metals onto its cell surface. Heavy metals are also known to bind with microalgal cell wall via phytochelatins, which aids in detoxification of heavy metal. FT-IR spectroscopy was performed to identify the functional groups involved in the biosorption of arsenic onto the microalgal cell surface **(Fig. 19)**. The FT-IR spectra of *Scenedesmus* sp. IITRIND2 loaded with As (III, V) indicated shifting of various peaks with respect to control.

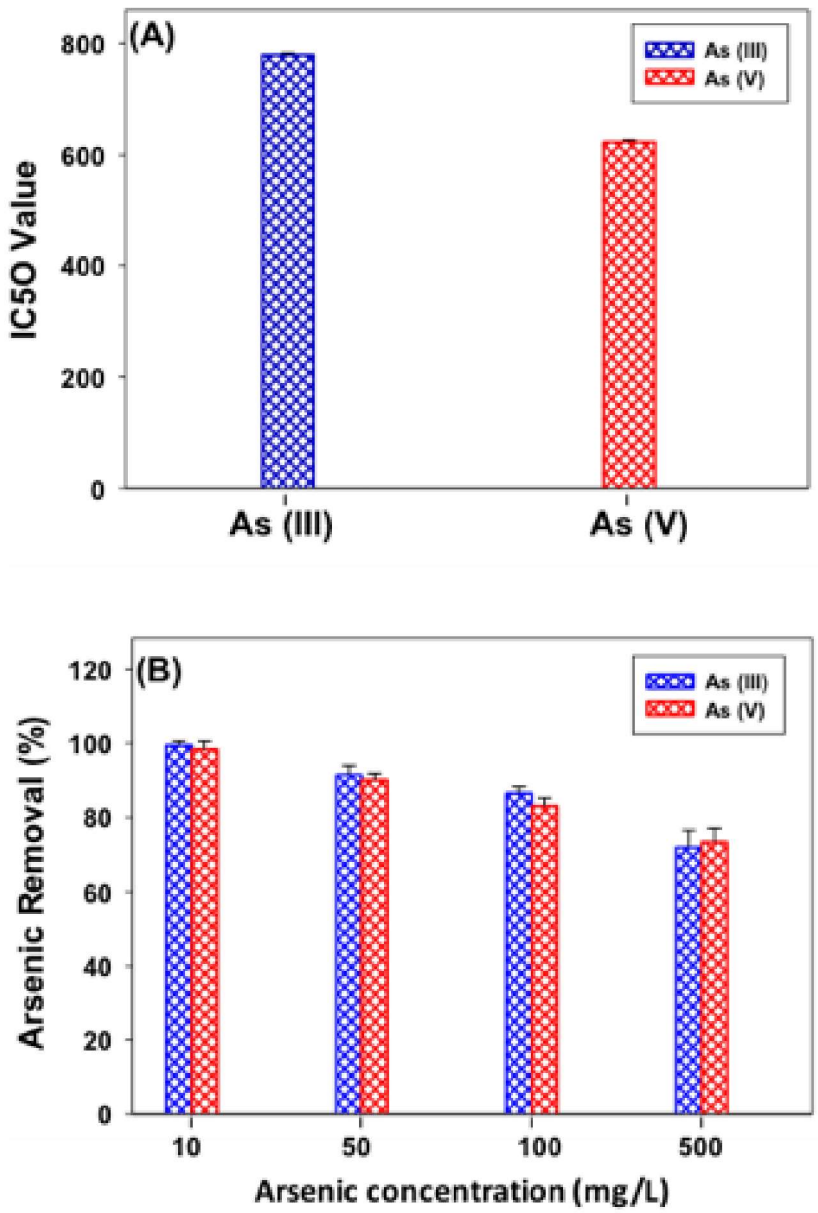

Figure 18: (A) IC_{50} value and, **(B)** arsenic removal efficiency of *Scenedesmus* sp. IITRIND2 different concentrations (0-500 mg/L) As (III) and As (V)

On spiking with As (III), the O-H and N-H stretching at 3307 cm^{-1}, shifted to a higher wavenumber (3428 cm^{-1}) indicating an alteration in the H bonding. A decrease in the shift at 2930 cm^{-1} in control to 2921 cm^{-1} designated interaction of As (III) with aliphatic C-H and aldehyde C-H stretching. Our study is in line with earlier reported studies on binding of As (III) with *Ulothrix cylindrium* and *Chlorella pyrenoidosa*. The absorption peak at 1660 cm^{-1} in control algal biomass shifted to 1641 cm^{-1} in As (III), corroborating H binding as an interaction bonding. Shift in peak from 1058 cm^{-1} in non-spiked biomass to 1039 cm^{-1} in arsenic spiked biomass attributing to the C–N stretching vibrations of amino groups indicating interaction between nitrogen of amino group with arsenic **(Fig. 19)**. Indeed, significant similarities existed between the spectra of algal biomass loaded with As (III) and As (V) in the prominent peaks at 2921 cm^{-1} and 1039 cm^{-1}. However, two notable differences existed between the FTIR spectra of As (V); an increase in the peak at 1256 cm^{-1} in control to 1265 cm^{-1} indicating bonding of sulphide linkages and a decreased in 559 cm^{-1} in control to 531 cm^{-1} signified involvement of aromatic amino acids for the biosorption of As (V) **(Fig. 19)**. Such a differential characteristic peak(s) shifting of amide and sulphide groups observed in As (III) and As (V) spiked microalgal biomass with respect to control indicates a distinct ion-exchange interaction between the algal surface with As III and As V.

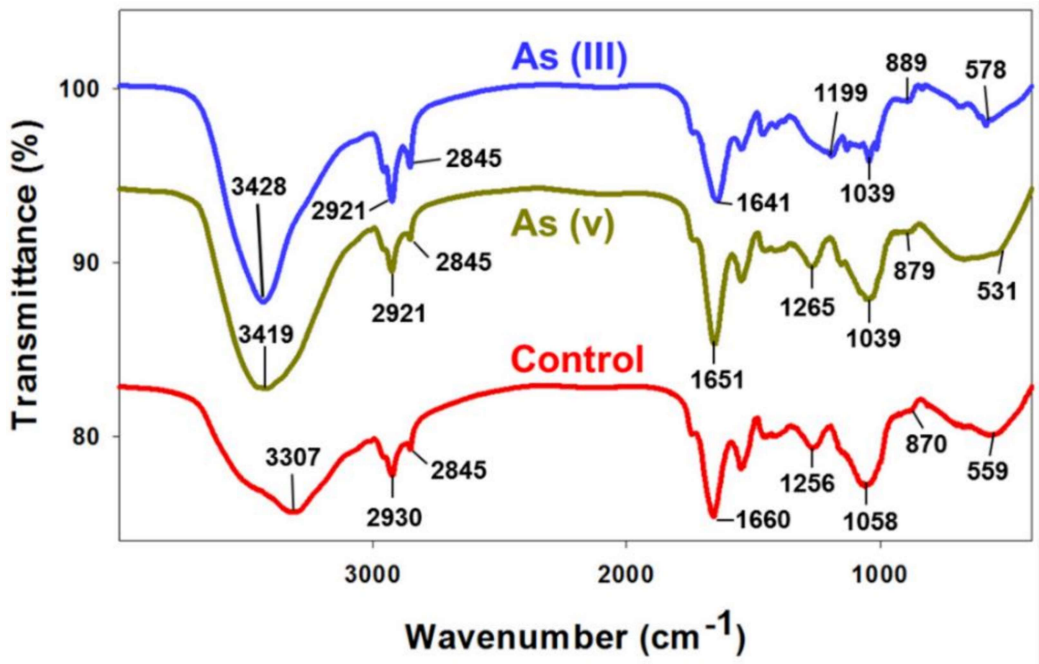

Figure 19: FTIR profiles of *Scenedesmus* sp. IITRIND2 cultivated in the absence and presence of 500 mg/L As (III) and As (V).

Effect of arsenic on morphology and cell surface of *Scenedesmus* sp. IITRIND2:

Interaction of As (III, V) with the surface markers of the microalga and their presence inside the algal cell can significantly influence its shape/size and morphology. In order, to elucidate the physical characteristics (cell size, cell shape, surface texture etc.) of As (III, V) spiked algal cells FE-SEM and AFM studies were performed. FE-SEM micrographs of As (III) and As (V) spiked *Scenedesmus* sp. IITRIND2 suggested that the microalgal cells retained their ellipsoidal shape **(Fig. 20 A-C)**. However, the surface of the cells appeared more ruptured, rough

with ridged textures as compared to control cells which were smooth **(Fig. 20 A-C)**. The resultant rigid texture of algal cell spiked with arsenic can be attributed to the adsorption of arsenic on to the cell surface, which was confirmed by EDX spectrum **(Fig. 20 D-F)**. The surface characteristics of the algal cells visualized by 3D AFM image suggested that the microalgal cell surface of control was smooth without drops, while on treatment with arsenic (III, V), the surface of the cell became rough, irregular with frequent drops throughout (**Fig. 20 G-I**). Thus, AFM analysis validated the aberrations caused by As (III) and As (V) to the surface of microalgal cells.

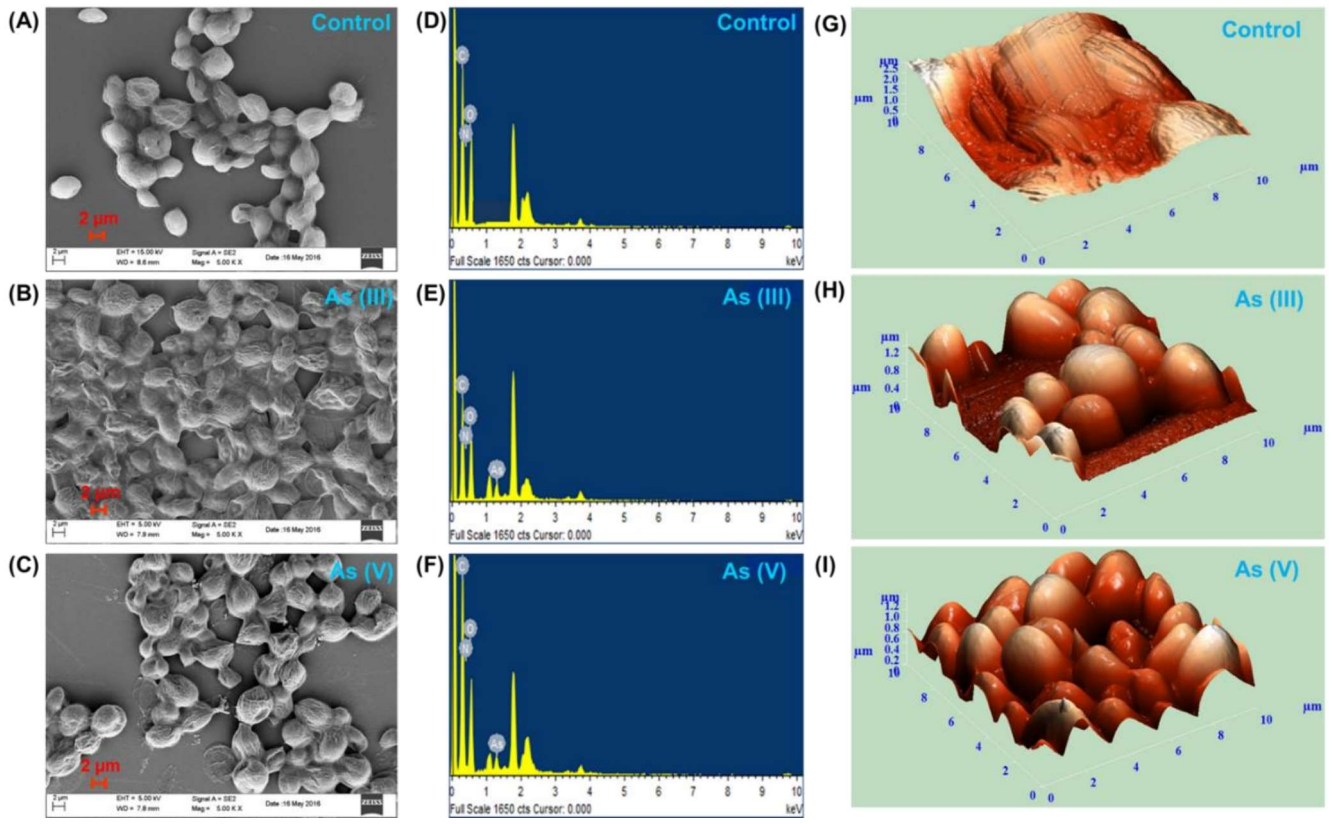

Figure 20: SEM-Scanning electron micrographs **(A-C)** EDX-Energy Dispersive X-Ray **(D-F)** analysis and (**G-I**) Atomic force microscopy of *Scenedesmus* sp. IITRIND2. Control - (**A,D,G**); As (III) - (**B,E,H**); and As (V) - (**C,F,I**). The images were collected at a concentration of 500 mg/L of As (III, V).

Metabolic changes observed in *Scenedesmus* sp. IITRIND2 upon exposure of As (III) and As (V) :

In order to gain in deep insights on the variable effects of As (III) and As (V) on *Scenedesmus* sp. IITRIND2, the metabolites obtained from aqueous methanolic extract of microalga were analyzed using NMR spectroscopy. The cumulative ^{1}H-NMR spectra (n=6 replicates) of *Scenedesmus* sp. IITRIND2 control polar extracts stacked up with that of cultures spiked with As (III) and As (V) metal systems was recorded (**Fig. 21A)**.

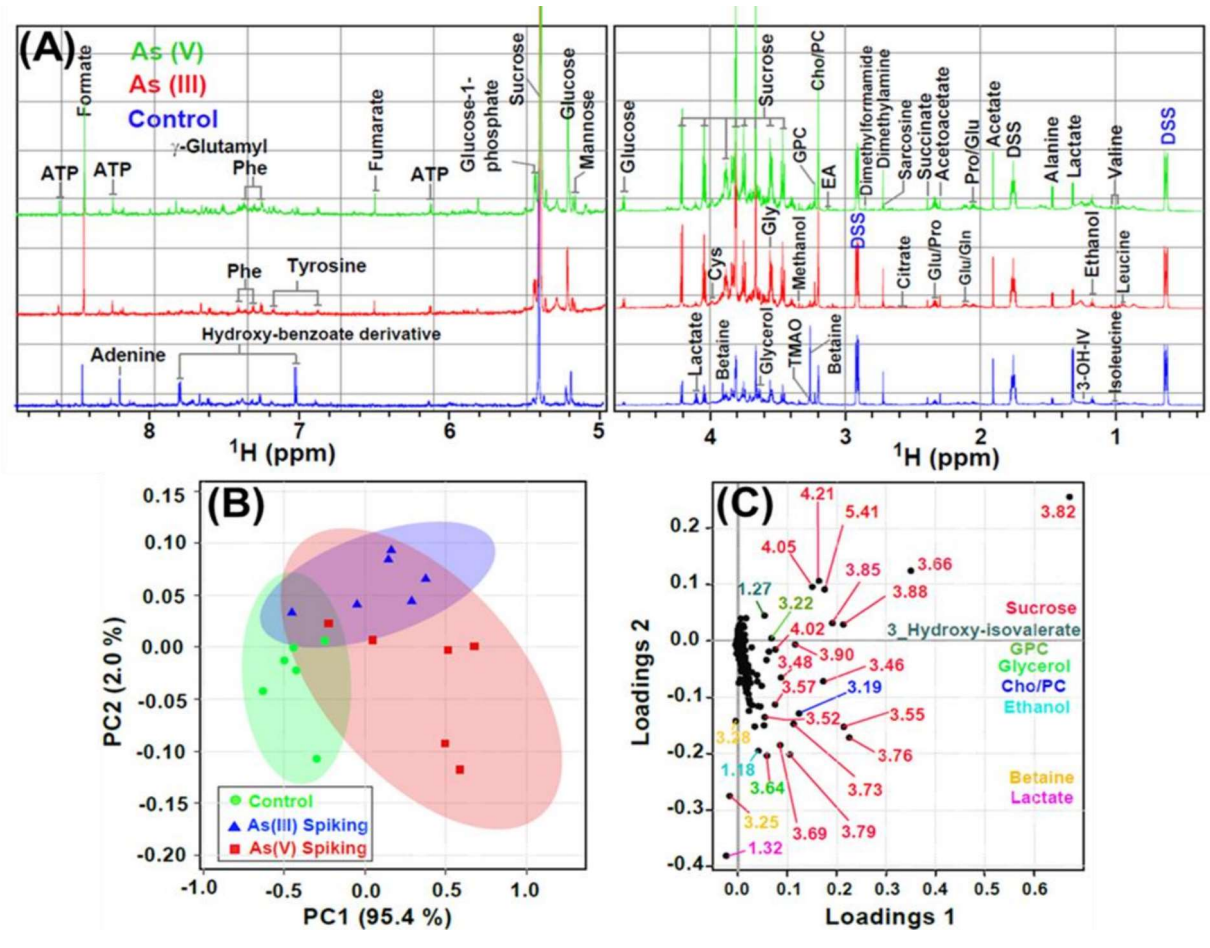

Figure 21: (A) The cumulative 1D ^{1}H NMR spectra (n=6) of *Scenedesmus* sp. IITRIND2 control polar extracts (**blue**) stacked up with that of cultures spiked with As (III) (**red**) and As (V) (**green**) metal systems. The spectral peaks were assigned for particular small-molecule metabolites. The water region at δ 4.6–4.9 was removed for clarity. The abbreviations used are: 3-OH-IV: 3-hydroxyisovalerate; Gln: Glutamine; Glu: Glutamate; EA: Ethanolamine; Cys: Cysteine; Cho: Choline; PC: Phosphocholine; GPC: Glycerophosphocholine, DSS: 4,4-dimethyl-4-silapentane-1-sulfonic acid; TMAO: Trimenthylamine-N-oxide; DMG: N,N-dimethylglycine; Phe: Phenylalanine; ATP: Adenosine Triphosphate. **(B)** The combined PCA 2D score plot resulted from the analysis of 1D ^{1}H CPMG spectra of *Scenedesmus* sp. IITRIND2 exposed to different metal treatments over a period of 10 days (**green** = Control; **blue** = As (III) spiking; **red** = As (V) spiking. The semi-transparent red and blue ovals represent the 95% confidence interval. **(C)** PCA loadings plot revealing the metabolites of responsible for the discrimination pattern, the more the metabolite is away from the origin (0,0) more it contributes in the group discrimination.

A total of 45 metabolites were identified which composed of carbohydrates/sugar (5), amino acids (17), organic acids (7), phosphagen (2), nucleotides (2), osmolytes (3) and others (9) **(Table 8)**. Several of the assigned metabolites were validated using the two-dimensional NMR experiments such as ^{1}H-^{1}H TOCSY, ^{1}H-^{13}C HSQC and 2D *J*-resolved (JRES). Representative plots for the metabolite assignments using these experiments were presented in **Fig. 22-24**. The assignment of metabolites using NMR data showed clear differences in the peaks of carbohydrates (sucrose, glucose, mannose), amino acids (leucine, alanine, valine, serine, cysteine), ATP, organic acids (fumarate, succinate, citrate, acetate) and nucleotides in control as compared to As (III) and As (V) algal extracts, and also between the two arsenic species **(Fig.**

21A). To validate these variabilities across the three treatments, multivariate analysis was performed using principal component analysis (PCA). The PCA analysis showed statistically significant clustering of the six biological replicates and distinct differences between the control and arsenic treated algal samples, as well as between As (III) and As (V), assuring a differential metabolic profiling in all the three cases **(Fig. 21B)**. The PCA loadings plot revealing metabolites responsible for the discrimination pattern along with the assignment of few relevant metabolites is shown in **Fig. 21C**. Univariate analysis was further performed to identify the relative change in the metabolite levels. Representative box-cum-whisker plots derived from the univariate analysis shown in **Fig. 25**, clearly revealed the quantitative variations of relative signal integrals for algal metabolites in response As (III) and As (V) treatment. The quantitative data of significantly altered algal metabolites were visualized using quantitative NMR analysis and hierarchically clustered heat maps to discern the dissimilarity between the three experimental groups **(Fig. 26)**. The results clearly established that the As (V) treated group was remarkably different in terms of the expression levels of metabolites compared to control and As (III) treated groups **(Fig. 26, Table 8)**. These metabolites include amino acids, organic acids, sugars and osmolytes are distinct between As (III) and As (V) species. Among the identified metabolites, 28 metabolites were overexpressed in both As (III, V) spiked microalgal cells, while only two metabolites (Betaine and TMAO) showed reduced levels as compared to control (**Table 8**). Apart from 28 mutually overexpressed metabolites of As (III, V), 12 metabolites were exclusively enhanced in As (V) treated microalgal cells (**Table 8**).

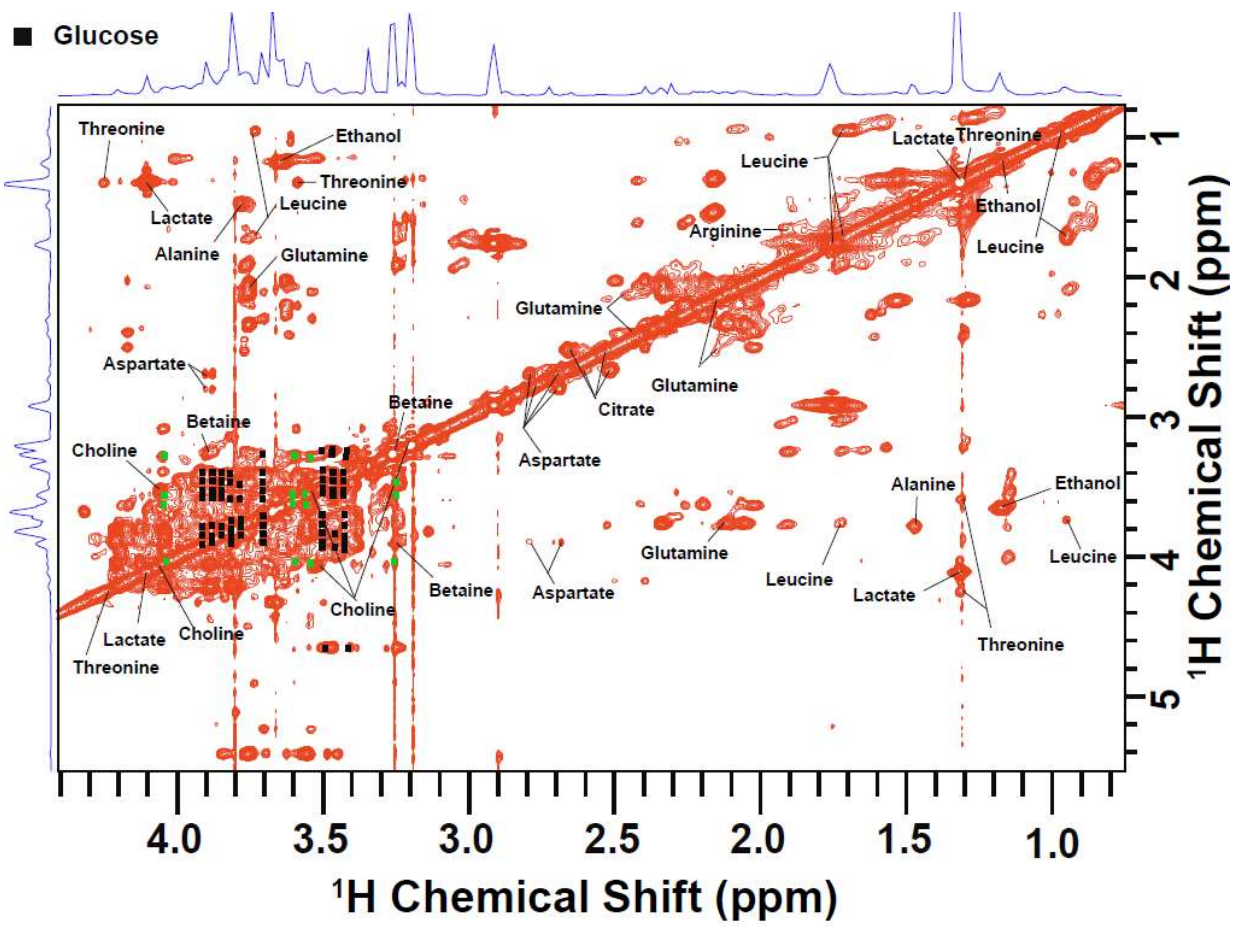

Figure 22: The representative 800 MHz ^{1}H-^{1}H TOCSY spectrum of *Scenedesmus* sp. IITRIND2 showing CH cross-peak assignments for various metabolites.

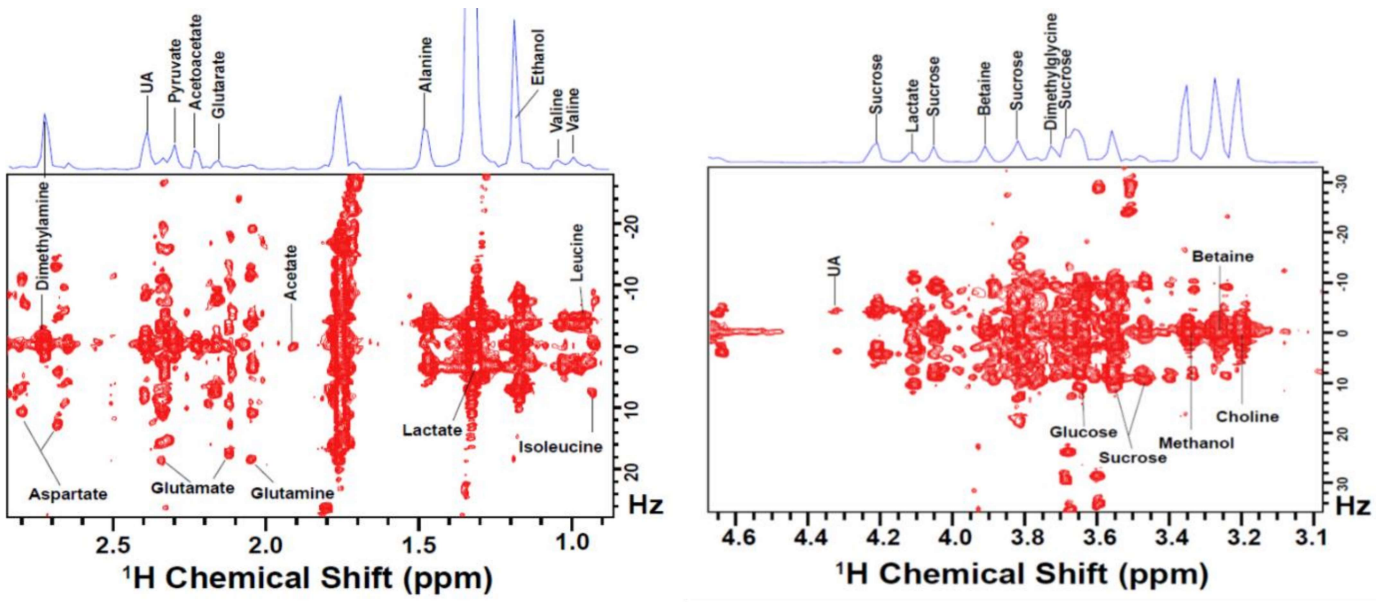

Figure 23: The representative 800 MHz ^{1}H-^{1}H J-Resolved (JRES) spectrum of *Scenedesmus* sp. IITRIND2 showing CH cross-peak assignments for various metabolites. Two different spectral region of the JRES spectrum are expanded for improved visualization: **Right Panel -** δ(0.9-2.8) ppm and, **Left Panel** - δ(3.1-4.6) ppm. Assigned peaks are annotated, whereas unassigned (UA) metabolite signals are labelled as UA.

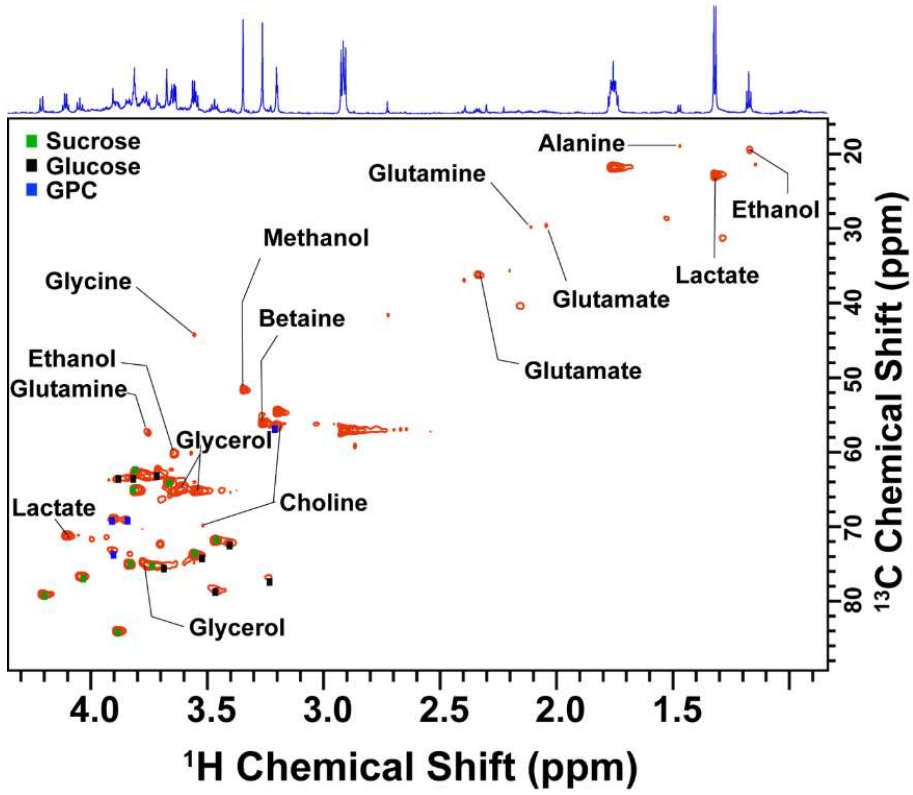

Figure 24: The representative 800 MHz ^{1}H-^{13}C HSQC spectrum of *Scenedesmus* sp. IITRIND2 showing CH cross-peak assignments for various metabolites. GPC – Glycerophosphocholine.

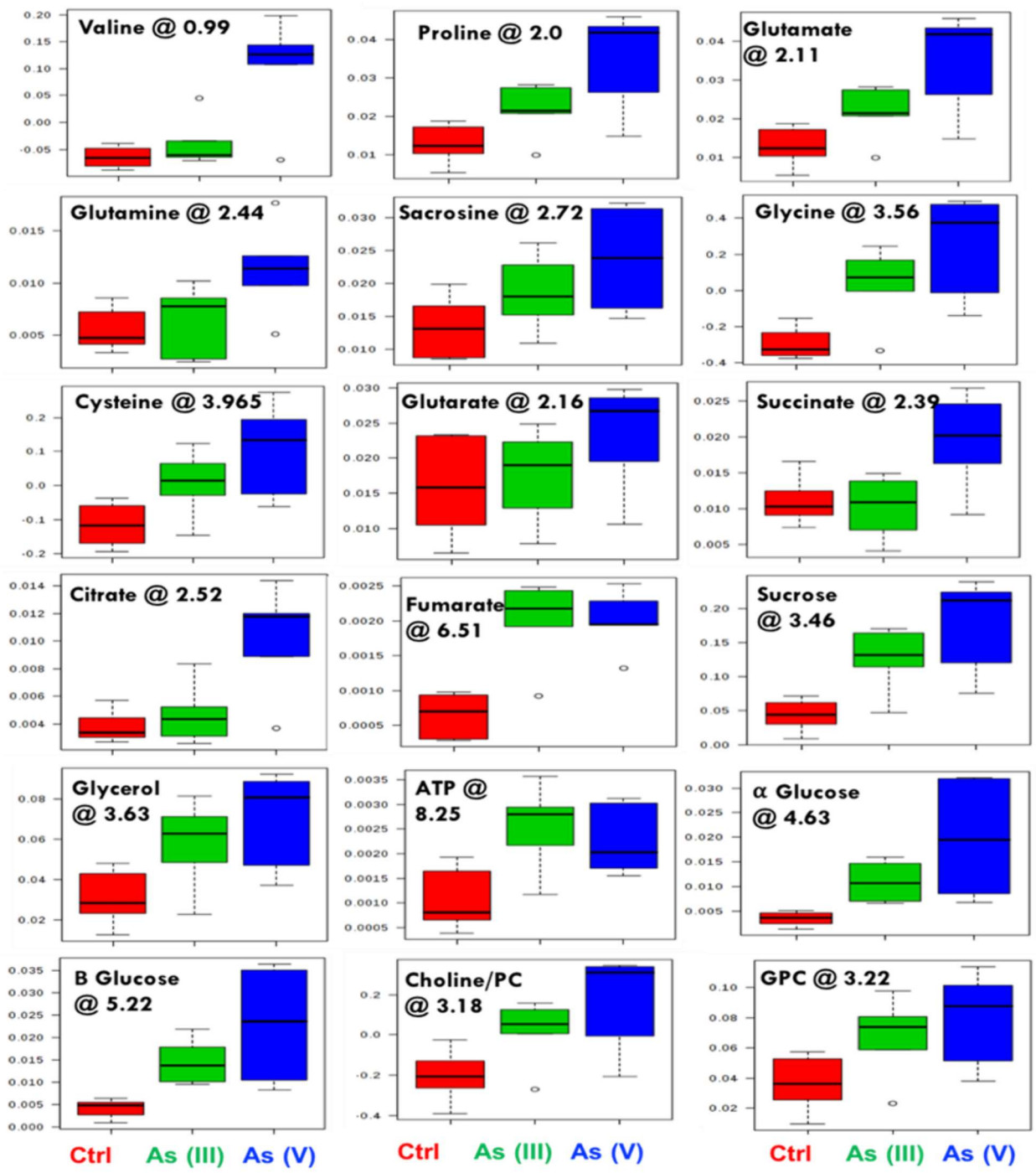

Figure 25: The box plots showing relative abundance of some of the metabolites showing significant variation after As (III) and As (V) spiking compared to normal algal culture. In the box plots, the boxes denote interquartile ranges, horizontal line inside the box denote the median, and bottom and top boundaries of boxes are 25th and 75th percentiles, respectively. Lower and upper whiskers are 5th and 95th percentiles, respectively. The corresponding chemical shift (in ppm) for each of the metabolites was also presented.

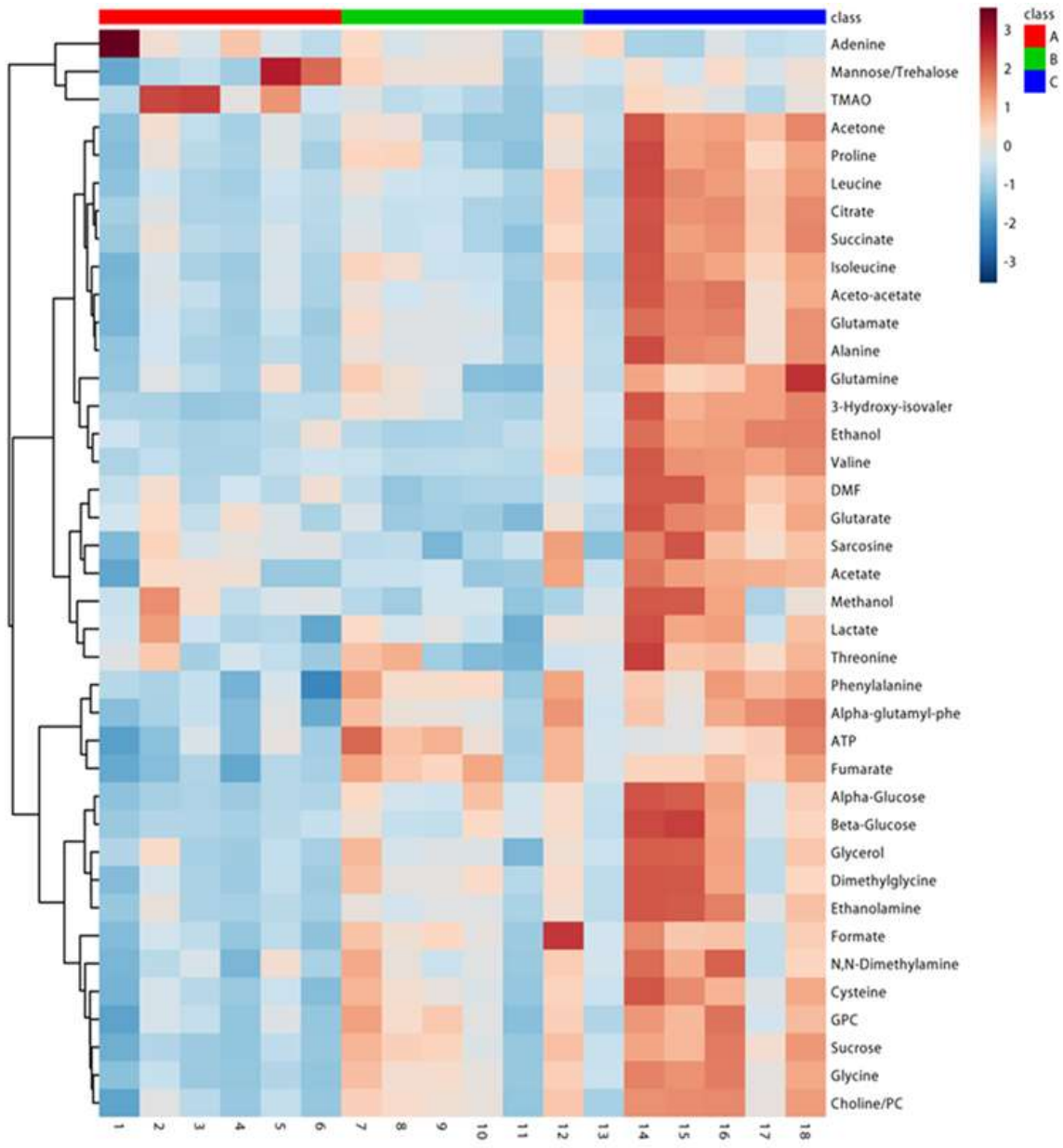

Figure 26: Heat maps showing z-scores of discriminatory metabolite entities altered in either As (III) or As (V) spiking compared to control algal culture. X-axis represents the six replicates of the culture (**A**) Control: lane (1-6) - red bar; (**B**) As (III): lane (7-12) - green bar; (**C**) As (V): lane (13-18) - blue bar. The colour scheme through signifies the elevation and reduction in metabolite concentration in As (III) or As (V) spiking compared to normal algal culture: dark blue: lowest; dark red: highest.

Among the identified differential metabolites, a total of 18 metabolites were then correlated for their role in As (III, V) bioremediation by the microalga. Out of these 18 metabolites, 13 were differentially regulated for both As (III, V). A two-fold increase in the levels of free amino acids involved in bioremediation such as glutamate, valine, glycine, proline and cysteine were recorded in As (V) treated microalgal cells in comparison to As (III) treatment **(Table 9)**.

Analogous to the results of the free amino acids, the levels of carbohydrates (sucrose, glycerol, and glucose) and ATP were higher in As (V) spiked cells as compared to As (III). The levels of fumarate, choline/PC (phytochelatin), GPC and (glycerophosphocholine) were also high

in As (V) as compared to As (III) spiked microalgal cells. Thus, the above metabolic responses established that As (V) was more toxic to the microalgal cells as compared to As (III). Such an enhanced toxicity indeed resulted in overexpression of five specific metabolites (sarcosine, succinate, citrate, glutarate and glutamine) exclusively under As (V) stress conditions (**Table 9**). Differential regulation of these extra four metabolites suggests that *Scenedesmus* sp. IITRIND2 has activated additional defense mechanism to cope up with the enhanced toxicity of As (V).

Table 8: List of metabolites along with their respective chemical shifts and their respective metabolic change patterns as a consequence of uptake of Arsenic III and V metal uptake. Two-way ANOVA followed by post-hoc Tukey's HSD was conducted to determine significant ($p < 0.001$) metabolic changes. The up (↑) and down (↓) arrows represent, respectively, increased and decreased metabolite levels.

Metabolite Name	Assignment	Chemical shifts (δ) in ppm	Relative Change*	
			As (III) Spiking vs Control	As (V) Spiking vs Control
Amino acids				
Leucine	δ-CH3 δ-CH3	0.95 (d) 0.96 (d) €	↑	↑↑
Isoleucine	γ-CH3 δ-CH3	0.93 (t) € 1.00 (d)	↑	↑↑
Valine	γ-CH3 γ-CH3	0.98 (d) 1.03 (d) €	--	↑↑
Threonine	γ-CH_3	1.29 (d) €	--	↑
Alanine	β-CH_3 α-CH	1.47 (d) € 3.79 (q)	↑	↑↑
Proline	γ-CH2 ½ β-CH2 ½ β-CH2	2.00 (m) € 2.06 (m) 2.34 (m)	↑	↑↑
Glutamate	β-CH_2 γ-CH_2	2.11 (m) € 2.34 (m)	↑	↑↑
Glutamine	β-CH_2 γ-CH_2	2.12 (m) 2.44 (m) €	--	↑
Sarcosine#	N-CH_3	2.71 (s)	--	↑
N,N-Dimethylamine (DMA)#	N-CH_3	2.72 (s)	↑	↑↑
N,NN,-Trimethylamine (TMA)#	N-CH_3	2.86 (s)	↑	↑
Glycine	α-CH_2	3.56 (s)	↑	↑↑
Cysteine	□-CH2 □-CH	3.07 (m) 3.97 (dd) €	↑	↑↑
N,N-dimethylglycine	N-CH3	3.71 (s)	↑	↑↑

Tyrosine	C2H & C6H C3H & C5H	6.88 (d) € 7.18 (d)	↑↑	↑
Phenylalanine	C2H & C6H C4H C3H & C5H	7.31 (m) 7.37 (m) 7.43 (m) €	↑	↑
γ -glutamyl-phenylalanine	C2H, C6H & C4H C3H & C5H	7.3 (m) € 7.4 (m)	↑	↑↑
Organic acids				
Lactate	*β*-CH_3 *α*-CH	1.32 (d) 4.10 (q) €	↑↑	↑
Acetate	CH_3	1.91 (s)	--	↑
Glutarate	B, δ- CH2	2.16 (t)	--	↑
Succinate	α, β-CH_2	2.39 (s)	--	↑
Citrate	½ γ-CH2 ½ γ-CH2	2.52 (d) € 2.69 (d)	--	↑
Fumarate	CH	6.51 (s)	↑	↑
Formate	CH	8.44 (s)	↑↑	↑↑
Carbohydrates/sugar				
Sucrose	C10H C12H C13H C11H C17H & C19H C5H & C9H C4H C3H C7H	3.46 (t) 3.55 (dd) 3.66 (s) 3.75 (m) 3.77 (m) 3.81 (dd) 4.04 (t) 4.21(d) € 5.40(d)	↑	↑↑
α-Glucose	C1H	4.63 (d)	↑	↑↑
β-Glucose	C1H	5.22 (d)	↑	↑↑
Mannose/Trehalose	C1H	5.19 (d)	↑	↑
Glucose-1-phosphate	C1H	5.55 (d,d)	↑↑	↑
Phosphagen				
Choline/PC	N–$(CH_3)_3$	3.20 (s)	↑	↑
GPC	N–$(CH_3)_3$	3.22 (s)	↑	↑

Osmolytes				
Glycerol	½ γ-CH2 ½ γ-CH2	3.63 (d) € 3.65 (d)	↑	↑↑
Betaine	N–$(CH_3)_3$ β-CH_2	3.26(s) 3.91 (s)	↓↓	↓
TMAO	N–$(CH_3)_3$	3.27(s) €	↓↓	↓
Nucleotides				
Adenine	C2H C6H	8.19 (s) € 8.19 (s)	--	↓
ATP	C7H C12H C2H	8.61 (s) € 8.25 (s) 6.13 (d)	↑↑	↑
Others				
Isopropanol	*β*-CH_3	1.16 (d)	--	--
Ethanol	CH3	1.17 (t)	--	↑↑
3-hydroxy-isovalerate	γ-CH3	1.24 (s)	↑	↑↑
Acetone	CH_3	2.22 (s)	--	↑
Aceto-acetate	δ-CH3	2.3 (s)	--	↑
N,N-Dimethyl-formamide (DMF)	N-CH_3	2.85 (s)	--	↑
Ethanolamine	N-CH_2	3.13(m)	↑	↑↑
Methanol	CH_3	3.34 (s)	↑	↑↑
Hydroxy-benzoate derivative	C2H & C6H C3H & C5H	7.02 (d) € 7.79 (d,d)	↓	↓↓

Note: All the values of the metabolites were statistically significant with p value 0.001 respectively. For visualization interpretation, single (↑,↓) and double (↑↑,↓↓) arrows are used to represent relative change in the mean value of metabolite concentration (as evaluated from their respective box-plots). "€" represents the metabolite peak used for evaluating the quantitative difference as represented here using up (↑) and down (↓) arrows in the case of multiple signals/chemical shift values. "#" The metabolites showing discrepancy in the box-plot calculation because of some outlier values.

All the above results concisely deduce the hierarchy of arsenic tolerance/ bioremediation **(Fig. 27)**. Firstly, arsenic gets adsorbed on microalgal by complexation with various functional groups present on its cell wall followed by slow intracellular metabolism. As (III) is reported to get transported across plasma membrane via aquaglyceroporine (AQP) and hexose permeases while As (V) competes with the phosphate transporters. Post internalization, As (V) is reduced to As (III) via methylation catalyzed by GSH while PC and its derivatives inside cell shield As (III) with S-H groups (increase in levels of cysteine, PC, glutamine, glutamate)**.** Arsenic inhibits the oxidative phosphorylation and its methylation results in buildup of oxidative stress inside microalgal cells causing perturbations in TCA cycle. To combat this oxidative stress, microalga starts accumulating proline, fumarate and trehalose which act as antioxidant molecules scavenging ROS. This can be synchronized with protein catabolism (increase in levels of free amino acids), carbohydrate and lipid biosynthesis (**Fig. 27**). These methylated compounds (DMA, MMA) are then converted to arsenosugars and arsenolipids followed by excretion from cells. An increase in the levels of glycerol and sucrose indicated the formation of arsenosugars. To gain detailed insights into the hierarchical activation of these multiple pathways of metabolites and mitigation of arsenic during the stepts **3-5** as in depicted in the schematic (**Fig. 27**), a future time course metabolomics analysis is quintessential. In a nutshell, this study demonstrated the effectiveness of using a metabolomics approach in answering environmental and in particular arsenic tolerance mechanism by microalgae which could lead successful deployment of microalgae via genetic engineering for bioremediation of arsenic from contaminated water sources.

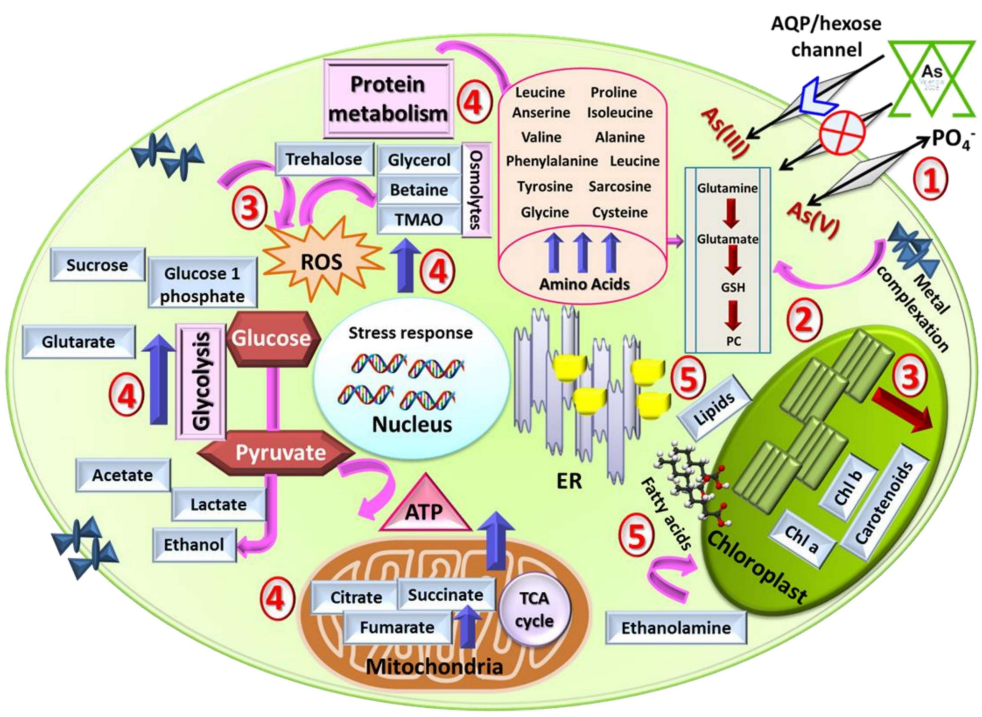

Figure 27: Schematic showing the hierarchy of arsenic (III, V) induced metabolic changes in the microalgal cells: **(1)**: Arsenic intake via AQP/hexose and phosphate channels **(2)** metal complexation by PC, **(3)** ROS generation in response to arsenic stress, **(4)** mitigating ROS stress by modulating protein metabolism, glycolysis and TCA **(5)** ER stress resulting in increase in lipid content.

Table 9: List of metabolites involved in bioremediation along with their respective chemical shifts and their respective fold change as a consequence of uptake of Arsenic III and V metal uptake. one-way ANOVA was conducted to determine significant ($p < 0.001$) metabolic changes. All the differentially expressed metabolites involved in bioremediation pathway of As (III, V) are represented in bold. Metabolites that are specific to As V mitigation are marked with bold and italics.

Metabolite Name	Assignment	Chemical shifts (δ) in ppm	Relative Fold Change*	
			As (III) Spiking vs Control	As (V) Spiking vs Control
Amino acids				
Valine	γ-CH3 γ-CH3	0.98 (d) 1.03 (d) €	--	4.1
Proline	γ-CH2 ½ β-CH2 ½ β-CH2	2.00 (m) € 2.06 (m) 2.34 (m)	1.3	2.3
Glutamate	β-CH_2 γ-CH_2	2.11 (m) € 2.34 (m)	1.7	2.8
Glutamine	β-CH_2 γ-CH_2	2.12 (m) 2.44 (m) €	--	2.1
Sacrosine	N-CH_3	2.72 (s)	--	1.3
Glycine	α-CH_2	3.56 (s)	2.2	(3.0)
Cysteine	□-CH2 □-CH	3.07 (m) 3.97 (dd) €	1.8	2.5
Organic acids				
Glutarate	*β*, δ- CH2	2.16 (t)	--	1.4
Succinate	α, β-CH_2	2.39 (s)	--	(2.2)
Citrate	½ γ-CH2 ½ γ-CH2	2.52 (d) € 2.69 (d)	--	2.7
Fumarate	CH	6.51 (s)	3.3	3.3
Carbohydrates/sugar				
Sucrose	C10H C12H C13H C11H C17H & C19H C5H & C9H C4H C3H C7H	3.46 (t) 3.55 (dd) 3.66 (s) 3.75 (m) 3.77 (m) 3.81 (dd) 4.04 (t) 4.21(d) € 5.40(d)	3.2	4.2
α-Glucose	C1H	4.63 (d)	2.7	5.1
β-Glucose	C1H	5.22 (d)	3.4	5.3

Phosphagen				
Choline/PC	N–$(CH_3)_3$	3.20 (s)	1.9	2.4
GPC	N–$(CH_3)_3$	3.22 (s)	1.8	2.2
Osmolytes				
Glycerol	½ γ-CH2 ½ γ-CH2	3.63 (d) € 3.65 (d)	1.3	1.6
Nucleotides				
ATP	C7H C12H C2H	8.61 (s) € 8.25 (s) 6.13 (d)	2.2	2.0

Note: All the values of the metabolites were statistically significant with p-value 0.001 respectively. "€" represents the metabolite peak used for evaluating the quantitative difference as represented here as fold changes.

Conclusions:

In a nutshell, we demonstrated the effectiveness of using proton NMR based metabolomics approach in answering environmental toxicological responses.

- The current study identified of an array of metabolites, which provided information on the arsenic mitigation mechanism by a hyper-tolerant microalga. In a recent study, ^{1}H NMR in conjunction with high resolution mass spectroscopy (HRMS) was deployed to identify and quantitate metabolites in bacteria on exposure to metal nanoparticles.
- The authors initially utilized ^{1}H NMR to tentatively assign metabolites by matching with an open-access *E.coli* Metabolome database (ECMDB) and structurally validated via HRMS.
- In the current study, we have developed an exclusive NMR (1D and 2D) metabolomics workflow to efficaciously assign algal metabolites which can serve as a starting framework for algal metabolome database. Such a database can be enriched with more metabolites using similarity search algorithms on plant, yeast and bacterial metabolite databases, and metabolites assigned using NMR/MS techniques.
- The workflow developed could be a utilized as a centralized source for robustly assigning algal metabolites, which can shed light on the different biochemical pathways, instrumental in exploiting algae on biotechnological platforms for flux analysis, and also to study the effect of environmental factors or any stress stimulus.

Concluding remarks:

- The present work demonstrated the screening of different microalgae species capable to tolerate high concentration of heavy metal ions such as Arsenic (As III, V), cadmium (Cd II), and lead (Pb II).
- Parallel to the screening of heavy metal tolerant algae, novel four novel microalgae candidate were also isolated form contaminated water near Haridwar ghats.
- The molecular identification of the two potent isolated strains were identified as *Coccomyxa* sp. and *Chlorella* sp.
- Among the two new isolate, *Coccomyxa* sp. showed excellent removal efficiency in presence of lead and cadmium.
- Based on all the screening results, Scenedesmus sp. IITRIND2 was found to be the most tolerant strain as it was able to tolerate around half a gram of both form of arsenic.
- Further to unravel the biochemical and molecular mechanism adopted by the microalgae cells, detailed NMR-based metabolomics studies were performed.
- The outcomes suggest that the cells rewired their carbohydrate pool towards lipid biosynthesis under high arsenic concentrations.
- Further, increase in levels of cysteine, phytochelatin (PC), glutamine, glutamate suggest the mechanism of chelation of heavy metal ions inside the microalgae cells
- Furthermore, enhanced level of trehalose, proline, and fumarate also suggest an active antioxidant system to maintain the osmotic balance and mitigate the ROS generated during arsenic stress.

Final report

A Detail Study to Understand the Non-Putrefying Property of River Ganga in both Water and Sediment

Sponsor
Ministry of Water Resources, River Development & Ganga Rejuvenation, New Delhi

CSIR-National Environmental Engineering Research Institute
Nehru Marg, Nagpur – 440 020

Indian Council of Medical Research
Ansari Nagar, New Delhi - 110029

Nov. 2017- Dec 2020

Health Component
All India Institute of Medical Sciences, New Delhi

Project Investigator:

Name	:	Dr. Rama Chaudhry
Designation	:	Professor and Head
Organization	:	All India Institute of Medical Sciences (AIIMS)
Address	:	Department of Microbiology, AIIMS, New Delhi, 110029
Tele Fax	:	011-26594795
E mail	:	drramach@gmail.com

Co- Project Investigator

Name	:	Dr. Bimal Kumar Das
Designation	:	Professor
Organization	:	All India Institute of Medical Sciences (AIIMS)
Address	:	Department of Microbiology, AIIMS, New Delhi
Telephone	:	9717315286,
E-mail	:	tezpur.bimal@gmail.com

Duration of the report: Nov 2017- Dec 2020

AIIMS Components – Objectives

1. Identification of bacteriophages against health care associated bacterial strains, clinical isolates, multi drug resistant bacterial strains, anaerobic and special pathogen bacteria of clinical significance.

2. Assessment of bacteriophage enriched water as an anti-infective agent to clean infected hospital setup including wards, ICU and operation theatre.

1. Methodology:

Objective One

1.1 Isolation and identification of aerobic bacterial pathogens:

1.1.a Sample collection and isolation of aerobic bacteria: To isolate the bacterial clinical isolates, the samples including blood, pus, urine, cerebrospinal fluid, Bronchoalveolar lavage etc. were obtained from different Out Patient Departments (OPDs), wards and ICU of AIIMS New Delhi. The samples were processed for bacterial isolation as per standard guidelines. Initially the samples were processed and inoculated on culture media; the obtained pure culture was further processed for Matrix Assisted Laser Desorption/Ionization Time of Flight (MALDI-TOF). The identified bacterial isolates were maintained by making glycerol stocks and kept at -80ºC, till further processing.

1.1.b Antimicrobial susceptibility testing of aerobic bacterial isolates: Antimicrobial susceptibility testing was performed in the Bacteriology section of Dept. of Microbiology, for aerobic bacterial isolates using Mueller–Hinton Agar (MHA) by the Kirby–Bauer disc diffusion method following standard procedures as per Clinical and Laboratory Standards Institute (CLSI) guidelines.

1.2 Isolation and identification of special bacteria pathogen:

1.2.a Isolation and isolation of Special Bacterial pathogen (*Legionella pneumophila*): The water samples were collected from different sites of All India Institute of Medical Sciences, New Delhi. Samples were collected by using a sterile cotton swab into the opening of the taps and rotating it along the inner sides of the nozzles or 100 ml from opening the tap.

Water sample processing: The 100 ml water sample was filtered through 0.22 micrometre polycarbonate membrane. The membrane through water was passed was kept in 5 ml of initial water sample and sonicated for 3 minutes.

Direct Seeding: The processed sample (0.2 ml) was seeded on buffered charcoal yeast extract (BCYE) agar plate supplemented with glycine (3 g/L), vancomycin (1 mg/L), polymyxin B (80,000 UI/L) and cycloheximide (80 mg/L)(GVPC) and L-cysteine (4%).

Acid treatment: Two ml of concentrated water sample was treated with 2 ml of HCl-KCl buffer for 5 minutes, and 0.2 ml of the processed sample was seeded on BCYE/GVPC plate.

Thermal treatment: Two ml of concentrated sample was heated at 50°C for 30 minutes and 0.2 ml was inoculated on BCYE/GVPC plate.

Processing of swabs: The swabs were suspended in 5 ml water collected from the same tap, from where swab was collected and directly, 0.2 ml of suspension was inoculated on BCYE/GVPC plate

All sample seeded plates were and incubated at 37°C with 5% at 48 hours and observed for typical colonies.

1.2.b Confirmation of *Legionella pneumophila*: The suspected colonies of *Legionella pneumophila,* obtained on BCYA/GVPC plates were further confirmed by PCR. DNA was isolated by boiling method. The PCR was performed with following reaction condition with primer of *mip* gene.

Primer sequence of *mip* gene:
Forward Primer: 5'GACAAGGATAAGTTGTCTTATAGC3'
Reverse primer: 5'ACGACCAGTGTATTCCACAG3'

Reaction Mixture for PCR of *L. pneumophila*

Component	**Volume in µl**
10x PCR buffer	2.5
dNTP mix (100mM)	0.5
Forward primer (10 pmol/µl)	0.5

Reverse primer (10 pmol/µl)	0.5
Taq Polymerase (5U/µl)	0.3
Genomic DNA (10ng)	5.0
Sterile water	15.7

The conditions in thermocycler for PCR: Initial denaturation at 95 ºC for 10 min, 40 cycles of 94ºC for 1 min, annealing at 55 ºC for 1 min, extension at 72 ºC for 1 min and Final extension at 72º C for 10 min.

1.2. c Antibiotic Sensitivity testing of *L. pneumophila*: The antibiotic sensitivity testing of isolates of *L. pneumophila* was done as per European Committee on Antimicrobial Susceptibility Testing (EUCAST) guidelines by gradient MIC method. In brief, a lawn of bacterial isolate was prepared by bacterial suspension of 0.5 McFarland standards in 9 cm plate. The plate was allowed to dry and one strip per plate was applied to the surface. Antimicrobial-gradient plastic strips (Himedia) with an MIC scale in a continuous-range concentration of each drug were used, MICs were read directly from a scale on the strip at the point where the ellipse of growth inhibition intercepted the strip after 48 hours of incubation as per EUCAST guidelines.

1.3: Isolation and Identification of Anaerobic organisms: Stool samples were obtained from different wards of AIIMS, New Delhi. In brief, the stool sample was treated with 1:1v/v absolute alcohol for 30-45 minutes or heated at 100 °C for 10 min for spore selection. The treated sample was inoculated in RCM bottle and incubated at 37°C for 24-48 hours. The content of RCM bottle was sub cultured on Blood agar (BA), Brain Heart Infusion Agar (BHIA) and Cycloserine Cefoxitin Fructose Agar (CCFA). Metronidazole (Mz) disk (5µg) was placed on the BHIA plates. The plate of BA was incubated in CO_2 candle jar under aerobic conditions for 24 hrs to grow facultative anaerobes while of BHIA and CCFA were for 48 hrs in anaerobic condition in whitley anaerobic work station (glove box) at 37°C for aerobes.

The plates kept in anaerobic condition were observed after 48 hrs of incubation for colonies.

The plates of BHIA were observed for large flat ground glass colonies while CCFA was looked for yellow colored colonies. The metronidazole sensitive colonies of desired characteristics were

suspected for *C. difficile*. Further confirmation of *C. difficile* was done by grams staining and standard biochemical method.

1.4. Bacteriophage Isolation and Characterization

1.4.a Water sample Collection and Bacteriophage isolation: The water samples have been collected from different Ganga ghats and processed for bacteriophage Isolation. In brief, the water sample has been treated with 1% chloroform (v/v) for 10 minutes followed by centrifugation at 10,000 rpm for 10 minutes. The supernatant (500 µl) has been added with 500µl of bacterial culture (log phase) and incubated overnight at 37° C. The suspension was treated with 1% chloroform with shaking for 10 minutes, centrifuged and the supernatant was tested for presence of bacteriophage by spot assay as well as plaque assay. On obtaining plaques, single plaque was further processed for scaling up of bacteriophages.

In addition to isolation of bacteriophages at AIIMS Delhi, we also received bacteriophages from Banaras Hindu University (BHU), Dept. of Microbiology and tested their lytic activity on bacterial strains, collected at AIIMS. Twenty bacterial clinical isolates were also sent to National Environmental Engineering Research Institute (NEERI) Nagpur for bacteriophage isolation. The NEERI also provided us the bacteriophages against clinical isolates, but the phages could not be revived at AIIIMS, New Delhi.

1.4.b Isolation of bacteriophages against *Legionella pneumophila:* The chloroform treated water samples were dropped on lawn of *L. pneumophila* on buffered charcoal yeast extract supplemented with glycine (3 g/L), vancomycin (1 mg/L), polymyxin B (80,000 UI/L) and cycloheximide (80 mg/L)(GVPC) and L-cysteine (4%) and allowed to dry**.** The plates were incubated overnight at 37°C with 5% CO_2 at 48 hours and observed for lytic zones. After 48 hours, the plate was washed with TMG buffer and suspension was treated with 1% chloroform, centrifuged at 10,000 rpm for 10 minutes, supernatant was collected and dropped again on lawn of *L. pneumophila and* incubated overnight at 37°C with 5% CO_2 at 48 hours and observed for lytic zones.

1.4.c Isolation of Bacteriophages for anaerobic pathogens: The 1% chloroform treated water samples were dropped on lawn on *C. difficile* and incubated at 37°C in anaerobic condition followed by observation for lytic zones after 24 and 48 hours.

1.4.d Bacteriophage lytic activity determination: The bacteriophages isolated at AIIMS New Delhi or obtained from Banaras Hindu University; Dept. of Microbiology were tested for their lytic activity on their respective bacterial clinical isolates. To observe the lytic activity of bacteriophages by spot assay, in brief, bacterial suspension of 2.0 OD was plated on Mueller Hinton Agar (MHA) plate and incubated at 37°C for 2 hours. The phages in 10 µl volume (10^5-10^6 PFU/ml) were dropped on bacterial lawn and incubated overnight to observe lytic activity.
A total of 51 strains of *Acinetobacter baumannii,* 40 strains of *Klebsiella pneumoniae*, 43 strains of *Escherichia coli,* 30 strains of *Pseudomonas aeruginosa* and 20 strains of *S. aureus* have been tested for lytic activity by bacteriophages.

1.5. **Electron Microscopic Analysis**: The purified bacteriophages; 1000 µl (10^7-10^8 PFU/mL) active against *A. baumannii* and *P. aeruginosa* were filtered through 0.22 µm-pore-size membrane filters, centrifuged at 25000g for 75 min, the pellet was washed with 0.1 M ammonium acetate (pH 7.0) and negatively stained using phosphotungstic acid, PTA (2% [w/v], pH 7.0). Briefly, 10 µl of phage preparation was added over the copper grid and allowed to absorb for 10 min followed by staining with 2% PTA solution (staining solution) for 5 min. The stained grid was visualized under Transmission Electron Microscopy at Sophisticated Analytical Instrumental Facility, AIIMS, New Delhi. The phage head/ tail lengths were measured using Image J software.

1.6 Molecular characterization of Bacteriophages

1.6a **Bacteriophage DNA Isolation:** Extraction of phage DNA was performed from three bacteriophages active against *A. baumannii* and two phages active against *P. aeruginosa*, using phenol:chloroform- isoamyl extraction method.

Ten ml bacteriophage lysate of 10^8 PFU/ml was treated with 1unit/µl DNase I (Thermo Scientific) and 10mg/ml RNase (Thermo Scientific), and incubated for 1 hour at 37°C followed

by addition of 20 µl EDTA (0.5M). Twenty µg/µl of Proteinase K was added to the mixture and incubated at 55°C for 1 hour. An equal volume of saturated phenol was added and mixed by inversion. Samples were centrifuged at 14,000 rpm for 10 min and the top aqueous layer was retained. The aqueous layer was added to an equal volume phenol: chloroform: isoamyl alcohol (25:24:1 v/v/v) and mixed, centrifuged at 14,000 rpm for 10 min and the top aqueous layer retained. The last step was repeated twice, first using phenol:chloroform:isoamyl alcohol, followed by one using chloroform:isoamyl alcohol (24:1 v/v). After the final purification, the DNA was precipitated using 2 volumes isopropanol and 0.4 volumes 7.5 M NaAcetate. Samples were incubated on ice for 1 hour or overnight at -20°C. DNA was pellet down following centrifugation at 14,000 rpm for 30 min at 4°C. The pellet was washed with 70% ethanol and air dried before re-suspension in either EB buffer (10 mM TrisCl, pH 8.5) or water.

DNA was quantified using a NanoDrop (Nanoquant) spectrophotometer and was visualized on 0.8% agarose gel by electrophoresis. Genomic DNA contamination was examined by PCR, using the universal primers 16S rRNA gene.
FP:AGAGTTTGATCCTGGCTCAG
RP:CCGTCAATTCCTTTRAGTTT

1.6 b Whole genome sequencing of bacteriophages: The whole genome sequencing of the bacteriophages was performed using Illumina HiSeq platform by Clevergene Biocorp Pvt. Ltd. Bangalore. The sequence data quality was checked using FastQC and MultiQC softwares. The data was also checked for base call quality distribution, % bases above Q20, Q30, %GC, and sequencing adapter contamination. The reads were processed using fastp to remove low quality bases and adapter sequences. The QC passed reads were used to assemble the genomes using Megahit genome assembler and contigs shorter than 1500bp were removed from the assembled genome. The phage annotation was performed using PHAge Search Tool Enhanced Release (PHASTER) server. The identified phage sequence was further was analyzed by NCBI Megablast to search for highly similar bacteriophage.

Objective Two

1.7 Bacterial collection and identification from the ward of AIIMS New and determination of bacteriophages activity on surface

1.7.a Collection of Floor samples from Ward: The floor samples from G ward, AIIMS New Delhi were collected from seven different sites. The sampling was done thrice on 15 days interval. The surface of 10x10 cm^2 was selected and marked, the cotton swab was dipped in normal saline and rubbed along selected surface. The swabs were immediately brought to laboratory and spread over luria Bertani (LB) agar plate. The plates were incubated overnight and observed next day. The colonies obtained on plates were further cultured to scale up and processed for MALDI-TOF analysis.

1.7.bTesting of bacteriophage Activity against the bacterial isoaltes obtained from G ward : The bacterial isolates from G ward AIIMS New Delhi, which were identified as *A. baumannii, K. pneumoniae,* and *S. aureus* have been tested for antibacterial activity by their respective bacteriopahges at AIIMS New Delhi. The phage activity was observed by performing spot assay.

1.8 Bacteriophage cocktail preparation and activity on plastic surface: The bacteriophages cocktail of 10^7 PFU/ml was prepared by using equal proportion of phages active against a specific host in normal saline. The bacteriophage cocktail (10^7 PFU/ml) was spotted on either individual bacterial lawn (against which the phage was isolated) or cocktail of bacteria (cocktail of bacteria against which the phages were isolated) to observe the lytic activity of the prepared bacteriophage cocktail.

The lysing effect of the bacteriophages cocktail on plastic surface was determined by CFU analysis as well as ATP monitoring. The petri plates (9 cm diameter) were used as plastic surface in experimental condition.

1.8. a CFU Analysis in presence of bacteriophage cocktail on plastic surface: The bacterial cocktail of *A. baumannii, K. pneumoniae*, *P. aeruginosa, E. coli* and *S. aureus* (200µl of $1x10^7$ CFU/ml) was spread on plastic surface, partially dried for 15 minutes, sprayed over with 200 µl of normal saline or bacteriophage cocktail (10^7 PFU/ml) and covered with lid to avoid drying. At

2 hours interval, the swabs were collected (Before collecting swab the surface was allowed to dry), suspended in 1ml normal saline and spread over MHA plates for CFU analysis.

1.8.b ATP monitoring in presence of bacteriophage cocktail on plastic surface: To observe the bioluminescence (ATP level) on the surface in the presence and absence of bacteriophages; the plastic surface was experimentally contaminated with bacterial cocktail and sprayed with normal saline or bacteriophage cocktail as mentioned for CFU analysis. The plastic surface was swabbed with UXL100 at 2 hours interval up to 6 hours and the ATP levels were observed using 3M™Clean-Trace™ Hygiene Monitoring system. The ATP production was measured as Relative Light Units (RLU), proportion to light emitted by bioluminescence assay.

1.9 Biostatistics Analysis: The comparative data analysis was statistically analyzed by Graph Pad Prism (version 5.0) using Bonferroni's posttests, $P<0.05$ and $P<0.001$ were considered significant.

2. Results:
Objective 1

2.1 Aerobic bacterial Isolates and antibiotic sensitivity pattern: A total of 210 aerobic clinical isolates were obtained from different wards and ICU of AIIMS New Delhi during the study. List of organisms identified is given in table 1 and resistance pattern of clinically significant pathogens is presented in Figure 1.

Table 1: List of aerobic bacterial pathogens isolated and identified during the study

Gram Negative Organisms		
SN	**Organism Identified**	**No. of Isolates**
1	*Acinetobacter baumannii*	52
2	*Klebsiella pneumoniae*	41
3	*Escherichia coli*	44
4	*Pseudomonas aeruginosa*	31
5	*Enterobacter cloacae*	3
6	*Enterobacter spp.*	1
7	*Enterobacter hormaechei*	1
8	*Proteus mirabilis*	1
9	*Klebsiella oxytoca*	1
10	*Klebsiella spp.*	1
11	*Proteus vulgaris*	1
12	*Providencia rettgeri*	1
13	*Sarratia marcescens*	1
Gram Positive Organisms		
14	*Staphylococcus aureus*	21
15	*Staphylococcus haemolyticus*	3
16	*Staphylococcus epidermidis*	2
17	*Enterococcus faecium*	2
18	*Staphylococcus spp.*	2
19	*Enterococcus spp.*	1
	Total	**210**

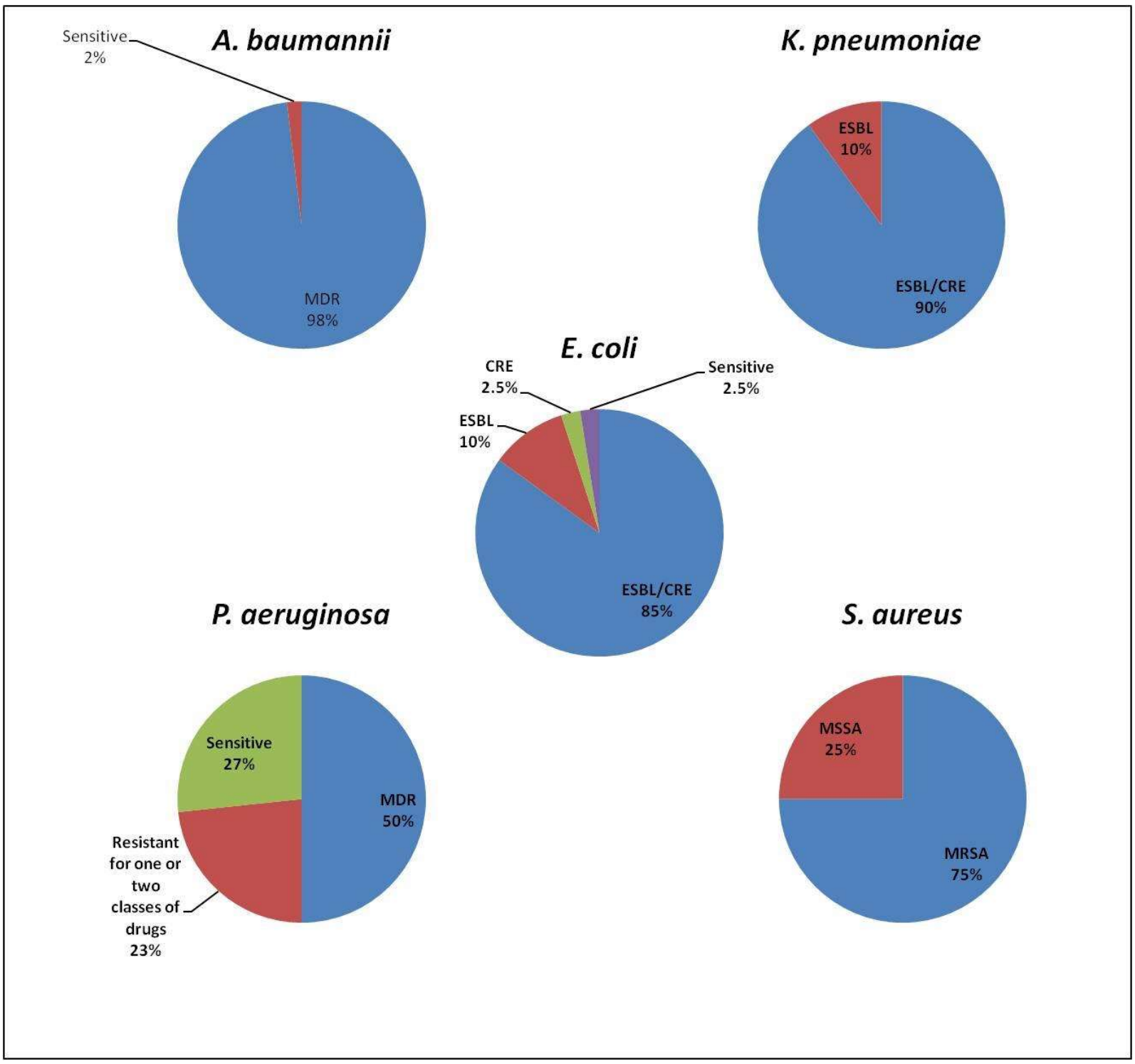

Figure 1: The resistance pattern of clinically significant pathogens.
MDR=Multidrug-resistant, ESBL=Extended-spectrum beta-lactamases, CRE=carbapenem-resistant Enterobacteriaceae, MRSA=Methicillin-resistant *Staphylococcus aureus*, MSSA= Methicillin-sensitive *Staphylococcus aureus*

2.2 Isolation of special bacterial pathogen: A total of 10 isolates of *L. pneumophila* were isolated from environmental water samples during Nov 2017 to till date by culture method (Figure 2A). The isolates were further confirmed by PCR and were processed for antibiotic sensitivity testing for the antibiotics; Azithromycin =AZM, Erythromycin = ERY, Ciprofloxacin =CIP, Levofloxacin =LVX Rifampicin =RIF, Doxycycline =DOX, Tigecycline =TGC as per EUCAST guidelines. All tested isolates were sensitive for all tested drugs as per EUCAST guidelines (Figure 2B).

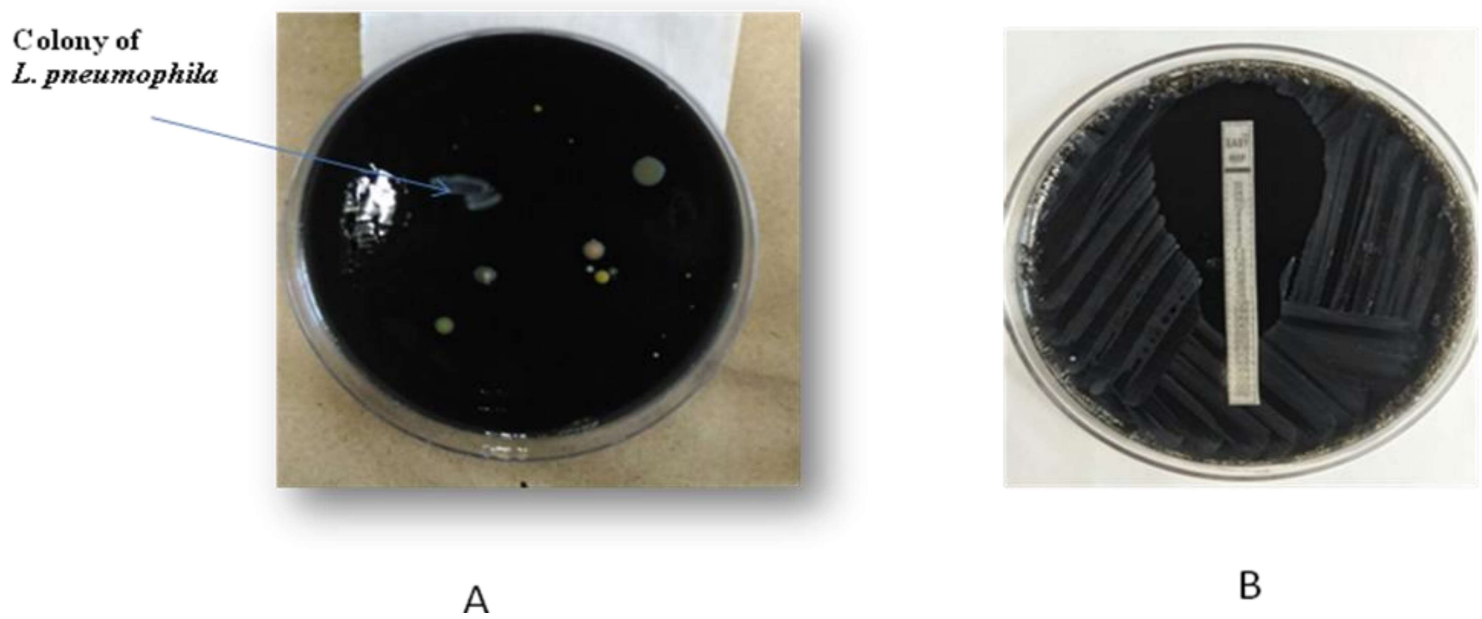

Figure 2: (A) – A representative plate having colony of *L. Pneumophila*, (flattened and grown overnight further to enlarge colony size), (B)-A representative picture of *L. Pneumophila* shown inhibited region in presence of rifampicin.

2.3 Isolation of anaerobic bacteria: Four bacterial isolate of *C. difficile* has been isolated and identified during the study period (Figure 3), that showed sensitivity to metronidazole.

Figure 3: A representative picture showing colonies of metronidazole sensitive *C. difficile* colonies on BHIA

2.4 Isolation and Characterization of Bacteriophages:

2.4.a Isolation and determination of lytic activity of Bacteriophages: The Ganga water samples have been collected from different Ganga ghats (Figure 4, Table 2) and processed at AIIMS New Delhi, bacteriophages have been isolated against bacterial clinical isolates. At AIIIMS New Delhi, seven bacteriophages against *A. baumannii* (AIIMS-Ab-A4, AIIMS Ab-A5, AIIMS- Ab-A6, AIIMS Ab-A7, AIIMS-Ab-A8-1, AIIMS-Ab-A8-2 and AIIMS-Ab-A8-3), four bacteriophages against *P. aeruginosa* (AIIMS-Pa-A1, AIIMS-Pa-A2, AIIMS-Pa-B1 and AIIMS-Pa-B2) and three bacteriophages against *E. coli* (AIIMS- Ec-A3-1, AIIMS-Ec-A3-2, and AIIMS-Ec-A3-3) have been isolated. For the nomenclature of the phages, first two alphabets represents and genus and species of bacterium first letter, followed by abbreviation of water sample lab number of phage isolate from specific ghat. All isolated bacteriophages showed clear lytic activity on performing spot assay, presented in Figure 5 (A), (B) and (C). The bacteriophages were spotted on bacterial isolates; their lytic activity is presented in figure 6.

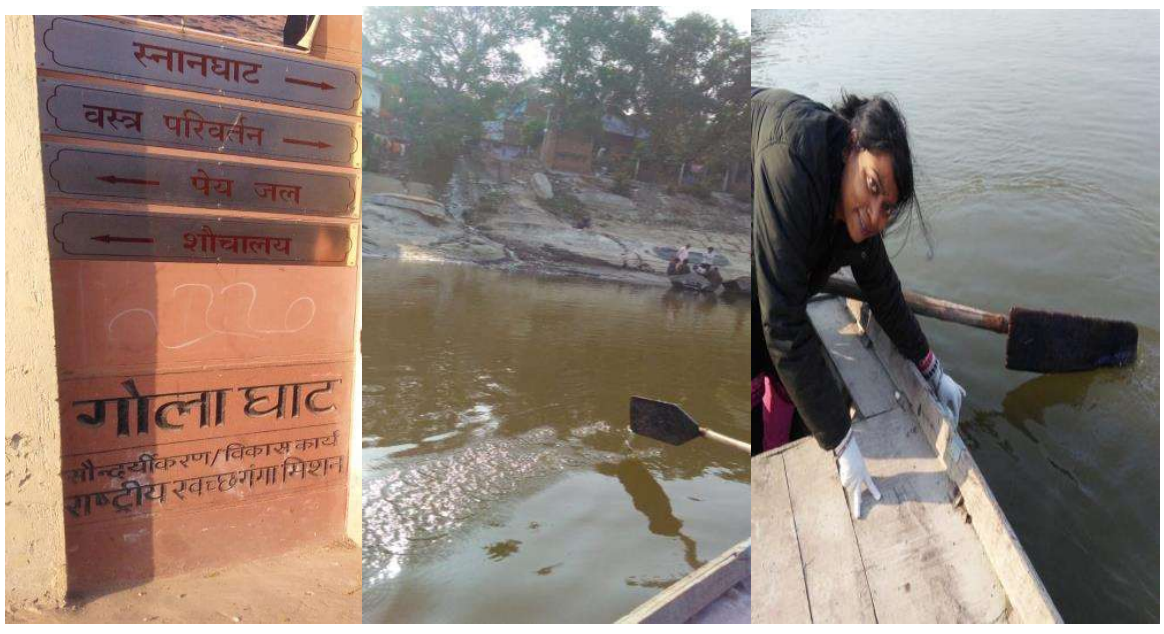

Figure 4: AIIMS New Delhi representative collecting the Ganga water sample from the Gola Ghat Kanpur, Uttar Pradesh.

Table 2: Details of water sample collection sites from the river Ganga

Place	Sample collection site	Abbreviation
Varanasi	Assi Ghat	A1
Varanasi	Dasashawmed Ghat	A2
Haridwar	Kankhal	A3
Kanpur	Parmat Ghat	A4
Kanpur	Bhairav Ghat	A5
Kanpur	Gola Ghat	A6
Kanpur	Sarsaiya Ghat	A7
Kanpur	Bhagwatdas Ghat	A8
Hapur	Garhmukteshwar	A9
Varanasi	Prahlad Ghat	B1
Varanasi	Panchganga Ghat	B2

2.4.b Activity of Bacteriophages obtained from collaborating Institutes: A number of bacteriophages have been received from BHU. They were tested for lytic activity on their respective host by spot assay. However, lytic had been shown by three bacteriophages against *K. pneumoniae* and two bacteriophages against *S. aureus*. Figure 5; (D) and (E) and one phage against *P. aeruginosa*. The bacteriophages were further subjected to Spot assay against their respective bacterial clinical isolates. The lytic spectrum of the bacteriophages is presented in figure 6.

From NEERI, we obtained bacteriophages against *K. pneumonia, P. aeruginosa and S. aureus* However, the phage activity could not be revived at AIIMS New Delhi.

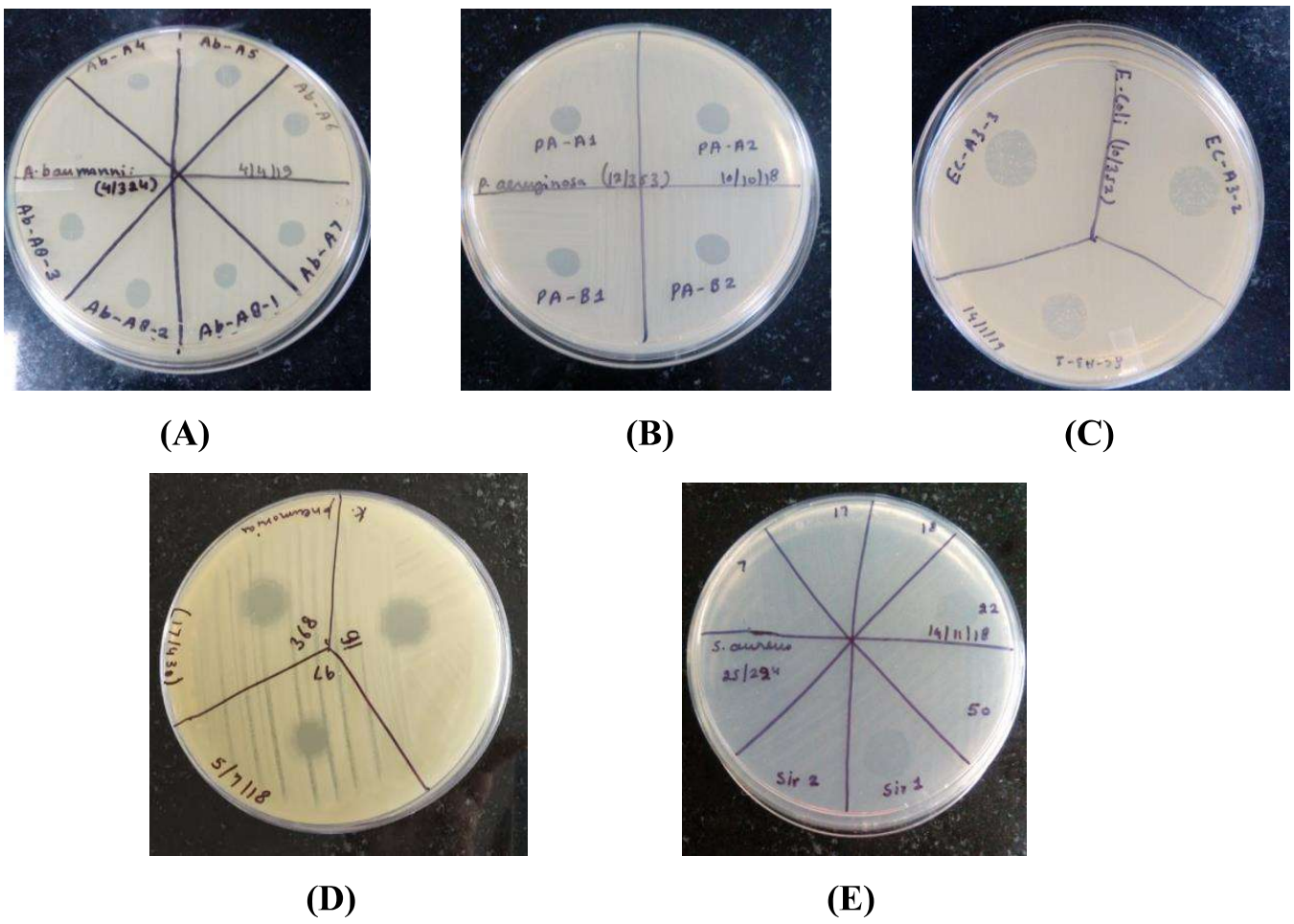

Figure 5: Representative pictures of MHA plate showing lytic activity of (A) Acinetobacter phages; AIIMS-Ab-A4, AIIMS-Ab-A5, AIIMS-Ab-A6, AIIMS-Ab-A7, AIIMS-Ab-A8-1, AIIMS-Ab-A8-2, AIIMS-Ab-A8-3 on *A. baumannii*; (B) Pseudomonas phages; AIIMS-Pa-A1, AIIMS-Pa-A2, AIIMS-Pa-B1 and AIIMS-Pa-B2 on *P. aeruginosa* (C) Escherichia phages; AIIMS-Ec-A3-1, AIIMS-Ec-A3-2, AIIMS-Ec-A3-3 on *E. coli* , (D) Klebsiella phages; BHU-91, BHU-97 and BHU-368 on *K. Pneumoniae* and (E) *Staphylococcus* phages BHU-22 and BHU-sir1 on *S. aureus.*

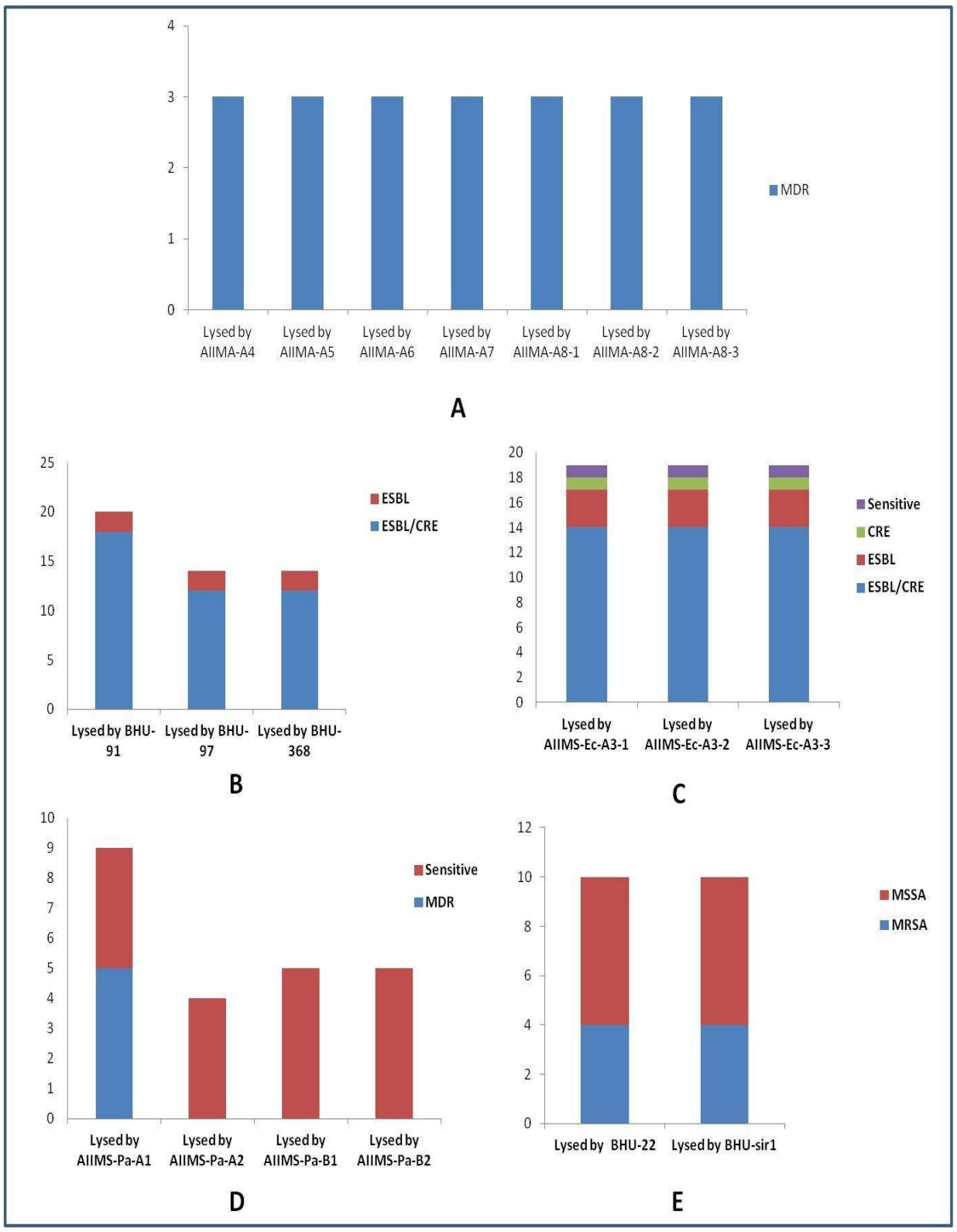

Figure 6: The lytic behavior of bacteriophages on their respective bacterial clinical isolates; Host Rang. A: *A. baumannii*, **B:** *K. Pneumoniae,* **C**: *E. coli*, **D** *P. aeruginosa*, and **E**: *S. aureus*. Multi-drug resistant (MDR), Extended Spectrum Beta-Lactamase (ESBL), Carbapenem-resistant Enterobacteriaceae (CRE), EBBL/CRE*:* Extended Spectrum Beta-Lactamase & Carbapenem-resistant Enterobacteriaceae, Methicillin-resistant *Staphylococcus aureus (*MRSA), Methicillin-sensitive *Staphylococcus aureus* (MSSA)

2.5. Microscopic morphology of Bacteriophages: The bacteriophages isolated against *A. baumannii and P. aeruginosa* at AIIMS, New Delhi; have been subjected to Transmission Electron Microscopy (TEM). The phages with hexagonal heads and long tails (Figure 7 and Figure 8); belonging to order Caudovirales. One pseudomonas phage AIIMS-Pa-A1 showed hexagonal head and small tail, the feature of order Caudovirales and family podovirideae.

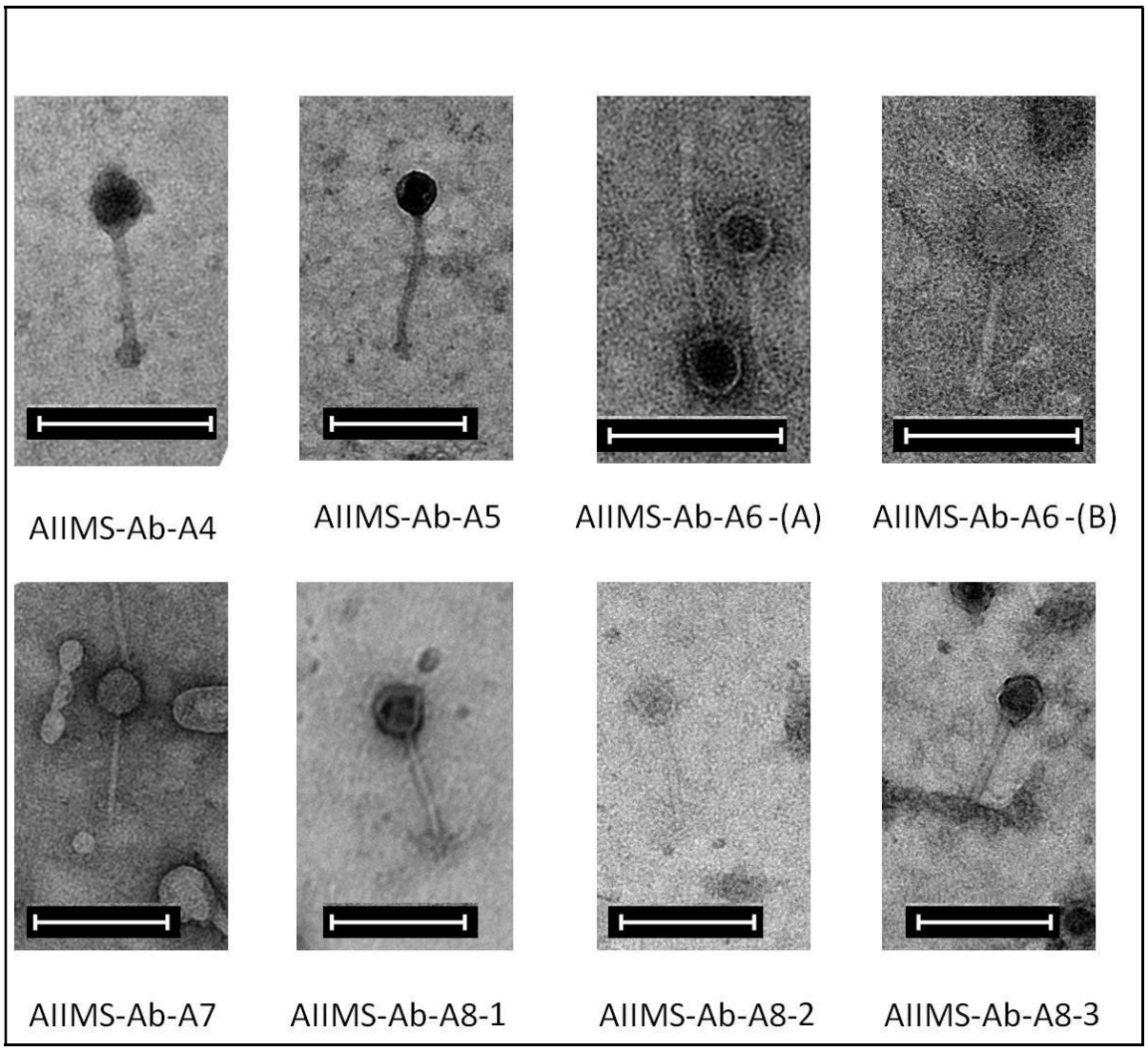

Figure 7: Microscopic morphology of Acinetobacter phages revealed by TEM; hexagonal heads and long tails. The scale bar is presenting 200nm.

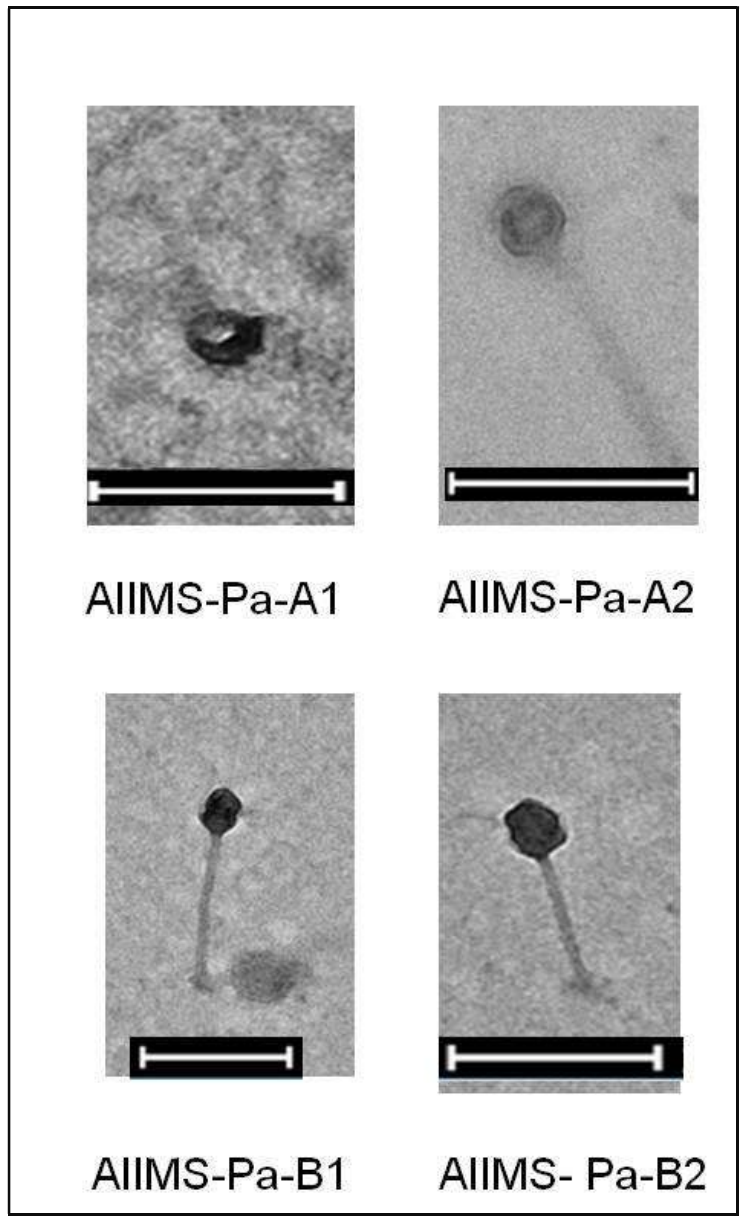

Figure 8: Microscopic observations of pseudomonas phages visualized by TEM. The phage AIIMS-Pa-A1 showed the hexagonal head and small tail while AIIMS-Pa-A2, AIIMS-Pa-B1 and AIIMS-Pa-B2 are having hexagonal head and long tail, scale bar is presenting 200nm.

2.5 Molecular characterization of bacteriophages:

2.5a Bacteriophage DNA: DNA has been isolated from three bacteriophages active against *A. baumannii*; AIIMS-Ab-A4, AIIMS-Ab-A5, AIIMS-Ab-A8-3 and two bacteriophages; AIIMS-Pa-A1 and AIIMS-Pa-B1, active against *P. aeruginosa* by phenol:chloroform:isoamyl alcohol extraction method. The DNA preparations were visualized on gel (Figure 9). The gel showed presence of intact DNA. The DNA samples were quantified by Nanoquant Infinite 200Pro. The whole genome sequencing of isolated DNA has been done by Clevergene Biocorp Pvt. Ltd.

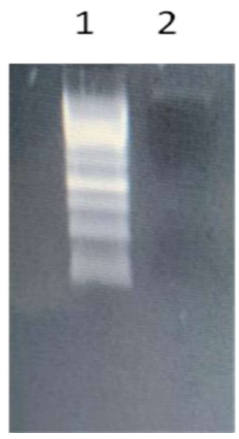

Figure 9: A representative picture of agarose gel showing DNA isolated from the bacteriophage AIIMS-Ab-A4: Lane 1: 1Kb DNA ladder (Thermo fisher) and Lane 2: Genomic DNA from Bacteriophage; AIIMS-Ab-A4.

2.5.b. Genome Sequence Analysis: The genome size of Acinetobacter phages; AIIMS-Ab-A4, AIIMS-Ab-A5, AIIMS-Ab-A8-3 and pseudomonas phages; AIIMS-Pa-A1 and AIIMS-Pa-B1, their GC content and number of Open Readings Frames (ORF) are listed in table 3.

Table 3: Details of bacteriophage whole genome sequences

Bacteriophage	Genome Size (in kb)	GC content (%)	Open Readings Frames
AIIMS-Ab-A4	32.93	39.9	28
AIIMS-Ab-A5	35.61	41.5	32
AIIMS-Ab-A8-3	63.6	41.12	119
AIIMS-Pa-A1	40.97	61.0	47
AIIMS-Pa-B1	37.57	64.5	51

Genome Analysis of bacteriophage AIIMS-Ab-A4: The whole genome sequencing of bacteriophage AIIMS-Ab-A4 showed 27 proteins as presented in figure 10.

Figure 10: The pictorial presentation of whole genome sequence of bacteriophage AIIMS-Ab-A4

Genome Analysis of bacteriophage AIIMS-Ab-A5: The whole genome sequencing of bacteriophage AIIMS-Ab-A5 (active against *A. baumannii*) showed 32 proteins as presented in figure 11.

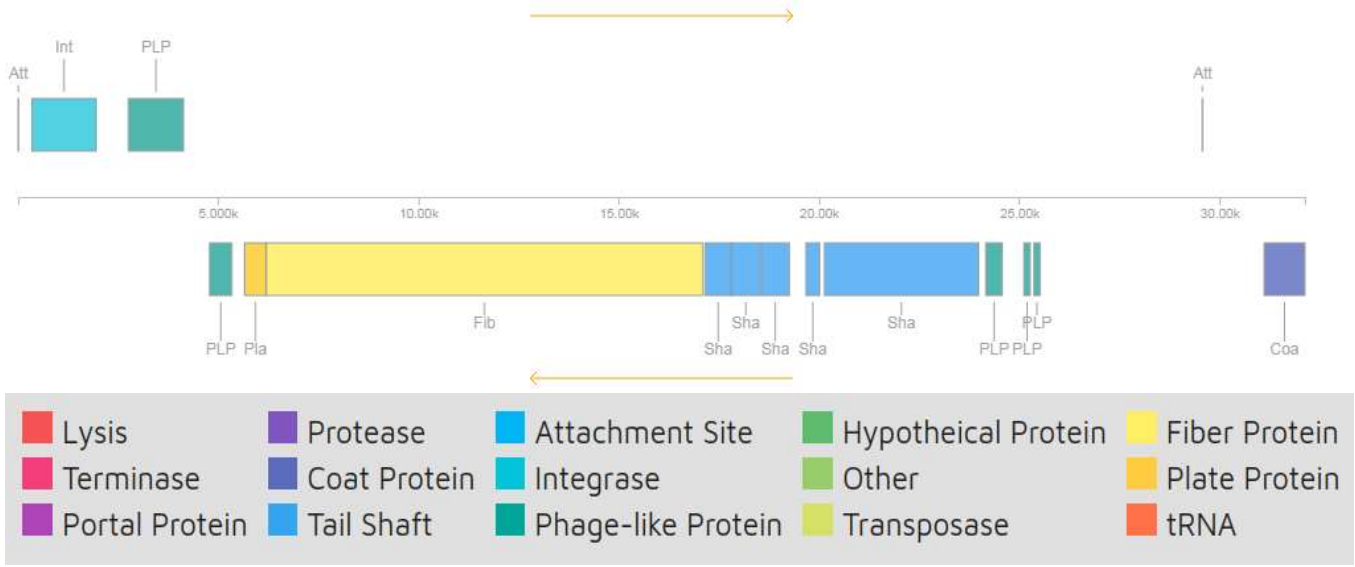

Figure 11: The pictorial presentation of whole genome sequence of bacteriophage AIIMS-Ab-A5

Genome Analysis of bacteriophage AIIMS-Ab-A8-3: The whole genome sequencing of bacteriophage AIIMS-Ab-A8-3 (active against *A. baumannii*) showed 119 proteins as presented in figure 12.

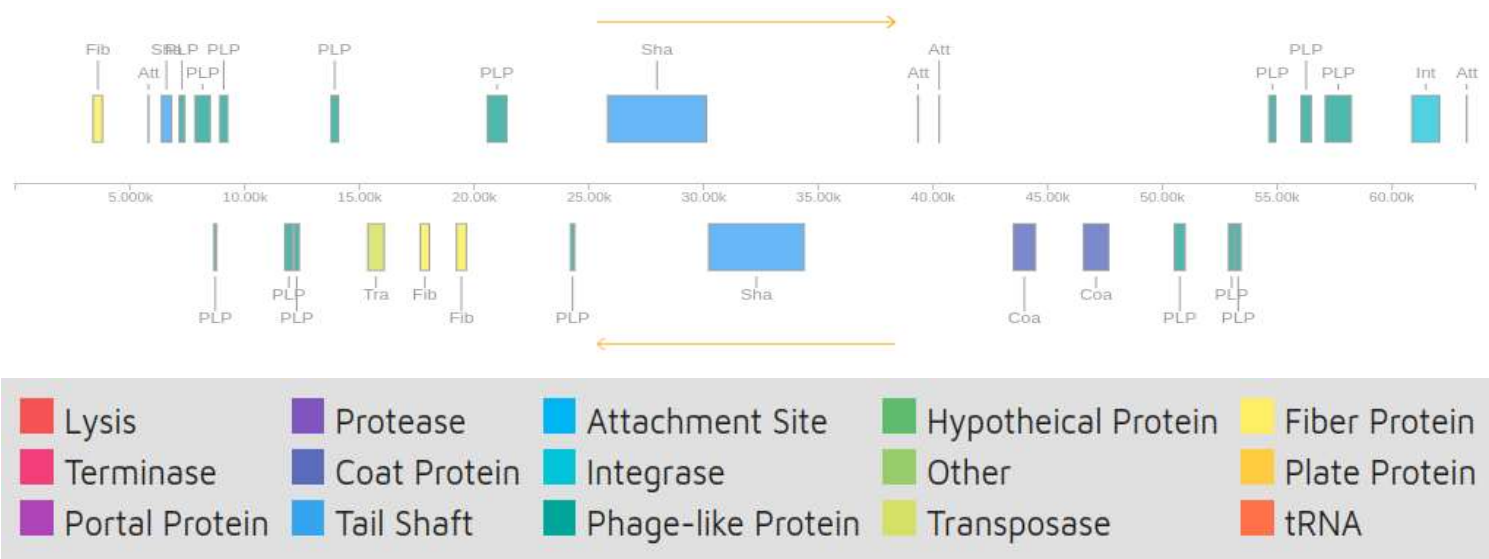

Figure 12: The pictorial presentation of whole genome sequencing of bacteriophage Ab-A8-3

Genome Analysis of pseudomonas phage AIIMS-Pa-A1: The whole genome sequencing of pseudomonas phage AIIMS-Pa-A1 showed 47 proteins including endolysin gene (Figure 13). The sequence has been submitted to NCBI (Accession No. MW117144)

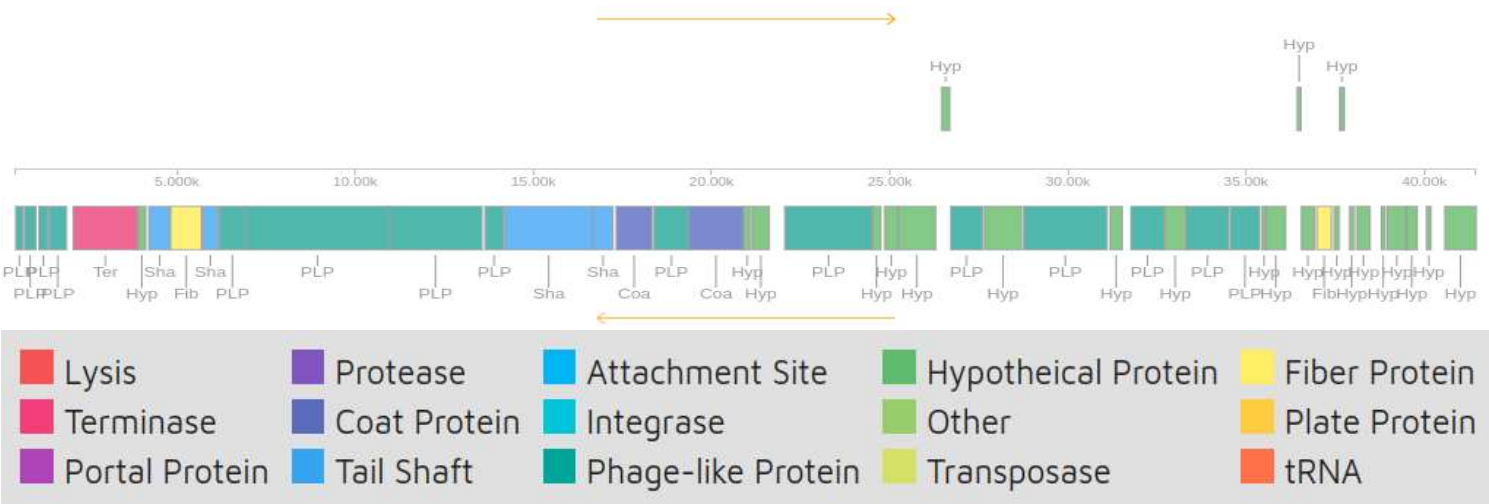

Figure 13: The pictorial presentation of whole genome sequence of pseudomonas phage AIIMS-Pa-A1.

Genome Analysis of pseudomonas phage AIIMS-Pa-B1: The whole genome sequencing of pseudomonas phage AIIMS-Pa-B1 showed 51 proteins including recombination endonuclease, RNA polymerase sigma factor, virion structural protein, ssDNA binding protein, virion morphogenesis protein, DNA helicase, exonuclease A and hypothetical proteins etc. as presented in figure 14. The sequence has been submitted to NCBI (Accession No. MW390886)

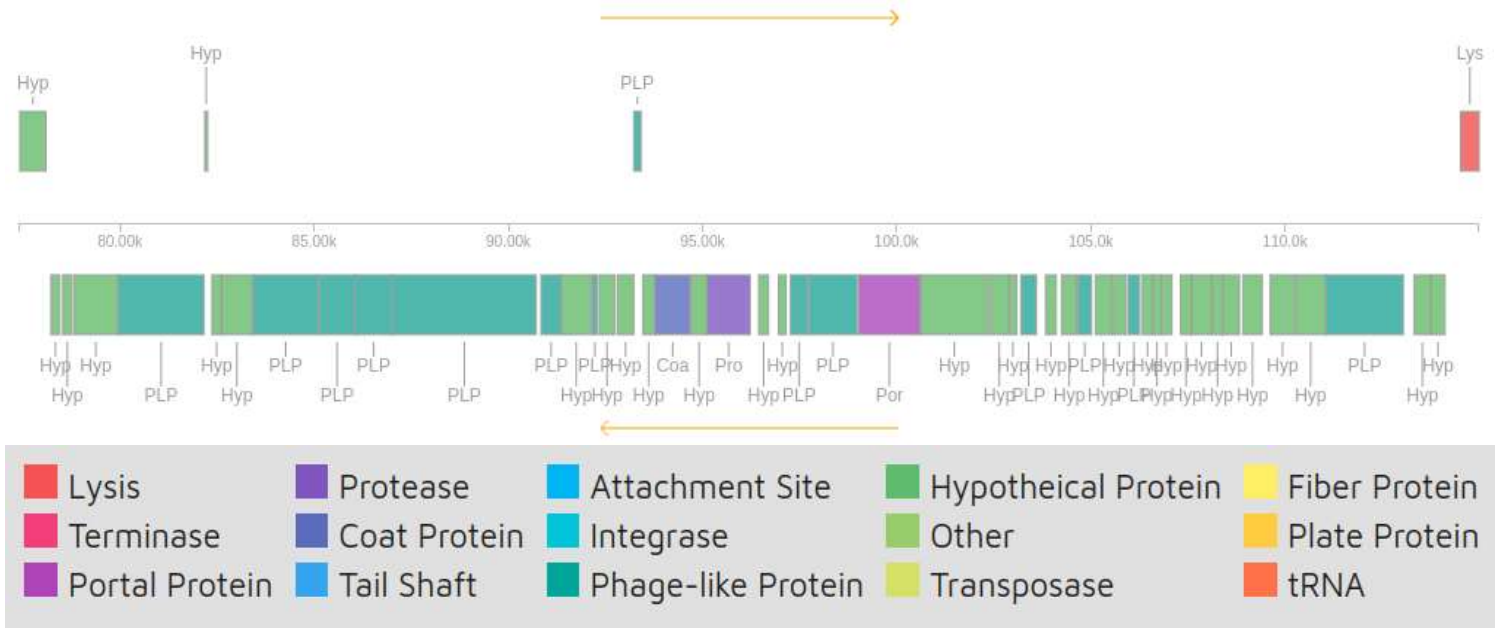

Figure 14: The whole genome sequence view of pseudomonas phage AIIMS-Pa-B1

Objective 2

2.5 Bacteria obtained from G ward: The swabs were collected from seven different sites of G wards at 15 days interval for three times (figure 15) and processed for bacterial isolation (Figure 16A). The bacterial colonies obtained on LB agar were culture further (Figure 16B) and identified by MALDI-TOF (table 5).

Figure 15: The ward surface sampling across 10x10 cm^2 area for bacterial isolation

16(A) 16(B)

Figure 16: (A) A representative picture showing colonies obtained from swabbing of floor samples of G ward AIIMS, New Delhi. (B) A representative picture showing grown cultures to be processed for identification.

The bacteria including belonging to genus Staphylococcus, Pseudomonas, Acinetobacter and Klebsiella have been isolated (Table 4).

Table 4: List of bacterial pathogens isolated and identified from floor of G ward, AIIMS, New Delhi

S No.	Bacterial Isolate	No of Isolates
1	*A. baumannii*	5
2	*Acinetobacter lwoffi*	1
3	*Aerococcus viridans*	1
4	*Bacillus group*	1
5	*Bacillus altitudinis*	1
6	*Bacillus altitudinis/pumilus*	1
7	*Bacillus cereus group*	1
8	*K. pneumoniae*	2
9	*Kocuria rhizophilia*	1
10	*Leclercia adecarboxylata*	1
11	*Pseudomonas stutzeri*	1
12	*Pseudomonas luteola*	1
13	*Pseudomonas oleovorans*	1
14	*S. aureus*	5
15	*Staphylococcus epidermidis*	2
16	*Staphylococcus haemolyticus*	9
17	*Staphylococcus hominis*	5
18	Staphylococcus arlettae	3
19	*Staphylococcus xylosus*	1
20	*Staphylococcus gallinarum*	2

2.6 Antibacterial activity of bacteriophages on bacterial samples collected from G ward: The lytic activity of bacteriophages against *A. baumannii*, *K pneumoniae* and *S. aureus* have

been tested by spot assay on their respective bacterial isolated from G ward AIIMS, New Delhi. However, no lytic activity was observed in any tested bacteria by any bacteriophage.

2.8 Antibacterial activity of bacteriophages cocktail on plastic surface: The spot assay of the bacteriophage cocktail (Table 5) showed efficient lysis of bacterial lawn of drug resistant bacterial mixture; presented in Figure 17.

Table 5: **The bacterial isolates and bacteriophages used to prepare drug resistant bacterial mixture and bacteriophage cocktail**

Bacterial strain used in bacterial cocktail against which phages have been isolated or scaled up	Source of Bacteriophage		Volume of each phage (of 10^7PFU/ml) for 1000 µl cocktail
	Bacteriophages isolated at AIIMS Delhi	Obtained from BHU	
A. baumannii (MDR)	AIIMS-Ab-A8-3	-	200 µl
K. pneumoniae (ESBL/CRE)	-	BHU-91 BHU-97 BHU-368	66 µl
P. aeruginosa (MDR)	AIIMS-Pa-A1 AIIMS-Pa-A2 AIIMS-Pa-B1 AIIMS-Pa-B2	-	50 µl
E. coli (ESBL/CRE)	AIIMS-Ec-A3-1 AIIMS-Ec-A3-2 AIIMS-Ec-A3-3	-	66 µl
S. aureus (MRSA)	-	BHU-22 BHU-Sir1	100 µl
Total number of phages used in cocktail			**13**

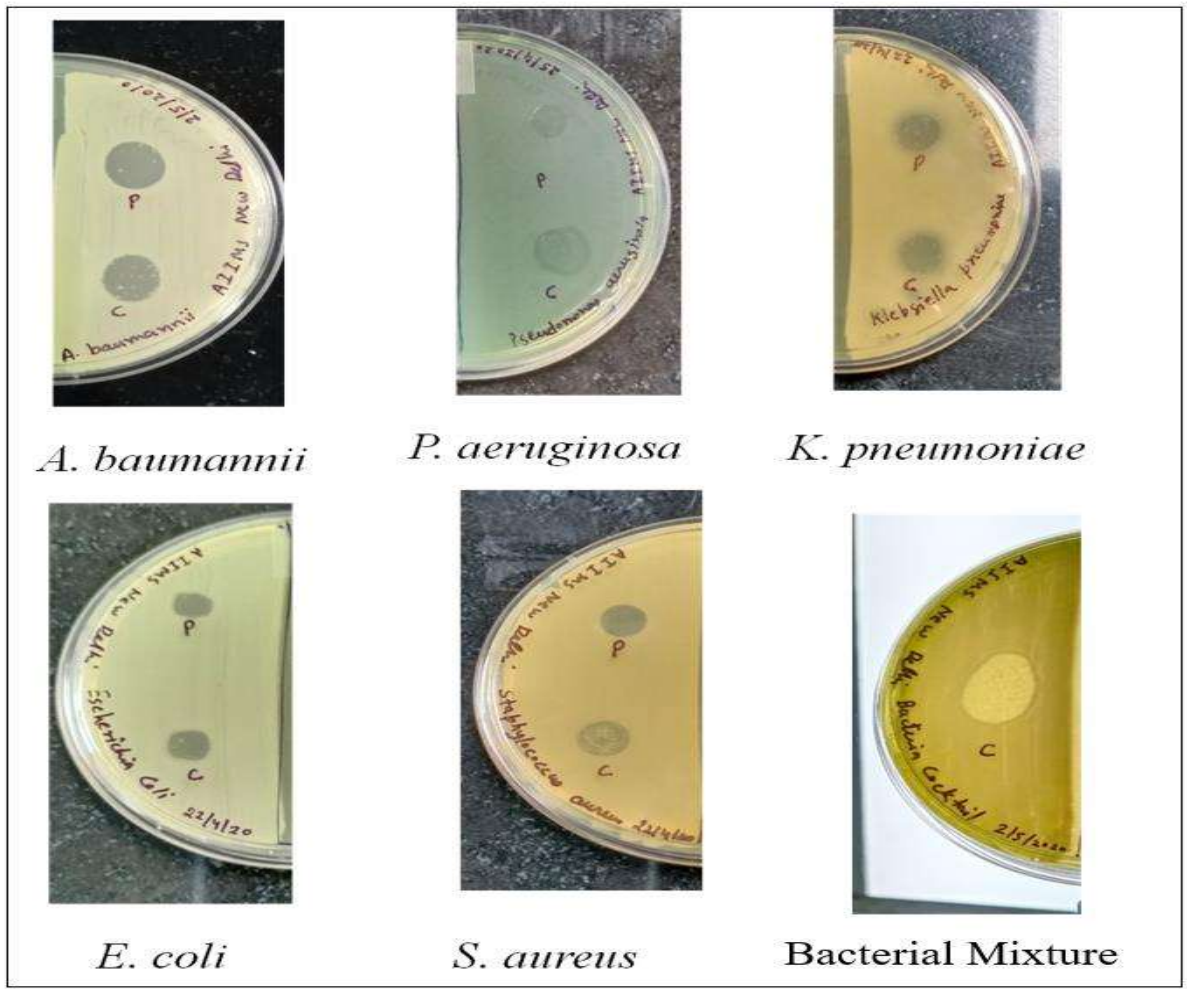

Figure 17. The bacterial lysis observed by spot assay. The bacterial lawn (Mixture of drug resistant *A. baumannii, P. aeruginosa, K. pneumoniae, E. coli* and *S. aureus)* spotted with their respective phage: P (positive control) and C (Cocktail of phages active against *A. baumannii, P. aeruginosa, K. pneumoniae, E. coli* and *S. aureus*).

To determine the antibacterial activity of bacteriophage cocktail on the plastic surface the blank petri plates were used. The spray bottle and 3M™Clean-Trace™ Hygiene Monitoring system (ATP monitor) used for the experiment is presented in figure 18 A and 18 B respectively.

The antibacterial activity of the bacteriophages on experimentally contaminated plastic surface was monitored by CFU analysis and by measurement of ATP produced. The bacteriophage cocktail reduced the bacterial CFU significantly at each time point (Table 6 and Figure 19) even

at t=0 (P<0.001). The significant CFU reduction at t=0 appeared in bacteriophages cocktail treated plate, due to phage to bacteria interaction during the processing of the experiment.

In the presence of bacteriophage cocktail, initially up to two hours, the ATP levels were higher than bacterial cocktail in presence of normal saline. However, the difference was not significant (P>0.05). After 4-6 hours of phage to bacteria interaction, declination in RLUs was observed on phage treated surface, suggesting lower bacterial load (P<0.001) (Table 7 and Figure 20).

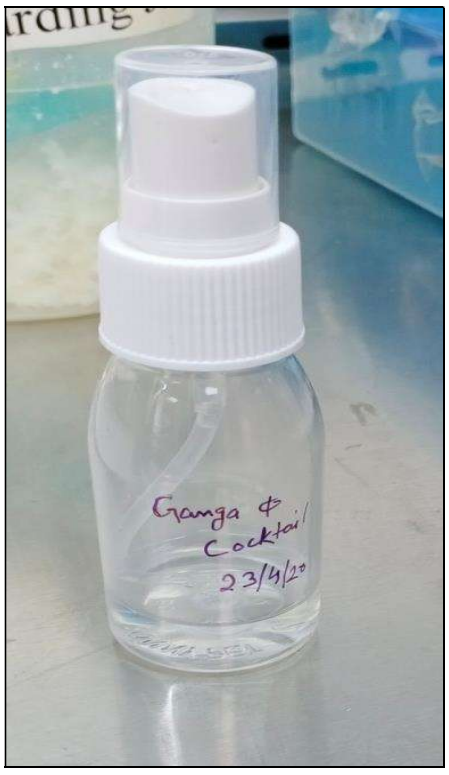

(A)

(B)

Figure 18: (A) The bottle used to spray bacteriophage cocktail (B) 3M™ Clean-Trace™ Hygiene monitoring system.

Table 6: **The bacterial load in the presence of bacteriophages cocktail on plastic surface (CFU analysis)**

Time Point in hours	10^4×CFU /ml CFU-B	10^4×CFU/ml CFU-P	P value
t=0	205	147	<0.001
t=2	500	29	<0.001
t=4	1760	28	<0.001
t=6	4680	5	<0.001

CFU-B: Colony forming units of drug resistant bacterial mixture in presence of normal saline
CFU-P: Colony forming units of drug resistant bacterial mixture in presence of bacteriophage cocktail

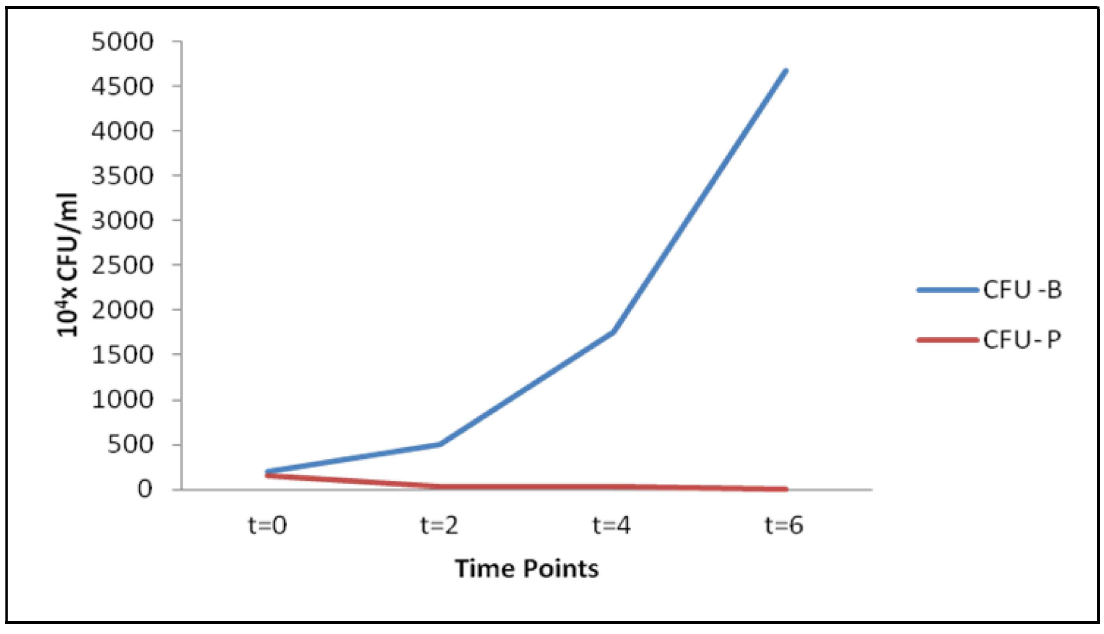

Figure 19: Comparison of CFUs of bacterial mixture in the absence and presence of bacteriophages.

CFU-B: Colony forming units of drug resistant bacterial mixture in presence of normal saline,

CFU-P: Colony forming units of drug resistant bacterial mixture in presence of bacteriophage cocktail.

A significant difference was observed at each time point in CFUs of bacterial cocktail in presence of bacteriophages (P<0.001).

Table 7: ATP monitoring (in terms of Relative light units) of experimentally contaminated plastic surface in the presence of bacteriophages; measured by 3M™ Clean-Trace™ Hygiene Monitoring system

Time Point in hours	RLU -B	RFU –P	P value
t=0	1265	1487	P>0.05
t=2	6757	8552	P>0.05
t=4	19659	5499	P<0.001
t=6	57598	1383	P<0.001

RFU-B: Relative light units of bacterial cocktail in normal saline
RFU-P: Relative light units of bacterial cocktail in presence of isolated bacteriophages cocktail.

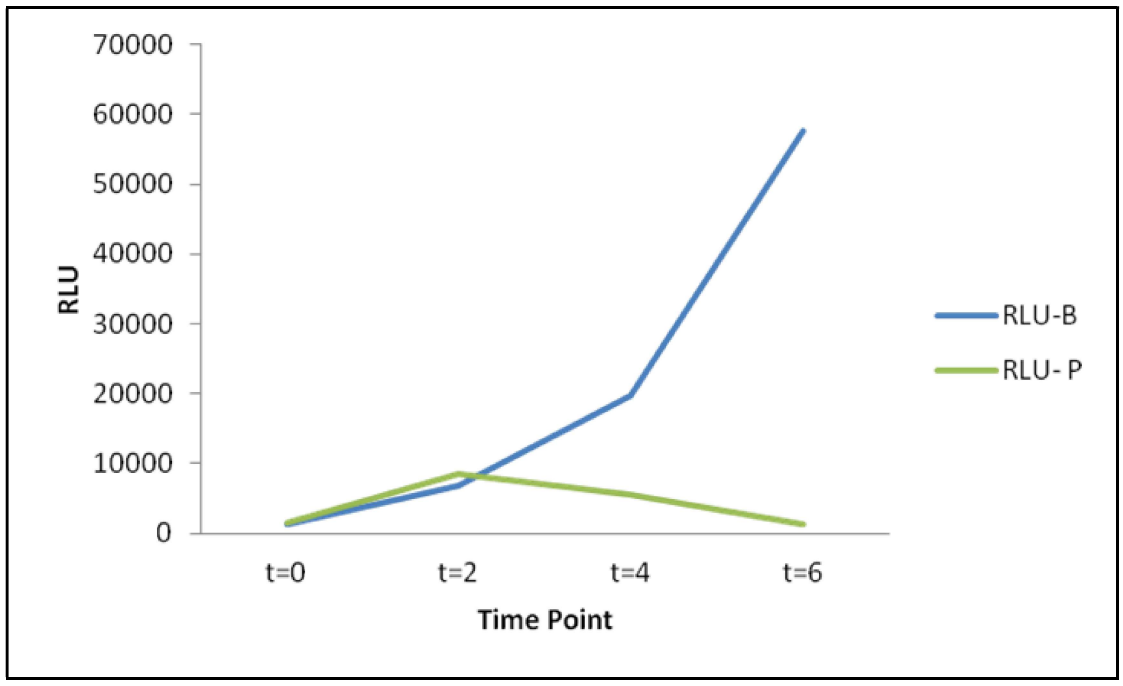

Figure 20. Comparison of ATP levels of Bacterial cocktail in the absence and presence of bacteriophages cocktail. **RFU-B**: Relative light units of bacterial cocktail in normal saline, **RFU-P**: Relative light units of bacterial cocktail in presence of isolated bacteriophage cocktail. A significant difference was observed in RLUs after 4- 6 hours of phages to bacteria interaction (P<0.001).

Summary and conclusions of work done:

- A total of 224 bacterial isolates including aerobic (210), anaerobic (4) and Special Bacterial pathogen; *Legionella pneumophila* (10) have been collected and identified. The antibiotic testing has been performed for aerobic pathogens and *L. pneumophila.*

- Eleven Ganga water samples have been collected from different sites and processed to isolate bacteriophages against collected bacterial pathogens.

- A total of 14 bacteriophages were isolated at AIIMS, New Delhi, including the phages active against *A. baumannii* (7 phages), *P. aeruginosa* (4 phages) and *E. coli* (3 phages). The Bacteriophages obtained from BHU (6 phages) also showed lytic activity on bacterial isolates at AIIMS New Delhi, against *K. pneumoniae* (3 phages), *S. aureus* (2 phages) and *P. aeruginosa* (1 phage).

- The phages against *A. baumannii* and *P. aeruginosa* were morphologically characterized by transmission electron microscopy; showed hexagonal heads with tails belonging to order Caudovirales.

- The molecular characterization has been performed for some Acinetobacter and pseudomonas phages by whole genome sequencing. The pseudomonas phage; AIIMS-Pa-A1 showed the presence of holing, endolysin and virion encoded RNA polymerase genes, contributing it highly lytic potential. The pseudomonas phages (AIIMS-Pa-A1 and AIIMS-Pa-B1) whole genome sequences have been submitted to NCBI.

- The ward floor samples have been collected and processed for bacterial isolation and identification; from ward surface, 45 bacterial isolates have been identified.

- The lytic activity of bacteriophages was tested on experimentally contaminated plastic surface with the bacteria against which the phages were isolated or enriched, to determine

the disinfectant property of the phages isolated from the water Ganga. The mixture of 5 drug resistant bacterial isolates (*A. baumannii, P. aeruginosa, K. pneumoniae, E. coli* and *S. aureus*) was subjected to bacteriophage cocktail on plastic surface. A significant reduction was observed in bacterial load within 2 hours of bacteriophage interaction evidenced by CFU analysis. The observation was further supported by significant ATP reduction on phage to bacteria interaction for 4-6 hours.

- **The results of the study indicated that the isolated bacteriophages from the river Ganga, significantly reduced the bacterial load of the drug resistant pathogens in *in-vitro* condition, present on plastic surface. The results suggest that the strategy to apply bacteriophages as disinfectant on hospital surface may be effectively used with having a large pool of bacteriophages cocktail active against the drug resistant pathogens, associated to Hospital acquired infections.**

Signature of the PI

Final report

A Detail Study to Understand the Non-Putrefying Property of River Ganga in both Water and Sediment

Sponsor:
Ministry of Water Resources, River Development & Ganga Rejuvenation, New Delhi

CSIR-National Environmental Engineering Research Institute
Nehru Marg, Nagpur – 440 020

Indian Council of Medical Research
Ansari Nagar, New Delhi - 110029

April 2nd 2018- September, 2021

Project Investigator:
Name : Dr Gopal Nath
Designation: Professor
Organization: Institute of Medical Sciences (IMS), BHU
Address: Department of Microbiology, Institute of Medical Sciences, BHU, Varanasi-221005

Tele Fax : 05452236578, mobile: 9335058394

E mail : : gopalnath@gmail.com, gnath@bhu.ac.in

Duration of study: 2 years

Duration of First annual report: April 2018 – September 2021 (The recruited staff could join on April 02, 2018)

IMS (BHU) Components – Objectives

1. Monitoring of source and spectrum of pathogenic and so called non pathogenic bacteria that interfere with the water quality of Ganga round the year in Varanasi.

2. Study on relevant bacteriophages (enumeration, isolation, characterization) with different seasonal variations.

3. Study on potentials of bacteriophage therapy in the infections caused by multidrug-resistant bacterial pathogens in animal and human infections.

1 Milestones

Phage therapy centre for pre-clinical investigations

Sr. No.	Milestone	Months						
		3	6	9	12	15	18	24
1.	Initiation of the project after receipt of initial funds i.e., the appointment of staff and procurement of consumables							
2.	Isolation and identification of bacterial pathogens from river water							
3.	Isolation, characterization and purification of Bacteriophages against different pathogenic bacteria of clinical origin							
4.	Evaluation of Bacteriophages dose in suitable animal models							
5.	Analysis and final data submission							

Detailed progress of the work carried out during the period

Objective 1:

Monitoring of source and spectrum of pathogenic and so-called non-pathogenic bacteria that interfere with the water quality of Ganga round the year in Varanasi.

Materials and Methods:

1. Isolation and enumeration of coliforms, faecal coliforms and faecal streptococci in Ganga water samples collected from ten different Ghats at Varanasi.

1.1 Sample collection: The water samples from Ganga were collected in a 500 mL bottle of rubber cap (usually available normal saline bottles – autoclaved) from 10 different Ghats at Varanasi to enumerate the coliforms and faecal coliforms was done. Samples were collected twice per month from April 2018 to June 2019.

Table- 1: Details of water sample collection sites from the river Ganga at Varanasi

S.N0.	Sample collection site	Abbreviation
1	Samne Ghat	G1
2	Asssi Ghat	G2
3	Jain Ghat	G3
4	Harishchandra Ghat	G4
5	Narad Ghat	G5
6	Dasashwamedh Ghat	G6
7	Manikarnika Ghat	G7
8	Gola Ghat	G8
9	Prahlad Ghat	G9
10	Panchganga Ghat	G10

1.2 Processing of water samples: The samples were processed for the coliform count and faecal coliform count by using multiple tube technique. The water samples were processed and inoculated in EC broth (*Escherichia coli* Broth) for the coliform count; positive tubes (turbidity with gas) were used to inoculate Brilliant green bile broth and kept at 44^0 C overnight. Samples that were positive for faecal coliform were cultured on a MacConkey agar plate. Positive EC broth tubes were also cultured on Sodium Azide agar plates for detection of faecal streptococci.

1.3 Confirmation of faecal coliform: Biochemical tests further confirmed the suspected faecal coliform colony obtained on MacConkey agar plates.

1.4 Isolation and Identification of bacterial pathogens from Ganga water

1.4a Isolation of Special Bacterial pathogens: Water samples were collected from 10 different Ghats at Varanasi (shown in the above table) were processed for different bacterial pathogens like *Salmonella spp.*, *Shigella spp., Vibrio spp*., *Aeromonas spp., Plesiomonas spp.*
i) Water sample processing: The 100 mL water sample was centrifuged at 13000 rpm for 15 min, the pellet was collected, and the supernatant was discarded.
ii) Acid treatment: Pellets of different water samples obtained after centrifugation were treated with 3.5 pH LB(Luria Bertani) broth for 10 min, after 10 min neutralized with an equal volume of LB of pH 10.5 and cultured on TCBS (selective growth of *Vibrio* spp.), XLD agar plates, MacConkey agar plates and DCA agar plates (selective for *Salmonella* spp.).

iii) Enrichment: Pellets having 500µL from different samples neutralized after acid treatment were inoculated into the SFB broth (for selective growth of *Shigella*) and Alkaline Peptone Water pH8.6 (for the enrichment of *Vibrio sp*.) incubated at 37^0C for 6 hours. After 6 hours selected on DCA and TCBS plates, respectively.

All the cultured plates were incubated at 37^0C for 24 hours and observed for yellow colonies on TCBS, black-headed or NLF colonies on DCA plates and pink, convex regular edge colonies on MacConkey plates.

1.5a Antimicrobial Susceptibility of environmental isolates of *Klebsiella pneumoniae*: Antimicrobial susceptibility was performed for 15 environmental isolates using Mueller Hinton Agar by the Kirby-Bauer disc diffusion method following the standard procedure Clinical and Laboratory Standards Institute (CLSI) guidelines. The antibiotics used for isolates are listed in table 2.

Table 2. Antibiotics used for antimicrobial susceptibility testing of *Klebsiella pneumoniae*

SN	Antibiotic disc	Abbreviation	Sensitivity range(mm)
1	Ampicillin (10µg)	3	≥17

2	Amoxicillin (20µg) + Clavulanic acid(10µg).	5	≥18
3	Cefazolin/Cephalexin (30 µg)	6/7	≥18
4	Cefuroxime (30 µg),	8	≥18
5	Cefotaxime/Ceftriaxone (30 µg)	9/10	≥26
6	Cefpirome/Cefepime (30 µg),	Cp	≥18
7	Gentamicin (10 µg)	12	≥15
8	Amikacin (30 µg)	14	≥17
9	Ciprofloxacin (5 µg)	18	≥21
10	Levofloxacin (5 µg)	LV	≥19
11	Trimethoprim (1.25 µg) +Sulfamethoxazole (23.75 µg)	22	≥16
12	Meropenem (10 µg)	Me	≥16
13	Imipenem (10 µg)	27	≥16
14	Ertapenem (10 µg)	Erta	≥22

Results

Enumeration of coliform, faecal coliform, and faecal streptococci : All the samples showed a higher MPN count ,collected from ten different Ghats at Varanasi from October 2018 to June 2019. MPN count of coliform, faecal coliform and faecal streptococci is given in table no 4.

Table 3: MPN count of coliform, faecal coliform, faecal streptococci in Ganga water sample.

GANGA GHATS	April 1st Round 2018			April 2nd Round 2018			May 1st Round 2018			May 2nd Round 2018		
	Coliform count /100mL	Fecal coliform count/ 100 mL	Enterococcus faecalis/ 100 ML	Coliform count /100mL	Fecal coliform count/100 mL	Enterococcus faecalis/100 ML	Coliform count /100mL	Fecal coliform count/ 100 mL	Enterococcus faecalis/ 100 ML	Coliform count /100mL	Fecal coliform count/100 mL	*Enterococcus faecalis*/100 ML
Samne Ghat	920	2	350	920	13	540	540	49	540	>1600	>1600	540
Assi Ghat	>1600	430	1600	240	49	240	>1600	130	1600	>1600	>1600	110

Jain Ghat	63	33	33	>1600	2	>1600	22	11	22	1600	1600	49
Harishchandra Ghat	23	13	45	>1600	4.5	>1600	23	45	7.8	540	540	11
Narad Ghat	>1600	31	11	920	<1.8	110	22	2	22	240	240	6.8
Dashshwamegh Ghat	>1600	34	13	1600	2	1600	63	23	23	170	170	31
Manikanika Ghat	>1600	>1600	540	22	<1.8	22	11	2	4.5	920	540	540
Panchganga Ghat	1600	920	33	17	<1.8	1.8	21	45	4.5	350	170	33
Gola Ghat	170	130	130	33	13	33	17	2	13	350	40	70
Prahlad Ghat	>1600	920	540	23	<1.8	7.8	11	4	7.8	>1600	1600	350

Ganga Ghats	**June 1st Round**			**June 2nd Round**			**July 1st Round**			**July 2nd Round**		
	Coliform count /100mL	Fecal coliform count/ 100 mL	*Enterococcus faecalis* /100 ML	Coliform count /100mL	Fecal coliform count/100 mL	*Enterococcus faecalis*/100 ML	Coliform count /100mL	Fecal coliform count/ 100 mL	*Enterococcus faecalis* /100 ML	Coliform count /100mL	Fecal coliform count/100 mL	*Enterococcus faecalis*/ 100 mL
Samne Ghat	79	49	6.8	920	430	13	1600	920	48	>1600	>1600	170
Assi Ghat	240	240	11	>1600	170	130	1600	1600	170	350	170	350
Jain Ghat	130	79	33	48	17	48	920	920	350	920	240	8.1
Harishchandra Ghat	130	130	7.8	49	13	49	1600	540	48	350	170	48
Narad Ghat	170	13	11	63	23	43	280	280	140	130	79	130
Dashshwamegh Ghat	170	170	7.8	13	7.8	4.5	280	280	11	70	70	13
Manikanika Ghat	170	33	33	33	4	4	130	130	41	920	540	25

Panchganga Ghat	22	4.5	17	33	33	27	38	32	3.6	79	79	6.8
Gola Ghat	>1600	1600	>1600	26	6.8	<1.8	920	350	1.8	31	23	7.8
Prahlad Ghat	49	7.8	11	170	4.5	4.5	280	130	49	33	17	17

GANGA GHATS	**August 1st Round**			**August 2nd Round**			**September 1st Round**			**September 2nd Round**		
	Coliform count /100mL	Fecal coliform count/ 100 mL	*Enterococcus faecalis*/100 mL	Coliform count /100mL	Fecal coliform count/ 100 mL	*Enterococcus faecalis*/100 mL	Coliform count /100mL	Fecal coliform count/ 100 mL	*Enterococcus faecalis*/100 mL	Coliform count /100mL	Fecal coliform count /100 mL	*Enterococcus faecalis* /100 mL
Samne Ghat	>1600	1600	<1.8	63	46	<1.8	540	540	<1.8	140	23	<1.8
Assi Ghat	>1600	>1600	1.8	540	170	<1.8	>1600	>1600	4	240	34	2
Jain Ghat	540	350	4	33	11	<1.8	>1600	>1600	<1.8	49	49	<1.8
Harishchandra Ghat	540	350	1.8	94	70	2	>1600	>1600	79	170	110	<1.8
Narad Ghat	1600	1600	<1.8	17	6.8	<1.8	>1600	>1600	1.8	350	130	<1.8
Dashshwamegh Ghat	>1600	>1600	<1.8	350	350	1.8	>1600	>1600	<1.8	350	350	<1.8
Manikanika Ghat	>1600	>1600	1.8	33	33	<1.8	>1600	>1600	<1.8	350	170	<1.8
Panchganga Ghat	>1600	>1600	<1.8	240	79	1.8	>1600	>1600	2	280	47	1.8
Gola Ghat	>1600	>1600	1.8	>1600	280	12	920	350	2	140	17	<1.8
Prahlad Ghat	1600	1600	3.7	110	110	<1.8	>1600	>1600	<1.8	49	23	<1.8

GANGA GHATS	October 1st Round			October 2nd Round			November 1st Round			November 2nd Round		
	Coliform count /100mL	Fecal coliform count/ 100 mL	Enterococcus faecalis/100 mL	Coliform count /100mL	Fecal coliform count/ 100 mL	Enterococcus faecalis/100 mL	Coliform count /100mL	Fecal coliform count/ 100 mL	Enterococcus faecalis/100 mL	Coliform count /100mL	Fecal coliform count/ 100 mL	Enterococcus faecalis/100 mL
Samne Ghat	27	27	<1.8	170	27	<1.8	280	280	<1.8	1600	920	<1.8
Assi Ghat	94	94	<1.8	>1600	>1600	<1.8	>1600	>1600	<1.8	>1600	>1600	<1.8
Jain Ghat	79	49	<1.8	920	920	<1.8	920	920	<1.8	>1600	920	<1.8
Harishchandra Ghat	110	110	<1.8	21	21	<1.8	>1600	>1600	<1.8	>1600	>1600	<1.8
Narad Ghat	170	32	<1.8	79	49	<1.8	1600	1600	<1.8	>1600	920	<1.8
Dashshwamegh Ghat	>1600	>1600	<1.8	350	350	<1.8	43	43	<1.8	>1600	>1600	<1.8
Manikanika Ghat	170	49	1.8	130	130	<1.8	280	920	<1.8	540	4.5	<1.8
Panchganga Ghat	540	79	4	79	79	<1.8	240	240	<1.8	1600	17	<1.8
Gola Ghat	220	22	<1.8	540	540	1.8	920	920	<1.8	>1600	>1600	<1.8
Prahlad Ghat	49	11	<1.8	70	70	<1.8	>1600	1600	<1.8	>1600	1600	<1.8

GANGA GHATS	December 1st Round			December 2nd Round			January 1st Round			January 2nd Round		
	Coliform count /100mL	Fecal coliform count/100 mL	*Enterococcus faecalis*/100 ML	Coliform count /100mL	Fecal coliform count/100 mL	*Enterococcus faecalis*/100 ML	Coliform count /100mL	Fecal coliform count/100 mL	*Enterococcus faecalis*/100 ML	Coliform count /100mL	Fecal coliform count/100 mL	*Enterococcus faecalis*/100 ML
Samne Ghat	>1600	>1600	<1.8	>1600	>1600	<1.8	170	170	<1.8	>1600	>1600	<1.8
Assi Ghat	>1600	>1600	<1.8	>1600	>1600	<1.8	1600	1600	2	84	84	<1.8
Jain Ghat	>1600	>1600	<1.8	130	130	<1.8	1600	>1600	<1.8	220	220	<1.8
Harishchandra Ghat	>1600	>1600	<1.8	920	280	<1.8	>1600	>1600	<1.8	79	49	<1.8
Narad Ghat	>1600	>1600	<1.8	540	540	<1.8	430	170	<1.8	13	13	<1.8
Dashshwamegh Ghat	>1600	>1600	<1.8	79	79	<1.8	280	220	<1.8	49	49	<1.8
Manikanika Ghat	>1600	>1600	2	>1600	>1600	<1.8	79	79	<1.8	79	79	2
Panchganga Ghat	>1600	>1600	<1.8	>1600	>1600	<1.8	23	23	<1.8	13	23	<1.8
Gola Ghat	170	170	<1.8	>1600	>1600	<1.8	23	23	<1.8	350	240	<1.8
Prahlad Ghat	>1600	>1600	<1.8	>1600	>1600	<1.8	23	23	<1.8	350	350	<1.8

GANGA GHATS	February 1st Round			February 2nd Round			March 1st Round			March 2nd Round		
	Coliform count /100mL	Fecal coliform count/100 mL	Enterococcus faecalis/100 ML	Coliform count /100mL	Fecal coliform count/100 mL	Enterococcus faecalis/100 ML	Coliform count /100mL	Fecal coliform count/100 mL	Enterococcus faecalis/100 ML	Coliform count /100mL	Fecal coliform count/ 100 mL	Enterococcus faecalis/ 100 ML
Samne Ghat	1600	<1.8	<1.8	280	220	<1.8	-	-	-	540	540	<1.8
Assi Ghat	920	<1.8	<1.8	170	170	<1.8	-	-	-	240	240	<1.8
Jain Ghat	38	13	<1.8	>1600	>1600	<1.8	-	-	-	920	920	<1.8
Harishchandra Ghat	110	4	<1.8	70	70	<1.8	-	-	-	79	79	<1.8
Narad Ghat	70	14	<1.8	22	22	<1.8	-	-	-	94	63	<1.8
Dashshwamegh Ghat	140	39	<1.8	17	17	<1.8	-	-	-	130	130	<1.8
Manikanika Ghat	140	24	<1.8	22	26	<1.8	-	-	-	280	280	2
Panchganga Ghat	47	17	<1.8	17	13	<1.8	-	-	-	94	94	<1.8
Gola Ghat	350	<1.8	<1.8	11	11	<1.8	-	-	-	7.8	7.8	<1.8
Prahlad Ghat	350	<1.8	<1.8	9.2	<1.8	<1.8	-	-	-	49	33	<1.8

GANGA GHATS	April 1st Round			April 2nd Round			May 1st Round			May 2nd Round		
	Coliform count /100mL	Fecal coliform count/100 mL	Enterococcus faecalis/100 ML	Coliform count /100mL	Fecal coliform count/100 mL	Enterococcus faecalis/100 ML	Coliform count /100mL	Fecal coliform count/100 mL	Enterococcus faecalis/100 ML	Coliform count /100mL	Fecal coliform count/ 100 mL	Enterococcus faecalis/ 100 ML
Samne Ghat	13	<1.8	<1.8	79	79	<1.8	>1600	>1600	3.6			
Assi Ghat	>1600	48	<1.8	>1600	>1600	<1.8	>1600	540	<1.8			
Jain Ghat	350	170	<1.8	170	3.6	<1.8	920	540	<1.8			
Harishchandra Ghat	540	7.8	<1.8	33	11	<1.8	210	140	<1.8			
Narad Ghat	23	7.8	<1.8	79	17	<1.8	1600	540	3.6			
Dashshwamegh Ghat	94	4.5	<1.8	23	130	<1.8	540	350	<1.8			
Manikanika Ghat	41	<1.8	<1.8	>1600	47	<1.8	110	14	<1.8			
Panchganga Ghat	17	7.8	<1.8	920	31	<1.8	350	94	4.5			
Gola Ghat	>1600	110	<1.8	>1600	130	<1.8	350	240	<1.8			
Prahlad Ghat	70	<1.8	<1.8	1.8	<1.8	<1.8	94	4.5	<1.8			

GANGA GHATS	June 1st Round 2019			June 2nd Round 2019		
	Coliform count /100mL	Fecal coliform count/100 mL	Enterococcus faecalis/100 ML	Coliform count /100mL	Fecal coliform count/100 mL	Enterococcus faecalis/100 ML
Samne Ghat	920	920	**<1.8**	23	13	23
Assi Ghat	84	84	**<1.8**	1600	1600	21
Jain Ghat	210	79	**<1.8**	7.8	<1.8	<1.8
Harishchandra Ghat	41	27	**<1.8**	<1.8	<1.8	<1.8
NaradGhat	240	130	**<1.8**	4.5	2	4.5
DashshwameghGhat	240	33	**<1.8**	350	41	33
Manikanika Ghat	130	34	**<1.8**	9.3	1.8	6.1
Panchganga Ghat	2	2	**<1.8**	49	33	11
Gola Ghat	79	49	**<1.8**	2	<1.8	<1.8

Prahlad Ghat	240	79	**<1.8**	2	2	2

Bacterial Isolates and antibiotic sensitivity pattern of environmental *Klebsiella pneumoniae*: A total of 16 bacterial pathogens were isolated from samples collected from ten different Ghats at Varanasi from April 2018 to June 2019. Many Unidentified isolates were kept for sequencing. The list of bacteria isolated are shown in table 5, and the antibiotic sensitivity pattern is presented in table 6.

Table- 4: List of bacterial pathogen isolated and identified at IMS, BHU, Varanasi

SN	Organism Identified	No of Isolates
1.	*Klebsiella pneumoniae*	200+
2.	*Salmonella spp*	2
3.	*Shigella spp*	-
4.	*Vibrio cholerae*	1
5.	*Vibrio spp*	2
6.	*Aeromonas spp*	10
7.	*Plesiomonas spp*	1

(-) showing, till the date, no bacteria is isolated.

Table 5: Antibiotic sensitivity pattern of *Klebsiella pneumoniae* isolated from Ganga water

S.No.	Strain	3	5	6	8	9/10	12	14	18	22	Lv	Cp	PTZ	27	Erta	Me
1.	K-1	R	R	R	R	R	R	S	R	S	R	R	S	S	S	S
2	K-2	R	R	R	R	R	R	S	R	S	R	S	S	S	R	S
3	K-3	R	R	R	R	S	S	S	R	S	S	S	S	S	S	S
4	K-4	R	S	S	R	S	S	R	S	S	S	S	S	S	S	S
5	K-5	R	S	R	R	S	S	R	R	S	S	S	S	R	S	S
6	K-6	R	S	R	R	S	S	R	S	S	S	S	S	S	S	S
7	K-7	R	S	R	R	S	R	S	S	S	S	S	S	R	S	S
8	K-8	R	R	R	R	S	S	S	S	S	R	S	S	S	R	S
9	K-9	R	S	S	R	S	S	S	S	R	S	S	S	S	S	S

10	K-10	R	R	R	S	S	S	S	S	S	S	S	S	S	S	S
11	K-11	R	S	S	R	S	S	S	S	S	S	S	S	R	S	S
12	K-12	R	R	R	R	S	S	S	S	R	S	S	S	S	S	S
13	K-13	R	S	S	R	S	S	S	S	S	S	S	S	R	S	S
14	K-14	R	R	R	R	S	S	S	S	S	S	S	S	S	S	S
15	K-15	R	R	S	R	S	S	S	S	S	S	S	S	R	S	S
16	K-16	R	S	S	S	S	S	S	S	S	S	S	S	R	S	S
17	K-17	R	R	R	R	S	S	S	S	S	S	S	S	S	R	S
18	K-18	R	R	R	R	R	S	S	S	S	R	R	R	S	R	S
19	K-19	R	R	R	R	R	S	S	R	R	R	S	R	S	R	S
20	K-20	R	S	S	R	S	S	S	S	S	S	S	S	S	S	S
21	K-21	R	S	S	R	R	S	S	S	S	S	S	S	S	S	S
22	K-22	R	R	R	R	R	S	S	S	S	S	S	R	S	S	S
23	K-23	R	S	S	R	S	S	S	S	S	S	R	R	S	S	S
24	K-24	R	S	S	R	S	S	S	S	S	S	S	S	S	S	S
25	K-25	R	R	R	R	R	R	S	R	R	R	R	S	S	R	S
26	K-26	R	S	S	R	S	S	S	S	S	S	S	S	S	S	S
27	K-27	R	R	R	R	S	S	S	S	S	S	S	S	S	S	S
28	K-28	R	R	R	R	S	R	S	S	S	S	S	S	S	S	S
29	K-29	R	R	R	R	R	S	S	S	R	S	R	S	S	R	S
30	K-30	R	R	R	R	S	S	S	S	S	S	S	S	S	S	S
31	K-31	R	R	R	R	S	S	S	S	S	S	R	R	S	S	S
32	K-32	R	R	R	R	S	S	S	S	S	S	S	S	S	S	S
33	K-33	R	R	R	R	S	S	S	S	R	S	S	S	S	S	S
34	K-34	R	S	S	R	S	S	S	S	S	S	S	S	S	S	S
35	K-35	R	S	S	R	R	S	S	S	S	S	S	S	S	S	S
36	K-36	R	S	S	S	S	S	S	S	S	S	S	S	S	S	S
37	K-37	R	S	R	S	S	S	S	S	S	S	S	S	S	S	S
38	K-38	R	S	S	S	S	S	S	S	S	S	S	S	S	S	S
39	K-39	R	S	R	S	S	S	S	S	S	S	S	S	S	S	S
40	K-40	S	S	S	S	S	S	S	S	S	S	S	S	S	S	S
S.No	**Strain**	**3**	**5**	**6**	**8**	**9/10**	**12**	**14**	**18**	**22**	**Lv**	**Cp**	**PTZ**	**27**	**Erta**	**Me**
41	K-41	R	S	S	S	S	S	S	S	S	S	S	S	S	S	S
42	K-42	R	S	S	S	S	S	S	S	S	S	S	S	S	S	S
43	K-43	R	S	R	R	S	S	S	S	S	S	S	S	S	S	S
44	K-44	R	S	S	S	S	S	S	S	S	S	S	S	S	S	S
45	K-45	R	S	S	S	S	S	S	S	S	S	S	S	S	S	S
46	K-46	R	S	R	S	S	S	S	S	S	S	S	S	S	S	S
47	K-47	R	S	S	S	S	S	S	S	S	S	S	S	S	S	S
48	K-48	R	S	S	S	S	S	S	S	S	S	S	S	S	S	S
49	K-49	R	S	R	R	S	S	S	S	S	S	S	S	S	S	S
50	K-50	R	R	S	S	S	S	S	S	S	S	S	S	S	S	S
51	K-51	R	S	S	S	S	S	S	S	S	S	S	R	S	S	S
52	K-52	R	S	S	S	S	S	S	S	S	S	S	S	S	S	S
53	K-53	R	S	S	S	S	S	S	S	S	S	S	S	S	S	S
54	K-54	S	S	R	S	S	S	S	S	R	S	S	S	S	S	S
55	K-55	R	S	S	S	S	S	S	S	S	S	S	R	S	S	S
56	K-56	R	S	S	S	S	S	S	S	S	S	S	S	S	S	S
57	K-57	R	S	S	S	S	S	S	S	S	S	S	S	S	S	S
58	K-58	R	S	R	R	R	S	S	S	R	S	S	S	S	S	S

59	K-59	R	S	S	S	S	S	S	S	R	R	S	S	S	S	S
60	K-60	R	S	S	S	S	S	S	S	S	S	S	S	S	S	S
61	K-61	R	S	S	S	S	S	S	S	S	S	S	S	S	S	S
62	K-62	R	S	S	S	S	S	S	S	S	S	S	S	S	S	S
63	K-63	R	S	S	S	S	S	S	S	S	S	S	S	S	S	S
64	K-64	R	S	R	R	R	S	S	S	S	S	R	S	S	S	S
65	K-65	R	R	R	R	R	S	S	R	S	R	S	R	S	S	S
66	K-66	R	S	S	S	S	S	S	S	S	S	S	S	S	S	S
67	K-67	R	S	S	S	S	S	S	S	S	S	S	S	S	S	S
68	K-68	R	S	S	S	S	S	S	S	S	S	S	S	S	S	S
69	K-69	R	S	S	S	S	S	S	S	S	S	S	S	S	S	S
70	K-70	R	S	R	R	R	S	S	S	R	S	S	S	S	S	S
71	K-71	R	S	R	R	S	S	S	S	S	R	S	S	S	S	S
72	K-72	R	S	R	S	S	S	S	S	S	S	S	S	S	S	S
73	K-73	R	S	R	R	R	S	S	S	S	S	S	S	S	S	S
74	K-74	R	S	R	R	R	S	S	S	R	S	R	R	S	R	S
75	K-75	R	S	S	S	S	S	S	S	S	S	R	S	S	S	S
76	K-76	R	S	S	S	S	S	S	S	S	S	S	S	S	S	S
77	K-77	R	S	R	R	R	R	S	R	R	S	R	S	S	S	S
78	K-78	R	S	S	S	S	S	S	S	S	S	S	S	S	S	S
79	K-79	S	R	S	S	R	S	S	S	S	S	S	S	S	S	S
80	K-80	R	S	S	S	S	S	S	S	S	S	S	S	S	S	S
81	K-81	R	S	S	S	S	S	S	S	S	S	S	S	S	S	S
82	K-82	R	S	R	S	R	S	S	S	R	S	R	S	S	S	S
83	K-83	R	S	R	R	R	S	S	S	R	S	R	R	S	S	S
84	K-84	R	S	R	R	R	S	S	R	R	S	R	R	S	S	S
85	K-85	R	S	R	S	R	S	S	S	S	S	S	R	S	S	S
86	K-86	R	S	R	R	R	S	S	S	R	S	S	S	S	S	S
S.No	**Strain**	**3**	**5**	**6**	**8**	**9/10**	**12**	**14**	**18**	**22**	**Lv**	**Cp**	**PTZ**	**27**	**Erta**	**Me**
87	K-87	R	S	S	S	S	S	S	S	S	S	S	S	S	S	S
88	K-88	R	S	S	S	S	S	S	R	R	S	R	R	S	S	S
89	K-89	R	S	S	S	S	S	S	S	S	S	S	S	S	S	S
90	K-90	R	S	S	S	S	S	S	S	S	S	S	S	S	S	S
91	K-91	R	S	R	R	R	R	R	R	R	R	R	R	S	S	S
92	K-92	R	S	S	S	S	S	S	S	S	S	S	S	S	S	S
93	K-93	R	S	S	S	S	S	S	S	S	S	R	S	S	S	S
94	K-94	R	S	R	R	R	S	S	S	R	S	R	S	S	S	S
95	K-95	S	S	R	S	S	S	S	S	S	S	S	S	S	S	S
96	K-96	R	R	R	R	R	S	S	S	S	S	R	S	S	S	S
97	K-97	R	S	S	S	S	R	R	R	R	S	R	S	S	S	S
98	K-98	S	S	S	S	S	S	S	S	S	S	S	S	S	S	S
99	K-99	R	S	R	R	R	S	S	S	S	S	S	S	S	S	S
100	K-100	R	S	S	S	S	S	S	S	S	S	S	S	S	S	S

K-1 to K-100 = *Klebsiella pneumoniae* isolates, 3= Ampicillin (10 µg), 5= Amoxicillin (20 µg)+Clavulanic Acid (10 µg), 6= Cefazolin/Cephalexin (30 µg), 8 = Cefuroxime (30 µg), 9/10 = Cefotaxime/Ceftiaxone (30µg) 12 = Gentamicin (10 µg), 14 = Amikacin (30 µg), 18 = Ciprofloxacin (5µg), 22 = Trimethoprim (1.25 µg) +

Sulfamethoxazole (23.75 µg), Lv = Levofloxacin (5 µg), Cp = Cefpirome/Cefepime (30 µg), PTZ=

27 = Imipenem (10 µg), Erta = Ertapenem (10 µg), Me = Meropenem (10 µg)

Figure 1: A representative plate showing antibiotic sensitivity pattern of an environmental isolate of *Klebsiella pneumoniae*

Objective 2:

Isolation, characterization and purification of Bacteriophages against pathogenic bacteria of clinical origin

2.1 Isolation of bacterial pathogens (*Klebsiella pneumoniae*) of clinical origin: The samples, including stool, pus, blood, urine etc., were obtained from OPD, indoor wards and ICU of Institute of Medical Sciences BHU, Varanasi to isolate clinical bacterial pathogens. The samples were processed for bacterial isolation as per standard guidelines. Initially, samples were cultured in a suitable medium; biochemical tests confirmed the obtained pure culture.

2.2: Antimicrobial Susceptibility of clinical strains of *Klebsiella pneumoniae*: Antimicrobial susceptibility was performed for 100 clinical isolates using Mueller Hinton Agar by the Kirby-Bauer disc diffusion method following the standard procedure as per clinical and Laboratory Standards Institute(CLSI) guidelines. The antibiotics used for isolates are listed in table 2.

2.3 Isolation and characterization of *Klebsiella pneumoniae* specific Bacteriophages:

2.3a Water sample collection and bacteriophage isolation: Many water samples have been collected (Table 2) and processed for bacteriophage isolation. In brief, the water samples were treated with 1% chloroform (v/v) for 10 min, followed by centrifugation at 10,000 rpm for 10 min. The supernatant was dropped on MHA plates having bacterial lawn (log phase) and incubated overnight at 37° C. Next day, plates were harvested in TMG, and the suspension was treated with 1% chloroform (v/v) with shaking for 15 min, centrifuged thrice and the supernatant was tested for the presence of bacteriophage by spot assay as well as plaque assay by soft agar overlay method. Phage plaques were differentiated based on plaque morphology. Single Plaque was further processed for the high count.

Table 1. Detail of water sample collection site for bacteriophage isolation

Serial No.	Sampling site	Date of sampling
1.	Ganga water- Assi ghat	15.05. 2018
2.	Ganga water NMCG old	14 .03.2017
3.	N CG old	14 .03. 2017
4.	Umang pharmacy	19 .05.2018
5.	Assi	15 .052018
6.	Narad	15 .05.2018
7.	Harishchandra	15 .05.2018
8.	Prahalad	15 .05.2018
9.	Harishchandra	15 .05.2018
10.	Prahalad	01.06.2018
11.	Jain	01.06.2018
12.	Umang BHU main tank	09.05.2018

13.	Assi	01.05.2018
14.	Pedia BHU	09.05.2018
15.	Sunbeam Lahartara	09.05.2018
16.	Umang pharmecy	09.05.2018
17.	Maduwadih sabji mandi	09.09.2018
18.	Sankat Mochan	09.05.2018
19.	Bhagwanpur	06.10.2018
20.	BHU Gausala 1st	20.10.2018
21.	BHU Gausala 2nd	20.10.2018
22.	Assi nala sundrpur	27.10.2018
23.	Aaditya Nagar	23.10.2018

2.3b Bacteriophage lytic activity determination: Many bacteriophages isolated from Ganga water collected from 10 different Ghats at Varanasi were tested for their lytic activity on their respective bacterial clinical isolate. To observe the lytic activity of bacteriophages, in brief, bacterial suspension of 2.0 OD was plated on Mueller Hinton Agar (MHA) plate and incubated at 37°C for 2 hours. The phages in 10 µl volume were dropped on the bacterial lawn and incubated overnight to observe the lytic activity.

2.3 c Broad spectrum activity of bacteriophages against clinical isolates of *Klebsiella pneumoniae*: Broad-spectrum activity of bacteriophages estimated against 70 clinical isolates of *Klebsiella pneumoniae* by spot assay.

2.3 Clinical isolates of *Klebsiella pneumoniae* and their antibiotic sensitivity pattern: A total of 101 positive samples were obtained from different wards and ICU of IMS, BHU from April 2018 to June 2019. Their resistance pattern is presented in table 6.

RESULTS:

Table 2: Showing the antibiotic sensitivity pattern of clinical isolates of *Klebsiella pneumoniae*

S.No	Strain	3	5	6	8	9/10	12	14	18	22	Lv	Cp	PTZ	27	Erta	Me

1.	K1	R	R	R	R	R	R	R	R	R	R	R	R	S	R	R
2.	K2	R	R	R	R	R	S	R	R	R	R	R	R	R	R	R
3.	K3	R	R	R	R	R	S	R	R	R	R	R	R	R	R	R
4.	K4	R	R	R	R	R	S	R	R	S	R	R	R	R	R	R
5.	K5	R	R	R	S	S	R	R	R	R	R	S	R	S	R	R
6.	K6	R	R	R	R	R	R	R	R	R	R	R	R	S	R	R
7.	K7	R	R	R	R	R	R	R	R	R	R	R	R	S	R	R
8.	K8	R	R	R	S	S	R	S	S	S	R	R	R	R	R	R
9.	K9	R	R	R	R	R	R	R	R	R	R	R	R	S	R	R
10.	K10	R	R	R	R	R	R	R	R	R	R	R	R	S	R	R
11.	K11	R	R	R	R	R	R	R	R	R	R	R	R	S	R	R
12.	K12	R	R	R	R	R	R	R	R	R	R	R	R	S	R	R
13.	K13	R	R	R	R	R	R	R	R	S	S	R	R	S	R	S
14.	K14	R	R	R	R	R	R	R	R	R	R	R	R	R	R	R
15.	K15	R	R	R	R	R	R	R	R	R	R	R	R	R	R	R
16.	K16	R	R	R	R	R	R	R	R	R	R	R	S	S	S	S
17.	K17	R	R	R	R	R	R	R	R	R	R	R	S	S	S	S
18.	K18	R	R	S	R	R	S	R	R	S	R	R	R	R	R	R
19.	K19	R	R	S	R	R	S	S	S	R	R	S	S	S	S	S
20.	K20	R	R	S	R	R	S	R	R	S	R	R	R	R	R	R
21.	K21	R	R	R	R	R	R	R	R	R	R	R	S	S	S	S
22.	K22	R	R	R	R	R	R	R	R	R	S	R	R	S	R	R
23.	K23	R	R	R	R	R	R	R	R	R	S	R	R	S	R	R
24.	K24	R	R	R	R	S	R	R	R	R	R	S	R	S	R	R
25.	K25	R	R	R	R	R	R	R	R	R	R	R	R	R	R	R
26.	K26	R	R	R	R	R	R	R	R	R	R	R	S	S	R	S
27.	K27	R	S	S	S	R	S	R	R	S	S	R	R	R	R	R
28.	K28	R	R	R	R	R	R	R	R	R	R	R	R	S	R	R
29.	K29	R	R	R	R	R	R	R	R	R	R	R	R	R	R	R
30.	K30	R	R	R	R	R	R	R	R	R	R	S	S	S	R	S
31.	K31	R	R	R	R	R	R	R	R	R	R	R	R	R	R	R
32.	K32	R	R	R	R	R	R	S	S	R	S	S	S	S	S	S
33.	K33	R	R	R	R	S	R	R	R	R	R	S	R	S	R	R
34.	K34	R	R	R	R	R	R	R	R	R	R	R	R	S	R	R
35.	K35	R	R	S	R	R	S	R	S	S	S	R	R	R	R	R
36.	K36	R	R	S	R	R	S	R	R	S	R	R	R	R	R	R
37.	K37	R	R	R	R	R	R	R	R	R	R	R	R	S	R	R
38.	K38	R	R	R	R	R	R	R	R	R	R	R	R	S	R	R
39.	K39	R	R	R	R	R	S	R	R	R	R	R	R	R	R	R
40.	K40	R	R	R	R	R	S	R	R	S	R	R	R	R	R	R
41.	K41	R	R	R	R	R	R	R	R	R	R	R	R	R	R	R
42.	K42	R	R	R	R	R	S	S	R	R	R	R	R	S	R	R
43.	K43	R	R	R	R	R	S	S	R	R	R	R	S	R	S	S
44.	K44	R	R	R	R	R	R	R	R	R	R	R	R	S	R	R
45.	K45	R	R	R	R	R	R	R	R	R	R	R	R	S	R	R
46.	K46	R	R	R	R	R	R	R	R	R	R	R	R	S	R	R
47.	K47	R	R	R	R	R	R	R	R	R	R	R	R	R	R	R
48.	K48	R	S	S	S	S	S	S	S	S	S	S	S	S	S	S
49.	K49	R	R	R	R	R	S	R	R	R	R	R	R	R	R	R
50.	K50	R	R	R	R	R	S	R	R	R	R	R	R	R	R	R
51.	K51	R	R	S	R	R	S	R	R	S	R	R	R	R	R	R
52.	K52	R	R	R	R	R	S	S	S	R	S	S	S	S	R	S
53.	K53	R	R	R	R	R	S	R	R	R	R	R	R	R	R	R

54.	K54	R	R	R	R	R	R	R	R	R	R	R	R	R	R	R
55.	K55	R	R	R	R	R	R	R	R	R	R	R	R	S	R	R
56.	K56	R	R	R	R	R	R	S	R	R	R	S	S	S	R	S
57.	K57	R	R	R	R	R	R	R	R	R	R	R	R	R	R	R
58.	K58	R	R	R	R	R	R	R	R	R	R	R	R	S	R	R
59.	K59	R	R	R	R	R	R	R	R	S	R	R	R	S	R	R
60.	K60	R	R	R	R	R	R	R	R	R	R	R	R	S	R	R
61.	K61	R	R	R	R	R	R	R	R	R	R	R	R	S	R	R
62.	K62	R	R	S	R	R	S	R	R	S	R	R	R	R	R	R
63.	K63	R	R	R	R	R	S	R	R	S	R	R	R	R	R	R
64.	K64	R	R	S	R	R	S	R	R	R	R	R	R	R	R	R
65.	K65	R	R	R	R	R	R	R	R	R	R	R	R	R	R	R
66.	K66	R	R	R	R	R	R	R	R	R	R	R	R	S	R	R
67.	K67	R	R	R	R	R	R	R	R	R	R	R	R	S	R	R
68.	K68	R	R	R	R	R	R	R	R	R	R	R	R	S	R	R
69.	K69	R	R	R	R	R	R	R	R	R	R	R	R	R	R	R
70.	K70	R	R	R	R	R	R	R	R	R	R	R	R	S	R	R
71.	K71	R	R	R	R	R	R	R	R	R	R	R	R	S	R	R
72.	K72	R	R	R	R	R	S	R	R	R	R	R	R	R	R	R
73.	K73	R	R	R	R	R	R	R	R	R	R	R	R	S	R	R
74.	K74	R	R	R	R	R	R	R	R	R	R	R	R	S	R	R
75.	K75	R	R	R	R	R	R	R	R	R	R	R	R	S	R	R
76.	K76	R	R	R	R	R	R	R	R	R	R	R	R	R	R	R
77.	K77	R	S	R	R	R	S	S	S	R	S	S	S	S	S	S
78.	K78	R	S	S	S	S	S	S	S	R	S	S	S	S	S	S
79.	K79	R	R	R	R	R	R	R	R	R	R	R	R	S	R	R
80.	K80	R	R	S	R	S	S	S	R	R	R	S	S	S	S	S
81.	K81	R	R	R	R	R	R	R	R	R	R	R	R	S	R	R
82.	K82	R	R	S	R	S	S	S	R	R	R	S	S	S	S	S
83.	K83	R	R	R	R	R	R	R	R	R	R	R	R	S	R	R
84.	K84	R	R	R	R	R	R	R	R	R	R	R	R	S	R	R
85.	K85	R	R	R	R	R	R	R	R	R	R	R	R	S	R	R
86.	K86	R	R	R	R	R	R	R	R	R	R	R	R	S	R	R
87.	K87	R	R	R	R	R	R	R	R	R	R	R	R	S	R	R
88.	K88	R	R	R	R	R	R	R	R	R	R	R	R	R	R	R
89.	K89	R	R	R	R	R	R	R	R	R	R	R	R	R	R	R
90.	K90	R	R	R	R	R	R	R	R	R	R	R	R	S	R	R
91.	K91	R	R	R	R	R	R	R	R	R	R	R	R	S	R	R
92.	K92	R	R	S	R	S	S	S	R	R	R	S	S	S	S	S
93.	K93	R	R	R	R	R	R	R	R	R	R	R	R	R	R	R
94.	K94	R	R	R	R	R	S	R	R	R	R	R	R	R	R	R
95.	K95	R	R	R	R	R	R	R	R	R	R	R	R	S	R	R
96.	K96	R	R	R	R	R	R	R	R	R	R	R	R	S	R	R
97.	K97	R	R	R	R	R	R	R	R	R	R	R	R	S	R	R
98.	K98	R	S	S	S	R	S	R	S	S	S	S	S	S	S	S
99.	K99	R	R	R	R	R	R	R	R	S	R	R	R	R	R	R
100.	K100	R	R	R	R	R	R	R	R	S	R	R	R	R	R	R
101.	K101	R	R	R	R	R	R	R	R	R	R	R	R	R	R	R

K.p 1to K.p 101 = *Klebsiella pneumoniae* isolates, abbreviations for antibiotics are given below table 5.

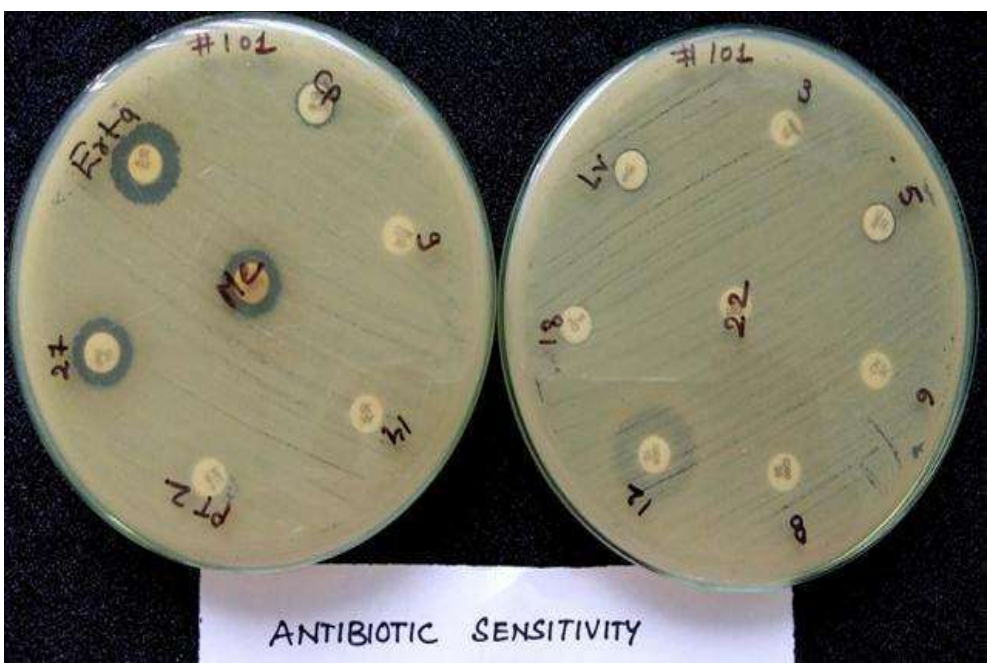

Figure 1: A representative plate showing antibiotic sensitivity pattern of clinical isolate of *Klebsiella pneumoniae*

(A)

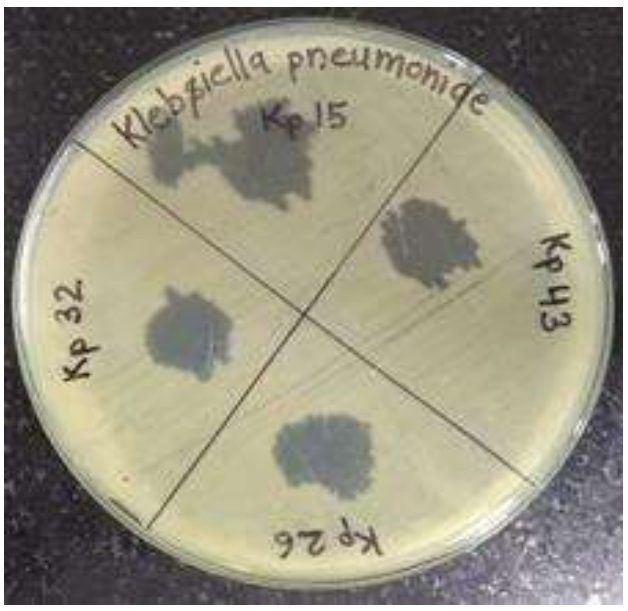

(B)

Figure 3: Representative pictures of MHA plate showing (A) Broad spectrum lytic activity of bacteriophages; Kp1- Kp50 and there is no lytic activity in Kp17 and Kp18 on *K. pneumoniae* (B) Activity of bacteriophages;Kp15,K43,K32 and Kp26 on *K. Pneumoniae.*

Table 3. Bacteriophage lytic activity against 70 clinical isolates of *Klebsiella pneumoniae*

	Bacterial Isolates →	K 1	K2	K 3	K4	K5	K6	K7	K8	K9	K10	K11	K12	K13	K14	K15	K16	K17
SN	**Phage isolates**																	
1.	Kp A1	–	–	+	+	–	+	+	+	–	–	+	–	+	+	–	+	+
2.	Kp A2	+	–	+	+	–	+	+	+	–	–	+	–	+	+	–	+	+
3.	Kp A3	+	–	+	+	–	+	+	+	–	–	+	–	+	+	–	+	+
4.	Kp A4	+	–	+	+	+	+	+	+	–	–	+	–	+	+	–	+	+
5.	Kp A5	–	–	+	+	+	+	+	+	–	–	–	–	+	+	–	+	+
6.	Kp A6	+	–	+	+	+	+	+	+	–	–	–	–	+	+	–	–	+
7.	Kp A7	+	–	–	+	+	+	+	+	–	–	–	–	+	+	–	+	+
8.	Kp A8	+	–	–	+	+	+	+	+	+	–	–	–	+	+	–	+	+
9.	Kp A9	+	–	+	+	+	+	+	+	+	–	+	–	+	+	–	+	+
10.	Kp A10	+	–	+	+	+	+	+	+	+	–	+	–	+	–	–	+	–
11.	Kp A11	–	–	+	–	+	+	+	+	+	–	–	–	+	–	–	–	–
12.	Kp A12	+	–	+	+	+	+	+	+	+	–	+	+	+	–	–	–	+
13.	Kp A13	+	–	+	+	+	+	+	+	+	–	+	+	+	–	–	+	+
14.	Kp A14	+	–	+	+	–	+	+	+	+	–	+	–	+	–	–	+	+
15.	Kp A15	+	–	–	–	+	+	+	+	+	–	–	–	+	–	–	+	+
16.	Kp A16	+	–	+	+	+	+	+	+	+	–	+	+	+	–	–	+	+
17.	Kp A17	+	–	–	+	+	+	+	+	+	–	–	+	+	–	–	+	+
18.	Kp A18	+	+	+	+	+	+	+	+	+	–	+	+	+	–	–	+	+
19.	Kp A19	+	–	+	+	+	+	+	+	+	–	+	–	+	–	–	+	+
20.	Kp A20	+	–	+	+	+	+	+	+	+	–	+	–	+	–	–	+	–
21.	Kp A21	+	–	+	+	+	+	+	+	+	–	+	–	+	–	–	–	+
22.	Kp A22	+	–	+	+	–	+	+	+	+	–	–	–	+	–	+	–	+
23.	Kp A23	–	+	+	+	–	+	+	+	+	+	+	+	+	–	+	+	+
24.	Kp A24	–	+	–	+	–	+	+	+	+	+	+	–	+	–	+	+	+
25.	Kp A25	–	+	+	+	+	+	+	–	+	–	–	–	–	–	–	+	+
26.	Kp A26	–	+	+	+	+	–	–	+	+	+	+	–	+	–	-	+	+
27.	Kp A27	+	+	+	+	+	+	+	+	+	+	+	+	+	–	–	–	–
28.	Kp A28	+	–	+	+	+	+	+	+	+	–	+	–	+	–	–	–	+
29.	Kp A39	+	–	+	+	+	+	+	+	+	–	+	–	+	–	–	+	+
30.	Kp A30	+	–	+	+	+	+	+	+	+	–	+	–	+	–	+	+	+
31.	Kp A31	+	–	+	+	+	+	+	+	+	–	+	–	+	–	+	+	–
32.	Kp A32	–	–	+	–	+	+	+	+	+	–	+	–	+	–	+	+	–
33.	Kp A33	+	–	+	+	+	+	+	+	+	–	–	–	+	–	+	+	+
34.	Kp A34	+	+	+	+	+	+	+	+	+	+	+	–	+	–	+	+	–
35.	Kp A35	+	–	+	+	+	+	+	+	+	–	+	–	+	–	–	+	–
36.	Kp A36	+	+	+	+	+	+	+	+	+	–	–	–	+	–	+	+	–
37.	Kp A37	+	+	+	+	+	+	+	+	+	–	+	–	+	–	+	–	–

38.	Kp A38	+	+	+	+	+	+	+	+	+	+	_	_	+	_	+	_	_
39.	Kp A39	+	+	+	+	+	+	+	+	+	_	_	_	+	_	+	+	_
40.	Kp A40	+	+	+	+	+	+	+	+	+	_	_	_	+	_	+	+	_
41.	Kp A41	+	+	+	+	+	+	+	+	+	+	+	_	+	_	+	+	_
42	Kp A42	+	+	+	+	_	+	_	+	+	_	_	_	+	_	_	+	_
43.	Kp A43	+	_	+	+	+	+	+	+	+	+	_	_	+	_	+	+	_
44.	Kp A44	+	_	+	+	+	+	+	+	+	_	+	_	+	_	+	+	+
45.	Kp A45	+	_	+	+	+	+	+	+	+	_	_	_	+	_	+	+	_
46.	Kp A46	+	_	+	+	+	+	+	+	+	_	+	_	+	_	+	+	_
47.	Kp A47	+	+	+	+	+	+	+	+	+	+	+	+	+	_	+	+	+
48.	Kp A48	+	+	+	+	_	+	+	+	+	_	+	_	+	_	+	+	_
49.	Kp A49	+	+	+	+	_	+	+	+	+	_	+	+	+	_	+	+	_
50.	Kp A50	_	+	_	_	_	+	_	+	+	_	_	_	+	_	+	+	_

S.N.	**Bacterial Isolates →**	K 18	K 19	K 20	K 21	K 22	K 23	K 24	K 25	K 26	K 27	K 28	K 29	K 30	K 31	K 32	K 33	K 34
	Phage Isolates↓																	
1.	Kp A1	_	+	+	+	+	+	+	+	_	_	+	_	+	_	+	_	_
2.	Kp A2	_	+	+	+	+	+	+	+	_	_	+	_	+	_	+	+	_
3.	Kp A3	_	+	+	+	+	+	+	+	_	_	_	_	+	_	+	+	_
4.	Kp A4	_	+	+	+	+	_	_	+	_	+	+	+	+	_	+	+	_
5.	Kp A5	_	_	+	+	+	+	_	+	_	_	_	_	+	_	+	+	_
6.	Kp A6	_	_	+	_	+	+	_	+	_	_	_	_	+	_	+	_	_
7.	Kp A7	_	+	+	+	+	+	+	+	+	_	+	_	+	_	+	+	+
8.	Kp A8	_	+	+	+	+	+	_	+	+	_	_	_	+	_	+	+	+
9.	Kp A9	_	+	+	+	+	+	+	+	_	_	+	_	+	_	+	+	+
10.	Kp A10	_	_	+	_	+	_	_	+	_	_	_	_	+	_	+	_	+
11.	Kp A11	_	+	+	_	+	+	_	+	_	_	_	_	+	_	+	_	+
12.	Kp A12	_	+	+	_	+	+	+	+	+	_	_	_	+	_	+	_	_
13.	Kp A13	_	+	+	+	+	_	+	+	_	_	+	_	+	_	+	_	+
14.	Kp A14	_	+	+	+	+	+	+	+	+	_	_	_	+	_	+	+	+
15.	Kp A15	_	_	+	+	+	+	+	+	_	_	+	_	+	_	+	+	+
16.	Kp A16	_	_	+	+	+	_	+	+	_	_	+	_	+	_	+	_	+
17.	Kp A17	_	+	+	+	_	+	_	+	+	+	_	+	_	_	+	_	_
18.	Kp A18	_	+	+	+	_	+	+	+	+	+	+	+	+	_	+	_	_
19.	Kp A19	_	_	+	+	+	+	_	+	+	_	+	_	+	_	_	_	+
20.	Kp A20	_	+	+	+	+	_	_	+	+	+	+	_	+	_	+	_	+
21.	Kp A21	_	+	+	+	+	_	+	+	+	_	+	_	+	_	+	_	_
22.	Kp A22	_	+	+	+	+	_	_	+	_	_	_	_	+	_	+	_	_
23.	Kp A23	_	_	+	+	+	_	_	+	_	_	_	_	+	_	_	_	+
24.	Kp A24	_	_	_	+	+	_	+	+	_	_	_	_	+	_	_	_	+
25.	Kp A25	_	_	+	_	+	_	+	_	+	_	_	_	_	_	+	_	+

26.	Kp A26	_	_	+	_	+	_	+	+	+	_	_	_	+	_	+	_	+
27.	Kp A27	_	+	+	+	+	_	_	+	+	_	_	_	+	_	_	_	+
28.	Kp A28	_	+	+	+	+	_	_	+	+	_	+	_	+	_	+	_	+
29.	Kp A39	_	+	+	+	+	_	_	+	_	_	_	_	+	_	+	_	+
30.	Kp A30	_	+	+	+	+	_	_	+	_	_	_	_	+	_	_	_	+
31.	Kp A31	_	+	+	+	+	_	_	+	_	_	_	_	+	_	_	+	+
32.	Kp A32	_	+	+	+	+	_	_	+	_	+	_	_	+	_	_	_	+
33.	Kp A33	_	+	+	_	+	_	+	+	_	+	_	_	+	_	_	_	+
34.	Kp A34	_	_	+	+	+	_	_	+	+	_	_	_	+	_	+	_	+
35.	Kp A35	_	+	+	+	+	_	_	+	+	+	_	_	+	_	+	_	+
36.	Kp A36	_	+	+	+	+	_	_	+	_	_	_	_	+	_	_	_	+
37.	Kp A37	_	+	+	+	+	_	+	+	_	+	+	_	+	_	_	_	+
38.	Kp A38	_	+	+	+	+	_	_	+	_	+	+	_	+	_	_	_	+
39.	Kp A39	_	_	+	+	+	_	_	+	_	_	_	_	+	_	_	_	+
40.	Kp A40	_	+	+	+	+	_	_	+	+	_	_	_	+	_	_	+	+
41.	Kp A41	_	+	+	+	+	_	+	+	_	_	+	_	+	_	_	_	+
42	Kp A42	_	_	_	+	+	_	+	+	+	_	_	_	+	_	_	_	+
43.	Kp A43	_	_	+	+	+	_	_	+	+	_	_	_	+	_	_	_	+
44.	Kp A44	_	_	_	+	+	_	_	+	+	_	_	_	+	_	_	_	+
45.	Kp A45	_	_	_	+	+	_	+	+	_	_	_	_	+	_	_	_	+
46.	Kp A46	_	+	_	+	+	_	+	+	_	_	_	_	+	_	_	_	+
47.	Kp A47	_	_	_	+	+	_	_	+	_	+	_	_	+	_	_	_	+
48.	Kp A48	_	_	+	+	+	_	_	+	+	_	+	_	+	_	_	_	+
49.	Kp A49	_	_	_	+	+	_	_	+	_	_	_	_	+	_	_	_	+
50.	Kp A50	_	_	_	+	+	_	_	+	_	_	_	_	_	_	_	_	+

S.N.	**Bacterial Isolates →**	K 35	K 36	K 37	K 38	K 39	K 40	K 41	K 42	K 43	K 44	K 45	K 46	K 47	K 48	K 49	K 50	K 51
	Phage Isolates↓																	
1.	Kp A1	_	+	_	+	+	+	+	+	_	+	+	_	+	_	_	_	_
2.	Kp A2	_	_	_	+	+	+	+	+	_	+	+	_	+	+	+	+	+
3.	Kp A3	_	_	_	+	+	+	+	+	_	+	+	+	+	+	+	_	_
4.	Kp A4	_	_	_	+	+	+	+	+	_	+	+	+	+	+	+	+	+
5.	Kp A5	_	_	_	+	+	+	+	_	_	+	_	+	_	+	+	_	+
6.	Kp A6	_	_	_	_	+	+	+	_	_	+	+	+	+	_	+	_	_
7.	Kp A7	_	_	+	+	+	+	+	_	+	+	+	+	+	+	+	_	+
8.	Kp A8	_	_	_	+	+	+	+	_	_	+	_	+	_	+	+	_	+
9.	Kp A9	+	_	_	+	+	+	+	_	_	+	_	+	_	+	+	_	+
10.	Kp A10	_	+	+	+	+	+	+	_	_	+	+	+	+	+	+	+	+
11.	Kp A11	+	+	_	+	+	+	+	_	_	+	+	+	_	+	+	+	+
12.	Kp A12	+	_	+	+	+	+	+	+	+	+	+	+	_	+	+	+	+
13.	Kp A13	+	_	_	+	+	+	+	_	+	+	+	+	+	+	+	+	+

14.	Kp A14	+	+	+	+	_	+	+	_	+	+	+	+	+	+	+	+	+
15.	Kp A15	+	+	+	+	_	+	+	+	+	+	+	+	+	+	+	+	+
16.	Kp A16	+	_	_	+	_	+	+	_	+	_	+	_	+	+	+	+	+
17.	Kp A17	+	_	_	+	_	+	+	_	_	+	+	_	+	+	+	+	+
18.	Kp A18	+	+	_	+	+	+	+	+	+	+	+	+	+	+	+	+	+
19.	Kp A19	_	+	+	+	_	+	+	_	+	+	+	+	+	+	+	+	+
20.	**Kp A20**	+	+	_	+	+	_	_	_	+	+	+	_	_	+	_	+	+
21.	**Kp A21**	+	+	_	+	+	_	_	_	_	+	+	_	+	+	+	+	+
22.	**Kp A22**	+	_	_	+	+	_	_	_	+	+	+	_	_	_	_	+	+
23.	**Kp A23**	+	+	+	+	+	+	+	_	+	+	+	_	_	+	_	+	+
24.	**Kp A24**	+	+	_	+	_	_	_	_	+	+	+	_	+	+	+	+	+
25.	**Kp A25**	+	+	_	+	_	_	_	_	+	+	+	_	_	+	+	_	+
26.	**Kp A26**	_	+	_	+	+	_	_	_	+	+	+	_	+	+	+	+	+
27.	**Kp A27**	+	_	_	+	+	_	_	_	+	+	+	_	_	+	+	+	+
28.	**Kp A28**	+	+	_	+	+	_	_	_	+	+	+	_	+	+	+	+	+
29.	**Kp A39**	+	+	+	+	+	_	_	_	+	+	+	_	+	+	+	+	+
30.	**Kp A30**	+	+	+	+	+	+	_	_	+	+	+	_	+	+	+	+	+
31.	**Kp A31**	+	+	_	+	+	+	_	_	+	+	+	_	+	+	+	+	+
32.	**Kp A32**	+	+	_	+	_	+	_	_	+	+	+	_	+	+	_	_	+
33.	**Kp A33**	+	+	_	+	_	_	_	_	+	+	+	_	+	+	+	+	+
34.	**Kp A34**	+	+	_	+	_	_	_	_	+	+	+	_	+	+	+	+	+
35.	**Kp A35**	+	+	_	+	+	_	_	_	+	+	+	_	+	+	+	+	+
36.	**Kp A36**	+	+	_	+	+	+	_	_	+	+	+	_	+	+	+	+	+
37	**Kp A37**	_	+	_	+	+	+	_	_	+	+	+	_	+	+	+	+	+
38	**Kp A38**	_	+	+	+	_	+	_	_	+	+	+	_	_	+	+	+	+
39	**Kp A39**	+	+	+	+	_	+	_	_	+	+	+	_	+	+	+	+	+
40	**Kp A40**	+	+	_	+	_	+	_	_	+	+	+	_	_	+	+	+	+
41.	**Kp A41**	+	+	+	+	_	+	_	_	+	+	+	_	+	+	+	+	+
42	**Kp A42**	+	+	_	+	_	+	_	_	+	+	+	_	+	+	+	+	+
43.	**Kp A43**	+	+	_	+	_	+	_	_	+	+	+	_	+	_	+	_	_
44.	**Kp A44**	+	+	_	+	_	+	_	_	+	+	_	_	_	+	+	+	+
45.	**Kp A45**	+	+	+	+	_	+	_	_	+	+	+	_	+	+	+	+	+
46.	**Kp A46**	+	+	+	+	_	+	_	_	+	+	+	_	+	+	+	+	+
47.	**Kp A47**	+	+	+	+	_	+	_	_	+	+	+	_	_	+	+	+	+
48.	**Kp A48**	+	+	+	+	_	+	+	_	+	+	+	_	_	+	+	+	+
49.	**Kp A49**	+	+	+	+	_	+	_	_	+	+	+	_	+	+	+	+	+
50.	**Kp A50**	+	+	+	+	_	+	_	_	+	+	+	_	+	+	+	+	+

S.N.	**Bacterial Isolate→**	K 52	K 53	K 54	K 55	K 56	K 57	K 58	K 59	K 60	K 61	K 62	K 63	K 64	K 65	K 66	K 67	K 68
	Phage Isolates↓																	
1.	Kp A1	_	_	_	_	+	_	+	_	_	_	_	_	_	_	+	+	+
2.	Kp A2	+	+	+	+	+	+	+	_	+	+	+	_	+	+	+	+	+

3.	Kp A3	+	+	_	+	+	+	+	+	_	+	_	_	_	+	+	+	+
4.	Kp A4	+	+	+	+	+	+	+	+	+	+	+	+	_	+	+	+	+
5.	Kp A5	_	+	+	+	+	+	_	+	+	+	+	+	_	+	+	+	+
6.	Kp A6	+	+	+	+	+	+	_	+	_	+	+	+	_	+	+	+	+
7.	Kp A7	_	_	+	+	+	+	_	+	+	+	_	+	+	+	+	+	+
8.	Kp A8	+	+	+	+	+	+	_	+	+	+	_	_	_	+	+	+	+
9.	Kp A9	+	_	_	+	+	+	_	+	+	+	_	_	_	+	+	+	+
10.	Kp A10	+	_	_	+	+	+	_	+	+	+	_	+	_	+	+	+	+
11.	Kp A11	_	_	+	+	+	+	+	+	+	+	_	+	_	+	+	+	+
12.	Kp A12	_	_	+	+	+	+	+	+	+	+	_	+	_	+	+	+	+
13.	Kp A13	+	_	+	+	+	+	+	+	+	+	_	+	_	+	+	+	+
14.	Kp A14	+	_	+	+	+	+	+	+	+	+	_	+	+	+	+	+	+
15.	Kp A15	+	_	+	+	+	+	+	+	+	+	_	+	+	+	+	+	+
16.	Kp A16	_	_	+	+	+	+	+	+	+	+	_	+	_	+	+	+	+
17.	Kp A17	_	_	_	_	+	+	+	_	+	+	_	_	_	_	+	+	+
18.	Kp A18	_	_	_	+	+	+	+	_	+	+	_	+	+	_	+	+	+
19.	Kp A19	_	_	+	+	+	+	+	+	+	+	_	+	+	+	+	+	+
20.	Kp A20	+	_	+	+	+	+	+	+	+	+	_	+	_	+	+	+	+
21.	Kp A21	+	_	+	+	+	+	+	+	+	+	_	+	+	+	+	+	+
22.	Kp A22	+	_	+	+	+	+	_	+	+	+	_	_	+	+	+	+	+
23.	Kp A23	+	_	+	+	+	+	_	+	+	+	_	+	+	+	+	+	+
24.	Kp A24	+	_	+	+	+	+	+	+	+	+	_	+	+	+	+	+	+
25.	Kp A25	+	_	+	+	+	+	_	+	+	+	+	+	_	+	+	+	+
26.	Kp A26	+	_	+	+	+	+	+	+	+	+	_	_	+	+	+	+	+
27.	Kp A27	+	_	+	+	+	+	+	_	+	+	_	_	_	+	+	+	+
28.	Kp A28	+	_	+	+	+	+	+	_	+	+	_	+	+	+	+	+	+
29.	Kp A39	+	_	+	+	+	+	+	+	+	+	_	_	+	+	+	+	+
30.	Kp A30	+	_	_	+	+	+	+	+	+	+	_	+	_	+	+	+	+
31.	Kp A31	+	_	_	+	+	+	+	+	+	+	_	+	+	+	+	+	+
32.	Kp A32	+	_	+	+	+	+	+	+	+	+	_	+	+	+	+	+	+
33.	Kp A33	+	_	+	+	+	+	+	_	+	+	_	+	_	+	+	+	+
34.	Kp A34	+	_	+	+	+	+	+	_	+	+	_	+	+	+	+	+	+
35.	Kp A35	+	_	+	+	+	+	+	_	+	+	_	+	+	+	+	+	+
36.	Kp A36	+	_	+	+	+	+	+	_	+	+	_	+	+	+	+	+	+
37.	Kp A37	+	_	+	+	+	+	+	_	+	+	_	+	+	+	+	+	+
38.	Kp A38	+	_	+	+	+	+	_	_	_	+	+	+	_	+	+	+	+
39.	Kp A39	+	_	+	+	+	+	_	_	+	+	+	+	_	+	+	+	+
40.	Kp A40	+	_	+	+	+	+	_	_	+	+	+	+	+	+	+	+	+
41.	Kp A41	+	_	+	+	+	+	_	_	+	+	+	+	+	_	+	+	+
42	Kp A42	+	_	+	+	+	+	_	_	+	+	+	+	+	_	+	_	+
43.	Kp A43	+	_	+	+	+	+	_	_	+	+	+	+	_	_	+	_	+
44.	Kp A44	+	_	+	+	+	+	_	_	+	_	+	+	_	_	+	_	+
45.	Kp A45	+	_	+	+	+	+	_	_	_	+	_	+	_	_	+	_	+
46.	Kp A46	+	_	+	+	+	+	_	_	+	+	_	+	+	_	+	_	+

47.	Kp A47	+	_	+	+	+	+	+	_	+	+	_	+	_	_	+	_	+
48.	Kp A48	+	_	+	+	+	+	+	_	+	+	_	+	_	+	+	_	+
49.	Kp A49	+	_	+	_	+	+	+	_	+	+	_	+	_	_	+	_	+
50.	Kp A50	+	_	+	+	+	+	+	_	+	+	_	+	_	_	+	_	+

S.N.	**Bacterial Isolates →**	K 69	K 70
	Phage isolates↓		
1.	Kp A1	+	_
2.	Kp A2	+	+
3.	Kp A3	+	+
4.	Kp A4	+	+
5.	Kp A5	+	+
6.	Kp A6	+	+
7.	Kp A7	+	_
8.	Kp A8	+	+
9.	Kp A9	+	_
10.	Kp A10	+	_
11.	Kp A11	+	_
12.	Kp A12	+	_
13.	Kp A13	+	_
14.	Kp A14	+	_
15.	Kp A15	+	_
16.	Kp A16	+	_
17.	Kp A17	+	_
18.	Kp A18	+	_
19.	Kp A19	+	_
20.	Kp A20	+	_
21.	Kp A21	+	_
22.	Kp A22	+	_
23.	Kp A23	+	+
24.	Kp A24	+	+
25.	Kp A25	+	+
26.	Kp A26	+	_
27.	Kp A27	+	_
28.	Kp A28	+	_
29.	Kp A39	_	_
30.	Kp A30	_	_
31.	Kp A31	_	+
32.	Kp A32	_	_
33.	Kp A33	_	_
34.	Kp A34	_	_

35.	Kp A35	_	_
36.	Kp A36	_	_
37.	Kp A37	_	_
38.	Kp A38	+	_
39.	Kp A39	+	_
40.	Kp A40	+	_
41.	Kp A41	+	_
42	Kp A42	+	_
43.	Kp A43	+	_
44.	Kp A44	+	_
45.	Kp A45	_	_
46.	Kp A46	_	_
47.	Kp A47	_	_
48.	Kp A48	_	_
49.	Kp A49	_	_
50.	Kp A50	_	_

+: Lytic activity present, –: No lytic activity, Kp is the abbreviation *for Klebsiella pneumoniae* phages, K1-K70.

Objective 3:

Study on the potentials of bacteriophage therapy in the infections caused by the multidrug-resistant bacterial pathogens (*Klebsiella pneumoniae*) in animal and human infections

Materials and Methods:

3.1 CFU counting of *Klebsiella pneumoniae:* Fifty milliliters of LB was inoculated with a single bacterial colony, incubated at 37 °C at 150 RPM, till the OD reached 0.60at 600nm. After that, we centrifuged it at 3000 rpm for 5 min. After centrifugation, the supernatant was discarded, and the pellet was dissolved in normal saline (0.85%) and washed again with normal saline to perform tenfold serial dilution for colony counting (CFU/mL).

3.2 To determine the LD100 for *Klebsiella pneumoniae* in immunocompetent mice

Table-1: Determination of the lethal dose in healthy mice by giving 1x 10^7CFU/mouse bacterial challenge

Date	Dose of bacteria	Mice condition	Death date and time
24/09/19	1x10^7 CFU/mouse	Active	No
25/09/19	-	Both were ill	No
26/09/19	-	Both died after 48 hours	Yes

After death, mice were dissected, and the samples from spleen, liver, heart and peritoneal fluid were cultured on MacConkey Agar and Blood Agar and incubated for 24hr. *Klebsiella pneumoniae* like growth could be observed, which was further confirmed biochemically. Antibiotic susceptibility was performed according to CLSI guidelines by the Kirby Bauer method (2018).

Thus, concluding that the lethal dose for healthy mice is 1x10^7CFU/mouse. Mice died after 48 hours of bacterial challenge (*Klebsiella pneumoniae*), without producing the immunocompromised state.

Table-2: To determine the lethal dose in healthy mice model by giving (8x 10^7 CFU/mouse) bacterial challenge

Date	Dose of bacteria	Mice condition	Death date and time
24/09/19	**8**x10^7 CFU/mouse	Active	No
25/09/19	-	Severe	Both died within 24 hour

After death, mice were dissected, and the samples from spleen, liver, heart and peritoneal fluid were cultured on MacConkey Agar and Blood Agar and incubated for 24hr. *Klebsiella pneumoniae* like growth could be observed, which was further confirmed biochemically. Antibiotic susceptibility was performed according to CLSI guidelines by the Kirby Bauer method (2018).

3.3 Bacteriophage cocktail dose determination for *Klebsiella pneumoniae* septicemia model

Table- 3 Administration of bacteriophage cocktail ($1x10^2$PFU/mouse) 24 hours after bacterial challenge.

Date	Dose of bacteria 100microlitre)	Dose of bacteriophage cocktail	Mice condition	Death date and time
07/01/20	$7x10^8$CFU/mouse	-	Active	No
08/01/20	-	$1x10^2$ PFU/ mouse	Severe illness, exudative accumulation around the eyes	No
09/01/20	-	-	Severe illness, lethargy, ruffled fur, exudative accumulation around the eyes	Two died 24 hours after bacteriophage dose.
10/01/20	-	-	Severe illness	Two died 48 hours after bacteriophage dose.
11/01/20	-	-	Severe illness	One died 52 hours after bacteriophage dose

Table- 3 Administration of bacteriophage cocktail ($1x10^3$PFU/ mouse) 24 hours after bacterial challenge.

Date	Dose of bacteria	Dose of bacteriophage cocktail	Mice condition	Death date and time
14/01/20	$1x10^8$CFU/ mouse	$1x10^3$ PFU/ mouse	Active	No
15/01/20	-	-	All were severe	One was dead 18 hour after bacteriophage dose
16/01/20	-	-	Slight illness	No
17/01/20	-	-	Active	No
18/01/20	-	-	Active	No

Table- 4 Administration of bacteriophage cocktail ($1x10^4$PFU/ mouse**) 24 hours after bacterial challenge.**

Date	Dose of bacteria	Dose of bacteriophage cocktail 6 hours after bacterial challenge	Mice condition	Death date and time
21/01/20	$1x10^8$ CFU/ mouse	100 µl (cocktail having $1x10^4$ PFU/ mouse)	Active	No
22/01/20	-	-	Severe illness, lethargy, ruffled fur, exudative accumulation around the eyes.	One was dead.
23/01/20	-	-	Moderate illness.	No
24/01/20	-	-	Normal	No
25/01/20	-	-	Active	No

Table- 5 Administration of bacteriophage cocktail ($1x10^5$PFU/ mouse) 6 hours after bacterial challenge

Date	Dose of bacteria	Dose of bacteriophage cocktail 6 hours after bacterial challenge	Mice condition	Death date and time
5/02/20	$8x10^7$ CFU/ mouse	$1x10^5$ PFU/ mouse	All were severe	No
6/02/20	-	-	Moderate illness	No
7/02/20	-	-	Normal	No
8/02/20	-	-	Normal	No
9/02/20	-	-	Normal	No
10/02/20	-	-	Normal	No

After death, mice were dissected, and the samples from spleen, liver, heart and peritoneal fluid were cultured on MacConkey Agar and Blood Agar and incubated for 24h. *Klebsiella pneumoniae* like growth could be observed, which was further confirmed biochemically. Antibiotic susceptibility was performed according to CLSI guidelines by the Kirby Bauer method (2018).

When bacteriophage efficacy was tested 6h after bacterial challenge in preventing the death, it was $1x10^5$PFU/mL concentration was safe. In the control group, mortality was 100%. In experimental groups, with $1x10^2$PFU/mL, the mortality rate was 80%, with $1x10^3$PFU/mL and $1x10^4$PFU/mL, the mortality rate was 20 %

Table- 6 ***Simultaneous administration of bacteria (8x10^7 CFU/ mouse) and bacteriophage cocktail (1x10^3 PFU/ mouse).***

Date	Dose of bacteria	Simultaneous dose of bacteriophage	Mice condition	Death date and time
14/01/20	7x10^{8}CFU/ ***mouse***	1x10^3 PFU/ mouse	Active	No
15/01/20	-	-	Severe illness, lethargy, ruffled fur, exudative accumulation around the eyes.	No
16/01/20	-	-	Three were slightly ill.	Two died after 48 h.
17/01/20	-	-	Two were normal	No
18/01/20	-	-	Normal	No

Table- 7 Simultaneous administration of bacteria (1x10^8 CFU/mL) and bacteriophage cocktail (1x10^5 PFU/mL)

Date	Dose of bacteria	Simultaneous dose of bacteriophage cocktail	Mice condition	Death date and time
21/01/20	(8x10^{7}CFU/mL)	1x10^5 PFU/mouse	Active	No
22/01/20	-	-	Severe illness, lethargy, ruffled fur, exudative accumulation around the eyes.	No.
23/01/20	-	-	Moderate illness.	No.
24/01/20	-	-	Normal	No
25/01/20	-	-	Normal	No

When bacterial challenge and bacteriophage cocktail was given simultaneously at the concentration of 1x10^5 PFU/mL, there was no mortality. However, with 1x10^3 PFU/mL dose, the mortality was 40%.

Table- 8 Administration of higher concentration of bacteriophage cocktail (1x10^{12}PFU/mouse) 6 hours after bacterial challenge

Date	Dose of bacteria	Dose of bacteriophage cocktail 6 hours after bacterial challenge	Mice condition	Death date and time
13/03/20	($8x10^7$CFU/mouse)	$1x10^{12}$ PFU/mouse	Moderate illness	No
14/03/20	-	-	Severe illness, lethargy, ruffled fur, exudative accumulation around the eyes.	No
15/03/20	-	-	All were severe, lethargy, ruffled fur, exudative accumulation around the eyes.	Two died.
16/03/20	-	-	The remaining two were severe, lethargy, ruffled fur, exudative accumulation around the eyes, and one was slightly ill.	Two died.
17/03/20	-	-	One was normal	No
18/03/20	-	-	Normal	No

When the bacteriophage cocktail at the 1x1012 PFU/mouse concentration was administered 6h after bacterial challenge, 80% mortality was observed.

Table- 9 Administration of higher concentration of bacteriophage cocktail ($1x10^{12}$PFU/mouse) 24 hours after bacterial challenge

Date	Dose of bacteria	Dose of bacteriophage cocktail 24 hours after bacterial challenge	Mice condition	Death date and time
13/06/20	$7x10^8$CFU/mouse		Active	No
14/06/20	-	$1x10^{12}$ PFU/mouse	All were severely ill, lethargy, ruffled fur, exudative accumulation around the eyes.	No
15/06/20	-	-	Moderate illness.	No
16/06/20	-	-	Slight illness	No
17/06/20	-	-	Normal	No
18/06/20	-	-	Normal	No
19/06/20	-	-	Normal	No

After death, mice were dissected, and the samples from spleen, liver, heart and peritoneal fluid

were cultured on MacConkey Agar and Blood Agar and incubated for 24hr. *Klebsiella pneumoniae* like growth could be observed, which was further confirmed biochemically. Antibiotic susceptibility was performed according to CLSI guidelines by the Kirby Bauer method (2018).

No mortality was observed when the bacteriophage cocktail at the 1x1012 PFU/mL

Experiment group	Number of mouse	Bacterial count (CFU/mouse)/100 µL	Survival rate (%)	Mortality rate (%)
Control group	5	Normal saline	100%	0%
I	5	3×10^7	100%	0%
II	5	5×10^7	100%	0%
III	5	7×10^7	60%	40%
IV	5	8×10^7	0	100% (between 24-48 h)
V	5	1×10^8	0	100% (between 16-17 h)

concentration was administered 24h after the bacterial challenge.

Table-10. Determination of LD100 of *Klebsiella pneumoniae* in mice septicemia model

Table 2.1. Efficacy of phage cocktail containing 1×10^2 PFU/mouse injected 6 h after bacterial challenge in mice septicaemia experimental group

Mice group	Phage cocktail with 1×10^2 PFU/mouse	Observed severity in septicaemia model after intervention with phage cocktail at the different time point (h)					
		6	12	24	48	72	96
I	Phage cocktail 6 h after bacterial challenge	4+4+4+4+4 (4.0)	4+4+4+4+4 (4.0)	4+4+4+5+5 (4.4)	4+5+5+5+5 (4.8)	5+5+5+5+5 (5.0)	5+5+5+5+5 (5.0)

Table 10. Efficacy of phage cocktail containing 1 x 10^3 PFU/mouse injected simultaneously and 6 h after bacterial challenge in mice septicaemia experimental groups

Mice group	Phage cocktail with 1 x 10^3 PFU/mouse	Observed severity in septicaemia model after intervention with phage cocktail at the different time point (h)					
		6	12	24	48	72	96
I	Simultaneous administration of phage and KpnBHU101	3+3+3+3+2 (2.8)	3+3+3+3+3 (3.0)	3+4+4+4+3 (3.6)	2+5+5+2+2 (3.2)	5+5+1+1+1 (2.6)	5+5+1+1+1 (2.6)
II	Phage cocktail 6 h after bacterial challenge	4+4+4+4+4 (4.0)	3+3+3+3+4 (3.2)	3+2+2+2+5 (2.8)	2+2+2+2+5 (2.6)	1+1+1+1+5 (1.8)	1+1+1+1+5 (1.8)

Table 11. Efficacy of phage cocktail containing 1 x 10^4 PFU/mouse injected 6 h after bacterial challenge in mice septicaemia experimental groups

Mice group	Phage cocktail with 1 x 10^4 PFU/mouse	Observed severity in septicaemia model after intervention with phage cocktail at the different time point (h)					
		6	12	24	48	72	96
I	Phage cocktail 6 h after bacterial challenge	4+4+4+4+4 (4.0)	3+3+3+4+4 (3.4)	3+3+3+3+4 (3.2)	2+2+2+2+5 (2.6)	1+1+1+1+5 (1.8)	1+1+1+1+5 (1.8)

Table 12. Efficacy of phage cocktail containing 1 x 10^{12} PFU/mouse injected 6 h and 24 h after bacterial challenge in mice septicaemia experimental groups

Mice group	Phage cocktail with 1 x 10^{12} PFU/mouse	Observed severity in septicaemia model after intervention with phage cocktail at a different time point (h)					
		6	12	24	48	72	96
I	Phage cocktail 6 h after bacterial challenge	4+4+4+4+4 (4.0)	4+4+4+4+4 (4.0)	4+4+4+5+5 (4.4)	5+4+4+5+5 (4.6)	5+3+3+5+5 (4.2)	5+2+2+5+5 (3.8)
II	Phage cocktail 24 h after bacterial challenge	4+4+4+4+4 (4.0)	3+4+3+3+3 (3.2)	2+3+2+2+2 (2.2)	1+2+1+1+1 (1.2)	1+1+1+1+1 (1.0)	1+1+1+1+1 (1.0)

Table 13. Efficacy of phage cocktail containing 1 x 10^5 PFU/mouse injected simultaneously, 6h before and after; 12h and 24h after bacterial challenge in mice septicaemia experimental groups

Mice group	Phage cocktail with 1 x 10^5 PFU/mouse	Observed severity in septicaemia model after intervention with Phage cocktail at the different time point (h)					
		6	12	24	48	72	96
I	Simultaneous administration of phage and KpnBHU101	2+2+2+2+2 (2.0)	2+3+3+3+3 (2.8)	2+2+2+2+2 (2.0)	1+1+1+1+1 (1.0)	1+1+1+1+1 (1.0)	1+1+1+1+1 (1.0)
II	Phage cocktail 6 h before bacterial challenge	1+2+2+1+2 (1.6)	2+2+2+2+2 (2.0)	1+1+2+1+2 (1.4)	1+1+1+1+1 (1.0)	1+1+1+1+1 (1.0)	1+1+1+1+1 (1.0)
III	Phage cocktail 6 h after bacterial challenge	4+4+4+4+4 (4.0)	3+4+3+3+3 (3.2)	2+2+2+2+2 (2.0)	1+1+1+1+1 (1.0)	1+1+1+1+1 (1.0)	1+1+1+1+1 (1.0)
IV	Phage cocktail 12 h after bacterial challenge	4+4+4+4+4 (4.0)	4+3+4+4+4 (3.8)	3+3+3+4+4 (3.4)	2+2+2+5+2 (2.6)	1+1+1+5+1 (1.8)	1+1+1+5+1 (1.8)
V	Phage cocktail 24 h after bacterial challenge	4+4+4+4+3 (3.8)	4+4+4+3+3 (3.6)	3+2+2+2+2 (2.2)	1+1+1+1+1 (1.0)	1+1+1+1+1 (1.0)	1+1+1+1+1 (1.0)

1 – Normal; 2 – Slight illness, lethargy, ruffled fur; 3 – Moderate illness, severe lethargy, ruffled fur and hunched back; 4- Severe illness with the above sign, exudative accumulation around eyes; 5- Death; Figure in parenthesis shows the average of the signs of all the five mice in a particular study group.

Table 14. Endotoxin and Il-6 levels in mice blood after administration of phage cocktail

Time	Mice (control)		*K. pneumoniae* (control)		Phage 10^5 PFU/mouse (control)		Phage 10^{12} PFU/mouse (control)		Phage 10^5 PFU/mouse		Phage 10^{12} PFU/mouse	
	Endotoxin (EU)	IL-6 pg/mL	Endotoxin (EU)	IL-6 pg/mL	Endotoxin (EU)	IL-6 pg/mL	Endotoxin (EU)	IL-6 pg/mL	Endotoxin (EU)	IL-6 pg/mL	Endotoxin (EU)	IL-6 pg/mL
0.5 h	-	-	-	-	-	-	-	-	1.41	840	1.31	280
3 h	-	-	-	-	-	-	-	-	1.51	340	1.28	1390
6 h	0	0	0.1	135	0	0	0.1	0	1.16	150	1.4	875
9 h	-	-	-	-	-	-	-	-	1.21	140	1.43	340
24 h	0	0	0.71	210	0	0	0	0	1.16	55	1.59	165

The symbol **(-)** represents the blood was not withdrawn at that time point.

Summary of work done and Findings:

The emergence of resistance against last-resort antibiotics, carbapenem and colistin-resistant in *Klebsiella pneumoniae* has been reported across the globe. Bacteriophage therapy seems to be one of the most promising alternatives. River Ganges water is an excellent source of a variety of phages. The project's primary objective was to optimize the quantity and frequency of bacteriophage cocktail dosage/s required to eradicate the *Klebsiella pneumoniae* bacteria in immunocompetent septicaemic mice.

Although, we isolated and purified more than 50 different bacteriophages against *Klebsiella pneumoniae*, we selected the three most active phages ϕKpBHU4, ϕKpBHU7 and ϕKpBHU14 which were characterized by molecular and TEM analysis constituted in the form of cocktail and was given intraperitoneally to mice model after inducing the septicaemia in mice with the constant dose of 8×10^7 CFU/mouse of *Klebsiella pneumoniae*. After that, the efficacy of the phage cocktail was analyzed at different dosages, i.e., in increasing, variable, constant and repeated dosage. Further, Interleukin - 6 and endotoxin levels were estimated with variable doses of phage cocktail.

We could elucidate that phage therapy is effective against the *Klebsiella pneumoniae* septicaemia mice model and a promising alternative to antibiotic treatments. Our work delineates that a single dose of phage cocktail with 1×10^5 PFU/mouse protects the mice from fatal outcomes from different stages of septicemia. However, the higher phage dosage of 10^{12} PFU/mice was fatal when given at the early hours of septicemia, while this high dose was safe at the late stages of septicemia. Moreover, multiple repeated dosages are required to eradicate the bacteria from peripheral blood. In addition, the IL-6 levels in the 1×10^5 PFU/mouse group remain lower, but in the 1×10^{12} PFU/mouse group remains high at all points, which were associated with fatal outcomes.

Our study showed that the optimized relatively lower and multiple dosages of phage cocktails with the strict monitoring of vitals in clinical settings might cure septicaemia caused by MDR bacteria with different severity of infection.

Any publications: Under communication with the title
"**Evaluation of bacteriophage cocktail on septicaemia caused by colistin-resistant *Klebsiella pneumoniae* in mice model.**"

Any patents applied for Nil

Date:

Signature of PI
(Prof. Gopal Nath)